Hydrology
A Science for Engineers

Benoît Hingray
Cécile Picouet
André Musy

HYDROLOGY

A Science for Engineers

HYDROLOGY
A Science for Engineers

Benoît Hingray
Laboratoire d'Etudes des Transferts en Hydrologie et Environnement–Grenoble
Centre National de la Recherche Scientifique (CNRS/France)
Grenoble, Cedex
FRANCE

Cécile Picouet
Expert in hydrological risks, water resources and regional planning
HYDRETUDES, Alpespace
FRANCE

André Musy
Professor Emeritus
Ecole Polytechnique Fédérale de Lausanne (EPFL)
SWITZERLAND

FOREWORD

"There does not exist a category of science to which one can give the name applied science. There are sciences and applications of the sciences, bound together as the fruit of the tree which bears it."

Louis Pasteur

Given the role of water in the Earth system, hydrology is a crucial branch of the environmental and earth sciences. Likewise, given the importance of water to humans and human welfare, hydrology forms a key component of engineering, providing a scientific basis for water resources development. One strives to understand the role of water in the Earth system and the other aims to use that understanding to solve societal problems. These two expectations on the science need not be in conflict, however, especially if hydrology is viewed as a "use-inspired" basic science, in the spirit of Louis Pasteur. Indeed, the intractability of many of the water challenges that face humanity demands more, not less, fundamental understanding of hydrologic variability and complexity, over a range of time and space scales, including the Earth system as a whole. It is in this spirit that Hingray, Picouet and Musy have brought out this new book, aimed at presenting hydrology as both a holistic earth science and engineering science.

Many current textbooks of hydrology tend to present a fragmented vision of hydrology, treating individual processes separately (e.g., precipitation, infiltration, runoff, evaporation), with inadequate emphasis on how many of these processes interact to produce an emergent whole system response. The fact is that the real world hydrologic systems we study, and have to then predict to support engineering designs or decision-making, are in essence whole systems, just as the real problems that we face, such as floods and droughts, are also holistic. This demands that the way we teach hydrology to a new generation of hydrologists must embrace this reality. Yet, historically, this has been difficult to achieve. This book goes a long way towards satisfying this long felt need.

First of all, the book has adopted the catchment as the organizing concept, which is already a major step towards overcoming fragmentation. The description of catchment processes, e.g., wetting, storage and release, are all presented in a holistic manner, being used to track the propagation of precipitation variability as it cascades through the various components of the catchment system. Processes such as interception, runoff generation and evaporation are certainly covered in detail, but without losing sight of the interactions and feedbacks between them, and focusing on how they contribute to the overall catchment

response. Lateral flow processes in the river network that impact on the timing of the runoff response are also covered at a fundamental level and yet these process-based descriptions are ultimately linked to holistic, catchment-scale representations, such as the unit hydrograph, thus ultimately connecting to engineering practice as well.

In fact, in respect of the holistic treatment, the book goes even further. The material presented is organized around the practice of catchment modeling. Modeling issues are introduced right at the beginning and are continued right through the book in a coherent manner. For example, after a brief introductory chapter, Chapter 2 already covers preparation of input data (both climatic and landscape) for model development and Chapter 3 presents both the science and the art of modeling, including a range of modeling approaches (lumped versus distributed, etc.), model calibration and parameter regionalization as well as uncertainty analysis. This is a novelty in so far as current hydrology textbooks are concerned, in that the notion of model-based synthesis is introduced right at the beginning and continued right through, so there is less chance for readers to become accustomed to a fragmented view of hydrology.

The treatment of hydrology as an engineering science demands a serious effort at bringing about a synthesis between science and practice. Being aware of the practical relevance of hydrologic science is important to keep us on track, to prevent us from wandering off to an ivory tower of hypothetical methods for idealized situations. Practice sharpens the focus on what is important and steers us towards adoption of targeted methods appropriate for a common set of problems. Advances in hydrologic process understanding and the ability to make predictions for the right reasons are the surest way to contribute towards improvements in water resources development and the alleviation of natural hazards. The book recognizes the importance of this by devoting four chapters to a comprehensive and state-of-the-art treatment of fundamental issues underpinning several mainstream hydrologic problems, such as low flow analysis, flood estimation, flood forecasting and methods of regionalization for predictions in ungauged basins.

Importantly, and on a related note, the book has been framed within the perspective of a modern hydrologic practitioner in the era of computers, satellites and electronic data transmission, channeling and synthesizing the major advances in hydrologic process understanding, including methodological advances that have been achieved in the past fifty years, into a unified treatment. For example, the final chapter introduces the reader to a broad coverage of the multi-scale climatic and meteorological drivers of catchment hydrologic responses and their connections to global and regional atmospheric and oceanic circulation patterns, including possible long-term climate changes. In doing so, the authors have succeeded in producing an advanced, up-to-date and comprehensive textbook for engineers and scientists. The book is an updated translation of an original version published in French. The material presented, including analysis methods, are universally applicable and the book will have wide appeal.

In conclusion, given the contents of the book and the strongly and long-felt need for a hydrology textbook dealing, in a holistic manner, with recent advances in both technological capabilities and process understanding, the publication of this book is very

timely. I congratulate the authors for an outstanding product of their labors. I am confident that the book will be warmly welcomed by hydrology teachers and practitioners and will be widely used.

Murugesu Sivapalan
Professor of Civil and Environmental Engineering
Professor of Geography and Geographic Information Science
University of Illinois at Urbana-Champaign
United States of America

PREFACE

The pressure exerted by man on the environment, in particular on water resources, is increasing every day. At the same time, exceptional hydroclimatic events are occurring more frequently in many parts of the world, often with catastrophic consequences. As a result, effective management of water resources and associated risks has become essential to satisfy the social and economic needs of our society while improving the protection of life and property and safeguarding our environment.

This growing need has raised new questions that call for a deeper understanding of underlying hydrological processes. Rigorous studies are now required to design, build and manage the diverse hydraulic works that go into service every year. Hydrological sciences and their different disciplines, including conventional hydrology, frequency analysis, hydrological processes and snow and glacier hydrology, are the source of methodological and technical developments aimed at building or regulating appropriate water resources engineering projects.

Progress in these diverse scientific disciplines has been a driving force behind the evolution of the education and training of engineers and specialists in natural and environmental sciences in the field of water resources. For example, over more than 20 years, HYDRAM, the former Hydrology and Land Improvement laboratory (now the ECHO Ecohydrology laboratory) of EPFL (Ecole Polytechnique Fédérale de Lausanne) has set up an educational program and forged a high level of expertise in these different fields.

Over the past decade, HYDRAM and PPUR (Presses Polytechniques Universitaires Romandes), the official publisher of the EPFL Press, has published three French-language books in the field of hydrology. These are "Hydrologie 1: une science de la nature" (A. Musy and C. Higy, 2004), "Hydrologie fréquentielle: une science prédictive" (P. Meylan, A.-C. Favre and A. Musy, 2008) and "Hydrologie 2: une science de l'ingénieur" (B. Hingray, C. Picouet and A. Musy, 2009). They expand on two other books published in French by PPUR in related fields, i.e. soil physics ("Physique du sol", A. Musy and M. Soutter, 1991) and water and soil engineering processes and projects ("Ingénierie des eaux et du sol: Processus et aménagements", M. Soutter, A. Mermoud and A. Musy, 2007).

The first two books on hydrology cited above have since been translated into English, published by Science Publishers in the USA and distributed by CRC Press under the titles "Hydrology 1: A Science of Nature" (Musy and Higy, 2011) and "Predictive Hydrology: A Frequency Analysis Approach" (Meylan *et al.*, 2012). The following English edition of the third book, entitled "Hydrology 2: A Science for Engineers", now completes this English-language series in Hydrology.

This third book complements the two other works. It is intended to serve as both an educational and operational resource in the field of hydrology and water resources engineering. It is made up of 12 chapters.

- Chapter 1 provides an introduction.
- Chapter 2 discusses the data required for hydrological analysis and modeling, a topic rarely treated on its own although fundamental to the development of any methodology.
- Chapters 3 to 6 present conventional aspects of water resources engineering with a special focus on hydrological models. Chapter 3 introduces the general principles of hydrological modeling while Chapter 4 deals with the modeling of rainfall excess and associated processes. Chapter 5 covers rainfall-runoff analysis and Chapter 6 discusses reservoir and streamflow routing.
- Chapter 7 presents the specifics of snow hydrology in mountainous regions.
- Chapters 8 to 10 cover aspects of a more operational nature related to the prediction or forecasting of specific hydrological variables. Chapters 8 and 9 deal respectively with the prediction of low flows and floods while Chapter 10 focuses on hydrological forecasting.
- Chapters 11 and 12 cover more recent problems of rising interest concerning regionalization as a way to deal with ungaged basins (Chap. 11) and the production of meteorological scenarios for hydrological analyses related to present or future climatic contexts (Chapter 12).

To help readers review their understanding of the material presented, the key points of the above topics are highlighted at the end of each chapter.

For all the topics, the methods and techniques presented are fully illustrated by numerous figures and examples. In addition, the French edition of this book is supplemented by a set of exercises prepared and presented in widely accessible computer formats, generally accompanied by solutions. This "Hydrothèque" includes more than 150 exercises, often based on concrete problems intended to explain in detail and reinforce the theoretical material presented. They provide a valuable learning resource for students, practicing engineers and scientists alike. Thanks to the extensive use of illustrations, these exercises are readily accessible even to non-French speakers. The Hydrothèque is presently accessible on the site of the LTHE laboratory of Université Grenoble Alpes (www.lthe.fr/ PagePerso/hingray/PAGES/Accueil.html).

Certain subjects of this book involve processes underlying the considered hydrosystems. Their descriptions are often based on material presented in the other books of the HYDRAM series mentioned above. The same is true for the scientific foundations of the statistical methods presented, often related to frequency analysis.

The original French edition of this book was the result of an extensive collective effort. Over and above the fundamental input of the three main authors, the book more widely reflects the work of a dedicated team, that of the former HYDRAM laboratory of the EPFL. Without naming all those who participated to varying degrees in any particular phase of the preparation of this book, I would like to sincerely and warmly express my gratitude to all the members of this laboratory who contributed in different ways, through their research and teaching missions, to the development of the methods and applications forming the basic material that was adapted and expanded as necessary to produce this book.

With regard to all this work, I must emphasize the high level of knowledge, scientific rigor and expertise of Benoît Hingray and the scientific and pedagogical competencies of Cécile Picouet. The scientific and pedagogical quality of this book is largely the result of their fine work and I am sincerely and deeply grateful to these researchers for their precious input.

The original French edition was highly innovative and virtually unique among French publications in the field. The present English version is intended to enhance existing English-language documentation. We hope it will provide an excellent resource for course work and that the wide range of topics covered will serve instructors and researchers as well as engineers and scientists working in hydrology and associated fields. In this way, we are confident that this work will be shared by many to fulfill the overall objective of serving society.

André Musy
Professor Emeritus, EPFL

ACKNOWLEDGEMENTS

CONTENTS

CHAPTER 1

INTRODUCTION

Hydrology is the science dealing with the water cycle in continental environments. This water cycle, often referred to as the hydrological cycle, involves many processes illustrated schematically in Figure 1.1. Understanding and describing these processes figure among the main objectives pursued by hydrologists.
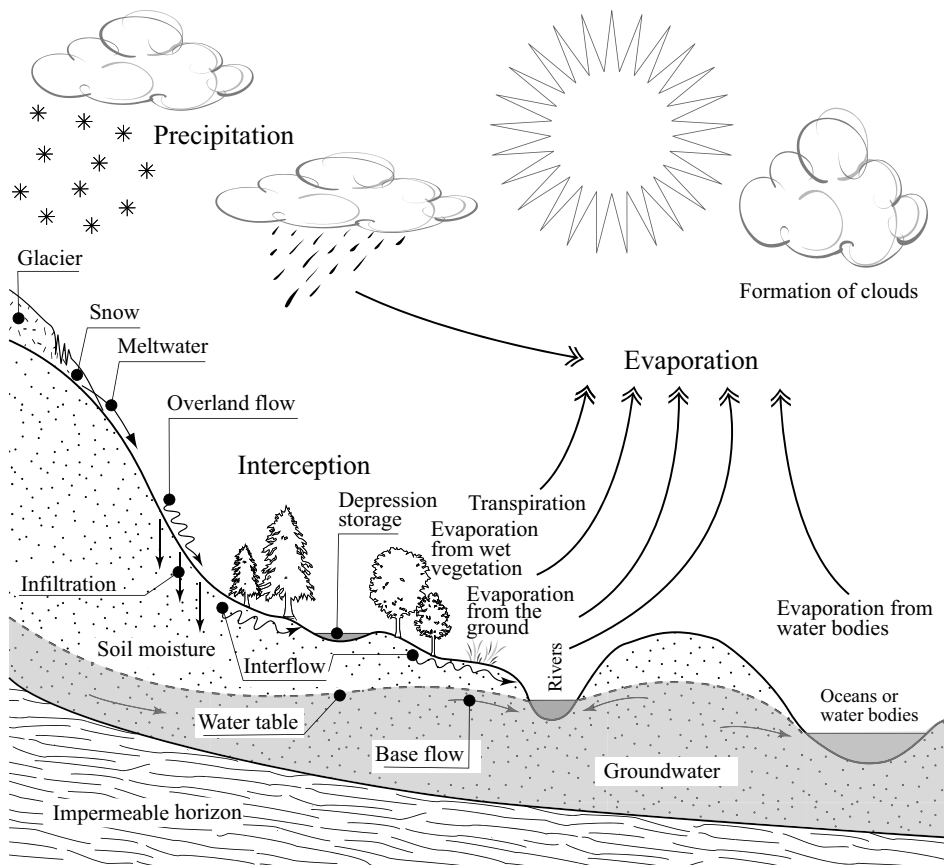
Fig. 1.1: Schematic representation of the water cycle.

Hydrology is however much more than a field of scientific research. It also aims to provide methods and tools to solve concrete problems related to the estimation of water resources and the assessment of hydrological risks.

The objective of this book is to provide the necessary basis for the analyses and modeling required for this estimation. It is a follow-up to the book "Hydrology—A Science of Nature" by Musy and Higy (2011) that presents in particular the various components of the hydrological cycle, drainage basins, factors affecting their hydrological response and the different hydrological regimes, as well as issues related to the measurement and control of hydrological data.

Section 1.1 of this introduction presents the main problems encountered in contemporary hydrology. Section 1.2 deals with the principles underlying the methods used to solve these problems. Section 1.3 presents the content of this book including the topics covered and the organization of the chapters.

1.1 KEY PROBLEMS IN HYDROLOGY

The management of water resources and associated hydrological risks (e.g. flooding, landslides, mudslides, erosion, droughts) is a major concern in our society. It involves many hydrological problems including the key ones presented below.

1.1.1 Prediction of Hydrological Variables

The prediction of certain hydrological quantities is part of the medium-term management of water resources and hydrological risks. Also referred to as «predetermination» in many French-speaking countries, it is generally used for the design of hydraulic works and the application of other measures, structural or non-structural, for the preventive management of hydrological risks. Prediction is also sometimes used to provide diagnostics concerning existing works or systems for which the effectiveness depends on the variability of water resources.

The objective of hydrological analyses conducted in this framework is the estimation of the values of certain hydrological quantities that could be observed at a given location over a given period. Whatever the hydrological variable concerned, the objective is never to estimate the date or time of occurrence.

Given that hydrological quantities vary greatly with time, their estimation is necessarily statistical. The estimation may concern the amount of resources available for a given use, for example the annual inflow for a run-of-river hydroelectric power plant. In this case, the estimation generally takes the form of an expected average value of the hydrological variable concerned along with a characterization of its temporal, seasonal and interannual variability. The estimation also often concerns the risks associated with exceptional hydrological events. In this case, the estimation is generally associated with the frequency of occurrence, exceedance or non-exceedance of certain hydrological variables characterizing these events. This is the case for example for maximum flood or minimum low-flow discharges. The frequency of occurrence of these variables is generally given in terms of a return period expressed in years.

1.1.2 Hydrological Forecasting

Hydrological forecasting is used in the real-time management of water resources and associated hydrological risks. The objective of hydrological forecasting is to estimate the future values of various hydrological variables, their date or time of occurrence or their change over a given time.

Hydrological forecasting is useful in many applications. For example, the use of water in a storage reservoir can be optimized on the basis of forecasted inflows for the *n* days or weeks to come. Forecasting can also be used to anticipate on risks associated with extreme hydrological events, in particular floods and low flows. In this case, the main objective is to reduce potential social and economic disruption, loss of life or injuries and property damage (e.g. via warnings or the operation of hydraulic control works).

1.1.3 Hydrological Impact of Human Activities

Since the dawn of time, human societies have adapted their natural environment and constructed a wide range of regulation works to optimize the management of water resources or reduce hydrological risks. Projects include, for example, the derivation of some or all of a watercourse to irrigate vast expanses of land or the building of dams to produce hydroelectric power or reduce flood peaks. These projects, and their operation, generally significantly modify the hydrological regime of watercourses or even, in certain cases, the hydrological cycle of the corresponding drainage basins.

The hydrological behavior of hydrosystems can also be modified indirectly by human activities. For example, this is the case for the deforestation of certain regions, often linked to local agricultural practices, or the impermeabilization of the ground surface that accompanies the widespread urbanization of drainage basins. Such land use modifications generally lead to major changes in the distribution of water transfers at the soil-vegetation-atmosphere interface, often intensifying extreme hydrological events (e.g. floods, low flows). Transportation and communication routes can also modify the natural boundaries of drainage basins and the corresponding flows.

Whatever the context considered, a major concern for communities is to be able to assess the hydrological impact of their existing or planned projects and activities. One of the key hydrological problems today is to propose methods and tools for such assessments.

1.1.4 Hydrological Impact of Climate Change

Global climate change, related in part to the increase in greenhouse gases resulting from human activities, is progressively modifying regional climates as well as the hydrological cycle and will continue to do so in the future. As a natural consequence, the continental surface, the hydrological behavior of hydrosystems and consequently the water resources and hydrological risks are expected to change to an extent that will vary depending on the region. These possible changes must be assessed to prepare the inevitable adaptations that our society will have to undertake

A hydrological analysis carried out in this context can have for example the objective of estimating changes in the intensity and/or frequency of extreme events or possibly assessing water resource modifications in terms of volumes and seasonal or interannual

variability. This important hydrological problem lies in the framework of the long-term management of water resources and hydrological risks.

1.2 METHODS

The data and methods required to solve these different problems are many and varied. A number of different scientific approaches can nevertheless be distinguished and are presented below.

1.2.1 Statistical Analysis of Observed Data

One of the most frequent hydrological tasks consists in estimating quantities of water that will be observed (e.g. discharges, volumes) at a given location over a given period. If a long series of observations is available for the variable concerned, this estimation can in principle be obtained by statistical analysis of the corresponding data.

Statistical analysis does not necessarily require knowledge of the hydrological phenomena and processes that drive the variation of a given variable with time. It does however require a stationary hydrosystem, which is rarely the case given the often major and repeated modifications to which it is subjected (e.g. development projects or natural modification of the soil cover). This limitation is of course even more important in the context of climate change.

Moreover, data are rarely available at the required locations. As a matter of fact, for many regions of the world, no hydrological data is available. Traditional statistical analysis of observed data is clearly impossible in such a context. It is also unsuitable for problems that require simulation of the hydrosystem's response to a given meteorological forcing. Under these different conditions, hydrological analysis implies estimating the required variables on the basis of other variables and data. Observations of various meteorological variables are for example very often used in this context. The methods associated with these alternative approaches are hydrological regionalization and hydrological modeling, which we will now be discussed.

1.2.2 Hydrological Regionalization

In most cases, hydrologists do not have all the data they need to analyze and/or model the hydrological variable of interest at a given site. In this case, the variable must be predicted or forecasted on the basis of other informative data available for the region or neighborhood of the target site. These data often include geographic and geomorphologic data characterizing the studied basin. They can also include various hydrometeorological variables observed within or near the basin. If the objective is to estimate, for example, a characteristic flood discharge, one possible approach is to use the characteristic flood discharges estimated for gaged basins of the same region.

Such approaches are referred to as regionalization methods. They represent a major portion of methodological and operational development work carried out in hydrology.

1.2.3 Hydrological Modeling

Many methods have been developed to produce unavailable hydrological information from available hydrometeorological data. Most of these methods are based on hydrological models. The majority of these models have been developed to simulate discharges resulting from various meteorological conditions, in particular precipitation. Some models can for example forecast discharges on the basis of meteorological forecasts, while others produce hydrological scenarios corresponding to meteorological scenarios selected or developed elsewhere (e.g. for present or future climatic conditions).

Hydrological models are many and varied. They are often classed according to their concepts, the logic and nature of the mathematical expressions that define quantitative relationships between the model input information (e.g. precipitation) and the model output information (e.g. discharges). From this viewpoint, modeling approaches are often divided into three types: physical, empirical and conceptual.

The physical approach uses the fundamental laws of physics to represent and explain the hydrological processes governing the behavior of the studied hydrosystem. These include the laws of conservation of mass, energy and momentum. They can be expressed in the form of partial differential equations with respect to time and space. If the initial conditions and boundary conditions of the corresponding system of equations were perfectly known, a physical model would be able to reproduce the change of the hydrosystem state variables at any point in space and at any time. This approach has several limitations. First of all, the physical characteristics of the natural environment exhibit high spatial variability that is very difficult or even impossible to describe. Furthermore, the hydrological processes that drive the hydrological behavior of the hydrosystem are so numerous and complex that they cannot all be described. In physically-based models, the description of the processes and the environment must therefore be simplified.

The opposite approach is empirical. Empirical models are based on the observed relationships between the inputs and outputs of the considered hydrosystem. They represent the relationship between system input and output variables (e.g. the rainfall-runoff relationship) by a set of equations developed and adjusted on the basis of data obtained on the system. In this type of model, the hydrosystem is considered as a "black box". The resulting representation can take into account various components of the hydrological cycle. The manner in which this representation works is generally very different from the real working of the hydrosystem. Empirical approaches are usually developed for easy use in operational mode, however they have a number of limitations. Based on the experience of the observer, they can omit one or more important factors affecting the hydrological behavior. Although they are often capable of suitably reproducing observations, it is difficult to use them in hydrometeorological contexts that are different from the ones for which they were developed.

So-called conceptual modeling lies between the two above approaches. Conceptual models are based on a simplified representation of the hydrosystem i.e. its geometry, its physical characteristics and the physical processes that govern its behavior. The representation is conceptual in that it is based on the way the hydrologist perceives the hydrological behavior of the basin. Many different simplifications are possible, leading to a whole series of models. When major simplifications are used, such models tend towards empirical models. On the other hand, minor simplifications lead to models that are similar

to their physically-based counterparts. Conceptual models are often easy to develop and apply. They must however be adjusted to a set of data observed on a given hydrosystem. For this reason, it can once again be difficult to use them in spatial and temporal contexts other than those for which they were developed. Conceptual models often describe the hydrosystem as a combination of conceptual reservoirs assumed to represent its different hydrological compartments (e.g. unsaturated and saturated zones of the drainage basin). These reservoirs are linked to one another by simple transfer relationships. Moreover, each reservoir is associated with a continuity equation. This equation, often referred to as the water balance or storage equation in hydrology, applies in fact to any closed hydrosystem (e.g. drainage basin, river reach or plot of land). It expresses the fact that the change of the volume of water stored in the system over a given time interval is equal to the difference between the sum of the inflows and the sum of the outflows over this time interval (Figure 1.2).
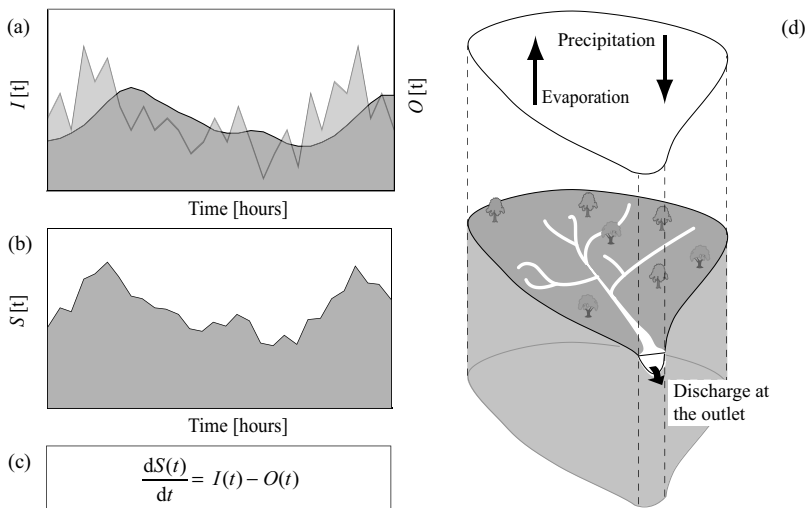
Fig. 1.2: Illustration of the principle of mass conservation of a hydrosystem. a) System inflows ($I(t)$) and outflows ($O(t)$) versus time. b) Changes in the amount of water stored in the system ($S(t)$). c) The continuity equation for the system. d) The spatial limits of the hydrological system considered (here the drainage basin) and some of the incoming and outgoing fluxes included in the overall balance.

1.2.4 Hydrometeorological Scenarios

To manage water resources and hydrological risks in an optimum manner on a medium- or long-term basis, it is necessary to know or determine the possible or probable hydrological scenarios for a given hydroclimatic context. Ideally, it is often necessary to be able to consider a whole series of scenarios to effectively take into account the existing hydrological variability. For most hydrological applications, as long as an appropriate hydrological model is available, the most widely used approach consists in simulating the required hydrological scenarios on the basis of meteorological scenarios identified or generated elsewhere for the given climatic context.

To manage water resources and hydrological risks, it must also be possible to anticipate on the probable changes of hydrological variables in the near future. In most cases, the hydrological forecasts required for this are obtained by hydrological simulations based on suitable meteorological forecasts.

Whether the problem is forecasting or prediction, the determination of meteorological scenarios is one of the key components of the analysis methods used by hydrologists.

1.3 CONTENTS OF THIS BOOK

1.3.1 Topics

This book has twelve chapters including the present introduction (Chapter 1). Chapter 2 presents the data that are necessary and/or generally available for hydrological analysis and modeling. They include time series that make it possible to follow the changes in the meteorological conditions and state variables of the studied system. They also include geographical (spatial) data used to describe the hydrosystem.

Chapters 3 to 7 deal with hydrological modeling. Chapter 3 introduces the general principles of the hydrological modeling approach. It discusses the various problems encountered when building a model and estimating and validating its parameters. Chapter 4 presents various models that can be used to represent and simulate certain processes that determine how precipitation is divided into various components at the soil-vegetation-atmosphere interface (i.e. interception by vegetation, surface storage, evaporation, evapotranspiration, infiltration and overland flow). Chapter 5 deals with the way the resulting direct runoff produces discharges at the outlet of a given basin. Chapter 6 presents aspects related to the propagation of flows along a river and routing of the discharges through lakes and artificial reservoirs. These three chapters deal respectively with what is commonly referred to as rainfall excess, rainfall-runoff analysis and routing (Figure 1.3). Chapter 7 discusses problems related to the hydrological modeling of drainage basins in mountainous regions with glaciers and seasonal snow cover.

Chapters 8 to 10 provide operational solutions to the problems of hydrological prediction and forecasting. Chapter 8 is devoted to the estimation and forecasting of low flows. Chapter 9 deals with the estimation of flood discharges and the determination of
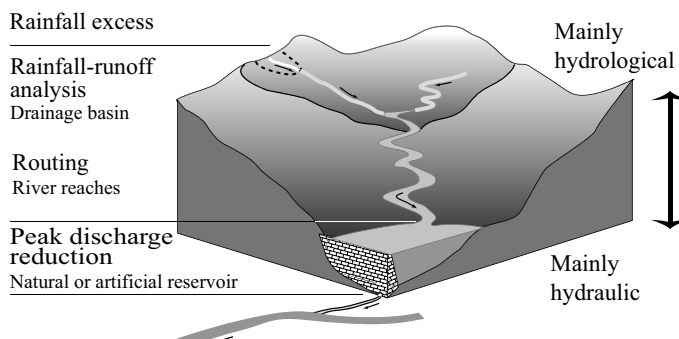
Fig. 1.3: The relative contributions of hydrological and hydraulic approaches in the simulation of discharges.

project flood hydrographs. Chapter 10 presents the different components required to develop an operational hydrometeorological forecasting model.

Chapters 11 and 12 deal with cross-functional hydrological problems. Chapter 11 covers the various possible hydrological regionalization methods. Chapter 12 discusses certain key problems encountered in hydrometeorology, for instance the production of meteorological forecasts and the determination of meteorological scenarios for a given climatic context (present, future) that satisfy the requirements of hydrological analysis and/ or modeling.

Other hydrological topics that are important for engineers could have been discussed in this book. The fact that they have been omitted does not signify that they are less important than those presented here. Various specialized publications devoted to them can be referred to. Readers can for example consult the works of Musy and Higy (2011) for the analysis of hydrological processes and Meylan *et al.* (2012) for frequency analysis and predictive hydrology. French-speaking readers can also consult Chocat (1997) for hydrology in urban environments, Soutter *et al.* (2007) for the management of water and soil and Gilli *et al.* (2004) for hydrogeology.

The French version of this book (Hingray *et al.*, 2009) comes with an interactive CD-Rom entitled "Hydrothèque" containing 150 exercises often corresponding to case studies encountered in environmental engineering practice.[1] Each exercise includes the problem statement along with documents and spreadsheets that provide the context, basic data, results and generally the detailed solutions. These exercises[2] were prepared for undergraduate courses in hydrology and water resources at the Ecole Polytechnique Fédérale de Lausanne (EPFL) and post-graduate courses dealing with these subjects and associated hydrological risks at EPFL and at the Universities of Lausanne and Geneva. They cover most of the topics dealt with in the present book as well as those presented in the book "Hydrology—A Science of Nature" (Musy and Higy, 2011), in the on-line "e-drology" courses prepared by Prof. André Musy and a number of his colleagues (2001)[2] and in the VICAIRE project (Virtual Campus of Hydrology and Water Resources) developed by Prof. Musy and his group and supported by specific Swiss and European research funds (2003).[3]

Some of the exercises focus on other key topics in hydrology that could be of interest to engineers, for example regarding water resources management, urban hydrology and frequency analysis of hydrological variables. A number of exercises deal in particular with preliminary design and diagnostics concerning common hydraulic structures.

These exercises are written and presented in French, however they are readily accessible to all engineers with a basic knowledge of the language of Voltaire.

1.3.2 Chapter Organization

Each chapter first presents the context of the topics covered and the associated problems, then the methods and/or models available to solve them. In some cases, guidelines are provided to help choose the most suitable method or model. The material presented in each

[1]Accessible free of charge at: http://www.lthe.fr/PagePerso/hingray/PAGES/Accueil.htm
[2]Accessible free of charge at: http://echo2.epfl.ch/e-drologie/
[3]Accessible free of charge at: http://echo2.epfl.ch/VICAIRE/index.htm

chapter is illustrated by figures and examples. Additional information can often be found in Addendums presented in boxes within the main text or in Appendices found at the end of the chapter.

The key points concerning each topic are summarized at the end of the corresponding chapter as a reminder.

CHAPTER 2

DATA REQUIRED FOR HYDROLOGICAL ANALYSIS AND MODELING

To understand, characterize and/or model the different phenomena and processes associated with hydrological systems, data are required. They can be divided into two categories:

- time series and historical data used to follow, in a continuous or discontinuous manner, the temporal evolution of meteorological conditions (e.g., precipitation, temperature, wind) and state variables of the hydrological system considered (e.g., discharges, soil moisture, water table level, snow cover, snowpack depth and water equivalent, storage level in natural and artificial reservoirs);
- geographic (i.e., spatial) data used to describe, at a given time, the studied hydrological system (e.g., physiographic characteristics of the drainage basin, characteristics of the hydrographic network, hydraulic structures).

These data are not always available or may be incomplete. When they exist, they may not correspond to the period of interest or may not cover it completely. Note however that the success of hydrological analysis and modeling strongly depends on the existence, accessibility and quality of data.

The objective of this chapter is not to review the different classical or modern data measurement and acquisition techniques—some of which are presented in Chapter 8 (Hydrological Measurement) of Musy and Higy (2011)—but rather to provide an overview of the main data that a hydrological engineer has or needs to carry out hydrological analysis and/or modeling. Sections 2.1 and 2.2 discuss precipitation and discharge data respectively. Section 2.3 deals with other types of meteorological and hydrological data. Section 2.4 presents information used to describe the drainage basin. Finally, Section 2.5 discusses data obtained by remote sensing.

Note that the type and quantity of data required depends on the purpose of the hydrological study (e.g., flood forecasting, low-flow studies, flood hazard mapping). Similarly, the availability and quality of these data, often limiting factors in hydrology, will determine the methods finally used to meet the targeted objective.

2.1 PRECIPITATION

Precipitation data are without a doubt one of the fundamental inputs to many hydrological models. Two main systems are presently used to obtain pertinent precipitation information: rain-gage networks and weather radar. Rain gages provide a direct measurement of precipitation on the ground at each instrumented site. Radar is a remote-sensing technique that provides an indirect estimate of precipitation and in particular its spatial structure.

The main problems facing engineers when using these data are discussed below, including the problem of estimating the total precipitation depth on the scale of the drainage basin, an essential hydrological task. In this regard, note that precipitation varies greatly in space and time. For a given region, this variability depends mainly on the meteorological situation observed on a given day. The reliability of an estimate of precipitation and its variability increases with the frequency and density of measurements.

In addition to precipitation data that have been observed or derived from observations, other types of precipitation data can be used by rainfall-runoff models. These include precipitation forecasts, precipitation scenarios obtained from frequency analysis of observed precipitation or scenarios obtained by simulation using an appropriate stochastic generator (Chapter 12).

2.1.1 Measurement Time Step and Basin Response Time

The appropriate or required time step for the description of precipitation often depends on the objective to be met and the response time of the analyzed system. A weekly or even monthly time step may for example be sufficient for problems related to the seasonal management of water resources (e.g., regulation of reservoirs for the generation of hydroelectric power) or for studies covering very large hydrological systems (e.g., drainage basins with sizes of several tens of thousands of km^2).

Shorter time steps are however required for most hydrological applications. For example, plant growth models require an evaluation of daily precipitation volumes. On the other hand, when sizing the components of a storm drainage network, data at an hourly or even shorter time step are often required.

When working with rainfall-runoff relationships, a first approximation of the required time step can be based on: 1) the time scale required for a good description of the main processes generating floods—related in particular to the production of direct runoff and 2) the responsiveness of the drainage basin, characterized by its concentration time. The latter depends on a variety of factors, in particular the size of the basin (Musy and Higy, 2011). For small and medium-sized drainage basins (i.e., areas up to 10,000 km^2), the required time step is generally less than 24 hours. It is therefore necessary to obtain precipitation data for time steps of one hour or less and even as short as a few minutes for small urban drainage basins that often have a very short response time.

2.1.2 Rain-gage Networks

Point measurements are often the only observations available for hydrological studies. Time series of daily precipitation measured by manual (i.e., non-recording) rain-gage networks generally cover longer periods than those providing hourly or shorter values

measured by recording rain-gage networks, although the density of the latter has increased since the 1970s. Certain daily time series go back to the 19th century.

The uncertainties of measurements and problems concerning their use to estimate precipitation depth over a given area are discussed below.

Uncertainties concerning ground measurements

Particular attention must be paid to the reliability of precipitation measurements carried out with rain gages. Although rain gages are technically simple, many factors can affect measurements (Musy and Higy, 2011). The volumes measured by these instruments depend on the location of the measurement station, the possible presence of obstacles to air currents around the instrument, the shape and orientation of the device and possible losses from evaporation, wind and splashing.

There are also errors inherent to the operation of certain rain gages—for instance the accuracy of a tipping-bucket rain gage is very sensitive to heavy rainfall. A report published by the World Meteorological Organization (WMO, 1994) deals with different aspects of hydrological practices. National weather services, the main providers of precipitation data, generally validate precipitation time series—often by jointly analyzing the diagrams produced by recording rain gages and the daily rain-gage values measured manually by observers.

Solid precipitation can also be poorly estimated even if the gage is equipped with a heating system to melt precipitation falling in the form of snow. In mountainous regions, precipitation measurements often greatly underestimate the real precipitation.

Precipitation measurements therefore include major uncertainties. The precipitation estimates derived from these measurements for use in most hydrological applications have even greater uncertainties. The reasons for this are the poor knowledge of the spatial variability of precipitation and the additional uncertainties introduced by the interpolation techniques used for its spatialization. The accuracy of such estimates depends greatly on the rain-gage network available for the given region (Lebel, 1997). In this respect, it is important to note that in absolute terms, there is no unique optimum rain-gage network. The optimal network for a given case depends in particular on the temporal and spatial resolution required for the hydrological analysis to be carried out—for instance, measurement networks in urban environments must be very dense.

Spatial interpolation and areal precipitation estimates

Most precipitation measurements available to hydrologists are point measurements obtained from a limited number of rain-gage stations. It is however often necessary to estimate, for a given rainfall event or period, the quantity of precipitation that has fallen at a given site for which no measurements are available,[1] or the amount that has fallen on a given area *A*—for example part or all of a drainage basin. The volume of rainfall falling on area *A* over a period Δt is often represented by the average precipitation per unit area or the precipitation depth P_A falling over the entire area. These variables are estimated using spatial interpolation techniques.

---

[1]This may be because the site has no instruments or because the instruments installed at the site were out of service during the period considered.

A wide variety of spatial data interpolation methods exist (Creutin and Obled, 1982). Considering the precipitation accumulated over a given time interval [*t, t+Δt*], the local precipitation $P_M(t)$ that has fallen at a given point $M(x_0, y_0)$, or the precipitation depth $P_A(t)$ falling on area *A*, is estimated by the most widely used methods using a weighted average of the point precipitation values $P_i(t)$ observed at the *n* rain-gage stations located at or near the point or area considered:

At point *M*: $P_M^*(t) = \sum_{i=1}^{n} \lambda_{M,i} \cdot P_i(t)$ (2.1)

On area *A*: $P_A^*(t) = \sum_{i=1}^{n} \lambda_{A,i} \cdot P_i(t)$ (2.2)

where the symbol * indicates an estimate and where $P_i(t)$ is the precipitation recorded at station *i* between times *t* and *t+Δt* and $\lambda_{.,i}$ is the weight associated with this station.

The simplest interpolation method is to assign the same weights λ_i to all neighboring stations having measurements over time interval [*t, t+Δt*]. This is equivalent to taking the arithmetic mean. This method, although seldom recommended, can be used in certain cases if the precipitation and the measurement stations are relatively uniformly distributed over the study region.

The weight λ_i is in fact often calculated as a decreasing function of the distance separating the station *i* from the point or area of interest. This method is often referred to as inverse distance weighted interpolation. Weighting can also be based on the discretization of the area of interest using Thiessen polygons. Another weighting method is based on the plotting of isohyets (contours of equal precipitation depth). All these methods are described in more detail in Appendix 2.7.1. Example 2.1 illustrates how they can be applied.

The inverse distance and Thiessen polygon methods are used widely in operational hydrology. They are particularly attractive because the weights assigned to the different stations do not vary with time (unless the measurement network is modified over the considered period). It is then easy to estimate the average precipitation falling over the successive time steps of a given period. Note however that these methods do not provide an optimal interpolation of the precipitation field from a statistical viewpoint.

On the other hand, geostatistical methods such as kriging, widely used in geoscience applications, provide a statistically optimal interpolation. They also provide the expected variance of the estimation error. The uncertainty concerning the precipitation falling on the considered area can thus be characterized and then used to estimate the resulting hydrological uncertainty. The principles and ingredients required for the application of geostatistical methods for the spatialization of precipitation are presented in Appendix 2.7.2. These methods are however seldom used operationally because they are more difficult to apply than the simple methods presented above. For example, the kriging method requires the fitting of a model (an analytical function) on the empirical variogram derived from observations of the considered field (Appendix 2.7.2). The fitting procedure is difficult to automate and must therefore often be carried out manually. Note that the empirical variogram can vary greatly with time, in particular from one rainfall event to another. It can also be anisotropic and depend on the direction considered. Consequently, kriging is mainly used for the interpolation of precipitation for a limited selection of events or for different mean interannual precipitation values (annual, seasonal). This method

can however be refined in different ways to make it more suitable for a wider range of applications (Appendix 2.7.2).

Marked topographic relief strongly influences the spatio-temporal variability of precipitation. Spatial interpolation of precipitation in this particular context is dealt with in Chapter 7 and, for kriging in particular, in Appendix 2.7.2.

Example 2.1

Annual rain-gage measurements were made at 7 stations located in or near a 57,500 m² drainage basin. The annual average precipitation depth for the basin was estimated successively using the: a) Thiessen polygon method, b) inverse distance method and c) isohyetal method. For each method, WSi is the calculated weight applied to the precipitation Pi measured at station i.
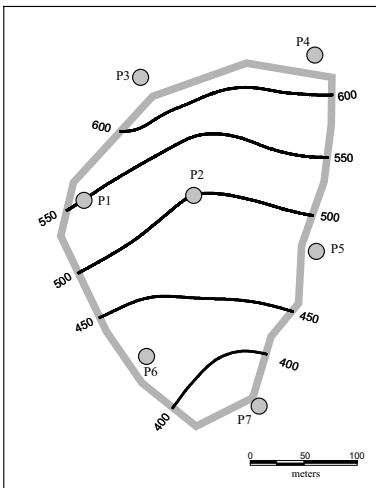
a) Thiessen polygon method

Station	Rain [mm]	Polygon area [m²]	WSi [-]	Pi·WSi [mm]
P1	550	7539	0.13	72
P2	500	6066	0.11	53
P3	625	4591	0.08	50
P4	610	16194	0.28	172
P5	490	3805	0.07	32
P6	425	8123	0.14	60
P7	375	11125	0.19	73
			P_{avg} =	512
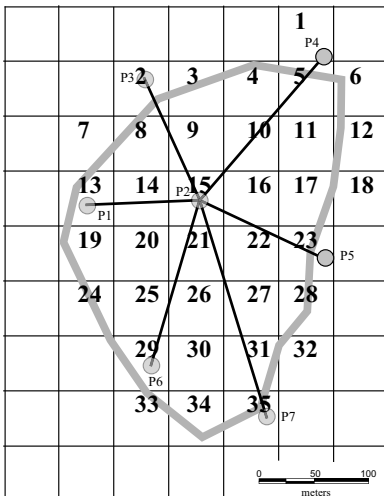
b) Inverse distance method

Station	Rain [mm]	Spatialized method WSi [-]	Spatialized method Pi·WSi [mm]	Basin centroid method WSi [-]	Basin centroid method Pi·WSi [mm]
P1	550	0.15	82	0.13	71
P2	500	0.17	84	0.18	90
P3	625	0.11	66	0.08	51
P4	610	0.07	45	0.07	41
P5	490	0.13	64	0.13	66
P6	425	0.19	81	0.26	112
P7	375	0.18	68	0.14	54
		P_{avg} =	491	P_{avg} =	485

In this example, the rainfall on grid cell 15 is calculated as:

$$\sum_{i=1}^{7} d_{i,M}^{-2} Pi \Big/ \sum_{i=1}^{7} d_{i,M}^{-2}$$

where M is the center of this grid cell. The average rainfall for the entire basin is then the weighted average of the values of all the grid cells (where the weight applied to each grid cell is proportional to its area).
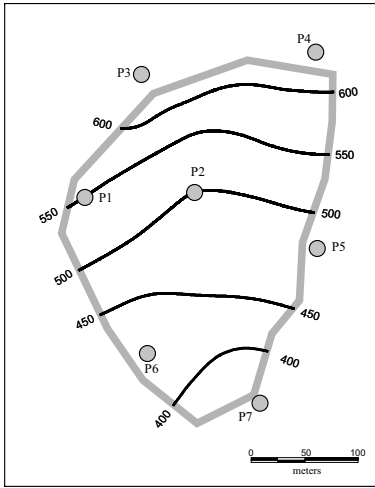
c) Isohyetal method

Inter-isohyets		Average rainfall between two isohyets	Area between two isohyets	WSi	Pi WSi
inf.	sup.	[mm]	[m2]	[-]	[mm]
350	400	375	3425	0.060	22
400	450	425	10146	0.177	75
450	500	475	16087	0.280	133
500	550	525	13974	0.243	128
550	600	575	10161	0.177	102
600	625	613	3651	0.064	39
				P_{avg} =	499

Whatever the spatial interpolation method used, only a rough estimate of the volume of precipitation that actually fell on a given area can be obtained. The uncertainty of the estimated areal precipitation increases as the density of the rain-gage network and the size of the time step considered decrease. Furthermore, the accuracy of the estimation varies from one rainfall event to another. It generally decreases with increasing spatial variability of precipitation (related to the nature of the event and topographic effects) and with decreasing spatial extent of the event.

Given the very local nature of certain precipitation fields, for instance those associated with thunderstorms observed in summer in temperate regions such as Europe, even relatively dense rain-gage networks may not record a precipitation event that causes flooding. An analysis carried out by Neppel *et al.* (2006) illustrates this problem. These authors determined the ability of the rain-gage network of the OHMCV[2] observation system to record different rainfall events. They generated a large number of events with different areas. They were assumed to be circular in shape and their position within the study area was assigned randomly (uniform distribution). The simulation showed that the present observation system, operating since 1960 with an average density of 11 rain-gage stations per 1000 km^2, does not "see" one out of two 80 km^2 diameter events (an event is "seen" if it is recorded by at least one of the stations). They also analyzed an older network operated on the same region from 1900 to 1940, with an average density of 2 stations per 1000 km^2. This less dense network could "see" only one out of two 250 km^2 diameter events. For example, as shown in Figure 2.1, it would not have seen the most intense part of the extreme event that occurred in the Aude department on 12 and 13 November 1999.

Note that all the interpolation methods presented above tend to smooth the real precipitation field. Given that hydrological processes are generally highly non-linear, this

---

[2]OHMCV is the French Cévennes-Vivarais Mediterranean Hydrometeorological Observation System (Delrieu *et al.,* 2005).
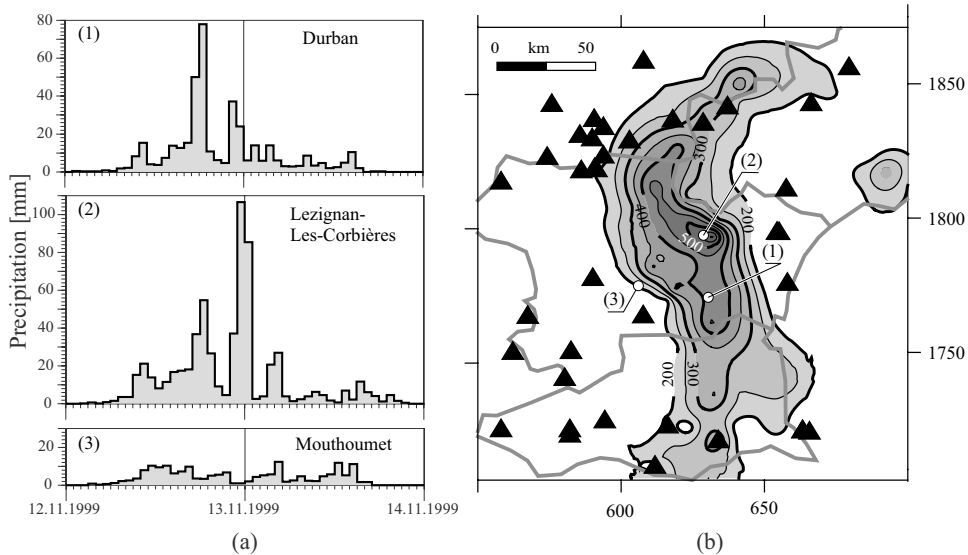
Fig. 2.1: Ability of a rain-gage network to see precipitation events. (a) Hyetographs observed on 12 and 13 November 1999 at three stations located within the OHMCV observation system. (b) Precipitation field estimated for this event based on the stations operated in 1999 (only isohyets greater than 200 mm are represented) and the locations of the stations of the 1930 rain-gage network (modified from Neppel *et al.*, 2006).

smoothing can lead to significant errors in subsequent hydrological analyses, for instance in the estimation of net precipitation and the resulting flood discharges (Vischel, 2006).

Recent and ongoing research tends to reduce these uncertainties. For example, in spite of major limitations, radar techniques can be used to improve the estimation of the spatial variability of precipitation (Section 2.1.3). Atmospheric re-analyses also help reduce uncertainties by providing information on the large-scale meteorological situation for the current day (Section 2.1.3). They provide a better understanding of the origin and regional context of precipitation, improving the incomplete information derived from local observations. Finally, stochastic models can be used to generate conditional random fields to produce different plausible rainfall scenarios and thus described some of the uncertainty related to the estimation of precipitation and its effects (Appendix 2.7.2 and Chapter 12).

2.1.3 Weather Radar

Principles

Radar[3] was initially developed in the 1930s for the detection of approaching aircraft. It is made up of a wave transmitter, a receiver and a signal processing system that can be used to detect a wide variety of objects. Radar transmits pulses of electromagnetic energy in the microwave frequency spectrum and "listens" for any return signal (wavelength generally between 1 and 10 cm) reflected by an object.

Conventional radar measures the power of the wave returned by the target object through backscattering. This power depends on the size and dielectric properties of the

---

[3]The term "RADAR" is an acronym for **RA**dio **D**etection **A**nd **R**anging.

target. The difference in time between the transmitted and received signal can be used to estimate the distance between the radar and the target. Doppler radar measures, in addition to the backscattered power, the phase of the transmitted and returned signals. This can be used to estimate the speed of the target along the line of site of the radar (Tabary, 2002). The direction in which the target is moving can be estimated from the data of two or more Doppler radars.

In recent years, ground radar has become an important instrument in hydrometeorology, in particular for the observation of convective events (Figure 2.2). The radar is designed to detect hydrometeors (water droplets, snowflakes, hailstones). The backscattered power is measured by the radar and converted into a radar reflectivity factor, often referred to simply as radar reflectivity, that characterizes the hydrometeors (Addendum 2.1). Dual polarization
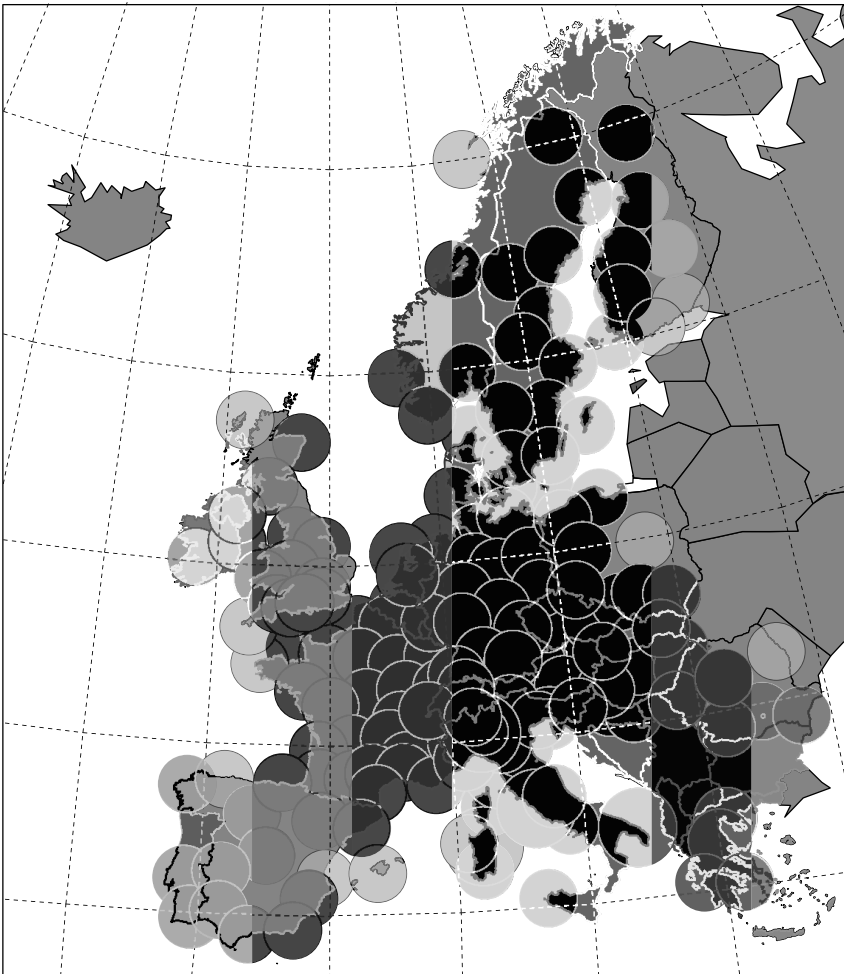
Fig. 2.2: Spatial coverage of Europe by different weather radar systems. The radii of the areas covered are between 150 km and 500 km (as of December 2002, data from the Internet site of the European Meteorological Services network (EUMETNET/OPERA project)). The hydrological visibility of the network is much less than the theoretical visibility presented in this figure (roughly 50% of the area covered by the circles, varying according to the region).

radar also detects the shape of the detected hydrometeors, making it possible to identify their type (water droplets, snowflakes or hailstones) (Sauvageot, 2000). Radar has one clear advantage over classical rain-gage networks in that it can provide a high-resolution estimate of the spatio-temporal variability of precipitation within the radius of a few tens to hundreds of kilometers. With each radar sighting, the estimated precipitation field is updated, thereby continuously monitoring the development and trajectory of precipitation events.

> **Addendum 2.1 Weather radar**
>
> Weather radar measures the backscattering of the transmitted radar wave by hydrometeors present in a given volume. When subjected to an electromagnetic field, water molecules form oscillating dipoles that capture and then retransmit an isotropic field with the same frequency. The most important factors affecting the detection of precipitation are: 1) the characteristics of the radar, 2) those of the target, 3) the atmospheric conditions between the radar and the target and 4) the distance between the radar and the target. For precipitation to be detected, the wavelength λ of the radiation used must be an order of magnitude greater than the size of the hydrometeors (i.e., λ between 1 and 10 cm).
>
> The main characteristics of radar that affect measurement resolution and measurement errors are the: 1) beam aperture, 2) elevation angle and 3) signal range. The wavelength λ used (X-band: $\lambda=3$ cm; C-band: $\lambda=5$ cm; S-band: $\lambda=10$ cm) determines the amount of attenuation error. Radar transmitting small wavelengths has high attenuation error. However, the associated equipment is smaller and less costly than that of longwave radar.
>
> Radar can explore the atmosphere by combining constant elevation-angle antenna rotations and/or constant azimuth vertical scans. Measurements are therefore made in polar coordinates. The atmosphere can be explored on the basis of several antenna rotations at increasing or decreasing elevation angles. The data are often processed by computerized post-processors for different vertical and horizontal cross-sections of the atmosphere. The measurements are then transformed into Cartesian coordinates on pixels that are often square-shaped with a horizontal resolution generally between 0.5×0.5 km and 4×4 km and a temporal resolution of 5 to 10 minutes.

Radar rainfall data and Z-R relationships

One sensitive aspect of radar precipitation measurements is the necessity of finding a relationship to convert the target reflectivity Z obtained by radar[4] into the rainfall rate R on the ground. Two main methods are used to determine rainfall rates from reflectivity data (Vieux, 2001a; Krajewski and Smith, 2002). One is based on measurements obtained from the ground rain-gage network and the other on the size distribution of the raindrops.

The first method directly compares the rainfall rates R_i measured by n rain gages to the n radar reflectivity values Z_i obtained at these rain-gage locations for the same time steps. An empirical *Z-R* relationship is deduced from these observations. This relationship is then used to estimate the intensity of the precipitation at every point of the area for which reflectivity data are available. The *Z-R* relationship established by Marshall and Palmer (1948), expressed as $Z = 200\ R^{1.6}$, is a relationship of this type.

---

[4]A reflectivity map serves as an initial source of purely qualitative information concerning the precipitation detected. Note that it corresponds to precipitation detected at altitudes that increase with the distance from the radar and that are integrated vertically. To obtain an estimate of rainfall rates on the ground, several conversion steps are required.

The second method is based on the fact that the two quantities, Z and R, depend on the size distribution of the raindrops, i.e., the frequency distribution of raindrop diameters, commonly referred to as the drop size distribution (DSD). Under certain assumptions, concerning in particular the shape of the DSD, a theoretical relationship between Z and R can be obtained (Addendum 2.2). In practice, the DSD is often estimated for different calibration events using a disdrometer—a measurement instrument used to estimate the number of rain drops of different sizes reaching the ground, which makes it possible to subsequently calculate Z and R.[5] A relationship of the form $Z = a\,R^b$ is established empirically for the different types of rainfalls commonly observed by the radar (stratiform and convective rainfalls).

These *Z-R* relationships show a high variability, reflected by different parameters a and b, from one region to another, from one precipitation event to another at a given location and within a given precipitation event. The formulas obtained by this method, and the resulting precipitation estimates, are therefore highly approximate. For this reason, rain-gage networks are often used when available to correct the precipitation fields derived from radar reflectivity fields. For this, a mean relative error is often calculated between the measured precipitation on the ground P_i and the precipitation R_i estimated by the radar on the basis of the reflectivity measured at the corresponding site. An average correction factor is then deduced and used to correct the set of precipitation values estimated using radar reflectivity (Example 2.2).

Addendum 2.2 Drop size distribution, reflectivity, rainfall rate and rainfall correction factor

Z-DSD relationship. The reflectivity Z measured by radar is the sum of the individual reflectivity values of all the raindrops contained in the target volume. This can be expressed as:

$$Z = \int_{D=0}^{D=\infty} N(D) \cdot \sigma_B(D) \cdot dD \tag{2.3}$$

where $N(D)$ is the drop size distribution (DSD) for raindrops of diameter D and $\sigma_B(D)$ is the effective backscattering cross-section of a raindrop, assumed to be spherical with diameter D. For a sufficiently long wavelength λ, the effective backscattering cross-section of the raindrop is roughly proportional to the 6th power of its diameter (Rayleigh approximation). The reflectivity measured by the radar can therefore be expressed as:

$$Z = C_Z \int_{D=0}^{D=\infty} N(D) \cdot D^6 \cdot dD \tag{2.4}$$

where C_Z is a constant that depends on the units. Note that other expressions are possible for the general case.

R-DSD relationship. The rainfall rate R for precipitation measured on the ground [mm/h] is related to the raindrop fall velocity. This can be expressed as:

$$R = C_R \int_{D=0}^{D=\infty} V_F(D) \cdot Vol(D) \cdot N(D) \cdot dD \tag{2.5}$$

where $V_F(D)$ and *Vol(D)* are respectively the fall velocity and volume of the raindrop of diameter D, $N(D)$ is the DSD of the event and C_R is a constant depending on the units.

---

[5] Rainfall intensity can obviously be obtained directly via conventional measurements.

Z–R relationship. Using different assumptions concerning the DSD and the shape of the relationship between the fall velocity and diameter of water drops, it is possible to derive a theoretical relationship between the two quantities Z and R.

Based on various measurements, Marshall and Palmer (1948) proposed a 2-parameter gamma distribution to model the DSD, i.e., $N(D) = N_0 \, e^{AD}$ where N_0 is the limiting value of the number of raindrops as their diameter tends to 0 and Λ is a parameter related to the median diameter D_0 of the raindrops and varying with the rainfall rate.

Atlas and Ulbrich (1977) proposed an empirical relationship between the fall velocity V_F [m/s] and its diameter D [m]: $V_F(D) = k \, D^a$.

For a given event, the reliability of the Z–R relationship obtained strongly depends on the pertinence of the DSD model and raindrop velocity model (proposed for atmospheric conditions without downdrafts or updrafts).

Rainfall correction factor F_R. The correction factor F_R is commonly estimated as either: 1) the mean of the station precipitation/radar precipitation ratios of all available stations or 2) the ratio of the mean precipitation estimated on the basis of all the rain-gage stations to the mean precipitation estimated on the basis of all the radar pixels corresponding to these stations.

The example below shows how to calculate the systematic error E of the radar estimates based on the correction factor F_R estimated using method (1) above.

Example 2.2

Precipitation values measured on the ground P_i and estimated by radar R_i at n sites of the study zone are indicated in the table below.

P_i [mm]	R_i [mm]
2.0	4.4
0.5	1.2
6.2	6.7
…	…
$\sum P_i = 12.4$	$\sum R_i = 15.7$

The correction factor F_R is estimated using the equation below. The mean difference between corrected radar estimates and ground measurements then gives an indication of the radar estimation error E.

$$F_R = \frac{\sum_{i}^{n} P_i}{\sum_{i}^{n} R_i} = \frac{12.4}{15.7} = 0.79 \quad E = \frac{1}{n}\sum_{i}^{n}\left|\frac{F_R . R_i - P_i}{P_i}\right| = 36\%$$

(2.6)

In the present case, the correction factor is 0.79 and the absolute value of the mean difference is 36% (+/– 18%). Different precipitation scenarios, and consequently discharge estimates, can be produced on the basis of this indication.

Perspectives and limits for hydrological applications

As opposed to the majority of conventional rain measurement techniques, weather radar can provide real-time measurements of precipitation over an entire drainage basin. It therefore has great operational potential for nowcasting forecasts of precipitation and therefore discharges (Chapter 12) and consequently for optimum management of certain hydraulic works (e.g., storm drainage networks). Radar can also be used to carry out a detailed a posteriori spatial and temporal analysis of storm events.

As for data from any measurement instrument, reflectivity data obtained by radar include certain measurement or interpretation errors. For example, the main problems encountered in hydrological applications include fixed echoes and masked zones resulting from obstacles such as buildings and topographic features (Pellarin *et al.*, 2002), high reflectivity gradients with altitude (Andrieu *et al.*, 1995),[6] attenuation phenomena (Délrieu *et al.,* 2000)[7] and updrafts or downdrafts in the atmosphere. As a result, radar data are particularly difficult to use in mountainous regions or in cities (Figure 2.3). In certain contexts, radar may fail to detect precipitation or detect precipitation when there is none. Radar measurements must therefore be appropriately processed before any comparison with ground precipitation measurements.

In spite of these limitations, weather radar will be used increasingly in operational hydrology. Many hydrological models already use radar rainfall measurements as input data in addition to measurement data from meteorological stations. For more details on weather radar, on how to interpret and manage the corresponding data and on future development perspectives, see for example Meischner (2003) and Bringi and Chandrasekar (2001). Polarimetric radar, capable of identifying and correcting many measurement and interpretation errors, should soon become the new standard in this field. Such radar systems have been dealt with widely by Bringi and Chandrasekar (2001).
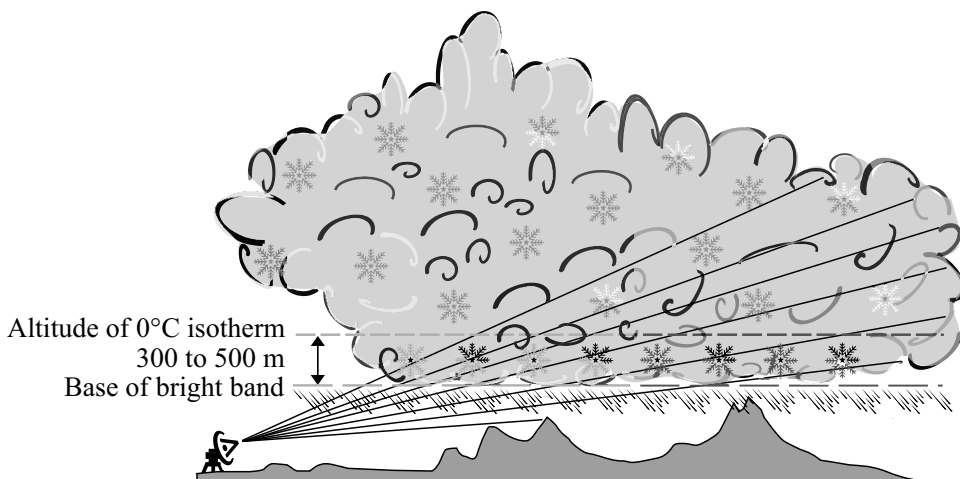
Fig. 2.3: Two main sources of error for radar rainfall measurements. 1) Relief error: Topographic features produces fixed echoes that can mask a downstream zone. 2) Vertical reflectivity profile error: Above the 0°C isotherm, reflectivity is lower than for liquid water drops, while below, the melting of snow crystals causes an increase in radar reflectivity corresponding to a bright band (when snow crystals melt, a film of water forms around each snowflake that radar interprets as very large water drops) (modified from Parent du Châtelet *et al.*, 2005).

---

[6]A *Z-R* relationship is determined assuming a constant vertical radar reflectivity profile (i.e., invariant with respect to altitude) while in reality precipitation may be subject to major modifications from the time it is detected by the radar to the time it reaches the ground.

[7]Water drops and other atmospheric particles between the target and the radar attenuate the radar signal by absorption and diffraction. Water can be present in the atmosphere in different forms (rain/snow/ice) and the proportion of each of these forms also influences radar signal attenuation.

2.1.4 Combining Rainfall Data

Daily data collected by rain-gage networks often provide insufficient temporal resolution. Rain-gage networks providing measurements for hourly or even shorter time steps are therefore indispensable. However—for cost and maintenance reasons—such networks are far less dense than those providing daily measurements. This density is often insufficient to provide a reasonable estimate of the spatial variability of precipitation.

Combining daily and hourly time series from ground measurements

In most hydrological applications, it is obviously of interest to use all available rain-gage information, i.e., information obtained from recording rain gages over short time steps to estimate the temporal variability of precipitation and daily measurements from all rain gages to estimate spatial variability. One possible method is to apply the temporal structure observed at a neighboring recording rain-gage station—for example the nearest—to the daily precipitation measured at a given non-recording rain-gage station. The daily precipitation $R_{S_m}(d)$ observed at station S_m on day d into hourly precipitation is thus "disaggregated" using the following equation:

$$R_{S_m}(d,h) = \left(\frac{R_{S_m}(d)}{\sum\limits_{h=1}^{24} R_{S_n}(d,h)} \right) \cdot R_{S_n}(d,h) \qquad (2.7)$$

where $R_{Sn}(d,h)$ and $R_{Sm}(d,h)$ are respectively the precipitation observed at station S_n and estimated at station S_m for hour h on day j.

Use of an averaged structure based on N neighboring stations around a recording rain-gage station is not recommended for such disaggregation. Such a procedure nearly always smoothes the real temporal structures, which can subsequently lead to an incorrect representation of the different hydrological processes studied.

Combining ground measurements and radar data

Whatever their density, ground measurement networks (e.g., non-recording and recording rain gages) provide only a partial view of the spatial variability of precipitation. Furthermore, data collected from these networks provide limited insight into the structure and movement of precipitation fields. On the other hand, data from radar imagery provides information on the structure and movement of precipitation fields but are hard to use to obtain reliable estimates of precipitation volumes. Note that radar images are obtained at a certain frequency and radar data can therefore only provide a discontinuous view of precipitation over time.

It is therefore useful to combine these two types of information: 1) conventional ground measurements that can be used to calibrate radar images and continuously monitor the process and 2) radar measurements that can be used to estimate the spatial variability of the process.

2.1.5 Rainfall Analysis

Combining different precipitation estimates is clearly a useful venture. Furthermore, new sensors and methods have been developed over the past 30 years to estimate rainfall. For example, imaging radiometers on board geostationary satellites are sometimes used to estimate rainfall activity from the temperature measured at the top of clouds.[8] However, these estimates have a very low spatial and temporal resolution (Section 2.5) and the percentage of rainfall variance explained by satellite measurements remains low—roughly between 50% and 75% even for large time intervals and areas. They are therefore of limited use in operational hydrological applications.

Precipitation has a marked influence on the attenuation of radio signals transmitted and received by cell-phone relays. It may therefore be possible to use these relays to measure precipitation (Messer *et al.*, 2006). The usefulness of this type of measurement stems particularly from the very wide coverage offered by mobile phone operators—sometimes even in mountainous regions—and the high density of relay stations, in particular in urban areas where precipitation must be estimated with a very high temporal resolution. As opposed to radar estimates, this technique does not provide direct access to the spatial variability of precipitation. Only the total precipitation falling between two relays can be estimated.

As long as the different estimates provide some reliable non-redundant information, it may be useful to combine them. For certain well-instrumented regions, such combinations have produced spatialized databases that use all sources of information in the best possible manner. The precipitation fields contained in these databases are sometimes used as "observed" values. The data from such rainfall analyses represent a reference for the concerned region. This reference can be used to study both the structural properties and dynamics of precipitation. It can also be used for hydrological studies (Delrieu *et al.*, 2005). However, such rainfall analyses are not widely used for the time being. Given the tedious nature of processing and merging the different sources of data, such analyses carried out to date often cover only a limited number of rainfall events.

2.2 DISCHARGES

When available, discharge or streamflow data can be used to carry out a statistical analysis of the hydrological regime of a given watercourse or to characterize certain hydrological risks such as those associated with low flows or floods (Chapter 8 and 9). Furthermore, discharge data are primordial for real-time hydrological forecasting (Chapter 10) and for the development of hydrological models, in particular for parameter calibration when needed (Chapter 3).

The quality of discharge data obviously influences the quality of the analyses carried out and/or the representativeness of the model used to reproduce observations—without good measurements, even the best analysis methods and models cannot give good results.

---

[8]An imaging radiometer measures the radiation reaching the satellite from an element of the Earth's surface or atmosphere. The instrument has a number of channels that correspond to different electromagnetic wavelength bands. Thermal radiation from the target can be obtained on the infrared channel. If clouds are present, the temperature immediately above them is measured and the altitude of the top of the clouds can be deduced from the known vertical temperature profile.

The purpose of this section is to present the different uncertainties related to discharge data and demonstrate their importance through several simple analyses.

2.2.1 Discharge Time Series and Uncertainties

Discharge time series can be obtained in a number of ways (WMO, 1994; Musy and Higy, 2011). Generally, continuous streamflow measurements are obtained indirectly by recording water-level variations at a given section (i.e., at a hydrometric station). The graph of stage versus time is converted into a graph of discharge versus time (hydrograph) using a rating curve that defines the stage-discharge relationship (for more information see Musy and Higy, 2011).

Over and above issues related to measurement uncertainty—which depends in particular on the equipment used and measurement conditions—two main problems affect the validity of rating curves. First of all, discharge measurements are seldom available for very low or high flows. According to Lang *et al.* (2006), the highest water level with a discharge measurement generally corresponds to a discharge with a return period of less than 10 years. Extrapolation of rating curves beyond measured discharges can lead to significant errors in the estimation of streamflows for rare events (often more than 20% for the hundred year flood discharge).[9]

The stage-discharge relationship can also vary with time. The validity of the rating curve is directly related to the stability of the control section and flow conditions at the measurement point. If the control section is a calibrated, stable and well-maintained artificial structure, the stage-discharge relationship may be accurate to within 5% and this accuracy will vary little with time. On the other hand, if no structure exists or if the structure is altered—for example by very heavy flood flows—the rating curve may become unreliable. The cause is sometimes heavy erosion or deposition of sediments at the station. Ideally, the rating curve should be checked regularly and updated if necessary. The time interval between these checks should depend on the stability of the discharge measurement control section.

The hydrological regimes of gaged watercourses are increasingly disturbed by hydraulic projects and/or other inflows and outflows upstream of the measurement site. These disturbances must be identified to determine the source of the observed streamflows. They can then be directly integrated in the model of the system. The observed discharges can also be corrected to reconstruct, for example, the discharges that would have been observed without these disturbances. Note however that certain disturbances are not necessarily identifiable (unauthorized pumping) or are not measured. In special case, the corresponding data may be confidential and consequently not available for hydrological study—sometimes the case for disturbances related to hydroelectric power plants. Moreover, these disturbances can change with time (hydraulic construction projects, modification of operating rules), resulting in non-stationary behavior of the system and non-homogeneous series of observed discharges (Figure 2.4).

---

[9]In France, average stream-gaging errors are around 1% for water levels and 3 to 5% for discharges (Lang *et al.*, 2006).
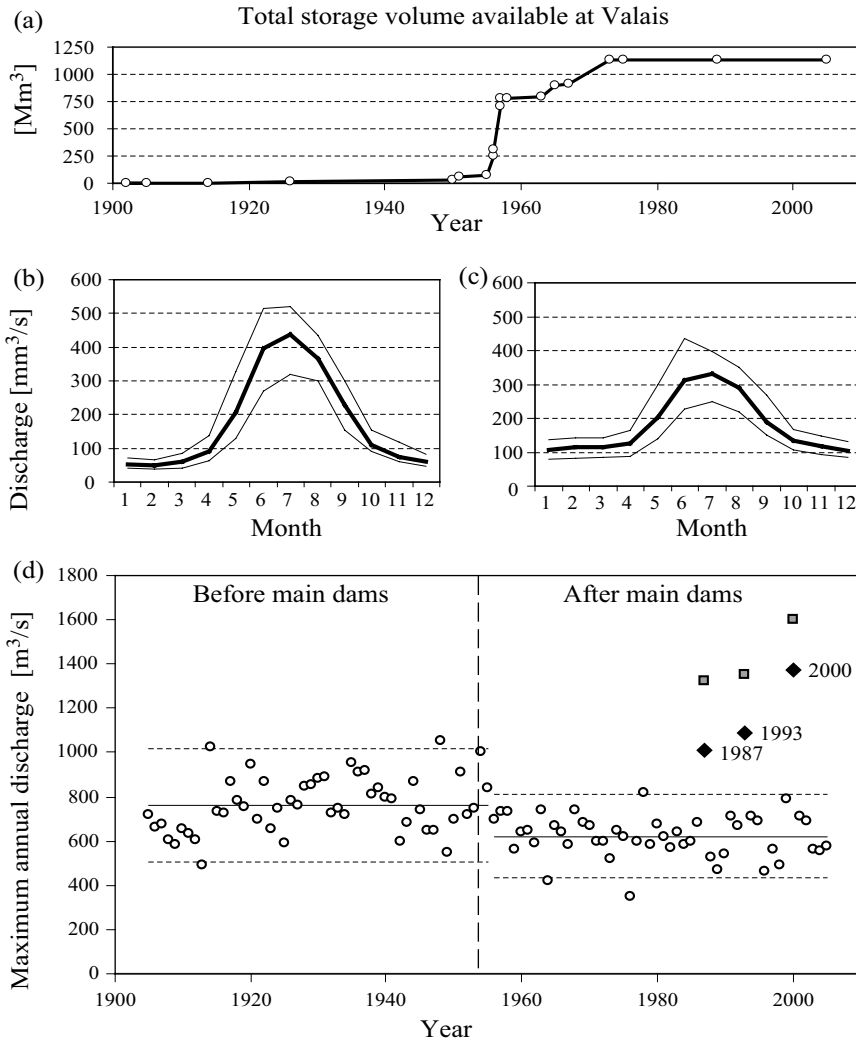
Fig. 2.4: Example of a non-homogeneous discharge time series. (a) Evolution of the total storage capacity of the reservoirs of hydroelectric power projects built in the canton of Valais of Switzerland during the 20th century (from 1905 to 2005). Two-thirds of the 1200 million cubic meters of storage available in 2005 corresponded to projects commissioned between 1955 and 1957 (Grande Dixence, Mauvoisin, Moiry, Tseuzier and Vieux Émosson dams). b) and c) Mean monthly discharges of the Rhone River at Porte-du-Scex (5220 km^2) before and after the construction of the main dams (i.e., 1905–1955 and 1955–2005 respectively). The three curves are the 10, 50 and 90% quantiles of mean monthly discharges. d) Maximum annual discharges of the Rhone River at Porte-du-Scex. The 1987, 1993 and 2000 floods were exceptional events. The diamonds correspond to the observed peak flows (i.e., mitigated by the reservoirs) and the squares are the discharges that would have been observed without the reservoirs, as estimated by the Swiss Federal Office for Water and Geology (OFEG)[10] on the basis of data provided by the reservoir operators (OFEG, 2002).

---

[10]This organization has now become the Federal Office for the Environment (FOEN).

2.2.2 Validation of Discharge Time Series

Even without disturbances upstream of the considered station, available data does not always give a true image of the real phenomena. A preliminary study should therefore be carried out to check their consistency (i.e., absence of contradictions). In addition to the analysis of certain "objective" evidences and information obtained from hydrometric station operators, various simple validation methods can be used (Appendix 2.7.3). These methods may be based on hydrological consistency studies or hydrological models.

2.2.3 Estimation of Discharges in the Absence of Measurements

Discharge time series are generally rare and limited to a small number of hydrometric stations located on the watercourses of a given region.

If no measurement station is present or if existing measurement stations are inoperative, the only way to obtain point information on discharges after an event is to estimate them indirectly (WMO, 1994). Hydraulic structures can for example provide a useful alternative for the estimation of discharges. Information recorded for the operation of hydraulic works (e.g., turbined, diverted and released discharges along with storage variations) can be used to calculate inflows and outflows. The three exceptional flood discharges plotted in Figure 2.4 were reconstructed using this approach. The uncertainty of such estimates can however be relatively high. For large reservoirs, for example, the uncertainty is related in particular to the accuracy of the measurements of the water-level variations used to calculate the changes in storage volumes. In some cases, this uncertainty can even lead to reconstructed inflows taking on negative values.

If all relevant meteorological data are available for a given basin, a discharge series can be reconstructed by simulation using a hydrological rainfall-runoff model. The quality of the reconstructed discharges obviously depends on the quality of the model and the input data—in particular precipitation data. Possible models and their components are dealt with in the following chapters. They require the estimation of a certain number of parameters. If no discharge measurements are available for a given basin, it will not be possible to estimate these parameters using classical calibration procedures (Chapter 3). Instead, regional estimation methods must be used, generally involving various physiographic and climatic characteristics of the basin. This aspect is dealt with in detail in Chapter 11.

Hydrologic studies do not necessarily always require discharge time series. For example, an estimate of the peak flow of a particular flood event may be sufficient. A number of hydraulic estimation methods are available for this, such as the Manning-Strickler equation. These methods do not necessarily require a hydrometric station in operation during the event. This is important given that, during extreme flood events, water-level measurement instruments are often damaged or destroyed by the flood flows. On the other hand, these methods require various data such as the profile of the flow cross-section, the roughness coefficient, the slope of the bed and observations of the high watermark or other indications. High watermarks are the marks or lines left on the river banks by silt or debris at the highest water level reached during a flood. High water indications include marks left on walls or poles.

These methods remain however very approximate given that they are based on a certain number of assumptions that are generally poorly satisfied, in particular for very

heavy floods. In spite of these limitations, these point discharge estimates are often used to add the missing discharges of extreme historical events to available discharge time series. They may also be used to check the relevance of data obtained elsewhere. The usefulness of historical series reconstructed in this manner has for example been demonstrated by Payrastre (2005) for the statistical study of flash floods in the Mediterranean region (Chapter 10).

2.3 OTHER METEOROLOGICAL AND HYDROLOGICAL DATA

Precipitation and discharges are the most widely available and most useful data for hydrological analyses. However, other data are often indispensable to define the state of the system considered, understand the phenomena involved or improve the associated description. Various meteorological data can, for example, be used to describe the conditions to which the considered system has been subjected. Other data may be used to identify the nature of the water volumes stored within the drainage basin and their spatial distribution.

2.3.1 Atmospheric Re-analyses

Many atmospheric measurements have been carried out for decades around the world. They come from ground measurement networks, measurement instruments on board aircraft or ships, weather balloons and various remote-sensing devices. The purpose of atmospheric re-analysis is to bring together all these data and analyze them simultaneously with a single and unique recent version of a meteorological model to propose a global and consistent vision of the atmosphere and its evolution over the considered period.[11]

This "data assimilation" technique (Appendix 2.7.4) can be used to interpolate measurements carried out around the world while respecting certain constraints imposed by physical laws governing the behavior of the atmosphere. This technique is applied a posteriori, i.e., not in real time. It ensures a certain spatial and temporal consistency of the considered variables and makes it possible to reconstruct the corresponding atmospheric and meteorological data, even for regions where measurements are scarce.

The quality of re-analyzed data obviously depends on the quality and density of available measurements. It therefore depends on the region considered. For example, data for the southern hemisphere was insufficient to suitably constrain models until the 1980s. Note that the quality of data tends to improve with time as a result of the assimilation of an increasing quantity and variety of data. However, this also means that re-analyzed data may lack homogeneity over the period covered by the re-analysis. For instance, the introduction of remote sensing in the 1980s resulted in a well-identified alteration in terms of homogeneity. Care must therefore be taken in this regard and changes observed in the products of these re-analyses should not be assimilated too hastily with real changes in the corresponding atmospheric variables (Sturaro, 2003; Sterl, 2004).

Note that the quality of re-analyzed data also depends on the variable considered (Bontron, 2004). Variables related mainly to the dynamic aspects of meteorological models tend to be relatively independent with respect to the model and thus essentially

---

[11]The main principles of meteorological models are presented in Chapter 12.

depend on the available measurements. This is the case, for example, for geopotential fields, temperatures and wind in the upper layers of the atmosphere. On the other hand, for physical aspects such as those related to the generation of precipitation, different models use different parameters and the related re-analyzed data are therefore less reliable. This is the case for nebulosity, precipitation, latent and sensible heat flux and, to a lesser extent, surface temperature or humidity. The robustness of the variables produced by these re-analyses therefore varies according to the degree of dependency of the variables on the measurements or on the model used.

A wide range of variables estimated on the ground (e.g., temperature, precipitation) and at different geopotential levels (e.g., geopotential altitude, temperature, relative humidity, precipitable water, zonal and meridional wind speed)[12] are available. Some atmospheric re-analysis archives have been accessible since 2008. The NCEP/NCAR archives, produced jointly by the National Center for Environmental Prediction (NCEP, US) and the National Center for Atmospheric Research (NCAR, US), are available for the period from 1948 on through to the last complete month of the current year (Kalnay *et al.*, 1996). They are available on 28 vertical levels at a T62 (~1.875°×1.875°) resolution. The ERA-15 and ERA-40 archives are produced by the European Center for Medium-Range Weather Forecasts, funded by the European Community and based in Reading, England (Uppala *et al.*, 2005). They are available for 60 vertical levels over the period 1957–2001 with a T159 (~1.125°×1.125°) resolution.[13] Figure 2.5 illustrates the type of data obtained by NCEP/NCAR re-analyses. Other atmospheric re-analyses are mentioned in Appendix 2.7.6.

Surface variables produced by these re-analyses are generally not suitable for use in hydrological studies. Their spatial resolution is too low and, in addition, they can be highly biased. Atmospheric re-analyses are however extremely useful in providing a regional vision of the atmospheric/meteorological context in which a given hydrological event occurred. They are also often used as a basis for analysis or simulation when local meteorological scenarios must be prepared from synoptic atmospheric situations. The corresponding methods are referred to as downscaling or adaptation. They can be used to produce meteorological forecasting scenarios for the *n* days to come (Obled *et al.*, 2002) as well as probable scenarios for the current climatic context (Buishand and Brandsma, 2001) or possible future climatic contexts (Wilby *et al.*, 1998). The variables mainly used to characterize the current synoptic situation are often related to atmospheric circulation—imposed by the spatial shape of the geopotential fields (Chapter 12).

2.3.2 Other Meteorological Data

Various other meteorological data often prove necessary for hydrological analysis and modeling. This is particularly the case for temperatures. Temperatures influence, for example, the form of precipitation (e.g., rain or snow) and snowmelt volumes. For this reason, they are indispensable when modeling mountainous regions (Chapter 7). More generally, all surface meteorological variables that influence in one way or another the

---

[12]A geopotential surface is a surface with a constant potential (constant pressure). Variables corresponding to 200, 500, 850 and 1000 hPa geopotentials are often used in hydrological applications. The highest available geopotential is 3 hPa for NCEP/NCAR re-analyses and 0.1 hPa for ERA-40 re-analyses.
[13]The T62 (resp. T159) resolution corresponds roughly to a 210 km (resp. 130 km) grid in central Europe.
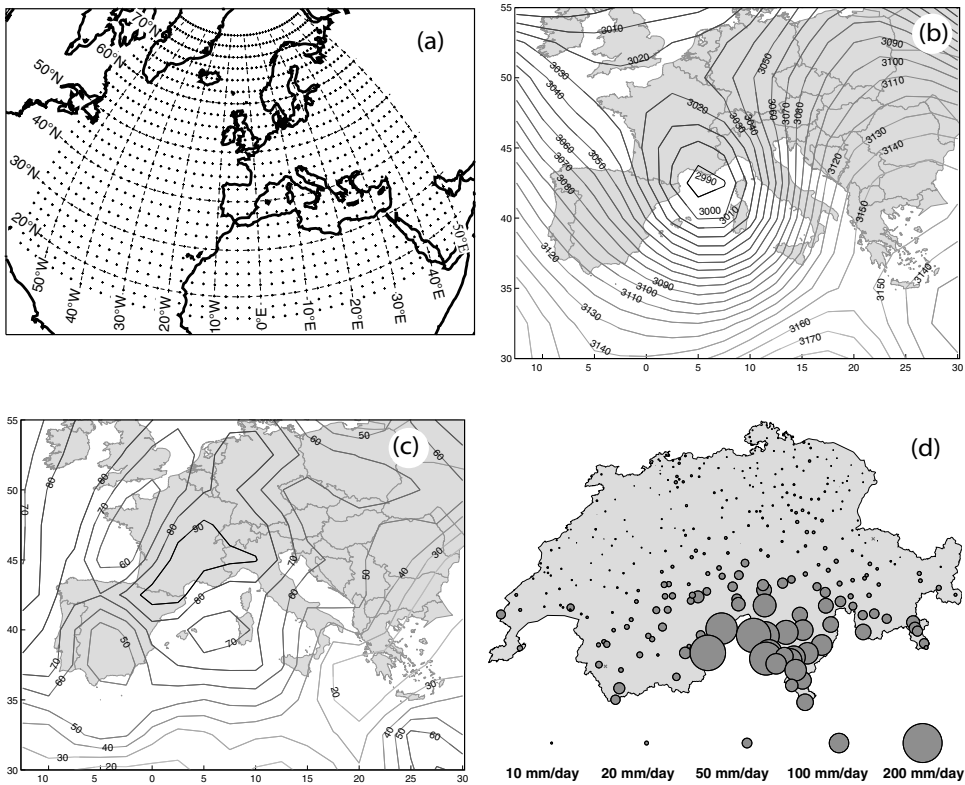
Fig. 2.5: Example of data from NCEP/NCAR re-analyses for 24 September 1993. (a) Storage grid of the archive for Europe. (b) Altitude of the 700hPa geopotential field. (c) Relative humidity field for the 850hPa geopotential. (d) Spatial distribution of daily precipitation observed in Switzerland (MeteoSwiss network).

energy and water balances at the soil-vegetation-atmosphere interface can be useful. This is in particular the case for the variables required for the estimation of evaporative fluxes, indispensable for example to estimate the evolution of basin saturation and in particular its initial state at the beginning of a given rainfall event.

Temperature data

Temperatures are classically measured continuously or recorded at regular intervals by an operator. Temperature time series are generally made up of instantaneous values that provide a good estimation of temporal variations if the sampling time is short enough (hourly or less). In open well-ventilated regions, spatial variations of temperatures are generally limited. Spatial interpolation of temperature measurements is therefore in principle easier than for precipitation. It is therefore often carried out using classical methods such as those presented in Appendices 2.7.1 and 2.7.2. Interpolation can however sometimes be a problem, in particular in regions with high relief. This is because temperature varies strongly with altitude and can also vary over short distances even at the same altitude, for instance in the presence of foehn winds. This aspect is dealt with in Chapter 7.

Different temperature data can also be obtained by remote sensing, which will be discussed at the end of the present chapter.

Data for the estimation of evaporative fluxes

Evaporative fluxes are of different types (Musy and Higy, 2011). They are determined by the surface energy and water balances. The type of data required to estimate these fluxes depends on the type of evaporating surface considered (e.g., soil type, free water surface, vegetation) as well as the estimation method used (Chapter 4).

For example, the estimation of evapotranspiration (ET) fluxes generally requires, in addition to an estimation of the availability of water in the ground, an estimation of the evaporative demand of the atmosphere, either for the considered vegetal cover (ETM) or for a reference vegetal cover (ET_0). This evaporative demand is part of the necessary input data to most hydrological models. It varies with time and is therefore described in the form of time series (e.g., series of mean daily or monthly values). It is generally estimated directly from measurements or using empirical or theoretical formulas based on various measured meteorological data. Depending on the method, these meteorological data include for example temperature, wind speed, air specific humidity and radiation measurements (Addendum 2.3). These data are often obtained from networks of meteorological or climatological stations that generally continuously record a wide range of meteorological variables.

On the scale of the drainage basin, the evaporative demand of the atmosphere is frequently estimated for the main types of vegetal cover present in the basin. Depending on the type of analysis or hydrological model subsequently used, the corresponding series are considered either separately or combined to obtain a series of average values for the basin. This estimation generally requires prior spatialization of the required climatic data. This spatialization is often a difficult task, in particular because the density of climatological stations is generally low. When several stations are present in or near the considered basin, simple interpolation methods such as those presented at the beginning of this chapter for the interpolation of precipitation are generally used (Section 2.3.3).

Various methods have also been developed to estimate and map actual evapotranspiration indirectly from satellite data (Bastiaanssen *et al.*, 2000; Courault *et al.*, 2005). These satellite data can also be used to estimate evaporation from lakes and other water bodies. The estimates obtained are relatively uncertain. This aspect is dealt with at the end of this chapter.

Addendum 2.3 Methods for estimating the evaporative demand of the atmosphere

The evaporative demand of the atmosphere over a given time interval is generally estimated using the so-called maximum evapotranspiration of the vegetal cover (ETM), i.e., the evapotranspiration that would be observed for the vegetation at different growth stages with sufficient water availability and other optimum agronomic conditions (fertility, plant health, etc.). ETM is often inappropriately referred to as "potential evapotranspiration (PET)" by hydrologists. To express this notion in a language familiar to hydrologists, PET will be used instead of ETM in Chapter 4 when dealing with the methods used to estimate evaporation and evapotranspiration losses. Reference evaporative demand or reference evapotranspiration (ET_0) is estimated for a reference vegetal cover (usually grass) that uniformly covers the soil at the maximum growth stage, with sufficient groundwater and optimal agronomic conditions.

These quantities can be evaluated by various measurement and estimation methods (Musy and Higy, 2011). The main estimation methods are summarized below.

Estimation of *ET*

The definition of *ET* (or here *ETM*) is highly dependent on the method and conditions used for its calculation. Operational hydrological methods for the estimation of *ETM* can be distinguished by the data they use:

- **Empirical methods based on temperature** (e.g., Thornwaite or Blaney-Criddle methods). These methods are based on equations that express *ET* as a function of temperature, air humidity and sometimes sunshine duration. Given their empirical nature, their use in a context (climate, time step) other than the one they were developed for is delicate. For this reason, these methods have been widely criticized although they are still very often used.
- **Empirical methods based on radiation** (e.g., Turc or Priestley-Taylor methods). These methods are generally based on the energy balance and use air temperature, relative humidity and wind speed data in addition to net or total radiation data. Given their empirical nature, they have the same limitations as the previous methods.
- **Combined methods based on the energy balance and mass transfer (e.g., Penman-Monteith method)**. Although it requires knowledge of many parameters—including meteorological data and vegetation characteristics—the Penman-Monteith equation is still a reference in the scientific community. It is presented in Appendix 4.8.2. *ET* can be estimated directly using this equation. The specific characteristics of the vegetation are used to estimate the model parameters (ASCE, 1996; FAO, 1998). *ETM* can also be estimated indirectly on the basis of the ET_0 estimated using the Penman-Monteith equation as defined in the recommendations of the FAO. The equation is:

$$ETM = k_c \cdot ET_0$$

(2.8)

where k_c is a crop coefficient that varies according to the vegetal cover and, for a given vegetal cover, according to its growth stage (i.e., physiological activity and ground cover ratio). This coefficient is estimated empirically using nomographs. The typical evolution of this coefficient is given by the FAO (1998) for different crops and by the ASCE (1996) for different types of natural vegetation.

Estimation of ET_0

ET_0 can be estimated on the basis of measurements made using lysimeters or evaporation tanks or by estimation equations. The FAO (1998) recommends ET_0 estimation using the Penman-Monteith method with 0.12 m high grass, a cover resistance of 70 s/m and an albedo of 0.23. The main reason for this recommendation is the necessity of having a standard international method for the estimation of crop water requirements that can be used to compare the evaporative demand of the atmosphere for different regions and meteorological contexts.

Radiation data

Radiation, in particular net radiation, is a key variable in the energy exchanges and consequently in the water phase change processes at the soil-vegetation-atmosphere interface. The net radiation affects for example the surface water evaporation and vegetation evapotranspiration rates as well as snowmelt volumes (Chapter 4 and 7). Estimation of net radiation requires estimation of the absorbed incident solar radiation (a function of the albedo of the ground surface), the absorbed downward infrared atmospheric radiation and the radiation emitted by the Earth's surface. Solar radiation is sometimes measured

continuously by climatological stations. Radiation from the atmosphere and from the Earth are however generally not measured. Various methods have been composed to estimate these variables on the basis of more accessible data. Some of these methods are presented in Appendix 2.7.5.

2.3.3 Analysis of Surface Meteorological Variables

Surface meteorological variables required for hydrological analysis should ideally be estimated at every point of the region studied. This estimation can be based on available point measurements using either of the interpolation methods already presented above (Section 2.1.2). This interpolation is generally not optimal because it does not take into account the spatial variability of the meteorological variables induced for example by the local characteristics of the Earth's surface.

To improve interpolation, spatialization is sometimes carried out by combining point observations with various other data that provide information on the spatial variability of the considered variables. This approach has already been presented for the spatialization of precipitation by merging data from different types of sensors such as recording and non-recording rain gages, radar and cell-phone relays (Section 2.1.4).

Data combination techniques can also be used to spatialize other meteorological variables. Generally this involves merging different types of data such as various types of observations and model output data. Based once again on data assimilation techniques, the approach is similar in principle to the approach used to re-analyze large-scale atmospheric variables (Section 2.3.1). In the present case, data combination techniques are sometimes used to carry out, for a given region, a meteorological analysis of various surface variables. An example of this are the SAFRAN analysis results proposed by Météo-France for the entire French metropolitan territory (Quintana-Segui *et al.*, 2008). These analyses are based on the assumption that the atmospheric variables are uniform within each of the 600 climatic zones defined for France, varying only as a function of topography. The analyses concern eight meteorological variables. For air temperature and humidity, wind speed and nebulosity, the spatial interpolation technique uses, in addition to observations, a first approximation of the field based on the outputs of an atmospheric model. For precipitation, additional information is derived from a climatological analysis of relationships between precipitation and altitude.

For surface variables, meteorological analyses provide valuable auxiliary meteorological data. In particular, they can be used to obtain a homogenized archive of spatialized data (8×8 km for SAFRAN) presenting the same time scale. Note that the quality of this analyzed data can vary greatly according to the variable, region and period considered. It depends on a number of factors including the source data used, the quality and density of available measurements and the complexity of the region considered. The quality of the analyzed data also depends on the nature of the meteorological variable. Given their high spatial variability, the quality of precipitation analyses obtained in this way is in particular often limited (Section 2.1.5). As for atmospheric re-analyses, the quality of meteorological analyses depends on the nature and quantity of data used and can therefore vary greatly over the re-analyzed period.

2.3.4 Other Hydrological Data

In addition to discharge data, other hydrological data can be useful or even necessary for hydrological analysis or modeling. For instance, data may be required to estimate the volume of water stored at the surface in natural or artificial water bodies (i.e., lakes and reservoirs) or in solid form (i.e., snow and ice). For lakes and reservoirs, water-level measurements can be easily converted into storage volumes using specific rating curves. It is however more difficult to estimate the volume of water stored in snow and ice. The reason for this is the heterogeneity of the snowpack and its high spatial and temporal variability. Various types of point and remote-sensing data can be used for this estimation (Chapter 7).

For certain drainage basins, other data are sometimes available. Common examples include water table height, soil moisture at different depths or physico-chemical composition of surface and sub-surface water (Jordan, 1992; Joerin, 2000; Talamba-Balin, 2004). Such data are generally used to improve identification of the mechanisms that generate floods. For example, soil moisture data provides information on the initial state of the drainage basin and on the separation of rainfall into infiltration, runoff and storage. These auxiliary data generally correspond to point measurements at a limited number of sites. This leads to two major problems regarding hydrological analysis and modeling. The first concerns the spatial representativeness of these measurements, for example at the scale of the drainage basin. The other problem is to determine how the corresponding information can be used, for example in hydrological models. Note that the basins for which such data are available are generally of the experimental type and relatively small (e.g., Haute-Mentue and Alptal in Switzerland, Orgeval and Real Collobrier in France, the upper Ouémé valley in Benin). These basins are therefore well-equipped in a manner that is far from representative of the vast majority of basins. Furthermore, such equipment is often installed only on a temporary basis, i.e., for intensive measurement campaigns. The corresponding data are therefore often available only for short periods.

Various remote-sensing data are also available to indirectly estimate and map some of these variables. Note however that the estimates obtained are relatively uncertain (Section 2.5).

2.3.5 Hydrometeorological Analysis

Hydrometeorological or hydrological analyses can also provide precious information. Based on the same principles as the re-analysis of meteorological and rainfall data, the aim of such analyses is to document certain hydrological events in a detailed manner. These analyses can concern some or all of the mechanisms and processes that have led to the hydrological response of the basin to a given meteorological event. For example, this may involve the temporal and spatial variations of meteorological forcing data, initial saturation conditions and their evolution or the mechanisms producing the discharges.

Hydrometeorological or hydrological analyses are carried out a posteriori for the selected events. They are based partly on all the hydrological and meteorological measurements carried out continuously on a given basin and partly on all the other hydrological information obtained by investigations conducted after the event (e.g., high watermarks, personal accounts). They generally also use different models to enhance or validate the

available data by simulations (Section 2.2.3). To provide relevant and useful information, hydrometeorological analyses must however be carried out carefully and consistently. A vast investigation of feedback obtained from real cases, carried out jointly by a number of European research institutes (Gaume, 2007), recently proposed a methodology aimed at satisfying these two criteria.

These analyses can be carried out on the request of local or national authorities after major floods that have produced or could have produced considerable damage in a given basin. The main objective is to obtain practical information concerning the zones affected by the event (e.g., feedback from the Swiss Federal Office for the Environment OFEV/ FOEN for the 2000 flood in the canton of Valais; OFEG, 2002). They may also be carried out by research organizations or technical services on their own account. In this case, the main objective is to understand the explanatory factors and predominant mechanisms behind the generation of floods (Gaume *et al.*, 2003; Delrieu *et al.*, 2005).

2.4 GEOGRAPHIC DATA CONCERNING THE DRAINAGE BASIN

All hydrological studies require information on the drainage basin and its hydrographic network. The basic data required depends however on the study objectives and can be classed in one of the following categories:

- topographic data,
- thematic data describing for example land-use, soils and geological characteristics,
- data on hydraulic projects and structures.

These basic data can be obtained in various manners, extending from field measurements to remote-sensing techniques. They are generally entered in geographic information systems (GIS) from which hydrological parameters of interest or used by simulation tools can be extracted. These geo-referenced data are often of the spatial type.

The above data are first used to characterize the drainage basin and its hydrographic network. For this, different descriptors that characterize the physiography of the drainage basin are generally extracted from them (e.g., average slope, percent forest cover). This characterization is often necessary to estimate the parameters required for application of a given empirical formula. It is also essential for any regionalization work related to the estimation of a characteristic hydrological variable on ungaged basins (Chapter 11).

The data mentioned above are also necessary whenever modeling the hydrological behavior of the basin. They are initially used to discretize the drainage basin into sub-basins or elements of hydrologically uniform behavior (Chapter 3 and 4). They can also be used to describe the topological structure and the various characteristics of the drainage network, whether completely natural, partially modified by reservoirs and/or collectors and diversion works or completely artificial as in urban storm drainage systems (Chapter 5 and 6). Finally, they can be used indirectly to estimate the values of certain parameters required by the model used.

All the required data are not necessarily always available and even when they are, their quality may be insufficient. Note that the available data generally correspond to the state of the system at a given time. They can therefore become unusable if the environment is later subject to anthropogenic or natural modifications. It may be indispensable to model such changes if the behavior of the system is to be simulated over a long period. In any case, it

is important to check the relevance of the geographic data used with respect to the study objectives and constraints.

2.4.1 Data Describing the Hydrographic Network

The hydrographic network, made up of all the natural and artificial watercourses, permanent or temporary which carry water through the drainage basin is one of the main constituents of the drainage basin. The ways in which it can be described have been discussed in detail by Musy and Higy (2011). Note that most hydrological studies require a description of the structure of the hydrographic network, i.e., the topological relationships between the different drainage elements that make up the network and the characteristics of these elements (e.g., geometry, length, slope, hydraulic roughness). In natural environments, it is often also necessary to describe the stream channel, for instance the main channel during normal flows and the flood plain during floods. These different types of information are partially accessible via topographic maps. They are frequently entered in the GIS. They can also be obtained from digital elevation models (DEM),[14] as presented in Section 2.4.2 below.

Various reservoirs or natural water bodies may be found in different parts of a given hydrographic network. As already mentioned in the beginning of this chapter, the hydrological behavior of drainage basins is increasingly often modified by the construction of various projects such as dams and reservoirs. The characteristics of the corresponding works are therefore clearly necessary for any hydrological study. They define the layout of the project within the basin, its geometry and the hydraulic characteristics of any associated equipment. For example, for a reservoir, the elevation-area and elevation-storage capacity relationships must be specified. Both can be estimated on the basis of the geometric characteristics of the project or the topography of the site (Chapter 6). In addition, the geometry and discharge coefficients of the various outlet works must be defined (low-level outlets, spillways, etc.), in addition to the discharge capacity of any pumps or turbines. When an artificial drainage network exists, its structure and the characteristics of the various collection and diversion works (dimensions, slope, roughness), its connections with the natural drainage network and any special works associated with it (overflow weirs, retention basins or stormwater infiltration basins) must also be described. In urban environments, these characteristics are often available via GISs created by local authorities to manage the corresponding drainage network.

2.4.2 Digital Topographic Data

Topography plays a key role in the distribution and propagation of flows within natural and anthropogenically modified systems. Progress in computing has led to the development of digital mapping. Digital elevation models (DEM) are now widely used

---

[14]The terms digital terrain model (DTM) and digital surface model (DSM) are also widely used in the literature, but no standardized definitions exist. These terms may used either as synonyms for DEM or have slightly different definitions. For instance, DTM sometimes refers to models that represent the bare ground surface as opposed to DSM that refers to models that represent the surface with all objects (e.g., buildings, trees). DEM will be used here as a generic term that includes DSMs and DTMs.

to analyze, represent and model drainage basins. With GIS spatial analysis functions, they can be used in particular to characterize the surface topography by automatic extraction of various derived variables. The quality of derived data is highly dependent on the format and quality of the DEM used, which is in turn dependent on the type and quality of source data, the procedures used to control and correct them and the method used for their spatial interpolation and final formatting.

The benefits of the combined use of DEMs and GISs in hydrology have been widely documented in the literature—see in particular Maidment (1993a), Vieux (2001b) and Bedient and Huber (2002). Given their availability on the web and their relatively low cost, DEMs are widely used in hydrological studies (Appendix 2.7.6). This is especially the case for raster DEMs that offer spatial resolutions varying from 50 to 1000 m.

Addendum 2.4 Availability of DEMs

Some cartography organizations offer free public access to large digital elevation databases via the web (Appendix 2.7.6). Free databases are however very few given that the organizations possessing this data are generally funded by selling the data. The situation is however improving because governments are becoming aware of the importance of these data in many civilian applications. For example, in September 2003, the government of the United States authorized the distribution of the files from the Shuttle Radar Topography Mission (SRTM). SRTM30 data (i.e., the updated version of GTOPO30 data) cover the entire globe with a resolution of 1 km and SRTM-3 data offer a resolution of 90 m for roughly 80% the Earth's unsubmerged surface.

Given the strategic importance of geographic information, certain data are however voluntarily altered before being made freely available. Moreover, the data are sometimes supplied in raw form or have not been subjected to the necessary corrections for the creation of a reliable DEM—this was the case in 2007 for SRTM data.

Data sources and methods

DEMs can be based on three types of data: 1) field surveys (x, y, z coordinates of points measured by triangulation), 2) cartographic data (elevation contours on maps) and 3) remote-sensing data (aerial photos or satellite images).

A number of DEMs have been generated by digitizing the elevation contours of topographic maps and then interpolating the data obtained. This method leads to significant errors in certain zones given that adjacent elevation contours always have the same fixed elevation difference, meaning that there are few contours in the flattest zones. It is still used in mountainous areas for which more powerful methods like interferometry are not always satisfactory. In recent years, a number of DEMs based on remote-sensing data have been developed.

Many types of data and processing methods are used to prepare DEMs (Table 2.1). The quality and accuracy of the resulting DEMs can therefore vary greatly. To illustrate this, Figure 2.6 shows five DEMs obtained for the flood plain of the Petite-Glâne River (Switzerland) using different data sources and interpolation methods. The quality of the DEMs is considered to increase from left to right. This classification is based on the visual appearance of the DEMs.

Aerial imaging produces DEMs with higher accuracy than those based on satellite imaging, however for relatively small areas. DEMs can be obtained by stereoscopy from pairs of aerial or satellite photos or by interferometry from pairs of aerial or satellite radar

Table 2.1: DEM characteristics for various data sources and techniques (modified from Dupont *et al.*, 1998).

	Planimetric accuracy	**Altimetric accuracy**
Topographic maps + digitization	10–100 m	5–50 m
Aerial photographs + photogrammetry	2–30 m	<4 m
SPOT satellite images + photogrammetry	20–40 m	10–20 m
Radarsat images + radargrammetry	30 m	15–25 m
ERS radar images + interferometry	30–40 m	5–20 m
LIDAR	0.2–1 m	10–20 cm

Fig. 2.6: DEMs obtained using different data sources and interpolation methods. From left to right: raster and TIN (Triangular Irregular Network) DEMs produced by the Swiss Federal Office of Topography, a raster DEM produced by IGUL (Institute of Geography of the University of Lausanne, Switzerland) and two raster DEMs based respectively on photogrammetry of aerial photographs and analysis of airborne laser measurements (Metzger, 2002). Spatial discontinuities related to roadways present in the area can be distinguished only on the last DEM (adapted from Metzger, 2002).

images. Radar imaging is the best method for regions with heavy cloud cover or little sunlight. In hydrology, airborne laser altimetry, referred to as LIDAR (Light Detection And Ranging), has generated a great deal of interest given the high density of observations (horizontal accuracy of 0.2 to 1 m) and very high altimetric accuracy (roughly 10 cm on flat terrain and less than 20 cm on slopes).

A DEM can be represented in different ways. The most common representations are elevation contours, the raster format and the TIN (Triangular Irregular Network) format (Addendum 2.5).

Addendum 2.5 Common digital elevation model (DEM) structures

The most common DEM structures are shown in Figure 2.7. Each has its own advantages and drawbacks that will be discussed below.
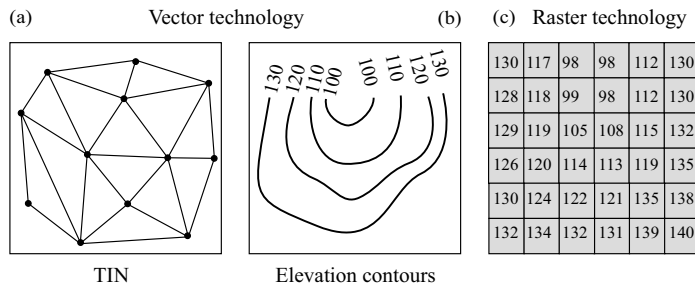
Fig. 2.7: Common digital elevation model (DEM) structures.

Elevation contour DEMs: As already discussed, a topographic representation using elevation contours is poorly suited to the morphology of the terrain. The distribution of data is highly irregular with numerous data along a given contour and no data between adjacent contours.

Raster DEMs: For DEMs based on the so-called raster or grid format (i.e., a regular grid made up of square cells), an elevation value is given either for each node or each cell of the grid, depending on the DEM construction method. Raster DEMs are the most commonly used in hydrological applications because cross-checking with other digital information sources is easy and because algorithms based on this format are easier to implement (Charleux-Demargne, 2001). However, the drawback of this format is that it does not reflect abrupt elevation changes and produces redundant information in areas with low slopes. This makes it difficult to determine flow paths. A number of studies have also emphasized the influence of the grid cell size on the data that can be derived from these DEMs (Charleux-Demargne, 2001).

TIN DEMs: The TIN (Triangular Irregular Network) format represents the topographic surface by a succession of adjacent triangular facets of different shapes and sizes. This irregular grid reduces redundancy in flat areas. The TIN format also allows integration of information given by characteristic points (e.g., orographic features such as summits, bowls and passes) or characteristic lines (e.g., ridge lines, thalwegs, slope break lines, lake contours). This is the best way of representing the morphology of the terrain. TIN DEMs are however much less practical to use than raster DEMs.

Note that it is sometimes necessary to convert from one format to another to satisfy software needs. In this case, it is important to make sure that no critical information (in particular in flat zones) has been lost in the conversion process.

Data derived for hydrological applications

DEMs represent a precious source of topographic information, in particular for identification and characterization of drainage basins and hydrographic networks. In hydrological modeling, they are used to extract model input parameters or as a geometric base for hydrological simulations (Chapter 3).

Many geomorphological parameters describing drainage basins and hydrographic networks can be extracted from DEMs. These parameters may be local (e.g., length and slope of a watercourse or basin, orientation, Strahler stream order) or global with a definition that is either intrinsic (e.g., upstream drainage area) or relative to a selected basin outlet (e.g., distance to the basin outlet, basin hypsometric curve) (Figure 2.8). It is also possible to extract various indexes such as the topographic index described by Beven (1977) used to identify the areas contributing to the production of runoff (Chapter 4).

Elevation   Slope   Orientation   Shade
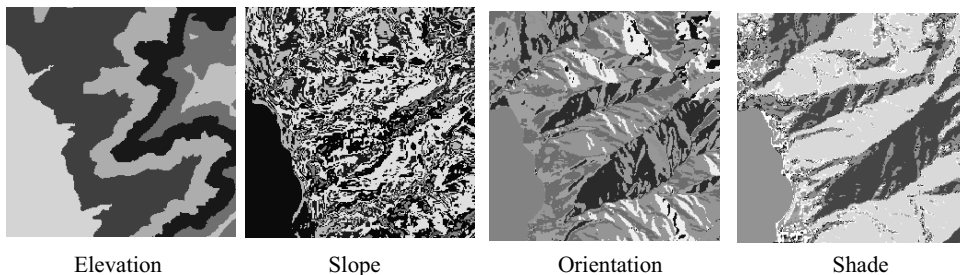
Fig. 2.8: A DEM and derived products. From left to right: DEM, slope (grid-based), orientation and shading of each grid cell.

Many methods have been proposed to automatically extract the hydrographic network and the boundaries of the drainage basins (topographic basins) using raster DEMs. The various steps of the extraction procedure are presented in Addendum 2.6. Note however that automatic extraction remains a delicate task. The relevance of the extracted data depends on the DEM used (format, resolution) and the extraction method. To improve the quality of automatic extractions, in particular for flat areas and sinks, it is generally useful to force the algorithms to use other sources of information. For example topographic maps can be used to obtain the hydrographic network in vector form. Moreover, a hydrographic network should not be extracted from a DEM with a resolution that is insufficient for the considered environment, for example more than 100 m in alpine areas.

It is also possible to determine hydrographic networks using TIN DEMs. Identification of the drainage network is however difficult. It consists in identifying the flow lines which must be perpendicular to the elevation contours at every point. Various software packages can be used for this extraction (e.g., THALES from Grayson *et al.*, 1995).

Note that for the time being, most of these extraction techniques are based on the underlying assumption that only topography influences the flow direction. However, it is known that other factors such as vegetation, geology and bedrock topography also play an important role. Furthermore, natural drainage networks and consequently the boundaries of natural drainage basins are often strongly modified by construction projects in the area, in particular those producing obstacles to flow (e.g., buildings, road embankments) and by artificial drainage elements (e.g., channels or collectors). This is particularly the case in urban environments where, according to certain authors, the size of the grid cells should not exceed one square meter!

In such situations, the hydrographic network and drainage basins can generally no longer be determined solely on the basis of elevation contours or remote-sensing data. The input of GISs, which contain the necessary information within transportation, structures or land-use layers, takes on great importance and vector type representations offer major advantages compared to raster representations.

Addendum 2.6 Deriving a hydrographic network from a raster DEM

1. Extracting the drainage network

When deriving a hydrographic network from a raster DEM, the first step is to extract the drainage network of the corresponding hydrosystem. The objective is to determine the path followed by a drop of water falling anywhere in the system. The drainage network therefore describes the flow directions at all points. For raster type DEMs, each grid cell has eight neighbors. This gives n possible flow directions corresponding to the n neighboring grid cells that are lower in elevation than the considered grid cell (where n is between 1 and 8 depending on the local topographic context). The problem is to determine how the flow must be distributed between these n directions (Figure 2.9). Tarboton (1997) compared different methods. Those based on the use of multiple directions (such as the method proposed by Quinn *et al.*, 1995) appear to be better than the simplest method based on the direction of the line of steepest downward slope (D8 method).

(a)   (b)
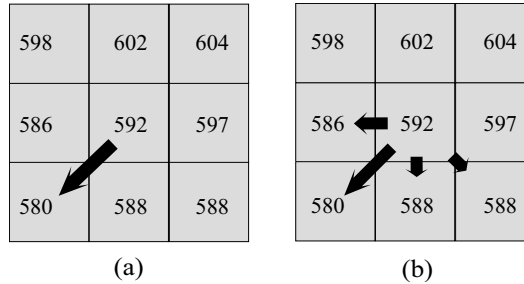
Fig. 2.9: Two possible ways of distributing flows on the basis of topographic data from a raster DEM: a) flow direction corresponding to the line of steepest downward slope and b) multidirectional flow.

2. Estimating upstream drainage areas and extracting the hydrographic network

The drainage network determined above can then be used to estimate the upstream drainage area for every point in the system. It is then possible to deduce the hydrographic network (which is supposed to correspond to the visible drainage network defined by the thalwegs and watercourses). One possible method consists in identifying the set of cells of the system that drain an area greater than a given threshold. This method makes it possible to distinguish between the cells of the drainage network and those of the hydrographic network (Figure 2.10). The value chosen for the threshold determines the complexity of the hydrographic network obtained (Figure 2.11).
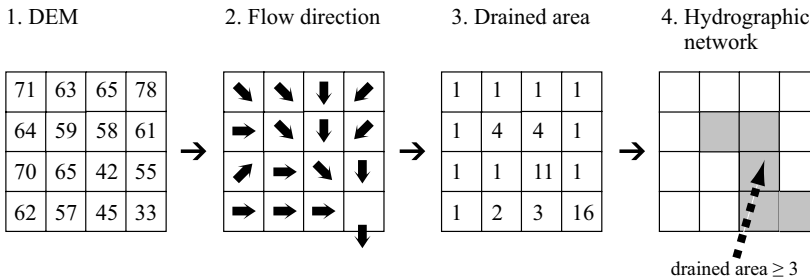
Fig. 2.10: Steps for the extraction of the hydrographic network: (1) DEM, (2) drainage network derived using the D8 method, (3) drainage areas and (4) the derived hydrographic network (the network cells are defined here as those that drain three or more upstream grid cells) (adapted from Charleux-Demargne, 2001).
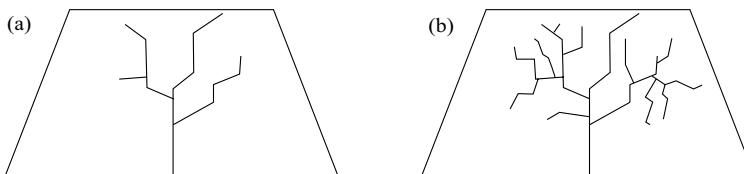
Fig. 2.11: Complexity of a hydrographic network derived from a DEM for two drainage area thresholds chosen for river identification. Threshold A is higher than threshold B (adapted from Payraudeau, 2002).

2.4.3 Thematic Data

Geomorphological information from DEMs can be extended by adding other spatial data from direct observations, traditional maps, remote sensing or any other source of information. The most important data for hydrological studies are those describing the surface (i.e., land-use and vegetation characteristics), soils (type and associated characteristics) and the sub-surface (geology). Some databases available on-line are mentioned in Appendix 2.7.6.

Soil type and associated characteristics

Infiltration parameters for the different types of soil in a drainage basin are required by hydrological models to calculate direct runoff and groundwater recharge. These parameters can be estimated using pedological maps and associated data (i.e., the main physico-chemical characteristics of the soil). Adjustments are however inevitable because the data gathered by pedologists and the data required by hydrologists are different. For hydrological modeling, soils are generally divided into various classes considered to be significantly different with respect to their effects on hydrological processes. The soil types indicated on pedological maps must therefore often be reclassified. In particular, each soil type must be associated with values of the infiltration parameters required by hydrological models. These values are generally taken from the literature or *in situ* measurements.

Vegetal cover

Information on the type of land use (e.g., bare ground, rock outcroppings, water bodies, glaciers, vegetal cover, buildings or pavement) is of capital importance in hydrology. It determines the water and energy balances at the surface. In particular, land use influences the distribution of precipitation between interception, evaporation, infiltration and surface runoff. The presence or absence of vegetation affects the quantities of water that will be returned to the atmosphere by evapotranspiration. The type of land-use also determines the roughness of the surface and therefore the runoff velocity.

Data on vegetal cover and land use are sometimes obtained by ground surveys but more generally by remote sensing. These data can be used to extract or derive various hydrological parameters. As for soil types, it is often necessary to transform thematic data into a form that can be used by hydrological models. Land-use and vegetation classes are for example assigned to new classes in which they are assumed to have similar hydrological behaviors. Each class is therefore characterized by different quantitative attributes (e.g., height of vegetal cover, root depth, leaf area index, albedo). These hydrological classes are often defined to correspond to the different classes mentioned in tables and nomographs already available for the estimation of the various parameters of the model used. The SCS-CN tables presented in Chapter 4 can be used for example to associate a certain runoff potential to each type of surface state. The table of Manning surface roughness coefficients, discussed in Chapter 5, is another typical example of this type of table.

Substratum geology

Data describing the geology of the substratum are also essential to the understanding of observed hydrological processes and to their modeling. The substratum geology first of all affects the flow of groundwater. It also influences soil and vegetal cover characteristics

and consequently the relative proportions of surface runoff versus groundwater. The characteristics of the surface drainage network also depend largely on the nature of the substrate. On highly permeable substrates, all water infiltrates and consequently no hydrographic network is formed. This is often the case for karstic rock and alluvial gravel deposits. On highly impermeable substrates, most of the water is evacuated by surface runoff and the hydrographic network is clearly formed and very dense. This is often the case, for example, for argillaceous substrates and unfissured magmatic rock (Parriaux, 2006).

2.5 DATA OBTAINED BY REMOTE SENSING

2.5.1 Why Remote Sensing?

Ground observations are generally scarce and seldom representative on a regional scale. They offer a very sparse spatial coverage and may not even exist for certain parts of the world. In comparison, remotely sensed data, in particular those obtained from satellites, provide spatialized information that can cover vast regions or even the entire surface of the globe.

Many methods have been developed to make effective use of certain remotely sensed observations and estimate, in an indirect manner, different variables of interest for hydrological analysis or modeling. These methods can be used to improve our understanding of the different physiographic characteristics of a given hydrological system such as topography, surface roughness, vegetal cover and land use (Huang *et al.*, 1995; Schumann *et al.*, 2007). They also provide a wide range of information on system state variables such as soil moisture (Owe *et al.*, 2001), the snow cover as well as the water equivalent of the snowpack (Rango, 1996), the leaf area index of vegetal cover (Guillevic *et al.*, 2002) and the extent of flooded areas (Bates, 2004).

Remote sensing can also provide useful information on the meteorological conditions to which the system is subjected (e.g., precipitation via weather radar), the evaporation rate of lakes and the evapotranspiration rate (Bastiaanssen *et al.*, 2000), surface temperatures (Becker and Li, 1990) and the temperature and humidity profiles of the atmosphere (Renault, 2004).

Schmugge *et al.* (2002) have reviewed remotely sensed data that can be used in hydrological applications. The signals used and the spatial and temporal resolution of the extracted variables depend on the variable considered, the characteristics of the measurement devices and their host (Table 2.2).

2.5.2 Constraints and Uncertainties

The use of satellite or radar observations represents a number of challenges for hydrologists and remote-sensing specialists. First of all, these data cannot be used directly. They require adequate processing for the interpretation and extraction of physical variables compatible with the needs of hydrological models—as already mentioned regarding the use of radar reflectivity for the estimation of precipitation.

Furthermore, remote sensing provides data with highly variable resolutions both in space (pixel size) and in time (dates and number of images), sometimes difficult to

conciliate with the resolutions used to model the rainfall-runoff process. As summed up by Puech (2000): "Hydrological parameters and techniques were designed and developed at a time when remote-sensing techniques did not exist. The parameters extracted from images rarely match those required by models in terms of type of information, accuracy and spatial and temporal scale".

Table 2.2: 2003 projection of hydrological observations expected to be available in 2010 (adapted from Walker *et al.*, 2003). Active sensors transmit waves towards a target and measure the signal returned by the target. Passive sensors measure only waves transmitted by the target. Note that the spatial and temporal resolution as well as the accuracy of possible estimates of a given variable depend on progress achieved in each technology.

Hydrological quantity	Remote-sensing technique	Temporal resolution	Spatial resolution	Accuracy considerations
Precipitation	Thermal infrared	1 hour 1 day 15 days	4 km 1 km 60 m	Tropical convective clouds only
	Passive microwave	3 hours	10 km	Land calibration problems
	Active microwave	30 days	10 m	Land calibration problems
Surface soil moisture	Passive microwave	1–3 days	25–50 km	Limited to sparse vegetation, low topographic relief
	Active microwave	3 days 30 days	3 km 10 m	Significant noise from vegetation and roughness
Surface skin temperature	Thermal infrared	1 hour 1 day 15 days	4 km 1 km 60 m	Soil/vegetation average, cloud contamination.
Snow cover	Visible/thermal infrared	1 hour 1 day 15 days	4 km 500 m–1km 30–60 m	Cloud contamination, vegetation masking, bright soil problems
Snow water equivalent	Passive microwave	1–3 days	10 km	Limited depth penetration
	Active microwave	30 days	10 m	
Water level/ velocity	Laser	10 days		Cloud penetration problems
	Radar	30 days		
Total water storage changes	Gravity changes	30 days	1000 km	Bulk water storage changes
Evaporation	Thermal infrared	1 hour 1 day 15 days	4 km 1 km 60 m	Significant assumptions

Note that estimates of hydrometeorological variables based on remotely sensed data are affected by errors induced by the sensors, atmospheric conditions, vegetal cover and parameterizations used to interpret the data. For certain variables, only the medium- and large-scale spatial structures over long periods are consistent with those obtained on the basis of ground measurements. Under certain conditions (e.g., very dense vegetal cover, observations during rainfall, heterogeneous land use), remotely sensed data may provide no usable information and it may therefore be impossible to extract certain variables (e.g., soil moisture cannot be estimated for very dry surfaces or frozen ground).

Furthermore, most observations are limited to parts of the terrestrial system that can be penetrated by electromagnetic waves transmitted in the microwave, infrared and

visible spectrums. The depth of penetration in the ground corresponds roughly to the wavelength considered. For example, temperature and soil moisture cannot be observed by existing satellite sensors below the first few centimeters of the ground or ocean surface. The estimates are also disturbed by any geometric objects for which the size exceeds the wavelength. Even if the estimate is based on the difference between measurements at two given times to work around this limitation—assuming for example that only soil moisture varies between these times—the residual error remains high.

2.5.3 Applications and Perspectives

In spite of the uncertainties and difficulties encountered on one hand and of acquisition and processing costs on the other, the use of remotely sensed data has a promising future in modern hydrology. A number of operational applications already exist. For example, evaporation from lakes and actual evapotranspiration (Bastiaanssen *et al.*, 2000) can be estimated on the basis of satellite data. Such information is often used for instance to obtain good estimates of crop water consumption over large agricultural regions, making it possible to optimize irrigation.

Various data are frequently used to initialize the state variables of hydrological forecasting models (e.g., snow cover extent, leaf area index). Other data are used to validate the outputs of certain models. For example, Ottlé *et al.* (2003) use maps of flooded areas obtained from radar or optical images to validate model simulations during flooding periods. Similarly, maps of evapotranspiration, snow cover or soil moisture can be used to validate certain modeled processes.

In addition to applications involving the quantitative or qualitative management of water resources, remotely sensed data will play an increasingly important role in meeting the new needs created by the development of global-scale hydrology and the modeling of the impact of climate change on hydrological regimes. Satellite measurements such as those to be supplied by the Global Precipitation Measurement mission are a good illustration of this (Testud, 2002).

Whether provided by point measurements or remote sensing, the quantity of data available is increasing steadily. In this light, it is important to consider the usefulness of continuously striving to obtain more information. Is this trend really improving the representation and modeling of the processes involved? According to Gendreau and Puech (2002), it is time to take a close look at the capacity of existing hydrological models to assimilate distributed data and, if necessary, develop ad hoc models. In addition, given the quantities of data coming from observations of the Earth, it is important to determine priorities to focus measurements on the most relevant hydrological variables.

2.6 KEY POINTS OF THE CHAPTER

- Many types of data are potentially useful for hydrological analysis and modeling. Depending on the region of the world, certain data may or may not be available.
- Most data available for hydrological analysis and modeling are point data and are subject to uncertainties.

- The data required for hydrological studies are not available for most drainage basins. This is particularly the case for streamflow data which, when available, are often highly disturbed by human activities.
- Verification of data quality and consistency is an essential preliminary step to any hydrological study.
- Hydrometeorological variables generally show high spatial and temporal variability. Point observations are often not very representative of regional or local values. Spatial interpolation methods smooth the real spatial variability and introduce additional uncertainties in the estimation of the necessary variables at the drainage basin scale.
- Various geographic data (e.g., altimetric, geological, pedological, physiographic, topological) are required when characterizing drainage basins and building hydrological models. These data concern the different hydrological compartments of the basins (e.g., subsoil, soil, surface, hydrographic network) and any hydraulic works that may be present (e.g., reservoirs, drainage works).
- Remote sensing (weather radar, satellite imagery) can provide, in an indirect manner, spatialized information concerning various characteristics of the basin cover and different hydrological variables. The associated uncertainties can be high.
- Geographic information systems are frequently used to manage data (editing, display). These GISs often form the basis for spatialized hydrological models.
- Digital elevation models are part of basic hydrological data. They are used to derive many types of physiographic data describing for instance basin slopes, the surface drainage network or basin boundaries. The results vary depending on the basic data and processing methods used.
- Today, many different types of data are freely accessible via the Internet. A number of links are indicated in Appendix 2.7.6.

2.7 APPENDICES

2.7.1 Common Interpolation Methods used to Determine Areal Precipitation

Note: The methods presented below do not allow optimum precipitation interpolation from a statistical point of view (Appendix 2.7.2).

Inverse distance weighted average method

To estimate the precipitation at a given point *M,* the weight $\lambda_{M,i}$ assigned to the precipitation measured at every station *i* is an inverse function of the distance between point M and station *i* such that:

$$\lambda_{M,i} = \left(\frac{1}{d_{M,i}} \right)^x / \sum_{i=1}^{n} \left(\frac{1}{d_{M,i}} \right)^x \qquad (2.9)$$

where *x* is a real positive number (often *x* =1 or 2).

To estimate the precipitation falling on a given area *A*, the weight $\lambda_{A,i}$ to be assigned to the precipitation measured at station *i* is often simply estimated as the average of the weights $\lambda_{M,i}$ obtained for all points *M* of the considered area. Another possibility is to base this weight on the distance between the center of gravity *G* of area *A* and station *i*.

This method has a number of limitations. First of all, the estimation is highly dependent on the value assigned to the power *x*. Secondly, the method does not take into account disparities in the spatial distribution of the measurement network (in terms of direction with respect to the point of interest and density). An area with a high density of stations will therefore have a greater influence on the interpolated value than another area located the same distance away but with a lower density of stations. Moreover, all available stations have non-zero weights. Furthermore, a station slightly further away from the point of interest than another station but located in the same direction with respect to the point of interest will have a similar weight (while it could be expected that the nearer station would be much more informative for the considered region).

Thiessen polygon method

The precipitation assigned to a given point *M* is the value measured at the nearest station *i* ($\lambda_{M,i}$ is equal to 1 for the station *i* and zero for all others). This interpolation method leads to the definition of isohyetal zones (corresponding to the so-called Thiessen polygons), each associated with a station *i*. The spatial variation of the interpolated precipitation is therefore discontinuous.
To estimate the precipitation falling on the total area *A*, the weight $\lambda_{A,i}$ assigned to each station *i* is the ratio A_i/A where A_i is the area of the Thiessen polygon surrounding station *i* and *A* is the total area.

Isohyetal method

The isohyets must first be plotted on the basis of point values measured near the region of interest. This is often carried out manually to take into account specific local or regional features (e.g., orographic effects, orientation of basins with respect to that of the main air mass movements).

To estimate the precipitation falling on area *A*, the weight $\lambda_{A,h}$ to be assigned to the precipitation falling on the hth isohyetal zone (often taken as the simple arithmetic mean of the two isohyetal contours delimiting this zone) is the ratio A_h/A where A_h is the area of the hth isohyetal zone and *A* is the total area.

2.7.2 Geostatistics and Regionalization of Precipitation

This appendix was prepared by Charles Obled, professor at the Grenoble Institute of Technology (Grenoble INP), France.

The objective of this appendix is to show why geostatistics have proven to be useful and well-suited to the regionalization of precipitation. To follow the explanations, the only prerequisite is a good understanding of simple and multiple regression techniques, which are related to geostatistics in a relatively straightforward manner.

Consider a precipitation field, for example the total precipitation *P* falling on a given region over time step $\Delta t = 24$ h. Point values of this field are generally available at rain-gage locations $t^i = (x_i, y_i)$ of a non-recording rain-gage network with a given density, made up of *N* stations ($i = 1,\ldots, N$). The two most common objectives are:

- precipitation mapping,
- estimation of the average rainfall falling on an area *A* (generally corresponding to a drainage basin or sub-basin) over time step Δt.

Let us first consider precipitation mapping.

To plot a precipitation map, it is first necessary to fill in a grid that should be as fine as possible. For any unmeasured point t^0 (the point t^0 will successively sweep through all points of the grid), a precipitation estimate $P^*(t^0)$ will be entered. This grid will then be used to plot contours of equal

precipitation (isohyets). The estimates required at every point t^0 are estimated using the available information, i.e., the precipitation values measured at stations $P(t^i)$.

If the model selected consists in linear weighting of the values at the rain-gage stations using weights λ_i^0, the precipitation estimates can be expressed as:

$$P*(t^0) = \sum_{i=1}^{N} \lambda_i^0 \cdot P(t^i) \qquad (2.10)$$

where λ_i^0 is the weight applied to the precipitation at station i with coordinates $t^i = (x_i, y_i)$ to estimate the precipitation at $t^0 = (x^0, y^0)$.

Other classical methods, although sometimes hard to justify, use different weights:

- $\lambda_i^0 = 1/N$, leading to the simple arithmetic mean of the observed values, which will be the same everywhere.
- $\lambda_i^0 = 1/n$, where n is the number of stations found in the neighborhood of the point t^0 to be estimated (therefore $n < N$). The difficulty here lies in how to delimit the neighborhood.
- A weight of 1 at station j nearest t^0 and a weight of zero elsewhere, i.e.,
  $\lambda_i^0 = 0 \ \forall \ i = 1, \ldots N, i \neq j$
  $\lambda_i^0 = 1$ for $i = j$.
  The problem here is that this leads to abrupt changes between two points that are associated with two different stations.
- A weight corresponding to the inverse or the square of the inverse of the distance d_{i0} between the point to be estimated and station i. But why this function rather than another?

Review of a classical statistics:

Another method that is easier to justify can be used. The objective is to ***explain*** a variable Y, often called the ***response***, using one or more explanatory variables, $X_1, X_2, \ldots, X_N$, called ***predictors,*** via a linear model with the form:

$$Y = \alpha_1 \cdot X_1 + \alpha_2 \cdot X_2 + \ldots + \alpha_N \cdot X_N + \alpha_0 + \varepsilon \qquad (2.11)$$

When using mean-centered values (i.e., Y and X_i adjusted to have means of 0), $\alpha_0 = 0$. The term ε accounts for the fact that the relation will not be perfect and that there will be a residual ε between the true value of Y and the value proposed by this relationship. This is called the ***estimation error.*** If the selected fitting criteria is to minimize the variance of ε (i.e., the expected value of the sum of the squares of the residuals), then it is necessary to know the ***correlation coefficients*** between:

- the variable Y and each of the variables X_i, $i = 1, \ldots N$, i.e., $\rho(Y, X_i)$,
- all the predictors variables X_i, X_j, i.e., $\rho(X_i, X_j)$

This provides the classical results defining the values of the weights α_i, or the regression coefficients, that can be used to calculate an estimate $Y*$ using the regression equation. In addition, a characteristic of the expected error is obtained, i.e., its variance σ^2_ε expressed as:

$$\sigma^2_\varepsilon = \sigma_Y \cdot (1 - R^2_{Y|X_1, X_2, \ldots X_N}) \qquad (2.12)$$

where $R^2 Y,[X_1, X_2, \ldots X_N]$ is the coefficient of determination, or the square of the multiple correlation coefficient between the variable to be predicted Y and the explanatory variables $X_1, \ldots X_N$.

In fact, this methodology provides and easy way of transforming the problem:

- the variable Y to be predicted is the unknown value of the precipitation $P(t^0)$ at point t^0,
- the candidates for the explanatory variables are the values measured at stations $P(t^i)$.

The equation: $Y = \alpha_1 \cdot X_1 + \alpha_2 \cdot X_2 + ... + \alpha_N \cdot X_N + \alpha_0 + \varepsilon$ then becomes:

$$P\left(t^0\right) = \sum_{i=1}^{N} \lambda_i^0 \cdot P\left(t^i\right) + \varepsilon \qquad\qquad (2.13)$$

and the estimated value

$$P*\left(t^0\right) = \sum_{i=1}^{N} \lambda_i^0 \cdot P\left(t^i\right)$$

will have an error variance $\sigma^2\varepsilon(t0)$ given by equation 2.12.

To sum up, the necessary ingredients are:

- the means of *X* and *Y*, which here are the means of the precipitation at every point of the field,
- the correlations between the precipitation at point *i* and the precipitation at point *j*, for all the measurement points,
- the correlation between the unmeasured point t^0 and all the measured points *i*.

From statistics to geostatistics:

When applying standard regression techniques, these ingredients are generally estimated using a sample of values y_p, x_{1p}, x_{2p}, …x_{Np} measured at the same time for a number of independently observed cases $k = 1…p$. When p is large, the estimates obtained for the necessary ingredients are robust.

At this point, the context becomes special, requiring a shift from classical statistics to geostatistics.

If the rain-gage network is relatively old, multiple realizations of precipitation fields are available for example on a daily basis. Unfortunately, they are not fully comparable. Some may have an average value of 5 or 6 mm over the region while others may have an average value of 70 or 75 mm. The variability is obviously significantly higher for the second case. In the first case, the values will range from 0 up to perhaps 20 or 25 mm, while in the second case, there will be few 0 values but the high values may extend up to for instance 200 mm.

The data should therefore often be standardized to make them comparable and provide a larger sample. However, although this will make it possible to calculate the correlations between precipitation values (possibly transformed) at stations t^i of the network, i.e., $\rho(t^i, t^j)$, it will still not be possible to calculate the correlations between any point t^0 and points t^i, i.e., $\rho(t^0, t^j)$.

For this, additional assumptions must be made. It will be assumed that *the variable is "regionalized" and organized in space* and that the correlation between two points *t* and *t'* depends only on the distance between them, i.e., $\rho(t, t') = \rho(d\,[t, t']) = \rho(d)$.

This can be checked using the samples corresponding to the different station pairs, i.e., $\rho(t^i, t^j) = \rho(\mathrm{d}[t^i, t^j]) = \rho(d_{ij})$ to see if the assumption appears be valid for the entire field and over the entire region. If this is the case, the ***correlation model $\rho(d)$***, i.e., the analytical function that gives the correlation between two points depending on the distance between them, can be accepted and used for all points t^0 of the grid by calculating $\rho(d_{i0})$. This makes it possible to fill in and solve a linear system providing the weights λ_i^0 to be assigned to each station to estimate $P*$ at t^0.

Going further towards geostatistics

These tools must now be adapted to the conditions most often encountered, while conserving the same estimation model at the base:

- linear weighting of observed values,
- weights calculated so as to minimize the expected value of the sum of the squares of the errors.

The objective of all these adaptations is to produce the ingredients required to solve the estimation problem, in particular the correlations or the covariances between two points, generally considered to depend only on the distance between them.

The first question appears if only a single measured field (one realization) is available or, even if a number of realizations are available, we consider that they are not comparable even after they have been normalized after an appropriate transformation. Each of these realizations must be treated separately to propose a $\rho(d)$ specific to it. In this case, it is possible to work with the covariance $C(d) = \rho(d)\sigma^2_P$ where σ^2_P is the variance of P in the field and $C(d)$ the covariance between two points separated by distance d, knowing that the $d = 0$, $C(0) = \sigma^2_P$ and $\rho(0) = 1$.

In practice, instead of working with the covariance function $C(d)$, it is preferable to work with the ***variogram***:

$$\gamma(d) = C(0) - C(d) \tag{2.14}$$

or:

$$\gamma(d) = C(0) - C(d) = \sigma^2_P \cdot (1 - \rho(d)) \tag{2.15}$$

Note that this normalized variogram $\gamma(d)/\sigma^2_P = 1 - \rho(d)$ is simply the ones' complement of the correlogram. However, it can also be shown that the variogram $\gamma(d)$ between two points t and t' separated by distance d can be interpreted as:

$$\gamma(d) = \gamma(t,t') = \frac{1}{2} \cdot E\left[\left\{P(t) - P(t')^2\right\}\right] \tag{2.16}$$

i.e., the expected value of the square of the difference of the values of two points separated by distance d. In practice, this approach involves calculating, in the field, the arithmetic mean of the square of the difference of values measured at the two points of the pair for a relatively large number of pairs (> 50) separated by a distance of approximately d. Note that if there are N stations, then there are $N(N-1)/2$ different pairs. They can be divided into classes containing pairs with roughly comparable distances of separation to estimate the value of $\gamma(d)$ corresponding to each of these classes. The practical advantage of working with the variogram is that it is unnecessary to explicitly calculate an empirical mean and standard deviation of the field (based on the N values of the network and therefore sometimes not very robust) before calculating the covariances.

An empirical variogram is therefore calculated for the considered field and fitted with an acceptable model (an analytical function satisfying certain criteria) to represent this variogram $\gamma(d)$. This is used to fill the system to be solved, which is totally analogous with the correlation system, with the $\gamma(d_{ij})$ and $\gamma(d_{i0})$ values it needs. The weights λ_i^0 of the estimator are then deduced along with the estimation variance $\sigma^2_{\varepsilon(t0)}$. Although very similar to a regression analysis, this estimation technique is called ***ordinary kriging***.

Other refinements can obviously be envisaged. For instance, it is possible to check whether the correlation (or change of the variogram) with distance depends on direction. If this is the case, the system is referred to as being ***anisotropic***. For example, the correlation can extend further in one direction than another if for instance during time step Δt, the precipitation system has enough time to move significantly and systematically in a dominant direction. In this case, the correlations will "spread" in this direction and have a longer ***range*** (the distance after which the correlation is null). The function then becomes $\gamma(d,\theta)$ where θ represents the direction.

Another possibility is to use a larger sample than the one that can be extracted from a single field by considering that a number of fields have, after processing to make them comparable (same variance and same mean), the same spatial relationship characteristics. For example, all the fields of the given season or a given type of weather can be grouped together. This makes it possible to calculate a ***climatological*** variogram that is standardized but averaged over a large number of fields. As a result, it is more robust, especially when considering direction. After the simulation stage for

each field, all that will be required is to "unstandardize" each field by multiplying it in general by the empirical variance of the field.

Another application concerns the calculation of the areal mean values (over area A) of the field sampled by the network of N stations at t^i. The variable to be predicted or estimated is then:

$$P_A = \frac{1}{A} \iint_A P(x,y) \cdot dx \cdot dy = \frac{1}{A} \cdot \int_A P(t) \cdot dt \qquad (2.17)$$

It must be explained or estimated using only the known values $P(t^i)$. Numerically, it can already be seen that it is possible to estimate:

$$P^*\left(t^0\right) = \sum_{i=1}^N \lambda_i^0 \cdot P\left(t^i\right) \qquad (2.18)$$

for all points t^0 of a grid covering area A and then calculate the sum and divide by the area A.

Theoretical developments beyond the scope of this book show that in the same way as above, it is possible to estimate the variable P_A by a linear relationship:

$$P_A^* = \sum_{i=1}^N \lambda_i^A \cdot P\left(t^i\right) \qquad (2.19)$$

where the weights are the solution of a linear system containing, as above, the covariances or correlations $\rho(t^i, t^j) = \rho(d_{ij})$ between the values measured at stations and also the correlations:

$$\rho\left(A, t^i\right) = \frac{1}{A} \int_A \rho\left(t^i, t\right) \cdot dt \qquad (2.20)$$

between the value $P(t^i)$ at t^i and the average value P_A of area A.

In practice, this is written using the variogram, therefore with the quantities:

$$\gamma\left(d_{ij}\right) \text{ and } \gamma\left(A, t^i\right) = \frac{1}{A} \int_A \gamma\left(t^i, t\right) \cdot dt \qquad (2.21)$$

In a similar manner, kriging calculates the variance of the error of estimation $\sigma^2_{\varepsilon\,A}$, which is in fact the variance of the difference between the true value P_A and its estimate P_A^*, i.e., $\varepsilon_A = P_A - P_A^*$. This is a theoretical value. It nevertheless provides a good order of magnitude estimate of the uncertainty to be expected.

It can be shown and checked that this formula is often optimal with respect to the other weighting formulas, in particular the arithmetic mean, where $\lambda_i^A = 1/N \; \forall i$, or the Thiessen formula $\lambda_i^A = A_A^i/A$, where A_A^i represents the area of the Thiessen polygon surrounding station i (for which all points are the closest to station i) and A is the total area.

It is therefore possible to provide as input, for example, to a semi-spatialized hydrological model, the precipitation depths estimated sub-basin by sub-basin along with their uncertainties. The latter depend on the network available stations and also on the position and shape of area A with respect to this network.

Taking into account additional information

At the beginning of this addendum, an example was considered involving a daily precipitation field measured by a non-recording rain-gage network. This can also be a network of recording rain-gages, which would make it possible to measure precipitation over shorter time steps Δt, for example 12h, 6h, 1h or less.

In this case, it is observed that the number of zero values (and thus the area without precipitation) increases as Δt decreases. The field is referred to as being **"intermittent"** and when the area without rainfall becomes significant, it requires special treatment. Note also that as Δt decreases, the correlation tends to decrease faster with distance. The reason is that the system does not have sufficient time to move significantly, while it is the advection of precipitation bands and their cells that generate a

portion of this correlation in space, i.e., two points have correlated precipitation values at time step Δt because the band that touched the point t also had the time to move and touch point t'.

The range d_0 of the variogram (the distance at which the correlation becomes null) should therefore be related to the precipitation measurement time step. Different formulas can be found in the literature. For example, the equation $d_0 = 25 \cdot \sqrt{\Delta t}$ with d_0 in km and Δt in hours can be used to calculate a good order of magnitude estimate of the range for heavy rainfalls that are quite strongly convective.

Similarly, depending on the region, a directional effect may be observed that depends on the time step. Although of little importance at an hourly time step (the displacement of the system is of the same order of magnitude as the size of the bands or cells), it is observed that starting from the 6h time step, the range can be twice as long in the direction parallel to the displacement than in the direction perpendicular to the displacement. In this case, it is better to use a directional (or an isotropic) variogram model $\gamma (d,\theta)$.

Another factor to take into account is ***orography***. Topographic relief strongly influences precipitation field maps, however in different ways depending on the type of weather. For example, easterly fronts produce heavier precipitation on the east side of the French Alps, while westerly fronts produce heavier precipitation on the west side. For such cases, additional variables such as elevation, distance from the sea, etc. could be added to the multiple regression model as predictors. In geostatistics, the corresponding technique is called ***cokriging***. However, even in its co-localized version that will not be dealt with here, this technique is difficult to implement.

The following approach is therefore preferred.

- First of all, known external information concerning the rainfall field is used. For example, it is known that there is a certain linear relationship with elevation (at least for relatively long time steps, i.e., daily or longer).
- Next, a regression analysis is carried out between precipitation and this elevation variable Z for the N available stations i. Subsequently, only the residuals $\varepsilon_z(t^i) = P(t^i) - P_z^*(t^i)$ are considered, i.e., the fraction of precipitation $P(t^i)$ not explained by elevation.
- These residuals are then mapped by Kriging, providing an estimate $\varepsilon_z(t^0)$ at every point t^0.
- Finally, these estimates are superimposed at every point t^0 on the first estimate $P^*z(z^0)$ deduced from elevation alone, giving the final estimate $P^*(t^0) = P_z^*(z^0) + \varepsilon z(t^0)$.

In this case, indirect secondary information or "proxy" data are first used to create a ***guess field,*** also referred to as a "footprint", that defines the major (regional) trend which is then fine-tuned with the measured values available for the considered field. This is called ***kriging with external drift*** **(KED)**. Another approach consists in stating that for a rainfall corresponding to a given type of weather, climatology can provide the rough shape of the field (in relative or normalized terms). The rough shape can also be estimated from a meteorological model or a radar image that is fine-tuned by injecting observed point data.

All these geostatistical techniques and their applications to precipitation fields have been introduced and discussed in publications starting in the late 1970s and continuing today. Recent developments concern in particular a new aspect that will now be discussed.

Stochastic simulation of different scenarios

The objective above was to propose the best estimate of the sampled field knowing only the values $P(t^i)$ at points t^0, i.e., $P^*(t^0)$. This made it possible to calculate an "expected" field. This field is however smoother than reality, because at t^0, the true value $P(t^0)$ is unknown but is in the neighborhood of $P^*(t^0)$ with a difference $\varepsilon(t^0)$ having a known mean (zero) and in particular standard deviation $\sigma^2\varepsilon(t^0)$. It is then possible to generate fields in which we enter, at every unmeasured point t^0, not the estimated $P^*(t^0)$ alone, but rather the estimated value $P^*(t^0)$ increased by the difference

$\varepsilon(t^0)$ drawn randomly from a distribution (generally Gaussian) with mean 0 and standard deviation $\sigma^2\varepsilon(t^0)$.

This gives fields that are much closer to the real field, that include the measured values $P(t^0)$ and that oscillate around the estimated value $P^*(t^0)$ at other points t^0, in an interval with a standard deviation of $\sigma^2\varepsilon(t0)$, specific to the point t^0 considered. By reconstructing the entire variability of the field in this way, more realistic fields are obtained, which can be an important factor when they are used as input to non-linear processes such as a rainfall-runoff model.

In addition, any number of scenarios can be generated, all different within the limits of the standard error of estimation, and all passing through the points $P(t^i)$, thus giving an idea of what is due to uncertainty, given that the field has only been sampled by a limited network. When these scenarios are used as model input, they make it possible to estimate the effect of variability that the corresponding uncertainty produces in terms of uncertainty in the output of the rainfall-runoff model for example.

A final challenge consists in generating scenarios that respect, as above, the spatial structure of the observed fields as well as, when the fields arrive sequentially one after the other, the temporal structure, in particular the spatio-temporal correlations between successive time steps. This is presently a very active field of research.

2.7.3 Validation of Hydrometric Data

Certain erroneous data are hard to detect, however, simple tests can be used to detect major errors (adapted from Beven, 2000; see also Musy and Higy, 2011).

- If storage variations within a given basin can be neglected, rainfall and streamflow measurements can be used to estimate evapotranspiration losses via the water balance of the basin. The data can be validated by comparing these estimates with evapotranspiration measurements or the usual values obtained for the region.
- It is also possible to validate the runoff coefficient (ratio of runoff to precipitation depth) by comparison with the characteristics of the drainage basin or by checking that it does not have obviously erroneous values (e.g., a value greater than 1 due to snow melt or inflows from outside the drainage basin). Inconsistencies can come from errors in rainfall or streamflow data or from the estimation of areal precipitation. Another source of inconsistencies can be non-concordance between the topographic and hydrogeological basins. The runoff coefficient can also be validated by checking that the values obtained for different periods of the year are consistent with the expected seasonal changes for a given region. For non-mountainous basins of the northern hemisphere, the runoff coefficients should be higher in winter than in summer as a result of the lower evapotranspiration losses in winter. On the basis of similar low-flow discharges, it is possible to select separate periods for which the streamflow volumes are not greatly affected by recession discharges.
- If several hydrometric stations are available on a given hydrographic network, data consistency can be checked by comparing the discharge per unit area calculated for the different basins or by plotting double mass curves to identify a possible break in the slope of the proportionality relationship between the running totals of the values measured at two stations.
- Estimates obtained by reconstruction (Section 2.2.3) are another way of checking the consistency of estimated streamflows.

Signs of invalid data

It is important to identify certain signs that indicate that the data for a given station may be partially or totally invalid.

- Errors related to the equipment used or its replacement.
- Errors related to data reconstruction (often carried out manually by the station manager in the

event of an equipment breakdown to avoid missing records in the time series).

- Errors related to stream-gage data (which affect accidentally the stage-discharge relationship) or the use of obsolete rating curves conserved by the station manager (even if it is not an easy task, the station manager should be encouraged to conserve old rating curves that provide a local history of the morphodynamics of the watercourse).
- Changes in the drainage basin and/or the hydrographic network (urbanization, major land use modifications, hydraulic projects, etc.).
- Changes in the rainfall-runoff relationships (caused for example by climate change).
- Sample heterogeneity detected by simple tests or double mass curves (identifying possible breaks in behavior).
- Regional hydrological heterogeneity.

2.7.4 Assimilation of Hydrological Data

Many observations of various types are carried out every day around the world. These include direct measurements by devices installed on the ground or on aircraft or ships and remotely sensed measurements by instruments installed on the ground or on aircraft, ships and satellites. Although these measurements and observations provide only a partial and inaccurate vision of the concerned physical variables, they often provide relevant supplementary information.

Moreover, a number of different models have been developed over recent decades to simulate many of the natural phenomena of interest (e.g., atmospheric, hydrological). They are based on basic physical principles (conservation of mass, energy and momentum) and on various equations regarded as laws for certain processes. These models can be used, in principle, to simulate the behavior of part or all of a terrestrial system in a physically plausible manner, in particular the spatial and temporal evolution of certain physical variables. They can therefore also be used to produce, on the basis of observed meteorological data, estimates of the physical variables of interest (e.g., streamflow at a given point, groundwater level).

The possibility of using different estimates together to make best use of all available information is crucial to improving the description, understanding and simulation of the state of the system at a given time as well as its changes over a past or future period. Information from models and observations can be merged using data assimilation methods. These techniques have considerable development perspectives for a wide range of hydrological applications (Bach and Mauser, 2003; Reichle *et al.*, 2005; Castaings *et al.*, 2006) and offer a number of advantages in terms of:

- *Independence of estimates.* Estimates of the state of the physical system based on ground, airborne or satellite observations and behavioral models are generally independent, with different data sources and processing.
- *Spatial and temporal coverage. In situ* observations offer limited regional or even local representativeness and low spatial coverage and are often confidential. In this respect, discharges are the most frequently available measurements. They integrate the spatial variability of the meteorological conditions to which the system is subjected as well as the spatial variability of the corresponding system responses. Remotely sensed data provides spatialized information covering vast regions, including areas without ground observations. The sampling time step for remotely sensed data is often long (from 12 hours up to several days for certain satellite observations), as opposed to ground observations that are often recorded continuously.
- *Spatial resolution and applications.* Spatial observations are often obtained with a resolution that is not optimal for the applications concerned. For example, soil moisture measured by the AMSR-E system (Advanced Microwave Scanning Radiometer for the Earth Observing System) has a resolution of 50 km, too coarse for operational hydrological applications. MODIS (Moderate Resolution Imaging Spectroradiometer) snowpack estimates have a resolution of 500 m, too fine for existing meteorological forecasting models.

- *Observability of considered variables.* Present remote-sensing systems can observe only surface variables as opposed to *in situ* measurements that can generally be performed at different depths.
- *Volume of data and redundant data.* The quantity of data acquired each day is considerable and only a small number are actually used. This is due to the difficulty of performing certain pre-processing procedures and the complexity of data combination methods. Certain observations made with similar instruments are regularly redundant but may be also be inconsistent due to measurement and interpretation errors.

Data assimilation methods are therefore useful and necessary to interpolate and extrapolate available data and carry out the changes of scale required by applications that use this data. They can be used to manage redundant and conflicting data or to combine different types of observations to provide a single estimate, i.e., the best possible, of the variables considered to make best use of available knowledge of the physical laws governing the spatial and temporal evolution of these variables.

The optimal combination of measurements and estimates produced by the selected physical model is based on the respective uncertainties of these measurements and model estimates. For example, for cases where certain remotely sensed data are very reliable and accurate, estimates provided by assimilation will be very close to these data. On the other hand, when no observations are available or when the quality of observations is poor, assimilation estimates will be close to those provided by the model.

Many assimilation methods have been developed with varying degrees of complexity. The main methods are based on optimal control theory (variational methods) or optimal estimation theory (stochastic methods) (Castaings *et al.*, 2006). For stochastic methods, the evolution of the model is considered to be a discrete random process. Its variables are estimated by correcting the state of the system in an iterative manner each time new observations become available. The Kalman filter or any of its generalized forms provides a solution to this problem.

2.7.5 Estimating Net Radiation R_n (FAO, 1998; Singh and Singh, 2001)

1. Definitions (see Musy and Higy, 2011, for further details)

Net radiation R_n. Net radiation R_n is the radiation received or emitted by a given surface on the earth depending on whether the following balance is respectively positive or negative:

$$R_n = (1-\alpha) R_S - R_b \tag{2.22}$$

where R_S is the incident shortwave solar radiation, α the albedo of the surface (bare ground, vegetation, water, snow, ice) and R_b the net longwave radiation emitted by the surface. $(1-\alpha) R_S$ is the net solar radiation received by the surface after subtracting shortwave radiation αR_S returned by the surface to the atmosphere. Note that albedo depends, rigorously speaking, on the wavelength of the radiation.

Solar radiation R_S. This is the shortwave radiation (< 4 µm) from the sun that reaches a given surface after absorption, reflection and scattering by the atmosphere. Solar radiation depends on the amount of extraterrestrial radiation R_A and cloud cover. For clear skies, solar radiation is roughly 75% of extraterrestrial radiation. In the presence of very dense cloud cover, up to 25% of the extraterrestrial radiation may still reach the Earth's surface (diffuse radiation). Solar radiation R_S, often referred to as global radiation, is the sum of direct and diffuse solar radiation.

R_S is generally measured continuously by climatological stations [W/m²]. If such measurements are not available, R_s can be estimated on the basis of extraterrestrial radiation R_A and an estimate of cloud cover for the considered time interval (see below).

Extraterrestrial radiation R_A. Extraterrestrial radiation R_A is the solar radiation received by a horizontal surface at the top of the atmosphere.

Net longwave radiation R_b. This is the longwave radiation emitted by a given terrestrial surface (R_T) minus the longwave radiation received by the surface from the atmosphere (R_a).

$$R_b = R_T - R_a \tag{2.23}$$

Outgoing terrestrial radiation R_T is generally greater than incoming atmospheric radiation R_a. The net longwave radiation R_b therefore generally represents an energy loss from the surface. In practice, R_b is first estimated for clear-sky conditions and then adapted according to the real cloud conditions (see below).

2. Estimating solar radiation in the absence of measurements

Estimation of clear-sky solar radiation (R_{s0}). For clear skies, the maximum solar radiation that can be received by a horizontal surface can be estimated from the extraterrestrial radiation R_A using the relationship:

$$R_{s0} = (a_s + b_s)\, R_A \tag{2.24}$$

where $a_s + b_s$ is the fraction of extraterrestrial radiation that reaches the Earth's surface. These parameters are mainly related to the average transmissivity of the atmosphere along the path of the solar rays and are generally calibrated for a given location. The mean daily transmissivity at sea level, equal to 0.75, is often used as a default value for $a_s + b_s$. This value increases with altitude and can therefore be corrected using the empirical equation: $a_s + b_s = 0.75 + 0.00002\, z$ where z is the elevation of the location [m].

Estimation for cloudy skies. The influence of clouds on solar radiation depends on the properties of the clouds (reflectivity, transmissivity) and the extent of the cloud cover. If cloud cover (also referred to as cloud fraction) is measured continuously, a rough approximation of the mean daily solar radiation can be obtained on the basis of the extraterrestrial radiation R_A and the actual sunshine duration n [h]:

$$R_s = (a_s + b_s * n/N)\, R_A \tag{2.25}$$

where a_s and b_s are the constants defined above and N is the maximum possible sunshine duration [h] for the considered day (see extraterrestrial radiation R_A for details on how to estimate this value). The constants a_s and b_s can be obtained by calibration if solar radiation and actual sunshine duration data are available. The FAO (1998) recommends the following default values if such measurements are not available: $a_s = 0.25$ and $b_s = 0.5$.

If cloud cover is not measured continuously, mean daily solar radiation can be estimated from minimum and maximum daily temperatures. The difference between the maximum (T_{max}) and minimum (T_{min}) daily temperature of the air depends on the degree of cloud cover at the considered location. On cloudy days, a significant amount of solar radiation never reaches the Earth's surface, reducing the maximum temperature during the day. At night, the net outgoing longwave radiation is reduced under cloudy conditions, thereby raising the minimum temperature with respect to clear-sky conditions. In the absence of other data, solar radiation can be estimated on the basis of these temperatures and the extraterrestrial radiation R_A using the Hargreaves empirical radiation formula:

$$R_S = k_{RS} \sqrt{\left(T_{max} - T_{min}\right)}\, R_A \tag{2.26}$$

where k_{RS} [°C$^{-0.5}$] is an adjustment factor that varies between 0.16 for interior locations and 0.19 for coastal locations.

Relative solar radiation R_S/R_{S0}. The relative solar radiation R_S/R_{S0}, where R_{S0} is the maximum possible value of solar radiation in the absence of cloud cover, provides an estimate of the degree of cloudiness of the atmosphere. This ratio generally varies between 0.33 (dense cloud cover) to 1 (clear sky). It can be estimated continuously if solar radiation R_S is measured. Its mean daily value can be estimated from the mean daily extraterrestrial radiation if the actual sunshine duration is known.

3. Estimating terrestrial and atmospheric radiation

Estimation for clear skies. For clear-sky conditions, a first approximation of atmospheric radiation R_a can be based on the emissivity ε_a and temperature T_a of the atmosphere. Similarly, the terrestrial radiation R_T can be estimated from the emissivity ε_s and temperature T_s of the considered surface. Net longwave radiation R_b for clear-sky conditions will be referred to as R_{b0}. Therefore:

$$R_a = \varepsilon_a \sigma T_a^4 \text{ and } R_T = \varepsilon_s \sigma T_S^4 \tag{2.27}$$

where T_a and T_S are expressed in degrees Kelvin [K] and σ is the Stefan-Boltzmann constant (5.67 x 10^{-8} Wm^{-2}K^{-4}).

The emissivity of the atmosphere depends on the vapor pressure e_a (in kPa) above the ground surface. The emissivity is 0.757 for the saturated vapor pressure and can be estimated using the following equation:

$$\varepsilon_a = a_1 + b_1 . e_a^{0.5} \tag{2.28}$$

where a_1 and b_1 are constants that depend on the region. According to ASCE (2005), $a_1 \in [0.55–0.65]$ and $b_1 \in [0.13–0.20]$. The FAO (1998) proposes default values of $a_1 = 0.66$ and $b_1 = 0.14$.

Table 2.3 Emissivities of different surfaces (Singh and Singh, 2001; Tardy, 1986).

Type de surface	Emissivity
Black body	1.00
Water (depending on depth)	0.95–0.99
Cultivated soil	0.90–0.95
Rock	0.95–0.98
Leaves	0.94–0.98
Snow	0.97–1.00

Estimation for cloudy days (R_b). If solar radiation R_S is measured and the net longwave radiation R_b is not, R_b can be estimated on the basis of the net longwave radiation for clear skies R_{b0} and the relative solar radiation R_S/R_{S0} using the following equation:

$$R_b = \left(a \frac{R_s}{R_{s0}} + b \right) R_{b0} \tag{2.29}$$

The coefficients a and b can be estimated empirically ($a+b = 1$). Smith *et al.* (1991) recommend the following default values: $a = 1.35$ and $b = –0.35$.

4. Estimating extraterrestrial radiation R_A

Extraterrestrial radiation R_A is a function of the solar altitude, i.e., the angle Φ between the direction of the sun's rays and the tangent to the Earth's surface at the point of observation:

$$R_A = G_{sc} \cdot d_r \sin(\Phi) \tag{2.30}$$

where R_A is extraterrestrial radiation [Wm^{-2}], G_{sc} the solar constant [1367 Wm^{-2} = 0.082 x 10^6 Joules m^{-2} min^{-1}], Φ the solar altitude [°] at a given time and d_r the inverse relative Sun-Earth distance. The intensity of solar radiation is maximum for Φ=90°. It decreases with solar altitude because the area intercepting the rays of the sun increases. The main factors affecting solar altitude are the time of day and the declination angle of the sun, while the latter depends on the day of the year and the latitude of the considered location.

The mean extraterrestrial radiation R_A [Wm^{-2}] received by a horizontal surface during daytime under clear skies over a time interval $[t_1; t_2]$ less than 24 hours can be estimated using the following expression (FAO, 1998):

$$R_A = \frac{12}{\pi} G_{sc} \cdot d_r \left[(w_2 - w_1) \sin(\varphi)\sin(\delta) + \cos(\varphi)\cos(\delta)\left(\sin(w_2) - \sin(w_1)\right) \right] \tag{2.31}$$

where ϕ is the latitude of the location [rad] (latitude <0 for the southern hemisphere), δ the solar declination [rad] and w_1 and w_2 the solar hour angles [rad] at respectively the beginning and end of the time interval.

The variables d_r and δ depend on the number of the day in the year D (D=1 on January 1)

$$\delta = 0.409 \ \sin\left(2\pi \frac{284 + D}{365}\right) \tag{2.32}$$

$$d_r = 1 + 0.033 \ \cos\left(\frac{2\pi}{365} D\right) \tag{2.33}$$

the solar hour angles w_1 and w_2 are respectively a function of t_1 and t_2:

$$w_1 = w(t_1) \text{ and } w_2 = w(t_2) \tag{2.34}$$

$$\text{with} \ \ w(t) = \frac{\pi}{12}\left[(t + 0.0667(L_z - L_m) + S_c) - 12\right] \tag{2.35}$$

where t is the standard decimal clock time [h] (t =14.75 h for 14:45), L_z the longitude [°] of the center of the time zone (L_z = 0° for the Greenwich time zone, 15° for Burkina Faso and 345° for France and Switzerland), L_m the longitude [°] of the site and S_c a seasonal correction for solar time:

$$S_c = 0.1645 \sin(2b) - 0.1255 \cos(b) - 0.025 \sin(b) \tag{2.36}$$

$$\text{where} \ \ b = \frac{2\pi(D - 81)}{364} \tag{2.37}$$

If $w(t) < -w_s$ or $w(t) > w_s$, where w_s is the sunset hour angle, the sun is below the horizon and extraterrestrial radiation is, by definition, zero. w_s is expressed as:

$$w_s = \arccos(-\tan(\delta)\tan(\varphi)) \tag{2.38}$$

The maximum possible sunset duration N for a given day of the year is expressed as:

$$N = \frac{24}{\pi} w_s \tag{2.39}$$

2.7.6 Non-exhaustive List of Web Links to Free-access Databases Concerning Hydrology

The web sites listed below provide free access to data. However, sometimes the free data is only available in the form of graphs and the source data must be paid for. Note that these services are continuously evolving and the addresses may change or disappear. Note also that although these

databases are free, they often have copyright restrictions. This list was last updated in October 2012.

Meteorological data for the recent climate

The ECMWF (European Center for Medium-Range Weather Forecasts) provides 3-day to 6-day weather forecasts for Europe.

http://www.ecmwf.int/

The NCDC (National Climatic Data Center—United States) provides a large number of climate data archives.

http://lwf.ncdc.noaa.gov/oa/ncdc.html

The CNRM (Météo-France) provides access to a wide range of climate data in the form of maps and graphs.

http://climat.meteofrance.com/chgt_climat2/accueil

Environment Canada provides public access to its national climate data and information archives in statistical form.

http://climate.weatheroffice.gc.ca/Welcome_e.html

MeteoSwiss (Swiss Federal Office of Meteorology and Climatology) provides access to various types of meteorological and climatological data.

http://www.meteosuisse.admin.ch/web/en/weather.html

NCAR (National Center for Atmospheric Research—United States) provides access to NCEP/NCAR re-analysis data (1948-), the NOAA-CIRES Twentieth Century Global Re-analysis (1869–2010) and other datasets

http://rda.ucar.edu/

The ECMWF (European Center for Medium-Range Weather Forecasts) provides access to ERA40 re-analysis data (1957–2001), the ERA-interim re-analysis (1989-present) and other datasets.

http://www.ecmwf.int/research/era/do/get/index

The Japan Meteorological Agency (JMA) provides access to the Japanese 25-year Re-analysis (JRA-25) (1979–2004). The JRA-55 re-analysis (1958–2012) will be available mid-2013.

http://jra.kishou.go.jp/JRA-25/index_en.html

Meteorological data from climate experiments (past/future climate scenarios)

Program For Climate Model Diagnosis and Intercomparison provides output of the latest climate experiments for past and future centuries.

http://cmip-pcmdi.llnl.gov/cmip5/availability.html

Hydrological data for the recent climate

The WMO (with support from Germany) provides daily and monthly data from more than 7000 locations around the world:

http://grdc.bafg.de/

The Swiss Federal Office for the Environment (FOEN/OFEV) provides hydrological data from 315 stations in Switzerland.

http://www.bafu.admin.ch/index.html?lang=en

The French HYDRO databank provides hydrometric and hydrological data for a very large number of watercourses.

http://www.hydro.eaufrance.fr/

ADES provides access to data on groundwater resources in France.

http://www.ades.eaufrance.fr/?CInfo=en-GB/

The Vigicrues system provides real-time access to flood-warning maps for France as well as the latest water level and streamflow measurements from many stations.

http://www.vigicrues.ecologie.gouv.fr/

Environment Canada provides public access to historical and real-time hydrometric data (water levels and streamflows) for more than 1200 sites in Canada.

http://www.wateroffice.ec.gc.ca/index_e.html

Wise-Hydro (Web Integrated Server for Enhanced Hydrological Data Release and Observation) is a hydrological Web server that can be used to display real-time streamflow variations in West and Central Africa.

http://aochycos.ird.ne

Spatial data

DEMs

Characteristics of some DEM data accessible free of charge via the web:

Name	Resolution	Geographic coverage	Publisher
ASTER DEM	30 m	Global (on request)	NASA
GTOPO30	30 arcsec (~ 1km)	Global	USGS/NASA
SRTM-3	90 m	80% of dry land	NASA/NIMA
7.5-minute DEMs	10 and 30 m	United States	USGS
1-degree DEMs	90 m	United States	USGS
CDED DEM	23 m and 90 m	Canada	CCOG

Name	Web site
ASTER DEM	http://asterweb.jpl.nasa.gov/
GTOPO30	http://eros.usgs.gov/
SRTM-3	http://www2.jpl.nasa.gov/srtm/
7.5-minute DEMs	http://eros.usgs.gov/
1-degree DEMs	http://eros.usgs.gov/
CDED DEM	http://www.geobase.ca

Drainage basins, rivers and lakes

HYDRO1k, developed by the USGS (U.S. Geological Survey), is a geographic database providing global topographic data on streams, drainage basins and ancillary layers derived from the GTOPO30 DEM.

http://eros.usgs.gov/#/Find_Data/Products_and_Data_Available/HYDRO1K

Ecrins, from the European Environment Agency, gives vector-based information on European catchments and Rivers network system (rivers, catchments and lakes).

http://www.eea.europa.eu/data-and-maps/data/european-catchments-and-rivers-network

The Digital Chart of the World (DCW) is a 1:1,000,00 scale geographic database developed initially by the U.S. Defense Mapping Agency.

http://www.maproom.psu.edu/dcw/ and/or http://data.geocomm.com/ (paid access)

SANDRE (Service d'Administration Nationale des Données et Référentiels sur l'Eau) provides an interactive map that can be used to find, consult and download data on water resources in France.

http://www.sandre.eaufrance.fr/atlascatalogue/

Remote-sensing data

NASA World Wind is an open-source virtual globe developed by NASA and the open source community from a number of data sources including satellite databases. It can be used to explore the Earth from space.
http://worldwind.arc.nasa.gov/

Land-cover data

The National Snow and Data Center distributes remotely sensed global snow cover data.

http://nsidc.org/data/modis/data_summaries/index.html#snow

POSTEL is French organization providing 300 m resolution maps of soil and vegetation at regional and global scale from satellite data.

http://postel.mediasfrance.org/

Corine Land Cover, from the European Environment Agency, gives Land Cover maps (vector data) for the year 2006 for European countries.

http://www.eea.europa.eu/data-and-maps/data/clc-2006-vector-data-version-2

GLOBCOVER is a 300 m resolution map of the Earth's global land cover mainly based on data from the Envisat satellite and made available by the European Space Agency for two periods: December 2004 - June 2006 and January—December 2009.

http://ionia1.esrin.esa.int/

GLC2000 is a global vegetation land cover map from the Joint Research Center of the European Commission.

http://bioval.jrc.ec.europa.eu/products/glc2000/glc2000.php

Other web sites providing hydrological data and knowledge bases

On-line course on General Hydrology from HYDRAM, the former Hydrology and Land Improvement Laboratory (now the ECHO: Ecohydrology laboratory) of EPFL (Ecole Polytechnique Fédérale de Lausanne).

http://echo2.epfl.ch/e-drologie/

Documents (e.g., theses), freeware and an International Hydrology Glossary in more than 10 languages. The web site is hosted by CNFSH via Ecole Nationale Supérieure des Mines de Paris.

http://hydrologie.org/BIB/bib1.htm and http://hydrologie.org/TER/ter.htm

The EauFrance web site (in French) provides a wide range of information on water resources and hydrological risks in France.

http://www.eaufrance.fr

The International Glossary of Hydrology provides translations in 11 languages of the main scientific and technical terms used in Hydrology.

http://webworld.unesco.org/water/ihp/db/glossary/glu/aglo.html

"Hydrothèque", a database containing 150 exercices and case studies for engineers with data and solutions published by Hingray *et al.* (2009) (in French) and hosted by the Laboratoire d'Etudes des Transferts en Hydrologie et Environnement (LTHE, France).

http://www.lthe.fr/PagePerso/hingray/PAGES/Accueil.html

PRINCIPLES OF HYDROLOGICAL MODELING

Hydrological modeling is one of the main techniques used to meet the challenges of predicting or forecasting hydrological variables. The aim of the hydrological model is essentially to estimate the various hydrological variables required for a given application, study or design project. Hydrological modeling is also used in addition to observations to reconstruct and/or verify observed data or as a complement to experiments in scientific research in hydrology.

Hydrological modeling consists in representing a given hydrosystem (and the corresponding hydrological phenomena) mathematically in order to simulate a part or all of its hydrological behavior. Hydrological modeling is generally carried out on the scale of a drainage basin, which is the scale that will be dealt with in particular in this chapter. In such a case, the objective of modeling is often to simulate, at the basin outlet, the runoff or discharges resulting from various meteorological forcing variables (e.g., precipitation, temperature). Precipitation is generally the main forcing variable, which is the reason that hydrological models are often referred to as rainfall-runoff models.

Section 3.1 of this chapter first describes the principles and objectives of hydrological modeling along with the main types of hydrological models and their structure and variables. Section 3.2 deals with methods and problems related to the representation of a given hydrosystem and the corresponding hydrological phenomena that occur within it. Section 3.3 presents the problems encountered when estimating the parameters of these models. Section 3.4 is devoted to the methods used to validate models and characterize the associated uncertainties. Section 3.5 provides some guidelines for choosing a suitable modeling approach.

For further information on any of the different aspects of hydrological modeling, the reader can refer to a wide range of publications devoted to this topic (ASCE, 1996; Ambroise, 1999; Beven, 2000; Singh and Woolhiser, 2002; Duan *et al.*, 2003).

3.1 INTRODUCTION

3.1.1 Principles and Objectives of Hydrological Modeling

Principles of hydrological modeling

A model is a simplified representation of a given physical system and the different processes that govern its operation. The system can be represented physically by a physical

model.[1] It is however more often represented mathematically. Such a representation is formalized by a set of equations expressing the laws or concepts considered to appropriately describe the behavior of the system.

The hydrosystem most often modeled in hydrology is the drainage basin. Smaller hydrological units can however be modeled (e.g., a given hill slope or parcel of land). Whatever the hydrosystem, the objective of hydrological modeling is to simulate part or all of its hydrological behavior.

The hydrological behavior of a given hydrosystem is extremely complex (Musy and Higy, 2011). This is mainly related to the complexity and heterogeneity of the physical medium itself (e.g., geomorphology of the basin, land use, soil properties, geology and characteristics of the hydrographic network). This explains the multitude of hydrological processes involved which, in addition, function on different spatio-temporal scales (Figure 3.1).
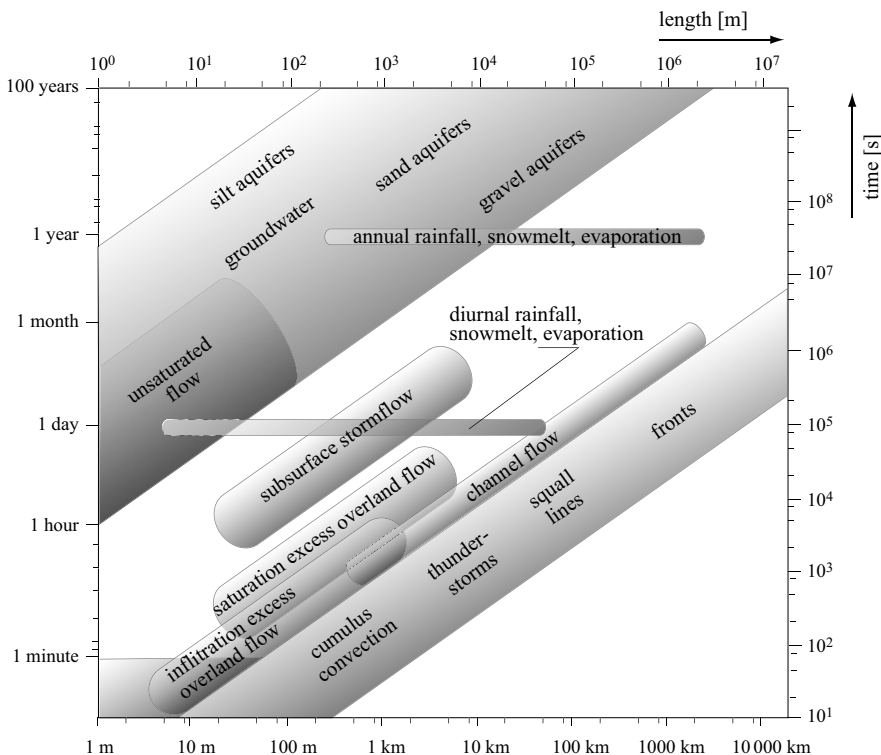
Fig. 3.1: Temporal and spatial scales of various hydrological processes (adapted from Bloschl and Sivapalan, 1995).

---

[1]In hydrology, physical models are scale models of hydraulic works, river reaches or drainage basins. They are used to quantify the influence of works such as discharge channels, spillways and retention basins in a simple manner for cases where solving mathematical equations would be excessively complex or impossible. The main difficulties encountered in the application and interpretation of these models are related to the scale and the transposition of results in the field. It is impossible to avoid distortion of the phenomena, which often leads to different scale ratios for the different runoff parameters. Analog physical models also exist. They are based on the similarity between the studied phenomenon (e.g., hydraulic head field and the flow of water in the ground) and another physical phenomenon and (e.g., electrical field and the flow of electrical current in an aqueous solution).

All hydrological models are consequently an extremely simplified representation of the real hydrosystem and its operation. For convenience, these models focus on the processes and spatio-temporal scales that are critical with respect to the hydrological phenomena to be studied. For example, a model developed to simulate the rainfall-runoff relationship during flood periods often ignores processes related to evaporation and groundwater recharge. On the other hand, these processes must be taken into account if the purpose of the model is to estimate the seasonality and interannual variability of water resources. Note however that for interannual variability, processes related to surface runoff can generally be neglected. A model is therefore highly dependent on the final objective of the simulation. Whatever the objective, there are many ways to simplify the representation of the physical medium and the associated hydrological processes. For this reason, there is a multitude of modeling possibilities for any given hydrosystem.

Note that the term model is often used incorrectly to designate a "modeling system". A modeling system corresponds to the computer code of generic or custom software developed to model the hydrological behavior of a drainage basin. The actual model corresponds to the application of this code to a particular site.

Objectives of hydrological modeling

Hydrological modeling can have many different objectives. From a scientific standpoint, the objective is to improve understanding of the behavior of hydrological systems by modeling the dynamics of the processes involved. As opposed to observations or experiments, modeling can be used to describe and represent, in their full complexity and variability, some or all of the many processes governing the hydrological behavior of one or all of the compartments of the considered hydrosystem. For a given hydrosystem and under certain conditions, such studies can be used to: 1) identify the most important processes and any non-linearities in the hydrological behavior of the hydrosystem, 2) test different hypotheses and conceptual frameworks and 3) identify any lack of understanding of the behavior of certain components. Modeling can also be used to simulate the hydrological behavior of the considered hydrosystem under changed conditions for which no observations are available.

Rainfall-runoff modeling also has operational objectives, for instance to simulate the hydrological response of the hydrosystem to a given forcing. How such simulations will be used depends on the analysis context.

Simulations can be used to reconstruct historical hydrological events that were observed but not measured (Chapter 1). They can also be used for hydrological forecasting, the objective being to estimate possible future changes of different hydrological variables (Chapter 10). In another application, simulations can be used to produce the hydrological scenarios required for medium- or long-term management of water resources and associated hydrological risks or to manage development projects. In this context, modeling can provide the hydrological information required for example to design hydraulic works (e.g., dams, drainage networks) or flood protection schemes (e.g., dikes). Simulations can also be used to estimate changes in the response of the considered hydrosystem resulting from modification of the characteristics of the drainage basin (e.g., future projects, changes in land use), modification of meteorological forcing (e.g., climate change) or other non-stationary conditions.

In hydrology, modeling can be implemented on other scales than that of the drainage basin. When coupled with general circulation models, hydrological models can be used for example to simulate water fluxes on the continental scale. On a given hill slope within a drainage basin, they can be used to simulate surface runoff and the associated erosion. For a given parcel of land, the can be used to estimate the water balance of the soil-vegetation-atmosphere system and the water requirements of the vegetation.

3.1.2 Structure and Variables of a Hydrological Model

The typical structure and variables of a hydrological model are summarized in Figure 3.2. The model, designated *G*, can be formally defined by the following expression:

$$\mathbf{Z}_{obs}(t) = G\,[\mathbf{X}(t), \mathbf{Y}(t), \mathbf{BC}(t), \boldsymbol{\theta}] + \boldsymbol{\varepsilon}_{Z}(t, \boldsymbol{\theta}) \tag{3.1}$$

where $\mathbf{Z}_{obs}(t)$ are the values observed at time t of the various output variables of the hydrological model and $\mathbf{X}(t)$, $\mathbf{Y}(t)$ and $\mathbf{BC}(t)$ are respectively the values of the various input variables, state variables and boundary conditions at time t. Furthermore, $\boldsymbol{\theta}$ is the vector of model parameters and $\boldsymbol{\varepsilon}_{Z}(t, \boldsymbol{\theta})$ the vector of model errors that are a function of time and parameter set $\boldsymbol{\theta}$. All these variables will be dealt with below.

Hydro-meteorological forcing	Input variables $X_1(t)$, $X_2(t)$, …

Hydrological model
- Schematic representation of physical medium
- Schematic representation of processes
- Parameters θ_1, θ_2, …
- State variables $Y_1(t)$, $Y_2(t)$, …

$+$

- Initial conditions $Y_1(t_0)$, $Y_2(t_0)$, …
- Boundary conditions $CL_1(t)$, $CL_2(t)$, …

Response of hydrological system	Output variables $Z_1(t)$, $Z_2(t)$, …
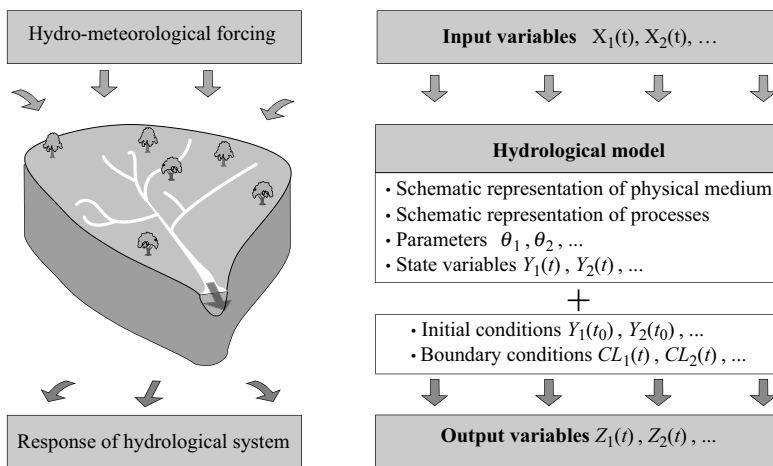
Fig. 3.2: Typical structure and variables of a hydrological model.

Input variables, output variables and model error

The variables used by a model to describe the hydrometeorological forcing phenomena represent the model inputs, $X(t)$. These variables, often referred to as forcing variables, are generally independent and the corresponding data are available in the form of time series. The variables used depend on the model but deal essentially with meteorological phenomena such as precipitation, reference evapotranspiration and temperature. The corresponding data are often available only at certain points corresponding to the different measurement stations located within the drainage basin (Chapter 2). In some cases, the data may reflect a spatial distribution, as is the case with precipitation fields derived from radar observations. Other model input variables include inflows such as those from upstream

drainage basins and outflows such as pumping for irrigation or diversion to neighboring drainage basins.

The model outputs, for which the values at time t are given by the formal expression $\mathbf{Z}_{sim}(t, \boldsymbol{\theta}) = G[\mathbf{X}(t), \mathbf{Y}(t), \mathbf{BC}(t), \boldsymbol{\theta}]$, are the variables that the model produces by simulation. The main output variable of any hydrological model is the discharge, or sometimes the water level, at one or more points in the hydrographic network. In addition, other variables of the hydrological cycle are often simulated (e.g., actual evaporation rate, water table height, snow cover and snowpack water equivalent).

The model outputs can be compared to the values observed for the corresponding hydrological variables, if available. The differences between the simulated outputs and the observed values of a given hydrological variable represent the model error, also referred to as residuals. The error varies with time. For output variable Z, it can be expressed by:

$$\varepsilon_Z(t, \boldsymbol{\theta}) = Z_{obs}(t) - Z_{sim}(t, \boldsymbol{\theta}) \tag{3.2}$$

where $\varepsilon_Z(t, \boldsymbol{\theta})$ is the error at time t for hydrological variable Z, $Z_{obs}(t)$ the value observed for this variable and $Z_{sim}(t)$ the value simulated for this variable by model G at time t. The error is a function of the parameter set $\boldsymbol{\theta}$.
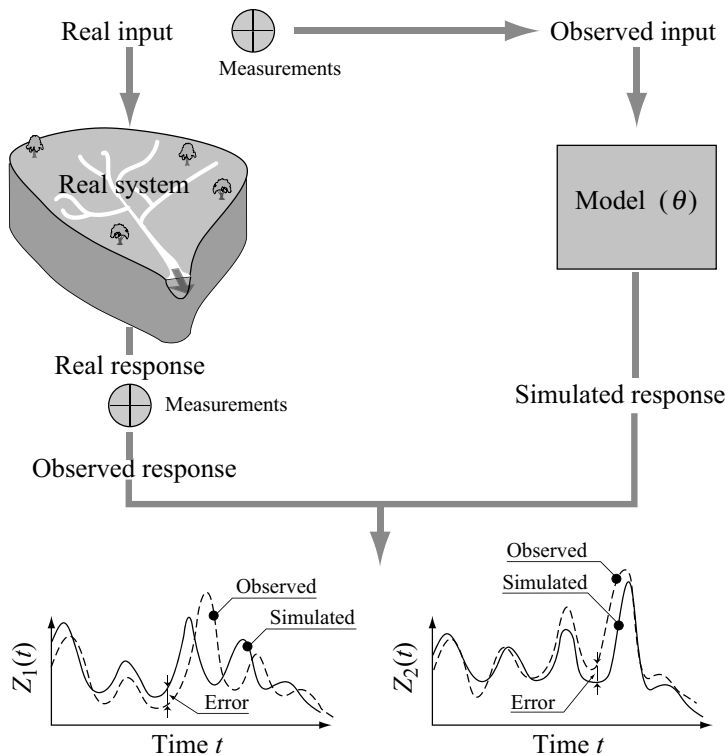
Fig. 3.3: Illustration of simulation error produced by a model for two output variables $Z_1(t)$ and $Z_2(t)$.

Model structure

The simplified representation of the hydrosystem used to transform the model input variables into output variables defines the structure of model *G*. It concerns:

- the representation of the physical medium defining the hydrosystem.
- the representation of the hydrological behavior of the hydrosystem with respect to the targeted hydrological phenomena, requiring the development of equations for certain hydrological processes.

The schematic representation of the physical medium concerns first of all the description of its geometry, including for example the elevation contours of the basin, the relief, the structure of the hydrographic network, the geometry of surface reservoirs and the spatial organization of the terrain. It also concerns the description of its physical properties (geology, soil types, land use). Representation of the physical medium requires its spatial discretization, i.e., division of the medium into distinct hydrological compartments, each governed by its own laws of behavior. These compartments may or may not correspond to real hydrologic entities of the system. Different types of spatial discretizations are presented in Section 3.2.3.

To represent the hydrological phenomena of interest for the considered hydrosystem, equations must be provided for certain processes. First of all, a choice must be made concerning the main hydrological processes to be represented to describe the behavior of the hydrosystem with respect to the phenomenon of interest. Then mathematical expressions that provide a "reasonable" representation of these processes must be chosen. The development of the equations also requires details on the nature of the interactions between the different spatial discretization elements selected to represent the medium. The equations typically used for this purpose are the laws of conservation of mass, energy and momentum, the state relationships (i.e., relationships between the different variables defining the state of the considered spatial unit) and the flux relationships expressing the various fluxes as a function of the pressure or pressure gradient. Different types of models are possible depending on the nature of the equations selected to represent the processes. These types of models are described in Section 3.2.2.

State variables and model parameters

Each of the equations used by a model expresses a relationship between different quantities, some of which vary with time. They define the model state variables, previously designated $\mathbf{Y}(t)$ (e.g., water volume or level, wetted perimeter). Some of these variables can represent model outputs (e.g., water table height at different points in the drainage basin).

Given the many simplifications in the representation of the medium and the phenomena, the state variables used to model the hydrosystem are rarely of the same nature as the variables used to describe the state of the true physical system. For example, the state of soil moisture, defined by its humidity profile, is often described in a simplified manner by a unique variable describing the average degree of saturation of the soil (Chapter 4). Similarly, the state of the snowpack, defined by different variables such as snow depth, density and degree of maturity, is often described simply by its water equivalent (Chapter 7).

The other quantities appearing in the equations of the model are constants.[2] Some of these are related to measurable physical characteristics of the medium (e.g., hydraulic conductivity of soils). Others are abstract quantities (e.g., storage capacity of the conceptual reservoirs). These various constants defined the model parameters, previously described by the vector $\mathbf{\theta}$. Depending on the nature of the discretization used to represent physical medium, both the state variables and the parameters of the model can vary in space.

Initial conditions and boundary conditions of the model

For a given hydrologic modeling application, it is always necessary to specify the initial conditions and boundary conditions of the simulation.

The initial conditions are the initial values assigned to the state variables $\mathbf{Y}(t)$, i.e., the values $\mathbf{Y}(t_0)$ that these variables take on the first simulation time step (e.g., values of water level at every point of the hydrographic network for $t = t_0$). The temporal evolution of the state variables subsequently depends on the boundary conditions specified for the simulation.

The boundary conditions $\mathbf{CL}(t)$ define the interactions between the boundaries of the considered hydrosystem and its neighborhood. They are used to estimate, for each time step of the period covered by the simulation, the values of the model state variables at the boundaries of the hydrosystem (e.g., lateral or vertical boundaries). The boundary conditions can specify the value of certain extensive variables such as water table height or intensive variables such as mass and energy flux exchanges across the boundaries of the hydrosystem. They can be defined in the form of a zero flux condition (e.g., no exchange of discharge between the considered drainage basin and neighboring drainage basins) or a functional relationship (e.g., equilibrium relationship between the outflow and the water level at the corresponding channel cross-section).

3.1.3 Main Types of Hydrological Models

A large number of hydrological models exist that vary in terms of their nature and the complexity. They are hard to classify into unambiguous types given the variety of possible classification criteria. Various classifications have been proposed in the literature (Singh, 1995; ASCE, 1996; Chocat, 1997; Refsgaard, 1997; Ambroise, 1999). They vary depending on the viewpoint adopted.

- Depending on the nature of the relationships used to represent the processes, models can be classed as empirical, conceptual or physically-based. These models are presented in Section 3.2.3.
- Depending on the manner in which the physical medium is represented and in particular depending on the nature of the spatial unit in which the equations used to describe the processes are solved, models can be classed as global, distributed, spatialized or semi-spatialized. These models are presented in Section 3.2.2.

---

[2]In certain hydrological models, referred to as dynamic, the constants can vary with time. This is the case for example for parameters used to describe the growth stage of a given vegetal cover or the degree of impermeabilization of a drainage basin subject to urbanization. Temporal variations of these constants are slow compared to those of hydrological state variables.

- Depending on the way the hydrological variables of the relationships between these variables are considered, models can be classed as deterministic or stochastic. The principle of these models is presented in Addendum 3.1.
- Depending on the nature of the time periods considered for the simulation, the models can be classified as event-based or continuous-simulation models. The principle of these models is also presented in Addendum 3.1.

Another distinction between models can be made on the basis of the time step selected for the simulation. For example, for flood forecasting models developed in urban hydrology, the time step can be infra-hourly. For models used to manage water resources on the scale of very large drainage basins, the time step can be weekly, monthly or even annual.

The principles of the various hydrological models currently used in different regions of the world (among many others) are illustrated in Appendices 3.8.1 to 3.8.5.

Addendum 3.1 Deterministic, stochastic, event-based and continuous-simulation models

Deterministic and stochastic models

Deterministic models stipulate that, for the given initial conditions and boundary conditions, the relationship between the inputs and the outputs of the system considered are unequivocal. In other words, for a given model input, there exists one and only one output.

Stochastic models simulate processes that are partially or totally random. For a given set of initial conditions and boundary conditions, different applications of the stochastic model give, for a given input, different outputs. The underlying assumption is that the considered phenomenon (e.g., precipitation, flood discharge, low-flow discharge) is the result of so many causes that are so complex that the relationship between the model inputs and outputs is not unequivocal. Stochastic models therefore generate a possible realization of the output variable, conditioned by the values of the model input variables. This realization results from the change, generally with time, of one or more appropriate random variables for the studied phenomenon.

Stochastic models are rarely used in hydrological modeling. Apart from autoregressive statistical models with exogenous variables (ARX) or autoregressive moving-average models with exogenous variables (ARMAX) (Box and Jenkins, 1970), that can be used stochastically, rainfall-runoff models are deterministic.

On the other hand, various stochastic approaches can be applied to estimate model parameters or the uncertainty related to a given model (Section 3.4.2). Similarly, numerous stochastic models have been developed to generate meteorological scenarios that are subsequently used as input to deterministic hydrological models (Chapter 12).

Deterministic and stochastic models are therefore increasingly often used together. In this case, the deterministic model makes it possible to simulate identifiable physical phenomena and the stochastic model takes into account phenomena of a predominantly random character (e.g., precipitation) as well as the uncertainty inherent to parameter estimation.

Event-based and continuous-simulation models

Event-based models are used to simulate selected hydrological events without considering periods between events. They are mainly developed to simulate the transformation of rainfall into runoff for flood discharge forecasting or prediction. Use of an event-based model requires estimation of the initial conditions the simulation for each event considered. This represents one of the main difficulties of event-based approaches. When simulating the design flood, average initial conditions can be used (Chapter 9).

Continuous-simulation models are used to simulate on a continuous basis the hydrological behavior of the basin. The simulation can be run over long time periods covering a variety of hydrometeorological situations extending from low flows to flood discharges. These models must consider all the processes significantly influencing the response of the drainage basin and not only the processes implied by particular hydrological phenomenon (e.g., the generation of floods). They also require estimation of the initial conditions. However, the influence of initial conditions on the expected results becomes negligible after a certain time (Section 3.3.5).

3.1.4 Approach for the Development of a Hydrologic Model

In any modeling approach, it is essential to first identify the modeling objective and framework, i.e., the hydrosystem and the nature of the hydrological phenomena to be modeled, the data available to describe the physical medium and the hydrometeorological variables of interest. This conditions the main hydrological processes to be considered, the possible spatial and temporal resolutions and the choice of realistic concepts and reasonable simplifications.

When the modeling framework has been defined, the general approach to be followed when developing a model follows three steps:

- Model construction
- Model calibration
- Model evaluation, implying in particular its validation

The principles of these three steps are presented below. They will be described in more detail in Section 3.2, 3.3 and 3.4.

Data preparation is also an important step in the development of the model. It is often carried out in parallel with model construction. It includes the mapping and preliminary processing of hydrometeorological data. Mapping aspects concern all the data required to describe the physical medium (Chapter 2). These data are often used for the discretization of the drainage basin or for the estimation of certain model parameters (Section 3.3). Data preparation also involves compiling valid hydrometeorological time series. These time series are then used either as model input or for the model calibration and validation steps.

Once all these steps have been carried out and the initial and boundary conditions specified, the model can finally be used for the targeted hydrological application.

Model construction principles

To build the structure of the model, the hydrosystem must be schematized and the mathematical and numerical problems related to its spatial discretization and to the concepts chosen to represent the physical medium and processes must be formulated. Model construction is necessarily accompanied by the development of the computer program that will be used to solve the associated mathematical and numerical problems. The construction of the model and development of the corresponding computer program is often based on existing modeling system. In this case, the modeling concepts along with the numerical tools required to solve the mathematical problem are reused. On the other hand, the schematization of the physical medium and its spatial discretization in particular must in principle be adapted to the hydrosystem targeted by the study.

Model calibration principles

The objective of model calibration is to: 1) optimize the structure of the model and in particular 2) estimate the parameters appearing in each of the model equations, in each of the spatial discretization elements. Some of these parameters can sometimes be derived from measured data or thematic maps available for the drainage basin. Most of the parameters must however be adjusted by calibration. Calibration is carried out by comparing, on the basis of selected criteria and for different hydrological variables, observed data and model output data obtained by simulation.

Model evaluation principles

Evaluation concerns the different quality criteria that must be satisfied by the model. The model must essentially be valid, parsimonious, robust and sensitive.

- Validity signifies that the representation of the physical medium and processes that occur within it is possible or acceptable. Validation is generally carried out by comparing, on the basis of selected criteria and for different hydrological variables, observed data and model output data obtained by simulation. This validation is carried out on a dataset that is different from the one used for model calibration. Validation concerns the structure selected to describe the physical medium and processes as well as the values assigned to the different model parameters.
- Parsimony refers to the complexity of the model. A model is parsimonious if it has few parameters and requires a limited quantity of input data. Parsimony is directly related to the choices made concerning the structure of the model.
- Robustness and sensitivity implies that the results obtained by simulation with the model: 1) do not diverge when the values of input variables are slightly modified, e.g., due to errors and uncertainties that are associated with them, but 2) are sensitive to variations of the factors for which the effects are to be estimated.
The approach for developing a hydrological model is summarized in Figure 3.4.

3.2 REPRESENTING THE PHYSICAL MEDIUM AND PROCESSES

Whatever the modeling objective, construction of a hydrological model is always based on the choice or design of its structure, i.e., the representation of the processes to be modeled and the spatial representation of the drainage basin.

3.2.1 Constructing a Model

Two main approaches can be followed when constructing a hydrological model.

The first approach is often referred to as the top-down approach and the modeling objectives in this case are limited to a few or often only a single objective. The model is developed to reproduce the measured hydrological response of the studied system in the simplest manner possible. The approach is inductive and systemic. Only the most important processes for the given objective are considered. The representation of the processes or the geometry of the drainage basin can be gradually refined as new observations become

```
                         ┌──────────────────┐
                         │  Define purpose  │
                         └──────────────────┘
                                  │
                                  ▼
┌──────────────┐         ┌──────────────────┐
│  Field data  │────────▶│ Conceptual model │
└──────────────┘         └──────────────────┘
                                  │
                                  ▼
                         ┌──────────────────┐
                         │  Code selection  │
                         └──────────────────┘
                                  │
                                  ▼
                         ╱────────────────╲        ╭─────╮
                        ╱  Existing code    ╲──────▶│ Yes │
                        ╲  suitable?        ╱       ╰─────╯
                         ╲────────────────╱             │
                                  │                      │
                                  ▼                      │
                               ╭─────╮                   │
                               │ No  │                   │
                               ╰─────╯                   │
                                  │                      │
                                  ▼                      │
                         ┌──────────────────┐            │
                         │ Code development │            │
                         └──────────────────┘            │
                                  │                      │
                                  ▼                      │
                         ┌──────────────────┐            │
                         │Model construction│◀───────────┘
                         └──────────────────┘
                                  │
                                  ▼
                         ┌──────────────────┐
                         │Performance criteria│
                         └──────────────────┘
                                  │
                                  ▼
┌──────────────┐         ┌──────────────────┐
│Comparison with│───────▶│Estimation /      │
│field data    │    ┌───▶│Calibration       │
└──────────────┘    │    └──────────────────┘
                    │             │
                    │             ▼
                    │    ┌──────────────────┐
                    └───▶│Evaluation /      │
                         │Validation        │
                         └──────────────────┘
                                  │
                                  ▼
                         ┌──────────────────┐
                         │    Simulation    │
                         └──────────────────┘
                                  │
                                  ▼
┌──────────────┐         ┌──────────────────┐
│  Field data  │────────▶│    Post-audit    │
└──────────────┘         └──────────────────┘
                                  │
                                  ▼
                         ┌──────────────────┐
                         │    Operation     │
                         └──────────────────┘
```
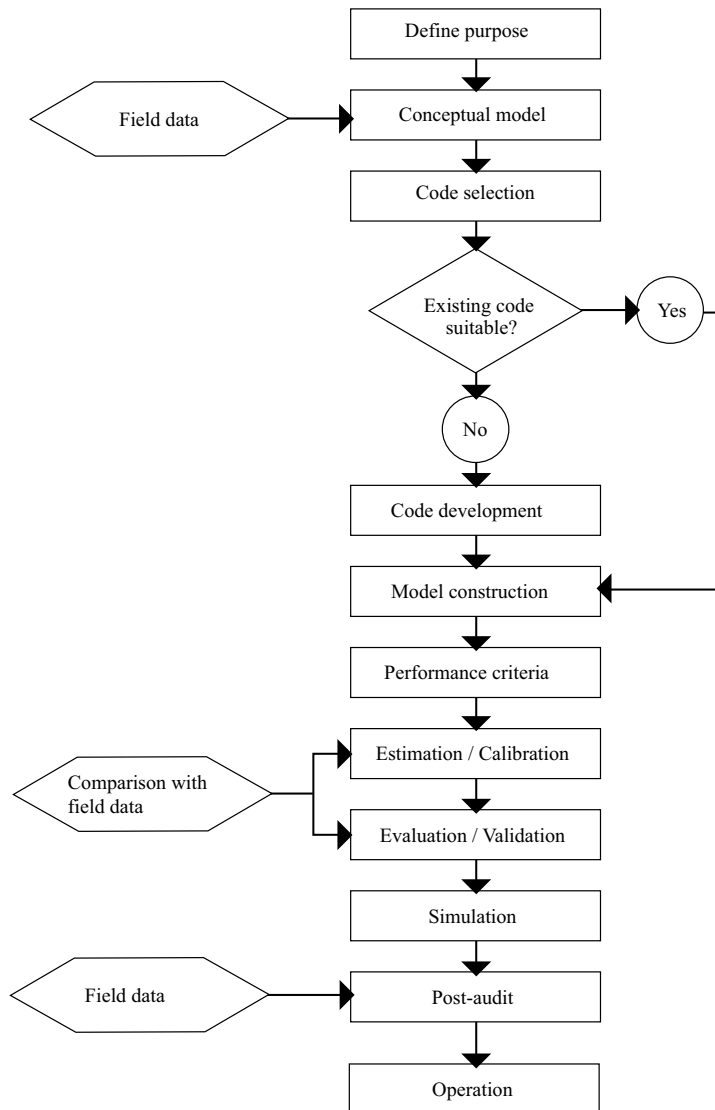
Fig. 3.4: Illustration of the approach used to develop a hydrological model (modified from Refsgaard, 1997).

available. This approach is often used in operational hydrology. It generally leads to the development of models that are relatively parsimonious and efficient for the targeted objective.

The second approach is referred to as the bottom-up approach and the modeling objectives in this case are not pre-defined. It is assumed that the behavior of the overall hydrosystem can be simulated properly as long as the processes governing the behavior of the hydrosystem are sufficiently known and these processes and their interdependence are correctly represented. The bottom-up approach is of a more scientific nature and mainly deductive. It leads to models with complex structures and that are difficult to assess

given that the required experimental data often do not exist. This perhaps explains why these models seldom leave the laboratories in which they are developed. To be used in operational hydrology, they often require a number of simplifications. Such models can be easily simplified a posteriori if one of the processes initially taken into account proves to have no significant influence on the targeted hydrological behavior.

Whatever the approach used, the construction of a hydrological model is ideally based on: 1) observation and experimentation of the targeted hydrological phenomenon and associated hydrological processes for the considered hydrosystem, 2) formulation of the assumptions required to represent the physical medium and these processes and 3) testing of these assumptions, i.e., their validation or invalidation.

These three successive steps often make up an iterative and a priori infinite cycle aimed at improving the mathematical description and knowledge of some or all of the components of the hydrological cycle.

3.2.2 Representing the Processes

The different approaches used to represent the processes leads to empirical, conceptual or physically-based models. The underlying principles of these models will now be reviewed.

Whatever the type of representation, the models are generally made up of different modules, each designed to describe, with a varying degree of independence, the main processes explaining the behavior of the drainage basin. The modules most commonly encountered are presented further on in this section under "Typical components of a hydrological model".

Empirical models

Empirical models are based on the relationships observed between the inputs and outputs of the considered hydrosystem. They express the relationship between the input and output variables of the system (e.g., rainfall-runoff relationship) using a set of equations developed and adjusted using data obtained for the system. An empirical model is not designed to describe the causes of the considered hydrological phenomenon nor to explain the operation of the hydrosystem. The hydrosystem is considered to be a black box.

Examples of empirical models include the SCS-CN model used to estimate the net rainfall resulting from a given total rainfall (Chapter 4) and the unit hydrograph model used to estimate the hydrograph of the runoff resulting from this net rainfall (Chapter 5). ARX type models can also be classed in this category (Chapter 5 and 10).

Physically-based models

Physically-based models represent the hydrological operation of the hydrosystem by coupling different sub-models, each dedicated to certain hydrological processes. They are generally based on a fine spatial discretization of the physical medium (Section 3.2.3). Whatever the nature and spatial resolution of this discretization, note that the spatial variability of the physical medium and processes can only be explicitly described for spatial scales that are larger than those of the discretization. For smaller scales, it must be described in a conceptual manner—which is not frequently the case (Addendum 3.2).

The development of physically-based models on the drainage basin scale goes back to the 1980s. One of the first physically-based models is the well-known European Hydrological System, often referred to as SHE for "Système Hydrologique Européen" (Abbott *et al*., 1986a,b). The underlying principles of this model are presented in Appendix 3.8.5. Several other models of this type have since been developed and are the subject of numerous publications (Noilhan and Planton, 1989; Habets *et al*., 2008; Liang *et al*., 1994; Wood *et al*., 1992).

Addendum 3.2 Representation of the internal variability within the discretization elements of physically-based models

The choice of the spatial resolution of a model determines the respective parts of the spatial variability that can be represented explicitly and implicitly. In practice, three main approaches can be used to account for the variability within the discretization elements of a given model.

The first consists in using so-called effective parameters in the equations describing the processes. These parameters are supposed to make it possible to simulate the overall behavior of the considered discretization element. An "effective" conductivity is for example often used to describe saturated flow in heterogeneous porous media (Figure 3.5). The difficulty of this approach lies in the estimation of the values of these effective parameters. For certain types of heterogeneity, an explicit relationship can be found between the value of the effective parameter and the spatial variability of the parameter within the discretization element. The method used most often to estimate the effective parameters is empirical, often implying the use of the calibration procedure. The use of effective parameters does not often provide full satisfaction, in particular if the processes are non-linear and/or conditioned by one or more operating thresholds (e.g., infiltration processes, see Chapter 4).
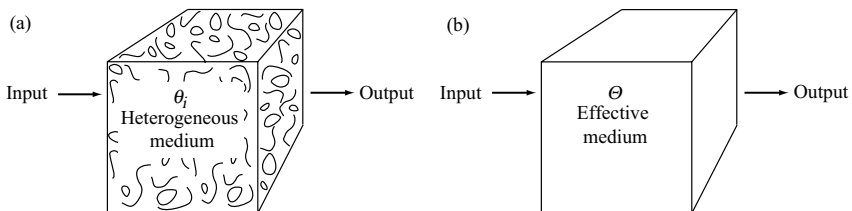
Fig. 3.5: Spatial variability of the physical properties of the medium (e.g., hydraulic conductivity) within a given discretization element (e.g., heterogeneous porous medium) and the effective parameter used in the model representation (e.g., equivalent hydraulic conductivity).

The second approach consists in using a statistical representation of the physical property considered. The statistical distribution of the property is used to define a set number of classes of behavior and the model is applied to each of them. This is the same principle as that of the distributed models presented below in Section 3.2.3. In certain cases, the distribution can be chosen to obtain an analytical solution of the targeted behavior, which simplifies the application of the model.

The third approach consists in proposing a parameterization for the targeted process, i.e., a conceptual model that can be used to represent the average behavior at the scale of the considered element. This parameterization can be derived from the corresponding fundamental physical laws. For common hydrological applications, free-surface flow can be modeled for example using the Barré de Saint-Venant model (Chapter 6). This model, derived from the Navier-Stockes equations, considers free-surface flows in an integrated manner over a flow section (the Navier-Stockes equations define the basic physical equations of hydrodynamics).

The equations that define the parameterization are not necessarily related to the equations that describe the processes at the scale of these processes. A classical parameterization is the Darcy model used to describe the mean flow velocity within saturated porous media. The associated parameter is a hydraulic conductivity of the spatial element considered. One difficulty of this approach lies in the fact that adequate parameterization depends in principle on the spatial and temporal resolutions used.

Conceptual models

Conceptual hydrological models are designed to represent the main hydrological processes in a reasonable manner without requiring parameterization of the physical laws that govern them. The representation is conceptual in that it is based on the hydrologist's perception of the hydrological behavior of the drainage basin. This perception is derived from the hydrologist's expertise and theoretical, empirical and/or intuitive understanding of the operation of the studied hydrosystem. For surface runoff, for example, one modeling concept assimilates the drainage basin with a rectangular inclined plane of constant slope. For such a configuration, it is possible to derive runoff equations in a simple manner (Chapter 5).

Most conceptual models consider the drainage basin can be represented by a combination of conceptual reservoirs linked together by various exchange relationships (Addendum 3.3). This is for example the case for the SWMM model with 8 reservoirs and 27 parameters developed at Stanford University for urban drainage basins (Crawford and Linsley, 1966) and the GR3J model with 3 reservoirs and 3 parameters developed for rural drainage basins in France by Cemagref[3] (Edijatno and Michel, 1989; Appendix 3.8.1). These reservoirs are sometimes considered to represent the main hydrologic compartments of the basin.

Addendum 3.3 Conceptual reservoir models

A wide variety of reservoir models are used in hydrological modeling (see the inventory proposed by Perrin, 2000). Reservoir models, also call "capacitive models", can first be differentiated by the way they describe the space. They are most often global but can also be distributed or semi-spatialized. Reservoir models can also be differentiated by the degree of simplification used to represent the processes involved and also by the number and type of reservoirs and the way in which the reservoirs are organized to represent these processes.

Whatever the reservoir implied in the structure of a reservoir model, its behavior is governed by a system of three types of equations:

• the continuity equation that expresses mass conservation of water in the reservoir,
• a storage equation that defines the volume of water stored in the reservoir for a given water level,
• various discharge equations expressing the inflows and outflows to and from other compartments of the modeled system as a function of the water level in the reservoir.

The variations of the water volume stored in a reservoir depend on the volumes of inflows and outflows. Inflows can be of many types (e.g., direct precipitation or surface runoff). The same is true for outflows (e.g., percolation or evapotranspiration).

---

[3]In 2012, Cemagref became Irstea, the French institute for research in environmental and agricultural sciences and technologies.

A reservoir can have a linear or non-linear behavior. Non-linearity often results from the non-linear character of one or more of the reservoir discharge equations, in particular for the outflows. For example, the outflow may be expressed as an exponential function of the storage or may depend on the value of certain water-level thresholds.

A reservoir can have different types of outlet works. For example, low-level outlets and bottom sluices provide continuous outflows that vary with time as long as the reservoir is not empty. On the other hand, overflow weirs produce outflows only when the water in the reservoir has exceeded a certain level.
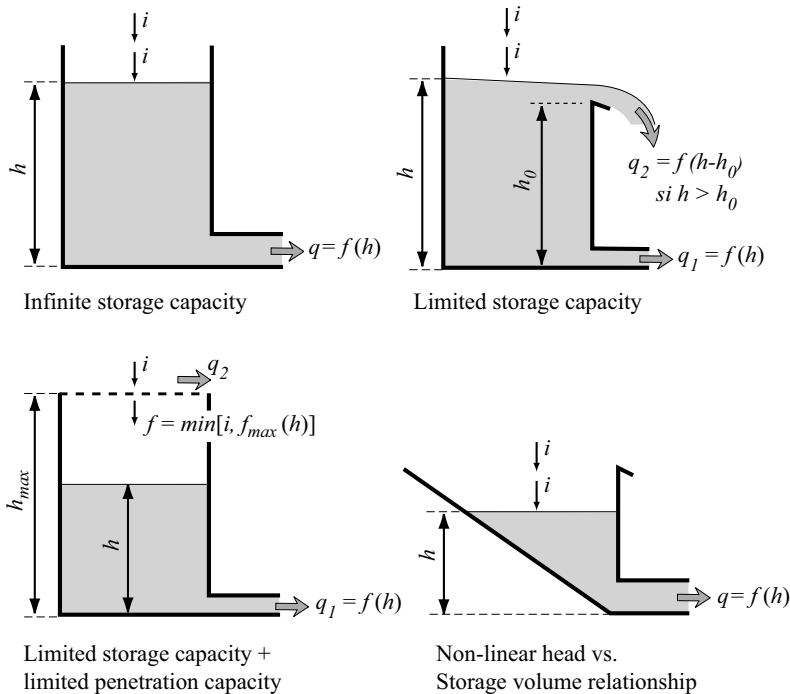
Fig. 3.6: Examples of conceptual reservoirs used in the structures of reservoir-type hydrological models.

Typical components of a hydrological model

When designed to simulate the hydrological behavior of hydrosystems, hydrological models, whether empirical, conceptual or physically-based, combine different modules or sub-models, each designed to represent one or more of the hydrological processes considered to be important.

Although sometimes interdependent, these modules are often independent, i.e., the output of one module is the input to another module. Depending on the hydrological model, some of these sub-models may not be considered or may be considered in an extremely simplified manner. Typical modules of a hydrological model are presented in Figure 3.7.

The first module is generally designed to transform available meteorological data into input data with the spatial and temporal resolution required by the simulation model. This
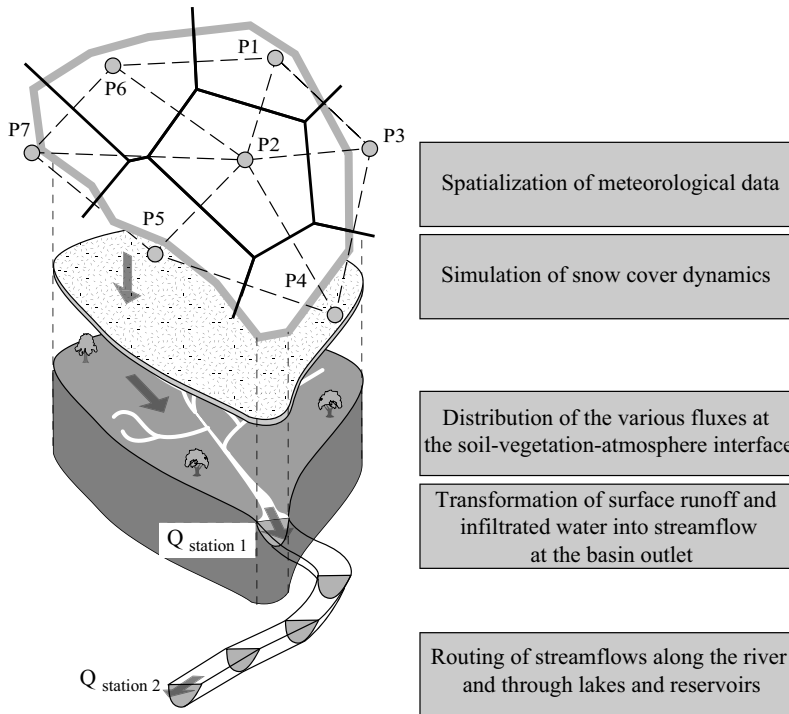
Fig. 3.7: Typical modules of a hydrological model.

module is often used to estimate meteorological forcing data for each element of the selected spatial discretization. It makes use of data combination and spatialization techniques such as those presented in Chapter 2.

The second module generally focuses on the processes that determine the distribution of the various water fluxes at the soil-vegetation-atmosphere interface. In varying degrees of detail, this module represents interception by vegetation, depression storage, evaporation from water bodies, evapotranspiration from vegetal cover and infiltration. In hydrological modeling, this module can be associated with the estimation of rainfall excess (Chapter 4), i.e., the net rainfall contributing to surface runoff.

The rainfall-excess module is often accompanied by a snowmelt module that treats phenomena related to the presence of solid precipitation, snow cover and ice surfaces. This aspect is dealt with in Chapter 7.

The way that surface runoff (resulting from the net rainfall calculated by the rainfall excess and, if applicable, the snowmelt modules) generates streamflow at the outlet of a given basin is modeled by another module, often based on what is referred to as the rainfall-runoff transformation function (Chapter 5).

Another module can be used to handle precipitation that has infiltrated in the soil and that percolates downward into the water table before entering the hydrographic network via base flow. Different approaches can be followed to represent the related processes. They are either hydrological, similar to those used for rainfall-runoff analysis (Chapter 5), or hydrogeological.

The propagation of streamflows along a river and through lakes, artificial reservoirs and hydraulic structures is handled by another complementary module often based on what hydrologists refer to as the "routing" function (Chapter 6).

Note that the modules related to rainfall excess and snowmelt deal with predominantly vertical processes while the modules related to the rainfall-runoff relationship and routing deal with predominantly lateral processes.

3.2.3 Representation of the Physical Medium and Spatial Discretization

As already mentioned, global, distributed, spatialized and semi-spatialized models can be distinguished by the way they represent the physical medium and, in particular, by the spatial unit in which the equations describing the processes are solved.

Global hydrological models describe the drainage basin as a single hydrological unit. The spatial variability of the hydrological processes considered to describe its behavior is therefore not taken into account. The GR3J model developed in France and a number of other models are of this type (Edijatno and Michel, 1989) (Appendix 3.8.1).

The drainage basin can also be represented in a discretized manner by dividing it up into distinct spatial units. Depending on the spatial discretization and the nature of the relationships between the discretization elements, the models are referred to as spatialized, semi-spatialized or distributed. These types of discretization are described below. A more detailed presentation can be found in the work of Grayson and Bloschl (2000) or Indarto (2002).

Spatialized models

Spatialized models attempt to represent the physical medium and in particular the surface of the drainage basin using a relatively fine spatial discretization that respects the spatial organization of the discretization elements. Most of them have been derived from work aimed at explaining the hydrological response of a considered basin on the basis of its geomorphology (Rodriguez-Iturbe and Valdes, 1979; Bérod *et al*., 1995; Rodriguez *et al*., 2003).

Spatialized models simulate the evolution of the system at every point of this discretization along with the exchanges of water with neighboring elements. Each element of the discretization is in principle characterized by its own parameters. Given the determining influence of topography on the displacement of water at the surface of a drainage basin, a discretization is mainly dictated by the manner in which the topography is described.

Different types of discretizations are possible (Figure 3.8). Some are based on elevation contours. Depending on whether the boundaries of the discretization elements are parallel or orthogonal to the elevation contours, these discretizations delimit bands of equal elevation (e.g., Topog model, Vertessy *et al*., 1993) or stream tubes (e.g., Thales model, Grayson *et al*., 1995). Other discretizations describe the drainage basin as a cascade of inclined planes (hill slopes) and drainage elements (channels) organized in a tree structure (e.g., Socont model, Bérod *et al*., 1995; Kineros model, Smith *et al*., 1995). The most widely used discretizations are based on spatially referenced digital elevation data (Chapter 2). Given that the raster format is the classical representation mode of Digital Elevation Models (DEM), the physical medium is most often spatially discretized into a
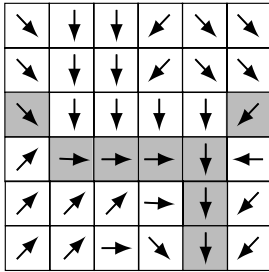
(a) Regular square grid   (b) Triangular irregular network (TIN)
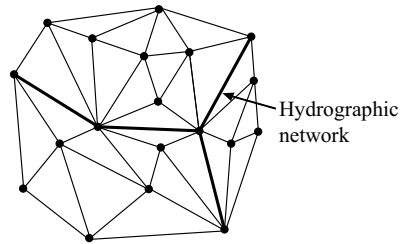
(c) Inclined planes and drainage elements   (d) Elevation contour bands
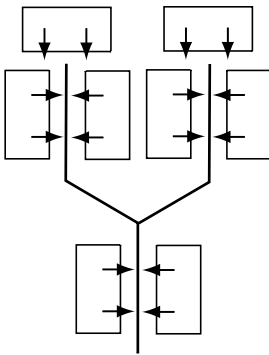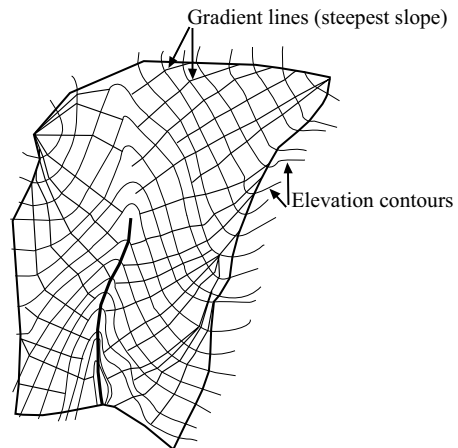
Fig. 3.8: Examples of possible discretization schemes for specialized hydrological model (modified from Grayson *et al.*, 2000).

regular grid of square cells (e.g., MODCOU, Ledoux *et al.*, 1989). One of the models the most representative of this type of discretization is the SHE model (Abott *et al.*, 1986a,b) (Appendix 3.8.5). The modeled space can also be divided up into irregular triangular grid cells on the basis of a TIN (Triangular Irregular Network) model but this method is less widely used (tRIBS physically-based model, Ivanov *et al.*, 2004).

These different discretization schemes each have their advantages and disadvantages. For example, a raster-type discretization can be used to identify the drainage network in a simple manner (Chapter 2) and makes it easier to develop algorithms to solve the associated equations. It however imposes a sub-optimal description of the basin boundaries, the layout of the hydrographic network and the spatial variability of the characteristics of the physical medium. On the other hand, a TIN-type spatial discretization generally requires fewer points to provide a very satisfactory representation of the topography and spatial variability of the characteristics of the medium. At the same time, however, it requires more complicated algorithms to solve the associated equations.

Semi-spatialized models

For a semi-spatialized model, discretization consists in delimiting hydrological units for which it is assumed that the behavior can be reasonably described by a global or distributed hydrological model. These hydrological units, generally assumed to function independently, are emptied one into another and/or into the hydrographic network that drains them from upstream to downstream. Many discretization methods and criteria are possible.

One possible type of discretization consists in delimiting Relatively Homogeneous Hydrological Units (RHHUs), i.e., zones in which the hydrological processes are comparable both in terms of their nature and relative impact. These hydrological units are generally identified on the basis of the most pertinent physiographic characteristics of the basin with respect to the key processes. The characteristics often used are those of the hydrographic network, topography (elevation, orientation, influencing the meteorological conditions, the drainage network), land use (e.g., characteristics of the vegetal cover, type of urbanization) and pedological and geological characteristics of the soils and subsoils (Amerman, 1965). The CEQUEAU model (Girard *et al.*, 1972) uses this type of discretization (Appendix 3.8.3). In general, RHHUs are also determined in such a way that meteorological forcing is not excessively heterogeneous within each of the RHHUs. In mountainous regions, this often leads for example to RHHUs based on elevation bands (Chapter 7).

For very large drainage basins, the hydrological units are generally sub-basins of the complete drainage basin. Most of the approaches used to delimit these sub-basins are empirical, based on the topography, structure of the hydrographic network and locations of the key points in the network. The sub-basins can for example be defined as the smallest spatial units in which it is possible to calibrate the hydrological model. In this case, the divisions depend greatly on the distribution of the stream-gage stations over the drainage basin. In another case, the sub-basins can be defined on the basis of the points of the hydrographic network where the model must be able to simulate discharge data. The divisions can also be conditioned by the locations of hydraulic structures that modify the natural behavior of the basin. This criterion can lead to relatively fine discretizations as is the case in urban environments where artificial drainage elements, impervious areas connected and not connected to the drainage network and special equipment such as stormwater infiltration/retention works must be considered separately.

The different partitioning criteria, based for certain on the homogeneity of the hydrological processes and meteorological forcing and for others on the presence of key points, can be considered in a combined manner. The GSM-SOCONT model (Hingray *et al.*, 2006b; see Appendix 7.6.4 of Chapter 7) has been used in this way to model the Rhone upstream of Lake Geneva (Figure 3.9).

Distributed models

In a distributed model, it is assumed that the hydrological behavior of the drainage basin can be explained on the basis of the behavior of a limited number of distinct hydrological units. These units are chosen to be representative of the main types of hydrological behaviors observed within the basin. They are generally referred to as hydrologically similar response units (HRUs) (Gurtz *et al.*, 1999).

The hydrological response of the drainage basin to a given meteorological forcing is simply obtained by a weighted sum of the hydrological responses simulated for the different

(a)

Porte du Scex

Martigny

Sion

Sierre

Viège

Brigue

Reckingen

N

0   10   20 km

(b)

Reckingen

Brigue

bv1

bv2

Sierre

Viège

Porte du Scex

Martigny

Sion

bv36

Production + transfer
Production + transfer + routing
● Analysis point
○ Discharge combination point
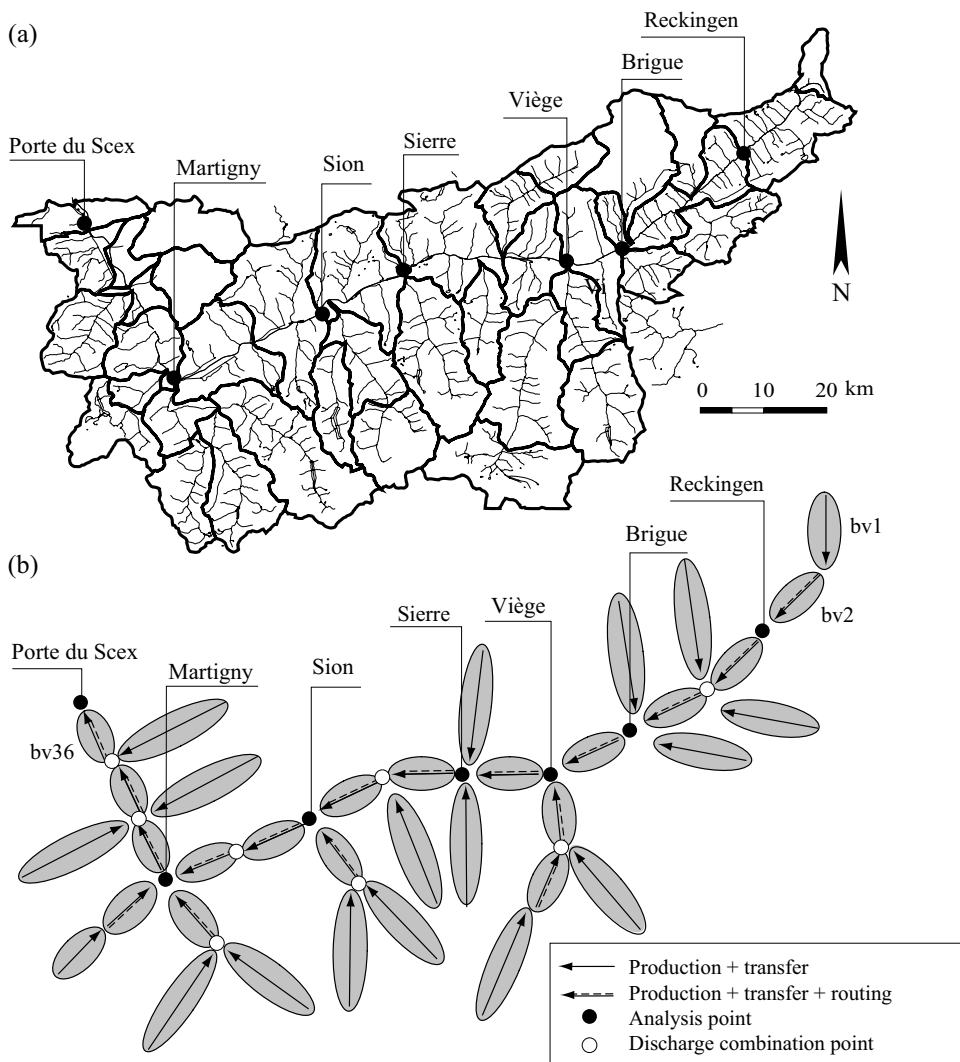
Fig. 3.9: Discretization of the Rhone drainage basin upstream of Lake Geneva into sub-basins (adapted from Hingray *et al.*, 2006b). a) The Rhone drainage basin (area: 5240 km^2 upstream of Porte du Scex), the hydrographic network and the 35 sub-basins selected for discretization. b) Structure of the hydrological model with: 1) sub-basins generating rainfall excess (production) and transforming it into streamflow (transfer) 2) river reaches used to route basin inflows. The discretization is based on: 1) the natural topographic boundaries of the basins, 2) the points in the network where it is possible to calibrate the model and 3) the points in the network where discharge simulations are required.

HRUs. The weight applied to the response of a given HRU is generally proportional to the area occupied by this unit within the drainage basin. This approach reduces the number of calculations required to simulate the behavior of the basin. Distributed models do not describe predominantly horizontal flows within the drainage basin or do so in an extremely simplified manner (e.g., assuming a permanent equilibrium between the levels

of the reservoirs used to represent groundwater storage within each unit). The units are often assumed to be independent of each other and their spatial organization is frequently ignored.

With this approach, each elementary area of the basin must be assigned to one of the HRUs. The physical characteristics used for this are mainly the same as those used to identify relatively homogeneous hydrological units (Section 3.2.3). They can be used in a combined manner (Figure 3.10).

In certain models, each elementary area is assigned to an HRU on the basis of a single characteristic. For example, for a drainage basin in a mountainous region, where the hydrological response is highly dependent on snow accumulation and snowmelt processes, assignment is often based on elevation alone (Chapter 7). This is for example the principle used for the HBV model (Bergström, 1976; Appendix 3.8.2). For TOPMODEL (Beven *et al*., 1984), assignment is based on a topographic index calculated at every point in the basin from the local slope and the upstream area drained at the point (Appendix 3.8.4). When the discretization is based on a single characteristic, a statistical distribution function is sometimes used to describe the distribution of this characteristic, hence the term "distributed" models.
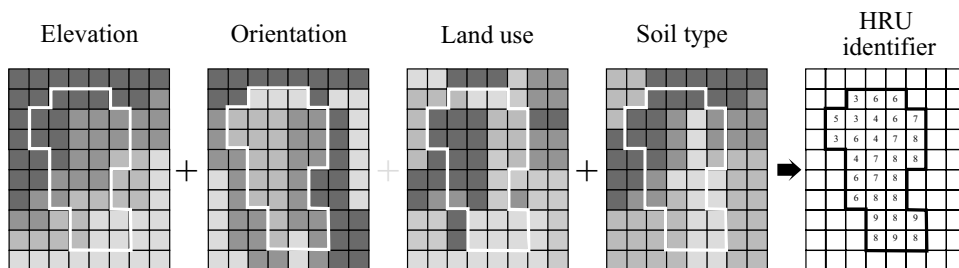
Fig. 3.10: Illustration of HRUs obtained on the basis of different characteristics of the physical medium described in raster format (modified from Zappa, 1999).

3.2.4 Compatibility Between Spatial Representations and Processes

A key question when constructing a hydrological model concerns the optimum level of complexity to be targeted. According to Grayson and Bloschl (2000), this depends on modeling objectives, knowledge of the system and the required level of validation.

Whatever the case, the level of complexity selected for the different model components must be well-balanced. This is because the pertinence and accuracy that can be achieved by the model is determined by the component with the coarsest representation. In other words, the different levels of complexity used to represent the different processes explaining the behavior of the hydrosystem must be compatible with each other in the same way as the levels of complexity used to represent the physical medium. They must also be compatible with the data available for model input, calibration and validation. Figure 3.11 illustrates various degrees of simplification that can be used when representing the geometry of the drainage basin and the transformation of surface runoff into a discharge at the basin outlet.

Arbitrary grid

Saint-Venant equations

$$\frac{\partial A}{\partial t} + \frac{\partial Q}{\partial x} = q$$

$$S_0 - S_f = \frac{\partial h}{\partial x} + \frac{1}{g}V\frac{\partial V}{\partial x} + \frac{1}{g}\frac{\partial V}{\partial t} - (k-1)\cdot\frac{q}{g}\cdot\frac{V}{A}$$

Combination of inclined planes

Kinematic wave model

$$\frac{\partial A}{\partial t} + \frac{\partial Q}{\partial x} = q$$

$$Q = \frac{1}{n}\cdot A(h)\cdot R_H(h)^{2/3}\cdot\sqrt{S_0}$$

Sub-basins

Sub-basin 1

Sub-basin 2

Sub-basin 3

Reservoir model

$$\frac{d\,S(t)}{dt} = I(t) - Q(t)$$

$$Q(t) = S(t)/K$$

Black box

Empirical equation

$$Q(t) = f(A, i, ...)$$

Reduction of the complexity of the representation and the amount of data needed
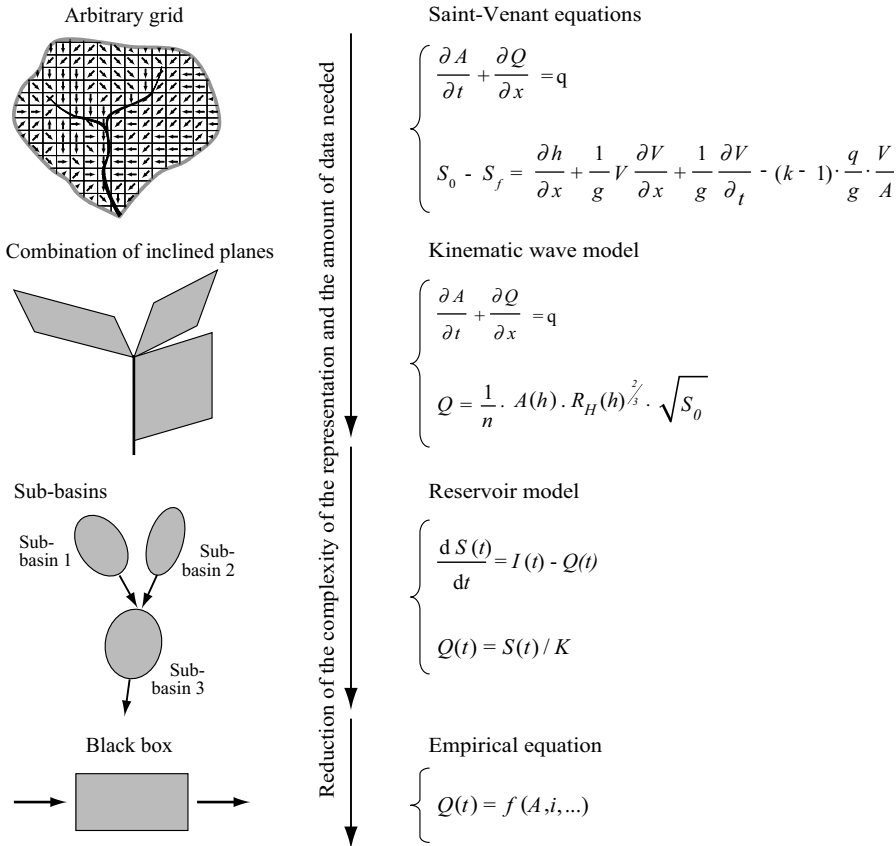
Fig. 3.11: Different degrees of simplification that can be used when representing the geometry of the drainage basin and the corresponding surface runoff.

The targeted level of complexity also depends on the optimal temporal and spatial resolutions for the considered hydrological problem. For a given type of model, the optimal resolutions depend on the available data and the dynamics of the hydrological processes considered. This problem has been relatively well analyzed for streamflow routing (Chapter 6) however this is not the case for modeling of the rainfall-runoff relationship. The approach proposed by Obled *et al*. (2009), based on analysis of the spatial variability of the precipitation, provides valuable insight into this issue. Their analysis is summarized in Addendum 3.4.

Addendum 3.4 Selecting the temporal and spatial resolution for the modeling of the rainfall-runoff transformation

The objective of the analysis proposed by Obled *et al*. (2009) was to determine the optimum time and space steps for the construction of the parsimonious conceptual model for the simulation of the rainfall-runoff transformation.

In their work, the authors first note that, for a given rain-gage network, the accuracy of the estimation of the precipitation falling on the unit area increases with the duration. On the other hand, the accuracy of the description of the hydrological dynamics of the drainage

basin increases as the considered time step decreases. The necessity of limiting uncertainties in the estimation of precipitation therefore leads to selecting the maximum duration that still represents the determining hydrological processes in a reasonable manner.

In process-oriented models, the optimum time step is the smallest time step required to represent all the processes. In certain contexts, this can be a few seconds (e.g., infiltration excess overland flow on steep drainage basins, erosion processes).

In conceptual hydrological models, the required time step depends on the dynamics of the output signal, the discharge. It is longer than for process-oriented models, the drainage basin filtering the high frequencies of the input signal (precipitation) and those of the processes related to the production of rainfall excess in the basin. To accurately represent the shape of the basin discharge response to a given precipitation input, Obled *et al*. (2009) suggest that, in this case, the maximum permissible time step Δt_o is roughly between a fifth and a third of the rise time t_r of the instantaneous unit hydrograph of the basin (Chapter 5). Therefore:

$$t_r/5 \leq \Delta t_o \leq t_r/3 \tag{3.3}$$

where Δt_o is the time step of the model and consequently the time step used to represent the input signal.

This analysis is based on the spatial correlation of the precipitation fields considered to be the most critical with respect to the generation of floods (Appendix 2.7.2). Geostatistical analyses of these fields has shown that the decorrelation distance between precipitation depths, i.e., the distance at which the correlation between precipitation depths becomes null, is a function of the time step Δt over which the precipitation has accumulated. In other words, the spatial variability of rainfall increases as the accumulation time decreases. The relationship identified for different regions in France is:

$$a = b \cdot \Delta t^c \tag{3.4}$$

where a is the decorrelation distance [km], Δt the accumulation time [hours] and b and c constants (b between 18 and 30, c between 1/3 and 1/2).

Using a classical decay model to describe the decreasing correlation with distance (e.g., exponential or spherical), it is possible to evaluate the maximum size for which a point precipitation value reasonably represents the mean precipitation value over a spatial domain centered on the point. For a spherical decay model, 80% of the variance of the mean value on a square with side length $a/2$ is explained by the value at the center of the square. The explained variance is 72% and 60% for a square with a side length of respectively $2a/3$ and a. The maximum space step for which it is possible to consider that the rainfall is reasonably uniform over a domain of area $A = (\Delta x)^2$ is therefore roughly between two values:

$$a/2 \leq \Delta x \leq 2a/3 \tag{3.5}$$

Given the maximum time step Δt_o that can be used to represent the flood dynamics of the considered basin, equations 3.4 and 3.5 can be used to estimate the maximum possible space step Δx or the maximum possible size A of the domain over which the rainfall can be assumed to be reasonably uniform.

$$100\,\Delta t_o \leq A \leq 400\,\Delta t_o \tag{3.6}$$

with A in km^2 and Δt_o in hours. This relationship between the maximum possible spatial and temporal resolutions is only valid from a statistical viewpoint for the context targeted by the analysis and under the assumptions of the analysis. Obled *et al*. (2009) discuss the precautions that must be taken when using such an approach.

Expression 3.6 answers the question concerning the optimal discretization of the drainage basin. If the area A of the domain is greater than the size of the basin, the basin can be described

by a global model. If not, it must be divided into sub-basins. The number of sub-basins to be considered can be determined in an iterative manner, the maximum permissible time step decreasing with the number of sub-basins. This is because the rise time of the instantaneous unit hydrograph of the basin increases with the size of the basin.

3.3 ESTIMATING MODEL PARAMETERS

All hydrological models include parameters that must be estimated. The number of parameters varies greatly with the degree of conceptualization of the model and the spatial discretization scheme. Global conceptual models generally have four to ten parameters while spatialized models may have several dozen or more.

Parameter estimation often refers to model calibration, one of the most delicate steps in the development phase. A number of publications and been devoted to this topic (e.g., Duan *et al*., 2003, 2006).

A wide variety of parameter estimation methods exists. This is because there are many types of parameters and no single estimation method has proved satisfactory for all of them. Parameter estimation implies making choices concerning a calibration strategy that of course depends on the modeling objectives. The strategy also depends on the experience, priorities and personal preferences of the modeler. It influences the way the hydrological simulation model represents the hydrosystem as well as the pertinence and performance of the model itself.

Model parameters can be estimated using either a deterministic or probabilistic approach. The first is the most widely used and is aimed at identifying the optimal set of parameters for the considered model and data. The second approach, more recent, has a statistical context and is aimed at identifying not only the best values for the parameters but also their probability distributions. This approach is closely related to the problem of modeling uncertainty and will be dealt with in Section 3.4.

The objective below is to provide an overview of: 1) certain problems related to parameter estimation using a deterministic approach and 2) certain methods widely used for parameter estimation. This presentation is not intended to be exhaustive and the reader can refer to numerous publications devoted to this problem for more information.

3.3.1 Nature of Parameters and Estimation Methods

As a first approximation, the estimation of parameters depends on their nature, the type of model and the available data. Two approaches are possible.

The first consists in assigning values on the basis of data describing the drainage basin. These data can be derived from measurements, field observations or thematic maps. This approach is often used to specify parameters that have a physical meaning. It can however be applied to estimate all types of parameters if appropriate regional models are available.

The second approach consists in estimating the parameters by means of a calibration procedure. This is carried out indirectly using hydrometeorological observations.

Specifying parameters that have physical meaning

Depending on the model, certain parameters may have physical meaning and are therefore directly related to the physical characteristics of the medium.

Some of them may be estimated relatively easily from thematic maps, DEMs or other data obtained by remote sensing. The type of land use on a given element of the discretization can for example be estimated from a land-use map. The slopes and upstream drainage areas at every point of the drainage network can be extracted from DEMs (Chapter 2).

Theoretically, some parameters can be estimated from measurements made on the studied drainage basin. This is for example the case for certain properties of the physical medium such as the hydraulic conductivity of the soil. However, two major difficulties are encountered.

- First of all, the physical medium within each discretization unit is generally very heterogeneous. Measurements, usually made at certain points, cannot be used directly to characterize the properties of the considered discretization element. Using the measurements requires that it is possible to: 1) find a method to describe the internal variability of the parameter and the associated behavior of the discretization element and 2) relate the point values to the associated model parameters (Addendum 3.2).
- Next, even if the above problem can be solved, it is impossible from a practical viewpoint to measure, at every point, the characteristics required for the estimation. Consequently, the point measurements must be spatialized using the classical spatial interpolation methods already discussed in Chapter 2. This spatialization leads to a very imperfect view of the real variability of the characteristics of interest, in particular because the point measurements are not necessarily representative.

These problems in terms of scale and representativeness explain why it is often necessary to calibrate parameters that have a physical meaning. This is for example the case for the physically-based SHE model (Abbott *et al.*, 1986a,b). Note that when an automatic calibration procedure is used for this, the physical meaning of certain parameters can be considerably modified or disappear altogether.

Specifying parameters using regional models

Whether or not they have physical meaning, the parameters can also be estimated on the basis of the characteristics of the physical medium when a regional model capable of predicting them is available.

These predictive models must be constructed by applying a hydrological regionalization procedure (Chapter 11). They are often available to estimate the parameters of hydrological models frequently used for a given region. Such models are of many different types. For example, pedotransfer functions (Soutter *et al.*, 2007) are predictive models relating the parameters describing the hydrodynamic properties of soils to various measurable pedological characteristics by means of appropriate mathematical functions (Addendum 4.6).

A similar predictive approach makes use of tables or nomographs proposing standard values or possible parameter ranges for different types of media. Each discretization unit chosen to represent the basin is matched to one of the classes figuring in these tables. The value indicated for the class is assigned to the corresponding discretization unit. Land-use maps are for example often used to estimate the values of certain parameters such as basin roughness coefficients affecting surface runoff. Different tables of this type will be found in Chapters 4, 5 and 6.

Note that estimates obtained using these predictive models can give poor simulation results. These prior estimates are consequently very often subsequently adjusted using a calibration/validation procedure as will be discussed below.

Estimating parameters by calibration

Whether they have physical meaning or not, many model parameters are determined using a calibration procedure. The objective of this deterministic approach is to adjust parameter values so as to obtain the best possible agreement between the simulation results obtained with the model and observed data. In other words, model calibration involves finding parameter values that minimize the simulation error $\varepsilon_z(t, \mathbf{\theta})$ for the various output variables considered (Figure 3.12).

The procedure used to calibrate hydrological models generally consists in choosing:

- the dataset to be used for the calibration,
- one or more criteria for the evaluation of the performance of the hydrological model,
- a method to identify optimum values of the parameters with respect to the selected performance criteria.

The calibration method always depends on the modeling objectives, type of model and available data. The parameter estimates obtained in this step along with the associated uncertainties must be evaluated in a subsequent validation step (Section 3.4).

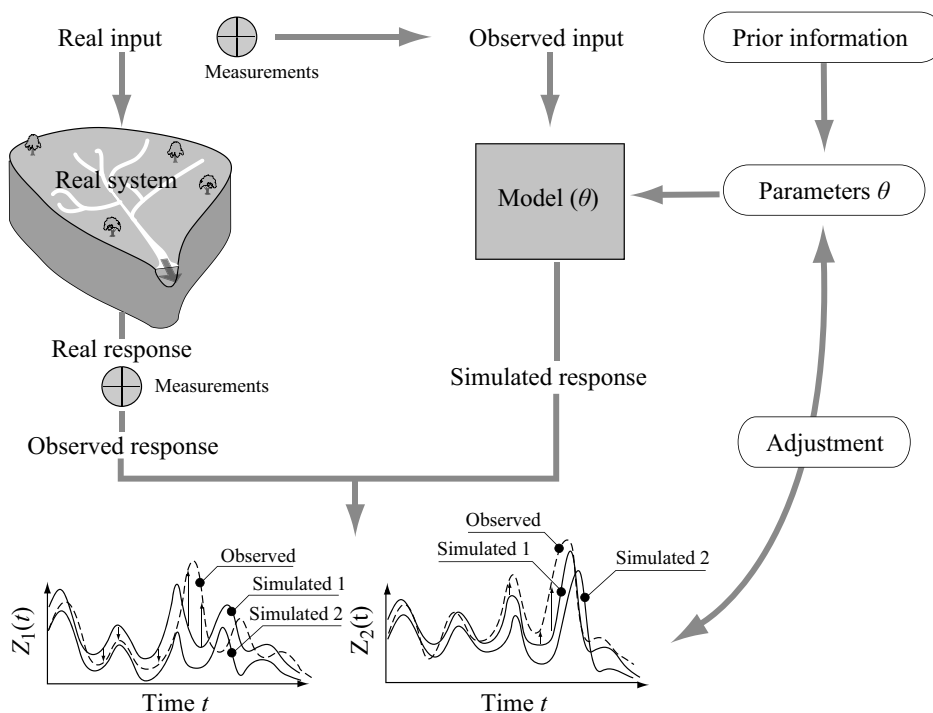
Fig. 3.12: Schematic procedure used to calibrate parameters θ of a hydrological model. Calibration involves minimizing the error between the observed and simulated values of various model output variables (e.g., $Z_1(t)$ and $Z_2(t)$).

3.3.2 Performance and Equifinality Criteria

Different possible criteria that can be used to assess model performance along with the main difficulties related to this assessment will now be discussed.

Model performance criteria

Before calibrating a hydrological model, one or more performance criteria must first be defined. Many criteria are possible. They can also be used in the model evaluation step.

Model performance can first be evaluated qualitatively by visually comparing observed and simulated values of a given variable on a graph. Several types of graphs can be considered, expressing for example:

- the temporal evolution of the variable of interest for different time steps and over a given temporal window,
- the spatial structure of the variable of interest at a given time if the model is spatialized or semi-spatialized and if the corresponding observations are available,
- the statistical distribution of the variable of interest (e.g., statistical distribution of the daily discharges or maximum flood discharges at an hourly time step).

Model performance can also be evaluated quantitatively using a given numerical performance criterion that is a mathematical function of the error obtained. It is generally based on a metric that can be used to estimate, for any hydrological variable of interest, the norm of the error vector $\boldsymbol{\varepsilon_Z}(\boldsymbol{\theta}) = \mathbf{Z}_{obs} - \mathbf{Z}_{sim}(\boldsymbol{\theta})$ (i.e., vector $[\varepsilon_Z(t_1, \boldsymbol{\theta}), \varepsilon_Z(t_2, \boldsymbol{\theta}), \dots \varepsilon_Z(t_n, \boldsymbol{\theta})]$) or, in other words, that can be used to measure the distance between the observed and simulated values of the considered variable. This function is often referred to as the objective function, criterion function, error function or likelihood function. This function F can be formally expressed as:

$$F(\mathbf{Z}_{obs}, \mathbf{Z}_{sim}(\boldsymbol{\theta})) = F(\mathbf{Z}_{obs}, G(\mathbf{X}, \boldsymbol{\theta})) \tag{3.7}$$

where $\mathbf{Z}_{obs}$ and $\mathbf{Z}_{sim}(\boldsymbol{\theta})$ are the vectors containing respectively the n observed and n simulated values of the variable $Z(t)$ for the considered simulation period T, $\boldsymbol{\theta}$ is the vector containing the p parameters of the model G and $\mathbf{X}$ is the vector containing the n values of the m model input variables.

Several of the most widely used objective functions are presented in Addendum 3.5. Other objective functions can be found in the literature (e.g., Singh, 1995). They reflect various optimization objectives that are sometimes conflicting. The most commonly encountered objectives are designed to obtain a good match between: 1) measured and simulated flow volumes over the simulation period, 2) observed and simulated discharges over time—whether for the entire simulation period or for certain selected events, 3) flood characteristics (e.g., peak discharges, rise time, flood volumes) and 4) low-flow characteristics (e.g., decay factors, available reserve).

> **Addendum 3.5 Some objective functions commonly used in hydrology**
>
> The main objective functions used to calibrate and evaluate hydrological models are described below. The corresponding mathematical expressions are indicated in Table 3.1. For all the expressions, $Q_o(i)$ and $Q_s(i)$ are respectively the observed and simulated discharges for time step i, n is the number of observations, $\bar{Q}_o$ and $\bar{Q}_s$ are the mean discharges for respectively the n observations and n simulated values, η is a fraction of the mean discharge to be defined

(e.g., $\varepsilon = \bar{Q}_o/20$), used to avoid problems related to null values and $Q_{po}(k)$ and $Q_{ps}(k)$ are respectively the observed and simulated peak flood discharges for event k. These formulations can of course be used for variables other than discharge. Sums appearing in certain expressions are weighted (e.g., higher weights for no-rain days when estimating parameters influencing the reconstruction of low flows).

Table 3.1: Mathematical expressions for a number of objective functions with discharge Q at the outlet of the considered basin as the variable of interest.

Criterion	Expression
Bias	$F = \dfrac{1}{n}\sum_{i=1}^{n}\left(Q_o(i) - Q_s(i)\right)$
Squared correlation coefficient	$F = \dfrac{\left[\sum_{i=1}^{n}\left(Q_o(i)-\bar{Q}_o\right)\left(Q_s(i)-\bar{Q}_s\right)\right]^2}{\sum_{i=1}^{n}\left(Q_o(i)-\bar{Q}_o\right)^2 \cdot \sum_{i=1}^{n}\left(Q_s(i)-\bar{Q}_s\right)^2}$
Least squares	$F = \sum_{i=1}^{n}\left(Q_o(i) - Q_s(i)\right)^2$
Nash-Sutcliffe	$F = 1 - \dfrac{\sum_{i=1}^{n}\left(Q_o(i) - Q_s(i)\right)^2}{\sum_{i=1}^{n}\left(Q_o(i) - \bar{Q}_o\right)^2}$
Nash-Sutcliffe with logarithms	$F = 1 - \dfrac{\sum_{i=1}^{n}\left(\ln\left(Q_o(i)+\eta\right) - \ln\left(Q_s(i)+\eta\right)\right)^2}{\sum_{i=1}^{n}\left(\ln\left(Q_o(i)+\eta\right) - \ln\left(\bar{Q}_o+\eta\right)\right)^2}$
Clabour-Moore	$F = \dfrac{\sum_{i=1}^{n}\left|Q_o(i) - Q_s(i)\right|}{\sum_{i=1}^{n}Q_o(i)}$
Peak flood discharges	$F = Q_{po}(k) - Q_{ps}(k)$

Bias criterion B

This criterion measures the tendency of a model to underestimate or overestimate the observed discharges. It must be minimized (the optimum value being zero). The bias criterion is often normalized by dividing it by the mean observed discharge. It then gives the relative error for the simulated and observed flow volumes at the basin outlet over the simulation period. This criterion is generally used to calibrate model parameters that condition the simulated hydrological balance in such a way that the balance is close to the one estimated on the basis of observations.

Least-squares criterion

This criterion is widely used in the field of statistics. It provides an unbiased estimate of the parameters as long as the errors are not correlated between themselves and are identically distributed according to a normal law with constant variance and a mean of zero. These

conditions are not generally satisfied in hydrology. To approach these conditions, the data should ideally first be transformed (e.g., logarithmic transformation of discharges, modeling of residuals using an autoregressive (AR) process).

Nash-Sutcliffe criterion (Nash and Sutcliffe, 1970)

This criterion expresses the fraction of the variance of the discharges explained by the hydrological model. In other words, it expresses the relative difference between the error of the tested hydrological model and the error of the reference model with respect to the mean of the discharges.

The closer the value of this criterion is to 1, the better the agreement between the simulation and observations. A negative value of this criterion indicates that it is better to use the mean observed discharge as the model rather than the model proposed with these parameters. A value of 0 indicates that the reference model and the proposed model offer the same performance.

This is one of the criteria most widely used by hydrologists. It is strictly equivalent to the least squares criterion (it therefore assumes the same conditions concerning the statistical structure of the errors). The great advantage of the Nash Sutcliffe criterion is that it is normalized. It can therefore be used to compare the performance of a model in different simulation contexts and for different drainage basins.

The disadvantage of this criterion is that high values are heavily weighted. To increase the weight of low values, the same formulation is sometimes used on the logarithm (Table 3.1) or square root of the variable. Such formulations should be preferred in particular when focusing on low flows.

Clabour and Moore criterion (Clabour and Moore, 1970)

This criterion weights all the residuals equally. It is therefore well suited to cases requiring good simulation of both high and low discharge values.

Peak flood discharge difference

The difference between observed and simulated values of peak flood discharges can be adapted by adding an error on the rising time of the flood hydrograph. This is generally not recommended when calibrating a hydrological model (Chapter 5).

The surface defined by the values of the objective function at every point in the parameter space is referred to as the response surface of this function. For a model with two parameters, this surface is 3-dimensional. For a model with N parameters, it has $N+1$ dimensions. For a model with two parameters, the surface is often represented graphically by iso-criterion curves, i.e., curves along which the value of the criterion is the same at every point (Figure 3.13). This representation is not possible for the general case, unless N-2 values of the N parameters are fixed.

Model calibration difficulties

The search for a set of optimal model parameters for a given performance criterion involves finding the set of parameters that gives the best value of this criterion.

If the criterion is numerical, this means finding the global optimum of the response surface for the corresponding objective function. Ideally, this set of parameters is located at the center of more or less circular and concentric iso-criterion curves (Figure 3.13a). It is
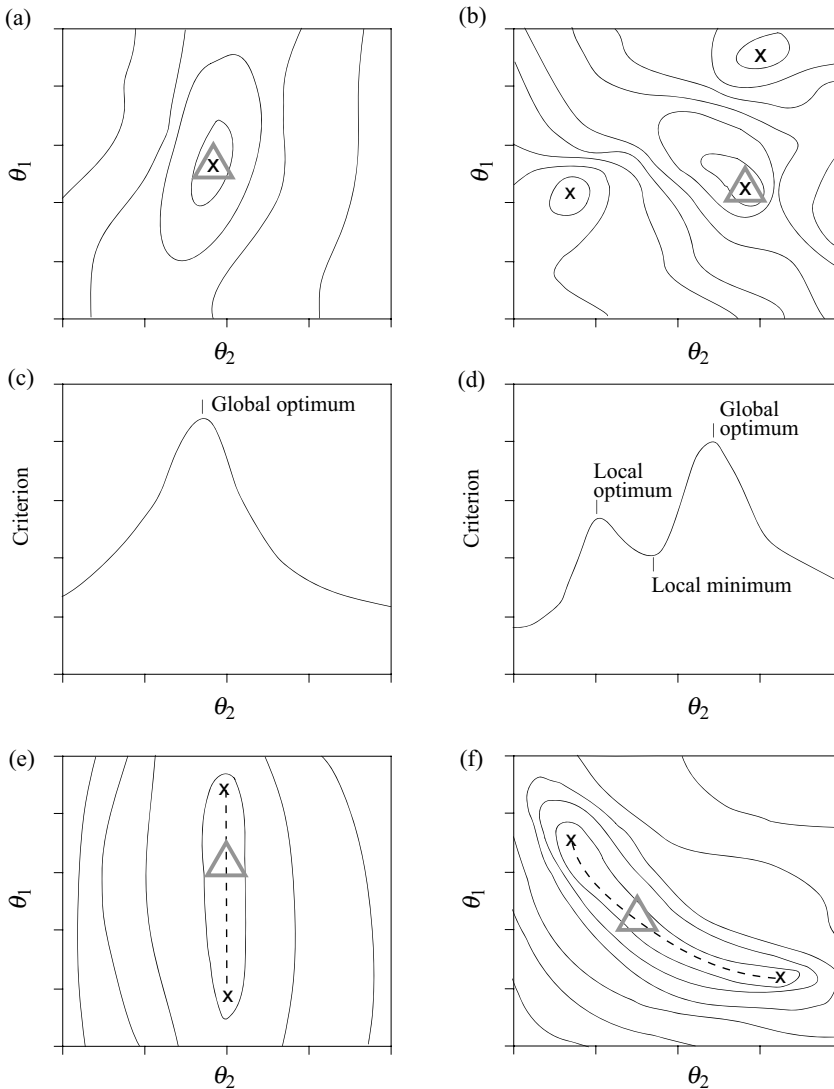
Fig. 3.13: Typical iso-criterion performance curves for two parameters θ_i and θ_j of a model. a) Curves for the ideal case where the response surface is convex. b) Case where different local optima exist. c,d) Cross-sectional views of the two response surfaces shown respectively in graphs a and b. e) Case where the selected performance criterion is insensitive to one of the two parameters (here the parameter θ_1). f) Case where the parameters are interdependent with respect to the performance criterion. The global optimum for each configuration is indicated by a triangle and any local or secondary optima by x's.

generally relatively easy to identify the corresponding point. In practice, various problems illustrated by the other response surfaces presented in Figure 3.13 can complicate this task.

- Possible existence of local optima (Figure 3.13b,d): Such optima correspond to parameter sets that provide better model performance than all their nearby neighbors, although not as good as that of the global optimum.

- Possible interdependence between certain model parameters (Figure 3.13f): When this is the case, model performance remains unchanged if the modification of one parameter can be compensated by modification of the other parameters.
- Low sensitivity of model performance to the modification of certain parameters (Figure 3.13d): If this is the case, a major change in the value of one parameter causes only weak changes in model performance.

In this context, a number of parameter sets can generally be found to give equivalent model performance for a selected performance criterion. This questions the concept of an optimal parameter set and introduces what is commonly referred to as the equifinality problem (Beven and Binley, 1992; Beven, 1996). This problem increases with the number of parameters.

3.3.3 Manual or Automatic Calibration

The model can be calibrated manually, automatically or by a combination of the two. Manual calibration consists in manually adjusting parameter values in an iterative manner. Model performance is evaluated after each adjustment. The operator stops the calibration when the performance reached is considered to be reasonable. This judgment is generally based on the combination of numerical and graphical performance criteria.

Automatic calibration methods are designed to identify the parameter set that provides the optimal value of a selected numerical performance criterion. Optimization is carried out by applying iterative and systematic changes to parameter values so as to minimize simulation errors for the corresponding objective function. Automatic calibration requires a mathematical optimization algorithm and the corresponding computer code. The optimization algorithms mainly follow two approaches referred to as local or global (Addendum 3.6). For more information on the topic, see the different publications by Duan *et al.* (2003, 2006).

Addendum 3.6 Principles and limitations of optimization algorithms

Local approaches

Local approaches have been developed for the ideal optimization case where the response surface is convex. These approaches explore the parameter space in a progressive and evolving manner starting from a prior initial parameter set. The space is explored in the direction in which it is possible to improve the value of the criterion function. It stops when it is no longer possible to produce a significant improvement.

Local optimization methods differ in particular according to the type of information used to explore the parameter space and the strategy adopted for this exploration (choice of direction and displacement length). Direct methods such as the Rosenbrock (1960), Pattern Search (Hooke and Jeeves, 1961) and Simplex (Nelder and Mead, 1965) methods are among the most widely used in hydrology. Gradient descent methods (e.g., Newton and conjugated gradient methods) proceed in the direction of the steepest slope from any point and converge faster than the direct methods. However, the objective function must be differentiable and the derivative must be continuous over the domain. Generally speaking, local methods are often limited for different reasons: 1) the parameter space generally contains several attraction zones where an algorithm can converge, 2) for each attraction zone, several local optima frequently exist and 3) the objective function and its derivative can exhibit major discontinuities over the explored domain.

Global approaches

Global optimization methods have been developed to remedy these limitations. They can be used to explore a much larger part of the parameter space and therefore in principle the optimal parameter set without stopping at any local optimum.

In deterministic global methods, the space is explored in a systematic manner on the basis of a fine discretization. The value of the objective function is calculated for each point of the discretization. Stochastic global methods explore the parameter space in a random or pseudo-random manner. This exploration can also involve a random choice of one or more starting points for the search algorithm. Some of these methods consist in modifying a population of parameter sets so as to identify the optimal set. Genetic algorithms are an example of this type of method. They use the notion of natural selection developed by Darwin to adapt the population (Holland, 1975). For an application in hydrology, see Franchini *et al*. (1998). Many other global optimization methods can be found in Duan *et al*. (2003).

Combined approaches

Optimization methods can also result from the combination of global and local methods. A good example of this is the relatively complex method proposed by Duan *et al*. (1992). This method combines the global method of the genetic algorithm type to randomly generate the starting points with a local method of the simplex type to find the associated optima.

The main limitation of global and combined methods is related to their complexity. For example, they generally include different parameters themselves that must be calibrated before the algorithm can find the optimum.

Whether manual or automatic, local or global, all these optimization methods are based on the assumption that there is a single real optimum on the response surface. However, in reality, many parameter sets offer equivalent performance. The major uncertainty related to the values assigned to model parameters has led certain hydrologists to alter their way of dealing with the estimation of model parameters. The methods proposed characterize this uncertainty and subsequently characterize the resulting uncertainty of the simulation results. This point will be discussed in more detail in Section 3.4.2.

3.3.4 Multi-criteria and Multi-objective Calibration

Advantages and principles

A model can be calibrated for a single objective and on the basis of a single criterion or on multiple objectives using multiple criteria. This choice influences the ability of the model to reproduce any or all of the hydrological variables to be simulated. For example, a Nash criterion calculated on the basis of all the discharge values obtained over a given time period leads to better results for the simulation of flood discharges to the detriment of low flows. Moreover, the Nash criterion provides no information on the ability of the model to reproduce the observed hydrological balance. On the other hand, a bias criterion can optimize the reproduction of the hydrological balance but provides no information on the ability of the model to reproduce the temporal evolution of the observed discharges.

Use of a single performance criterion therefore provides only a very partial view of model performance, even if the model is evaluated only for a single simulation objective (e.g., good reproduction of recessions). Because it does not make full use of the information contained in the data, single-criterion and single-objective calibration necessarily produce

a sub-optimal parameter set with respect to all the variables simulated by the model. For this reason, the calibration procedures should be multi-criteria and multi-objective. One or more criteria are then assigned to each of the targeted objectives (e.g., good reproduction of peak flood discharges AND could reproduction of recessions).

There are many possible objectives and criteria. However, the method only works well if they are independent. Ideally they should concern:

- different characteristics of a given model output variable (e.g., flood discharges and low flows),
- different output variables (e.g., discharge, water table height, snow cover extent and snowpack depth),
- different temporal windows and time scales (e.g., specific seasons or events, hourly, weekly and monthly time steps),
- different spatial resolutions if the spatial variability of the variable is simulated by the model (e.g., runoff volumes for the complete drainage basin and its sub-basins).

The temporal windows to be considered can for example concern periods of the year during which the dominant processes have been identified to occur. For certain drainage basins in mountainous areas, for example, spring discharges are mainly related to snow melt, summer discharges to glacier melt and autumn discharges to groundwater releases, while rainfall events throughout the year affect numerous specific temporal windows.

The time scales considered can correspond to the time scales of certain processes. For example, mean annual discharge series can be evaluated to test the ability of a model to correctly describe, on the average, meteorological forcing (e.g., basin precipitation) or reasonably simulate the processes that influence the annual hydrological balance (e.g., interception, evapotranspiration). On the other hand, mean monthly discharge series can be evaluated to focus on highly seasonal processes (e.g., snow melt, groundwater recharge or discharge). Finally, the evaluation of hourly discharge series looks mainly at infra-daily processes (e.g., melting, evapotranspiration) or those related to the generation of flood discharges (e.g., infiltration and spatial redistribution of sub-surface water).

The use of multiple objectives is of interest in so far as model parameters often strongly influence a limited number of model processes or modeled hydrological phenomena. In conceptual models, for example, the parameters of the rainfall excess module determine a major part of the hydrological balance. This is for instance generally the case for the storage capacity of reservoirs used to manage sub-surface water reserves. On the other hand, the hydrological balance is not influenced at all by the parameters of the rainfall-runoff model. These parameters however determine the shape of the flood hydrograph.

Implementation strategies and limits

Even if the advantages of multi-criteria calibration are now widely accepted its implementation leads to an optimization problem that is far more complex than for single-criterion calibration. First of all, the different criteria have objectives of varying importance with respect to the final objective of the hydrological model. Next, the different criteria do not generally lead to the same optima or to the same acceptable regions within the parameter space (Figure 3.14a). Finally, the criteria are often conflicting. Improvement of one criterion is nearly always achieved at the detriment of another (Figure 3.14b). It

is for this reason that no unique optimal parameter set exists but rather different optimal parameter sets in the sense of Pareto optimality.[4] Note however that for practical reasons, it is generally impossible to identify all Pareto optima.

The main difficulty of multi-criteria approaches is therefore to find a method that makes it possible to combine conflicting information produced by different criteria and to take into account the relative importance of the objectives targeted by each. Once again, many strategies can be followed to achieve this (Fenicia *et al.*, 2007).

One strategy consists in transforming the multi-criteria optimization problem into a single-criterion optimization problem with the sole criterion to be optimized based on a combination of individual criterion. A wide variety of rules can be devised to implement the combinations (e.g., arithmetic weighting of the different criteria, rules based on fuzzy logic). The search for the optimum value of the selected global criterion can then be carried out using classical optimization methods. This approach is relatively convenient from a practical viewpoint. It is however of limited interested in that it globalizes the optimization and does not allow differentiated improvement of the different components of the model.

Another strategy consists in carrying out the calibration in several steps. An example is illustrated schematically in Figure 3.15.

Each new step is aimed at estimating the values of the different supplementary parameters so that these values are optimal with respect to one or more selected criteria. The optimum values of the parameters calibrated in a previous step are eventually adjusted
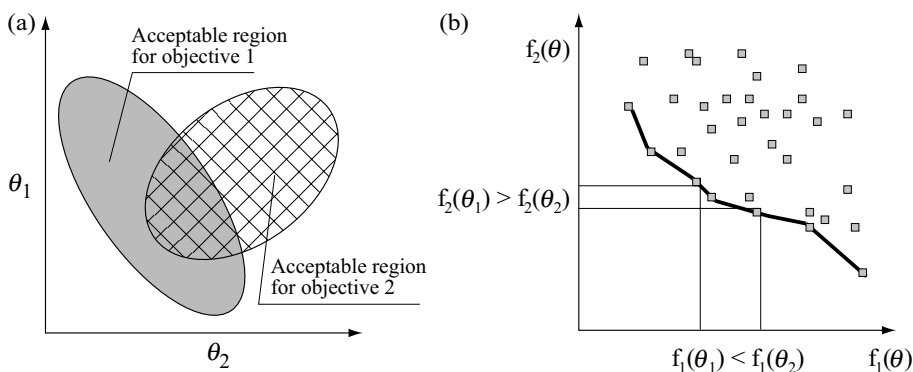
Fig. 3.14: Typical problem related to a multi-criteria optimization. a) For a two-parameter space (parameters θ_1 and θ_2), this graph shows two regions that are acceptable for a certain level of performance with respect to two distinct criteria. b) For a two-criteria space (criteria f_1 and f_2), this graph shows the set of optimal parameter sets in the sense of Pareto optimality (solid line).

---

[4]A Pareto optimum is a set of parameters for which model performance cannot be improved with respect to a given criterion without reducing performance with respect to another criterion. According to this notion, the parameter space can be divided into two sub-spaces. The first concerns parameter sets for which it is possible to improve certain criteria by modifying the value of one or more parameters without deteriorating other criteria. The second sub-space concerns parameter sets for which improvement of one or more criteria leads to deterioration of at least one other criteria. This sub-space defines the Pareto set for the problem. For concrete problems, it is not possible to obtain an approximation of the Pareto set. The difficulty lies in the fact that it is impossible to distinguish between "good" pairs and "better" pairs. One method proposed to solve this problem consists in transforming the multi-objective calibration into a series of single-objective calibrations by aggregating the various objective functions considered (Yapo *et al.,* 1998).
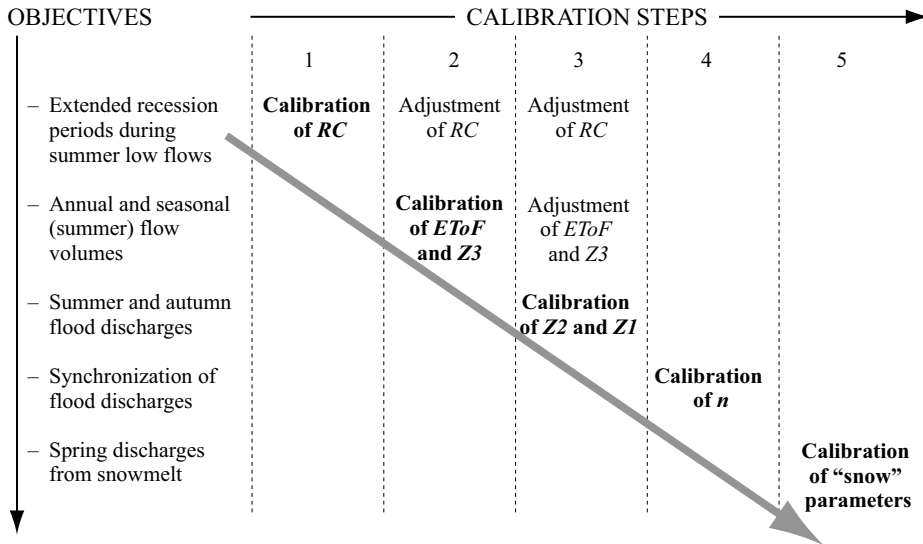
Fig. 3.15: Schematic representation of a carefully reasoned sequential and multi-objective calibration process (adapted from Turcotte *et al.*, 2003). Bold text: Main iterations used to estimate the indicated parameters on the basis of specific criteria. Normal text: Secondary iterations used to readjust the indicated parameters and satisfy the preceding criteria. *CR* is a recession coefficient. The evapotranspiration multiplication factor ET_0F and the total depth $Z3$ of the soil layer control the flow volumes. $Z2$ and $Z1$, respectively the depths of the second and first soil layers, determine the division of surface runoff as well as the redistribution of water in the ground. The Manning coefficient n governs the flow velocity of surface runoff.

so as to optimize the performance of the model for the n first steps. In this sequential approach, calibration can be manual, automatic or semi-automatic depending on the step. To be optimal, the calibration must be carefully reasoned (Turcotte *et al*., 2003; Peugeot *et al*., 2003; Hingray *et al*., 2010). For example, it is often of interest to start by calibrating the parameters that affect the processes with the longest time scales (e.g., the rainfall excess parameters affecting the hydrological balance of the basin). Furthermore, to estimate the parameter(s) targeted in a given step of the calibration process, it is first necessary to identify the hydrological quantities that are most informative. This approach therefore requires a high level of modeling expertise. It generally makes best use of some or all of the information available in the available time series.

3.3.5 Choosing a Calibration Method and other Considerations

Influence of initial conditions on calibration

The initial conditions can influence the output of the model for a certain time during simulation (Figure 3.16). The duration depends on the response time of the associated processes. For example, the influence of initial conditions related to the amount of water stored in the hydrographic network can last from several hours to several days depending on the drainage basin. The influence of initial conditions related to soil moisture, snow cover or groundwater storage can last several weeks to several months.

(a) (b)
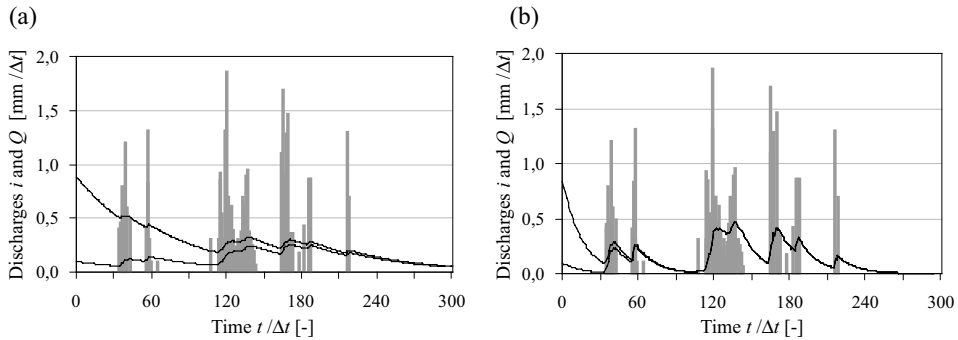
Fig. 3.16: Influence of initial conditions on the outputs of a conceptual linear reservoir (Chapter 5) for different reservoir time constants K [h]: a) $K = 60\Delta t$ and b) $K = 15\Delta t$ (graph b therefore represents a faster system response than graph a). The inflow $i(t)$ into the reservoir is described by the gray histograms (in mm/Δt) and the outflow $q(t)$ from the reservoir by the black curves (in mm/Δt). The initial conditions are defined by the value of the reservoir outflow discharge $q(t)$ at time $t = t_0$. For each value of K, the simulated system response is given for two initial conditions: $q_0 = 0.1$ mm/Δt and $q_0 = 0.9$ mm/Δt.

For the calibration of event-based models, the initial conditions are commonly considered as additional parameters to be calibrated. On the other hand, for continuous simulation models, if the simulation period is long enough, the influence of the initial conditions on the simulation results becomes negligible after a certain time. The results of a continuous simulation are therefore always evaluated without taking into account the results obtained for the first time steps of the simulation. The excluded period, which may last from a few days to a few months, depending on the context, is referred to as the initialization or warm-up period.

Whatever the simulation context, it is always important to carefully estimate the initial conditions of a model. Field observations can sometimes be used for this. If the hydrological behavior of the drainage basin is very seasonal, another possibility is to use the mean values of the state variables estimated by simulation over a number of years (e.g., 10 years) or for the first month of the simulation. Note that system initialization is easier if the start of the simulation period is chosen within the period of the year in which storage volumes in the different compartments of the basin are known or assumed to be known (e.g., snow cover is for instance inexistent at the end of the snowmelt period).

Predicting calibration parameters

Most conceptual models have 5 to 15 parameters. Physically-based models often have several dozen parameters. A pertinent manual or automatic calibration is therefore generally not possible. In this case, a good approach is to predict as many parameters as possible on the basis of observations, measurements, thematic maps, regional models (Chapter 11) or the expertise of the modeler. The remaining parameters can then be obtained by calibration (Fortin *et al*., 1995; Szilagyi and Parlange, 1999). The values of predicted parameters can if necessary be adjusted during this calibration phase.

In all cases, it is important to start calibration with reasonable prior estimates of the different model parameters (Fortin *et al*., 1995; Szilagyi and Parlange, 1999). This often makes it possible to take full advantage of the expertise acquired during past hydrological studies and to obtain a final parameter set that is consistent with the optimal configurations

of parameters used for these studies. The need for such consistency is in particular essential for model parameter regionalization work that may be undertaken in a later phase (Chapter 11).

Calibrating a spatialized or semi-spatialized model

Hydrological model calibration complexity increases with the number of elements selected for discretization of the drainage basin. Even if the structure of the model is the same for all the elements of this discretization, it is generally necessary to estimate the values of each of the parameters differently for each of these elements.

If this estimation involves calibration, it rapidly becomes a tedious operation. To simplify the procedure, the default method often used consists in assigning a unique value to one or another of the parameters for all the sub-basins. A better strategy consists in using an assumed relationship between the parameter and various known characteristics of the sub-basins. For example, as a first approximation, it is reasonable to consider that the rainfall-runoff model parameter expressing the basin response time with respect to surface runoff increases with the size of the basin and decreases with the slope. This relationship can for example be formalized by a regional shape model:

$$\theta\,(X_1,\,X_2) = \theta_0 \cdot X_1^a \cdot X_2^b \tag{3.8}$$

where θ is the rainfall-runoff parameter to be estimated and X_1 and X_2 are respectively the size and mean slope of the basin. Estimating parameter θ for the different sub-basins of the model then consists simply in calibrating the parameters of the regional model, i.e., calibrating the scaling parameter θ_0 and the two exponents a and b of the scaling relationship in the present case.

This approach is particularly advantageous if the number of sub-basins is high and if a pertinent relationship of this type is expected to exist. First of all, it reduces the number of parameters to be estimated (here the three parameters θ_0, a and b instead of the n parameters θ_i corresponding to the n sub-basins). It subsequently ensures regional consistency in the spatial variation of the parameter.

Numerical or visual evaluation of performance

Objective functions measure modeling performance in a global, objective and reproducible manner. They are generally appreciated for these reasons. However they have a number of drawbacks. For example, given their global character, it is impossible to identify the reason for the good or poor performance of the model. A model that simulates flood discharges well but low flows poorly can produce the same performance value as a model offering average performance for both flood discharges and low flows. Moreover, numerical criteria are often used to estimate the ability of a model to reproduce discharges over long time periods (typically daily discharges observed over one or two decades). This practice is far from optimal. It only assesses the ability of the model to reproduce the average behavior of the basin. It provides no information on its ability to produce exceptional events. Note that the reason for developing a model is often related precisely to such events. Furthermore, it is often these events that, by revealing flaws in the modeling concept, offer the possibility of improving it.

Evaluation of model performance on the basis of objective functions must therefore always be accompanied by a graphical evaluation. In particular, it is essential to use graphs

to evaluate the ability of a model to reproduce the considered variables over time, in particular for selected events. This technique can detect certain anomalies that are difficult or even impossible to detect with numerical criteria. It can however be extremely tedious for long simulations. For this reason, graphical evaluation is often limited to certain specific or representative events.

Choosing the right level of calibration automation

Manual calibration is intrinsically subjective. The result of this type of approach therefore depends entirely on the expertise of the modeler. The modeler must therefore understand the hydrological behavior of the basin to be modeled and the modeling concept on which the model is based. This approach takes full advantage of the results of calibrations that the modeler may have already carried out for example on other basins. Fundamentally, manual calibration is a multi-criteria method and gives very good results when the modeler has sufficient expertise. It also makes it possible to improve the modeling concept by allowing identification of certain shortcomings of the initial model (Fenicia *et al*., 2008). Manual calibration is in practice the method that is most widely used by hydrologists. It can however rapidly become difficult or tedious to implement for models with 3 to 5 parameters.

The great increase in the processing power of recent computers has led to the widespread use of automatic calibration methods. These methods allow a certain level of objectivity in the adjustment of the calibration parameters. They can easily be developed for simple cases on the basis of any of a number of existing optimization methods. They generally allow fast calibration and account for uncertainties in the values of the parameters.

The development of multi-criteria and multi-objective automatic calibration methods is however difficult. Ultimately, these methods always require the expertise of the hydrologist to assess the pertinence of the calibration. The importance of this expertise increases with the number of parameters to be specified. For cases with many parameters, automatic calibration can lead to a set of parameters that gives satisfactory results for the wrong reasons (Klemes, 1986; Grayson *et al.*, 1992).

Ideally, hydrological models should be calibrated using a semi-automatic approach combining automatic and manual optimization methods.

3.4 EVALUATING A MODEL

A model must be evaluated to ensure that it meets the objectives for which it was developed. This evaluation consists first in validating the model by testing the plausibility of its structure and the parameter sets obtained during its calibration. The next step is to analyze and, if possible, to characterize the uncertainties of the model. These different aspects of the evaluation process are discussed below.

3.4.1 Validating a Hydrological Model

Validation versus verification

Model validation is not equivalent to model verification. The objective of verification is to check that the model is "realistic", i.e., that it provides a representation that is as close

as possible to reality. Validation, on the other hand, will be considered to consist only in checking that the model provides a reasonable representation of this reality, adapted to the targeted objective.

In fact, whatever the ability of the model to reproduce the basin response for a given set of observations, it is never possible to conclude that the model is exact (or fully "realistic"). For example, it is always possible that future observations will be obtained for major hydrological events that will reveal a hydrological behavior that could not be identified on the basis of past observations and therefore could not be accounted for in the development of the model.

It is therefore impossible to verify that a model is fully realistic. It is however possible to conclude that it is not if one or more observations cannot be explained by the model. On the other hand, it is in principle possible to validate a model, i.e., to check that it is reasonable for the targeted objective. However, no universal method exists for such a validation. Validation schemes and criteria used to evaluate the validity of models vary greatly.

Validation schemes

To systematize model evaluation, hydrologists have proposed various validation schemes that have different restrictions. The schemes are principally based on one or another of the five tests presented below. The type of test or tests that are best suited depends on the modeling context. It also depends on data availability and on the stationarity of the processes over the period covered by these data. This stationarity depends in particular on the stationarity of the basin characteristics and the hydrometeorological context. The five tests are:

- the split sample test,
- the proxy basin test,
- the differential split sample test,
- the proxy basin differential split sample test,
- the blind validation test.

The ***split sample test*** (Klemes, 1986) consists in testing the model over a time period that was not used for calibration. In practice, available data are split into two datasets. For continuous simulation models, the two datasets correspond to two sub-series of the initial series. For event-based models, the two datasets come from catalogs of distinct observed events. The catalogs are constructed either by randomly sampling pertinent events or in such a way as to provide a complete range of events of varying magnitudes in each catalog. In both cases, one of the datasets is used for model calibration and the other for model validation or vice versa. The results must be similar for both datasets. The way the two datasets are split can be modified as desired. The split sample test can be applied to a drainage basin for which the duration of the available series is sufficiently long. The hydrometeorological context and characteristics of the basin must be stationary over the considered period.

The ***proxy basin test*** (Klemes, 1986) consists in testing the model on a basin providing data that has not been used for calibration. Calibration is carried out on one basin and then the parameters are transferred to the other basin for validation. The two basins must have comparable hydrological behaviors and sufficient data for model implementation and

evaluation. This test requires a stationary hydrometeorological context over the considered period. It is often used when the calibration basin does not have enough data to both calibrate and validate the model. This test is always used in hydrological regionalization studies (Chapter 11). In such a case, several basins are used to calibrate the hydrological model to be regionalized and several others to validate it.

The ***differential split sample test*** (Klemes, 1986) consists in testing the model on a time period that has a different hydrometeorological context than the corresponding calibration period. This test is carried out when the model must simulate the behavior of a basin in a disturbed or non-stationary hydrometeorological context (e.g., climate change, land-use change). For example, if the objective is to estimate the change of the hydrological regime that would result from a wetter climate in the future, the test would include: 1) identification of wet and dry periods in historical data, 2) calibration of the model using the dry period and 3) validation on the wet period. The model must show that is capable of performing well for both contexts. The characteristics of the basin must be stationary over the considered period.

The ***proxy basin differential split sample test*** (Klemes, 1986) is similar to the previous test except that the basin used for validation is different than the basin used for calibration. This test can be used when there is not enough data for the basin of interest and when the objective is to simulate the behavior of a basin under non-stationary conditions. This approach is for example used to study the impact of climate change on the hydrological regime of ungaged drainage basins.

In ***blind validation*** (Ewen and Parkin, 1996), model performance is evaluated by a third-party once the parameters have been estimated. The modeler receives the data required to describe the drainage basin and prepare the model input data, but does not receive the observation data that the model is supposed to simulate. Once the model parameters have been estimated, the model is used in simulation mode. The simulation results are then transmitted to the third-party that compares them with the observed data. The hydrometeorological context and the basin characteristics must be stationary over the considered period.

Internal and external validation

Whatever the test used, hydrologists distinguish between internal and external validation.

Internal validation is designed to test the ability of the model to reproduce the basic variables for which it was calibrated. This validation can use the same evaluation criteria as those used for calibration (Sections 3.3.2 and 3.3.4). The robustness of the model is generally quantified by the difference (usually a decrease) between the average performance obtained in the calibration and validation phases. Internal validation is the most widely used approach. The data used are traditionally measurements of the discharge at the basin outlet. There are two reasons for this: 1) discharge is the most frequently measured hydrological variable and 2) it integrates all the hydrological processes that determine the behavior of the drainage basin.

External validation is designed to test the ability of the model to reproduce the variables or hydrological behaviors that were not considered in the calibration phase. Examples include fluxes other than discharges (e.g., evapotranspiration, sediment transport), state variables of certain drainage basin compartments (e.g., water table height, soil moisture,

snow depth), hydrological variables integrated over different time steps (e.g., daily and monthly discharges) and the spatial variability of certain hydrological variables (e.g., discharges, water table height).

External validation based on the spatial organization of hydrological variables is for example possible when measurement stations exist for the same variable at different points in the drainage basin (e.g., discharges on nested sub-basins). Spatial data obtained by remote-sensing techniques can also be used in this way. They are however often limited by the fact that they do not provide a direct measurement of hydrological variables and that they often include high uncertainties (Chapter 2). Confidence in the model is increased if external validation tests are passed.

3.4.2 Uncertainties

Simulations carried out with a given hydrological model are obviously imperfect. For each model output variable that can be compared with observations, this imperfection produces errors that vary with time (Section 3.1.2). These errors are often considered as realizations of random variables. Ideally, they should be homoscedastic, independent and normally distributed with a mean of zero. Whatever the nature of the errors, they always imply that the simulated value of a given variable is uncertain.

Although not widely done, it is extremely important to characterize the uncertainties associated with hydrological model outputs. This makes it possible for example to assign a confidence interval to the simulated values or estimate the significance of performance tests (Pappenberger and Beven, 2006). The following sections deal with sources of uncertainty, possible methods to analyze the importance of uncertainties and to characterize the uncertainty on model parameters and on the associated simulations. For more information on this topic, see the work of Zin (2002).

Sources of uncertainty

There are many sources of error and uncertainty. They are mainly related to: 1) the model itself and 2) the data used to calibrate, validate and more generally use the model operationally.

Uncertainties related to the hydrological model concern its structure and its parameters. Uncertainties induced by the structure are the consequence of simplifications used in the model to represent the physical medium and processes. Whatever the approach used, a model is always a rough representation of a complex natural system. Hydrological processes can therefore be simulated only in a very imperfect manner. Uncertainties in the parameters result from the fact that the optimal parameter set depends on the calibration strategy used, the performance of the calibration algorithm and the calibration data sample. They are partly related to equifinality questions already discussed in Section 3.2.2. Note also that the ability of a model (structure + parameters) to represent the hydrological behavior of the physical medium and processes varies with time, particularly because the relative importance of the hydrological processes operating within the hydrosystem also varies with time. Consequently, the statistical properties of the errors can vary greatly with time.

Uncertainties related to model input data and variables are many and varied (Chapter 2 and 7). They are in part related to:

- measurement errors (e.g., solid precipitation) and the poor spatial representativeness of certain point measurements (e.g., physiographic characteristics of the medium, precipitation),
- data acquisition and processing errors (e.g., estimation of discharges on the basis of water levels),
- errors induced by the aggregated representation of certain variables at the spatio-temporal scales of the model (e.g., basin precipitation),
- the imperfection of models used to calculate unobservable input data (e.g., reference evapotranspiration),
- lack of knowledge of certain anthropogenic disturbances of system behavior (e.g., diversions, irrigation off-takes).

Other sources of error include those related to the initial state of the considered hydrosystem and, in the case of a drainage basin for example, the state of basin saturation and water stored at the surface (e.g., soil moisture, extent of saturated zones, extent and density of snow cover).

In general, the majority of uncertainties are often related to the estimation of these state variables and meteorological forcing variables (e.g., precipitation and temperature).

Analyzing uncertainties

For a given modeling context, the effects of all potential sources of uncertainty in the simulations should ideally be analyzed. Then, the main sources should be characterized and a method found to take them into account and combine them, propagating them if necessary, to determine the overall uncertainty of each model output.

In practice, it is often impossible to take into account all sources of uncertainty and deal with them simultaneously. Most the time, only one or another of the sources is identified and considered. Moreover, characterization of the sources of uncertainty is not necessarily obvious, often due to a lack of knowledge. Finally, propagating the sources of uncertainties to deduce the uncertainties on output variables requires an appropriate sampling and simulation strategy, often difficult to implement. Then, even when only a single source of uncertainty is concerned, uncertainty analyses are limited to a sensitivity analysis designed to estimate the influence of the source of uncertainty on the model outputs—or possibly on the estimation of model parameters.

Analyses of uncertainties related to model input data and variables often depend on such a sensitivity analysis. For precipitation, for example, a sensitivity test can be used to assess the influence of different point data spatialization schemes or the influence of the number of stations used as a basis for this spatialization (Obled *et al*., 1994; Arnaud *et al*., 2002; Vischel and Lebel, 2007). For evapotranspiration, the influence of the method used to produce the reference evapotranspiration time series may be tested (Andréassian *et al*., 2004). When carried out, characterization of the uncertainty in the output variables resulting from the uncertainty in the input variables concerns mainly precipitation. This requires an error model capable of producing different precipitation scenarios that can each be used as input to the simulation model to provide different possible realizations of the hydrological variable of interest (Kelly and Krzysztofowicz, 2000; Zin, 2002). Such a set of realizations, that can also be obtained by taking into account other sources of

uncertainty, represents what is commonly referred to as an ensemble prediction or forecast, depending on the simulation context.

Analyses of uncertainty concerning the model structure are relatively rare. They generally consist in: 1) calibrating different types of models or different versions of the given model over a given period and 2) comparing results of their simulations in another context (Butts *et al*., 2004; Schaefli, 2005). Uncertainties related to model structure are often taken into account using a multi-model approach. Different models are applied to the basin of interest and the corresponding simulation results are combined, possibly with different weights, to provide different possible realizations of the variable of interest (Butts *et al*., 2004; Schaefli, 2005). Analyses of uncertainties more often concern uncertainties associated with model parameters. These analyses can be designed to identify the most important parameters in the model, i.e., those that have the greatest influence on the simulation results. They can also be used to identify interdependencies between these parameters. In this case, they mainly involve analysis of the sensitivity of model performance to parameter variations. Performance is evaluated by a selected numerical evaluation criterion. The response surface associated with this criterion is described for a given domain within the parameter space. In a two-parameter space, this produces curves such as those presented in Figure 3.13. At each point of the considered domain, the variations of the values of this function with respect to the relative variations of the values of one of the parameters determine the sensitivity of model performance to this parameter. In other words, the sensitivity S_i, at point M, of performance criterion C with respect to parameter θ_i is defined by:

$$S_i = \frac{dC/d\theta_i}{\theta_i} \tag{3.9}$$

where the values of all the other parameters $\theta_{j,j \neq i}$ are constant. For more information on the methods associated with this type of analysis, see the work of Singh (1995) or the more general work of Saltelli *et al*. (2000).

Analyses of uncertainties related to parameters is also and in particular aimed at estimating the uncertainty of the resulting simulation. This point will be discussed below.

Characterizing simulation uncertainties related to parameters

In practice, to characterize simulation uncertainties induced by uncertainties in parameters, different parameter sets are sampled in the parameter space according to a method and selected criteria. For each, the hydrological model is then applied to simulate an estimate of the hydrological variable(s) of interest—and possibly any changes with time. The *n* estimates provided by the *n* considered parameter sets are then combined to estimate the probability distribution of each of these hydrological variables. In this way, these distributions can be used to characterize the associated uncertainties.

The difficulty in deriving the required probability distribution lies in the choice of parameter sets to be considered and/or the weights to be assigned to the results produced by each. All parameter sets do not have the same probability. Those that produce good model performance are intuitively more likely than those that produce poor performance.

Two types of approaches are used in this context. From a very schematic point of view, the first consists in uniformly sampling the "entire" possible parameter space and then assigning a weight to each of the considered parameter sets depending on its likelihood.

This is the principle of the methods proposed by Van Straten and Keesman (1991) and by Beven and Binley (1992). The second approach is referred to as Generalized Likelihood Uncertainty Estimation (GLUE). Both these methods have three important drawbacks. The first is that their results depend strongly on the choice of the likelihood function used to weight the simulations (Gelman *et al.*, 1995). The second is the excessive number of parameter sets that must be considered to obtain a sufficiently dense sample of the parameter space. The importance of this problem increases with the number of parameters. The third drawback is related to the necessity of choosing a threshold for selection of the parameter sets that lead to simulations considered satisfactory with respect to observations. This choice can only be subjective.

The other type of approach consists in identifying the probability distribution of the parameter sets using a Bayesian inference process. In this case, prior knowledge of the model and the probable values of the parameters are used to define a so-called prior probability distribution of these parameters. This prior distribution can for example be produced on the basis of values obtained for these parameters on drainage basins other than the basin of interest. The likelihood between the observations and the outputs of the hydrological model is then used to revise or update this prior distribution and produce the posterior distribution of the parameters. Bayesian updating can be formally expressed as follows:

$$f(\boldsymbol{\theta}|\mathbf{Z}) = \frac{f(\mathbf{Z}|\boldsymbol{\theta}) \cdot f(\boldsymbol{\theta})}{\int f(\mathbf{Z}|\boldsymbol{\theta}) \cdot f(\boldsymbol{\theta}) \cdot d\boldsymbol{\theta}} \tag{3.10}$$

where $f(\boldsymbol{\theta}|\mathbf{Z})$ is the posterior distribution of $\boldsymbol{\theta}$ if the observations $\mathbf{Z}$ are known, i.e., it is the probability distribution that is to be determined for the parameters. $f(\mathbf{Z}|\boldsymbol{\theta})$ is the likelihood of observations $\mathbf{Z}$ if $\boldsymbol{\theta}$ is known, i.e., it is the information concerning $\boldsymbol{\theta}$ that is provided by the data. $f(\boldsymbol{\theta})$ is the priori probability distribution of $\boldsymbol{\theta}$. The denominator, representing the likelihood of the data sample, is a constant. The likelihood $f(\mathbf{Z}|\boldsymbol{\theta})$ of observations $\mathbf{Z}$ knowing $\boldsymbol{\theta}$ is equivalent to the likelihood of the error model $\varepsilon_Z(\boldsymbol{\theta}) = \mathbf{Z}\text{-}G(\mathbf{X}, \boldsymbol{\theta})$ knowing $\boldsymbol{\theta}$. The latter can be determined by considering that the errors are realizations of a random variable that can only be described by a stochastic model. Given the structure of equation 3.10, the effect of updating the prior distribution clearly depends on the pertinence of the information available in the observations. If there are very few observations, for example, the posterior distribution will be greatly influenced by the prior distribution and little influenced by the data itself and vice versa if many observations are available.

This posterior distribution of $\boldsymbol{\theta}$ knowing observations $\mathbf{Z}$ does not have an analytical expression for the general case. The value of $f(\boldsymbol{\theta}|\mathbf{Z})$ for a given parameter set $\boldsymbol{\theta}$ is a function of the error values $\varepsilon_Z(\boldsymbol{\theta})$ and the stochastic model chosen to describe them. Different algorithm schemes can however be used to reconstruct this distribution $f(\boldsymbol{\theta}|\mathbf{Z})$, including Metropolis (Metropolis *et al.*, 1953) and Metropolis-Hastings (Hastings, 1970) type algorithms. These algorithms can be used to sample the parameter space in such a way that the final sampling density corresponds at every point in space to the posterior probability density of the parameters (Addendum 3.7). These Bayesian inference methods are increasingly used in the hydrology community for a wide range of applications (Overney, 1997; Kuczera and Parent, 1998; Talamba, 2004; Schaefli *et al.*, 2007). Among other advantages, they correctly represent distributions that are bimodal or strongly conditioned

by the interdependence of certain parameters. They are also relatively easy to implement. They still however require careful reasoning on the part of the hydrologist concerning the parameter estimation procedure. The identification of informative and pertinent prior distributions is in particular a crucial step for this estimation.

Addendum 3.7 Principles of Metropolis type algorithms

Metropolis algorithm schemes combine Monte-Carlo and Markov chain simulations to sample the parameter space from a posterior distribution of $\boldsymbol{\theta}$, knowing observations $\mathbf{Z}$. At the nth step of the Markov chain, n parameter sets $\boldsymbol{\theta}_0, \boldsymbol{\theta}_1, \boldsymbol{\theta}_2, \ldots \boldsymbol{\theta}_n$ are available. To select parameter set $\boldsymbol{\theta}_{n+1}$, the algorithm proceeds via the following steps:

1. A parameter set candidate $\boldsymbol{\theta}^c$ is drawn randomly from a multivariate and symmetrical probability distribution $J(\boldsymbol{\theta}^c | \boldsymbol{\theta}_n)$ depending on the values of the two parameter sets $\boldsymbol{\theta}_n$ and $\boldsymbol{\theta}^c$.
2. Parameter set candidate $\boldsymbol{\theta}^c$ is selected as the parameter set for step $n+1$ on the basis of its acceptance probability defined by the probability of transition from $\boldsymbol{\theta}_n$ to $\boldsymbol{\theta}^c$:

$$p(\boldsymbol{\theta}^c | \mathbf{Z}) = \min\left(\frac{f(\boldsymbol{\theta}^c | \mathbf{Z})}{f(\boldsymbol{\theta}_n | \mathbf{Z})}, 1 \right) \tag{3.11}$$

where $f(\boldsymbol{\theta}^c | \mathbf{Z})$ and $f(\boldsymbol{\theta}_n | \mathbf{Z})$ are the posterior distributions of respectively $\boldsymbol{\theta}^c$ and $\boldsymbol{\theta}_n$, knowing observations $\mathbf{Z}$.
3. To determine if $\boldsymbol{\theta}^c$ is accepted or refused, a random number u is drawn from a uniform distribution over the interval [0,1] and compared to the above transition probability as follows:

if $\;p(\boldsymbol{\theta}^c | \mathbf{Z}) > u\;$ then $\boldsymbol{\theta}_{n+1} = \boldsymbol{\theta}^c$ $\tag{3.12}$

if not, remain at current position, i.e., $\boldsymbol{\theta}_{n+1} = \boldsymbol{\theta}_n$ $\tag{3.13}$
4. n is incremented and the procedure is repeated from step 1 as long as $n<N$.

The result of the algorithm is a sequence of parameter sets $\boldsymbol{\theta}_0, \boldsymbol{\theta}_1, \boldsymbol{\theta}_2, \ldots \boldsymbol{\theta}_N$ for which the probability distribution corresponds, if the chain is sufficiently long, to the posterior distribution of $\boldsymbol{\theta}$, knowing observations $\mathbf{Z}$. Given that the result is relatively sensitive to the parameter set $\boldsymbol{\theta}_0$ used to initialize the chain, the algorithm should generally be applied several times using different initial parameter sets $\boldsymbol{\theta}_0$. Moreover, the first part of the chain generated by the Metropolis algorithm should not be taken into account for the inference.

The distribution $J(\boldsymbol{\theta}^c | \boldsymbol{\theta}_n)$, referred to as the transition function, is defined as being symmetrical when $J(\boldsymbol{\theta}^c | \boldsymbol{\theta}_n) = J(\boldsymbol{\theta}_n | \boldsymbol{\theta}^c)$. A multivariate normal distribution $N(\boldsymbol{\theta}_n, \Sigma)$ is generally used as the transition function, where Σ is the covariance matrix of $\boldsymbol{\theta}$, updated during the process if necessary to take into account intermediate results of the chain. An asymmetrical distribution is sometimes used for the transition function, in which case the Metropolis-Hastings criterion must be used to calculate the acceptance probability of the new parameter set (Hastings, 1970).

The acceptance/refusal phase is the key step in the Metropolis algorithm. The algorithm will always move towards a parameter set providing better performance than the parameter set $\boldsymbol{\theta}_n$. However there is also a non-zero probability (probability $p(\boldsymbol{\theta}^c | \mathbf{Z})$) of moving towards a parameter set providing poorer performance. This makes it possible to explore in a dense manner the high-probability regions of the parameter space and also the regions of lower probability. This algorithm also avoids the problem of local optimum zones.

For further information on this algorithm and on precautions to be taken when implementing it, see for example Kuczera and Parent (1998) or Gaume (2007).

3.5 USING A MODEL

Once a hydrological model has been developed, calibrated and successfully validated, it is ready to be used. The way it is used obviously depends on the objectives of the study for which it was developed (Section 3.1.1). In all cases, using the model implies taking into account a number of constraints that will now be discussed.

3.5.1 Initial Conditions and Boundary Conditions

First of all, the initial conditions and boundary conditions of the simulation must be specified.

The way to specify initial conditions depends on the type of application. For example, if the model is to be used to simulate a design flood resulting from a given design meteorological event, the initial conditions are generally defined in such a way that they correspond to the average initial state of the drainage basin during a typical hydrological year (Chapter 9). If the model is to be used to forecast flood discharges over the coming hours, initial conditions are estimated in such a way that they correspond to the initial state of the drainage basin when the forecast is made (Chapter 10). However, if the model is used to simulate the system response over a long time period, estimation of the initial conditions is less critical given that they influence only the initial time steps of the simulation (Section 3.3.5). For subsequent analysis of the simulation results, the corresponding initialization period, of specified duration, must however be removed from the total simulation period. Whatever the case, initial conditions must be determined with careful reasoning.

The way to specify boundary conditions and input variables also depends on the simulation context. For example, meteorological forcing input can come from observed data or various scenarios constructed elsewhere (e.g., design rainfall or meteorological forecasts, see Chapter 12). In all cases, the quality of the input data is a critical factor given that it determines the quality of the model output data.

3.5.2 The Importance of Recognizing the Difficulties Inherent to Modeling

Over recent decades, note that progress in hydrology has been driven much more by computers and hydrological models than by scientific research aimed at improving the understanding of associated processes. Although hydrological modeling remains at the technological forefront, this must not lead us to forget certain weaknesses that are inherent to hydrological models. Final decisions related to the technical aspects of a given project cannot be based solely on the output of models, however sophisticated they may be. The interpretation and application of model output always requires the know-how and expertise of hydrologists and engineers.

It is important to recognize and expose the difficulties inherent to modeling. Although the performance of models presented in scientific publications and study reports is outstanding, it often concerns relatively straightforward drainage basins and events, i.e., those for which the model encounters no particular problem. The real world is often very different. Difficulties in correctly simulating observations are relatively frequent. Sooner or later, hydrologists encounter a hydrological event that the selected model cannot correctly reproduce or a drainage basin for which the behavior cannot be simulated. Note that such

failures should never be concealed, as is often the case, as this can make users overconfident with respect to simulation results. Hiding failures also prevents the modeler from having the opportunity to subsequently deal with a problem, for example by modifying the modeling concept or refining the strategy used to observe the variables required for the description of meteorological forcing or the state of the system.

Moreover, care must be taken not to extract more information from the simulations than they really contain. In particular, model outputs for which the simulation cannot be validated due to a lack of appropriate observations should be treated with caution. This is for example the case for discharge series produced at various intermediate ungauged stations of the spatialized or semi-spatialized model.

Whatever the context and target application, it is recommended ultimately to inform users of modeling imperfections. It is also important to deliver not only the output variables required for the project, but also the associated uncertainties. If all the uncertainties cannot be characterized, at least the most important must be (Section 3.4.2). Ensemble simulations are relatively easy to implement and should be more widely used to obtain rough estimates of these uncertainties.

3.5.3 Extrapolation and Spatial and Temporal Transposition

In general, a model should never be used for a hydrometeorological context that is too different from the one for which it was developed. In particular, a model should not be used to extrapolate to exceptional hydrometeorological events not considered in the calibration/validation phases. Neither should a model be used for spatial transposition (e.g., to ungaged basins) or temporal transposition (e.g., to a climate context different from that of the calibration period). If a model is nevertheless used in one of these contexts, different tests must be carried out to determine to what degree the results are pertinent (Section 3.4.1). In practice, such tests are unfortunately seldom carried out.

Note that all past and present hydrological studies (e.g., frequency analysis, modeling) are based on the assumption that the hydrological operation of drainage basins is stationary (Milly *et al.*, 2008; Meylan *et al.,* 2012). This assumption is however far from reasonable for many applications. This is obviously the case for studies aimed at assessing the hydrological impact of climate change (Addendum 3.8). Is also the case for most studies concerning recent decades. The behavior of drainage basins has often been modified continuously over the years by various development projects (e.g., urbanization, hydraulic works) or by the management of natural resources and land use (e.g., agriculture, forestry). In the absence of anthropogenic influence, the behavior of drainage basins can also be modified by changes in meteorological conditions or the natural evolution of the physical environment (Renard, 2006). Modification of the behavior of the drainage basin can in fact be accompanied by a modification in the main processes that cannot be represented correctly by the hydrological model used. It is therefore always necessary to keep this supplementary source of difficulty in mind, in particular because modifications of the behavior of the basin are not necessarily visible to hydrologists.

Addendum 3.8 Hydrological modeling and climate change

One of the key problems in hydrology today is the assessment of the hydrological impact of climate change. The current approach for this consists in producing the required hydrological scenarios by simulations based on meteorological scenarios generated for the considered climate change scenario (Chapter 12). The simulation is carried out using a hydrological model developed for the considered hydrosystem from observations and information available for the present climate context.

This approach supposes that a hydrological model that is valid for the present climate remains reasonably valid for a modified climate, which implies that the hydrological behavior of the hydrosystem is stationary. This assumption is obviously unreasonable if the climate changes. If the regional climate and consequently the local meteorological conditions are modified, the surface of drainage basins will also be modified (e.g., vegetal cover, temporary and permanent drainage networks). The same is true for the water stored at the surface and sub-surface (e.g., snow cover, ice surfaces, soil moisture). The hydrological processes that are preponderant today and which serve as a basis for developing hydrological models may no longer be preponderant tomorrow. The question may therefore be posed as to the pertinence of using existing hydrological models to simulate a given future state.

In fact, there is no way of guaranteeing that today's models will be reasonable tomorrow. A number of analyses can however be carried out to obtain useful information in this concern. For example, it is essential to at least check that the model can reproduce the behavior of the basin for different meteorological contexts observed in the past (e.g., validation of temporal transposition between wet and dry years, see Section 3.4.1). Similarly it is important to check that the model can reproduce unusual situations sometimes observed in the present context but that could occur more frequently in the future (e.g., situations corresponding to basin saturation conditions and weather types that will be more probable in the future or extreme events that are expected to become more frequent).

As mentioned above, it is likely that a presently valid modeling concept will be inappropriate for a future changed climate context. When assessing the impact of future changes, it is therefore judicious to devise and apply a different modeling concept for the targeted basin, based on experience acquired on other basins for which the present behavior could resemble the future behavior of the target basin. In this approach, it is necessary to define pertinent similarity criteria to identify, among basins observed today, those that can reasonably be thought to resemble the target basin tomorrow. The search for analog basins simply on the basis of geographic or physiographic similarity criteria (Chapter 11) is obviously insufficient here.

In all cases, producing hydrological scenarios for a given basin in the future climate context requires a description of what the basin could resemble tomorrow. Some expected modifications to the system can be estimated by simulations with an external model (e.g., glacier retreat model, Gerbaux *et al*., 2005; Schaefli, 2005; vegetal cover model, D'Almeida *et al*., 2006; Ishidaira *et al*., 2008) or on the basis of scenarios produced by an expert. These scenarios can also concern development projects carried out within the basin (e.g., urbanization, construction of hydroelectric projects, extension of irrigation parameters) or future resource management modes (e.g., adopted to a modified future demand). The production of these scenarios represents one of the most critical and uncertain aspects of such impact analyses.

3.6 CHOOSING A HYDROLOGICAL MODEL

The great diversity of existing hydrological models makes choosing a model a difficult task. As pointed out throughout this chapter, this choice first of all depends on the objective

of the hydrological study. Obviously, it must also be based on the ability of the chosen model to satisfy robustness, parsimony and validity criteria. Given two models offering equivalent robustness and validity, preference should in principle be given to the most parsimonious model (which does not necessarily mean a simplistic model).

Other criteria can of course also be taken into consideration. For instance, a model can be required to explicitly take into account the spatial variability of meteorological conditions or certain hydrological processes. It can also be required to be applied to a different meteorological context than the one for which it was developed. In certain contexts, it may be necessary to easily transpose the model spatially, for instance to basins without data.

Other aspects to be considered include data availability, the type of drainage basin analyzed, the adequacy of the model with respect to the main hydrological processes that explain its hydrological behavior and the required nature and quality of results.

Other less scientific criteria may also affect the choice of a model, for example the experience of the modeler, the fact that the model has been used successfully elsewhere and the available time and budget. The final choice often results from a compromise between these different criteria. In practice, the decision is often highly subjective, depending for instance on criteria imposed by the user. Whatever the criteria, it must be possible to justify the choice for each analysis carried out. Several aspects related to this requirement will now be discussed.

3.6.1 Data Availability, Model Complexity and Performance

As already mentioned in Section 3.2.4, the choice (or construction) of a model must be based on a balance between the degree of complexity required in the model structure (which depends on the objectives of the study) and the degree of complexity that is compatible with available data.

In other words, a model that is too simple to use all the information that can be derived from available data is sub-optimal. On the other hand, it is of no use to choose a model with an internal structure that is too complex to be verified on the basis of the available data. This principle is illustrated in Figure 3.17.

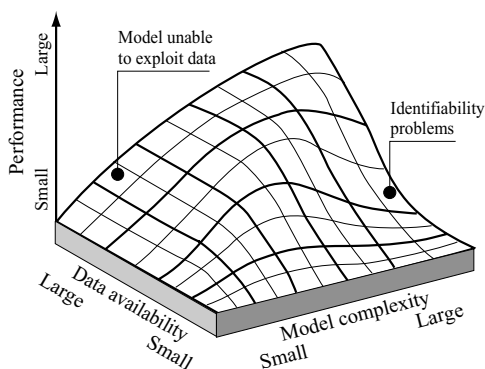**Fig. 3.17:** Schematic representation of the relationship between data availability, model complexity and performance (adapted from Grayson and Bloschl, 2000). For a fixed level of data, the performance of a hydrological model is optimal for a certain degree of complexity. For a given model, an increase in data availability increases model performance up to a certain threshold above which performance is no longer improved.

Note that most of the time, the data required for the construction of a hydrological model do not exist. In such a context, it is best to choose parsimonious models for which the parameters can be predicted using regional models (Chapter 11).

3.6.2 Model Output Requirements

The required model output variables can also greatly influence the choice of a certain type of model.

A distributed or global conceptual approach may be sufficient if only the discharges at the outlet of the given basin must be estimated. Such an approach is however inappropriate if the discharges must be estimated at different stations within the hydrographic network. Spatialized or semi-spatialized models are indispensable in such a case.

Almost all hydrological models can simulate discharges. However, many cannot simulate other hydrological variables that may be indispensable to certain hydrological studies. Examples of such secondary variables include river stage, flow velocity and water table height. Physically-based models are often the only models that can be used to estimate such variables.

3.6.3 Choosing a Type of Model

The different possible types of hydrological models are presented in Section 3.1.3. The choice of a certain type of model and then the choice of the model itself depends first of all on the objectives and available resources (data as well as computer and financial resources).

Conceptual or physically-based approaches?

The literature is rich in discussions comparing the respective virtues and shortcomings of conceptual and physically-based models (Beven, 1989, 1993; Grayson *et al*., 1992).

Conceptual models, in particular the so-called reservoir models, are widely used in operational hydrology. They offer many advantages. First of all, they are generally easier to develop and implement. They require little data and often have few parameters. For a generally moderate investment in terms of personnel and cost, they usually provide very satisfactory results for common hydrological applications.

Their main limitation is related to their representation of the processes that is often far from reality. This representation is often based solely on the law of mass conservation, neglecting the conservation of momentum and energy. Although these models can reproduce observed behavior after calibrating the parameters, nothing ensures they can reproduce behavior that has not already been observed. It is even highly probable that they will be unable to do so. Such models are therefore a priori not transposable to different hydrometeorological contexts (application to a basin configuration modified by development projects, extrapolation to unobserved events, applications to another drainage basin). For the same reasons, they cannot be used under non-stationary conditions, for example for impact studies concerning changes in land use or climate.

Physically-based models are not in principle subject to these limitations. As long as it is possible to accurately describe the physical medium, these models should be able to function "blindly" without calibrating their parameters. They are thus supposedly able to

simulate, in a realistic manner, the behavior of the considered hydrosystem for a modified hydroclimatic context. However as already mentioned, sub-grid parameterization of the elementary processes is inevitable and these models therefore generally require calibration of some of their parameters. In this respect, it would be misleading to think that it is sufficient to increase the spatial resolution of the discretization and improve the physical description of the processes to achieve an accurate representation of the hydrological operation of the drainage basin. It is in fact impossible to describe the complete structure of the physical environment and the spatial variability of the physical characteristics that govern its hydrological behavior. The difficulties encountered in defining the surface drainage network are a patent example. Over and above permanent drainage paths, how can temporary drainage channels or those that are only used, sometimes on a micro-scale, during flood periods be identified and described? Similarly, it is impossible to describe all the hydrological processes that coexist within the basin by means of physical equations. For example, the Darcy model, even generalized, is unable to represent the preferential flows that occur in various networks of conduits or macropores that can exist below the surface. It is important to remember that physically-based models are still only models and are therefore subject to the same limitations as conceptual models, even if to a lesser extent.

In practice, physically-based models are mainly used to study and understand processes taking part in the hydrological cycle. Useful for developing an understanding of these processes, they are widely used in the academic world and in scientific research (Higy, 2000). Their complexity however makes their development and use a tedious task. The considerable quantity of data required for the description of the physical medium and the estimation of their parameters represents the most severe obstacle. They also require a great deal of computing time. This stands in the way of any automatic calibration approach or any attempt to characterize the uncertainties in parameters and in the corresponding simulations.[5] Given the complexity and difficulties inherent to their calibration, these models can generally only be developed by specialists. Although seldom used in operational hydrology over past decades, this situation is rapidly changing today. Physically-based models are especially suited to studies aimed at assessing the impact of modifications of the physical environment on the behavior of drainage basins.

Global, spatialized or distributed modeling?

The choice of spatial discretization rather than global or distributed modeling depends on the way the processes are represented. Spatial discretization is for example required if the hydrological model is process-oriented. Global, distributed or semi-spatialized models are always of the conceptual type. The choice of spatial discretization is also closely related to the objectives for which the model was developed.

Global models are very widely used in operational hydrology. They offer a number of advantages. They are generally very easy to develop and implement. They require very little data and include very few parameters. Their key advantages are parsimony and robustness. Under certain conditions, they offer satisfactory results for common

---

[5]With the computer resources of their time, Yang *et al.* (2000) indicated for example that the simulation of two years of data at an hourly time step required 72 hours of calculations for the MIKE SHE physically-based model and only 2 minutes on the same machine for the TOPMODEL distributed conceptual model.

hydrological applications. They are for example used to check observed data and reconstruct missing data or to extend historical discharge series by simulations (when longer time series of meteorological variables are available). They are also used to generate flood scenarios for development projects and design studies (e.g., hydraulic works, roadway culverts), to evaluate water resources by simulating hydrological balances or to carry out real time hydrological forecasting (for management of water resources and the associated hydrological risks).

Global models have a number of drawbacks that are specific to conceptual models. In addition, because they consider the drainage basin as a single and unique hydrological entity, they cannot account for the heterogeneity of the physical medium or the spatial variability of the inputs, meteorological forcing and hydrological processes. Neither can they account for the phenomena that spatially redistribute surface and sub-surface water nor the influence of hydraulic works located within the basin on discharges. They are therefore not suitable for very large basins or basins in which meteorological forcing exhibits high spatial variability. They are also unsuitable for basins subject to a high level of anthropogenic activities or presenting high spatial heterogeneity. For instance, a global conceptual model cannot represent the behavior of a drainage basin made up of a rural part and an urbanized part. The hydrological behavior of the two parts of the basin is too different.

Distributed models present roughly the same advantages and disadvantages as global models. The only advantage of distributed models is that they can account for different types of hydrological behavior within the drainage basin (e.g., TOPMODEL, Chapter 3). They cannot however take into account the spatial variability of meteorological forcing.

Spatialized models do not have the limitations of global or distributed models. The main advantage of spatialized models is precisely that they can take into account the spatial variability of meteorological forcing, initial conditions and the characteristics of the physical medium that influence hydrological behavior. Spatialized models make it possible to simulate the hydrological variables of interest at any point within the spatial discretization of the system and in particular at any point of the hydrographic network described by the model.

The main drawback of spatialized models lies in the quantity of information required to describe the drainage basin. The spatial variability of the characteristics of the physical medium is for this reason often taken into account in a very simplified manner. In addition, meteorological forcing variables must be estimated at every point of the discretization, requiring a suitable method to spatialize the observed local variables. The inevitable uncertainties related to this spatialization can greatly reduce the interest of the spatialized description of the medium. Another difficulty lies in the discretization of the basins which remains a delicate task in spite of the use of DEMs and GISs. The implementation difficulties associated with spatialized models, in particular when physically-based, limited their use in operational applications.

Semi-spatialized models generally represent a good compromise between global (or distributed) approaches and spatialized approaches, in particular when modeling large drainage basins. They are generally easy to develop and implement. They require a large quantity of data but can partially take into account the spatial variability of meteorological forcing and state variables of the physical medium. The spatial variability of hydrological behavior can also often be taken into account. This is for example the case when model

parameters can be estimated on the basis of the key characteristics of the medium available elsewhere (e.g., average slope of the basin, percentage of impervious ground surface) and a scaling factor.

Whatever the approach considered, the spatial discretization resolution can vary with the level of detail required. In all cases, the basin is often divided up in such a way that all the different spatial units have roughly the same area. This ensures a certain consistency in the representation in the same way as it is necessary to ensure a certain compatibility between the levels of complexity used to represent the physical medium and processes. The choice of the average size of the units depends on the modeling objective and, as already mentioned, the information available to characterize the variability of the medium and the processes. Ideally, the choice should be made in such a way as to limit, within each unit, the spatial variability of the key meteorological variables, the characteristics of the medium and the dominant processes. This aspect was already discussed in Section 3.2.4.

Event-based or continuous simulation models?

The choice between an event-based or a continuous simulation model depends largely on the modeling objectives.

An event-based model is generally sufficient to simulate discharges resulting from a given meteorological event. This is for example the case when determining a design flood on the basis of a given design rainfall (Chapter 9). In such situations, the various other related hydrological processes (e.g., evapotranspiration) can generally be neglected.

Continuous simulation models can be used to simulate the evolution of state variables (e.g., soil moisture) and output variables (e.g., discharge) over several hydrological years. It is therefore possible to simulate flood discharges, low flows and hydrological regimes as well as frequencies of failure related to the operation of existing or future hydraulic structures and projects. This is the main advantage of this type of model. The main difference with respect to event-based models is that certain processes that can be neglected during an event cannot be neglected in a continuous simulation because they become predominant between events. This is for example the case for evaporative fluxes that can be neglected in simulations of given rainfall-runoff events but which are preponderant during dry periods that separate rainfall events. Consequently, continuous simulation models require more data to describe the climatic forcing that determines the basin response (e.g., temperature, radiation and wind speed in addition to precipitation). Give their numerous advantages over event-based models, the use of continuous simulation models is growing rapidly (Boughton and Droop, 2003).

3.6.4 Comparing the Performance of Hydrological Models

The choice of a hydrological model is generally guided by its performance with respect to a given objective. Many studies have been carried out to evaluate the performance of individual models. However, relatively little work has focused on comparing objectively the performance of different types of models for a given application.

Intercomparison projects mostly concerning a limited number of models applied to a limited number of basins for a given time step, climate context and type of application (simulation, forecasting, transposition; see Refsgaard and Knudsen, 1996; Jiang *et al.*, 2007). Larger scale intercomparison projects have also seen the day. One example concerns

the intercomparison projects initiated by the World Meteorological Organization (WMO) focusing on the ability of different reservoir-type global models to simulate observed discharges (WMO, 1986) or forecast discharges in real-time (WMO, 1992). More recently, Perrin (2000, 2002) compared the simulation performance of a large number of reservoir-type global models. The models were evaluated over more than a thousand drainage basins located around the world. In the USA, the Distributed Model Intercomparison Project (DMIP) compared in particular the performance of different spatialized models for operational discharge forecasting and evaluated the interest of an ensemble forecast obtained by combining associated individual forecasts (Smith *et al*., 2004; Georgakakos *et al*., 2004).

These analyses show that no universal model structure exists. Furthermore, the models are often well-suited to the hydrometeorological contexts for which they were designed but show much poor performance when they are applied to other contexts.

3.6.5 Other Considerations

In practice, an important selection criterion is the cost of developing and implementing a model. Costs and time requirements related to acquiring and preparing data, constructing calibrating and validating the model and interpreting the simulation results increase greatly with the degree of sophistication of the model.

Model development for a given basin is much easier if it is possible to use an existing user-friendly modeling system. The cost of such a system, including the license and user training, can however be prohibitive and impose the development of an in-house model.

The user-friendliness of the modeling system software interface can also be an important selection criterion. The user manual for certain modeling systems is sometimes insufficient for the user to understand and easily implement the corresponding model. Furthermore, the preparation of input data files and even the reading of output files can be extremely tedious for certain modeling systems.

The existence of a user-friendly interface does not eliminate the difficulties inherent to any hydrological modeling work. These difficulties are simply masked by the interface. Care must be taken to never sacrifice the understanding of the hydrological phenomena and the various representations proposed by the selected model. In other words, it is important to use a model only if all its modules are fully understood.

3.7 KEY POINTS OF THE CHAPTER

- The development of a model requires: 1) selection and development of a structure (and associated computer code) to represent the physical medium and processes of the modeled system, 2) estimation of the model parameters and 3) validation and characterization of the associated uncertainties.
- The different approaches that can be used to represent the processes lead to empirical, conceptual or physically-based models.
- The different approaches that can be used to represent the physical medium lead to global, distributed, spatialized or semi-spatialized models. They can be distinguished in particular by the nature of the spatial unit within which the equations describing the processes are solved.

- A hydrological model is made up of different modules that are often independent. The most common modules are used to convert input data into the required format, distribute the various water fluxes at the soil-vegetation-atmosphere interface, generate discharges at the basin outlet and route streamflows along the river and through lakes and reservoirs.
- The level of complexity used for the different representations or components of a model must be well-balanced. Processes must be represented in a manner that is compatible with the spatial and temporal resolutions of the model.
- Model parameters can be predicted on the basis of measurements, field observations or thematic maps, for instance using regional models. They are generally estimated by calibration.
- A model can be calibrated manually, automatically or semi-automatically. The objective of calibration is to determine the set of parameters that minimizes the differences between simulated values and observations. Calibration must always be subject to careful reasoning.
- Performance criteria can be qualitative or quantitative and based on an objective function.
- Ideally, calibration should be multi-criteria and multi-objective. To calibrate each of the different components of a model in a differentiated and optimal manner, the calibration must consider different variables, time scales, temporal windows, etc.
- A number of parameter sets can generally be found to produce equivalent model performance, leading to an equifinality problem.
- Model validation is intended only to check that the model provides a reasonable representation of reality, adapted to the targeted objective. Validation can be of the internal and/or external type.
- Validation schemes can be based on split sample tests, proxy basin tests, differential split sample tests, proxy basin differential split sample tests or blind validation tests.
- Model validation does not indicate that the model represents the hydrosystem in a pertinent manner. This is especially true for its behavior in extreme situations that have not yet been observed.
- The main sources of uncertainty in variables simulated by a model are related to its structure, its parameters and the data used.
- Simulation uncertainties are often characterized by combining the results of simulations produced for different sets of parameters sampled in the parameter space. Bayesian algorithms such as the Metropolis algorithm are well-suited for this sampling.

3.8 APPENDICES

3.8.1 Example of a Global Conceptual Model—the GR4J Model

Developed at Cemagref[6] (France), the GR4J model (French for *Génie Rural 4 paramètres Journaliers*) is a 4-parameter daily model designed for environmental and agricultural engineering applications. It is the most recent version of the GR3J model proposed by Edijatno and Michel (1989) and subsequently improved by Nascimento (1995), Edijatno *et al*. (1999) and Perrin *et al*. (2003).

---

[6]In 2012, Cemagref became Irstea, the French institute for research in environmental and agricultural sciences and technologies.

Drainage basin description

GR4J is a global model. It can be used in semi-spatialized mode (Baudez *et al*., 1999).

Process descriptions

The model is made up of rainfall excess, rainfall-runoff and routing functions. Four parameters must be estimated.

- Rainfall excess (one parameter): Reservoir with limited storage capacity, infiltrated rainfall and actual evapotranspiration as a function of present storage and respectively total rainfall and reference evapotranspiration.
- Rainfall-runoff (one parameter): Two unit hydrographs in parallel.
- Routing (two parameters): Non-linear reservoir with limited storage capacity.

Other characteristics

- Time step: Daily for the GR4J model and also hourly, monthly and annually for other models of the GR model family.
- Data requirements: Precipitation, reference evapotranspiration and discharge series.
- Parameter estimation: In principle by calibration but possible also using regionalizations.
- Resource requirements: Low computer, human resource and time requirements.
- Applications: Many drainage basins around the world.
- Web site: http://fresno.cemagref.fr/webgr/IndexGB.htm (last visited in November 2012).

3.8.2 Example of a Distributed Conceptual Model—the HBV Model

The HBV model (Swedish for *Hydrologiska Byråns Vattenbalansavdelning,* i.e., Water Resources section of the Hydrology Bureau) was initially developed by Bergström (1973, 1976, 1992). It is the standard hydrological forecasting model used in Nordic European countries.

Drainage basin description

HBV is a distributed rainfall-runoff model in which the discretization of the basin is based on elevation and the characteristics of the vegetation cover. Version HBV-96 is a semi-spatialized version that allows division of the drainage basin into sub-basins. The description of certain processes (e.g., snow accumulation and snowmelt, evapotranspiration) has been modified.

Basic model description (HBV)

The HBV model is a 5-reservoir model with 7 to 9 parameters that must be estimated. It is made up of 4 modules.

- Snow module (3 parameters): Reservoir with accumulation and degree-day type snowmelt.
- Interception module (no parameters): Storage reservoir for forested surfaces.
- Rainfall excess module (6 parameters): 3 reservoirs in series (soil, intermediate and groundwater reservoirs; linear and non-linear reservoirs, with or without storage capacity and with or without overflow).
- Rainfall-runoff module (1 parameter): Unit hydrograph.

Other characteristics

- Time step: Daily with possibility of shorter time steps.
- Parameter estimation: 9 parameters to be optimized, possible also using regionalizations.

- Data requirements: Moderate; precipitation, reference evapotranspiration (Penman, 1948), discharge and air temperature (for the snow module) series. In forecasting mode, the model requires air temperature and precipitation forecasts.
- Applications: Many drainage basins around the world.
- Well-suited in particular to mountainous and Nordic drainage basins strongly influenced by snow.
- Resource requirements: Low computer, human resource and time requirements.
- Web site: http://www.smhi.se/sgn0106/if/hydrologi/hbv.htm (last visited in November 2012)

3.8.3 Example of a Spatialized Conceptual Model—the CEQUEAU Model

The CEQUEAU model, named after the "CEntre QUébécois des Sciences de l'EAU" was developed initially by Girard *et al*. (1972). The corresponding software is available from the "Eau, Terre, Environnement" center of the "Institut National de la Recherche Scientifique" (INRS) (Quebec, Canada).

Drainage basin description

The drainage basin is divided up into elementary areas ("whole squares") which are in turn divided up into "partial squares" (depending on the water divides).

Model description

The conceptual model has 28 distributed parameters that must be calibrated. It implements two main functions.

- Rainfall excess (27 spatialized parameters to be calibrated): Vertical balance conceptual model including 3 to 4 reservoirs. The water balance is carried out on each whole square and at each time step. The model deals with snow accumulation and snowmelt using a degree-day function for a ripe snowpack (monitoring of cold storage), evaporation and evapotranspiration, water in unsaturated zone, saturated zone and lakes.
- Rainfall-runoff (1 parameter to be calibrated): Conceptual model designed to forward the volume of water produced within each whole square from one partial square to the next until reaching the basin outlet.

Other characteristics

- Time step: 1, 2, 3, 4, 6, 8, 12 and 24 hours.
- Parameter estimation: From 11 to 28 parameters to be calibrated.
- Data requirements: Extensive; liquid/solid precipitation and air temperature (maximum and minimum) series along with discharges, daily reference evapotranspiration, physiographic (DEM) and thematic data for the drainage basin.
- GIS interface.
- Applications: Many drainage basins, in particular in Canada.
- Well-suited to drainage basins are very different sizes.
- Resource requirements: Relatively high computer, human resource and time requirements.
- http://www1.ete.inrs.ca/activites/modeles/cequeau/aindex.html/

3.8.4 Example of a Distributed Physically-based Conceptual Model: TOPMODEL

TOPMODEL (*TOPography based hydrological MODEL*) was initially developed by Beven *et al.* (1984). A number of versions exist. For English-speaking readers, a detailed description of TOPMODEL, including its background and limitations, can be found in Beven (2012). For French-speaking readers, an instructive presentation of the basic version can be found in Obled and Zin (2004).

Drainage basin description

The description is based on hydrological response units (HRUs) determined on the basis of a topo-hydrological similarity index calculated at each point of the basin from the local slope β_i and upstream drainage area a_i. Parts of the basin that have the same values of this index are assumed to have a similar hydrological behavior.

Process description

TOPMODEL is based on physical principles for certain processes but uses conceptual reservoirs to represent others. It includes 3 parameters to be calibrated for the simplest versions. The model has two components.

- Rainfall excess: Based on the concept of a variable contributing area that is determined at each time step on the basis of the value of the local saturation deficit. This deficit depends on the average saturation deficit on the basin scale and the local value of a topographic index. The vertical balance is estimated for each index class from this local deficit using conceptual reservoirs connected in series.
- Rainfall-runoff: Different conceptual or empirical methods are used depending on the version (linear reservoirs, unit hydrographs).

Other characteristics

- Time step: Daily or shorter.
- One parameter is determined by field measurements (the topographic index and its distribution) and the others by calibration (e.g., conductivity at saturation at the top of the first layer, decay parameter for hydraulic conductivity at saturation, root storage depth, evaporation and interception rate, rainfall-runoff parameters).
- Data requirements: Moderate; precipitation series along with discharges, Penman evaporation and the distribution of the topographic index for the basin (currently obtained from DEMs).
- GIS interface.
- Applications: Many drainage basins around the world.
- Well-suited in principle to drainage basins with highly pervious soils.
- Resource requirements: Relatively high computer, human resource and time requirements.

3.8.5 An Example of a Spatialized Physically-based Hydrological Model: The SHE Model

SHE (French for *Système Hydrologique Européen*) is a hydrological model that was developed back in the early 1980s (Abbott *et al.*, 1986a,b). More user-friendly and modular versions (e.g., MIKE-SHE) are commercially available from the *Danish Hydraulic Institute* (DHI).

Drainage basin description

The basin is divided into regular square grid cells. The spatial resolution is in principle chosen to match the particularities of the drainage basin however in practice it is limited by the resolution of the supporting DEM and available computer resources.

Modeled processes

SHE solves the water balance on the drainage basin entirely on the basis of physical equations and spatialized parameters. The equations used and the other characteristics of SHE include:

- Snow: Accumulation and melt using energy balance or degree-day method.
- Interception: Rutter model.
- Evapotranspiration: Penman and Penman-Monteith model.
- Infiltration and percolation: One-dimensional Richards model for vertical fluxes in unsaturated soil and two-dimensional Darcy model for groundwater flow.
- Streamflow routing: One-dimensional Barré de Saint-Venant model.

Other characteristics

- Time step: Flexible (from a minute to a day).
- Calibration: In principle no parameters to calibrate but calibration is possible.
- Data requirements: Very extensive; meteorological data, discharge series (if calibrated), DEM, thematic data for the drainage basin, measurable soil characteristics, special features of the hydrographic network (hydraulic works, lakes).
- GIS interface.
- Applications: Many drainage basins and sub-basins around the world (in particular with derived models).
- Effective for modeling complex drainage basins.
- Resource requirements: Very high computer, human resource and time requirements.
- Requires purchase of license and updates.

CHAPTER 4

RAINFALL EXCESS AND ASSOCIATED PROCESSES

To describe the hydrological response of a drainage basin to meteorological forcing, it is first necessary to understand and estimate the various water fluxes at the soil-vegetation-atmosphere interface.

In the past, the objective was generally to estimate the net rainfall alone, i.e., the precipitation contributing to direct runoff after subtracting what is commonly referred to as rainfall losses from the total rainfall.[1] The main phenomena associated with these losses are interception by vegetation, depression storage and infiltration. Net rainfall, generally estimated for subsequent determination of a design flood, has often been determined in this context by different simplified methods using a so-called rainfall-excess function.

More recently, the necessity of continuously simulating the hydrological behavior of drainage basins, in particular during flood and low-flow periods, has changed the way hydrologists deal with the rainfall-excess notion. In particular, it is now necessary to consider and estimate all the components of the water balance at the soil-vegetation-atmosphere interface, even during periods between rainfalls. This has changed, for example, the way of dealing with fluxes related to evapotranspiration from vegetal cover.

This chapter presents the concepts and models used to estimate the main water fluxes at the soil-vegetation-atmosphere interface in view of estimating the different runoff components (e.g., fast and delayed runoff). Section 4.1 presents the different components of the surface and sub-surface water balance at land parcel and drainage basin scales. Section 4.2 discusses the different approaches and methods used to estimate the fraction of precipitation intercepted by the vegetal cover and/or stored in surface depressions. Section 4.3 describes the methods used to estimate evaporation and evapotranspiration losses. Although these losses are often neglected for flood-related problems, they can greatly affect the evolution of drainage basin saturation. Section 4.4 focuses on the estimation of infiltration. In temperate climates, infiltration often accounts for the majority of losses at the flood scale and also has a preponderant effect on the evolution of antecedent soil moisture conditions. This section also discusses the methods used to estimate infiltration at the scale of a parcel of land and even more importantly how to deal with the difficult

---

[1]No general consensus exists among hydrologists as to the use of the terms "total rainfall" and "gross rainfall". In this book, the term "total rainfall" refers to the precipitation falling above the vegetation canopy and "gross rainfall" refers to the precipitation reaching the ground, i.e., "total rainfall" minus rainfall intercepted by vegetation.

problem of its spatial variability over the drainage basin. Finally, Section 4.5 provides some guidelines for choosing a suitable approach.

4.1 INTRODUCTION

4.1.1 Water Balance at the Land Parcel Scale

At the scale of a parcel of land, the water balance at the soil-vegetation-atmosphere (SVA) interface can be divided into a surface and sub-surface balance. Figure 4.1 illustrates the different water storage and flux components of these balances.
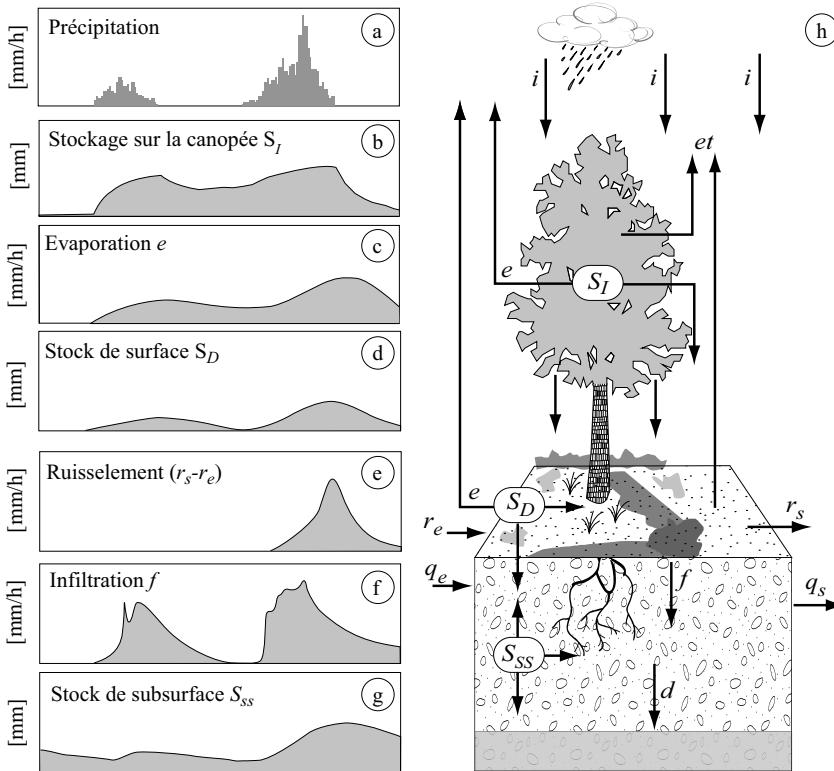
Fig. 4.1: Some of the terms of the water balance equation at the soil-vegetation-atmosphere interface versus time. a) Total rainfall. b) Water stored in the vegetal cover by interception. c) Losses from the vegetal cover by evaporation. d) Water stored in surface depressions. e) Runoff corresponding to the net rainfall (or rainfall excess) on the considered unit area. f) Infiltration. g) Water stored in the unsaturated zone. h) Schematic representation of the different components of the water balance at the scale of a parcel of land.

Surface water balance and rainfall excess

At the land parcel scale, the surface water balance at the soil-vegetation-atmosphere interface can be expressed per unit area in the following simplified manner:

$$\frac{\partial S_s}{\partial t} = i - f - E + r_{in} - r_{out} \tag{4.1}$$

where $\partial S_s/\partial t$ is the variation of the volume of water stored in solid or liquid form between the soil surface and the canopy of the vegetal cover, i the intensity of the total rainfall, f and E the intensity of infiltration and evaporation losses (from free water surfaces), r_{in} and r_{out} are respectively surface runoff inflows from upstream and outflows in the downstream direction either per unit area [l/s/m²] or in mm/h.

The volume of water stored between the soil surface and the top of the vegetation canopy can be broken down into two components as follows:

$$S_s = S_I + S_D \tag{4.2}$$

where S_I is the volume of water stored in the vegetal cover by interception and S_D the volume of water stored in surface depressions on the ground.

The relative magnitude of the different terms of the surface water balance varies with time. Figure 4.1 shows schematically an example of the possible temporal variations of some of these terms. A number of general trends can be observed.

- At the beginning of a rainfall event, the main terms of the water balance are the volumes stored in the vegetal cover and surface depressions. The intensity of these rainfall losses to storage (positive $\partial S_s/\partial t$) generally decreases as the rainfall event continues given that the storage volumes cannot exceed the maximum storage capacity of the medium. After the initial storage phase at the beginning of the rainfall, a storage release phase (negative $\partial S_s/\partial t$) follows, gradually restoring the storage capacity of the medium. The storage releases are driven by different processes that become predominant at the end of the rainfall event (e.g., evaporations, dripping, melting, infiltration or surface runoff).
- The evaporation rate E depends on the energy fluxes at the SVA interface and the rate of renewal of the air in the atmosphere (that can vary greatly during the event). The surface water balance can therefore not be dissociated from the energy balance at the SVA interface.
- The intensity of infiltration losses f depends on the infiltration capacity of the soil that generally decreases during a rainfall event as the soil becomes saturated. It can be restored between two consecutive events by the effect of drainage by gravity. The f term can be negative in the event of exfiltration.
- The difference $(r_{in}-r_{out})$ corresponds to the rainfall excess produced per unit area. In other words, it defines the intensity of the net rainfall i_n on the considered unit of area. The productivity of the parcel of land is the ratio between the intensity of the net rainfall and the intensity of the total precipitation. It increases during a given rainfall event as a result of the temporal evolution of the other terms of the water balance. The production of surface runoff is said to be Hortonian when the intensity of the supply (i.e., upstream runoff, storage releases and rainfall on the ground) is greater than the infiltration capacity of the soil. It is said to be Hewlettian when the soil is fully saturated and no more water can infiltrate.[2]

---

[2]Surface runoff produced by a Hortonian process is referred to as infiltration excess overland flow or infiltration excess runoff. Runoff produced by a Hewlettian process is referred to as saturation excess overland flow or saturation excess runoff (Hewlett, 1961; Hewlett and Hibbert, 1967). Note that this process was first described by Cappus (1960) and subsequently by Dunne and Black (1970). For this reason, French-speaking hydrologists often refer to this process as Cappusian rather than Hewlettian.

The storage and release of water at the SVA interface and the inflow of runoff from the upstream basin means that evaporation, infiltration and rainfall excess can occur on a unit area of land even in the absence of precipitation.

Infiltration and sub-surface water balance

The intensity of the water flux that infiltrates at the soil surface and then propagates in the underlying soil profile depends on the degree of saturation of the soil and more precisely on its moisture profile. The moisture profile describes the change of water content θ with soil depth. It varies with time as a result of infiltration itself and the processes that redistribute the water in the ground (horizontal and vertical redistribution by gravity and capillary forces). The variation of the soil moisture profile with time also depends on the evaporation of sub-surface water that returns to the surface by vapor diffusion or capillary action and on the evapotranspiration of water drawn from the ground by plants.

At the scale of the land parcel, the water balance of the unsaturated zone in the upper soil layers per unit area can be expressed in the following simplified manner:

$$\frac{\partial S_{ss}}{\partial t} = f - ET - d + q_{in} - q_{out} \tag{4.3}$$

where $\partial S_{ss}/\partial t$ is the change in the volume of water stored in the considered soil layer, f the intensity of infiltration of part of the surface water, ET the intensity of evapotranspiration losses (i.e., evaporation of sub-surface water and transpiration of the vegetation through the root system) and d, q_{in} and q_{out} respectively the outflows at the base of the considered soil layer and the lateral inflows and losses related to sub-surface runoff.

The change in storage $\partial S_{ss}/\partial t$ can be expressed as the change in the soil moisture profile. When the flux flowing out at the base of the soil layer is positive, it recharges the underlying water table (percolation flux d). This flux can also be negative when water flows upwards from the water table by capillary action.

During a rainfall event, the change in storage $\partial S_{ss}/\partial t$ is generally positive as a result of inflows from infiltration and sub-surface runoff coming from the upstream part of the basin. Storage periods are followed by release periods resulting from spatial redistribution processes and evapotranspiration (more details concerning these processes can be found in Musy and Soutter 1991).

Factors affecting the water balance

At the land parcel scale, the distribution between surface and sub-surface fluxes depends on different physiographic and agro-pedo-geological factors. These factors are discussed in detail in Musy and Higy (2011). The main factors are soil cover type, vegetal cover type and density, slope and the hydrodynamic characteristics of the soil.

As already mentioned, the distribution of the fluxes is also largely determined by meteorological forcing, the energy fluxes at the SVA interface and the soil humidity profiles. Furthermore, the type of precipitation (liquid and/or solid) and the presence of snow cover or frozen ground can modify the different processes affecting the distribution of these fluxes. This point will be dealt with in Chapter 7.

At the land parcel scale, runoff results from these factors. At a larger scale, the spatial heterogeneity of the characteristics of the medium and of the hydro-meteorological context influences the relative importance of the different terms of the water balance.

4.1.2 Hydrological Balance at the Drainage Basin Scale

At the scale of a drainage basin, it is preferred to refer to the hydrological balance rather than the water balance. The hydrological balance can also be divided into surface and sub-surface components. The different terms of the surface and sub-surface hydrological balances are relative to a given time interval. They correspond to the integral of the instantaneous fluxes observed at every point of the basin over time and over the area of the considered drainage basin. The corresponding volumes are expressed either in cubic meters or as an equivalent water depth in millimeters over the total area of the drainage basin.

Surface hydrological balance and rainfall excess

At the scale of a drainage basin, when there are neither inflows from or outflows to neighboring basins, the surface hydrological balance can be expressed in the following simplified manner:

$$\Delta S_S = \Delta S_D + \Delta S_I = P - F - E - V_R \tag{4.4}$$

where, for the considered time interval, S_s is the volume of water stored between the surface of the basin and the top of the vegetation canopy (including interception ΔS_I and depression storage ΔS_D), P the total precipitation falling on the considered hydrological unit above the vegetal cover, V_R the volume of direct runoff (i.e., runoff that rapidly reaches the basin outlet) and E and F the respective quantities of water loss through evaporation of free surface water and infiltration. The total precipitation P above the canopy minus interception is the gross rainfall (P_g) reaching the ground.

At the scale of a given rainfall-runoff event, ΔS_I and ΔS_D are also considered as rainfall losses. By definition, the volume of direct runoff (V_R) is equal to that of the net rainfall (P_n). For a given rainfall-runoff event, the surface hydrological balance determines the basin runoff coefficient, defined as the net rainfall divided by the total rainfall.

The runoff coefficient, in principle less than one, describes the productivity of the basin with respect to rainfall excess and therefore surface runoff. It can vary from one event to another. The average productivity of the basin depends, for a given climatic context, on its characteristics, in particular topography, land use and soil types. Runoff coefficients have been compiled for different types of media (e.g., ASCE, 1996).

Infiltration and sub-surface hydrological balance

At the drainage basin scale, the sub-surface hydrological balance can be expressed in the following manner:

$$\Delta S_{ss} = F - ET - D \tag{4.5}$$

where ΔS_{ss} is the change in sub-surface storage, F the inflow from infiltration and ET and D respectively evapotranspiration and deep percolation losses. Deep percolation supplies the underlying water table from which the later release of water produces delayed runoff and base flow at the outlet of the drainage basin.

Factors affecting rainfall excess at the drainage basin scale

The various factors that affect rainfall excess at the scale of the drainage basin are far more numerous and complex than those at the scale of a parcel of land. For more

information on this topic, the reader can refer to the Cosandey and Robinson (2000) or Musy and Higy (2011).

The difficulty in representing rainfall excess processes at the drainage basin scale is first of all related to the high variability of the physical characteristics of the medium, as already discussed. This leads to very large spatial disparities in the interception, infiltration and evapotranspiration processes.

The difficulty is also related to the importance of spatial redistribution processes of surface and sub-surface water, in particular in the horizontal direction. These processes depend greatly on the spatial organization and properties of the different soils that make up the basin from upstream to downstream. Spatial redistribution often leads to the saturation of certain parts of the drainage basin. These saturated zones are highly active in terms of surface runoff. They also take part in the processes that produce the exfiltration of water from the soil under certain sub-surface runoff conditions. However, the surface runoff that they produce does not necessarily contribute to the fast runoff observed in the hydrographic network because it can re-infiltrate before reaching the watercourse (Corradini *et al.*, 1998). It is therefore necessary to distinguish between active saturated zones that contribute to fast runoff and those that do not (Ambroise, 1999).

Re-infiltration can also affect surface runoff produced by a Hortonian process on other parts of the drainage basin. A typical spatial configuration of runoff processes is illustrated in Figure 4.2.

The relative importance of drainage basin runoff production mechanisms also varies greatly with time, whether at the scale of a rainfall event or of a hydrological year. For example, Figure 4.3 illustrates the extension of saturated zones during a rainfall event.
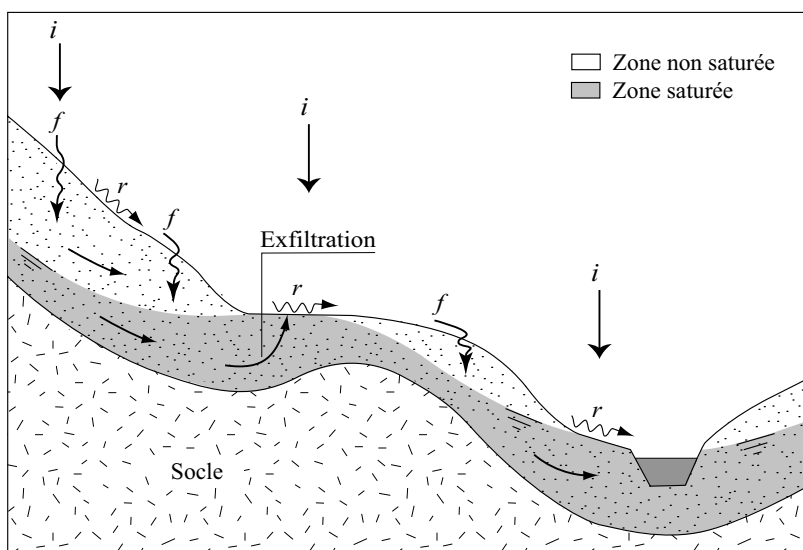
Fig. 4.2: Example of the spatial configuration of the different processes leading to the production of surface runoff in a drainage basin. At the top of the basin, runoff is produced by infiltration excess (Hortonian overland flow) followed by re-infiltration. In the middle of the basin, runoff is produced on saturated surfaces with exfiltration of sub-surface runoff followed by re-infiltration (non-contributing active saturated zones). At the bottom of the drainage basin, runoff is produced on contributing active saturated surfaces (Hewlettian processes) and accompanied by active sub-surface runoff (modified from Cosandey and Robinson, 2000).
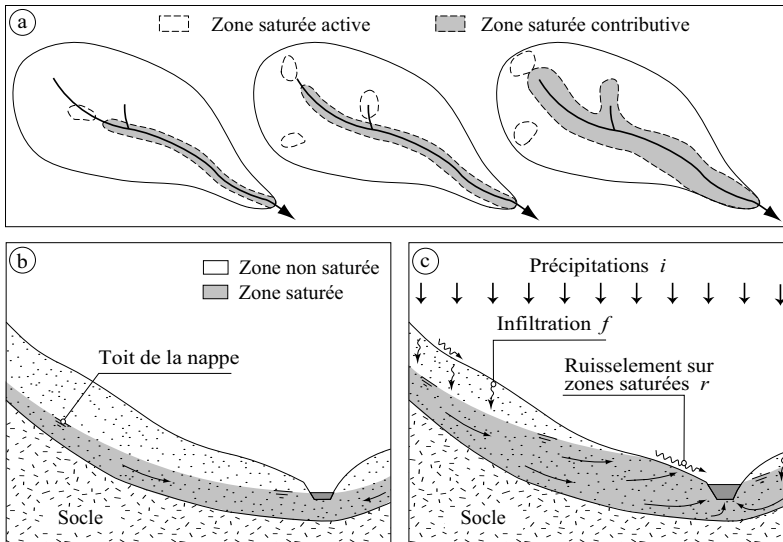
Fig. 4.3: Typical extension of contributing saturated zones during a rainfall-runoff event. a) Plan view of the drainage basin. b) and c) Cross-sectional views.

On an annual scale, the seasonal variability of runoff sources is generally even greater. For example, in temperate climates, abundant winter rainfalls often lead to partial or total saturation of drainage basins. Consequently, surface runoff and flood flows are mainly the result of precipitation on saturated surfaces. In such a context, the physical characteristics of the medium (vegetal cover, soil) have a negligible influence on the production of rainfall excess (although not on the transfer of runoff). In summer, on the other hand, the basins are far less saturated. Floods are therefore mainly generated by rainfall excess overland flow during intense storms. The runoff produced on the basin in this context is highly dependent on the physical characteristics of the medium and of the hydrographic network.

Given that the contribution of these runoff sources varies spatially and seasonally or as a function of the rainfall event sequences, they are often qualified as "variable active areas" or "variable contributing areas" when the runoff participates in the discharge at the drainage basin outlet.

4.1.3 Rainfall Excess Modeling Approaches

It may be necessary to estimate the distribution of water fluxes at the SVA interface in a number of analysis and modeling contexts. At the scale of a land parcel, for example, the water balance can be used to estimate the water demand of cultivated agricultural areas (e.g., Soutter *et al*., 2007). At the scale of a drainage basin, the different terms of the hydrological balance can be used to estimate groundwater recharge or the hydrological response of the basin to different meteorological forcing contexts. The balance at the SVA interface can also be estimated at the sub-continental scale or for all land surfaces of the Earth to define boundary conditions for meteorological or climate models.

Many hydrological approaches can be used to estimate water fluxes at the SVA interface. They depend on the scale at which the surface and sub-surface balances must be

estimated, the accepted degree of simplification, the objectives and the available data for the medium and for the meteorological forcing variables.

The purpose of this chapter is not to provide an exhaustive review of existing methods. It focuses on methods that have been developed for the simulation and in particular the continuous simulation of the hydrological behavior of a drainage basin in a given hydro-meteorological context (Sections 4.2, 4.3, 4.4). Several traditional methods used to estimate the net rainfall for subsequent estimation of a design flood are also presented (Section 4.5).

4.2 INTERCEPTION AND DEPRESSION STORAGE

Interception by the vegetal cover and storage in depressions at the surface of the basin can be described roughly by the same principles, i.e., storage and release of a fraction of the precipitation but with different and specific release processes. Whether for interception or depression storage, the different factors that affect either the storage capacity of the medium or the release processes are relatively well known. They remain however somewhat difficult to quantify and describe. The corresponding models are consequently often rudimentary and the associated parameterizations highly uncertain. Several modeling methods will now be presented.

4.2.1 Interception

Processes and definitions

Interception corresponds to the fraction of precipitation (liquid or solid) captured by the vegetal cover (or by any surface above the ground, e.g., roofs) before reaching the ground. The storage capacity of the vegetal cover is generally expressed in millimeters of water per unit of area on the ground.

Part of the precipitation intercepted by the vegetal cover enters the drainage basin by dripping from leaves (canopy dripping) or by flow along branches, stems and trunks (stemflow). The high spatial variability of the process implies that canopy dripping and stemflow can start before the maximum storage capacity of the vegetal cover has been reached. Water reaching the ground through canopy dripping or stemflow represents delayed precipitation.

Some of the precipitation intercepted is returned to the atmosphere by evaporation or sublimation. This corresponds to a loss for the basin and for surface runoff in particular.

Magnitude of the process

For individual rainfall events, interception losses due to storage and evaporation are generally very low (< 2 mm). On the other hand, on an annual basis, these losses (due in this case to evaporation alone) can represent a non-negligible component of the hydrological balance (Musy and Higy, 2011). Cosandey and Robinson (2000) pointed out the very high variability of results obtained by numerous studies aimed at estimating the percentage of precipitation intercepted, whether at the event, seasonal or annual scale. Certain forest stands can intercept from 20 to 50% of annual precipitation (e.g., Picea Abies). Natural prairies covered mainly by grass intercept no more than 20%. In urban environments,

losses to interception, often referred to as wetting losses, can be considerable. They concern surfaces above the ground such as rooftops as well as impervious surfaces such as roads and parking lots. In Nordic environments, the interception of snow by vegetation can strongly affect the distribution of water fluxes and the associated balance.

Explanatory factors

The many factors that influence the interception process have been discussed in detail by Cosandey and Robinson (2000) and Musy and Higy (2011). To sum up, the magnitude of the interception process depends partly on the characteristics of the precipitation (i.e., nature, duration, intensity, total depth and frequency) and various other meteorological variables including those that determine the evaporative capacity of the air (mainly wind speed and radiation). For the same evaporative demand, the percentage of precipitation intercepted decreases with increasing precipitation depths. For the same precipitation depths, interception losses decrease with increasing precipitation intensity.

The magnitude of the interception process also depends on the characteristics of the vegetal cover such as its type (e.g., coniferous, deciduous, herbaceous), structure (e.g., degree of ramification, inclination, density), density, growth stage and age. In principle, these characteristics make it possible to determine the different quantities required for the estimation of the interception process, for example: 1) the amount of covered area, i.e., the fraction of the horizontal ground surface masked by the vegetation, 2) the leaf area index (LAI), i.e., the surface area of leaves per unit of covered area, 3) the storage capacity and ease with which stored water can be conveyed to the ground and finally 4) the aerodynamic resistance of the vegetal cover.

The variability and diversity of the physical characteristics that affect these quantities make them difficult to estimate. Different values have been proposed in the literature to estimate the storage capacity, leaf area index and aerodynamic resistance of various types of vegetal cover. They are generally estimated by measuring fluxes on certain experimental parcels (e.g., Dunkerley, 2000) or by calibration of the simulation model to reproduce the water balance on these parcels (e.g., Holwerda *et al*., 2006). Their spatial transposition is always the source of major uncertainties. According to Crockford and Richardson (2000), it is generally difficult to determine standard values that can be used for a particular vegetal cover and climate. Estimations obtained experimentally almost always depend on the type of rainfall and other meteorological conditions during the study period.

Estimating interception losses

At the scale of a rainfall event, different empirical relationships have been proposed to estimate interception losses. The most simple express the intercepted depth as an increasing linear function of the total rainfall depth (e.g., Horton, 1940). The most sophisticated relationships generally take into account both the fact that the storage capacity of the vegetation is limited during a given rainfall event and the fact that interception losses increase with rainfall duration and evaporative demand. Total interception losses per unit area at the scale of a drainage basin are in this case estimated by summing up the amount stored in the vegetal cover between the beginning and end of the event and the amount evaporated during the event:

$$I = \Delta S_I + (1 - p) \cdot \bar{E} \cdot \Delta t$$

(4.6)

where I is the total interception loss [mm]; ΔS_I the quantity stored on the surface of vegetal cover [mm] (the volume stored in the vegetal cover divided by the area of the basin), $\overline{E}$ the average rate of evaporation from the vegetal cover during the event [mm/h] (Section 4.3.4), Δt the duration of the rainfall event [hours] and p the fraction of the rain that passes through the vegetal cover.

The fraction p is often assumed to be equal to 1-c, where c is the fraction of the basin area covered by vegetation. ΔS_I is generally estimated by the equation proposed by Merriam (1960) or an equation of similar form. This equation stipulates that the residual storage capacity of the vegetal cover at the end of the rainfall event, i.e., the difference between the maximum storage capacity of the vegetal cover S_{Imax} and the total volume stored during the rainfall event ΔS_I, is a decreasing exponential function of the total precipitation P that has fallen since the beginning of the event:

$$\Delta S_I = S_{Imax} \left(1 - \exp\left(-\frac{P}{S_{Imax}} \right) \right)$$

(4.7)

where P, ΔS_I and S_{Imax} are expressed in mm. This event-based approach has often been used (e.g., Morgan *et al*., 1998). The Merriam equation can also be used to estimate interception losses for each time step of the considered rainfall event as shown in Example 4.1.

Different empirical relationships have been proposed to express S_{Imax} from measurable vegetal cover characteristics. They often have a form similar to the following equation:

$$S_{Imax} = c \cdot f \cdot \text{LAI}$$

(4.8)

where LAI is the leaf area index and f the storage capacity per unit of leaf area (between 0.05 and 0.2). The orders of magnitude of parameters c and S_{Imax}/c (i.e., the storage capacity per unit of covered area) are indicated for different vegetal covers in Table 4.1.

The above event-based approaches often assume that the quantity of water stored by the canopy at the beginning of the rainfall event is zero. However this is not always the case. In order to estimate interception losses for all types of situations, it is necessary to use a model that is capable of continuously simulating the temporal evolution of the water volumes intercepted by the vegetal cover.

Table 4.1: Orders of magnitude of the storage capacity per unit area of vegetal cover and the vegetal cover fraction for different types of surfaces.

Type of vegetal cover	S_{Imax}/c [mm]	c [-]	Reference
Dense pine forest	0.8–1.2	0.7–1.00	Gash *et al*., 1980
Sparse pine forest	0.56–0.64	0.45–0.64	Gash *et al*., 1995; Valente *et al*., 1997
Amazonian rain forest	~ 0.8	~ 0.92	Lloyd *et al*., 1988
Eucalyptus forest	~ 0.35	~ 0.60	Valente *et al*., 1997
Prairie (0.1 to 0.5 m high grass)	~ 0.43–2.8		Merriam, 1961

Example 4.1

This example shows how to estimate possible interception losses using the formula proposed by Merriam (1960). Consider a configuration in which the fraction of rainfall

falling through the vegetal cover p is 30% and the maximum storage capacity of the vegetal cover S_{Imax} is 1.0 mm. The precipitation depths are 0.5 mm over the period [17:00, 19:00], 1.3 mm over the period [19:00, 21:00] and 0.7 mm over the period [21:00, 23:00]. The average rate of evaporation from the vegetal cover during the event $\bar{E}$ is 0.2 mm/h and the rainfall event duration Δt is 6 h.

The total precipitation depth for this rainfall event is $P = 2.5$ mm. Equations 4.6 and 4.7 give:

Water stored during the rainfall event $\Delta S_I = 0.92$ mm

Water evaporated from the vegetal cover $E = (1-p)\bar{E}\,\Delta t = 0.8$ mm

Water lost at the basin scale by interception $I = 1.7$ mm

Equation 4.7 also allows discretization of interception losses. At 19:00, 21:00 and 23:00, the total precipitation depths from the beginning of the rainfall event are respectively $P_1 = 0.5$ mm, $P_2 = 0.5+1.3 = 1.8$ mm and $P_3 = 2.5$ mm. For the fraction of precipitation falling on the vegetal cover, the amounts stored over the corresponding time steps are respectively $\Delta S_{I1} = 0.39$ mm, $\Delta S_{I2} = 0.83 - 0.39 = 0.44$ mm and $\Delta S_{I3} = 0.92 - 0.83 = 0.09$ mm.

Modeling the interception process

The modeling of the interception process is still a subject of much debate and research within the scientific community (e.g., Savenije, 2004; Keim and Skaugse, 2004). Various approaches are possible.

The first consists in continuously simulating the temporal evolution of the volumes stored in the vegetal cover and the resulting interception. This is for example the principle of the versions of the already mentioned Merriam (1960) event-based approach adapted by Rosnoblet (2002) and Kozak *et al.* (2007). It is also the approach of the model proposed by Rutter (Rutter *et al.*, 1975) and the derived Gash model (Gash and Morton, 1978).

The corresponding models are mainly conceptual and are made up of one or more reservoirs. In the simplest approach, a single reservoir is used. Its behavior is governed by a continuity equation, used to calculate the water volume stored in the vegetal cover versus time, combined with various empirical equations used to estimate losses by evaporation, canopy dripping and stemflow. The continuity equation is the following:

$$\frac{\partial S_I}{\partial t} = (1-p) \cdot i - E(S_I) - d(S_I) \tag{4.9}$$

where $\partial S_I/\partial t$ is the change in the volume of water stored in the vegetal cover [mm] and i the intensity of precipitation on the basin [mm/h]. Evaporation losses E and water drained to the ground by canopy dripping and stemflow d [mm/h] are a function of the stored volume S_I.

Reservoir models sometimes distinguish between interception by leaves, branches and stems or trunks. n reservoirs are then used to calculate the volumes stored on these media versus time. Each reservoir has a maximum storage capacity to be estimated or calibrated. In these approaches, the actual evaporation rate $E(t)$ is generally estimated as a fraction of the evaporative capacity determined for the considered wetted vegetal cover. This fraction is an increasing function of the water stored $S_I(t)$ on the considered medium at time t (Section 4.3.4). The same is often true for the canopy dripping and stemflow components. Such models remain however difficult to apply in practice given the large

number of parameters. They are often integrated in physically-based distributed models (e.g., SHE model, Abbott *et al.*, 1986a,b; DHSVM, model, Wigmosta, 2002).

A block diagram of the Rutter model, based the principles presented above, is shown in Figure 4.4. It is described in detail in Appendix 4.8.1. Figure 4.5 illustrates the different terms of the water balance obtained by applying this model to a given rainfall sequence.

To estimate the intercepted volumes in a continuous simulation, another much simpler approach is often used. It consists in comparing, at each time step, the total rainfall P above the canopy with the total evaporative capacity E_0 to be determined elsewhere for the considered vegetal cover.

- If the total rainfall P is greater than E_0, enough water is available to satisfy the evaporative capacity. Consequently, the actual evaporation is assumed to be equal to E_0 and the gross rainfall P_g is equal to the total rainfall P minus E_0.
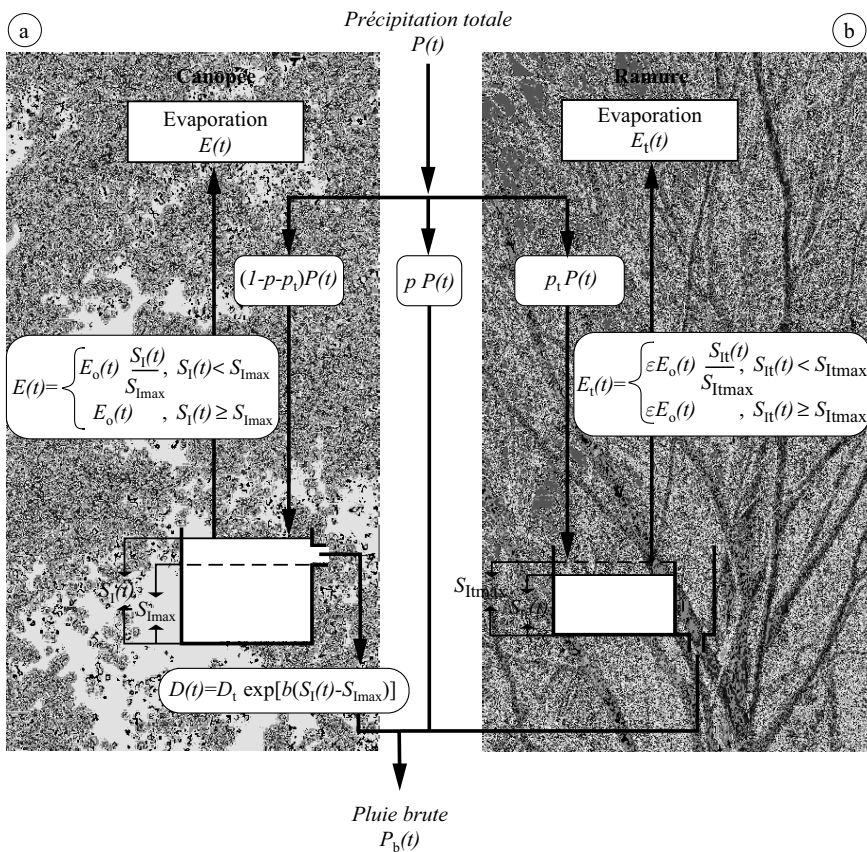
Fig. 4.4: Structure of the Rutter interception model (adapted from Gash and Morton, 1978). The model is a reservoir-based conceptual model. It distinguishes between interception processes on the leaves of the canopy and on the branches and trunks. The reservoirs used to monitor the storage volumes in each of these components each have a maximum storage capacity. The quantity of water $S_{I_*}(t)$ stored in each reservoir can evaporate at a rate $E_*(t)$ (less than or equal to the evaporative capacity $E_0(t)$ or $\varepsilon E_0(t)$, depending on the component) or be drained towards the ground (at rate $D_*(t)$ for the canopy) (see Appendix 4.8.1 for a detailed description of the variables and parameters involved).
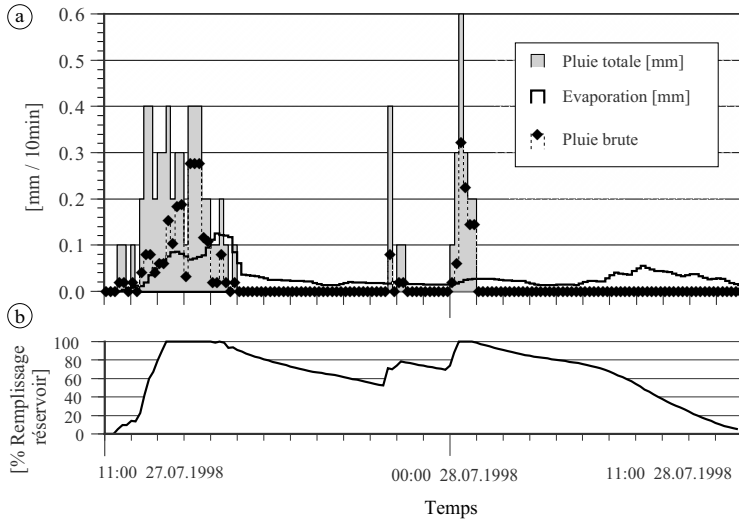
Fig. 4.5: Simulation of the interception process by the Rutter model for a fictitious vegetal cover with parameters $p = p_t = 0.2$; $S_{lmax} = 1.2$ mm; $S_{ltmax} = 0.8$ mm (see Appendix 4.8.1 for definitions of these parameters). a) Total rainfall (above the canopy), gross rainfall (on the ground) and quantity of water evaporated. b) Variations of storage in vegetal cover (in % of maximum storage capacity).

- On the other hand, if the total rainfall P is less than E_0, all the rain is assumed to be evaporated. The gross rainfall is therefore zero. In this case, there is not enough water to satisfy the evaporative capacity. The residual evaporative capacity E_b is therefore assumed to be equal to the initial evaporative capacity minus the total rainfall. The final value for the evaporation will depend on the amount of water the soil supplies through the evaporation processes. The residual evaporative capacity E_b will be fully or partially satisfied depending on the state of sub-surface reserves (Section 4.3.4).

The equations used in this approach are the following:

$$\text{if} \quad P \geq E_0 \qquad \text{then} \quad \begin{cases} P_g = P - E_0 & \text{and} \quad E_b = 0 \\ E_1 = E_0 & \text{and} \quad E_2 = f(E_b, S_{ss}) = 0 \end{cases} \tag{4.10}$$

$$\text{if} \quad P < E_0 \qquad \text{then} \quad \begin{cases} P_g = 0 & \text{and} \quad E_b = E_0 - P \\ E_1 = P & \text{and} \quad E_2 = f(E_b, S_{ss}) \geq 0 \end{cases} \tag{4.11}$$

where, at time t, E_0 is the total evaporative capacity, E_1 the evaporative flux resulting from evaporation of intercepted rainfall, E_b the residual evaporative capacity and E_2 the evaporative flux resulting from evapotranspiration, P and P_g are respectively the total rainfall and the gross rainfall and S_{ss} the state of the sub-surface water reserves. Storage in the vegetal cover is not considered in this approach. This approach has the major advantage of not requiring the estimation of parameters.

4.2 Depression Storage

Processes and definitions

Depression storage corresponds to the filling of surface relief or micro-relief[3] by a fraction of the precipitation and/or runoff coming from upstream. For pervious surfaces, depression storage takes place when the inflow to the depressions exceeds the infiltration capacity of the soil. The volume that can be stored depends on the storage capacity of each depression.

Any additional inflow to a depression leads to overflow that can feed other depressions further downstream or produce surface runoff. The high spatial variability of ground topography and micro-typography means that the emptying of certain depressions can lead to surface runoff before all the depressions are full.

Part of the water stored in depressions is returned to the atmosphere by evaporation or sublimation, which corresponds to a loss for the basin and runoff. For pervious soils, another part of depression storage infiltrates with a certain time lag.

Magnitude and explanatory factors

On an annual or inter-annual scale, documentation on the effect of depression storage on the hydrological balance is in fact scarce. Depression storage lost by evaporation is likely less than the volumes intercepted by the vegetal cover and far less than the volumes lost by infiltration. One of the main reasons for this is that depression storage is concentrated and consequently offers a much lower contact area with the atmosphere, which is necessary for water vapor exchanges. Except in certain special cases (e.g., swamps, lakes, etc.), it is therefore reasonable to consider that depression storage does not greatly affect the hydrological balance on time scales greater than that of the rainfall-runoff event.

However, at the rainfall-runoff event level, the magnitude of depression storage losses has been pointed out and studied by various authors in urban, cultivated or lake areas (e.g., Linsley *et al*., 1975; Viessman *et al*., 1977; Kidd, 1978; Mitchell and Jones, 1978; Onstad, 1984; Kamphorst *et al*., 2000). For a given rainfall event, these losses can amount to several millimeters expressed in terms of precipitation depth over the area of the type of surface considered (Table 4.2).

The main factors influencing depression losses are topography, type of surface (i.e., soil type, vegetal cover and land use), slope and the degree of saturation of the depressions at the beginning of the rainfall event.

Estimating depression storage losses

Event-based approaches to estimate depression storage losses are similar to those used to estimate interception losses. The maximum storage capacity of the medium S_{Dmax} is generally the main parameter to be estimated. For example, Linsley *et al*. (1975) propose an expression similar to that of Merriam (1960):

---

[3]Microrelief refers to roughness at the scale of 1 to 10 cm.

Table 4.2: Orders of magnitude of depression storage capacities per unit area for different types of surfaces and moderate slopes.

Type of surface		Storage [mm]	Reference
Sand		5.0	Hicks (1944)
Loam		3.8	
Clay		2.6	
Pervious		6.5	Tholin and Keifer (1960)
Impervious		1.5	
Urban basins		1.5–4.0	Viessman *et al.* (1977)
Impervious areas		0.5–2	Kidd (1978)
Flat roofs		2.5–7.5	
Yard lawns		10	
Pasture		5.0	ASCE (1992)
Forest litter		7.5	
Pervious with:	slope <3%	15	Chocat (1997)
	slope >3%	3	
Impervious with:	slope <3%	3	
	slope >3%	0.2	

$$\Delta S_D = S_{D\max}\left(1 - \exp\left(-\frac{P_g - F}{S_{D\max}}\right)\right)$$

(4.12)

where ΔS_D is the quantity of water stored in depressions since the beginning of the event, S_{Dmax} the maximum depression storage capacity of the considered medium [mm] and P_g-F the cumulative difference between gross rainfall P_g and infiltrated rainfall F since the beginning of the event [mm].

The maximum storage capacity is difficult to evaluate since it depends directly on the topography of the medium. In general, it increases with the roughness of the ground surface. It also increases as the slope of the terrain decreases. Various authors have developed empirical relationships expressing the maximum depression storage capacity (Addendum 4.1) as a function of different roughness and/or slope indices of the considered medium estimated from relatively simple field measurements. For example, Kidd (1978) proposed the following equation involving only the slope:

$$S_{DMax} = k\, J_0^{-0.5}$$

(4.13)

where S_{DMax} is the storage capacity [mm], J_o the mean slope of the terrain with values between 0.005 and 0.04 [m/m] and k [mm] a coefficient that depends on the type of surface (0.07 for an impervious surface 0.28 for pervious surface). The empirical relationship proposed by Onstad (1984) uses a roughness index:

$$S_{DMax} = a\, RR + b\, RR^2 + c\, RR\, J_0$$

(4.14)

where RR is the random roughness of the surface[4] and a, b, c are multiple regression parameters ($c > 0$).

---

[4]Random roughness is due to aggregates that are apparently randomly distributed over the surface. Many indices can be found in the literature to describe the random roughness (Kamphorst *et al.,* 2000).

The use of such semi-empirical expressions is almost always limited to event-based urban drainage models. They are mainly used to estimate the wetting losses that occur on impervious surfaces (e.g., SWMM model, Rossman, 2005). The losses are in this case often treated as a calibration parameter that can be used to adjust the runoff volumes simulated by the model. Depression storage is also treated in soil erosion models (e.g., WEPP model, Lane and Nearing, 1989; EUROSEM, Morgan *et al*., 1998; LISEM, De Roo *et al*., 1996). In hydrological studies aimed at estimating design floods, however, depression storage is most often combined with interception losses to define an overall initial runoff loss (Section 4.5.1).

Addendum 4.1 Estimation of S_{Dmax} on the basis of a DEM

A reference method used to estimate depression storage capacity S_{Dmax} is based on digital elevation models (DEMs). A DEM constructed for the considered surface is filled virtually with water by an appropriate algorithm (e.g., Planchon and Darboux, 2002). The depression storage capacity is obtained by subtracting the "empty" DEM from the "full" DEM. The quality of this estimate depends greatly on the resolution of the DEM, which may offer only a very poor representation of reality, in particular for micro-topography.

Using this method and studying a large range of agricultural situations and soils, many authors have developed empirical relationships to estimate depression storage capacity as a function of various roughness and/or terrain slope indices (e.g., Onstad, 1984; Hansen, 2000; Kamphorst *et al*., 2000).

Modeling depression storage

In continuous simulation approaches with natural media, depression storage is generally not modeled. As already mentioned, the main effect of depression storage is to delay the infiltration of part of rainfall or runoff. Furthermore, the uncertainties associated with modeling of infiltration are already very high at the drainage basin scale (Section 4.4). Consequently, it is often assumed that the modeling of depression storage will not significantly improve model performance. In addition, depression storage modeling would inevitably increase the complexity of the hydrological model, which is never recommended (Chapter 3).

However, for special cases such as those with lakes and swamps covering a large area of the drainage basin, continuous simulation of the depression storage process may be necessary. As for the interception process, the corresponding model often uses a reservoir with a limited capacity corresponding to the maximum depression storage capacity and specific functions to model the fluxes associated with infiltration and evaporation losses (e.g., CEQUEAU model, Morin *et al*., 1995).

4.3 EVAPORATION AND EVAPOTRANSPIRATION

At the drainage basin scale, various evaporation fluxes can be distinguished. They correspond to: 1) evaporation of water stored at the surface in the form of a liquid (lakes, watercourses, micro-depressions) or a solid (snow, ice), 2) evaporation of water intercepted by vegetation, 3) evaporation of water contained in the soil and 4) water losses related to the transpiration of plants. For the parts of the basin covered by vegetation, the term evapotranspiration combines the processes of evaporation of water from the soil and transpiration of water by plants.

Evaporation and evapotranspiration processes have been discussed for instance in Brustaert (2005) or Soutter *et al*. (2007). This section reviews the principles and methods most widely used to estimate these processes in the context of hydrological modeling.

4.3.1 Evaporation of Water from a Free Surface

The transformation of water from a liquid phase to a gaseous phase (water vapor) by the evaporation process requires sufficient energy to allow certain water molecules to escape from the liquid mass into the atmosphere (Figure 4.6). It also requires a mechanism (e.g., turbulent fluxes) to transport these molecules away from the immediate vicinity of the water surface to prevent them from returning back into the liquid mass by condensation.

These two conditions have led to the development of two types of methods to estimate the rate of evaporation from a free water surface.

- Methods based on the energy balance at the SVA interface, expressing the equilibrium between the balance of radiation exchanges and the balance of heat exchanges, whatever the value of energy storage variations (Addendum 4.2). Evaporation results from the latent heat flux.[5]
- The so-called mass transfer methods based on the description of vapor transfer mechanisms in the boundary layer of the atmosphere above the ground. These mechanisms are the result of a water vapor partial pressure gradient between the evaporation zone and the atmosphere (Figure 4.6). Based on the work of Dalton (Dalton, 1802a,b), the evaporation rate E can be expressed as a function of this gradient and the rate of renewal of the air mass above the water mass:

$$E = f(u) \cdot \left(e_s - e_a\right) \tag{4.15}$$

where u is the wind speed, e_a the effective or actual water vapor pressure and e_s the saturated water vapor pressure that can be expressed as a function of air temperature. The term $(e_s - e_a)$ is the air saturation deficit above the evaporation surface.
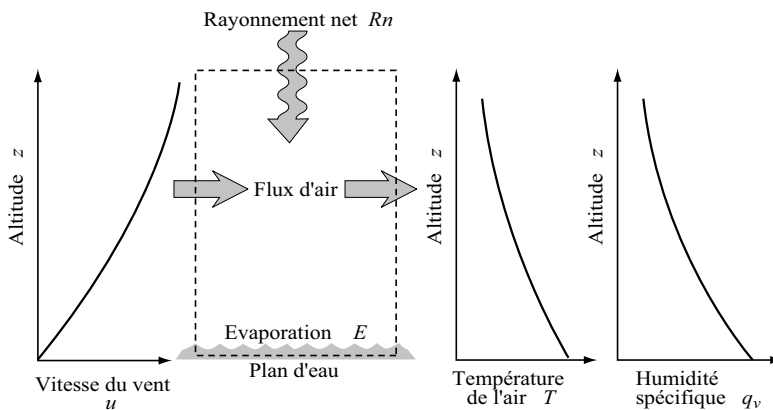

Fig. 4.6: Main mechanisms and explanatory variables determining evaporation fluxes at the SVA interface (adapted from Chow *et al*., 1988).

---

[5]The latent heat flux is the product of the water vapor mass flux resulting from evaporation and the latent heat of vaporization of water (λ = 2.3 x 106 J/kg).

Many formulations are used by hydrologists to estimate the intensity of evaporation fluxes (Xu, 2003). Most of them are based on one of the two approaches presented above. With varying degrees of simplification, they take into account some or all of the many meteorological factors (e.g., relative humidity of the air, wind speed profile, radiation flux) and physical characteristics (e.g., salinity, water depth, albedo) that affect the evaporation process. One formulation that is widely used and described in detail in a publication of the Food and Agriculture Organization (FAO, 1998), is that of Penman, which combines the energy balance and mass transfer approaches. A review of this method can be found in Appendix 4.8.2.

The other formulations are empirical, based on easily measured meteorological variables such as relative humidity and air temperature.

Evaporation fluxes related to evaporation from an open water surface are mainly estimated when the considered drainage basin includes a sufficient area of natural and/or artificial water bodies such that these fluxes modify the hydrological balance of the basin. The behavior of such water bodies can require specific modeling, in particular to estimate the variations of the surface area of the water bodies with time. Models available for this are described in Chapter 6.

Addendum 4.2 Energy balance: inputs, losses and storage

For a given closed system, the energy balance is based on the energy conservation principle. For the SVA interface, it expresses the equilibrium between the balance of radiation exchanges and the balance of heat exchanges, whatever the value of energy storage variations. For many hydrological applications, it can be written in the following form:

$$\frac{\partial W}{\partial t} = R_n + A_h - G - \lambda E - C - M \tag{4.16}$$

where $\partial W/\partial t$ is the variation of energy per unit area in the considered layer, R_n the net incident radiation, A_h the incoming energy flux by advection (expressed as a specific flux), G the heat flux penetrating into the soil, E the water vapor mass flux (evaporation), C sensible heat flux (convection) and M the part of radiation energy converted into chemical energy by plants through photosynthesis. λ is the latent heat of vaporization of water.

For most hydrological applications, the energy balance is often applied to a thin layer of soil, water or vegetal cover. The energy variation $\partial W/\partial t$ is in this case often neglected. The term A_h includes all possible energy inputs or losses related to water inputs or losses for the system. It is often negligible except possibly for the case of liquid precipitation on snow cover or solid precipitation on a free water body. Radiant energy used for photosynthesis does not exceed a few percent of the net radiation and the corresponding term is often neglected. For a more detailed description of these terms and methods to estimate them, see for example Brustaert (2005).

For snow or ice layer, the term $\partial W/\partial t$ can include the energy consumed by melting and the latent heat of vaporization λ can be replaced by the latent heat of sublimation. The corresponding energy balance equation is given in Chapter 7.

4.3.2 Evaporation from Bare Soil

Evaporation from bare soil is influenced both by the evaporative demand of the atmosphere (determined by meteorological factors) and the availability of water in the soil, in particular the capacity of the soil to transmit water to the surface (Soutter *et al*., 2007). The actual evaporation regime is determined by the smallest of these two parameters.

At the scale of a land parcel and when the water fluxes in the soil can be considered to be essentially vertical, the surface evaporation fluxes can be estimated by solving numerically the Richards partial derivative equations (Addendum 4.4). In practical hydrology, except for areas without any vegetation (e.g., certain Nordic regions), evaporation from the soil is often estimated jointly with transpiration from vegetation (see 4.3.3).

4.3.3 Evapotranspiration from Vegetal Cover

Evapotranspiration refers to water lost by transpiration from plants and by evaporation from the soil. The factors governing evapotranspiration are therefore: 1) the evaporative demand of the atmosphere, 2) the availability of water in the soil and also 3) the growth phase of the vegetal cover. With respect to bare soil or a free surface of water, the evaporative demand of the air in the presence of the vegetal cover is limited by the aerodynamic resistance of the vegetal cover to the movement of air masses. The fluxes related to transpiration by plants are also limited by the resistance of the surface of the canopy to the movement of water through stomata.

Estimation of so-called "actual" evapotranspiration from vegetation-covered surfaces is difficult, in particular when the availability of water in the soil is a limiting factor. This is a problem common to agronomists, hydrologists and meteorologists. A wide range of estimation models have therefore been developed (Dingman, 2002; ASCE, 1996; FAO, 1998; Brutsaert, 2005; Soutter *et al.*, 2007) that vary depending on their objective and the considered time and space scales.

The approach most widely used by hydrologists to estimate actual evapotranspiration (*ET*) is based on 1) the average level of saturation in the root zone and 2) the maximum evapotranspiration rate (*ETM*) commonly referred to by the hydrology community as the potential evapotranspiration (*PET*) for the considered vegetal cover.[6] This approach, along with a less widely used approach based on a complementarity principle, is described below.

Estimating ET on the basis of the water content in the root zone

In this approach, *ET* is expressed as a fraction of *PET*:

$$ET(t) = f\left(S_r(t)\right) \cdot PET(t) \tag{4.17}$$

where $S_r(t)$ is the water content of the root zone t [mm] and f an increasing function of S_r that depends in particular on soil type. In common hydrological applications, f can be a function of varying complexity (Xu, 2003; Oudin, 2006a,b). It is often expressed in the following form:

$$f = \begin{cases} 0 & S_r(t) \leq S_1 \\ \left(\dfrac{S_r(t) - S_1}{S^* - S_1}\right)^b & S_1 < S_r(t) < S^* \\ 1 & S_r(t) > S^* \end{cases} \tag{4.18}$$

---

[6]Methods for estimating ETM or *PET* are presented in Addendum 2.3 of Chapter 2. The reference evapotranspiration ET_0 estimated for a very specific reference vegetal cover is often used as a default value.

where S_1 [mm] is the average water content of the root zone below which evapotranspiration stops, S^* [mm] is the average water content of the root zone above which $ET(t)$ is equal to the evaporative demand $PET(t)$ and b is a shape parameter.

In other words, in the ideal case with sufficient water available in the soil to satisfy the evaporative demand, ET is simply equal to the potential evapotranspiration PET for the given vegetal cover z. If not, ET is less than PET and becomes zero below the threshold S_1. At the scale of a land parcel, this threshold is sometimes considered to correspond to the wilting point.

The values of parameters b, S_1 and S^* are often estimated by calibration. The value of parameter b, which depends on the type of soil, can be used to adjust the difficulty of satisfying the evaporative demand for low levels of saturation. It is however often set to a value of 1. Other similar formulations have been proposed (Laio *et al*., 2001; Guswa *et al*., 2002).

The water content of the root zone $S_r(t)$ at time t is often estimated using a conceptual reservoir with behavior governed by a combination of the continuity equation and different empirical equations used to estimate the incoming and outgoing fluxes of the reservoir. A typical configuration of such a conceptual reservoir is illustrated in Figure 4.7.

The incoming fluxes are generally limited to recharge deduced from the infiltration rate f. The outgoing fluxes include losses related to actual evapotranspiration ET, percolation in the underlying soil layer d and eventually a lateral drainage term r. When the latter term is neglected, the continuity equation can be expressed as:

$$\frac{\partial S_r}{\partial t} = f(S_r) - ET(S_r) - d(S_r) \tag{4.19}$$

where $\partial S_r/\partial t$ is the variation of the volume of water stored in the root zone and outgoing and incoming fluxes depend on the average water content of the root zone reservoir. Various expressions for $f(S_r)$ are given in Section 4.4. The rate of percolation (drainage by gravity) is often considered to be zero for storage values less than a threshold S_2. At the scale of a land parcel, this threshold is sometimes considered to correspond to the
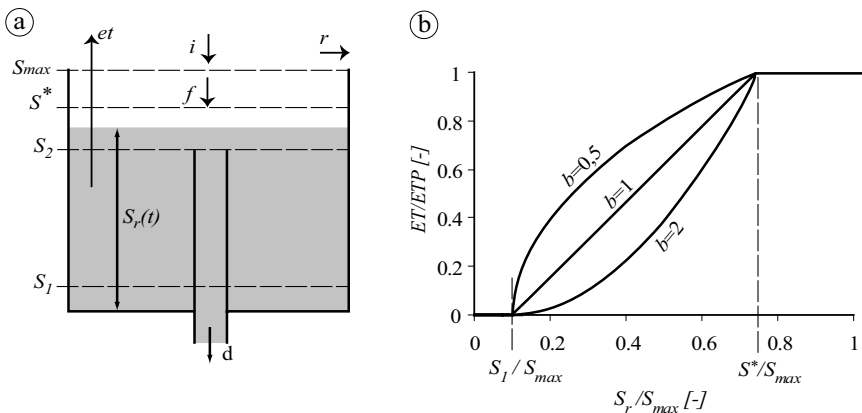
Fig. 4.7: A conceptual root zone reservoir used to estimate the actual evapotranspiration flux related to the presence of the vegetal cover. a) Typical reservoir structure, incoming flux (infiltration, i) and outgoing fluxes (evapotranspiration ET, percolation d and sub-surface runoff q). b) Typical functional relationship between the saturation level of the root zone reservoir and the degree of satisfaction of the evaporative demand.

field capacity of the soil. If *d* is not considered to be zero, it is often assumed to increase with storage S_r according to a power law ($d(S_r) = aS_r^b$) or an exponential law similar to the relationship often proposed between hydraulic conductivity and soil moisture content (Laio *et al.*, 2001).

The root zone reservoir is also often assumed to have a maximum storage capacity S_{max} (greater than the threshold S_2).

Estimating ET on the basis of the complementarity principle

Another approach has been developed to estimate actual evapotranspiration at the drainage basin scale. At this scale, complex interactions take place between the availability of water in the basin and climate variables. The related phenomena were identified and set to equations by Bouchet (1963) and later by Morton (1969), leading to evapotranspiration estimation models referred to as complementarity models (Addendum 4.3).

Addendum 4.3 Methods based on the Bouchet hypothesis

Bouchet (1963) identified negative feedback between *ET* and *PET*. Under constant energy conditions, *ET* is less than *PET* when water availability becomes a limiting factor. Bouchet assumed that a certain quantity of energy $\Delta H = PETW - ET$ was not used for evaporation under these conditions, where *PETW* is the reference evapotranspiration that would be observed in a wet environment. This energy is assumed to be available in the form of sensible heat, thereby increasing turbulence, temperature and humidity of the air above the evaporating surface. These increases are then assumed to increase in turn *PET* in proportion to the amount of energy made available: $PET = PETW + \Delta H$. This approach leads to a symmetrical relationship between potential evapotranspiration *PET* (i.e., the evaporative demand above the soil) and the actual evapotranspiration *ET*. This so-called complementary relationship is described by the following equation:

$$ET(t) + PET(t) = 2PETW(t) \tag{4.20}$$

PETW defines an equilibrium value observed when the soil is saturated with water. It represents the maximum possible value of *ET* and the minimum possible value of *PET* (with therefore $ET = PET$).

The advantage of this method is that it depends only on the meteorological parameters used to estimate *PET* and *PETW* (i.e., requires no information on soil moisture or canopy surface resistance). For more details on this approach, please refer to the cited literature.
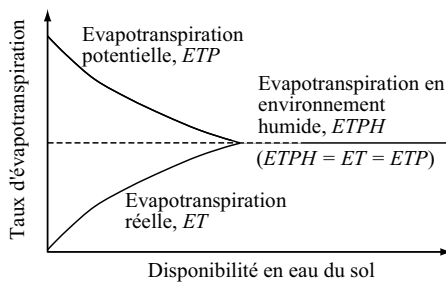

Fig. 4.8: Illustration of the complementary relationship between *PET* and *ET* (adapted from Bouchet, 1963).

The models based on this approach differ according to the equations used to calculate *PET* and *PETW* which are in turn used to deduce *ET* (Brutsaert, 2005; Xu and Chen, 2005; McMahon *et al.*, 2013). Xu and Chen (2005) have shown that the complementary relationship gives estimates of the actual evapotranspiration that are as good as those obtained from lysimeters. The Bouchet hypothesis should a priori offer good perspectives for the modeling of evapotranspiration at a regional scale (e.g., Brutsaert and Stricker, 1979; Hobbins *et al.*, 2001; Ramirez *et al.*, 2005; Xu and Singh, 2005). For example, Boughton and Chiew (2007) have successfully used *PET* values calculated by this method to estimate the daily discharges of ungaged basins in Australia.

However, application of the complementary relationship to rainfall-runoff modeling at the drainage basin scale has for the time being given mixed results (e.g., Chiew and McMahon, 1991; Oudin *et al.*, 2005). The main drawback is the difficulty in accurately delimiting the representative area of the obtained estimate. Note also that the use of the Bouchet hypothesis generally requires reformulation of the structure of the rainfall-runoff models and the equations they use (Oudin *et al.*, 2005).

4.3.4 Evaporation of Water Intercepted by the Vegetal Cover

Evaporation of water stored on the vegetal cover by interception involves the same mechanisms as evaporation from the free water surfaces of the drainage basin. The evaporative demand of the air is however modified by the aerodynamic resistance of the vegetal cover. The evaporative flux is also limited by the difficulty encountered in mobilizing the water trapped in the canopy.

Evaporation (E) of water intercepted by a given vegetal cover is often estimated on the basis of an evaporative capacity (E_0) determined for the considered wetted vegetal cover and the ratio of the volume of water intercepted (S_I) to the maximum storage capacity of the vegetal cover (S_{Imax}):

$$E(t) = f\left(S_I(t)\right) \cdot E_0(t) \tag{4.21}$$

The function f is often defined in the following manner (e.g., Rutter *et al.*, 1975; Figure 4.4; Appendix 4.8.1):

$$f = \begin{cases} \dfrac{S_I(t)}{S_{Imax}} & 0 < S_I(t) < S_{Imax} \\ 1 & S_{Imax} \le S_I(t) \end{cases} \tag{4.22}$$

The evaporative capacity E_0 can be estimated using the Penman-Monteith formula in which the surface resistance of the vegetal cover r_c is set to zero, which expresses the fact that the surface is wet (Appendix 4.8.2). The evaporative capacity of the wet vegetal cover is in principle greater than the evaporative capacity of the dry vegetal cover (see Example 4.2).

Many hydrologists consider that evaporation by interception is an alternative and not an addition to evapotranspiration. The main argument for this is that the energy available at the SVA interface cannot be used twice, i.e., once to evaporate water intercepted by

the vegetal cover and a second time to satisfy the evapotranspiration process (Penman, 1963). The validity of this theory or the adverse theory, according to which evaporation by interception adds to evapotranspiration losses, remains uncertain (e.g., Cosenday and Robinson, 2000).

An intermediate empirical approach often used to estimate the evaporation flux consists in considering that the evaporative demand is global and that it tends to be totally satisfied first by evaporation of intercepted water and then if necessary by evapotranspiration. In this scheme, the fraction of evaporative capacity E_0 that can be satisfied by evaporation of part of the water stored at the surface is first determined (e.g., via equations 4.10 in 4.11). The fraction not satisfied represents a residual evaporative demand E_b, already discussed, that can in turn be totally or partially satisfied by the evapotranspiration process.

Example 4.2

For conditions in which the availability of water is not a limiting factor, use the Penman-Monteith formula to estimate the evaporation rate for a grass-covered surface when the grass is wet and when the grass is dry. The characteristics of the vegetal cover are: height $h = 0.12$ m, surface resistance $r_c = 70$ s/m and albedo $\alpha = 0.23$. The meteorological data are: wind speed $u = 1.5$ m/s, air temperature $T = 11.1°C$, solar radiation $R_S = 187.9$ W/m^2 and the relative humidity of the air $R_H = 65.0\%$.

The equations of Appendix 4.8.2 give:
Net radiation R_n : 144.65 [W/m^2]
Saturated vapor pressure e_s : 1325.50 [Pa]
Slope of the vapor pressure curve Δ : 88.00 [Pa/°C]
Actual vapor pressure e_a : 861.62 [Pa]
Vapor deficit $\delta e = (e_s - e_a)$: 463.89 [Pa]
Aerodynamic resistance r_a : 101.4 [s/m]

ET is deduced using the Penman-Monteith equation. If the vegetation is dry, $ET = 3.8 \times 10^{-5}$ mm/s (3.29 mm/day). If the vegetation is wet, the surface resistance r_c is zero and $ET = 4.93 \times 10^{-5}$ mm/s (4.26 mm/day).

4.4 INFILTRATION

Infiltration takes place when precipitation reaches the soil surface or when this surface is exposed to submersion. Once infiltrated, the water can be recovered by the vegetal cover through the root system, return to the atmosphere by evaporation, flow laterally as sub-surface runoff or percolate deeper to recharge the water table. The infiltration process therefore affects different aspects of hydrology, agronomy and hydrogeology. For this reason, it has been the subject of many theoretical and experimental studies both in the field and in the laboratory.

This section presents different approaches that can be used to model the infiltration rate versus time at land parcel and drainage basin scales.

4.4.1 Processes and Explanatory Factors

Infiltration at land parcel scale

Infiltration is the process by which water flows through the top layers of the soil under the forces of gravity and pressure. During submersion or a rainfall event, two cases may be encountered.

- If the water supply rate is sufficient and the soil deep and well-drained, the infiltration rate is limited by the infiltration capacity of the soil, i.e., the maximum water flux that the soil is capable of absorbing. When the soil is initially unsaturated, the infiltration capacity (or infiltrability) decreases as the wetting zone moves deeper into the soil (saturation from the top down). If the soil is well-drained, it tends towards a lower bound often equal to the saturated hydraulic conductivity of the soil (Figure 4.9a). The fraction of the supply of water that cannot be infiltrated produces Hortonian runoff.
- If the water supply rate is less than the infiltration capacity of the soil, all the incoming water is infiltrated. In this case, the infiltration rate is determined solely by the water supply rate and no runoff is produced (Figure 4.9b).

When the water supply is interrupted or stops completely, or when the supply rate is less than the infiltration capacity, the latter can be partially restored. Infiltration capacity recovery is due to the redistribution processes that dispatch the water in the soil and also, if applicable, to evapotranspiration.

In general, the water supply rate over time can be alternately less than and greater than the infiltration capacity. Consequently, the infiltration rate can vary greatly with time (Figure 4.9b).

If the soil is not sufficiently pervious to evacuate infiltrating water or water received from upstream—for example due to an impervious underlying layer—it can be saturated from the bottom up. If it is totally saturated, it blocks all infiltration and produces Hewlettian type runoff. In a drainage basin, bottom-up saturation of certain soils often results in sub-surface inflows coming from upstream parts of the basin.

The infiltration process depends on many factors, the most important of which concern the hydrodynamic characteristics, texture and structure of the soil. It also strongly depends on the initial moisture conditions, the water supply (e.g., gross rainfall, irrigation, upstream
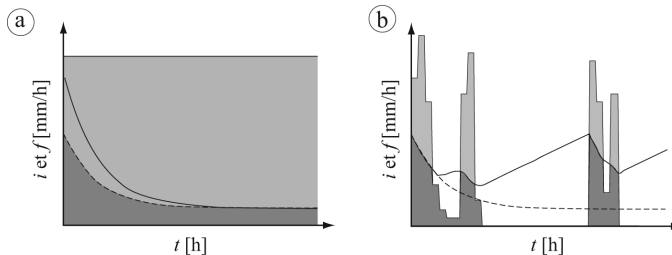
Fig. 4.9: Intensity of gross rainfall (*i*) and soil infiltration rate (*f*) for different rainfall events and initial soil saturation conditions. a) Hypothetical case in which the water supply rate is always greater than the infiltration capacity for an initially dry well-drained soil (solid curve) and an initially wet soil (broken curve). b) Infiltration rate (dark gray zone) and infiltration capacity with recovery (solid curve) when the supply rate is alternately less than and greater than the infiltration capacity and infiltration capacity for a supply rate that is always greater than the infiltration capacity (broken line).

runoff) and the water redistribution processes in the soils. These factors are discussed in detail in Musy and Higy (2011) and Soutter *et al.* (2007). Note also that infiltration processes can be greatly modified by partial or complete freezing of the soil. This aspect is dealt with in Chapter 7.

Infiltration at drainage basin scale

Estimation of the infiltration flux at the scale of a drainage basin is a complex task. This complexity is first of all induced by the high spatial variability of the hydrodynamic characteristics of the soils (e.g., Avissar and Pielke, 1989; Merz and Plate, 1997; Liang and Xie, 2001).

The main consequence of this variability is a non-linear hydrological response of the basin to the precipitation intensity or depth. Consider the case in which the production process is purely Hortonian at every point in the basin and local infiltration percolates deep into the soil. Runoff will be produced locally only if the precipitation intensity exceeds the local infiltration capacity, in which case the infiltration rate no longer depends on the precipitation intensity. On the other hand, at the scale of a drainage basin, the observed infiltration capacity varies between a minimum and maximum value and can be characterized by a statistical distribution function such as the one described in Figure 4.10a. At the scale of the basin, runoff is therefore produced as soon as the gross rainfall intensity exceeds the minimum infiltration capacity observed within the basin. Moreover, the infiltrated volume increases with this intensity as long as the latter remains less than the maximum infiltration capacity observed on the basin.

Figure 4.10 provides a simple illustration of the non-linearity of the hydrological response at the drainage basin scale for the hypothetical case in which: 1) the gross rainfall is uniformly distributed over the entire drainage basin and 2) the net rainfall at a given point within the basin does not re-infiltrate along its path towards the basin outlet. The non-linearity shown in the figure is due to the variability of the infiltration capacity at this scale. The infiltration and runoff volumes (corresponding to the light and dark gray zones
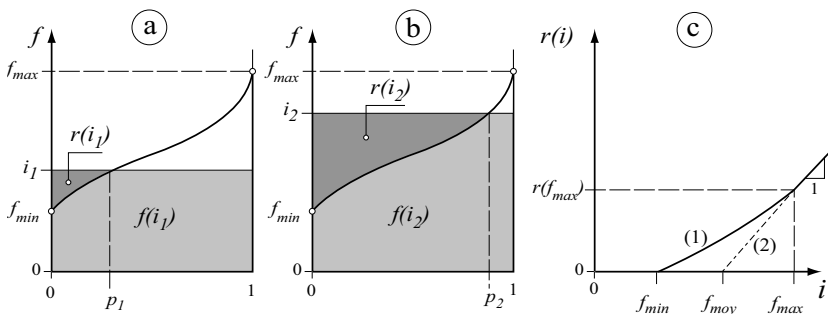
Fig. 4.10: Effect of the spatial variability of infiltration capacity on rainfall excess and infiltration losses at the drainage basin scale when the processes leading to rainfall excess are exclusively Hortonian. Runoff (dark gray zones) and total infiltration (light gray zones) at a given time for gross rainfall intensities: a) i_1 and b) $i_2 > i_1$. The resulting curves represent the statistical distribution function of the soil infiltration capacity for the drainage basin at a given time (infiltration capacity f not exceeded for a fraction c of the total basin area). The potential maximum infiltration rate at the considered time corresponds to the integral under the curve. c) Runoff volumes at the basin scale as a function of gross rainfall intensity considering: (1) the variability of local infiltration capacities and (2) only the average value of the corresponding distribution.

respectively) for the two supply rates i_1 and i_2 (with $i_1 < i_2 < f_{max}$ where f_{max} is the maximum infiltration capacity observed on the basin at the considered time) are indicated in Figure 4.10. For supply rate i_1, the soil infiltration capacity is exceeded on a fraction $p_1 < 1$ of the basin area. The fraction p_2 of the basin area obtained for supply rate i_2 is greater than p_1. This leads to both a greater runoff volume and a greater infiltrated volume.

A consequence of the non-linearity discussed above is that the hydrological behavior of the basin cannot be represented by an average Hortonian process at the basin scale even if the production process is Hortonian at every point in the basin. To illustrate this, Figure 4.10c compares the runoff volume versus time that would be produced by the hypothetical basin above for increasing rainfall intensities with those that would be simulated with the Hortonian scheme corresponding to an excess with respect to the mean capacity of the basin (mean of the infiltration capacities as described by the statistical distribution shown in Figure 4.10a).

The same type of non-linearity is obviously observed if the process is exclusively Hewlettian. In this case, the non-linearity is related to the spatial variability of the storage capacity (or soil saturation deficit) within the basin.

The non-linearity effects mentioned above increase with the spatial variability of the precipitation in terms of intensity (for Hortonian processes) or cumulative precipitation (for Hewlettian processes) (Obled *et al*., 1994; Koren *et al*., 1999; Arnaud *et al*., 2002).

The complexity of calculating rainfall excess at the basin scale is not due only to the reasons mentioned above. It also results from the spatial organization of the different terrains that can lead to re-infiltration of some of the runoff produced upstream. In addition, it is induced in particular by the processes that redistribute sub-surface water and that lead to a high spatial variability of the basin saturation conditions and consequently infiltration rates (Section 4.1.2).

Different approaches can be followed to estimate rainfall excess at the scale of a land parcel, drainage basin or any other hydrological unit. The complexity of these approaches varies according to the simplifications used to present the processes. Some of these approaches will now be discussed in detail.

4.4.2 Modeling at the Land Parcel Scale

At the scale of a land parcel and when infiltration can be considered to be essentially vertical, the infiltration flux in unsaturated soil can be described and modeled, with various simplifying assumptions, by the one-dimensional partial differential equation proposed by Richards (Addendum 4.4). This model is seldom used for typical hydrological applications.

Most hydrologists use simplified infiltration models. These are reservoir-type conceptual models or models based on infiltration capacity decay functions.

Addendum 4.4 The Richards equation

Assumptions and equations

The Richards equation is based on the following main assumptions:

- Water vapor fluxes in the soil are negligible.
- It is possible to express the relationship between moisture content θ, capillary pressure head h and the hydraulic conductivity of the soil K using unequivocal mathematical functions

$\theta(h)$ or $\psi(\theta)$ and $K(h)$ or $K(\theta)$. Among available functions, those proposed by van Genuchten (1980) are the most widely used.

- For saturated and unsaturated media, water velocity is assumed to be a linear function of the gradient of hydraulic head as defined by the following Darcy model:

$$\mathbf{q} = -K(\theta) \cdot \mathbf{grad}\left(H(\theta)\right) = -K(\theta) \cdot \mathbf{grad}\left(h(\theta) - z\right) \tag{4.23}$$

where $\mathbf{q}$ is the vector of water flux in the soil, θ the soil moisture content, $H(\theta)$ the hydraulic head resulting from gravity z and capillary pressure head $h(\theta)$. The pressure head is an increasing function of the moisture content of the soil. It has a negative value that increases (i.e., decreases in absolute value) as θ increases (Figure 4.9).

Note that the conservation of liquid in a porous medium is expressed by the following continuity equation:

$$\frac{\partial \theta}{\partial t} = -div(\mathbf{q}) + r_w \tag{4.24}$$

where r_w represents inflows or losses if applicable (e.g., water removed by vegetation or local evaporation of liquid water). This term depends in particular on the moisture content and local characteristics of the medium. It varies with depth.

The Richards partial differential equation results from the combination of the Darcy model and the continuity equation. Subject to the assumptions mentioned above, it governs the dynamics of water in porous media and can be expressed as follows:

$$\frac{\partial \theta}{\partial t} = div\left[K(\theta) \cdot \mathrm{grad}\left(h(\theta) - z\right)\right] + r_w \tag{4.25}$$

In unsaturated media, the fluxes related to the movement of water in the soil are essentially vertical. Consequently, it is reasonable to describe them using the following one-dimensional Richards equation:

$$\frac{\partial \theta}{\partial t} = -\frac{\partial q}{\partial z} + r_w = \frac{\partial}{\partial z}\left(K(\theta)\frac{\partial h(\theta)}{\partial z}\right) - \frac{\partial}{\partial z}K(\theta) + r_w \tag{4.26}$$

Solving the equation and application difficulties

To solve these equations for a given soil column, the soil must be discretized into different horizontal layers and appropriate numerical schemes must be used (Soutter *et al.*, 2007). Over and above the difficulties inherent to implementing these schemes and estimating model parameters, solving the equation is complicated by the parabolic nature of the Richards equation and the strong non-linearity of the relationships between the hydrodynamic properties of the soil and its moisture content.

Another major difficulty in applying the Richards equation is the specification of boundary conditions (Van Dam and Feddes, 2000). For example, for moderate precipitation and moderately saturated soil, the evaporation flux is often assumed to have an upper bound equal to the evaporative demand (flux condition). During extended dry conditions, the evaporation flux is governed by the hydraulic head in the soil which is mainly a function of the suction potential (head condition). During very wet conditions, the hydraulic head of water accumulated at the surface determines the infiltration rate (head condition). At the bottom of the considered soil column, the main difficulty lies in the estimation of the depth of transition between saturated and unsaturated zones and its spatial and temporal evolution.

Infiltration capacity decay functions

When the infiltration rate is limited by the infiltration capacity of the soil, a classical approach is to use an infiltration function. These functions assume that the infiltration capacity is a decreasing function of time. The functions proposed by Philip or Horton[7] are widely used (Table 4.3). Many other similar functions exist (Ravi and Williams, 1998; Musy and Higy, 2011). Infiltration functions can also be deduced from the simplified simulation of the advance of the wetting front in the soil using the Green and Ampt method, described in detail by Soutter *et al*. (2007).

Table 4.3 Three widely used $f(t)$ functions describing the infiltration capacity of the soil as a function of time.

Function	Infiltration capacity	Parameters
Horton	$f(t) = f_c + (f_0 - f_c) \cdot e^{-ct}$	f_0 and f_c [mm/h] are respectively the initial and limiting infiltration capacities and c [h^{-1}] is a decay constant.
Philip	$f(t) = \frac{1}{2} S \cdot t^{-0.5} + A$	S is the sorptivity [cm s$^{-1/2}$], which depends on the initial saturated moisture content and A is the gravitational component [cm s^{-1}], which depends on soil properties and the initial and saturated moisture content. A approaches the saturated hydraulic conductivity for very high infiltration durations.
Green-Ampt	$f(t) = K_s \left(1 + \dfrac{h_0 - h_f}{z_f(t)} \right)$	h_0 and h_f are respectively the pressure head at the surface and at the wetting front and $z_f(t)$ is the depth of the wetting front reached at time t.

The two main limitations of infiltration functions are that they do not take into account the possibility of 1) bottom-up saturation of the soil and 2) recovery of the infiltration capacity of the soil. Infiltration functions are therefore most often used for event-based simulations.

A number of adaptations have however been proposed to at least partially solve these limitations. The modified Horton method, for example, can be used to partially simulate the possible recovery of the infiltration capacity estimated on the basis of the total infiltrated precipitation since the beginning of the rainfall (ASCE, 1996—Chapter 9). The principle of this method is equivalent to that of the infiltration excess reservoir model (IEM) when $f_{max}(S) = f_0 - cS$. This model is described in Section 4.4.2. The Green and Ampt model has also been adapted to account for the redistribution of moisture in the soil (Ogden and Sahafian, 1997; Downer *et al*., 2002).

Note that application of an infiltration function also requires estimation of the parameters associated with these methods, e.g., initial infiltration capacity, initial soil saturation state, which is often far from straightforward. The values of these parameters can come directly from laboratory or field measurements of the hydrodynamic properties of the soils of the studied site. They have however often been compiled for different types of initially dry soils that are assumed to be homogeneous. Note that these parameters are in principle estimated under conditions in which the water supply rate is greater than or equal to the infiltration capacity.

---

[7]The Philip equation in fact expresses the solution of the Richards equation under various simplifying assumptions (Soutter *et al.,* 2007). The Horton equation result from the assumption that the rate of change of the infiltration capacity is proportional to the difference between the actual value of the infiltration capacity f and its limiting value when the soil is saturated f_c. In other words, it expresses the fact that $df/dt = - c(f - f_c)$.

A wide selection of typical values is available in the abundant corresponding literature (Van Genuchten, 1980; Hillel, 1982; Rawls *et al*., 1992; ASCE, 1996; Leij *et al*., 1996; Ravi and Williams, 1998; Williams *et al*., 1998). For example, the following tables provide indications of values for the Horton and Philip infiltration models.

Table 4.4: General indication of values of the parameters of the Horton equation for different soil types (adapted from Horton, 1940, as cited in ASCE, 1996).

Type of soil	f_0 [mm/h]	fc [mm/h]	c [min^{-1}]
Standard agricultural (bare)	280	6–220	1.6
Standard agricultural (turfed)	900	20–290	0.8
Peat	325	2–20	1.8
Fine sandy clay (bare)	210	2–25	2.0
Fine sandy clay (turfed)	670	10–30	1.4

Table 4.5: General indication of values of the parameters of the Philip's equation for different texture categories.

Texture classes	Sorptivity S [cm s$^{-1/2}$]	A [cm s^{-1}]
Coarse sand	1.7×10^{-1}	1.3×10^{-3}
Fine sand	7.3×10^{-2}	3.5×10^{-4}
Sandy loam	6.5×10^{-2}	2.1×10^{-4}
Sandy silt	4.9×10^{-2}	6.2×10^{-5}
Loam	4.0×10^{-2}	4.6×10^{-5}
Sandy- clay loam	6.5×10^{-2}	1.9×10^{-4}
Silty- clay loam	2.1×10^{-2}	1.4×10^{-5}
Clay loam	1.6×10^{-2}	8.8×10^{-6}
Light clay	3.6×10^{-2}	3.4×10^{-5}
Loam clay	1.4×10^{-2}	9.8×10^{-6}
Heavy clay	6.5×10^{-3}	1.7×10^{-6}
Peat	2.5×10^{-2}	2.2×10^{-6}

Reservoir-type models

The principle of reservoir models is to estimate infiltration rate on the basis of the average volume of water stored in the sub-surface soil layer. The evolution of this storage volume with time can be simulated using a global conceptual model. This model combines the continuity equation and various other equations expressing the different sub-surface fluxes as a function of the volume stored in the reservoir:

$$\frac{\partial S}{\partial t} = f(S,i) - ET(S,PET) - q(S) \tag{4.27}$$

where S is the reservoir storage volume at time t [mm], I and PET respectively the intensity of gross rainfall and the potential evapotranspiration, $f(S,i)$, $ET(S,PET)$ and $q(S)$ respectively the infiltration, actual evapotranspiration and deep percolation fluxes [mm/h]. The equations typically used for the $ET(S, PET)$ and $q(S)$ functions are indicated in Section 4.3.2.

The simulated infiltration rate depends on the variation of meteorological forcings (i, PET) with time. The existence of release terms ET and q makes it possible to take into account infiltration capacity recovery, in particular during periods without precipitation.

A wide variety of behaviors can be simulated depending on the chosen nature of the different functions f, ET and q. The following two reservoir models can be used for example to simulate radically different behaviors. They in fact describe two types of processes that can produce runoff. The infiltration excess model (IEM) describes rainfall excess produced exclusively by precipitation exceeding the infiltration capacity while the storage excess model (SEM) describes rainfall excess produced exclusively by precipitation exceeding the storage capacity (Figure 4.11).

Neglecting evaporation losses, they are based on the following equations:

IEM: $f(S,i) = \text{Min}\left(f_{\max}(S), i\right)$ and $q(S) = f_c$ \hfill (4.28)

SEM: $f(S,i) = \begin{cases} i & \text{if } S < S_{\max} \\ 0 & \text{if not} \end{cases}$ and $q(S) = f_c$ \hfill (4.29)

where f_c is the reservoir outlet discharge by percolation, assumed constant, and S_{max} is either the maximum storage capacity of the reservoir (for the SEM) or a decreasing function of reservoir storage (for the IEM), defining the maximum infiltration capacity of the soil.

For the SEM, all rainfall can be infiltrated as long as the reservoir is not full. If the reservoir is full, all rainfall (after subtracting losses by percolation from the reservoir) produces surface runoff. Infiltration does not depend on a given infiltration capacity but rather uniquely on the available storage volume for infiltration. This volume is called the "soil saturation deficit" in many approaches of this type.

The IEM defines, at each instant, a critical intensity and the infiltration capacity of the soil. Any excess with respect to the latter produces surface runoff. The infiltration capacity decreases as the reservoir fills. Filling continues without any limitation as long as the rainfall intensity is greater than the reservoir drainage rate. When the supply rate is always greater than the infiltration capacity and when initial storage is zero (S=0 at
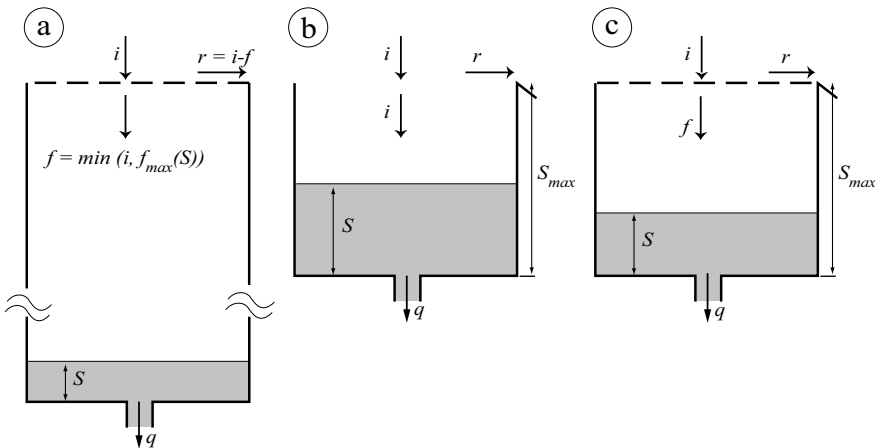

Fig. 4.11: Three typical structures of reservoir models used to simulate infiltration at the land parcel scale. a) Infiltration excess model (IEM). b) Storage excess model (SEM). c) Combined model (IEM + SEM).

t=0), note the analytical solution of the IEM obtained for two particular expressions of the $f_{max}(S)$ function:

- When $f_{max}(S) = f_0 - cS$, the model leads to the Horton infiltration equation where f_0 is the initial infiltration capacity and c the decay constant (see Table 4.3).
- When $f_{max}(S) = f_c + B/S$ with a constant B, the expression of the infiltration capacity is $f = f(t) = f_c + (0.5B/t)^{0.5}$, clearly related to the Philip equation given in Table 4.3.

As opposed to the Horton and Philip equations, these two models can be used to simulate soil infiltration capacity recovery when the supply rate is less than the infiltration capacity. This is illustrated in Figure 4.12 obtained on the basis of Example 4.3.

Various other models are possible. For example, the Holtan (1961) model combines an SEM and an IEM with infiltration capacity $f_{max} = f_c + B/S$ and storage capacity S_{max}. As with many other similar models, it can be used to produce one or other of the processes causing runoff depending on the supply rate and the level of reservoir saturation. If the reservoir is initially empty, a constant rainfall intensity i produces runoff by saturation if $f_c < i \leq f_c + B/S_{max}$ and by infiltration capacity excess if $i \geq f_c + B/S_{max}$.

For the different models, note that the volume and duration required to produce runoff depends on the rainfall intensity and the initial reservoir storage volume.
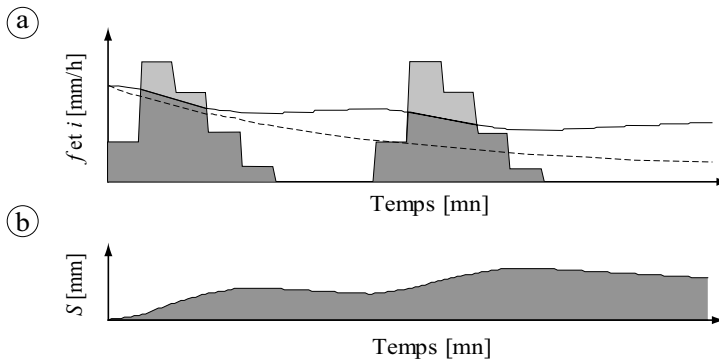

Fig. 4.12: Simulation of infiltration with an IEM type reservoir model where $f_{max}(S) = f_0 - cS$. a) Hyetographs of gross and infiltrated rainfall, simulated potential infiltration capacity (solid curve) with the IEM and infiltration capacity according to the Horton model $f(t) = f_c + (f_0 - f_c)e^{-ct}$ (dotted curve). b) Change of storage in the soil reservoir S with time.

Example 4.3

Estimation of infiltration rate for two infiltration models

Consider an initially dry soil with an infiltration capacity that decreases according to the Horton model if the supply rate is sufficient. The corresponding parameters are: $f_0 = 80$ mm/h, $f_c = 10$ mm/h and $c = 0.8$ h^{-1}. The soil is exposed to a rainfall corresponding to the hyetograph given in Table 4.6 for a 10-minute time step. The objective is to compare the net rainfall hyetographs for this event that would be obtained: 1) using the Horton model (with the above parameters) and 2) using the IEM (with f_{max} expressed in the form $f_{max}(S) = f_0 - cS$). It is assumed that water that cannot infiltrate at a given time step is evacuated instantaneously by surface runoff (i.e., no sub-surface storage). The calculations are carried

out for a 1-minute time step). Application of the Horton model (infiltration decay function) is immediate. The total infiltered depth is 56 mm. The net rainfall hyetograph is shown in Figure 4.12.

For the IEM, the potential infiltration $f_{max}(S_i)$ and sub-surface storage S_i must be determined for each time step in order to deduce the actual infiltration $f(S_i, i_i)$. At $t_0 = 0$, the value of the initial storage S_0 and initial infiltration potential $f_{max}(S_0)$ can be calculated as follows:

$$S_0 = S_{-1} + (f_{max}(S_{-1}) - f_e) \cdot \Delta t = S_{-1} + (f_0 - f_c) \cdot \Delta t = 0 + (80 - 10) \cdot (1/60) = 0.38 \text{ mm}$$

$$f_{max}(S_0) = f_0 - cS_{-1} = 80 - 0.8 \cdot 0 = 80 \text{ mm/h}.$$

This value of the potential infiltration is then compared to the rainfall intensity on the same time step ($i_0 = 33$ mm/h). The actual infiltration $f(S_0, i_0)$ is equal to the smallest of the two values, in this case $f(S_0, i_0) = 33$ mm/h. This procedure is repeated for the following time steps. The results are given in Table 4.6 (indicated only every 10 minutes). The corresponding net rainfall hyetograph is presented in Figure 4.12. The total infiltrated depth is 68.2 mm. The Horton model underestimates total infiltration by 18%. The underestimation is greater for the second rainfall event (-33%) than for the first rainfall event (–5%).

Table 4.6: Potential infiltration rate f_{max} and actual f obtained with the Horton and modified Horton (IEM) models.

Time [min]	Rainfall i [mm/h]	$f_{max}(t)$ (Horton) [mm/h]	$f(t)$ (Horton) [mm/h]	$f_{max}(S_i)$ (IEM) [mm/h]	$f(S_i, i_i)$ (IEM) [mm/h]	$S_i(t)$ (IEM) [mm]
0	33	80.0	33.0	80.0	33.0	0.4
10	100	71.3	71.3	76.9	76.9	4.9
20	75	63.6	63.6	68.5	68.5	15.3
30	40	56.9	40.0	61.2	40.0	24.0
40	10	51.1	10.0	57.2	10.0	28.5
50	0	45.9	0.0	57.2	0.0	28.4
60	0	41.5	0.0	58.5	0.0	26.7
70	0	37.5	0.0	59.8	0.0	25.0
80	33	34.1	33.0	61.2	33.0	23.9
90	100	31.1	31.1	58.1	58.1	28.2
100	75	28.5	28.5	52.1	52.1	35.6
110	40	26.1	26.1	46.8	40.0	42.0
120	10	24.1	10.0	42.8	10.0	46.5
130	0	22.4	0.0	42.8	0.0	46.4
140	0	20.8	0.0	44.1	0.0	44.7

4.4.3 Modeling Infiltration at the Drainage Basin Scale

To simulate the infiltration process at the scale of a drainage basin, most hydrologic applications use simplified models. These models are generally conceptual reservoir-type, global or distributed models (Chapter 3). Several hydrological models however use physically-based infiltration models (e.g., SHE model, Abbott *et al.*, 1986a,b).

Spatialized physically-based infiltration modeling

Physically-based models simulate the infiltration process with the one-dimensional Richards equation for the unsaturated zone and the three-dimensional Richards equation for the saturated zone. Solving these equations in principle makes it possible to simulate the lateral redistribution of the water in the soil related to sub-surface flows and flows in the saturated zone. It is therefore generally possible to simulate the main processes for runoff mechanisms, Horton mechanisms and those related to the formation of saturated zones. It is generally assumed that the runoff produced is not re-infiltrated.

For this type of model, the description of the drainage basin must necessarily be spatialized and multilayer (e.g., SHE model). The hydrodynamic characteristics of the soils, described by the relationships $\theta(h)$ or $\psi(\theta)$ and $K(h)$ or $K(\theta)$, must be specified for each element of the discretization. They are generally estimated on the basis of the nature of the soils using appropriate pedotransfer functions (Addendum 4.5).

The pertinence of the Richards equations when simulating infiltration at the scale of a given grid cell of the discretization of the drainage basin is highly open to question. The Richards equations are valid in the laboratory on columns of homogeneous soil. However, the characteristics of the medium often vary greatly within each the discretization elements of a basin. Within a parcel of a few hundred square meters, for example, the hydraulic conductivity can vary by 1 to 2 orders of magnitude if the soils are homogeneous and 4 to 5 orders of magnitude if this is not the case. Note that the infiltration process is very non-linear if the characteristics of the medium vary in space (Section 4.4.1). In the general case, infiltration modeling using the Richards equations does not account for this non-linearity —even if an effective conductivity is used (e.g., Hansen *et al*., 2007). These equations are therefore not very appropriate for most hydrological applications. Moreover, the production of rainfall excess at the scale of a drainage basin involves many other processes than those described by these equations (e.g., preferential flow through micropores).

Addendum 4.5 Pedotransfer functions

Pedotransfer functions (PTF) are models developed to estimate the hydraulic characteristics $\theta(h)$ or $\psi(\theta)$ and $K(h)$ or $K(\theta)$ of the soil from pedological characteristics that can be more easily measured (e.g., texture, chemical or mechanical properties). Numerous PTFs been developed (e.g., van Genuchten, 1980; Schaap *et al*., 2001; Wösten *et al*., 2001) that can be divided into two types.

The first type can be used for example to express the moisture content θ for different values of *h*. It takes the form of multiple regressions for which the explanatory variables are related to the measured soil characteristics. One of the analytical functions proposed in the literature to describe $\theta(h)$ is then fitted to (θ,*h*) pairs obtained on the basis of these equations for the considered medium.

The second PTFs can be used to directly predict the adjustment parameters of analytical functions describing for example the variations of θ with *h*. Many PTFs have for instance been developed to estimate the parameters of functions proposed by van Genuchten (1980), e.g., Wösten *et al*., 2001.

Global reservoir models

Rainfall excess at the drainage basin scale is most often estimated using global reservoir models. Threshold-based global models, such as the SEM (based on a saturation threshold)

and IEM models (based on a infiltration capacity threshold) presented in Section 4.4.2, are generally not appropriate because they cannot represent the major non-linearities discussed in Section 4.4.1. Various types of structures of reservoir models have nevertheless been proposed to partly solve this limitation (Perrin, 2000).

For a single reservoir used to simulate rainfall excess at the drainage basin scale, infiltration is generally estimated as a function of the fraction of the reservoir capacity that is filled (Figure 4.13).

This function often has the following form:

$$f(S) = \left(1 - \left(\frac{S}{S_{max}}\right)^a\right)^b \cdot i_b(t) \tag{4.30}$$

where S is reservoir storage, S_{max} the maximum storage capacity, i_b the intensity of gross rainfall and a and b are parameters determined empirically or by calibration (e.g., $a = 2$, $b = 1$ in the case of the Cemagref GR4J model; Edijatno *et al*., 1999). Infiltration is maximum when the reservoir is empty (all the rainfall is infiltrated) and zero when the reservoir is full (all rainfall produces runoff). The advantage of this formulation is that the net rainfall and infiltration are both an increasing function of gross rainfall. Note also that the net rainfall i_n can in this case be expressed in the following form:

$$i_n = i_b - f = i_b \cdot A(S / S_{max}) \tag{4.31}$$

where i_g is the intensity of gross rainfall and where the function $A(S/S_{max})$ can be obtained easily from equation 4.30. Certain authors suggest that such a model is therefore mainly Hewlettian, where the fraction of the basin area producing surface runoff $A(S/S_{max})$ (saturated areas), is assumed to be an increasing function of the average fill fraction of a global soil reservoir for the basin (e.g., Kavetski *et al*., 2003).

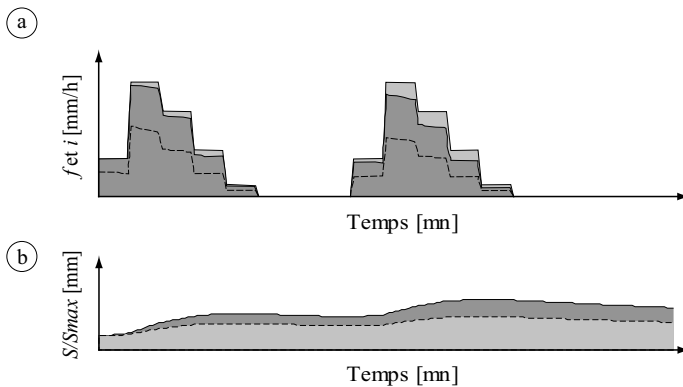**Fig. 4.13:** Simulation of infiltration by a global reservoir model with $f(S)=(1-(S/S_{max})^a) \cdot i_b(t)$ and $Q(S) = S/K$ ($K = 5$ h; $S(t_0) = 20$ mm; $S_{max} = 160$ mm). a) Hyetographs of gross rainfall and infiltrated rainfall obtained for $a = 0.5$ (gray curve) and $a = 2$ (broken curve). b) Storage in the soil reservoir S versus time for $a = 0.5$ (gray curve) and $a = 2$ (broken curve).

Distributed models

The high spatial variability of the physical characteristics of the medium and soil saturation conditions along with the non-linearity of infiltration processes with respect to precipitation have led to the development of different types of distributed models (Chapter 3).

In this context, rainfall excess produced in the basin is often simulated on the basis of the unique reservoir model structure for different hydrological units that are generally assumed to be independent of one another. The spatial organization of these units is in particular generally neglected. The hydrological units correspond to each element of a selected spatial discretization of the drainage basin. In this case, the model parameters are estimated for each unit on the basis of the local hydrodynamic soil characteristics (CEQUEAU, Girard, 1975; Szilagyi and Parlange, 1999). These units can also be of a limited number, selected so as to be representative of the main types of hydrological behavior observed within the basin. This is the principle of hydrologically similar response units (HRUs) described in Chapter 3 (Gurtz *et al.*, 1999). This approach makes it possible to reduce the number of calculations to be carried out to simulate the behavior of the basin.

Another approach consists in describing the spatial heterogeneity of the hydrological response of the basin using a function $f(c)$ that represents the statistical distribution of the key characteristic of the basin with respect to the production of rainfall excess. This characteristic is often the storage capacity of the soil (e.g., PDM model, Moore and Clarke, 1981; VIC, Liang *et al.*, 1994; Xinanjiang model, Zhao, 1992; ARNO model, Todini, 1996). In this case, the net rainfall at a given time is determined by the excess with respect to the soil saturation deficit of some of the storage elements described by this distribution. This is illustrated in Figure 4.14 for the PDM model for precipitation P falling on an initially dry basin. The local soil saturation deficit is updated at each time step on the basis of an average

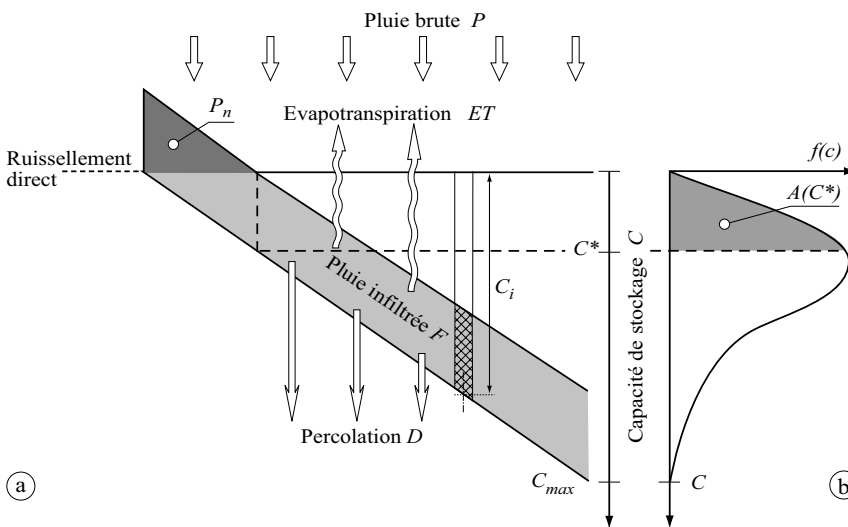**Fig. 4.14:** Principle of estimation of infiltration by the Probability Distributed Model (PDM) of Moore and Clarke (1981). a) Storage elements with insufficient storage capacity to absorb the gross rainfall (dark gray area). These elements determine the net rainfall and the fraction of saturated areas. b) The distribution function used to describe the spatial variability of storage capacity over the basin.

soil saturation deficit for the basin—or in an equivalent manner on the basis of average sub-surface storage. This updating requires various assumptions related in particular to the sub-surface redistribution of infiltrated water. The temporal evolution of the average soil saturation deficit (or average sub-surface storage) is estimated using a hydrological balance carried out at the scale of the basin. The balance equation is the same as equation 4.27. In addition to inputs by infiltration, the balance generally takes into account losses related to deep percolation and evapotranspiration.

The distribution function $f(c)$ takes on different forms depending on the model. In Topmodel (Beven *et al.*, 1984), this distribution is determined on the basis of a topographic index. This index is first calculated at every point in the basin on the basis of the local slope β_i and the upstream area a_i drained at this point. For one of the versions of this model, it is defined as follows (Ambroise *et al.*, 1996):

$$\delta_i = a_i/\tan \beta_i \tag{4.32}$$

High values of the index correspond to the parts of the basin with the lowest storage capacity. With the various assumptions of the model, the local soil saturation deficit D_i (corresponding to the local storage capacity) can be expressed as follows:

$$D_i = \overline{D} + m\left[\gamma - \ln(\delta_i)\right] \tag{4.33}$$

where $\overline{D}$ is the average soil saturation deficit over the drainage basin, m a parameter of the assumed exponential decrease of the hydraulic conductivity at saturation with depth and γ the spatial average of the logarithm of the topographic index. The simulation is carried out for a discrete number of increments of this index (Figure 4.15). The spatial extension of the saturated parts varies with time as a function of the dynamics of the saturated zone at the scale of the basin. These dynamics are assumed to rapidly lead to equilibrium where local storage depends on the average storage at the basin scale and on this index.
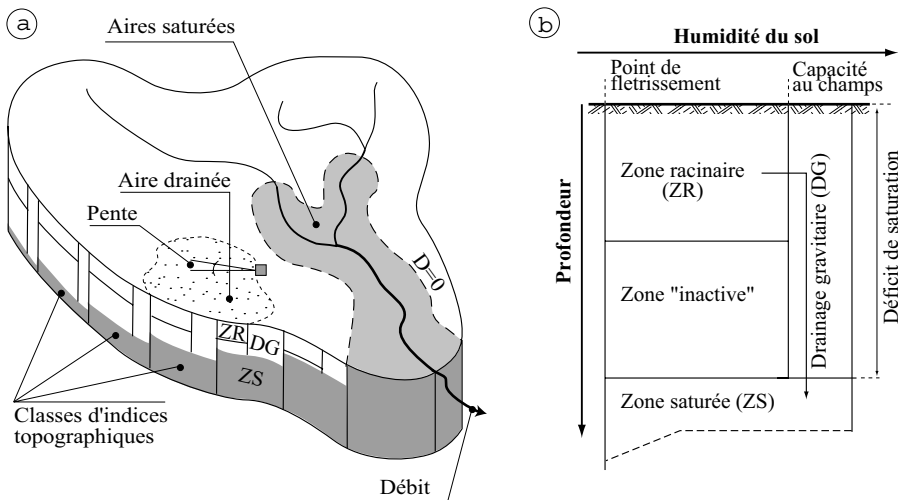
Fig. 4.15: Rainfall excess concept for the Topmodel distributed model (Beven *et al.*, 1984). a) The characteristics used to locally define the value of the topographic index, topographic index classes and saturated areas of the basin at a given time (areas defined by the parts of the basin where the value of the index implies a zero soil saturation deficit at the considered time). b) Schematic representation of the model used to simulate the behavior of each topographic index class.

The distribution function $f(c)$ does not necessarily have any particular hydrological justification other than that it allows the heterogeneity of the medium to be taken into account. The shape of this function is in fact often selected so that the model can be solved analytically.

For the PDM, ARNO and VIC models, for example, the Pareto distribution is used in a cumulative form expressed as follows:

$$F(c) = 1 - \left(1 - \left(\frac{c}{c_{max}} \right) \right)^a \tag{4.34}$$

where $F(c)$, the cumulative distribution function of the function $f(c)$, represents the fraction of the basin area in which the infiltration capacity is less than c, c_{max} is the maximum value of the storage capacity over the basin and a is a shape parameter. This distribution makes it possible to establish an analytical relationship at the scale of the drainage basin between the average instantaneous sub-surface storage, average instantaneous net rainfall and average instantaneous infiltrated rainfall. The simulation therefore does not have to be carried out for different increments of the distribution $f(c)$. Models of this type are in fact similar to global models. The parameters c_{max} and a of the function $F(c)$ must be calibrated.

A statistical distribution function can also be used to describe the spatial variability of the infiltration capacity. The distributed description of the infiltration capacity combined with the distributed description of the storage capacity has been proposed in an extension of the VIC model (Liang and Xie, 2001).

The main advantage of these distributed models is their parsimony in terms of calculations. In addition, they make it possible to consider some of the heterogeneity of the behavior within a given hydrological unit. They are therefore widely used for grid-based parameterizations in surface schemes of atmospheric or climatic models.

4.5 ESTIMATION OF DESIGN NET RAINFALL

By definition, the volume of precipitation (V_R) that flows directly on the surface of the terrain during a rainfall event is equal to the net rainfall (P_n). The estimation of the net rainfall hyetograph resulting from a given event has long been and still is a major concern of hydrologists. The objective is to determine both the fraction of the design precipitation that produces fast runoff and its temporal structure in order to subsequently estimate the resulting design flood.

This estimation can be made by combining several of the simulation models presented in the previous sections. The difficulty lies in the estimation of the parameters and initial conditions (i.e., initial storage volumes in the different reservoirs of the combined model).

Very simplified approaches developed for event-based simulations and engineering needs are frequently adopted. They are based on the estimation of rainfall losses. Two types of losses are considered: initial and continuous losses. Both these losses are estimated globally, in a manner that may be more or less empirical depending on the case, on a unit of area that can be from a parcel of land up to the entire drainage basin. A number of factors that can be used to assess the various approaches proposed for these estimations are indicated in Appendix 4.8.4.

4.5.1 Initial Losses

To estimate a design net rainfall, interception losses are often combined with depression storage losses in a unique term referred to as "initial losses" or "initial abstraction". These initial losses correspond in fact to the sum of storage losses ΔS_I and ΔS_D found in the equation of the hydrological balance of the basin (Section 4.1.2). In the context of this analysis, it is not necessary to know the origins of these losses. The corresponding quantities are however generally non-negligible and can be considered as rainfall losses with respect to runoff.

In practice, it is commonly accepted that the initial losses, generally designated I_a ("a" for abstraction) affect only the beginning of a rainfall event. They must be satisfied before runoff can take place. In other words, until the total precipitation that has fallen since the beginning of the event is equal to these losses, the net rainfall is assumed to be zero. The initial losses are therefore subtracted from the first increments of the hyetograph of total rainfall.

The value of I_a is generally estimated from values found in the literature. It is sometimes obtained in an empirical manner by calibration on various observed rainfall-runoff events. The choice of the value of these losses must always take into account the context of the study, in particular the antecedent soil moisture conditions prevailing on the studied basin. If the soil is already saturated by antecedant precipitation, the initial losses are practically zero. Other considerations must be taken into account such as the nature of the soils and vegetal cover (e.g., rural or urban drainage basin), the slope of the basin, the season and the return period of the design rainfall. There is no proven method for the determination of initial losses except possibly for the so-called global method presented in section 4.5.2. As a general indication, initial losses are often taken to be 10 to 20% of total rainfall for a forest or 2 to 5 mm for an urban drainage basin.

4.5.2 Continuous Losses

Continuous losses include those related to evaporation and infiltration. When the objective of the study is to estimate a design flood, evaporation from free surface water stored in the SVA interface and evapotranspiration from the vegetal cover are generally neglected. Only infiltration losses are therefore generally estimated in this context.

Methods based on Hortonian processes

These methods, based on an infiltration capacity decay function, have already been presented in Section 4.4.2 for the estimation of the infiltration rate of a land parcel. They are still often used to estimate rainfall excess at the basin scale. They are based on the assumption that surface runoff is produced by an exclusively Hortonian process that can be modeled by a unique infiltration function that is representative of all parts of the basin. Note that this assumption is generally not valid (Appendix 4.8.4).

Methods deduced from the runoff coefficient

When the runoff coefficient of the drainage basin can be estimated elsewhere, the net rainfall hyetograph can be estimated on the basis of the value of this coefficient (Figure 4.16). For this, it is necessary to estimate the way that the rainfall losses (i.e., initial losses
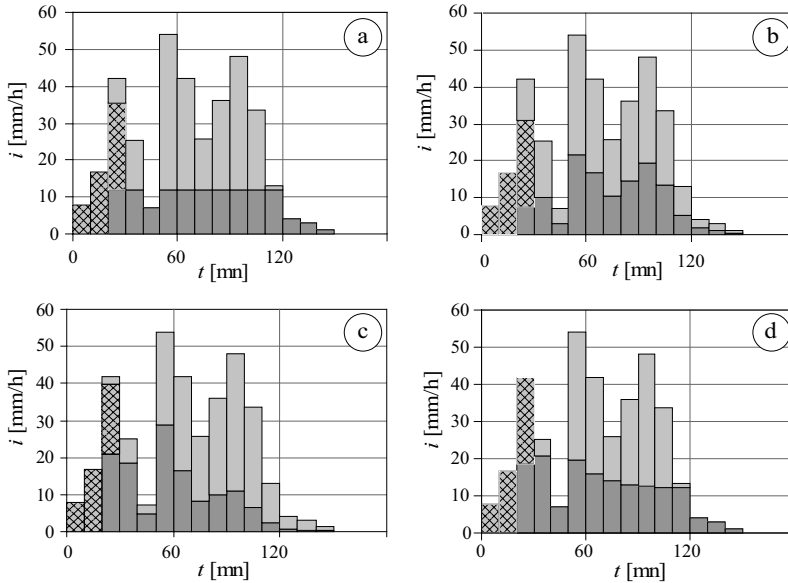
Fig. 4.16: Different possible schemes to estimate the temporal distribution of initial losses and continuous losses by infiltration (cross-hatched zones = initial losses; light gray= net rainfall; dark gray = infiltrated rainfall). The runoff coefficient of the basin as well as the initial losses are the same for all four schemes. a) φ index method with initial losses. b) W index method with initial losses. c) SCS-CN method (Appendix 4.8.3 and Example 4.4). d) Modified Horton method (IEM described in Section 4.4.2).

I_a and infiltration losses F) are distributed with time. These losses are defined using the hydrological balance at the scale of the drainage basin as follows:

$$F + I_a = P - P_n = P \cdot (1 - C_r) \tag{4.35}$$

where P and P_n are the depths of total and net rainfall respectively, C_r is the considered runoff coefficient, F is the depth of infiltrated rainfall from the event and I_a represents the initial losses (Section 4.5.1).

One method widely used to calculate F is the so-called constant continuous losses or φ index method in which the infiltration capacity is assumed to be constant with time, equal by definition to φ. In another method referred to as the W index method (introduced by the Institute of Hydrology, Wallingford, UK), the amount of infiltrated rainfall and consequently the net rainfall is assumed to be proportional to the total rainfall for each time step. The φ index, as for the W index, is estimated in such a way that the depth of the net rainfall corresponds to the selected runoff coefficient C_r. For example, the value of the φ index is determined by successive iterations with adjustment of φ and the number M of time intervals Δt such that the net rainfall is equal to the runoff R. This can be expressed as follows:

$$R = \sum_{k=1}^{M} (i_{n,k}) \cdot \Delta t \ \text{ with } \begin{cases} i_{n,k} = i_k & \text{if } \ i > \phi \\ i_{n,k} = 0 & \text{if not} \end{cases} \tag{4.36}$$

where $i_{n,k}$, and i_k are respectively the net and gross rainfall [mm] falling on the kth time step Δt.

To apply these two methods, the initial losses are often considered to be negligible compared to infiltration losses. This is a reasonable assumption for very large rainfalls. If this is not the case, initial losses are subtracted from the gross rainfall at the beginning of the event. The φ or W indices are adjusted appropriately.

SCS-CN method

Introduced around 1950, the so-called SCS-CN method of the US Soil Conservation Service (USDA-SCS, 1972) is the fruit of more than 20 years of analyses of rainfall-runoff relationships on small rural drainage basins. The main assumption of this method is that, for a given rainfall-runoff event, the ratio of the actual runoff (V_R) to the actual infiltration losses (F) is equal to the ratio of the potential maximum runoff to the maximum possible infiltration losses (F_{max}) for initially saturated conditions on the considered basin. Moreover, the potential maximum runoff for the considered event is assumed to be equal to the gross rainfall P_g, i.e., the total rainfall P minus the initial losses I_a. This is expressed by the following equation:

$$\frac{V_R}{F} = \frac{P_g}{F_{max}} = \frac{P - I_a}{F_{max}} \tag{4.37}$$

Many observations carried out by the SCS have made it possible to relate the initial losses I_a to the infiltration potential F_{max} and subsequently relate this infiltration potential to the soil moisture conditions prevailing on the basin at the beginning of the event. This second relationship involves a dimensionless number with a value between 40 and 100, referred to as the Curve Number (CN). This number is provided in tables for different types of land use. The surface runoff increases with the Curve Number. For CN = 100, net rainfall equals the gross rainfall (Figure 4.17).

Note that this method makes it possible to express the variation of infiltration rate with time using a decay function and consequently the net rainfall hyetograph. This method is demonstrated in Example 4.4 and presented in detail in Appendix 4.8.3.
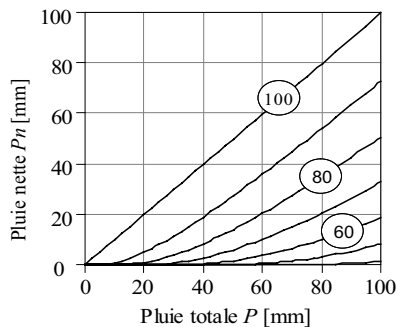

Fig. 4.17: Net rainfall depths obtained using the SCS-CN method versus total rainfall depths for different values of CN.

Example 4.4

A drainage basin with an area of 34.5 ha includes 25.5 ha in a commercial zone and 10 ha of open space (soil type B with 60% grass cover). For a rainfall with a hyetograph corresponding to the data in Table 4.7, the objective is to use the SCS-CN method for normal antecedent soil moisture conditions in order to estimate the direct runoff volume. Initial losses are assumed to be equal to 20% of the potential maximum infiltration losses.

The first step is to determine a Curve Number (CN) that is representative of the studied basin. A widely used approach is to calculate an average CN weighted by the different areas. From Table 4.8 of Appendix 4.8.3, CN(open spaces) = 69 and CN(commercial) = 95, giving CN(weighted average) = 87.5. For normal antecedent soil moisture conditions, the potential maximum losses by infiltration are therefore:

$$F_{max} = 25400/CN - 254 = 25400/87.5 - 254 = 36.5 \text{ mm.}$$

Knowing F_{max} and I_a ($= 0.2\ F_{max}$, $= 7.26$ mm), it is possible to calculate the cumulative infiltration F for each time step from the cumulative gross rainfall P_g. As long as the cumulative sum of initial losses has not been reached, there is no infiltration. Once this value has been reached (at the third rainfall increment), F is obtained using equation 4.51 of Appendix 4.8.3. The net cumulative rainfall is obtained by subtracting the initial cumulative losses and cumulative infiltration from the cumulative gross rainfall, giving the net rainfall increments (in mm/h).

Table 4.7 shows the results of this calculation. The temporal evolution of initial losses, continuous losses and net rainfall is represented in Figure 4.16c.

Table 4.7: Total rainfall, initial losses, infiltration and net rainfall.

Time [min]	Total rainfall [mm/h]	Cumulative rainfall P [mm]	Cumulative initial losses [mm]	Cumulative infiltration [mm]	Cumulative net rainfall [mm]	Net rainfall [mm/h]
0–10	7.8	1.3	1.3	0.0	0.0	0
10–20	16.8	4.1	4.1	0.0	0.0	0
20–30	42	11.1	7.3	3.5	0.4	2.2
30–40	25.2	15.3	7.3	6.6	1.5	6.5
40–50	7.2	16.5	7.3	7.4	1.9	2.5
50–60	54	25.5	7.3	12.1	6.1	25.4
60–70	42	32.5	7.3	14.9	10.4	25.5
70–80	25.8	36.8	7.3	16.3	13.3	17.4
80–90	36	42.8	7.3	18.0	17.6	26.0
90–100	48	50.8	7.3	19.8	23.8	37.0
100–110	33.6	56.4	7.3	20.9	28.3	27.1
110–120	13.2	58.6	7.3	21.3	30.1	10.9
120–130	4.2	59.3	7.3	21.4	30.7	3.5
130–140	3	59.8	7.3	21.5	31.1	2.5
140–150	1.2	60	7.3	21.5	31.2	1.0
150–160	0	60	7.3	21.5	31.2	0.0

4.6 CHOOSING AN ESTIMATION METHOD

Many models can be used to simulate the various processes related to the production of rainfall excess at the scale of a drainage basin. Selection criteria for choosing the right method for a given case are too numerous to be mentioned exhaustively here. It is however possible to provide a few helpful guidelines.

4.6.1 The Necessity of a Coupled Model

As emphasized throughout this chapter, the processes involved in the hydrological balance at the SVA interface (i.e., interception, evapotranspiration, infiltration) are highly interdependent. Consequently, to model the distribution of the different water fluxes at this interface, it is generally necessary to consider these processes in a combined manner.

A typical combined approach is that of the so-called Soil-Vegetation-Atmosphere Transfer (SVAT) models. These models, also referred to as surface schemes, model all the energy (Addendum 4.2) and mass exchanges at the SVA interface in a coupled manner (e.g., Olioso *et al.*, 1999). For this, the upper soil layers and surface strata—including vegetation if present—are divided into different horizontal layers for which inflows and losses generally correspond to the processes described by a physically-based behavior model (Figure 4.18).

SVAT models require characterization of conditions related to the state of the soil (e.g., temperature and humidity), plants (e.g., photosynthesis, chlorophyll content, leaf temperature, leaf area, phenology) and the atmosphere (e.g., air temperature, air relative humidity, net radiation, wind speed). A great deal of work has been focused on these models since the end of the 20th century.[8] They were initially developed for problems related to crop growth (e.g., SiSPAT model; Braud *et al.*, 1995) or to provide the boundary conditions for atmospheric and climate models (CLASS model, Verseghy, 1991, Verseghy *et al.*, 1993; BATS model, Gao *et al.*, 1996; ISBA model, Manzi and Planton, 1994; SiB2 model, Sellers *et al.*, 1996).

The description provided by surface schemes is generally one-dimensional. It neglects lateral advection in the atmosphere and soil. The way in which these schemes consider runoff production is often too simplistic for most hydrological applications. For this reason, they are rarely used in hydrology (for an example of the hydrological application, see for instance the VIC model; Lohman *et al.*,1998).

To estimate the distribution of water fluxes at the SVA interface at the scale of a drainage basin, most hydrological approaches also model the different processes in a coupled manner by combining interception, evapotranspiration and infiltration models (plus a depression storage model if necessary). The sub-models used are however simplified models such as those presented in the previous sections. The typical rainfall excess scheme used in hydrological models is based on a combination of reservoirs (Figure 4.19): a surface reservoir to estimate interception and one or more root zone or sub-surface reservoirs.

---

[8]The Penman-Monteith (1965) equation, explicitly involving parameters related to the vegetation characteristics, can be considered to be the first attempt to develop a schematic representation of the soil-vegetation-atmosphere transfers and remains the simplest SVAT model to implement.
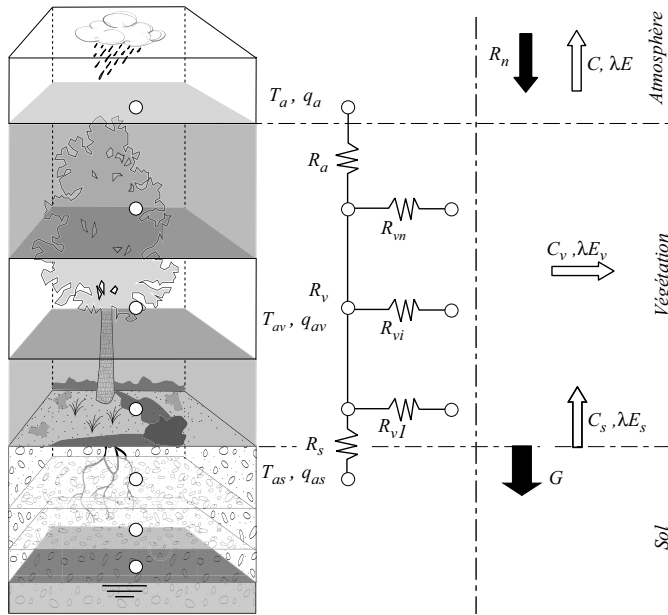
Fig. 4.18: Typical multilayer structure of an SVAT model along with associated parameters and energy fluxes. *n* compartments are used to describe the atmospheric boundary layer and in particular the vegetal cover and *m* compartments to describe the soils and sub-soils. R_n is net radiation, G the heat flux entering the soil, C and λE are respectively the sensible and latent heat fluxes, R_a, R_v and R_s are the resistances related to the atmosphere, vegetation and soil, T is temperature and q is humidity. Indices *s*, *v* and *a* designate respectively the soil, vegetation and atmosphere (*av* is the atmosphere within the vegetation).
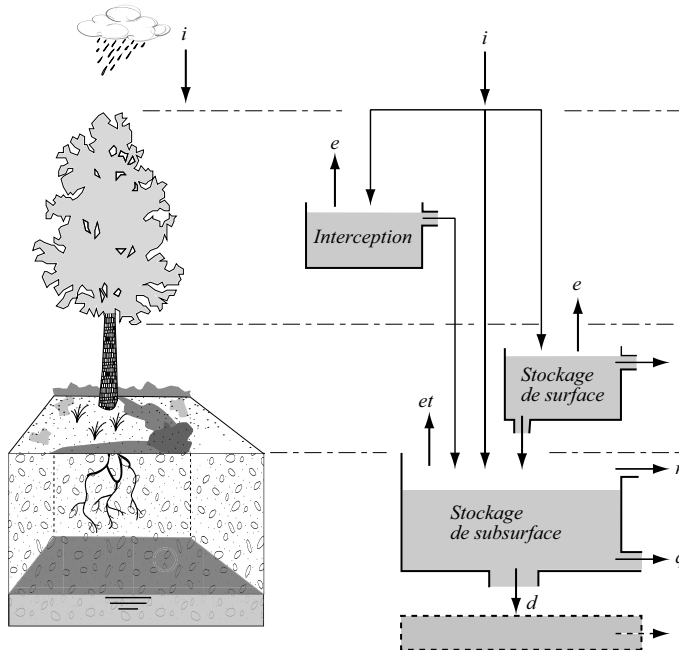

Fig. 4.19: Possible structure of the rainfall excess module of a hydrological model of a drainage basin.

The latter are used in particular to calculate the soil saturation level versus time, necessary for the estimation of net rainfall, evapotranspiration and sub-surface fluxes (lateral fluxes, percolation).

4.6.2 The Interest of Continuous Simulation Approaches

The distribution of fluxes at the SVA interface depend on the state of saturation of the system. The state is determined in particular by the water volume stored in surface depressions and the vegetal cover and by the extension of saturated zones and the moisture profile of unsaturated soils.

For the determination of a design net rainfall, the distribution of fluxes is generally estimated for typical saturation conditions. In most other cases, this approach is unsuitable. For hydrological forecasting or a posteriori simulation of past events, for example, saturation conditions must be estimated to represent as accurately as possible those prevailing on the basin for the considered hydrological event.

The initial saturation conditions of the basin have often been estimated in a simplified manner on the basis of an antecedent precipitation index, calculated on the basis of past precipitation. Various expressions have been proposed to account for the history of antecedent precipitation, in particular to estimate the current saturation conditions of the medium. One index often used is defined as follows:

$$API_i = \alpha \cdot API_{i-1} + P_{i-1} \tag{4.38}$$

where API_i is the antecedent precipitation index at time step i, API_{i-1} the index at the previous time step, P_{i-1} the total precipitation at the previous time step and α a constant that depends on the response time of the basin and the considered time step (Musy and Higy, 2011). Note that the expression for the *API* is very similar to the recurrent expression of the linear reservoir model often used to model the draining of sub-surface water (Chapter 5). Consequently, the coefficient α is naturally similar to the parameter of this model, i.e., $\alpha = \exp(-\Delta t/K)$, where Δt is the time step for which precipitation data are available and K the time constant of the sub-surface reservoir. For basins with time constants between 100 and 600 hours, α varies from 0.75 to 0.95 for a daily time step and from 0.99 to 0.998 for an hourly time step.

It is often difficult to identify a clear and robust dependency relationship between an antecedent precipitation index such as the one mentioned above in the real saturation conditions of the system (Peugeot *et al*., 2003). This is partly related to the fact that the index is calculated on the basis of total rainfall and not the rainfall that actually participated in saturating the medium (e.g., intercepted rainfall, infiltered rainfall). This approach is consequently seldom used.

To obtain the necessary saturation conditions, a better approach now widely used consists in continuously simulating, with a selected hydrological model, the temporal (and often spatial) evolution of liquid and solid water volumes stored in the different compartments of the SVA interface.

In this regard, it is important to remember that although evaporation fluxes are negligible at the scale of a given rainfall-runoff event, they represent a non-negligible part of the inter-event hydrological balance. The quality of estimates of these fluxes between rainfall events therefore strongly affects the quality of estimates of the basin

water reserves and therefore the forecasted or simulated discharges. Continuous simulation approaches are of course also used to simulate the discharges produced by a basin over long periods, for instance to characterize the hydrological regime. The quality of estimates of evaporation fluxes between rainfall events strongly conditions the quality of simulated discharges both between rainfalls and during floods. In particular, if the evaporation fluxes are underestimated between two rainfall events, the model compartments used to simulate the degree of saturation of the basin—and the root zone in particular – will be drained too slowly. Consequently, the rainfall excess of the drainage basin will probably be overestimated for the second rainfall event and vice versa.

4.6.3 Model Consistency with Respect to the Processes Involved

The consistency of the model with respect to the main processes involved in the production of rainfall excess on the basin is also an important criterion to be considered when choosing a model. For the infiltration process, for example, it is in particular necessary to identify whether the generation processes are mainly related to infiltration excess and/or the presence of saturated zones.

One of the first elements to be considered is the nature and depth of the soils and sub-soils. Hortonian runoff is typically produced on soils with very low permeability. Over and above the special case of urban basins, which are highly impervious, these conditions are found for example in clayey and marly soils. Hortonian runoff can also be produced on crusted soils[9] or soils that have been compacted by certain agricultural practices (e.g., frequent passage of tractors, high concentration of livestock). On the other hand, for soils with high infiltration capacities (e.g., sandy substrates), the majority of precipitation will infiltrate in drainage basins and supply the underlying water table which can then produce saturated zones at outcrops or at the bottom of thalwegs. The presence of an impervious layer near the surface also favors the creation of saturated zones.

The density of vegetal cover also affects the type of rainfall excess production. Dense vegetal cover generally reduces the risk of surface crusting. Furthermore, it increases the time required for runoff to reach the basin outlet. Consequently, even if runoff is initially produced by a Hortonian process, its prolonged presence at the surface of the basin will favor re-infiltration and the main process producing rainfall excess can in the end be mainly related to basin saturation.

Another key factor that must be considered is the precipitation regime to which the basin is subjected. A model simulating a Hewlettian process is a priori not suited to contexts involving infrequent but very intense rainfalls (e.g., Sahel regions). In such situations, runoff is produced more by excess with respect to the infiltration capacity of the soils (even if the infiltration capacity is non-negligible) than by saturation of the medium. A Hewlettian type model should however be well-suited to regions subject to frequent rainfalls of low intensities (e.g., Great Britain). Conversely, a model simulating Hortonian production process should be better for regions with infrequent but intense rainfalls and ill-suited to regions with frequent low-intensity rainfalls.

---

[9]Crusting is the result of the gradual closing of pores by the spatial redistribution of surface particles moved by the kinetic energy of raindrops. This phenomenon is for example often observed in Sahel regions on lateritic soils with sparse vegetation and exposed to very intense precipitation.

Note that most drainage basins are exposed to different rainfall contexts at different times of the year. In Europe, for example, drainage basins are affected mainly by Hortonian processes in summer and Hewlettian processes in winter (Section 4.1.2). Consequently, it is often necessary to use a model capable of reproducing these two types of processes in a combined manner.

4.6.4 Taking into Account the Spatial Heterogeneity of the Processes

Ideally, the flux distribution model should be able to take into account the high spatial heterogeneity of the processes. Note that a model that is appropriate to represent a given process locally is generally not appropriate when the same process is considered at the scale of a hillslope or drainage basin. This has already been illustrated for the infiltration process which is highly non-linear at the scale of a drainage basin as a result of the heterogeneity of the medium (Section 4.4.1). All the processes involved in the distribution of fluxes at the SVA interface present this type of non-linearity when they are no longer considered locally. This is the case, for example, of processes partly governed by a threshold (e.g., canopy storage capacity excess for the interception process).

The spatial heterogeneity of the interception process and evaporation fluxes depends on the type of vegetal cover and the evaporative demand of the atmosphere. It is therefore possible to estimate the potential evapotranspiration rate for the main types of vegetation present in the basin, most often based on an estimate of a reference evapotranspiration ET_0 and an appropriate crop/vegetation coefficient (Section 4.3.3). Depending on the type of analysis or hydrological model, the resulting evapotranspiration series can be either: 1) combined to obtain a series of average potential evapotranspiration values or 2) considered separately. The combined approach is the most widely used, in particular when the basin is modeled globally. It however assumes a linear behavior of the basin response with respect to the infiltration and evaporation processes, which is generally not the case. The second approach is often adopted when a spatialized (e.g., arbitrary regular grid) or semi-spatialized (e.g., independent sub-basins or homogeneous hydrological units) basin description is used. This makes it possible to consider the spatial variability of other factors (e.g., depth of the root zone, availability of water) that determine the actual evaporation rate. In practice, non-linearities, and therefore heterogeneity, related to interception and evaporation processes are seldom taken into account, in particular in global hydrological approaches.

On the other hand, the spatial heterogeneity of processes related to infiltration, the main source of non-linearity with respect to rainfall excess production on the basin, must be considered. In particular, the infiltration model should be able to simulate the variability of infiltration modes. This variability can be high given: 1) the spatial variability of the hydrodynamic characteristics of the soils and 2) the processes involved in the spatial redistribution of water at the surface (re-infiltration) and sub-surface (saturation, exfiltration). The redistribution of water is difficult to simulate except with physically-based spatialized models, however such models are generally too demanding for simple operational use.

The spatial heterogeneity of the medium can be more easily taken into account using distributed approaches or indirectly using certain non-linear global approaches. The possibility offered by a model to take into account the spatial variability of precipitation

can therefore be another model selection criterion. This is particular the case when rainfall excess processes are essentially Hortonian because the basin response to rainfall events is highly non-linear in this context (Koren *et al*., 1999; Vischel, 2006). As opposed to spatialized or semi-spatialized approaches, the global or distributed approaches presented in this chapter are not generally capable of considering the effect of the spatial heterogeneity of precipitation on rainfall excess at the scale of a drainage basin.

4.6.5 Advantages of Simple Approaches

Physically-based methods generally have a wider field of application than conceptual or empirical models. This explains for example the success of the Penman-Monteith formulation, considered by many hydrologists to be the most physically appropriate for the estimation of fluxes related to evapotranspiration. However, the factors intervening in these formulations can vary greatly within a given drainage basin and it is generally impossible for models to take this variability into account. Generally speaking, processes related to rainfall excess on drainage basins are highly complex and exhibit high spatial variability. This complexity is virtually impossible to describe or at best can only be described in a very partial manner. Consequently, physically-based models do not necessarily give better simulations in terms of discharges than simple empirical or conceptual approaches.[10]

When choosing a model, one key factor to be considered is obviously the availability of the necessary data for the meteorological variables of the model and the possibility of spatializing them over the entire basin. Another important selection criterion is the number of parameters in the model and the possibility of estimating them simply by calibration or on the basis of regional models (e.g., tables, pedotransfer functions).

For common hydrological applications, note that the final objective of modeling is generally to simulate the discharges at the basin outlet. However, these discharges, when observed, often constitute the only data that can be used to calibrate the model parameters. In other words, it is nearly impossible to independently estimate the parameters of interception, infiltration and evaporation models, especially when they must be estimated in a differentiated manner for different hydrological units of the considered basin. The uncertainty of parameter estimates increases with the number of parameters and with the generally high uncertainty of the input variables. For this reason, hydrologists most often prefer the simplest models involving few parameters (Chapter 3).

4.7 KEY POINTS OF THE CHAPTER

• The distribution of fluxes at the soil-vegetation-atmosphere (SVA) interface determines the water balance at the scale of a land parcel or the hydrological balance at the scale of a drainage basin. It influences in particular groundwater recharge and discharges in the hydrographic network during flood and low-flow periods.

• At the scale of a drainage basin, the distribution of fluxes is complex given the spatial variability of the meteorological forcings and the spatial heterogeneity of the

---

[10]Concerning the estimation of reference evapotranspiration, for example, a study by Oudin *et al.* (2005) carried out on a sample of 308 basins in Australia, France and North America suggests that the simplest methods based on extraterrestrial radiation and daily mean air temperature offer equivalent performance, in terms of the quality of simulated discharges, to that of more complex formulations such as that of Penman and other derived equations.

characteristics of the medium and the processes driving the spatial redistribution of surface and sub-surface water.

- Some of the precipitation intercepted by the vegetal cover produces delayed precipitation while the rest is returned to the atmosphere by evaporation. Evaporation of intercepted precipitation can represent a significant part of the annual hydrological balance.

- Some of the water stored in surface depressions produces delayed infiltration in the soil. Depression storage and interception by vegetation represents non-negligible initial losses with respect to fast runoff.

- Evaporation fluxes (evaporation from free water surfaces and evapotranspiration), although generally neglected at the rainfall-runoff event scale, cannot be neglected between events. They determine the state of the sub-surface water reserves and in particular the initial saturation of the basin for floods.

- Surface runoff can be produced by infiltration excess on unsaturated soils (Hortonian process) or by the blocking of infiltration in soil saturated from the bottom up (Hewlettian process).

- The production of rainfall excess can be either mainly Hortonian or on the contrary mainly Hewlettian for certain specific hydro-meteorological contexts. However, in most cases, both types of processes are present on a given basin.

- The high spatial and temporal variability of the processes involved makes the hydrological behavior of drainage basins with respect to the transformation of total rainfall to net rainfall highly non-linear.

- The distribution of the fluxes at the SVA interface is necessarily simulated by coupled approaches combining models representing the interception, depression storage, evapotranspiration and infiltration processes.

- Operational modeling of the processes related to the production of rainfall excess is carried out using simple conceptual models. The typical structure combines a surface reservoir to estimate interception and one or more root zone or sub-surface surface reservoirs to estimate the soil saturation level over time. The root zone and/or sub-surface reservoirs are necessary to estimate net rainfall, evapotranspiration and sub-surface fluxes.

- In distributed models, the spatial variability of the production of rainfall excess is often taken into account by: 1) modeling different homogeneous hydrological units considered to be representative of the basin or 2) a distribution function for the key characteristic of the drainage basin with regard to the production of rainfall excess (e.g., local storage capacity).

- Global models often offer similar performance to that of more sophisticated models.

- The basin rainfall excess production function depends greatly on the initial saturation state of the basin. The state is generally estimated by continuous simulation.

- The parameters of the flux distribution model are generally estimated at the same time as the other parameters of the complete hydrological model in order to reconstitute the discharges observed at the basin outlet as accurately as possible.

- A design net rainfall can be determined using very simplified approaches capable of estimating initial losses and continuous losses by infiltration for typical basin saturation conditions.

4.8 APPENDICES

4.8.1 Rutter Model

Rutter *et al*. (1972, 1975, 1977) were the first to move away from a purely empirical approach for interception modeling. They developed a reservoir-type conceptual model based on the balance of water fluxes at the surface of the leaves and branches of the canopy and the tree trunks (Figure 4.4). This model has served as a basis for many other analytical or semi-analytical models (Gash, 1979; Liu, 1997; Gash *et al*., 1995). A fraction p of the total rainfall P [mm/h] passes through the canopy and reaches the ground without any interception. The remaining fraction (1-p) falls on the canopy and can be temporarily stored, evaporated into the atmosphere or drained to the ground. Part of the intercepted precipitation is intercepted by branches and trunks (fraction p_t of the total precipitation). The other part is intercepted by leaves (fraction 1-p_t-p). The change in water storage on leaves with time $S(t)$ can be estimated using the following continuity equation:

$$\frac{dS_I(t)}{dt} = (1 - p - p_t) \cdot P(t) - E(t) - D(t) \tag{4.39}$$

where $S_I(t)$ is the quantity of water stored on the leaves [mm], $P(t)$ the precipitation intensity at the top of the vegetation [mm/h], $E(t)$ the intercepted precipitation returned to the atmosphere by evaporation [mm/h] and $D(t)$ the intercepted precipitation that drips through the canopy to the ground [mm/h]. All these variables are expressed in units that are divided by the total area of the considered basin.

When the water stored in leaves $S_I(t)$ reaches the maximum storage capacity of the leaves S_{Imax}, evaporation E from the vegetal cover takes place at a rate equal to the evaporative capacity $E_0(t)$. If not, the evaporation rate is reduced proportionally:

$$E(t) = \frac{S_I(t)}{S_{Imax}} E_0(t) \tag{4.40}$$

The Penman equation (Appendix 4.8.2) is well-suited to estimating the evaporative capacity because evaporation takes place in this case from the leaves and the stomata are not involved (this is equivalent to a zero canopy resistance in the Penman-Monteith equation).

Canopy dripping D varies depending on the phase of the interception process. It is assumed to be zero when $S_I(t)<S_{Imax}$ (although this assumption is a frequent source of criticism of the model). If $S_I(t)>S_{Imax}$, canopy dripping can be calculated by the following empirical relationship:

$$D(t) = D_s \, \exp\big(b\big(S_I(t) - S_{Imax}\big)\big) \tag{4.41}$$

where D_s and b are empirical constants derived from observations. Other dripping functions have been developed (e.g., Massman, 1983).

The system composed of trunks and branches can be modeled in the same way (Figure 4.4), the "trunk" reservoir being filled by the rainfall fraction $p_t P(t)$. When the reservoir is full (i.e., when the water stored $S_{It}(t)$ reaches the maximum storage capacity of the trunk system S_{Imaxt}), it empties by evaporation at a rate equal to the evaporative capacity $E_{0t}(t)$. If not, the evaporation losses are once again reduced proportionally:

$$E_t(t) = \frac{S_{It}(t)}{S_{Imaxt}} E_{0t}(t) \tag{4.42}$$

Moreover, the evaporative capacity for the trunks $E_{0t}(t)$ is assumed to be a linear function of the evaporative capacity of the canopy $E_0(t)$. As opposed to dripping from the canopy, excess water in the trunk reservoir is considered to flow instantaneously towards the ground. To simplify the

canopy dripping model, Valente *et al*. (1997) considered that excess water in the canopy reservoir was drained immediately. This implies that dripping stops when precipitation stops.

The key parameters of this model are, a priori, the fraction of the surface covered by vegetation (1-*p*) and the total maximum storage capacity (S_{Imax} + S_{Imaxt}). The first determines the part of the precipitation that reaches the ground directly and the second determines mainly the amount that is evaporated, in particular when the system is very wet.

In all, the Rutter model requires values for 6 characteristics of the vegetation structure (S_{Imax}, S_{Imaxt}, *p*, p_t, *b*, D_s) that can be obtained indirectly through field studies. The value of the maximum storage capacity of the canopy S_{Imax} is for example a generally obtained by statistical regression between measured interception *I* and total rainfall *P* for individual rainfall events with intensities exceeding the storage capacity (e.g., Gash and Morton, 1978; Klaassen, 1998). An alternative approach is to describe the canopy structure using standard density indices such as the leaf area index (LAI). The storage capacity of the canopy can then be calculated by a linear relationship with the LAI (van Dijk and Bruijnzee, 2001).

The Rutter model and its derivatives give good results for different types of vegetal cover and are generally used in forest ecology and agronomy. However, given their complexity and the large quantity of data required to estimate or calibrate the different parameters, such models are difficult to apply from a strictly operational viewpoint. Furthermore, the choice of a value for a given parameter based on literature data is difficult given the diversity of results that can be found for a given type of vegetal cover (see Deguchi *et al*. (2006) for a review of parameters estimated in many studies carried out around the world). On the other hand, simplified reservoir models based on the concepts already presented are often integrated in process-oriented hydrological models of the Mike SHE type (Refsgaard and Storm, 1995) or in surface-based schemes (SVAT type models, see Section 4.6.1).

4.8.2 Penman and Penman-Monteith Equations

Penman equation

The equation proposed by Penman (1948, 1963) to estimate evaporation (in mm/s) from an open water surface can be expressed as follows:

$$E = \frac{1}{\lambda} \cdot \frac{\Delta\left(R_n - G\right) + \gamma \cdot \left(e_s - e_a\right) \cdot W}{\left[\Delta + \gamma\right]} \text{ with: } W = 0.26 \cdot \left(1 + 0.54 \cdot u_2\right) \tag{4.43}$$

The way to estimate the different terms of this equation is discussed below. Valiantzas (2006) has proposed a simplified formulation of this equation that limits the explanatory variables to air temperature, solar radiation and extraterrestrial radiation, making it possible to estimate the evaporation rate even without wind data.

Penman-Monteith equation

The Penman-Monteith equation used to estimate (in mm/s) actual or potential evapotranspiration (*PET*) from a given vegetal cover or reference evapotranspiration ET_0 (for a specific grass) can be expressed as follows:

$$ET = \frac{1}{\lambda} \cdot \frac{\Delta\left(R_n - G\right) + \gamma \cdot \left(e_s - e_a\right) \cdot W}{\left[\Delta + \gamma\left(1 + r_c / r_a\right)\right]} \text{ with } W = \frac{\rho \cdot c_p}{\gamma \cdot r_a} \tag{4.44}$$

The Penman and Penman-Monteith formulations have a similar form. The difference lies in: 1) the expression of the *W* term in the numerator that involves the aerodynamic resistance r_a for the Penman-Monteith equation and 2) the presence of a ratio of surface resistance to aerodynamic resistance r_c/r_a in the denominator. The Penman-Monteith equation can be used to estimate evaporation

of water intercepted by the vegetal cover. In this case, the surface resistance of vegetal cover r_c is considered to be zero.

Associated terms: definitions and estimation for standard conditions

The different terms appearing in the two above expressions are defined as follows for standard conditions:

Δ the slope of the vapor pressure curve at air temperature, given by:

$$\Delta = \frac{4098 \cdot e_s(T)}{(T + 237.3)^2} \qquad [\text{kPa/°C}]$$

T daily mean air temperature   [°C]

R_n net radiation flux   [J/s/m²]

            (estimation of the different terms of net radiation is discussed in Appendix 2.7.5).

G heat flux transmitted to the soil   [J/s/m²]

            G is negligible if evapotranspiration is evaluated over a full day. For time steps of less than a day, G can be approximated as follows on the basis of net radiation R_n:

                       During the day: $G = 0.1\, R_n$
                       During the night: $G = 0.5\, R_n$

            More refined expressions have been proposed by the ASCE (1996).

ρ density of the air $\rho = 1.246$ [kg/m³]

c_p specific heat of the air $c_p = 1013$ [J/kg/°C]

e_s saturation vapor pressure at air temperature T, given by:

$$e_s(T) = 0.6108 \exp\left(\frac{17.27 \cdot T}{T + 237.3}\right) \qquad [\text{kPa}]$$

e_a the actual vapor pressure in the air, given by:

            $e_a = e_s R_H / 100$ [kPa]

R_H daily mean relative humidity of the air   [%]

r_a aerodynamic resistance, given by:

$$r_a = \frac{\ln\left(\dfrac{z_m - d}{z_{0m}}\right) \ln\left(\dfrac{z_h - d}{z_{0h}}\right)}{\kappa^2 \cdot u(z)} \qquad [\text{s/m}]$$

            where $u(z)$ [m/s] is the wind speed measured at height $z_m = 2\text{m}$, d [m] is the zero plane displacement height of the logarithmic relationship between wind speed and height (generally $d = 2/3 \cdot h$, h [m] being the height of the vegetation), z_{0m} [m] is the roughness length for momentum transfer, i.e., the height above d at which the actual wind speed is zero ($z_{0m} = 0.13 \cdot h$), z_h [m] is the height at which air humidity is measured, z_{0h} [m] is the roughness length of the vegetation for heat and vapor transfer ($= 0.1 \cdot z_{0m}$) and κ is the von Karmann constant ($= 0.41$).

u_2 wind speed 2 meters above the ground surface   [m/s]

r_c canopy resistance to vapor transfer, which must be calibrated on the basis of ET_0 values measured on grass.

λ latent heat of evaporation of water: $\lambda = 2477000$ [J/kg]

γ the psychometric constant: $\gamma = 0.0652$ [kPa/°C]

4.8.3 SCS-CN Method

The so-called SCS-CN method of the US Soil Conservation Service (USDA-SCS, 1972), assumes that the distribution of gross rainfall between runoff (V_R) and infiltration (F) must respect an equilibrium condition with respect to the associated potential maximum volumes (respectively the

gross rainfall P_g and the maximum possible losses by infiltration F_{max}). Considering that the actual runoff V_R is equal to the net rainfall P_n and expressing the actual losses by infiltration (F) on the basis of the hydrological balance for the considered event, this equilibrium, expressed by equation 4.37 in the main text, has the following form:

$$\frac{P_n}{P - I_a - P_n} = \frac{P - I_a}{F_{max}} \tag{4.45}$$

where I_a represents the initial losses or abstraction (interception and depression storage) and P is the total precipitation falling on the basin (all terms of the equation are expressed in mm). The expression for net rainfall P_n can be deduced from the previous expression as follows:

$$P_n = \frac{\left(P - I_a\right)^2}{P + F_{max} - I_a} \tag{4.46}$$

According to the work of the SCS, the initial abstraction I_a can be expressed as a function of potential maximum infiltration losses F_{max} using the following empirical relationship: $I_a = 0.2\, F_{max}$. The net rainfall can then be written:

$$P_n = \frac{\left(P - 0.2 \cdot F_{max}\right)^2}{P + 0.8 \cdot F_{max}} \quad \text{if} \quad P > 0.2\, F_{max} \tag{4.47}$$

$$P_n = 0 \qquad\qquad\qquad \text{if not}$$

The empirical relationship subsequently used to express the potential infiltration losses as a function of the antecedent soil moisture conditions involves a dimensionless parameter referred to as the Curve Number (CN) and can be written as follows:

$$F_{max} = \frac{25400}{CN} - 254 \tag{4.48}$$

where CN varies from 40 to 100 and F_{max} is in mm. CN is given in tables for so-called "average" Antecedent Moisture Conditions (AMC) and different types of land uses (Table 4.8). If a drainage basin is characterized by different soil types (associated with areas), it is possible to calculate an average value of CN weighted by the areas corresponding to each soil type. The CN for drying (CN_I) or wet (CN_{III}) AMCs can be estimated on the basis of the CN for average AMCs (CN_{II}) using the following expressions (Chin, 2000):

$$CN_I = \frac{4.2 \cdot CN_{II}}{10 - 0.058 \cdot CN_{II}} \tag{4.49}$$

$$CN_{III} = \frac{23 \cdot CN_{II}}{10 + 0.13 \cdot CN_{II}} \tag{4.50}$$

It is therefore possible to deduce the value of F_{max} and then P_n for a given AMC. AMCs are determined on the basis of an antecedent precipitation index. In its initial version, this index was the cumulative precipitation of the 5 previous days. In more recent versions, an Antecedent Precipitation Index (API) is used (Section 4.6.2).

It is also possible to establish an expression for the infiltration rate. By replacing the net rainfall term in equation 4.4.5 by its expression deduced from the hydrological balance of the basin ($P_n = P - I_a - F$), the expression for the infiltrated water depth since the beginning of the rainfall event (F) is

obtained, after a number of simplifications, as a function of the total precipitation depth (P) since the beginning of the event:

$$F = \frac{F_{max} \cdot (P - I_a)}{P - I_a + F_{max}} \tag{4.51}$$

The infiltration rate $f(t)$ is obtained by differentiating the above equation with respect to time t:

$$f(t) = \frac{dF(t)}{dt} = \frac{F_{max}^2}{\left(P(t) - I_a + F_{max}\right)^2} \cdot \frac{dP(t)}{dt} \tag{4.52}$$

where the exact derivative of $dP(t)/dt$ is none other than the intensity $i(t)$ of the total precipitation at time t.

Table 4.8: Values of the Curve Number (CN) of the so-called SCS-CN method for average antecedent soil moisture conditions (condition II) and I_a =0.2 F_{max} (adapted from ASCE, 1996; USDA-SCS, 1972).

Land use	Soil groups*			
	A	B	C	D
Agricultural land				
Crops in good condition	72	81	88	91
Crops in poor condition	62	71	78	81
Pasture, grassland or range				
Good condition	68	79	86	89
Poor condition	39	61	74	80
Meadow/brush	30	58	71	78
Woods				
Sparse forest cover	30	58	71	78
Dense forest cover	25	55	70	77
Open spaces, lawns, golf courses, cemeteries:				
- more than 75% grass cover	39	61	74	80
- 50 - 75 % grass cover	49	69	79	84
Commercial (85% impervious area)	89	92	94	95
Industrial (72% impervious area)	81	88	91	92
Residential:				
500 m² lots (65% average impervious area)	77	85	90	91
1000 m² lots (38% average impervious area)	61	75	83	87
1500 m² lots (30% average impervious area)	57	72	81	86
2000 m² lots (25% average impervious area)	54	70	80	85
4000 m² lots (20% average impervious area)	51	68	79	84

Table 4.8: contd....

Table 4.8: contd.

Land use	Soil groups*			
	A	B	C	D
Parking lots, roofs and paved surfaces	98	98	98	98
Streets and roads:				
Paved with curbs and storm sewers	98	98	98	98
Gravel	76	85	89	91
Surface in poor condition or dirt	71	82	87	89

Soil types are defined in the following manner:

Group A: Low runoff potential. Infiltration is high even when the soil is very wet. The soil is excessively well-drained with a high hydraulic conductivity.

Group B: Moderate infiltration rate when wet. The soil is well-drained with a wide grain size distribution from find course and the moderate hydraulic conductivity.

Group C: Low infiltration capacity when wet. The soil has a fine to very fine grain size distribution and the low hydraulic conductivity.

Group D: High runoff potential. Very low infiltration when the soil is wet. The soil is composed mainly of clay with a very low hydraulic conductivity.

4.8.4 Choosing a Method to Estimate Design Net Rainfall

For a given basin, the runoff coefficient generally increases with 1) the depth of total precipitation and 2) the initial basin saturation level. Moreover, rainfall losses generally increase with increasing rainfall duration and intensity. This is the case for initial losses (Sections 4.2.1 and 4.2.2) and for infiltration losses (Section 4.4.3). It interesting to look at the behavior of three types of global methods that can be used to estimate design net rainfall from these two viewpoints.

Rainfall excess versus total rainfall

Considering only one type of soil, Hortonian methods give infiltration losses that are independent of rainfall intensity. Conversely, the estimated net rainfall is a linear function of the total rainfall depth. The non-linearity of the basin rainfall excess with respect to total rainfall cannot in fact be reproduced using a single infiltration function of the Horton, Philip or Green and Ampt type. Unless the intensity of precipitation exceeds the infiltration capacity at every point of the basin, the only solution would be to consider the spatial variability of the medium explicitly, which is never done. The pertinence of the results coming from the application of this method should therefore be treated with caution.

Methods based on the runoff coefficient often use a typical coefficient estimated on the basis of the characteristics of the medium. With rare exceptions (mostly involving urban basins, see IEAust, 1987), the runoff coefficient does not depend on the precipitation depth. In particular, it does not tend towards 1 for extreme rainfalls. Conversely, infiltration losses are proportional (or nearly so if initial losses are considered) to the intensity and depth of total precipitation. They are not limited by the maximum storage capacity of the medium. The pertinence of the results obtained with this method is therefore also relative.

For the SCS-CN method, it is easy to demonstrate using the equations in Appendix 4.8.3 that the infiltration losses and runoff coefficient are both an increasing function of total rainfall depths. The infiltration losses tend towards the maximum possible infiltration losses (F_{max}) and the runoff

coefficient tends towards 1 for extreme total rainfall depths. From this point of view, this method is more satisfying than the other two described above.

Rainfall excess versus antecedent soil moisture conditions

For Hortonian methods, the values used for the model parameters, in particular for parameters influencing the initial infiltration capacity, are often the default values given in tables. They are often obtained experimentally at the scale of a land parcel by simulation on initially dry soil, i.e., soil moisture conditions that are generally different from those for which the estimation must be made.

Similarly, the runoff coefficient is given in tables for average antecedent moisture conditions. Runoff coefficients for other soil moisture conditions can be estimated when concomitant precipitation and discharge data are available for the basin of interest, thereby allowing a statistical analysis of the corresponding runoff coefficients.

For the SCS-CN method, curve number (*CN*) values have been tabulated for different configurations of antecedent moisture conditions including the following typical conditions: dry, average and wet (Appendix 4.8.3).

When looking at a particular hydro-meteorological configuration, it is not possible to use the above methods with typical parameters corresponding to standard initial saturation configurations. Adaptation of the initial conditions and corresponding parameters is necessary. This is however difficult task. For Hortonian methods, the initial infiltration capacity is sometimes estimated on the basis of an estimate of the saturation level of the drainage basin (Chahinian *et al*., 2005). Both the runoff coefficient and curve number (*CN*) are sometimes estimated empirically using an antecedent precipitation index related to the precipitation that has fallen over a certain period preceding the event.

CHAPTER 5

RAINFALL-RUNOFF ANALYSIS

Rainfall-runoff analysis is used to transform groundwater, sub-surface and surface water produced in the different parts of the drainage basin into a hydrograph at the basin outlet.

In the past, rainfall-runoff analysis referred to the transformation of net rainfall—obtained at every point of the drainage basin by applying an appropriate method to determine rainfall excess—into a direct runoff hydrograph at a given station of the hydrographic network. More recently, the need for continuous simulation of the hydrological behavior of drainage basins, in particular during flood and low-flow periods, has extended the domain of rainfall-runoff analysis to include the generation of all components of streamflow observed at a given hydrometric station (e.g., surface runoff, groundwater and sub-surface flows).

For this, rainfall-runoff analysis requires the use of appropriate models for each streamflow component or at least the main components. Some of the models used for this purpose are based on similar concepts while others differ significantly. For groundwater flow, for example, models are often based on the hydrodynamic equations describing flow in porous media. Belonging more to the field of hydrogeology, they will not be described here. For more information on this topic, readers are invited to consult specialized works (e.g., Castany, 1998; Gilli *et al*., 2004).

This chapter presents the concepts and models used for rainfall-runoff analysis. Some of these approaches may be adopted to model other flow components. Section 5.1 demonstrates how the transformation of net rainfall to streamflow, influenced by the geomorphology of the considered basin, is closely related to: 1) the time it takes for runoff to travel to the basin outlet and 2) the temporary storage of water within the basin. The expression for the rainfall-runoff transformation, identified within a formal and general mathematical framework, is also presented. Section 5.2 describes unit hydrograph theory, the associated basic assumptions and the way it can be applied. Various other rainfall-runoff models are then presented. In particular, Section 5.3 deals with the so-called translation models, based on a geomorphological approach, while Section 5.4 discusses reservoir models, based on a systemic approach. The linear reservoir model and its derivatives, which play an important role in many of today's hydrological modeling applications, are described in detail. Section 5.5 provides guidelines for choosing the most suitable model and for estimating the model parameters.

5.1 INTRODUCTION

5.1.1 Rainfall-runoff Transformation and Travel Times

The hydrograph observed at the drainage basin outlet for a given period is the sum of a number of flow components. For flood discharges, fast flow associated with surface and sub-surface runoff produced by rainfall excess are added to slow flow components. The hydrograph component corresponding to fast runoff is represented by the direct runoff hydrograph. The transformation of net rainfall into a direct runoff hydrograph at a given basin outlet is associated with a number of timing parameters illustrated in Figure 5.1a.

- Time-to-peak (t_p): The time between the beginning of direct runoff and the peak of the direct runoff hydrograph. It is also referred to as the rise time or rising-limb time.
- Recession time (t_r): The time between the peak and the end of the direct runoff hydrograph. It is also referred to as the falling-limb time.
- Concentration time (t_c): The time between the end of the net rainfall and the end of the direct runoff hydrograph.
- Lag time (t_l): The time between the centers of mass of the net rainfall and the direct runoff hydrograph.
- Time base (t_b): The total duration of the direct runoff hydrograph ($t_b = t_p + t_r = \theta + t_c$ where θ is the duration the net rainfall).

The asymmetrical bell shape of the direct runoff hydrograph observed at the basin outlet reflects the shift in time of the arrival of fast flow components produced in different parts of the basin. The runoff produced by the net rainfall is therefore associated with the statistical distribution of the travel times required for fast runoff to flow between its production location and the considered basin outlet. This distribution is bounded by the basin concentration time. For a given increment of instantaneous net rainfall, this distribution defines the fraction of the total area of the drainage basin that will have contributed to fast runoff at the basin outlet t hours after the beginning of this increment. The curve describing the increase of this fraction as a function of time t is referred to as the time-area curve[1] (Figure 5.1d).

The statistical distribution of travel times is also associated with isochrones for the basin (Figure 5.1c) for the considered net rainfall increment. The statistical distribution of fast runoff travel times, the corresponding time-area curve as well as the isochrones in principle vary during the rainfall event.

5.1.2 Factor Influencing Rainfall-runoff Transformation

The relationship between rainfall and runoff on a drainage basin corresponds to the statistical distribution of the travel times of flows between their origin and the basin outlet. The travel time of a particle of net rainfall produced at any point in the basin is in fact fully determined by 1) the path traveled by this particle of water to reach the basin outlet and 2) its velocity at every point along this path.

---

[1]The time-area curve is sometimes defined by the density function of the fraction of the drainage basin area contributing to direct runoff at the basin outlet at time t when the basin is subjected to an instantaneous net rainfall.
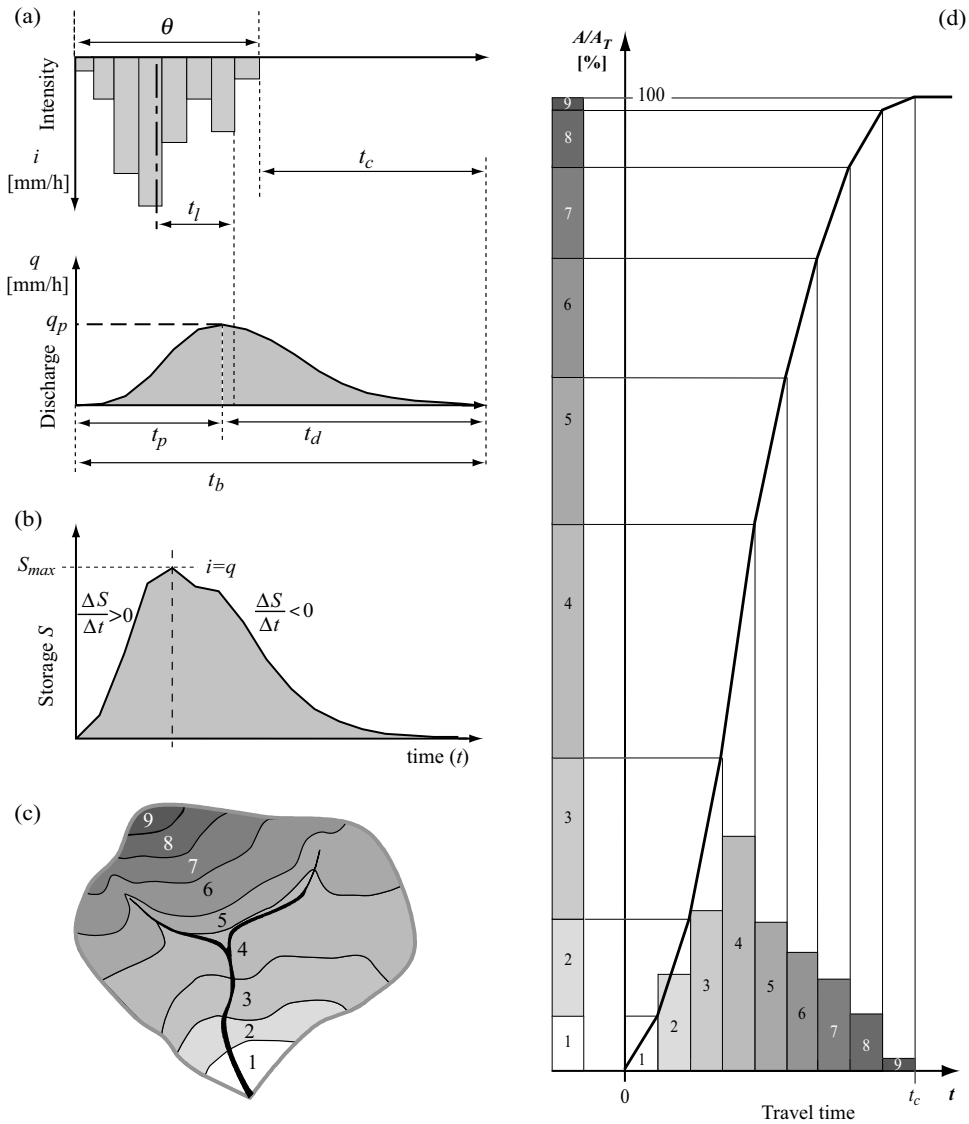
Fig. 5.1: Transformation of a net rainfall hyetograph into a direct runoff hydrograph. a) Net rainfall hyetograph and direct runoff hydrograph (see text for definitions of the various time parameters). b) Surface storage in the drainage basin during the rainfall-runoff event. c) Drainage basin and isochrones describing the time required for the net rainfall to travel to the basin outlet. d) Density function of travel times for a given instantaneous net rainfall showing the percentage of the drainage basin area contributing to the discharge at the basin outlet versus time *t*. The black curve is the time-area curve.

The rainfall-runoff relationship therefore depends largely on the geomorphology of the drainage basin including the characteristics of its slopes and the corresponding hydrographic network. The different factors involved are discussed in Musy and Higy (2011). The shape of the basin is a key factor: the lag between rainfall and runoff will be greater for an elongated basin than for a shorter basin. The steepness and type of soil

cover on the various slopes of the basin also influence runoff flow velocity and therefore the travel time. Other important factors include the topology, density, slope and surface roughness of the drainage network.

In general, the relationship between net rainfall and runoff also depends on the meteorological conditions causing the flood. For this reason, the relationship is generally non-linear. For example, the responsiveness of a given basin generally increases with precipitation intensity.[2]

5.1.3 Rainfall-runoff and Storage Within the Basin

For a given hydrological system, the relationship between rainfall and runoff is associated with not only the travel time of runoff within the system, but also with the difference between system outflow $q(t)$ and inflow $i(t)$ resulting from storage variations $S(t)$ within the system. For the case of runoff, storage is related to the temporary presence of each drop of runoff water in the basin for a period equal to the time required for it to travel from its point of origin to the basin outlet. These storage variations are related to the system input and output fluxes by the classical continuity equation:

$$\frac{dS(t)}{dt} = i(t) - q(t) \tag{5.1}$$

Storage variations typically observed during a rainfall-runoff event are illustrated in Figure 5.1b.

In general, storage can also be related to the inflow, outflow and their derivatives by the so-called storage equation:

$$S(t) = f(i, \frac{di}{dt}, \frac{d^2i}{dt^2}, ..., q, \frac{dq}{dt}, \frac{d^2q}{dt^2}, ...) \tag{5.2}$$

The continuity and storage equations determine the response of the system to the forcing variable $i(t)$. The function f characterizes the rainfall-runoff relationship and depends on the system considered.

5.1.4 Rainfall-runoff Modeling Approaches

Since the 1980s, many studies have attempted to link the rainfall-runoff relationship of the drainage basin to the geomorphology of the latter, leading to so-called geomorphological rainfall-runoff analysis. According to this theory, it is possible to obtain a good estimation of the basin rainfall-runoff relationship if it is possible to describe, in a sufficiently fine manner, at each instant in time: 1) the path traveled by each particle of net rainfall from the point where it falls to the basin outlet and 2) the runoff flow velocity at every point along its path.

---

[2]It is important to distinguish between the responsiveness of a basin and its response to meteorological forcing. For instance, the basin response to a given rainfall event of course always increases with the magnitude of the event, i.e., the more it rains, the higher the discharge at the basin outlet. Its responsiveness refers to the speed of the response. The fact that basin responsiveness also increases with rainfall intensity is in particular expressed by a generally decreasing relationship between the time-to-peak and the intensity of net precipitation, i.e., the heavier it rains, the faster the basin responds.

This approach can be used for certain specific configurations including for example concentrated runoff observed in a permanent and well-channeled hydrographic network or sheet flow runoff from a given rainfall flowing on an impervious inclined plane (Figure 5.2). For such configurations, the equations governing the temporal and spatial variations of flow or runoff are the fundamental equations of open-channel hydraulics (i.e., energy conservation and continuity equations). These equations can be solved numerically to estimate the average flow velocity and depth at every point of the network or plane and in particular at the outlet (see Chapter 6). Concentrated runoff and sheet flow runoff have been the object of much research and development in urban hydrology. Concentrated runoff is typical in storm drainage networks. Sheet flow runoff can be observed on various impervious surfaces in urban environments (e.g., roads, parking lots and airport runways). The research mentioned above has led to different rainfall-runoff models including, for example, the adaptation of the kinematic-wave model for the modeling of sheet flow runoff (Appendix 5.7.1).
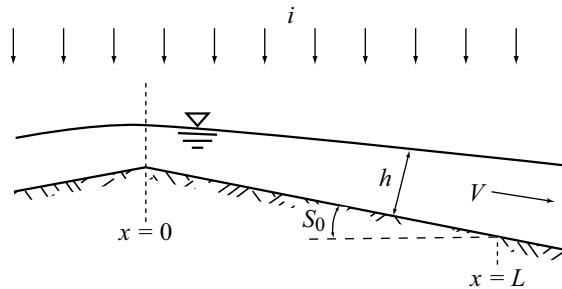
Fig. 5.2: Longitudinal profile at time t of the water surface corresponding to sheet flow runoff on an impervious inclined plane receiving a rainfall of intensity i. S_0 and L are the slope and length of the inclined plane and h and V the depth and velocity of the flow at abscissa x.

Outside these highly restrictive configurations, the modeling of the fast rainfall-runoff process cannot be based on a physical approach. For example, fast runoff is not necessarily the result of surface runoff alone. It can also include flows conveyed by macro-pores or produced by the piston effect (Musy and Higy, 2011), both of which cannot be modeled. Moreover, the complexity of the possible paths that can be taken to reach the basin outlet makes it impossible to provide a meaningful deterministic description of the detailed structure of the surface drainage network. In addition, this structure can change with time due to: 1) the disappearance and appearance of drainage paths induced respectively by erosion and accumulation processes and 2) temporary activation of certain drainage paths, for example during flooding periods.

In general, rainfall-runoff modeling is either physically-based or conceptual. Various approaches are possible. They can be distinguished by the point of view adopted.

The rainfall-runoff transformation can be viewed solely as the result of runoff traveling along paths within the basin. The corresponding rainfall-runoff models use a simplified description of the drainage network. They require a spatialized description of the drainage basin. Often referred to as translation models, they correspond to a simplified geomorphological approach. They are described in Section 5.3.

The rainfall-runoff transformation can also be viewed solely as the result of the storage and release of surface or sub-surface water by the drainage basin. The corresponding rainfall-runoff models are referred to as capacitive models and often use a global description of the drainage basin. These models, corresponding to a more systemic approach, are described in Section 5.4.

Rainfall-runoff models can also use a global empirical approach. For example, hydrologists often explicitly or implicitly assume that the transformation of net rainfall into a runoff hydrograph can be modeled by a linear time-invariant transfer function. In this case, the rainfall-runoff transformation can be fully characterized by what is referred to as a system response function. The most widely used functions of this type are the unit pulse, impulse and step response functions (Addendum 5.1). Various approaches have been proposed to model rainfall-runoff under such time-invariance and linearity assumptions, including in particular the unit hydrograph approach. The corresponding theory is detailed in Section 5.2.

The need to consider or not the possible non-linearity of the relationship between net rainfall and runoff is dealt with in Section 5.5 of this chapter. Although the relationship between net rainfall and direct runoff can in many cases be reasonably modeled by a linear operator, it is important to remember that the overall rainfall to runoff transformation is largely non-linear. Most of the non-linearity comes from the runoff production phase. It is therefore important to insist on the fact that direct runoff can only be studied or modeled after estimating the rainfall excess (Chapter 4) and adding, in mountainous regions, any water produced by the melting of snow or ice (Chapter 7).

Addendum 5.1 Response functions of a linear invariant system

Rainfall-runoff models often consider that the behavior of the hydrological system is linear and time-invariant. A system for which the behavior can be described by the continuity and storage equations is said to be linear and time-invariant if the storage equation can be expressed in the form:

$$S(t) = a_0 i + a_1 \frac{di}{dt} + a_2 \frac{d^2 i}{dt^2} + ... + b_0 q + b_1 \frac{dq}{dt} + b_2 \frac{d^2 q}{dt^2} + ... \qquad (5.3)$$

where $a_0, a_1, ..., a_n, b_0, b_1, ... b_n$ are constant parameters. Time-invariance signifies that the way the system responds to the forcing variable $i(t)$ does not change with time. The linearity and time-invariance assumptions imply two properties of interest:

- proportionality, i.e., if the system response to forcing i is q, then the system response to forcing ki is kq (where k is a constant),
- superposition, i.e., if the system responses to forcing i_1 and i_2 are respectively q_1 and q_2, then the system response to i_1+i_2 is q_1+q_2.

Moreover, a linear time-invariant system is entirely characterized by one of its response functions. The most widely used functions are its unit pulse, impulse and step response functions. The superposition and proportionality properties make it easy to change from one to another. They also make it possible to calculate the system response to a complex forcing $i(t)$. This calculation involves a mathematical convolution for which the expression varies depending on whether the system is described in a continuous or discrete manner. These different notions are presented in greater detail below.

Impulse response

This is the response of the linear system to a unit impulse. The unit impulse is defined by an input of unit height applied instantaneously to the system at time τ. The impulse response of the system at time $t > \tau$ is described by the function $u_0(t-\tau)$, where t-τ is the time that has elapsed since the impulse.

The proportionality and superposition principles make it possible to estimate the system response to a series of discrete impulses. For example, as illustrated in Figure 5.3, the response $q(t)$ of the system to an impulse of height 3 applied at time τ_1 and to an impulse of height 5 applied at time τ_2 is:

$$q(t) = 3u_0(t-\tau_1) + 5u_0(t-\tau_2) \tag{5.4}$$

The response $q(t)$ of the system to a continuous input defined by the function $i(\tau)$, which is equal to the sum of an infinitude of infinitesimal impulses, is obtained by convolution of input $i(\tau)$ and the impulse response function $u_0(t-\tau)$. The expression for this convolution is:

$$q(t) = \int_{t=0}^{\tau=t} i(\tau) \cdot u_0(t-\tau) \cdot d\tau \tag{5.5}$$

The product ($i(\tau) \cdot u_0(t-\tau) \cdot d\tau$) corresponds to the response of the linear system generated by the volume ($i(\tau) \cdot d\tau$) of input $i(\tau) \cdot$ between times τ and $\tau + d\tau$ (Figure 5.4). It is assumed that $q(t = 0) = 0$. The above convolution integral is also referred to as the Duhamel integral.
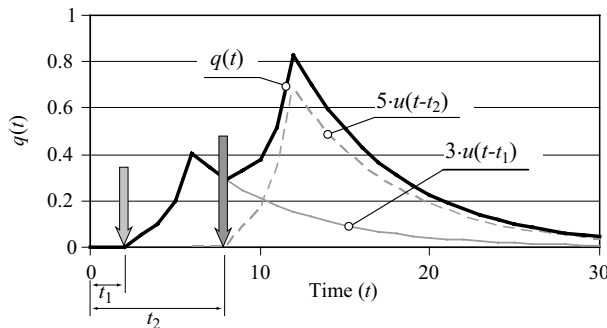

Fig. 5.3: Response $q(t)$ to two impulses of heights 3 and 5 respectively.

The impulse response $u_0(t)$ of the system is equal to the limit of the unit pulse response of the system $u_{\Delta t}(t)$ as the unit pulse duration Δt approaches 0. Moreover, $u_0(t)$ is also the first derivative of the step response $s(t)$ of the system (see the definitions of these two functions below).

$$u_0(t) = \lim_{\Delta t \to 0} \left(u_{\Delta t}(t) \right) = \frac{ds(t)}{dt} \tag{5.6}$$

Step response

The step response $s(t)$ is the response of a linear invariant system to a unit step increase of input $i(t)$. The unit step (also referred to as the Heaviside unit step function $H(t)$) is defined by:
- $i(t) = 0$ for $t < 0$
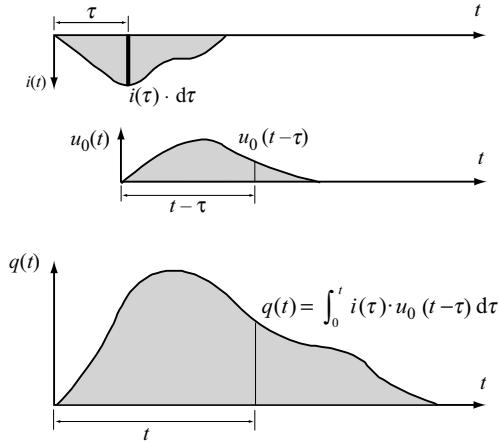- $i(t) = 1$ for $t > 0$

Fig. 5.4: Response $q(t)$ obtained by convolution of input $i(\tau)$ with the impulse response $u_0(t\text{-}\tau)$.

The step response (Figure 5.5) can be obtained by convolution of the unit step $i(\tau)$ and the impulse response $u_0(t\text{-}\tau)$ (see equation 5.5) or by superposition of an infinitude of unit pulse responses $u_{\Delta t}(t+k\Delta t)$, where $k = 0,1,\dots$, shifted by Δt and each multiplied by Δt.
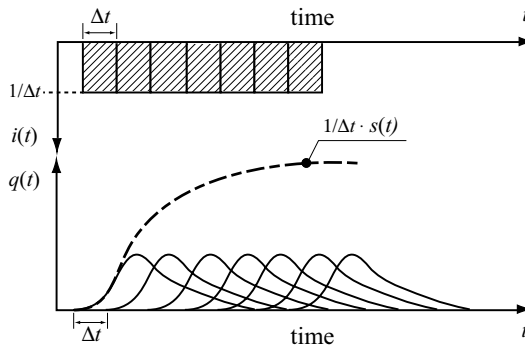

Fig. 5.5: Step response $s(t)$ obtained by the superposition of an infinitude of unit pulse responses $u_{\Delta t}(t+k\Delta t)$, with $k \geq 0$, shifted by Δt and each multiplied by Δt.

Unit pulse response

The unit pulse response $u_{\Delta t}(t)$ is the response of a linear invariant system to a unit pulse at input $i(t)$ (duration Δt, volume 1). The unit pulse is defined by:

- $i(t) = 0$ for $t < 0$
- $i(t) = 1/\Delta t$ for $0 \leq t < \Delta t$
- $i(t) = 0$ for $t > \Delta t$

The unit pulse response (Figure 5.6) can be obtained by convolution of the unit pulse $i(\tau)$ and the impulse response $u_0(t\text{-}\tau)$ or by calculating the difference between two step responses $s(t)$ shifted by Δt (Figure 5.6).

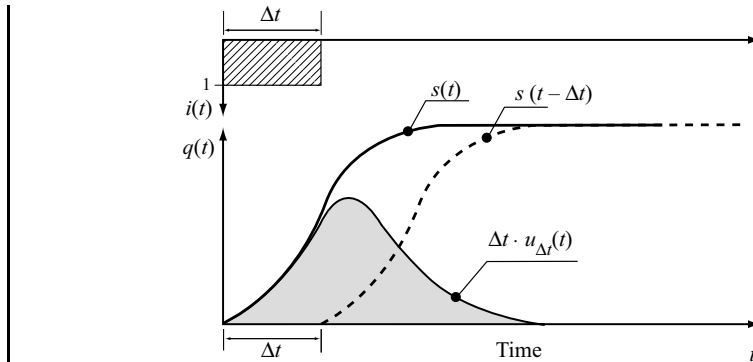$$u_{\Delta t}(t) = \frac{s(t) - s(t - \Delta t)}{\Delta t} \tag{5.7}$$

Fig. 5.6: Unit pulse response $u_{\Delta t}(t)$ obtained by calculating the difference between two step responses $s(t)$ and $s(t-\Delta t)$.

5.2 UNIT HYDROGRAPH MODEL

First proposed by Sherman (1932), unit hydrograph theory can be used to estimate the hydrograph of direct runoff from net precipitation. It is a semi-empirical approach, i.e., no attempt is made to describe the causes—in terms of flow or storage within the basin—of the transformation of net rainfall into streamflow.

5.2.1 Assumptions

Unit hydrograph theory is based on the following assumptions:

- Negligible spatial variability of precipitation. The response of the drainage basin to the net rainfall can therefore be described in a global manner.
- Linear response of the drainage basin to net rainfall. For a net rainfall of a given duration τ, the ordinates of the direct runoff hydrograph are therefore proportional to the depth d of net rainfall (Figure 5.7b).
- Time-invariant response of the drainage basin to net rainfall. The response of the drainage basin to a given increment of net rainfall is therefore the same whatever the time of occurrence of this net rainfall (Figure 5.7c).

These three assumptions imply that the drainage basin system can be considered to be a linear time-invariant operator and consequently that the properties of proportionality and superposition associated with such systems are valid. With respect to its response to net rainfall, the drainage basin system can therefore be characterized by one or more linear system response functions (Addendum 5.1). In hydrological jargon, the three response functions mentioned in the introduction are, for this approach, the unit hydrograph (unit pulse response), the instantaneous unit hydrograph (impulse response) and the S hydrograph (step response).
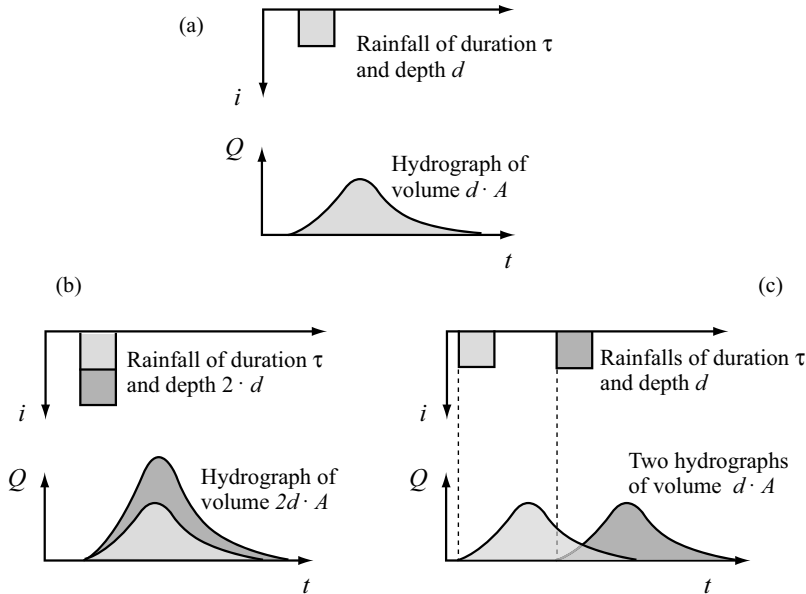
Fig. 5.7: Assumptions of the unit hydrograph method. a) Reference net rainfall and corresponding runoff hydrograph. b) Linear response for a given rainfall duration. For a given rainfall duration, the ordinates of the runoff hydrograph are therefore simply multiplied by 2 if the net rainfall depth is increased from 1 to 2. c) Time-invariant response. The response of the basin to two identical rainfalls at times t and $t+\Delta t$ is the same, shifted by Δt (with i expressed in mm/h, Q in m³/s and the area A of the drainage basin in km²).

5.2.2 Unit Hydrograph

For a given reference duration τ, the unit hydrograph of the drainage basin is the unit response $u_\tau(t)$ of the basin for this duration in relation to the transformation of net rainfall into streamflow (Addendum 5.1). In other words, the unit hydrograph (UH) of a drainage basin is the direct runoff hydrograph resulting from a net rainfall of depth d and duration τ, uniformly distributed in space and with constant intensity over duration τ.

The main characteristics of the UH for a reference duration τ are the time-to-peak (t_p), recession time (t_r), concentration time (t_c), lag time (t_l) and time base ($t_b = t_p + t_r = \tau + t_c$) (Figure 5.8). For a given reference duration τ and unit depth d, the characteristics of the corresponding UH are time-invariant.

The term "unit" designates here the reference duration τ of the rainfall (e.g., 30 minutes, 1 hour, 6 hours, etc.). Variations of the reference duration τ or the unit depth d lead to a different UH. In particular, the volume of direct runoff depends on these variables.

The properties of proportionality and superposition of the UH make it possible to easily calculate the direct runoff hydrograph resulting from a long and complex rainfall discretized with a time step equal to the reference duration τ of the unit rainfall. This operation involves the discrete convolution of UH $u_\tau(t)$ and the net rainfall corresponding to this rainfall $i(t)$. The discrete convolution principle is detailed in Addendum 5.2.
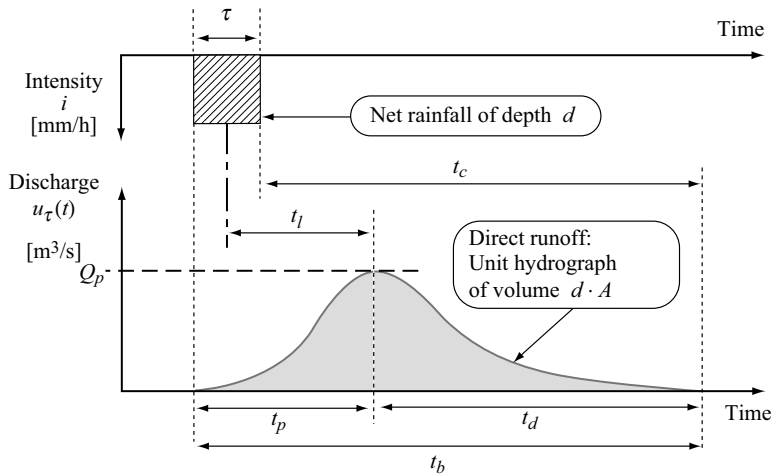
Fig. 5.8: Definitions of unit hydrograph characteristics. The timing parameters are defined in the same way as in Section 5.1.1.

Addendum 5.2 Discrete convolution of net rainfall with the UH

In the following, the UH for a unit net rainfall of reference duration τ and depth 1 mm is assumed to be known.

Consider first of all a complex rainfall for which the hyetograph can be divided into a series of simple rainfalls of duration τ. This hyetograph is defined by a set of M values (i_1, i_2, ..., i_M) corresponding respectively to the mean intensities of the net rainfall over time steps $[0, \tau]$, $[\tau, 2\tau]$, ...,$[(M-1)\tau, M\tau]$. For each of these M rainfalls, the resulting runoff hydrograph can be determined by applying the linearity principle. Note that each of these hydrographs has a time shift of duration τ with respect to the hydrograph resulting from the simple rainfall observed at the previous time step (e.g., the runoff hydrographs corresponding to rainfalls i_2 and i_3 are shifted by a duration of 1τ and 2τ respectively with respect to the hydrograph resulting from rainfall i_1). The hydrograph resulting from the complex rainfall is determined by summing the hydrographs obtained for each of the individual rainfalls. Figure 5.9 summarizes the different steps of the convolution.

To simplify the notation, the ordinates of the unit hydrograph of reference duration corresponding respectively to times τ, 2τ, 3τ, ... $k\tau$ are u_1, u_2, ... u_k. The discharge obtained after convolution of the net rainfall and the unit hydrograph for time $t = n\tau$, can be expressed as follows:

- If time t is greater than the rainfall duration ($n\tau > M\tau$)

$$q_n = i_1 u_n + i_2 u_{n-1} + ... + i_m u_{n-m+1} + ... + i_M u_{n-M+1} \tag{5.8}$$

or expressed more concisely:

$$q_n = \sum_{m=1}^{M} i_m u_{n-m+1}$$

- If time t is less than the rainfall duration ($n\tau < M\tau$)

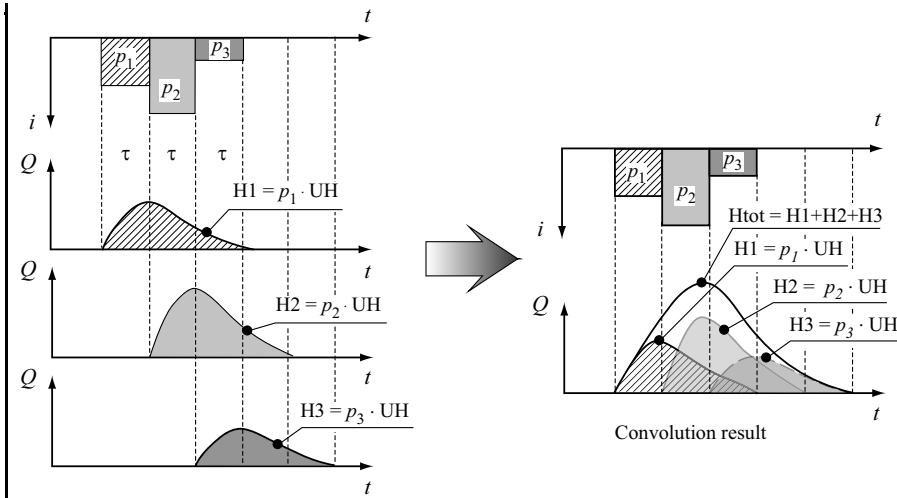$$q_n = \sum_{m=1}^{n \leq M} i_m u_{n-m+1} \tag{5.9}$$

Fig. 5.9: Discrete convolution of a net rainfall (i1, i2, i3) with the UH (u1, u2, u3, u4) to produce the total direct runoff hydrograph (q_1, q_2 ,..., q_7). The UH corresponds to a net rainfall depth of 1 mm and a reference duration of τ.

Table 5.1 illustrates the different terms taken into account for each time step for a net rainfall defined by intensities (i_1, i_2, i_3) and a unit hydrograph with a time base duration of 4τ and defined by the values (u_1, u_2, u_3, u_4).

Table 5.1: Discrete convolution of net rainfall with the UH.

Time	τ	2τ	3τ	4τ	5τ	6τ
$i_1 \cdot$ **UH**	$i_1 u_1$	$i_1 u_2$	$i_1 u_3$	$i_1 u_4$		
$i_2 \cdot$ **UH**		$i_2 u_1$	$i_2 u_2$	$i_2 u_3$	$i_2 u_4$	
$i_3 \cdot$ **UH**			$i_3 u_1$	$i_3 u_2$	$i_3 u_3$	$i_3 u_4$
Hydrograph	$\sum = q_1$	$\sum = q_2$	$\sum = q_3$	$\sum = q_4$	$\sum = q_5$	$\sum = q_6$

5.2.3 S-hydrograph

The S-hydrograph of the drainage basin is the particular step response $s(t)$ of the basin in relation to the transformation of net rainfall into streamflow (Addendum 5.1).

In other words, the S-hydrograph—also referred to as the S-curve—is the runoff hydrograph of the continuous uniform rainfall with a constant intensity ($i = 0$ for $t < t_0$; $i = i_0$ for $t \geq t_0$) and a duration greater than the concentration time of the drainage basin. Beyond t_c, the runoff discharge is constant and maximum given that it is supplied by the entire area of the drainage basin. This curve is obtained for example by the convolution of n unit rainfalls of duration τ with the UH corresponding to this duration (Figure 5.10).

Note that subject to normalization with respect to drainage basin area, the S-curve is equivalent to the time-area curve of the drainage basin (Figure 5.1d).

Calculating the difference between two S-curves shifted by time interval T gives the ordinates of the UH corresponding to a rainfall of depth of $d \cdot T/\tau$ and duration T (Addendum 5.1).
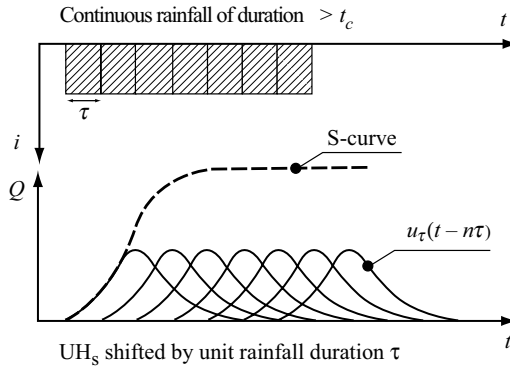
Fig. 5.10 Construction of an S-curve.

5.2.4 Instantaneous Unit Hydrograph

The instantaneous unit hydrograph (IUH) is the impulse response $u_0(t)$ of the drainage basin in relation to the transformation of net rainfall into streamflow (Addendum 5.1).

In other words, the IUH of the drainage basin is the UH for a unit rainfall of infinitesimal duration. The IUH $u_0(t)$ is the limit of the UH $u_\tau(t)$ as the duration of the unit rainfall τ approaches 0 (Addendum 5.1). The IUH is also the first derivative of the S-curve:

$$u_0(t) = \lim_{\tau \to 0} u_\tau(t) = \frac{ds(t)}{dt} \tag{5.10}$$

The IUH eliminates the dependence of the shape of the UH on the reference duration of the rainfall used to define the UH. The IUH is sometimes normalized so that the corresponding runoff volume is equal to unity. This normalization eliminates the dependence of the volume of the IUH on the depth of the unit rainfall. It also makes it possible to compare IUHs obtained for drainage basins of different sizes.

Convolution of the IUH $u_0(t)$ and the net rainfall $i(t)$ expressed in a continuous form gives the direct runoff hydrograph. The principle of this convolution is indicated in Addendum 5.1.

5.2.5 Identifying the UH of a Drainage Basin

Identification methods

Identification of the UH of a given basin consists in estimating the p values (u_1, u_2, …, u_p) that define it for the chosen reference duration D.

It is possible to identify the UH using a geomorphological approach. This requires development of a translation model as discussed in Section 5.3. Theoretically, this approach makes it possible to obtain the UH even if no concomitant precipitation and discharge data are available (Moussa, 1997; Shamseldin and Nash, 1998). It does however require adequate information concerning the geomorphology of the basin and its drainage network (Section 5.3).

The UH is more often identified on the basis of an observed rainfall-runoff event for which concomitant precipitation and discharge data are available at the same time step

D. It must first be possible to estimate the direct runoff hydrograph and the net rainfall that produced the hydrograph. To estimate the direct runoff hydrograph, a hydrograph separation technique is generally used (Chapter 8). The net rainfall is estimated using a rainfall-excess function considered to be appropriate for the considered event (Chapter 4). In addition, the rainfall event must have produced a significant flood on the drainage basin and have a homogeneous spatial distribution.

Different methods can be used to identify the unit hydrograph. They are based on the deconvolution technique.[3] If the net rainfall and runoff hydrograph are described respectively by M mean intensities i_m and N discharge values Q_n, then N equations can be formulated for Q_n, $n=1,\ldots, N$. They produce the $N-M+1$ unknowns u_k that define the unit hydrograph. The identification method to be used depends on whether the net rainfall is concentrated on a particular time step or spread over different time steps. It also depends on whether the time step used to discretize the hyetograph is equal to the required reference duration or not. Appropriate methods for these different situations are briefly discussed in Appendix 5.7.2.

In spite of the linearity and time-invariance assumptions inherent to the UH method, the UH of a basin can vary from one rainfall-runoff event to another. For a given basin, the identification procedure can be repeated for a certain number of events in order to reveal families of UHs corresponding for example to different hydrometeorological contexts. For a given family, a mean UH can then be considered if the non-linearity between events is not excessive. The selected UH is generally the average of the UHs obtained for different events. It is obviously necessary to first adjust all the event-based UHs so that they reflect the same reference duration τ and the same net rainfall depth d.

Limitations related to the estimation of UHs

Current methods to identify the UH corresponding to a given rainfall-runoff event require the estimation of the direct runoff hydrograph and the net rainfall (volume and temporal structure). Different methods can be used for these estimations. The reader can refer to Chapters 4 and 8 for more information on this topic. However, no general criterion exists for the selection of the most appropriate estimation method or technique. Consequently, the UH identified for a given rainfall-runoff event is highly dependent on the assumptions and methods used for the pre-processing of the associated data. This is illustrated in the example presented in Appendix 5.7.2.

The so-called First Differenced Transfer Function (FDTF) method introduced by Duband *et al*. (1993) alleviates these limitations. The classical process used to estimate the UH consists first in determining the net rainfall based on the gross rainfall and then identifying, on the basis of the direct runoff hydrograph, the impulse response. The UH therefore depends on the results obtained in the first step. With the FDTF method, the function describing the transformation of rainfall into runoff is first estimated using the gross rainfall as an initial estimate of the net rainfall. This function is then used together with certain constraints to obtain a better estimate of the net rainfall. These two steps are performed iteratively until the various estimates stabilize.

---

[3]Deconvolution is the inverse of the convolution operation presented above for the calculation of the runoff hydrograph from the net rainfall and the UH and described in Addendums 5.1 and 5.2.

Determination of the UH finally consists in estimating its *N-M+1* ordinates. These ordinates are in principle highly correlated, in particular in the part of the curve corresponding to the recession. Identification methods are generally unable to take this correlation into account, sometimes leading to the identification of UHs with strong oscillations. To avoid this problem, different constraints can be imposed on the shape of the UH (e.g., Natale and Todini, 1977) or the shapes obtained for different rainfall-runoff events can be averaged.

5.3 TRANSLATION MODELS

5.3.1 Principles

The so called "translation models" are rainfall-runoff models that consider that the transformation of rainfall to runoff results solely from fast runoff at the surface of the drainage basin (Figure 5.11). This is a geomorphological approach as described in Section 5.1.2.

Various approaches have been proposed to explain the rainfall-runoff transformation on the basis of the geomorphology of the considered basin. The first looked at the problem from a probabilistic viewpoint, assuming that the structure of the drainage network and consequently the statistical distribution of the travel times of water particles at the surface of the basin could be described by appropriate probability distributions. More recent approaches generally adopt a deterministic viewpoint. They derive the rainfall-runoff relationship from an explicit description of the surface drainage network of the basin along with the runoff propagated through it. The corresponding physically-based or conceptual models use a georeferenced spatial discretization of the drainage basin. These different approaches are described below.

Note that subject to normalization with respect to the drainage basin area, the direct runoff hydrograph obtained for an instantaneous rainfall with any of these models is equivalent to the statistical density of the time it takes for water particle to travel through the drainage basin. Consequently, these translation models provide a simple way of producing the isochrones and the time-area curve for the drainage basin.
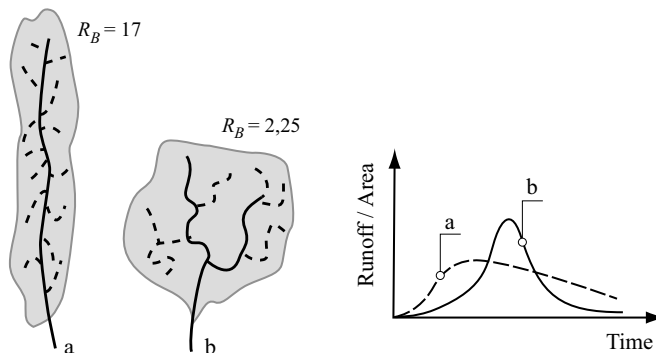

Fig. 5.11: Influence of basin geomorphology and drainage network topology on the unit hydrograph. Hypothetical drainage basins with different bifurcation ratios R_B and the corresponding unit hydrographs (adapted from Chow *et al.*, 1988).

5.3.2 Statistical Models: The Geomorphological Unit Hydrograph

In this approach, the translation model is based on a statistical and synthetic description of the drainage network topology and associated travel times. For this purpose, Rodriguez-Iturbe and Valdés (1979) adopted a Markovian view of the runoff process as described in Appendix 5.7.3. By introducing the Horton-Strahler geomorphological parameters, the proposed approach produces the so-called geomorphological unit hydrograph (GUH).

For the general case, the expression for the GUH is complex and changes with the order of the drainage basin. This approach is therefore not very practical to use. The GUH is therefore often approximated by a simpler model (e.g., a triangular UH or the Nash model), for which the parameters are estimated on the basis of the geomorphological parameters of the basin (Appendix 5.7.3).

Note that the time-to-peak and the peak discharge of the GUH depend on the mean velocity in the watercourse. The rainfall-runoff model is therefore non-linear. The term geomorphological unit hydrograph would therefore appear to be improper given that the UH concept implies linearity and invariance properties, as already discussed. It is however reasonable if the mean velocity in the watercourse can be considered constant throughout a given rainfall-runoff event.

5.3.3 Physically-based Deterministic Models

Physically-based translation models are often based on an explicit description of the main reaches of the hydrographic network and an explicit description of the topological organization. The hydrographic network is represented by a tree structure in which the bottom of the trunk corresponds to the basin outlet and the rest of the trunk and the branches correspond to the different reaches of the network. The degree of detail of the description of the drainage network depends on the size of the drainage elements chosen to represent the outermost branches. Moreover, the drainage basin is divided up into independent spatial units of variable size and shape, each connected to a branch of the tree. The drainage network within each of these units, considered to be less important, is neglected.

With this type of representation, the transfer of fast flows is often calculated using the Barré de Saint-Venant equations for open-channel one-dimensional gradually-varied flow (Chapter 6). Each of the spatial units supplying the network is generally assimilated to an inclined plane and the corresponding runoff is estimated by the diffusion-wave approximation or the Barré de Saint-Venant kinematic-wave approximation for sheet flow.[4] When entering the hydrographic network, runoff at a given point is combined with runoff coming from the upstream network and is then propagated downstream in the network. The diffusion-wave or kinematic-wave approximations for concentrated flows are often used for this (e.g., SOCONT model, Bérod *et al*., 1995; URBS-UH model, Rodriguez *et al*., 2003).

Physically-based rainfall-runoff models are not necessarily based on the type of representation described above. The basin can also be discretized into regular square grid,

---

[4]If the main hydrographic network is described in sufficient detail, a frequent simplification consists in considering that the runoff at the outlet from these spatial units is simply the net rainfall delayed by a certain network entry time that must be determined.

each cell representing a plane with given slopes in the *x* and *y* direction. The runoff on these grid cells, sometimes referred to as drainage cells, is transferred from the upstream to downstream cells until reaching the entry point to the main hydrographic network. The diffusion-wave or kinematic-wave approximations for sheet flow is generally used for this. The description of the network and the modeling of flows propagated in it are then carried out in the same way as in the previous representation (e.g., IHDM model, Calver, 1988; SHE model, Abbott *et al.*, 1986a,b).

Even if they are physically-based, these different approaches often require the calibration of various parameters such as the roughness of the different discretization cells.

The kinematic-wave model is presented in Appendix 5.7.1 for the simplified case of shallow flow on a rectangular inclined plane. Similarly to the case with other physically-based models, the rainfall-runoff model obtained with this approach is non-linear. In particular, the concentration time t_c of a uniform inclined plane obtained with the kinematic-wave model is a decreasing function of the net rainfall (rainfall excess) intensity i_e:

$$t_c = \frac{6.9}{i_e^{0.4}} \left[\frac{n \cdot L}{\sqrt{S_0}} \right]^{0.6} \tag{5.11}$$

with t_c in minutes and i_e in mm/h and where *n, L* and S_0 are respectively the roughness, length [m] and slope of the inclined plane.

5.3.4 Conceptual Deterministic Models

Conceptual deterministic translation models are generally based on a drainage model and a velocity model, both applied to a spatial discretization of the drainage basin (Figure 5.12).

The drainage model estimates the direction of runoff at any point of the basin discretization. It can easily be derived from a digital elevation model (DEM) (Chapter 2). For a DEM produced for a regular square grid, the drainage direction used for each grid cell is often chosen among the 8 possible elementary directions and generally corresponds to the direction of steepest slope. The drainage network corresponding to the drainage model provides the path traveled by any particle of water falling on the basin (Figure 5.12b).

The velocity model is used to estimate the time required for a particle of rain falling at any point in the basin to pass through each grid cell encountered on its path to the basin outlet. Each particle of water is generally assumed to move from its production location to the basin outlet independently with respect to the other water particles. Velocity models often distinguish between basin grid cells and network grid cells that exhibit higher velocities (Zech *et al.*, 1993; Muzik, 1996). The runoff velocity can also depend on the hydraulic head (Lhomme *et al.*, 2004).

The time T_m it takes a particle of water falling at a given point *m* in the basin to travel to the basin outlet (Figure 5.12c) is finally obtained by summing the times required to pass through the different grid cells encountered on its path:

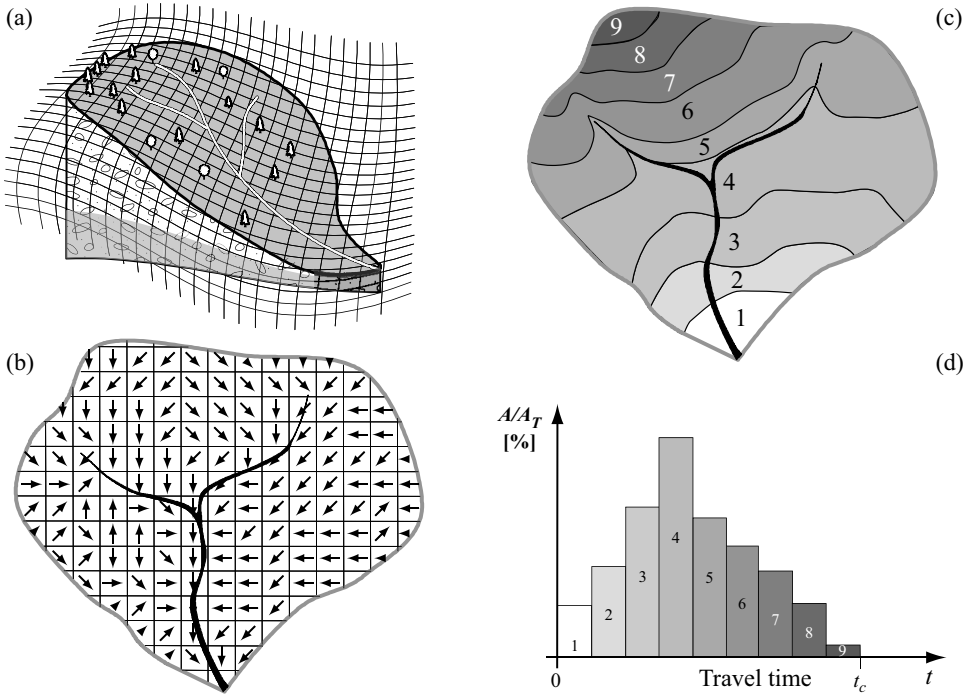$$T_m = \sum_{k=1}^{p} \frac{l_k}{v_k} \tag{5.12}$$

Fig. 5.12: Principle followed by the conceptual translation model to estimate the rainfall-runoff relationship using a drainage model and a velocity model. a) Drainage basin and digital elevation model. b) Drainage network derived from the drainage model. c) Travel time to the basin outlet derived from the drainage and velocity models (isochrones). d) Density function (discretized) of the travel time for an instantaneous net rainfall.

where l_k is the distance traveled on the kth grid cell on the path and v_k is the velocity on this cell. This approach also requires calibration of the different parameters including those of the velocity model.

5.3.5 Linear Translation Models and the Unit Hydrograph

A translation model can be a linear transfer function if: 1) the water particles from rainfall flow through the drainage network independently of other particles and 2) the flow velocities within the different grid cells depend only on the position of the grid cell within the basin and not on precipitation intensity or the fluxes in transit on the cell. The second condition above is satisfied for example when the velocity model expresses the flow velocity as a function of the grid cell slope and roughness alone.

If the translation model is linear, it is easy to obtain the response functions related to UH theory.

- The statistical density of the travel time of a particle of water falling on the drainage basin is, subject to normalization with respect to the drainage basin area, equivalent to a IUH of the drainage basin (Figure 5.12d).
- The time-area curve of the basin is, subject to normalization with respect to the drainage basin area, equivalent to the S-curve of the drainage basin (Figure 5.1d).

For the case of a linear model, the areas between the drainage basin isochrones, separated by a given duration Δt, can be deduced from the time-area curve. Convolution of the histogram of these areas and the net rainfall can be used to obtain the corresponding direct runoff hydrograph. This method is often referred to as the isochrone method. It is described in detail in Musy and Higy (2011).

If the translation model is non-linear, the statistical density of the travel time and the time-area curve vary with time and cannot be related to the response functions related to UH theory. In this case, the isochrone method cannot be used.

5.4 RESERVOIR MODELS

5.4.1 Principle

As opposed to the case of translation models, for reservoir models, the drainage basin is not necessarily discretized and can be considered globally. In this case, rainfall-runoff is simulated solely by temporary storage, within one or more conceptual reservoirs, of the net rainfall that has fallen in previous time steps. This is therefore not a geomorphological approach. Nevertheless, the parameters of such models can sometimes be derived from certain geomorphological characteristics of the medium.

The variety of reservoir models, also referred to as capacitive models, is almost infinite, as illustrated by the inventory proposed by Perrin (2000). They have different degrees of complexity, depending on the number of reservoirs used, their respective types and their organization. The general principles of these models are described in Section 3.2.2 of Chapter 3.

Figure 5.13 shows different types of reservoirs that are frequently used, sometimes in combinations, to model the rainfall-runoff process. Figure 5.14 illustrates some of the possible combinations used.

For the general case, simulation of the rainfall-runoff process with a reservoir model is relatively easy. An appropriate numerical scheme must be developed (e.g., finite differences) to estimate the temporal variations of storage and the different associated fluxes in each of the reservoirs.

Only certain reservoir models will be described in detail here, in particular the linear reservoir and Nash models. Their behavior provides a good illustration of the potential of this type of representation. Furthermore, because they are linear, these models are easy to use.

5.4.2 Linear Reservoir Model

The linear reservoir model is by far the most widely used in rainfall-runoff analysis. The behavior of the reservoir is governed by only two equations: a continuity equation and a storage-discharge equation. Linearity is expressed by the storage-discharge equation, in which the outgoing discharge (i.e., the outflow) is assumed to be a linear function of the depth (or volume) of water stored in the reservoir:

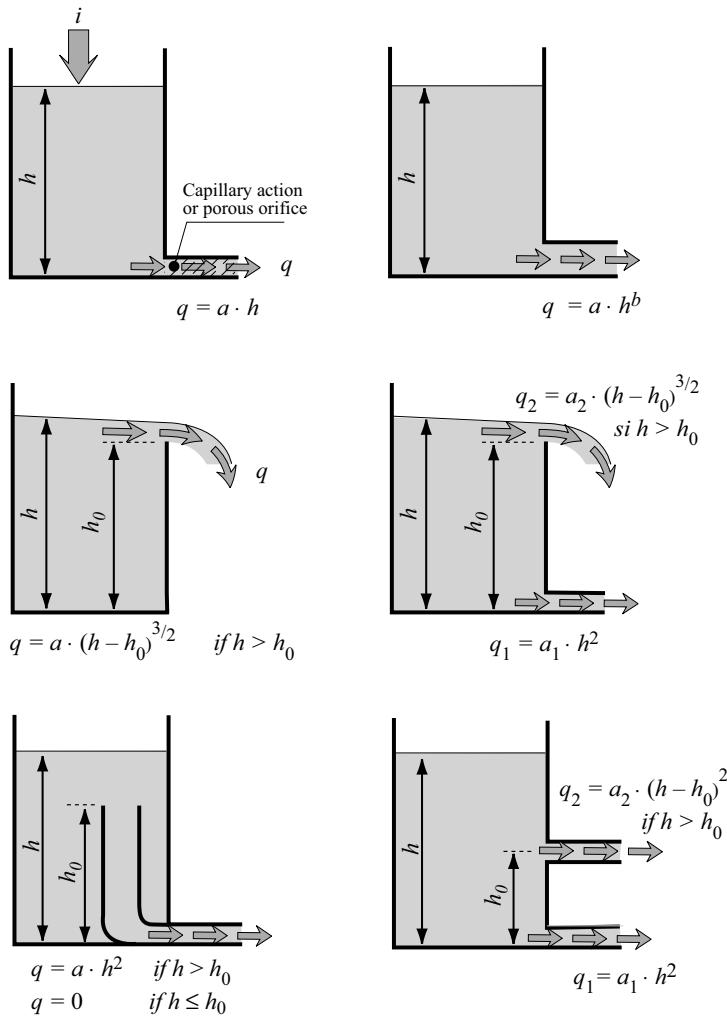Continuity equation: $\dfrac{dS(t)}{dt} = i(t) - q(t)$ (5.13)

Fig. 5.13: Typical reservoirs used to model part or all of the rainfall-runoff transformation (adapted from Ministère de l'Environnement, France, 1985).

Storage-discharge equation: $q(t) = S(t) / K$ (5.14)

where $S(t)$ is the water volume stored in the reservoir at time t and $i(t)$ and $q(t)$ are respectively the reservoir inflow and outflow, expressed in the same units. K is the time constant for the model, the only parameter to be estimated. If basin storage is represented by a water level (i.e., water depth), the units for these different variables are often mm for S, mm/hour for i and q and hours for K. The flows are then expressed in units of velocity, for example precipitation intensity for i and specific discharge for q. If storage is represented by the volume of water stored within the basin, the units are often m^3 for S, m^3/s for i and q and seconds for K.
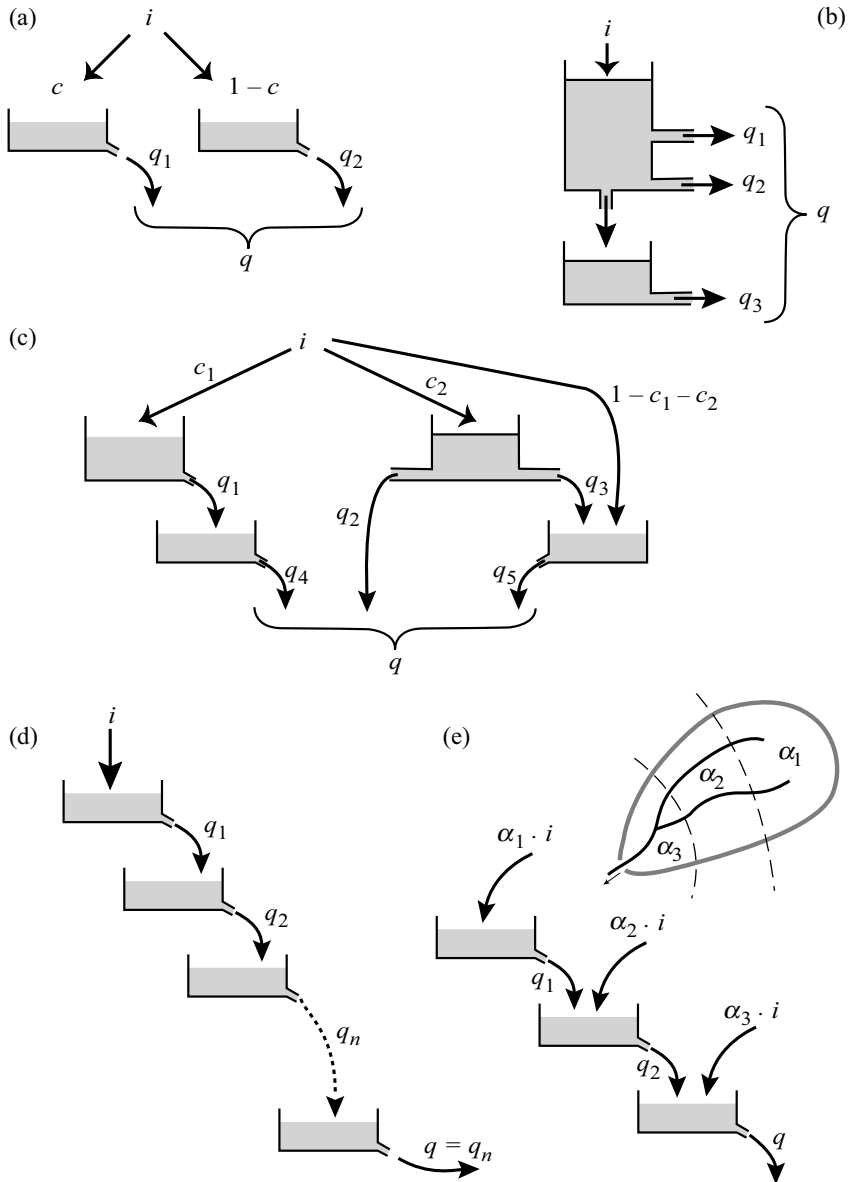
Fig. 5.14: Typical reservoir models representing the rainfall-runoff transformation. a) Linear reservoirs in parallel (e.g., IHACRES model, Jakeman *et al.*, 1990; SOCONT model, Bérod *et al.*, 1995; Schaefli *et al.*, 2005). b) Different reservoirs in series (e.g., HBV model, Bergstrom and Forsman, 1973). c) Hybrid configuration (e.g., MODGLO model, Servat and Dezetter, 1991). d) Cascade of linear reservoirs (e.g., Nash model, Nash, 1957). e) Configuration partially accounting for the spatial variability of basin inflows (e.g., Sugawara and Maruyama, 1956).

By combining the continuity and storage-discharge equations, a first-order linear differential equation is obtained to represent the linear reservoir:

$$K \cdot \frac{dq}{dt} + q = i \tag{5.15}$$

This equation has an explicit solution that can be obtained by separating the variables. The outflow $q(t)$ (e.g., the specific discharge at the basin outlet) resulting from the inflow $i(t)$ (e.g., the net rainfall) is:

$$q(t) = q(t_0) \cdot e^{\frac{t_0 - t}{K}} + \int_{t_0}^{t} \frac{i(\tau)}{K} e^{-\frac{t - \tau}{K}} d\tau \tag{5.16}$$

where $q(t_0) = q(t = t_0)$. This is a special case of the general expression obtained for a linear invariant system (Addendum 5.1). The instantaneous unit hydrograph of the model is deduced directly from this expression and gives the following exponential decay function:

$$u_0(t) = \frac{1}{K} e^{-\frac{t}{K}} \tag{5.17}$$

It is then easy to deduce the equations for the unit hydrograph corresponding to a net rainfall of reference duration τ:

For $0 < t < \tau$: $u_\tau(t) = \frac{1}{\tau}\left(1 - \exp(-\frac{t}{K})\right)$ \hfill (5.18)

For $\tau < t$: $u_\tau(t) = \frac{1}{\tau}\exp(-\frac{t}{K})\left(\exp(\frac{\tau}{K}) - 1\right)$ \hfill (5.19)

According to this model, the concentration time for the drainage basin is infinite. The time constant K estimated for a given basin nevertheless provides information on the basin responsiveness: 67% of the volume injected instantaneously in the reservoir at time $t = 0$ is discharged before time $t = K$. The constant K is sometimes assimilated to the concentration time of the basin.

Over and above the fact that it requires the estimation of only one parameter, the main advantage of the linear reservoir model is the possibility of obtaining an explicit and exact discrete expression for the rainfall-runoff relationship (Appendix 5.7.4). The average outflows q_n, $n = 1...N$ over time interval $[n\Delta t, (n+1)\Delta t]$ can be obtained on the basis of the initial condition and the following recurrence relationship:

$$\begin{cases} q_n = q_0 & \text{for } n = 0 \\ q_n = \alpha \cdot q_{n-1} + (1-\alpha) \cdot \left(\frac{i_n + i_{n-1}}{2}\right) & \text{for } n > 0 \end{cases} \tag{5.20}$$

with $\alpha = \exp(-\Delta t / K)$ \hfill (5.21)

where q_0 is the initial average outflow and i_n the average inflow over time interval $[n\Delta t, (n+1)\Delta t]$. The average flows q_n and i_n are expressed in the same units (e.g., in mm/h). The same is true for the constants K and Δt (e.g., in hours). This model is very easy to apply and is therefore widely used (Example 5.1).

5.4.3 Linear Reservoir Combinations

Nash model

The behavior of the rainfall-runoff process is sometimes modeled by a succession of n linear reservoirs connected in series and having the same storage coefficient K (Figure 5.14c). This cascade of linear reservoirs is known as the Nash model (Nash, 1957).

The instantaneous unit hydrograph of the Nash model is obtained by successively solving the linear reservoir equation for each of the reservoirs (Appendix 5.7.5). Solving the equation $dq/dt=0$ gives the expressions for the time-to-peak t_p and the peak discharge q_p:

$$t_p = K(n-1) \tag{5.22}$$

$$q_p = \frac{1}{K \cdot \Gamma(n)}(n-1)^{(n-1)} \cdot e^{1-n} \tag{5.23}$$

The Nash model has only two parameters, n and K, but can accommodate a wide variety of hydrograph shapes. Figures 5.15 and 5.16 illustrate the sensitivity of the model to these two parameters: n mainly influences the shape of the IUH while K affects the position of the peak.

The product nK is equal to the shift in time between the center of mass of the inflow and the center of mass of the signal obtained at the outlet of the nth reservoir. For a given fixed time shift (e.g., $nK=1$), the peak discharge increases and the IUH becomes narrower as the number of reservoirs increases (Figure 5.17).

A cascade of a finite number of linear reservoirs is in fact an intermediate case between the two extreme models, i.e., the pure storage model ($n=1$) and the pure translation model ($n\rightarrow\infty$) (Brutsaert, 2005). In other words, a cascade of a finite number of reservoirs can accommodate the effects of both storage and translation on the basin and in the network. This model provides a practical way of adjusting the simulated responsiveness of the drainage basin in terms of the time-to-peak of the unit flood and in terms of the time shift between the centers of mass of the net rainfall and the resulting direct runoff hydrograph.
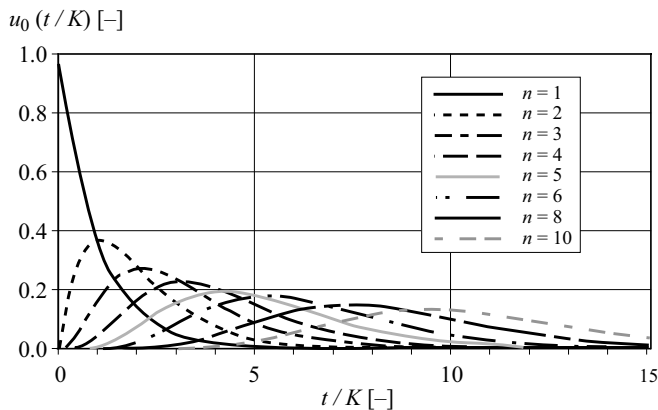

Fig. 5.15: Unit response function $u(t/K)$ of the cascade of linear reservoirs for different values of parameter n.
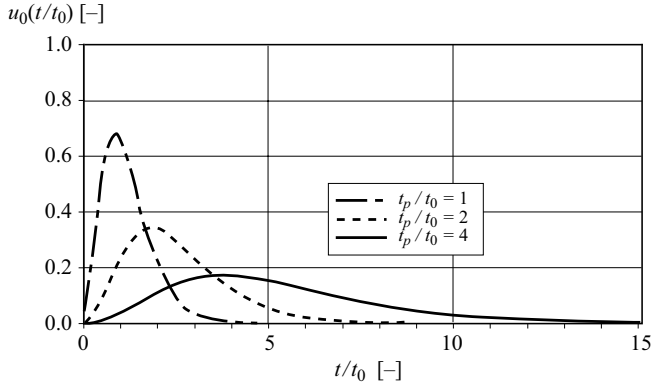
Fig. 5.16: Unit response function $u(t/t_0)$ of a cascade of linear reservoirs ($n=4$) for different values of the ratio t_p/t_0 (and therefore for the different values of $K=t_p/(n-1)$).
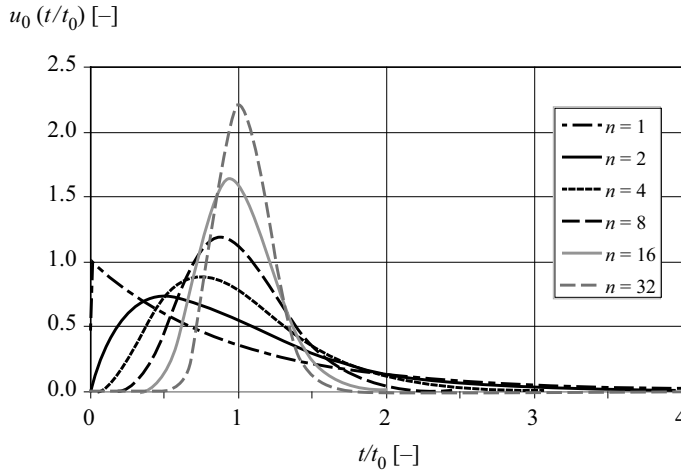

Fig. 5.17: Instantaneous unit hydrograph of a cascade of linear reservoirs for different values of the parameter n when the product Kn is constant and equal to 1.

Example 5.1

Let us use a Nash model made up of two linear reservoirs to simulate the direct runoff hydrograph resulting from the net rainfall described in Table 5.2 for a 100 km^2 drainage basin. The time constant for each reservoir is estimated to be 90 minutes.

Table 5.2: Net rainfall hyetograph and outflow hydrographs of the two reservoirs r_1 and r_2 in series.

t [h]	0	1	2	3	4	5	6	7	8	9	10	11	12
i_n [mm/h]	0	2	4	6	1	0	2	5					
$q_{r1,n}$ [mm/h]	0	0.5	1.7	3.3	3.4	2.0	1.5	2.5	2.5	1.3	0.7	0.3	0.2
$q_{r2,n}$ [mm/h]	0	0.1	0.6	1.5	2.4	2.6	2.2	2.1	2.3	2.1	1.5	1.0	0.7

The hydrograph of outflows from the first reservoir is obtained by applying the following equation in an iterative manner with $\alpha = 0.513$ and $q_{r1,0} = 0$.

$$q_{r1,n} = \alpha \cdot q_{r1,n-1} + (1-\alpha) \cdot \left(\frac{i_n + i_{n-1}}{2} \right) \tag{5.24}$$

The hydrograph of the outflows from the second reservoir is obtained by applying the following equation in an iterative manner with $\alpha = 0.513$ and $q_{r2,0} = 0$.

$$q_{r2,n} = \alpha \cdot q_{r2,n-1} + (1-\alpha) \cdot \left(\frac{q_{r1,n} + q_{r1,n-1}}{2} \right) \tag{5.25}$$

The resulting hydrograph has two flood peaks (Figure 5.18), a time-to-peak of 5 hours and a maximum hourly mean discharge of 2.6 mm/h, i.e., 35.5 m³/s.
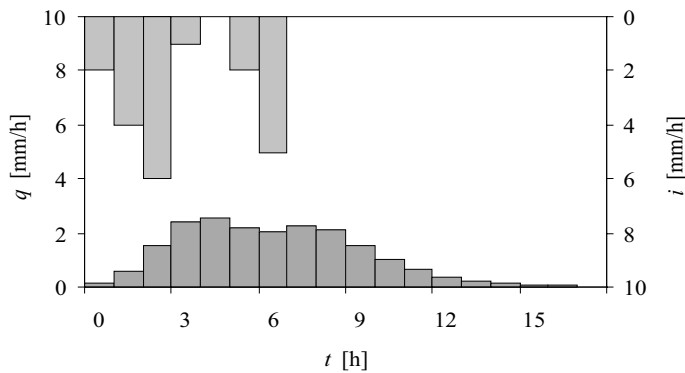

Fig. 5.18: Net rainfall hyetograph and direct runoff hydrograph obtained by simulation with a cascade of two linear reservoirs.

Reservoirs in series with different constants K

It is also possible to combine reservoirs with different time constants in series. For the case of two reservoirs, with respect to the time constants K_1 and K_2, the corresponding IUH is the product of the following convolution:

$$u_2(t) = \int_0^t \frac{1}{K_1 \cdot K_2} \exp\left[-\tau / K_1 \right] \cdot \exp\left[-(t - \tau)/ K_2 \right] \cdot d\tau \tag{5.26}$$

which gives

$$u_2(t) = \frac{\exp\left[-t / K_1 \right] - \exp\left[-t / K_2 \right]}{K_1 - K_2} \tag{5.27}$$

From equation 5.20, the mean discharge over time interval $[n\Delta t, (n+1)\Delta t]$ produced by the two reservoirs in series with respective time constants K_1 and K_2 can be estimated using the following recurrence equation:

$$q_n = (\alpha_1 + \alpha_2) q_{n-1} - \alpha_1 \alpha_2 q_{n-2} + (1-\alpha_1)(1-\alpha_2)(i_n + 2i_{n-1} + i_{n-2})/4 \tag{5.28}$$

with

$$\alpha_1 = \exp(-\Delta t / K_1) \text{ and } \alpha_2 = \exp(-\Delta t / K_2) \tag{5.29}$$

For a given number of reservoirs, the corresponding IUH in fact mainly depends on the sum of the time constants $K_1 + K_2 + \ldots K_n$ which determines the total shift in time between the centers of mass of the inflow and outflow. For a fixed sum $K_1 + K_2 + \ldots K_n$, the shape of the IUH depends very little on the respective values of each time constant. For this reason, this type of model is not of great interest compared to the Nash cascade, given that it requires the determination of different constants K_1, K_2, $\ldots K_n$ instead of the unique parameter K for the Nash model.

Reservoirs in parallel

Another reservoir structure often used to model the rainfall-runoff process is a combination of linear reservoirs connected in parallel (Figure 5.14a). The different reservoirs are described by different time constants used to represent processes generating runoff flows with different velocities. Most of these representations are restricted to two reservoirs intended to represent respectively slow and fast flows. In many cases, such a representation already provides reasonable performance.

These models require a distribution function to divide the net rainfall between the different reservoirs. For example, in the ABCD model (Thomas, 1981) or the IHACRES model Jakeman *et al*., 1990), the net rainfall is distributed between the slow and fast reservoirs on the basis of a coefficient that must be calibrated. The distribution can also vary with time. It therefore often depends on the fill fraction of one of the reservoirs as in the TOPMODEL (Beven and Kirby, 1979) and SOCONT (Schaefli *et al*., 2005) models.

Note that the number of parameters to be estimated increases with the complexity of the structure of the reservoir model. For example, a function designed to distribute the net rainfall between reservoirs always leads to an additional parameter to be calibrated.

5.4.4 Non-linear Reservoir Models

Non-linear reservoir models are also frequently used to model the rainfall-runoff process. This is particularly the case in urban environments because in principle they can reproduce the greater responsiveness of such drainage basins as rainfall increases. The non-linearity most often resides in the storage-discharge equation, which is often of the following type:

$$q(t) = a \cdot h(t)^b \tag{5.30}$$

where a and b are two constants that must be estimated. The parameter b determines the degree of non-linearity while the parameter a is related to basin responsiveness (in the general case, a is no longer the inverse of a time). The value of 5/3 is often used for parameter b, in particular for urban basins.[5] The equation describing the behavior of the reservoir is then:

$$\frac{dh(t)}{dt} + a \cdot h(t)^b = i(t) \tag{5.31}$$

---

[5]With b=5/3, the non-linear reservoir model is often assimilated to a formulation approaching the kinematic-wave model where friction is modeled as proposed by Manning. Consequently, the parameter a of the non-linear reservoir is often expressed in the form: $a = WS^{0.5}/(nA)$ where n, S, W and A are respectively the surface roughness, slope, equivalent width and area of the drainage basin. The responsiveness of different basins can be compared using this parameter a.

As opposed to the equation for a linear reservoir, this equation has no explicit solution and can only be solved using numerical techniques such as finite differences. In the absence of recent inflows ($i(t)$=0 for $t>t_0$), it is possible to determine the analytical expression for the recession curve produced by this reservoir. This expression varies depending on the value of b (Chapter 8, Section 8.3.1).

5.5 CHOOSING A MODEL AND ESTIMATING MODEL PARAMETERS

Many different models can be used to simulate the transformation of net rainfall into runoff at the outlet of a drainage basin. The choice of the best model for a given case and the method to estimate its parameters depends on too many criteria for them all to be discussed here. It is nevertheless possible to provide a few guidelines concerning these choices.

5.5.1 Choosing the Type of Model

UH approach versus translation or storage models

Unit hydrograph theory was widely used in the past to model the rainfall-runoff transformation. This is no longer true today. Its use has many limitations (e.g., those related to identification of the UH) and the approach is incompatible with many of the constraints imposed by recent hydrological modeling applications (e.g., continuous simulation).

At present, rainfall-runoff modeling is based mainly on a physical or conceptual representation of the processes operating in a drainage basin. Reservoir models are without a doubt the most widely used, offering great simplicity while generally maintaining suitable performance. Such models are also parsimonious (i.e., they require very few parameters). Their parameters must however be calibrated (Section 5.5.2). Consequently, these models cannot be used to estimate the influence of drainage network modifications (e.g., due to urbanization) on the rainfall-runoff transformation. Another disadvantage is that they consider the drainage basin from a global viewpoint. They are not well designed to take into account the spatial variability of meteorological forcing and/or the physiographic characteristics of the basin. This approach implies either restricting application of the model to small drainage basins or a division of the drainage basin into sub-basins with separate application of the model to each sub-basin. These remarks are also true for the modeling of the rainfall-runoff process using the unit hydrograph method.

The development of geographical information systems (GIS) and digital elevation models (DEM) has made it possible to extract the drainage network and some of its characteristics. These resources also make it easier to take into account the spatial variability of meteorological forcing and the physiographic characteristics of the basin. For this reason, spatialized models have become increasingly popular since the end of the 20th century. Physically-based and conceptual translation models have also become more popular in spite of the fact that their development and use is often tedious. The main advantage of these models is that the rainfall-runoff relationship can in principle be derived solely from the geomorphological characteristics of the medium. Consequently, the rainfall-runoff relationship can be easily updated to account for modifications affecting the

drainage network. In practice, certain parameters of these models must often be estimated by calibration (Section 5.5.2).

Note that both these approaches, storage and translation, are not incompatible and that certain rainfall-runoff models are in fact hybrid versions. A translation model can for example be used to combine the discharges produced in different parts the basin by associated reservoir models (Bérod *et al.*, 1995).

It is also important to mention that another approach is sometimes used to model the rainfall-runoff transformation. It is based on identification and optimal control methods used in signal processing (Longchamp, 2006). In hydrology, this empirical method is used almost exclusively for flood forecasting (Chapter 10). This approach is reviewed in Appendix 5.7.6.

Linear versus non-linear and pseudo-linear modeling

The responsiveness of the basin should tend to increase with the intensity of the net rainfall. For the rainfall-runoff relationship, various studies have been carried out in attempt to demonstrate this non-linearity. Apart from those that focus on the urban environment, where non-linearity today appears to be widely accepted, these studies have never been conclusive and have often led to contradictory conclusions.

Minshall (1960) published one of the rare studies demonstrating, for a rural drainage basin, that the characteristics of the unit hydrograph vary progressively with the mean intensity of the net rainfall, i.e., when the net rainfall increases, the peak discharge of the unit hydrograph increases and the time-to-peak decreases (Figure 5.19).

The necessity of taking into account the possible non-linearity of the rainfall-runoff relationship for rural basins is however not obvious. Some studies have shown that the use of a non-linear approach does not significantly improve the quality of results. If this is the case, there is no advantage in using a non-linear rainfall-runoff model that is always more
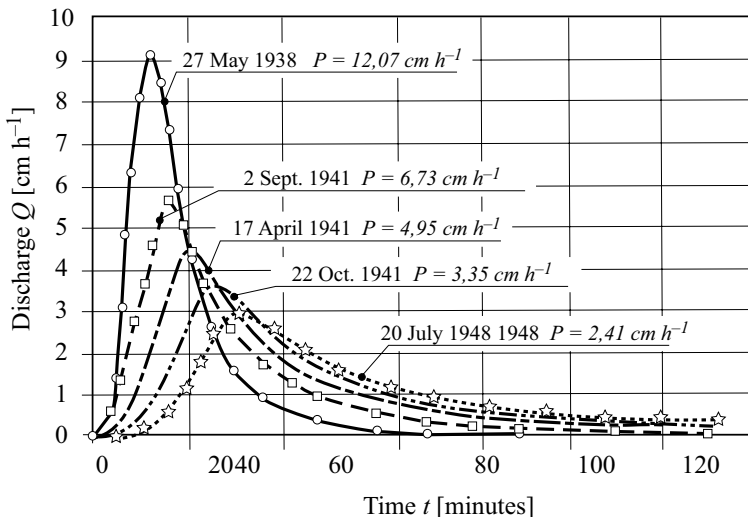

Fig. 5.19: Illustration of the possible non-linearity of the unit response to net rainfall. Results obtained for a small (11 ha) rural basin in the United States. The reference duration of the net rainfall is approximately the same for the different events (roughly 15 minutes) (according to Minshall, 1960).

complicated to apply than a linear relationship. Finally, note that intermediate models exist between linear and non-linear models. For these pseudo-linear models, the response of the drainage basin to the net rainfall is assumed to satisfy the conditions of linearity and time invariance during a given rainfall-runoff event but not necessarily between two events. This makes it possible to use the simple solution techniques available for linear models while at the same time taking into account some of the assumed non-linearity between events.

For example, various authors propose to use the value obtained on the basis of the expression below for the time constant of a linear reservoir. This is in fact the expression for the concentration time obtained for an inclined plane of length L, roughness n and slope S_o, under the various assumptions of the kinematic-wave model. This formulation is for example used by OTTHYMO (Wisner and P'ng, 1983) and MOUSE (Danish Hydraulic Institute) hydrological modeling software.

$$K = \frac{6.9}{i_e^{0.4}}\left[\frac{n \cdot L}{\sqrt{S_0}}\right]^{0.6} \tag{5.32}$$

where i_e is the maximum mean intensity of the considered net rainfall (Appendix 5.7.1). Similar equations expressing the dependence of this parameter on precipitation characteristics have been proposed. They are generally based on a regionalization of the parameters obtained by calibration of different urban drainage basins and for different rainfall events (e.g., Kidd, 1978, for the United States; Desbordes, 1984, for France). Pseudo-linear models are in fact relatively unsuited to today's requirements for continuous simulation and the trend is therefore to their replacement by other approaches.

5.5.2 Estimating Model Parameters

The techniques used to estimate model parameters depend on the type of model used for rainfall-runoff simulation and the availability of data.

Estimating parameters for gaged basins

Unit hydrograph identification methods and the associated difficulties have been described in Section 5.2.5 and will not be dealt with here.

The parameters of geomorphological approaches, based on a translation model, can in principle be extracted from geographic information available for the basin. Geographic information systems (GIS) represent a valuable source of information for this purpose. The type of soil cover and topography are often the main information used (e.g., Table 5.3 and Bérod *et al.*, 1995). Automatic extraction of the drainage network and its characteristics is however generally a difficult task (Chapter 2). For urban environments, however, the various data required for the description of the artificial storm drainage network—made up of streets on the surface and storm sewers underneath, are often accessible via GISs set up by the municipality or city to manage the environment and specific works (Rodriguez *et al.*, 2003).

Table 5.3: Values of the roughness coefficient *n* as a function of the type of surface proposed by the Institution of Engineers of Australia (IEAust, 1987) for use with kinematic-wave models in urban environments.

Type of surface	n_{min}	n_{max}
Concrete or asphalt	0.010	0.013
Bare sand	0.010	0.016
Graveled surface	0.012	0.030
Bare clay-loam (eroded)	0.012	0.033
Sparse vegetation	0.053	0.130
Short grass prairie	0.100	0.200
Lawn	0.170	0.480

Whatever the rainfall-runoff model developed, i.e., translation or reservoir model, it is generally necessary to estimate or adjust certain parameters by calibration. When concomitant data for precipitation and discharges are available, the parameters of conceptual rainfall-runoff models are classically estimated by minimizing the error obtained between simulated and observed hydrographs. The reader can refer to Chapter 3 for more details on the different aspects of the standard estimation procedure. Note however that the hydrologist generally confronted with the problems inherent to separation of the hydrograph and estimation of net rainfall, necessary tasks for the prior estimation of the net rainfall hyetograph and the direct runoff hydrograph that it is assumed to produce.

For this reason, it is not recommended to calibrate model parameters with the priority of reproducing the rising limb of the hydrograph and its maximum discharge. These characteristics are in fact largely determined by the shape and maximum intensities of the net rainfall hyetograph. For this reason, calibration with the objective of reproducing these characteristics generally leads to biasing of the rainfall-runoff model to compensate for imperfections related to the estimation of rainfall on the basin (depth and spatial variability) and runoff losses that are always determined by necessarily simplified and imperfect models (see Chapter 2 and 4). The resulting estimates of rainfall-runoff parameters may no longer be highly pertinent. On the other hand, calibration carried out in such a way that the model correctly reproduces the shape of the falling limb generally leads to a more reasonable and robust estimation of the rainfall-runoff parameters since less sensitive to net rainfall estimation errors.

Given these difficulties, the trend for the estimation of rainfall-runoff model parameters is to no longer separate the estimation of rainfall excess from its transformation to runoff. The resulting hydrological model is therefore designed to represent all the main processes leading to the total discharge observed at the basin outlet. The different parameters for the production of rainfall excess and its transformation to runoff are estimated during a unique calibration procedure—possibly of the hierarchical or multi-signal type. This approach can be used in both event-based and continuous modeling (Chapter 3).

Estimating parameters for ungaged basins

Estimating model parameters for ungaged drainage basins is based on the regionalization techniques described in Chapter 11. The principle is to use information available from gaged basins of the region in the considered ungaged basin. For this, all the drainage basins must belong to a homogeneous hydroclimatic region.

Many studies have been carried out to regionalize parameters for a given rainfall-runoff model. The explanatory variables frequently used to explain the variability of rainfall-runoff model parameters from one basin to another are first of all its area or a related parameter (e.g., basin perimeter or length of the hydrographic network) as well as its slope (Perrin, 2000). For example, regional expressions to predict the time constant K of a linear reservoir are often similar to those proposed for the basin concentration times. For example, the following expression is commonly used for areas with marked relief:

$$K = K_0 \left(\frac{n}{n_0} \right)^a \left(\frac{A}{A_0} \right)^b \left(\frac{S}{S_0} \right)^{-c} \tag{5.33}$$

where A, S and n are the area, slope and average surface roughness of the considered ungaged basin, A_0, S_0 and n_0 are the area, slope and surface roughness of the reference basin for which the time constant is K_0 and a, b and c are three constants to be estimated (b and c often have values of around 0.5).

Other parameters related to the nature of the soil cover also appear in these regional expressions. They influence the responsiveness of the drainage basins via the roughness of the slopes. The explanatory power of these variables for the rainfall-runoff parameters is generally high and the coefficients of determination between optimal parameters obtained by calibration and regional parameters estimated with the regional model are often greater than 0.7.

Whatever the model selected, to use these expressions in a pertinent manner, it is important to carefully consider the configuration of the drainage basin. For instance, these regional expressions are often used erroneously when the drainage basins are made up of similar sub-basins supplying the considered hydrographic station in parallel (Example 5.2).

Example 5.2

The objective is to simulate, using a linear reservoir model, the direct runoff hydrograph resulting from a net rainfall on a drainage basin made up of two identical parallel sub-basins (Table 5.4 and Figure 5.20). The complete drainage basin has an area $2A$ of 1000 km^2 and is ungaged. The following regional expression is available to estimate the time constant K of the model. This expression is based on the time constants determined by calibration for different gaged basins within the region and not divided into sub-basins.
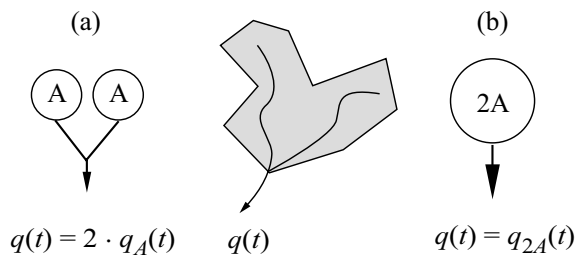

Fig. 5.20: Real drainage basin (middle) and studied schematic representations: a) Two distributed sub-basins. b) One global basin.

Table 5.4: Net rainfall hyetograph.

t [h]	0	1	2	3	4
i [mm/h]	5	8	15	7	2

$$K(A) = K_0 \left(\frac{A}{A_0} \right)^{2/3} \tag{5.34}$$

where A is the area of the considered basin and $K_0 = 8$ h the time constant corresponding to a basin with a reference area of $A_0 = 1000$ km². The use of this equation to estimate the time constant necessary for the required simulation is detailed below.

Two different schematic representations are considered: a) configuration with two sub-basins modeled separately (the discharge of the complete basin is then calculated as the sum of the respective contributions) (Figure 5.20a) and b) configuration with the basin considered globally (Figure 5.20b).

The value of parameter K obviously differs depending on the basin configuration modeled. For the 1000 km² basin considered here, the values obtained for K are 8 h for $A = 1000$ km² and 5 h for $A = 500$ km².

The distributed configuration (Figure 5.20a) leads to a hydrograph with a shorter time-to-peak and a higher peak discharge than the global configuration (Figure 5.21b). The distributed configuration is obviously more pertinent.
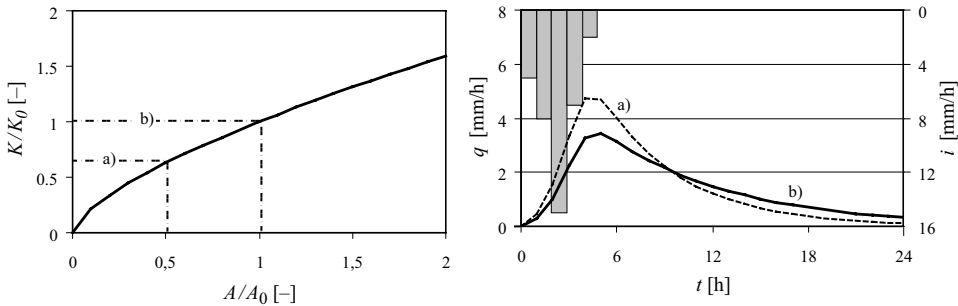

Fig. 5.21: Left: Regional model $K/K_0 = f(A/A_0)$. Right: Direct runoff hydrographs obtained by simulation for configurations (a) and (b) of Figure 5.20.

Synthetic or regional unit hydrograph

It is also often possible to determine a regional UH for a given homogeneous region. This regional UH, also referred to as a synthetic UH, is based on the average UHs identified for the different gaged basins of the region. The calculation involves a normalization. This consists in plotting the average UHs of the different gaged drainage basins in a dimensionless diagram of $u(t)/u_p$ versus t/t_p where t_p is the time-to-peak for each basin and u_p the ordinate of the average UH of this basin. The dimensionless average UHs of the different basins considered must correspond to the same normalized reference duration D_0/t_p (the reference duration used to determine the average UHs of the different drainage basins must therefore be adapted for this purpose). Figure 5.22 illustrates this principle.

The advantage of using synthetic UHs is that their main parameters can in principle be explained as a function of the various measurable characteristics of the drainage basins.
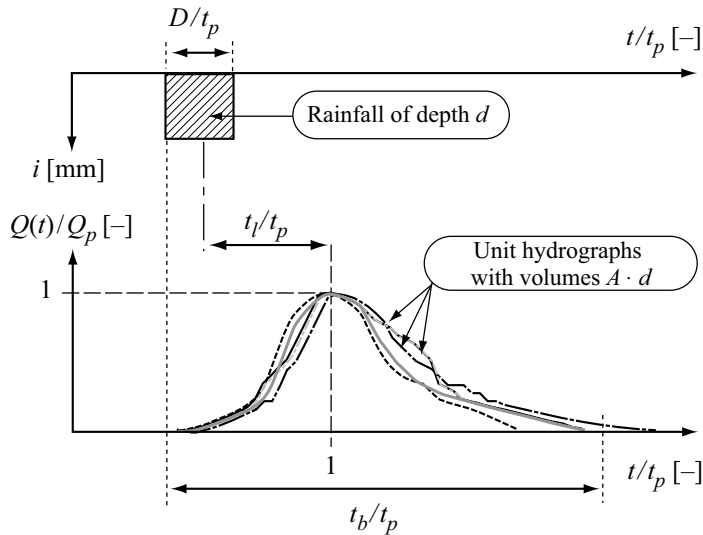
Fig. 5.22: Principle of the synthetic or regional unit hydrograph. The UHs obtained for the different drainage basins of the region are normalized with respect to their time-to-peak and peak discharge.

This approach once again makes use of the regionalization techniques described in detail in Chapter 11. Consequently, it is possible to estimate the UH of any ungaged basin belonging to the study region as long as the characteristics necessary for the determination of the UH parameters can be identified. This approach has for example been used by the US Soil Conservation Service (SCS) to produce the most well-known set of synthetic UHs (Appendix 5.7.7).

5.6 KEY POINTS OF THE CHAPTER

- Rainfall-runoff analysis involves the different components of the flow observed at a given point of the hydrographic network. It is related to storage and flow phenomena within the drainage basin.
- Fast flow components are many determined by the geomorphology of the basin, the characteristics of its slopes and its hydrographic network.
- The properties of a linear invariant system include superposition and proportionality. The corresponding rainfall-runoff transformation can be described by any of the following three response functions: unit pulse response, impulse response or step response.
- The hydrological behavior of drainage basins in relation to the transformation of net rainfall into runoff is a priori non-linear and non-stationary. It is nevertheless often assumed to be linear and invariant.
- The response functions of a linear invariant basin are respectively its unit hydrograph, instantaneous unit hydrograph and S-hydrograph.
- The transformation of net rainfall into a direct runoff hydrograph is related to the statistical distribution of the travel time of flows or runoff between the production location and the considered basin outlet.

- Translation models are based on a geomorphological approach to the rainfall-runoff transformation. They consider this transformation to be solely the result of the paths traveled by the flows within the basin. Such models are based on a spatialized representation of the drainage basin. They are frequently non-linear.
- Translation models can be used to produce the isochrones and the time-area curve for the basin. When the translation model is linear, the time-area curve is directly related to the S-curve of the basin.
- Reservoir models represent a systemic approach to rainfall-runoff analysis. They consider the transformation of rainfall to runoff to be solely the result of the storage and release of surface or sub-surface water by the drainage basin. They generally consider the entire basin in a global manner.
- The time constant of a linear reservoir model is equal to the time shift between the centers of mass of the net rainfall and the corresponding direct runoff hydrograph.
- A cascade of linear reservoirs can be used to adjust both the time-to-peak of the IUH and the time shift between the centers of mass of the net rainfall and the corresponding direct runoff hydrograph.
- Non-linear rainfall-runoff models do not necessarily offer better performance than linear models.
- The parameters of a rainfall-runoff model are sometimes estimated on the basis of a preliminary estimation of the net rainfall hyetograph (using an appropriate rainfall excess model) and on the estimation of the direct runoff hydrograph (by an appropriate hydrograph separation). This approach is generally the source of major uncertainties.
- Estimates of the parameters of a rainfall-runoff model are more robust when carried out at the same time as the estimation of the other parameters of the complete hydrological model (in particular the rainfall excess model).
- The best estimation of the parameters of a rainfall-runoff model is not necessarily the one that leads to the best simulation of the rising limb and flood peak.
- Models based on the unit hydrograph are rarely used today. Hydrologists generally prefer to use translation models, reservoir models or a hybrid combination of the two.

5.7 APPENDICES

5.7.1 Kinematic-wave Model for a Rectangular Inclined Plane

General formulation for runoff on a plane surface

The unidirectional Barré de Saint-Venant equations (conservation of mass and momentum) can be used to simulate the flow of surface runoff produced by a net rainfall of intensity $i(t)$ on a rectangular inclined plane with slope S_0, length L and width W.

Mass conservation: $\dfrac{\partial h}{\partial t} + \dfrac{\partial}{\partial x}(V \cdot h) = i_e$ (5.35)

Momentum conservation: $\dfrac{\partial V}{\partial t} + V\dfrac{\partial V}{\partial x} + g(\dfrac{\partial h}{\partial x} + S_f - S_0) = -\dfrac{i_e.V}{h}$ (5.36)

where V and h are the mean velocity and depth of flow, g acceleration due to gravity and S_f the friction slope. For the general case, the inflow is $i_e(t) = i(t) - f(t)$ where $i(t)$ is the precipitation intensity and $f(t)$ infiltration losses. The problem is fully defined if the initial conditions and boundary conditions are known. This is true if the plane is assumed to be initially dry:

For $0 \leq x \leq L$ and $t = 0$: $V = 0$ and $h = 0$ (5.37)

For $x = 0$ and $t > 0$: $V = 0$ and $h = 0$ (5.38)

Kinematic-wave model

Assuming that the terms related to the force of gravity balance the forces of friction at the surface of the plane and that the other terms of the equation are zero, a simplified model is obtained, referred to as the kinematic-wave model (see also Chapter 6).

$$S_0 = S_f \tag{5.39}$$

A friction model (e.g., Manning, Chézy) can be used to relate the discharge per unit width of the plane to the flow depth h in an unequivocal manner.

$$q = \alpha \cdot h^m \tag{5.40}$$

Combining the mass conservation equation (where $Vh = q$) with this discharge equation gives the kinematic-wave equation:

$$\frac{\partial h}{\partial t} + \alpha \cdot m \cdot h^{m-1} \frac{\partial h}{\partial x} = i_e \tag{5.41}$$

For the general case, the problem does not have any explicit solution. It must therefore be solved numerically. Assuming uniform and constant rainfall intensity $i(t)$ simplifies the problem. Note that equation 5.41 can be written in the following full differential form:

$$\frac{\partial h}{\partial t} + \frac{dx}{dt}\frac{\partial h}{\partial x} = \frac{dh}{dt} \quad \text{with} \quad \frac{dx}{dt} = \alpha \cdot m \cdot h^{m-1} \quad \text{and} \quad \frac{dh}{dt} = i_e \tag{5.42}$$

Consequently, for an observer moving at velocity:

$$c = \frac{dx}{dt} = \alpha \cdot m \cdot h^{m-1} \tag{5.43}$$

the relationship between water depth h and i_e is:

$$\frac{dh}{dt} = i_e \tag{5.44}$$

The two above equations are ordinary differential equations the can be solved by the method of characteristics (Eagleson, 1970). Solutions are only valid on the characteristic curves defined by equation 5.43. For an initially dry surface, integration of equations 5.44 and 5.43 give respectively:

$$h = h_0 + i_e \cdot t = i_e \cdot t \tag{5.45}$$

$$x = x_0 + \alpha \cdot i_e^{m-1} \cdot t^m \tag{5.46}$$

where x_0 is the abscissa of the point where the characteristic starts (at $t = 0$). Finally the discharge equation (eq. 5.40) gives the discharge at any point on the characteristic:

$$q = \alpha \cdot \left(i_e \cdot t \right)^m \tag{5.47}$$

The last three equations can be used to estimate the concentration time, the profile of the water surface at equilibrium and the evolution of the discharge at the outlet of the plane (i.e., for $x = L$).

Concentration time

Assuming that $t = t_c$ for $x – x_0 = L$, equation 5.46 expresses the concentration time:

$$t_c = \left(L / a \ i_e^{m-1} \right)^{1/m} \tag{5.48}$$

The concentration time is the time taken by the wave to travel the length L of the inclined plane. It is not the travel time of a particle of water coming from the top of the inclined plane. If the Manning friction model is used, the expression for the concentration time becomes:

$$t_c = \frac{6.9}{i_e^{0.4}} \left[\frac{n \cdot L}{\sqrt{S_0}} \right]^{0.6} \tag{5.49}$$

where t_c is expressed in minutes, i_e in mm/h, L in meters and S_0 is dimensionless.

Steady-state water surface

Steady state is reached when $\dfrac{\partial h}{\partial t} = 0$. The expression for the water surface is obtained by solving equation 5.41:

$$h(x) = \left(i_e \cdot x / \alpha \right)^{1/m} \tag{5.50}$$

where $h(x)$ is the depth of water obtained at the abscissa x in steady state and the x-axis is parallel to the slope and oriented from the top to the bottom. The discharge equation (eq. 5.40) for the abscissa $x = L$ gives the outflow per unit width of the inclined plane:

$$\text{at } x = L: \ q = \alpha \cdot h(L)^m = i_e \cdot L \tag{5.51}$$

Note that the total outflow from the inclined plane is:

$$Q = W \cdot q = W \cdot i_e \cdot L = A \cdot i_e \tag{5.52}$$

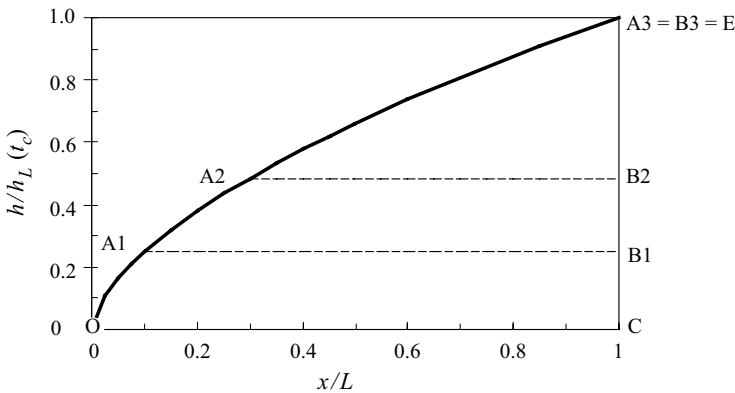where A is the area of the inclined plane and i_e is the intensity of the net precipitation.

Fig. 5.23: Dimensionless profile of the water surface. Profile obtained for steady state (OA$_3$C) and at two times before reaching steady state (OA$_1$B$_1$C and OA$_2$B$_2$C) using the kinematic-wave model where $h_L(t_c)$ is the depth below the water surface at time $t = t_c$ at the outlet from the inclined plane (i.e., at $x = L$).

5.7.2 Unit Hydrograph Identification Methods

General case: matrix inversion

Different methods can be used to identify the unit hydrograph. They are based on the deconvolution technique. If the net rainfall and runoff hydrograph are described respectively by M mean intensities i_m and N values of discharges Q_n, then N equations can be formulated for Q_n, $n=1,\ldots$,N. These equations involve $N-M+1$ unknowns u_k that define the unit hydrograph (note that Q_{N+1} $= 0$ and therefore the terms $u_{N-M+2} = u_{N-M+3} = u_{N-M+4} = u_N = u_{N+1}$ are zero). The system of equations can be written in matrix form as follows:

$$
\begin{bmatrix}
i_1 & 0 & 0 & \ldots & 0 & 0 & \ldots & 0 & 0 \\
i_2 & i_1 & 0 & \ldots & 0 & 0 & \ldots & 0 & 0 \\
i_3 & i_2 & i_1 & \ldots & 0 & 0 & \ldots & 0 & 0 \\
. & . & . & \ldots & . & . & \ldots & . & . \\
. & & & \ldots & & & \ldots & & \\
. & & & \ldots & & & \ldots & & \\
i_M & i_{M-1} & i_{M-2} & \ldots & i_1 & 0 & \ldots & 0 & 0 \\
0 & i_M & i_{M-1} & \ldots & i_2 & i_1 & \ldots & 0 & 0 \\
. & & & \ldots & & & \ldots & & . \\
. & & & \ldots & & & \ldots & & . \\
. & & & \ldots & & & \ldots & & . \\
0 & 0 & 0 & \ldots & 0 & 0 & \ldots & i_M & i_{M-1} \\
0 & 0 & 0 & \ldots & 0 & 0 & \ldots & 0 & i_M
\end{bmatrix}
\cdot
\begin{bmatrix}
u_1 \\
u_2 \\
u_3 \\
\\
\\
u_{N-M+1}
\end{bmatrix}
=
\begin{bmatrix}
Q_1 \\
Q_2 \\
Q_3 \\
. \\
. \\
. \\
Q_M \\
Q_{M+1} \\
. \\
. \\
. \\
Q_{N-1} \\
Q_N
\end{bmatrix}
\tag{5.53}
$$

or in the following condensed form:

$$[i] \cdot [u] = [Q] \tag{5.54}$$

where $[u]=[u_1, u_2, \ldots u_{N-M+1}]^T$, the vector of the $N-M+1$ values defining the required unit hydrograph.

In general, the system of equations is overdetermined given that the number of equations (N) is greater than the number of unknowns ($N-M+1$).

Let $[\hat{u}]$ be an estimate of the UH giving the estimate $[\hat{Q}]$ of the observed hydrograph $[Q]$ by convolution with the net rainfall $[i]=[i_1, i_2, \ldots i_M]$. Identification of the UH consists in finding the estimate $[\hat{u}]$ that minimizes the error ε between the simulated hydrograph $[\hat{Q}]$ and the observed hydrograph $[Q]$. Given that the system is generally overdetermined, classical numerical optimization methods can be used for this. These methods do not however guarantee that all the ordinates of the identified UH are positive (Chow *et al.*, 1988).

Special case of block-type net rainfall

Identification of the unit hydrograph of a given basin is simplified if it is possible to select a rainfall-runoff event with a net rainfall possessing a well-marked middle part. In this case, it possible to consider that the rainfall hyetograph: 1) is concentrated on a short duration τ and 2) has a constant intensity over this duration. The different steps of the identification procedure are summarized below and illustrated in Example 5.3 at the end of this appendix.

For each time step, the ordinate of the direct runoff hydrograph, obtained by a given hydrograph separation method, is normalized with respect to the runoff depth ($D_R=V_R/A$ where V_R is the runoff

volume and A the area of the basin). The hydrograph obtained is the unit hydrograph produced by the unit rainfall of depth $d = 1$ and for which the reference duration corresponds to the duration τ of the observed increment of net rainfall.

Identification for any given reference duration

The reference duration of the UH identified by any of the above methods is determined by the available data (in principle, it is equal to the time step of the data). If the reference duration (e.g., τ) does not correspond to the required reference duration (e.g., T), the required UH can be calculated using the S-curve.

The S-curve is first produced from the UH corresponding to a rainfall of depth d and reference duration τ. The difference between two S-curves shifted by time interval T gives the ordinates of the UH corresponding to a rainfall of depth $d \cdot T / \tau$ and duration T (Figure 5.5). To obtain the ordinates of the UH corresponding to a rainfall of depth d and duration T, the ordinates of the above UH must be divided by the ratio T/τ.[6] This procedure is illustrated in Example 5.3.
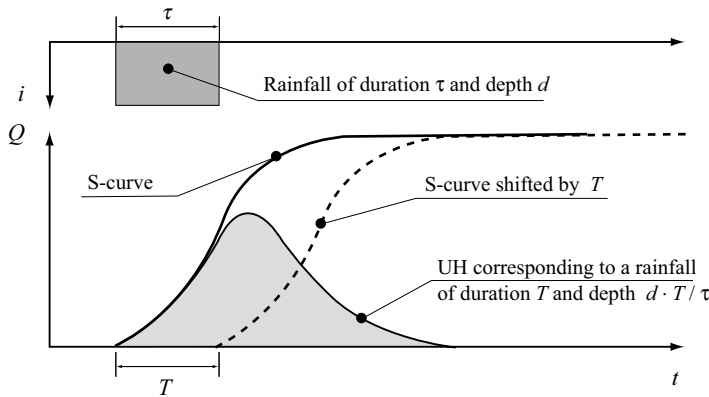

Fig. 5.24: Shifting of the S-curve to calculate the UH for any given reference duration T.

Example 5.3

The objective here is to identify the unit hydrograph of a flood observed on 31/08/1975 on the Parimbot river in Switzerland (drainage basin area = 380 ha). This example is provided only as an illustration given that the conditions required for the application of the identification method are rarely satisfied in practice.

The 31/08/1975 flood plotted below is assumed to satisfy the conditions mentioned above, i.e., it is considered to result from a net rainfall concentrated on a short duration (30 minutes).

Separation of direct runoff and base flow makes it possible to extract the ordinates of the direct runoff hydrograph ($Q(t)$ in the table below), estimate the volume of direct runoff (V_R = 2030 m³) and therefore the runoff depth ($D_R = V_R / A$ = 0.53 mm). The separation method used here is based on the identification of an inflection point on the logarithmic plot of the discharges (see Chapter 8). For each time step, the ordinates of the UH for a net rainfall of 1 mm are estimated by multiplying it by $1/D_R$.

The duration of the reference rainfall corresponds to the duration of the observed net rainfall hyetograph. Given the low runoff depth (0.53 mm), the net rainfall is concentrated in the middle of the gross rainfall hyetograph. Assuming a constant infiltration capacity (method of constant continuous losses or φ index method, Chapter 4), only the peak of the hyetograph between times 06:30 and 06:45

---

[6]It is easier to obtain a UH corresponding to a reference duration of $T = n.\tau$ (where n is a whole number) using the convolution principle.
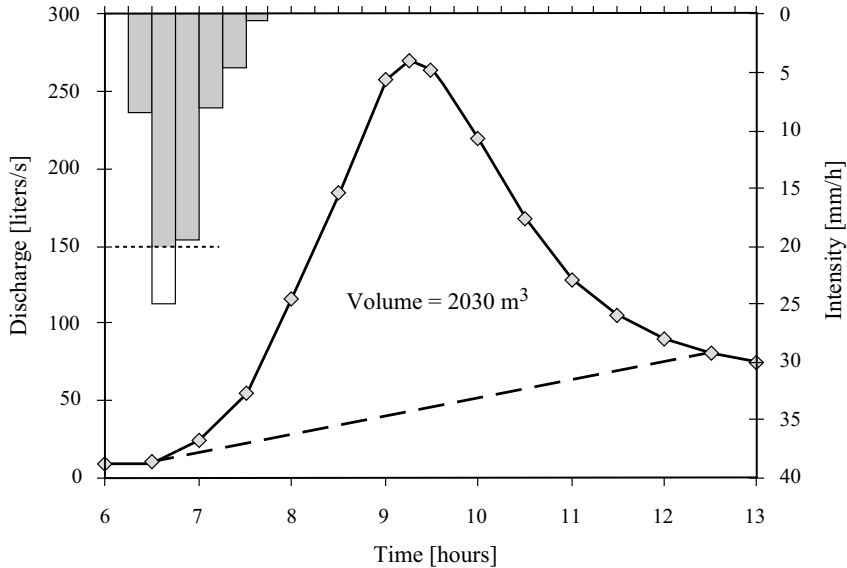
Fig. 5.25: Flood observed on 31/08/1975 on the Parimbot river (Switzerland).

generates runoff. This gives a reference duration of 15 minutes. A decrease in the infiltration capacity with time is however more probable. For this reason, it is preferable to consider that the entire peak of the rainfall is at the origin of the runoff between 06:30 and 07:00. A duration of 30 minutes is therefore adopted for the unit rainfall. The corresponding UH is normalized ($u_{30,1}(t)$) in Table 5.5.

The S-hydrograph of the drainage basin for a net rainfall of 2 mm/h is obtained by summing n UHs $u_{30,1}(t)$ shifted by 30 minutes each. The S-hydrograph reaches a constant value after 5 hours.

The UH for a 2 mm deep net rainfall with a reference duration of 1 hour ($u_{60,2}(t)$) can be determined by calculating the difference between two S-curves shifted by $T = 1$ hour. For each time step, the difference is multiplied by τ/T, where $\tau = 30$ minutes and $T = 60$ minutes. This gives the UH for a 1 mm deep normalized rainfall with a reference duration of 1 hour ($u_{60,1}(t)$).

Table 5.5: Estimation of the unit hydrograph for the flood observed on 31/08/1975 on the Parimbot river (Switzerland).

t [h]	$Q(t)$ [l/s]	t [h]	$u_{30,1}(t)$ [l/s]	$s(t)$ [l/s]	$s(t\text{-}T)$ [l/s]	$u_{60,2}(t)$ [l/s]	$u_{60,1}(t)$ [l/s]
06:30	0	0	0	0		0	0
07:00	10	0.5	19	19		19	9.5
07:30	34	1	64	83	0	83	41.5
08:00	88	1.5	166	249	19	230	115
08:30	160	2	302	551	83	468	234
09:00	216	2.5	408	959	249	710	355
09:30	218	3	411	1370	551	819	410
10:00	168	3.5	317	1687	959	728	364
10:30	110	4	208	1895	1370	525	263
11:00	62	4.5	117	2012	1687	325	163
11:30	33	5	62	2074	1895	179	90
12:00	12	5.5	23	2097	2012	85	43
12h30	0	6	0	2097	2074	23	12

5.7.3 Geomorphological Unit Hydrograph

Principle and assumptions

Depending on the path of a raindrop in the illustration in Figure 5.26, where a circle represents the set of watercourses of order *i* (or a state *i* of the system) according to the Horton-Strahler classification system (see definition below or in Musy and Higy (2011)).

In this example, the starting point of the raindrop can be a watercourse of order 1, 2 or 3. Assuming a random starting point, the probability that the drop of water starts its path at 1, 2 or 3 is respectively p_{01}, p_{02} and p_{03}. These probabilities p_{0i} correspondent to the initial state of the system.

Let us now follow the flow of a drop of water in the hydrographic network. For example, p_{12} is the probability that a drop of water flows from a watercourse of order 1 to a watercourse of order 2. The probability of a transition from state *i* to state *j* is defined as p_{ij}, where $p_{ij} = 0$ when $j < i$ given that water does not flow backwards in the network ($j = i$ corresponds to the conservation of a drop of water in a watercourse of the same order). To simplify the working of the system, the following assumptions are made:

- The net rainfall falls only on the land surfaces and not on the watercourses of the drainage basin.
- The net rainfall that falls on a land area of order *u* is drained exclusively by a watercourse of order *u+1*. The corollary of this is that water moves only from upstream to downstream.
- A transition from one state to another can only take place if the order of the new state is greater than the order of the previous state.
- All drops of water flow to the basin outlet. This eliminates the possibility of any endorheic phenomena (such phenomena are related to drainage basins with a particular shape such that their hydrographic network is not linked to any other hydrographic network). The passage from one state to another (i.e., from one watercourse to another) depends only on the location of the drop of water at that time, meaning that the drop of water has no memory of the path it took to reach its present watercourse.
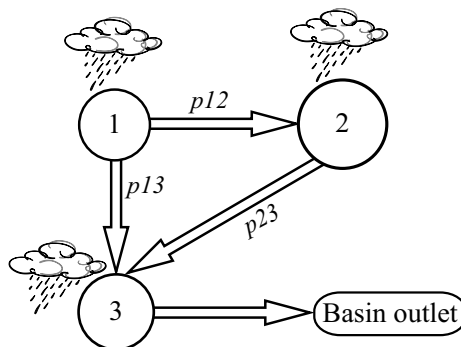

Fig. 5.26: Schematic representation of a 3rd order drainage basin and probabilities of the transition of a watercourse of order *i* into a watercourse of order *j > i* (adapted from Rodriguez-Iturbe and Valdés, 1979).

Approximations

The expression for the geomorphological unit hydrograph (GUH) is in this case generally complex and depends on the order of the drainage basin. For this reason, the GUH is often approximated by a simpler model for which the parameters are estimated on the basis of the geomorphological parameters of the basin. If the approximation model is a triangular UH (see for Example 5.7.7), its parameters (time-to-peak t_p and discharge Q_p) are given by the following equations:

$$Q_p = \frac{1.31}{L} \cdot R_l^{0.45} \cdot v \tag{5.55}$$

$$t_p = \frac{0.44 \cdot L}{v} \cdot R_b^{0.55} \cdot R_a^{-0.55} \cdot R_l^{-0.38} \tag{5.56}$$

where Q_p and t_p are respectively the peak discharge [h^{-1}] and time-to-peak [h] of the UH, v the mean velocity in the main watercourse [m/s], L the length of the main watercourse [km] and R_a, R_b and R_l the Horton-Strahler ratios (see below).

If the approximation model is a Nash model, its parameters (the number of reservoirs n and time-to-peak t_p) can be estimated using the following equations (to obtain the equations for the two parameters n and t_p, the product $(q_p t_p)$ of the Nash hydrograph must be equated with that of the GUH):

$$n = 3.29 \left(\frac{R_b}{R_a} \right)^{0.78} \cdot R_l^{0.07} \tag{5.57}$$

$$t_p = (n-1) \left[0.7 \cdot \left(\frac{R_a}{R_a \cdot R_l} \right)^{0.48} \cdot v^{-1} \cdot L \right] \tag{5.58}$$

The parameters t_p and q_p are a function of the mean velocity in the watercourse.

Horton-Strahler ratios R_b, R_l and R_a.

R_b is the proportionality constant between the number of tributaries of order u and the number of tributaries of order $u+1$:

$$R_b = \frac{N_u}{N_{u+1}} \quad \textit{(bifurcation ratio)} \tag{5.59}$$

where N_u is the number of tributaries of order u and N_{u+1} the number of tributaries of order $u+1$.

R_l is the proportionality constant between the length of tributaries of order u and the length of tributaries of order $u+1$:

$$R_l = \frac{L_{u+1}}{L_u} \quad \textit{(length ratio)} \tag{5.60}$$

where L_u is the length of tributaries of order u and L_{u+1} the length of tributaries of order $u+1$.

R_a is the proportionality constant between the area of tributaries of order u and the area of tributaries of order $u+1$:

$$R_a = \frac{A_{u+1}}{A_u} \quad \textit{(area ratio)} \tag{5.61}$$

where A_u is the area of tributaries of order u and A_{u+1} the area of tributaries of order $u+1$.

These different quantities are sometimes derived from the fractal properties of the drainage network (Rodriguez-Iturbe and Rinaldo, 1997).

5.7.4 Discrete Solution of the Linear Reservoir Model

With the linear reservoir model, the expression for the outflow $q(t)$ (e.g., the specific discharge at the basin outlet) resulting from the inflow $i(t)$ (e.g., net rainfall) is given by the following convolution:

$$q(t) = q(t_0) \cdot e^{\frac{t_0-t}{K}} + \int_{t_0}^{t} \frac{i(\tau)}{K} e^{-\frac{t-\tau}{K}} \, d\tau \tag{5.62}$$

Recurrence relation for the instantaneous outflow q(t)

If the inflow $i(t)$ is constant over the time interval $[t-\Delta t, t]$, then based on the expression above and calculating the integral associated with the term $A(t) = q(t) - \exp(-\Delta t/K) \cdot q(t-\Delta t)$, it is possible to express the outflow $q(t)$ at time t as a function of the outflow $q(t-\Delta t)$ at time $t-\Delta t$ and the mean inflow over the interval $[t-\Delta t, t]$:

$$q(t) = \alpha \cdot q(t - \Delta t) + (1 - \alpha) \cdot \overline{i_{t-\Delta t,t}} \tag{5.63}$$

where

$$\alpha = \exp(-\Delta t / K) \tag{5.64}$$

and $\overline{i_{t-\Delta t,t}}$ is the mean of the inflow $i(t)$ over time interval $[t, t+\Delta t]$. The variables $q(t)$ and $\overline{i_{t-\Delta t,t}}$ are expressed in the same units (e.g., in mm/h). The same is true for the parameter K and the time step Δt (e.g., in hours).

Recurrence relation for the mean outflow $[n\Delta t, (n+1)\Delta t]$

By integration, an explicit and exact expression for the rainfall-runoff relationship can be obtained for the input and output variables described at time step Δt by their mean values over each time interval. This equation is obtained on the basis of the exact expression for the instantaneous discharge (eq. 5.63), by calculating the following two integrals and considering that they are equal:

$$\int_{\tau=0}^{\tau=\Delta t} \left(q(t+\tau) - \exp(-\Delta t/K) \cdot q(t-\Delta t+\tau) \right) \cdot d\tau$$
$$= \int_{\tau=0}^{\tau=\Delta t} \left((1 - \exp(-\Delta t/K)) \cdot \overline{i_{t-\Delta t+\tau,t+\tau}} \right) \cdot d\tau \tag{5.65}$$

where the expression for the mean inflow over interval $[t-\Delta t+\iota, t+\iota]$ is:

$$\overline{i_{t-\Delta t+\tau,t+\tau}} = (\Delta t - \tau)/\Delta t \cdot \overline{i_{t-\Delta t,t}} + \tau/\Delta t \cdot \overline{i_{t,t+\Delta t}} \tag{5.66}$$

To calculate the second integral of equality 5.65, it must be assumed that the inflow is constant over the entire time interval $[n\Delta t, (n+1)\Delta t]$.

Integration of the two members of equation 5.65 gives the expression for the mean outflow q_n over the time interval $[n\Delta t, (n+1)\Delta t]$. This is a weighted average of the outflow q_{n-1} over the previous time interval and the mean inflows i_n and i_{n-1} over the current and previous time intervals. The output signal $q(t)$ over the time step Δt (i.e., its mean values $q_1, q_2, ..., q_m$ over Δt) resulting from an input signal $i(t)$ (described by its mean values $i_1, i_2, ... i_n$ over Δt) can be determined on the basis of the following initial condition and recurrence relation:

$$\begin{cases} q_n = q_0 & \text{for } n = 0 \\ q_n = \alpha \cdot q_{n-1} + (1 - \alpha) \cdot \left(\dfrac{i_n + i_{n-1}}{2} \right) & \text{for } n > 0 \end{cases} \tag{5.67}$$

where q_0 is the initial mean value of the outflow, q_n and i_n are expressed in the same units (e.g., mm/h), K and Δt are expressed in the same units (e.g., hours) and α is defined by equation 5.64. Note that this expression is a special case of the general expression for a linear transfer function (Appendix 5.7.6).

Recurrence relation for the net rainfall-runoff relationship

The recurrence relation to estimate the hydrograph $Q_1, Q_2, ..., Q_m$ at time step Δt resulting from a net rainfall $I_1, I_2, ... I_n$ can be expressed as:

$$
\begin{cases}
Q_n = Q_0 & \text{for } n = 0 \\
Q_n = \alpha \cdot Q_{n-1} + (1-\alpha) \cdot A.u.\left(\dfrac{I_n + I_{n-1}}{2}\right) & \text{for } n > 0
\end{cases}
\tag{5.68}
$$

where Q_n is the mean discharge and I_n the mean intensity of the net rainfall over the interval [$n\Delta t$, $(n+1)\Delta t$], A the area of the drainage basin and u a units conversion constant (u=0.00278 if A is expressed in ha, Q in m³/s and P in mm/h).

5.7.5 Cascade of Linear Reservoirs (Nash model)

By successively solving the linear reservoir equation for each of the reservoirs of the Nash cascade, it is possible to obtain the expression for the instantaneous unit hydrograph of the Nash model. Let K be the reservoir storage coefficient [hours] and n the number of reservoirs. For an instantaneous unit rainfall, the outflow from the first reservoir is the IUH of the linear reservoir given by equation 5.17:

$$
u_1(\tau) = \frac{1}{K} \cdot e^{\left(\frac{-\tau}{K}\right)}
\tag{5.69}
$$

When this function is used as the inflow to the second reservoir, the outflow of the second reservoir, obtained by convolution of this inflow and the IUH of the second reservoir (also equal to $u_1(t)$), can be expressed as:

$$
u_2(t) = \int_0^t i(\tau) \cdot u(t - \tau) \cdot \mathrm{d}\tau = \int_0^t u_1(t) \cdot \frac{1}{K} \cdot e^{\left(\frac{-1}{K}(t-\tau)\right)} \cdot \mathrm{d}\tau
\tag{5.70}
$$

$$
u_2(t) = \frac{t}{K^2} \cdot e^{\left(\frac{-t}{K}\right)}
\tag{5.71}
$$

Reiterating the calculation process for each of the n reservoirs gives immediately the expression for the outflow of the nth reservoir, i.e., the IUH of the Nash model:

$$
u_n(t) = \frac{1}{K \cdot \Gamma(n)} \cdot \left(\frac{t}{K}\right)^{(n-1)} \cdot e^{\left(\frac{-t}{K}\right)}
\tag{5.72}
$$

where $\Gamma(n)$ is the gamma function defined by:

$$
\Gamma(n) =
\begin{cases}
(n-1)! & \forall n \in \mathbb{N} \\
\int_0^\infty u^{n-1} \cdot e^{-u} \cdot \mathrm{d}u & \forall n \in \mathbb{R}
\end{cases}
\tag{5.73}
$$

5.7.6 General Expression for a Linear Transfer Function

If at time *t,* the model input signal is designated $u(t)$, $t = 1, 2, .., N$ and the output signal $y(t)$, and if we assume that the input and output signals are related by a linear system, then the relationship between the input and output can be written in the following form (Ljung, 1999):

$$y(t) = G(q) \cdot u(t) + H(q) \cdot e(t) \tag{5.74}$$

where $e(t)$ is a white noise at time t, q a lag operator and $G(q)u(t)$ and $H(q)e(t)$ the condensed expressions of:

$$G(q)u(t) = \sum_{k=1}^{\infty} g(k)u(t-k) \text{ and } H(q)e(t) = \sum_{k=1}^{\infty} h(k)e(t-k) \tag{5.75}$$

with:

$$G(q) = \sum_{k=1}^{\infty} g(k)q^{-k}, \ H(q) = \sum_{k=1}^{\infty} h(k)q^{-k} \text{ and } q^{-k}u(t) = u(t-k) \tag{5.76}$$

The numbers $\{g(k)\}$ are called the impulse response of the system. In other terms, $g(k)$ is the system output at time k if the input is a single impulse at time $t = 0$.

Assuming that the functions $G(q)$ and $H(q)$ can be expressed in the form $G(q) = B(q)A^{-1}(q)F^{-1}(q)$ and $H(q) = C(q)A^{-1}(q)D^{-1}(q)$, the general expression for a linear system can be obtained, commonly referred to as the transfer function of the system.

$$A(q)y(t) = \frac{B(q)}{F(q)}u(t-n_k) + \frac{C(q)}{D(q)}e(t) \tag{5.77}$$

where n_k represents the time shift between input $u(t)$ and output $y(t)$. The polynomials $A(q)$, $B(q)$, $C(q)$, $D(q)$ and $F(q)$ include a finite number of terms (respectively n_a, n_b, n_c, n_d and n_f) and are defined as follows:

$$A(q) = 1 + a_1 q^{-1} + ... + a_{n_a} q^{-n_a} \tag{5.78}$$

$$B(q) = b_1 + b_2 q^{-1} + ... + b_{n_b} q^{-n_b+1} \tag{5.79}$$

$$C(q) = 1 + c_1 q^{-1} + ... + c_{n_c} q^{-n_c} \tag{5.80}$$

$$D(q) = 1 + d_1 q^{-1} + ... + d_{n_d} q^{-n_d} \tag{5.81}$$

$$F(q) = 1 + f_1 q^{-1} + ... + f_{n_f} q^{-n_f} \tag{5.82}$$

For a model with several inputs (*nu*), equation 5.77 can also be written in the form:

$$A(q)y(t) = \frac{B_1(q)}{F_1(q)}u_1(t-n_{k_1}) + ... + \frac{B_{nu}(q)}{F_{nu}(q)}u_{nu}(t-n_{k_{nu}}) + \frac{C(q)}{D(q)}e(t) \tag{5.83}$$

where the polynomials $B_k(q)$ and $F_k(g)$ are defined by:

$$B_k(q) = b_1^k + b_2^k q^{-1} + ... + b_{n_{b_k}}^k q^{-n_{b_k}+1} \quad (k = 1...nu) \tag{5.84}$$

$$F_k(q) = 1 + f_1^k q^{-1} + \ldots + f_{n_{f_k}}^k q^{-n_{f_k}} \quad (k = 1\ldots nu) \tag{5.85}$$

According to Ribeiro *et al*. (1998), the general structure of equation 5.77 includes the expression of 32 types of different linear model structures. Among these models, the most widely used in hydrology are those for which $n_d = n_f = 0$. The advantage of this simplification is easier parameter estimation. The corresponding models are the so-called autoregressive models (Box and Jenkins, 1970), briefly discussed in Appendix 10.7.1.

5.7.7 SCS Regional Synthetic Unit Hydrograph

The US Soil Conservation Service (SCS) has compiled a large number of average UHs identified on drainage basins of different regions in the United States (USDA-SCS, 1972). The UHs are described in dimensionless plots of $q(t)/q_p$ versus t/t_p (where t_p is the time-to-peak and q_p the peak discharge of the UH). The regional synthetic UH resulting from the corresponding analysis and S-curve is given in Figure 5.27.
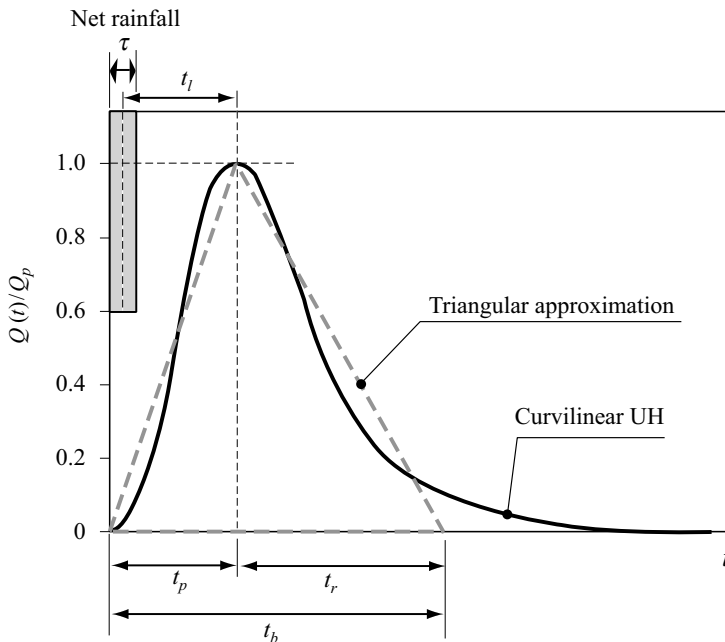

Fig. 5.27: Dimensionless synthetic unit hydrograph proposed by the SCS and its triangular approximation (adapted from USDA-SCS, 1972).

To simplify the use of the synthetic unit hydrograph, the SCS proposes a triangular approximation that depends on just two parameters: q_p and t_p. For a given basin, the SCS proposes to estimate these parameters with the following regional equations:

$$t_p = \frac{D}{2} + 0.6 \cdot t_c \tag{5.86}$$

$$q_p = \frac{1.5 \, V_R}{(D + 1.2 \, t_c)} \tag{5.87}$$

where D is the duration of the reference unit rainfall producing the hydrograph, V_R the runoff volume and t_c the concentration time of the basin (defined here as the time elapsed between the end of the rainfall and the inflection point on the recession limb).

Both these equations come from a combination of different equations based on experience and different relationships between the variables describing the triangular synthetic UH:

Flood volume: $V_R = \dfrac{q_p}{2}\left(t_p + t_r\right)$ (5.88)

Time-to-peak: $t_p = \dfrac{D}{2} + t_l$ (5.89)

where t_r is the recession time and t_l the basin lag time between the center of mass of the net rainfall and the hydrograph peak. The SCS estimates that, for the United States, t_l equals approximately $0.6 \cdot t_c$ and that 37.5% of the flood volume occurs before the hydrograph peaks (consequently $t_p/t_b = 0.375$ and $t_b = 2.67\,t_p$ where t_b is the time base of the hydrograph).

RESERVOIR AND STREAMFLOW ROUTING

The previous chapters presented various methods to estimate the way that precipitation is distributed between the different compartments of a drainage basin and the way the resulting groundwater, sub-surface water and surface water is transformed into a hydrograph at the basin outlet. This chapter will present methods designed to estimate the way discharges are propagated through streams, lakes and reservoirs and in particular the way the shape of the hydrograph changes from upstream to downstream. The models used for this are often referred to as reservoir and streamflow routing models.

The propagation of flows is clearly a problem related more to hydraulics than hydrology. This chapter is not intended to cover all aspects of this scientific discipline. For more information on this topic, the reader can consult any of the many works dealing with open-channel hydraulics, for example Chadwick and Morfett (1998), Graf and Altinakar (1998) or Sturm (2001) in English or Lencastre (1999) or Graf and Altinakar (2000) in French. The purpose of this chapter is to review the main elements required to understand and estimate the routing of flows and discharges.

Section 6.1 identifies the main effects of flow propagation. Section 6.2 presents several approaches that can be used to route flows through lakes and reservoirs. The next two sections focus on streamflow routing models, Section 6.3 dealing with hydraulic routing models and Section 6.4 with hydrological routing models. The first are derived from the basic hydraulic equations of open-channel one-dimensional gradually-varied flows that govern the variation of discharges in space and time. Hydrological routing models, on the other hand, are based on a more conceptual approach. Section 6.5 presents models that can be used for two-dimensional flows observed in certain contexts such as bank overflow. Section 6.6 indicates various criteria the can be used to identify the best methods for a given context.

6.1 INTRODUCTION

6.1.1 Flow Propagation and Streamflow Routing

Streamflows resulting from groundwater, surface and sub-surface runoff are governed by the topography and physical characteristics of the basin. These streamflows are three-dimensional and characterized by different variables, in particular their velocities in the *x*,

y and z directions (V_x, V_y, V_z) and the water depth at every point in the considered domain. These quantities obviously vary in space and time. For the general case, their description and in particular their modeling (based on hydrodynamic equations) are complex.

The description of flows for common hydrological applications can however be simplified. For streamflows, for example, they are often considered to be one-dimensional and described at every point x along the curvilinear abscissa of the watercourse by the flow depth, mean velocity and discharge observed at time t. A highly detailed description of the flows is generally unnecessary. A more lumped description of the effect of a hydraulic system on the discharges is often sufficient.

The actual propagation of flows is therefore not generally modeled as such. Instead, flow routing techniques are often designed simply to estimate the change in the shape of the hydrograph from upstream to downstream. For one-dimensional streamflows for example, the routing model is used to estimate discharge variations with time (and possibly flow velocity and velocity variations) at certain selected locations along the watercourse. For reservoirs, the purpose of the routing model is generally simply to estimate the temporal variations of the volume of water stored in the reservoir and the outflows resulting from the inflows and reservoir operating rules.

6.1.2 Reservoir Routing

Reservoir routing cannot be dissociated from the effects of reservoir storage and release operations. Variations of the stored volume $S(t)$ are related to the inflows $I(t)$ and outflows $Q(t)$ by the following continuity equation:

$$\frac{dS(t)}{dt} = I(t) - Q(t) \tag{6.1}$$

When inflows are greater than outflows, the reservoir fills. In the opposite case, it empties. Due to storage and releases, the outflow hydrograph does not have the same shape as the inflow hydrograph. In particular, it is attenuated and shifted in time, i.e., the peak outflow is lower than the peak inflow and occurs later.

For uncontrolled reservoirs, as long as the water surface can be considered horizontal at all times, the outflow is simply a function of the volume stored in the reservoir. Consequently, the outflow is maximum when the volume stored in the reservoir is maximum. Moreover, the maximum outflow observed at time t_p is equal to the inflow at that time. Typical temporal variations of inflow, outflow and reservoir storage volume are illustrated in Figure 6.1.

For controlled reservoirs, the outflow is not only a function of the volume stored in the reservoir. It also and especially depends on: 1) the management objectives imposed by the different users of the water stored reservoir and 2) the regulation strategy determined by the reservoir manager to reach those objectives. The effect of reservoir control on outflows is therefore highly variable and depends on the case. The outflow hydrograph is generally different from that of the uncontrolled case illustrated in Figure 6.1. Except under special circumstances, a controlled reservoir always attenuates the flood peak of reservoir inflows.
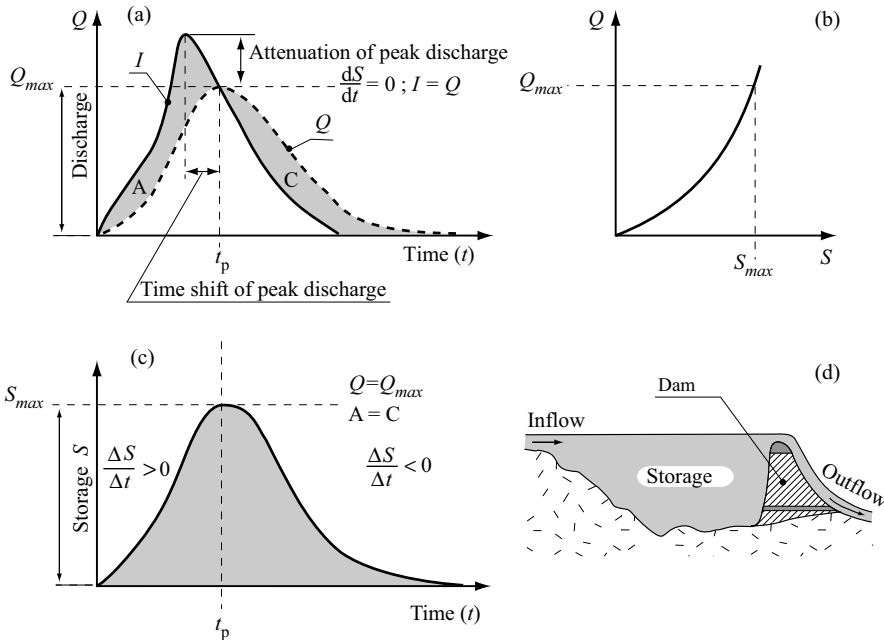
Fig. 6.1: Routing of a flood through an uncontrolled reservoir. a) Inflow and outflow hydrographs. b) Relationship between stored volume and outflow. c) Variation of storage volume with time. d) Longitudinal cross-section of the reservoir (adapted from Bedient and Huber, 2002, with modifications and additions).

6.1.3 Streamflow Routing

Streamflow routing is also influenced by the effects of storage and release within the considered channel reach. However, it also depends on the effects of inertia and energy losses by friction along the reach. The outflow does not depend on the stored volume alone, but also on the inflow. Consequently, it generally shows positive hysteresis (i.e., clockwise direction) as illustrated in Figure 6.2b, showing in particular the rising and recession phases of the flood. The flood peak will be particularly attenuated if the river overflows its banks, i.e., if some of the volume leaves the main channel and flows into a floodway or the natural flood plain.

For one-dimensional flows, the method used for streamflow routing can be either of the hydrological or hydraulic type.

- Hydrological streamflow routing considers flow propagation in a lumped manner and generally only provides an estimate of the mean discharge flowing through the different sections considered. The corresponding models are relatively simple and easy to use.
- Hydraulic streamflow routing is based on the fundamental equations of open-channel hydraulics. It provides not only estimates of the discharges, but also various other flow variables such as velocity and depth. For the case of gradually-varied flows, the corresponding model is referred to as the Barré de Saint-Venant model. Generally speaking, the corresponding system of equations does not have an analytical solution and numerical methods must be used.
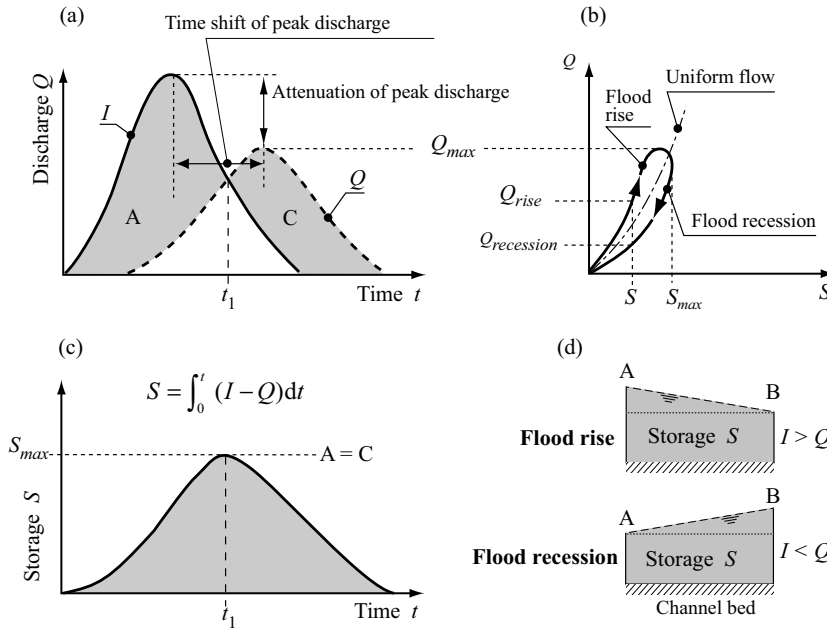
Fig. 6.2: Routing of a flood through the reach of a river. a) Inflow and outflow hydrographs. b) Indirect hysteresis between outflows from and storage in the channel reach. c) Variation of storage volume with time. d) Water surface within the considered channel reach during flood rise and recession (adapted from Bedient and Huber, 2002, with modifications and additions).

6.1.4 Objectives

Flow routing is clearly of great use when the objective is to estimate how a flood is propagated from upstream to downstream through rivers, lakes and reservoirs. This estimation makes it possible to characterize the downstream hydrograph (in terms of time-to-peak or peak discharge) and, in the event of failure of the hydrographic network, the consequences of overbank flow (in terms of flooded area as well as the depth and duration of flooding). Such estimations are required both for flood prediction and forecasting. In the first case, the results are used for the design of the river regulation or flood-protection works, risk mapping and land-use planning (Chastan *et al*., 1994; Metzger, 2002). In the second case, the objective is to forecast the discharges on the basis of hydrographs observed or estimated at different points on the upstream hydrographic network. Such forecasting makes it possible to take preventive measures to reduce potential flood damage, for example precautionary drawdown of upstream reservoirs to increase the peak attenuation potential for the expected flood (Chapter 10).

Flow routing can also be used for other problems not related to flooding, for instance optimized management, often in real time, of simple or complex hydraulic systems related to the operation or protection of resources (e.g., hydropower). Flow routing can also be used for low flows either in a prediction or forecasting context (Chapter 8).

Routing can also be used in simulations to propagate and combine various discharges produced by different parts of a given hydrological basin over a long period of time. This

approach is for example necessary when reconstructing the hydrological conditions of a large drainage basin by simulation or when simulating the effects of different land-use and/or climate change scenarios.

This chapter focuses on methods used to simulate the routing of flows through rivers, lakes and reservoirs. It will not deal with all of the various problems that can be encountered, although some of them may be mentioned below. Readers interested in more details concerning any of these problems can consult the many works published in the corresponding specialized field.

In the urban environment, flows from storm runoff are propagated mainly within the artificial drainage network. The storm drainage network may be separate from the wastewater network or combined with it. Most routing models use in this context are the same as those used for streamflow routing, however with some refinements when, for example, modeling flows under pressure (in closed conduits) or assessing the consequences of overflow if certain hydraulic works become saturated or fail. For more information on this topic, the reader is invited to consult for example Butler and Davies (2000) or Mays (2001) in English or Chocat (1997) in French.

This chapter does not deal either with the problem of real time management of reservoirs or the various other hydraulic works constructed on the hydrographic network. For reservoirs, such management is generally associated with various stakes and constraints often implying many players with frequently conflicting needs. Reservoir management and more generally the management of any regulated drainage network make use of regulation techniques or optimization methods based on optimal control theory (e.g., linear or dynamic programming). For more information on this subject, the reader can consult Becker and Yeh (1974), Litrico (1999) or Labadie (2004).

6.2 RESERVOIR ROUTING

Natural and artificial reservoirs modify the temporal evolution of discharges. Inflows are held in the reservoir for a variable period of time. This time can be just a few hours for certain flood-control works (e.g., storm retention basins in urban drainage networks) or up to a few months for reservoirs designed for seasonal or annual management of water resources (e.g., hydropower projects in mountainous regions, water supply or irrigation reservoirs).

Simulation of reservoir routing is a relatively easy task given that the outflow is either controlled by outlet works or a function of the water level in the reservoir. A model designed to route a hydrograph through a reservoir mainly requires three types of equations: 1) a continuity equation, 2) a storage equation and 3) one or more discharge equations.

6.2.1 Model Equations

Continuity equation

The continuity equation expresses the conservation of the mass of water for the considered system. It relates variations in the volume of water $S(t)$ [m^3] stored in the reservoir at time t to the various inflows $I(t)$ and outflows $Q(t)$ [m^3/s].

$$\frac{dS(t)}{dt} = \sum I(t) - \sum Q(t) \qquad (6.2)$$

Inflows include streamflows supplying the reservoir, runoff entering the reservoir directly, precipitation falling on the reservoir and any water that may be diverted to the reservoir from neighboring basins or watercourses. Outflows include discharges via natural outlets from the reservoir, outlet works (e.g., sluiceways, crest gates, siphons, weirs), offtakes (e.g., pumping for irrigation or water supply, penstocks to supply turbines) and losses to infiltration and evaporation (Figure 6.3).

Depending on the context, some of these inflows and outflows may not be present or maybe negligible. Direct precipitation on the water surface and evaporation losses are for example often neglected for studies focusing on flood discharges. However, the can generally not be neglected when studying the behavior of the system over long time periods and/or when the surface area of the reservoir is large with respect to the surface area of the drainage basins (Picouet, 1999).
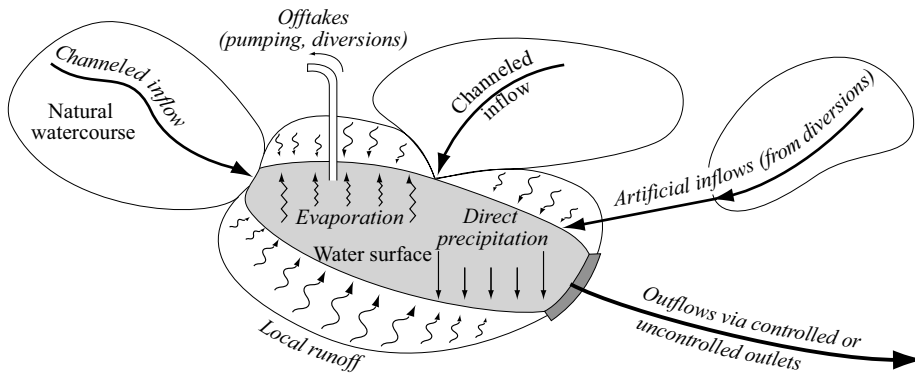

Fig. 6.3: Illustration of the different inflows and outflows for a natural or artificial reservoir.

Storage equation

The storage equation defines the volume of water S [m³] stored in a reservoir for a given water level elevation h [m]. In principle, the equation is time invariant.

$$S = g(h) \qquad (6.3)$$

This relationship, also referred to as the storage-elevation or reservoir capacity equation, is determined by the topography of the reservoir site or the reservoir geometry if the walls have been constructed artificially. It is related to the change in reservoir surface area A_r with respect to the water level h by one of the following two equations:

$$A_r(h) = \frac{dS(h)}{dh} \quad \text{or} \quad S(h) = \int A_r(h) \cdot dh \qquad (6.4)$$

The surface area of the reservoir is required for example for the estimation of evaporation losses. Figure 6.4 illustrates these relationships for an artificial reservoir with a simple geometry.
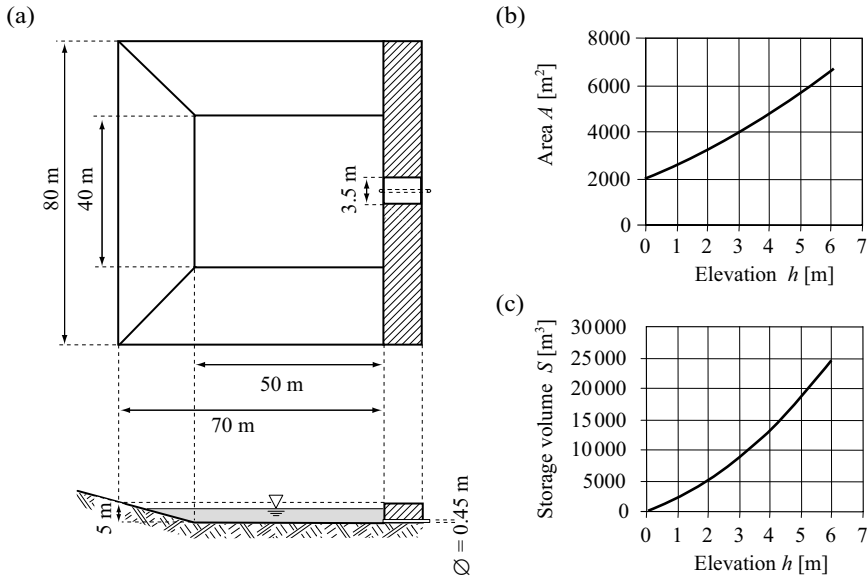
Fig. 6.4: Illustration of the storage equation for an artificial reservoir. a) Reservoir geometry. b) Area-elevation curve. c) Storage-elevation curve.

Discharge equations

A reservoir with a number of different outflow possibilities will have a number of discharge equations. Outflows corresponding to evaporation losses must be estimated on the basis of physically-based or empirical models (Musy and Higy, 2011).

For controlled reservoirs, the outflow is regulated by one or more adjustable outlet works (e.g., gates, pumps, adjustable weirs, etc.). Reservoir regulation is generally based on rules designed to optimize the operation of the outlet works with respect to the different objectives that have been assigned. The controlled outflow can therefore depend on different variables (e.g., reservoir level), downstream constraints (e.g., low-water releases imposed to maintain minimum downstream flows or maximum releases imposed to protect downstream areas against flooding) and constraints related to demand or financial considerations (e.g., water supply requirements, kilowatt-hour prices). For this type of reservoir, the controlled outflow can vary with time in a cyclical or non-cyclical manner. Cyclical variations can be daily, weekly or annual (Figure 6.5).

For uncontrolled reservoirs, the discharge equation is generally a relationship between water level and outflow. This relationship is generally empirical and in principle time invariant. The equation is of the following type:

$$Q = Q(h) \tag{6.5}$$

This relationship depends on the flow regime and the geometry of the flow control section at the reservoir outlet. For an artificial reservoir, it depends on the type of outlet works (Figure 6.6). Depending on the flow regime, the relationship can also involve the water level downstream of the outlet works (Carlier, 1972; Sinniger and Hager, 1989). Note that several outlet works can be used at the same time (e.g., normal and emergency outlet works).
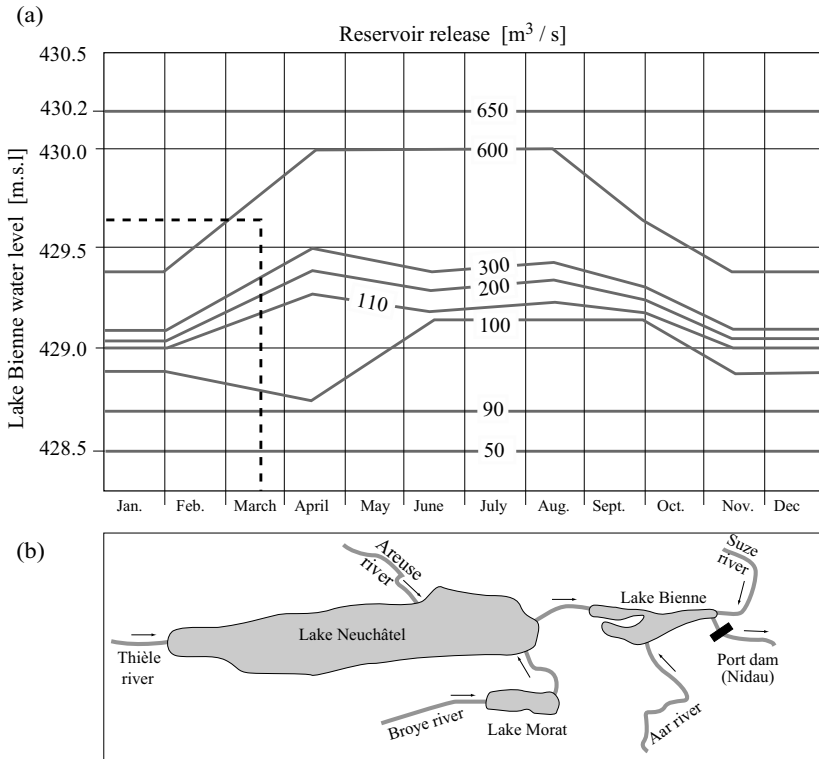
(a)

(b)

Fig. 6.5: Diagram used to control water levels in a system of three Jura lakes (Neuchâtel, Morat and Bienne) on the Swiss Plateau. The main inflows are streamflows from the Thièle, Broye, Areuse, Aar and Suze rivers and direct precipitation on the lakes. The water levels are controlled by a regulating dam built at Port (Nidau). The controlled outflows are set in accordance with special regulations laid down by the Swiss federal government (VAW, 1996). They depend on the water level observed in Bienne Lake and the day of the year. The regulation rules have been optimized to take into account various constraints related to agriculture, flood risks, hydropower production, ecosystems and recreational uses of the lakes.

6.2.2 Solving the Equations

Generally speaking, the behavior of a reservoir is simulated by numerically solving the system of equations made up of the continuity, storage and discharge equations. The system of equations must always be solved in a discrete manner to estimate the state variables of the system (water levels h, outflows Q) at time $t = i\Delta t$ as a function of the variables estimated for the previous time $t = (i-1)\Delta t$.

In certain cases (e.g., when the outflow is controlled), the system has a trivial solution that can be used to express the variables to be estimated explicitly as a function of the variables estimated for the previous time step.

In the general case, the two variables to be estimated are dependent and it is therefore not possible to obtain an explicit expression. Assuming that outflow is a unequivocal function of outlet discharge and that the storage equation can be written in the following form:
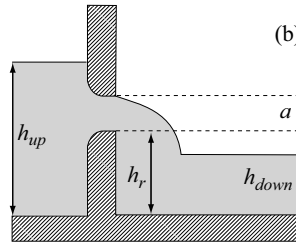
Flow over a weir   (a)

$$Q(h) = \frac{2}{3\sqrt{3}} \cdot m \cdot L \cdot \sqrt{2g} \cdot \left(h - h_r\right)^{3/2}$$
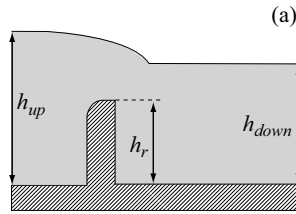
Flow through an orifice

                                                                                        (b)

$$Q(h) = m \cdot A_o \cdot \sqrt{2g} \cdot \sqrt{(h - h_r)}$$

Flow through a culvert [1]

$$Q(h) = m \cdot A_o \cdot \sqrt{2g / D} \cdot (h - h_r)$$
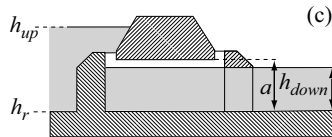
                                                                                        (c)

Fig. 6.6: Examples of discharge equations for different types of outlet works. a) A broad-crested weir of length L [m] and height h_r [m]; b) An orifice or sluice with cross-sectional area of flow A_O [m²] and height h_r [m] (A_O depends on the opening a); c) A culvert (inlet control) with cross-sectional area of flow A_O [m²] and height h_r [m]. D is the vertical dimension of the culvert (diameter if circular or height if rectangular section). In the above equations, Q is the discharge flowing through the outlet [m³/s], $h = h_{up}$ = water elevation upstream of the outlet [m], m is a dimensionless discharge coefficient and g acceleration due to gravity [ms⁻²]. These equations are valid for free flow conditions and a negligible velocity of approach. Free flow conditions exist for example if $(h_{up} - h_r)$ > 3/2 $(h_{down} - h_r)$. Otherwise the flow conditions are referred to as submerged (as illustrated in 6.6a). The equations for submerged flow depend on the downstream water elevation h_{down} (Carlier, 1972; Sinniger and Hager, 1989). If the velocity of approach is non-negligible, the hydraulic head must be considered instead of the water elevation. In this case, the relationship between Q and h is no longer unequivocal.

$$dS = A_r(h) \cdot dh \tag{6.6}$$

where dS is the change in storage volume for a water level variation dh and $A_r(h)$ is the surface area of the reservoir for water level h, then the continuity equation can be expressed in terms of the first derivative of the water level with respect to time:

$$\frac{dh}{dt} = \frac{I(t) - Q(h)}{A_r(h)} \quad \text{or} \quad \frac{dh}{dt} = f(h_n, t_n) \tag{6.7}$$

where the only variable to be estimated at time t_n is the water level in the reservoir h_n.

This differential equation is non-linear and must therefore be solved using a numerical scheme or some other appropriate method. The Puls method commonly used for this will be described below. The Runge-Kutta method is a numerical technique the can be used to

---

[1]For a culvert, the discharge equation provides an approximation based on linear fitting on the culvert inlet control curve (Anctil *et al.*, 2005).

solve many differential equations. It is also frequently used in this context. When applied at a sufficiently high order (e.g., fourth order), the Runge-Kutta method gives results similar to the Puls method. It is often preferred because, as opposed to the Puls method, it provides an explicit numerical scheme for the simulation. However, it is not unconditionally stable and may require a variable time step. The principle of the Runge-Kutta scheme is reviewed in Appendix 6.8.1.

6.2.3 Puls Method

With the Puls method, the continuity equation is discretized to approximate the relationship between inflow, outflow and storage at time steps j and $j+1$ (Figure 6.7). The approximation of the change in storage between these two time steps is:

$$S_{j+1} - S_j = \frac{I_j + I_{j+1}}{2}\Delta t - \frac{Q_j + Q_{j+1}}{2}\Delta t \qquad (6.8)$$

Equation 6.8 has two unknowns S_{j+1} and Q_{j+1}. These unknowns can be placed on the same side of the equation to give the following expression, where Y_{j+1} is a new variable for which the value at time $(j+1)\Delta t$ is known given that all the terms on the right-hand side of the equation are known:

$$Y_{j+1} = \left(\frac{2S_{j+1}}{\Delta t} + Q_{j+1}\right) = \left(I_j + I_{j+1}\right) + \left(\frac{2S_j}{\Delta t} - Q_j\right) \qquad (6.9)$$

Moreover, the combination of the reservoir storage and outflow equations can be used to construct an unequivocal relationship expressing the outflow Q as a function f of the variable $Y = 2\,S/\Delta t + Q$. Knowing the value of Y_{j+1} obtained at time step $j+1$ on the basis of equation 6.9, this relationship can be used to obtain the required value of outflow Q_{j+1}:

$$Q_{j+1} = f\left(Y_{j+1}\right) \qquad (6.10)$$

To estimate the outflow at time step $j+2$, it is necessary to know the variable $2\,S/\Delta t - Q$ at time step $j+1$ (in order to subsequently use equation 6.9 to estimate Y_{j+2}). The value of this variable can be determined in a simple manner using the following equation:

$$2\,S_{j+1}/\Delta t - Q_{j+1} = (2\,S_{j+1}/\Delta t + Q_{j+1}) - 2Q_{j+1} \qquad (6.11)$$
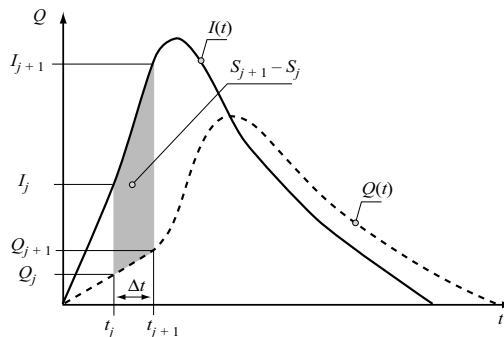

Fig. 6.7: Estimation of the change in reservoir storage over time interval $[j\Delta t, (j+1)\Delta t]$ induced by a variation of inflow and outflow.

Storage value S_{j+1} can also be deduced from the following equation:

$$S_{j+1} = \frac{\Delta t}{2}\left(\frac{2S_{j+1}}{\Delta t} + Q_{j+1}\right) - \frac{\Delta t}{2}Q_{j+1} = \frac{\Delta t}{2}\left(Y_{j+1} - Q_{j+1}\right) \tag{6.12}$$

Table 6.1 indicates the calculation steps necessary to route a hydrograph using this method.

Table 6.1: Summary of required calculations to route a hydrograph through a reservoir using the Puls method (Q_0 and S_0 are known).

j	I_j	$I_j + I_{j+1}$	$2\,S_j/\Delta t - Q_j$	Y_{j+1}	Q_{j+1}	S_{j+1}
(1)	(2)	(3)	(4)	(5)	(6)	(7)
					Q_0	S_0
0	I_0	$I_0 + I_1$	$2\,S_0/\Delta t - Q_0$	Y_1	Q_1	S_1
1	I_1	$I_1 + I_2$	$2\,S_1/\Delta t - Q_1$	Y_2	Q_2	S_2
2	I_2	$I_2 + I_3$	$2\,S_2/\Delta t - Q_2$	Y_3	Q_3	S_3
3	I_3	$I_3 + I_4$	$2\,S_3/\Delta t - Q_3$	Y_4	Q_4	S_4
4	I_4	$I_4 + I_5$	$2\,S_4/\Delta t - Q_4$	Y_5	Q_5	S_5

The curve of Y versus Q corresponding to the function f is referred to as the Storage Indication Curve (SIC) and the corresponding method is referred to as the Storage Indication method. The way the curve is constructed is illustrated graphically in Figure 6.8. For a natural reservoir, the elevation-storage curve cannot generally be described in an analytical manner. Consequently, the SIC must be described in a discrete manner by a finite number of pairs (Y_k, Q_k) and determination of the outflow Q_{j+1} corresponding to the value Y_{j+1} requires an iterative procedure.
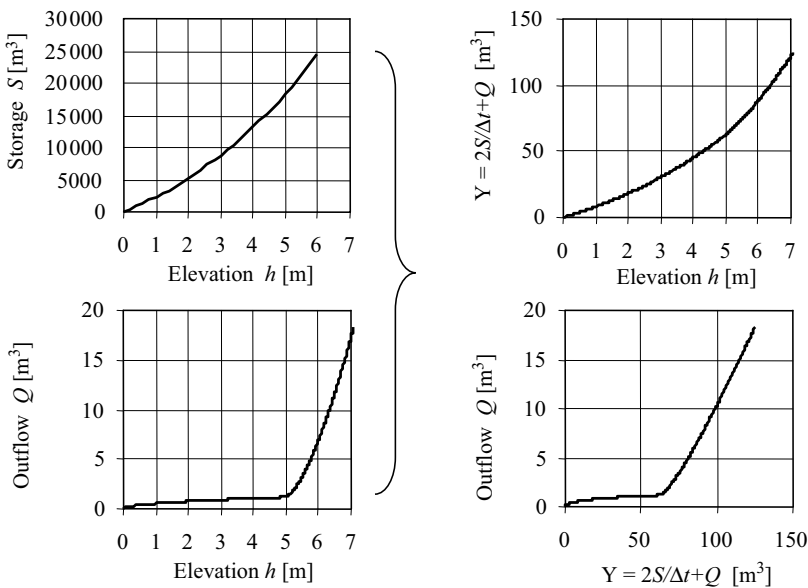

Fig. 6.8: Method for constructing a Storage Indication Curve (SIC) where $Y = 2\,S/\Delta t + Q$.

Example 6.1

Flood routing through a reservoir using the Puls method

Consider a reservoir built for flood mitigation purposes in a shopping center. Its geometrical characteristics are indicated in Figure 6.4. The outlet is an orifice (discharge coefficient $m = 0.75$ and cross-sectional area $A_0 = 0.16$ m²) located at the bottom of the reservoir ($h_0 = 0$). A spillway in the form of a weir with a crest elevation of 5 m is also provided to handle any overflows ($h_s = 5$ m; discharge coefficient $m = 1.6$; length perpendicular to the direction of flow $L_{weir} = 3.5$ m).

The objective is to determine the flood hydrograph resulting from the routing of the inflow hydrograph described in column 2 of Table 6.3 through the reservoir. The reservoir is assumed to be initially empty. The outflow is not influenced by backwater effects (free flow conditions). Flood routing is carried out using the Puls method. The solution obtained using the 4th-order Runge-Kutta method is described in Appendix 6.8.1 for the same case.

To apply the Puls method, it is first necessary to plot, for the chosen time step (Δt=10 min), the Storage Indication Curve (Figure 6.8). The straightforward geometry of the reservoir (Figure 6.4) makes it possible to obtain the following analytical expressions for the elevation-area and elevation-storage relationships:

$$A(h) = (L + m \cdot h)(l + 2m \cdot h) \qquad (6.13)$$

$$S(h) = L \cdot l \cdot h + 1/2 \cdot m \cdot (l + 2L) \cdot h^2 + 2/3 \cdot m^2 \cdot h^3 \qquad (6.14)$$

where L is the reservoir bottom length, l the reservoir bottom width and m the run-to-rise ratio of the reservoir banks, respectively 50 m, 40 m and 4 in Figure 6.4.

The expressions for the discharges are given in Figure 6.6 for the two outlet works. The can be used to estimate the outflow via the orifice if h <5 m or via the spillway if h >5 m. The orifice discharges are assumed to obey the indicated equation, even for low hydraulic head (the elevation-discharge analysis for the reservoir could be refined if this assumption is not valid). The Storage Indication Curve values are indicated in Table 6.2 for different water level elevations h.

Table 6.2: Storage Indication Curve (SIC) values for Δt =10 min.

Elevation h [m]	Volume S [m³]	Orifice outflow $Q_0(h)$ [m³/s]	Spillway outflow $Q_S(h)$ [m³/s]	Total outflow $O(h)$ [m³/s]	SIC $Y(h)$ [m³/s]
0.0	0	0.00	-	0.00	0
0.2	411	0.24	-	0.24	1.61
0.4	845	0.33	-	0.33	3.15
0.6	1303	0.41	-	0.41	4.75
0.8	1784	0.47	-	0.47	6.42
…	…	…	…	…	…
4.8	17230	1.16	-	1.16	58.59
5.0	18333	1.18	-	1.18	62.29
5.2	19471	1.20	0.50	1.70	66.61
5.4	20644	1.23	1.42	2.65	71.46

To route the flood through the reservoir, the identified SIC is used together with the continuity equation expressing storage as a function of outflow and variable Y (eq. 6.12). At $t_0 = 0$, it is known that $I_0 = 0$, $S_0 = 0$ and $Q_0 = 0$ (stated initial conditions). Consequently, $I_0 + I_1 = 6$ m³/s and $2S_0/\Delta t - O_0 = 0$ m³/s. For $t = t_1 = 10$ minutes, it is possible to calculate the value of $Y_1 = 2S_1/\Delta t + O_1 = (I_0 + I_1) + (2S_0/\Delta t - O_0) = 6 + 0 = 6$ m³/s and the value of outflow O_1 using the SIC values in the table, i.e., $O_1 = 0.46$ m³/s (interpolating if necessary between the two neighboring values). The value of the term $2S_1/\Delta t - O_1$, necessary for the estimation of the variables at the following time step ($t_2 = 20$ minutes), is $2S_1/\Delta t - O_1 = Y_1 - 2O_1 = 6 - 2 \cdot 0.46 = 5.1$ m³/s. The calculation is repeated over the entire time period [0, 120 min]. The calculations for the complete procedure are indicated in the table below.

Table 6.3: Input hydrograph and calculation of the output hydrograph using the Puls method.

j	I_j [m³/s]	$I_j + I_{j+1}$ [m³/s]	$2S/\Delta t - Q_j$ [m³/s]	Y_{j+1} [m³/s]	Q_{j+1} [m³/s]
0	0.0	6.0	0.0	6.0	0.5
1	6.0	24.8	5.1	29.9	0.9
2	18.8	45.7	28.1	73.8	3.1
3	26.9	46.7	67.6	114.3	14.8
4	19.8	36.0	84.7	120.7	16.8
5	16.2	28.6	87.2	115.8	15.2
6	12.4	22.8	85.3	108.1	12.8
7	10.4	19.0	82.5	101.5	10.7
8	8.6	14.8	80.1	94.9	8.8
9	6.2	9.8	77.3	87.1	6.6
10	3.6	6.2	74.0	80.2	4.7
11	2.6	4.8	70.8	75.6	3.6
12	2.2	4.4	68.4	72.8	2.9

Figure 6.9 shows the output hydrographs obtained using the Puls (Example 6.1) and Runge-Kutta (Appendix 6.8.1) methods. Note that the two methods give similar results.
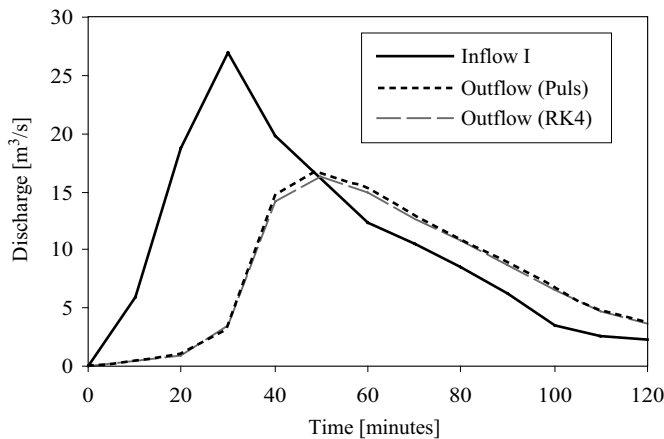

Fig. 6.9: Inflow and outflow hydrographs obtained by hydrological routing using the Puls method (Example 6.1) and the 4th-order Runge-Kutta (RK4) method (Appendix 6.8.1).

6.3 STREAMFLOW ROUTING

6.3.1 Description of the Problem

Variables to be estimated and equations

For transient and gradually-varied flow conditions, unidirectional flow in a watercourse can be described hydraulically, under certain simplifying assumptions, on the basis of a system of five equations implying five state variables.

Unless the model is further simplified, the five state variables are the flow depth h, mean water velocity V, wetted perimeter P, flow area A and head loss due to friction h_f. These variables are estimated for each of the cross-sections selected for the description of streamflows.

The five equations include two state relationships (one between flow depth and wetted perimeter and the other between flow depth and flow area), two balance equations expressing the conservation of mass and energy and finally a process dynamics equation expressing the relationship between flow velocity and friction slope. The two balance equations are commonly referred to as the Barré de Saint-Venant equations (1871).

The discharge through a given section is the product of the flow area and the mean flow velocity ($Q=AV$). The friction slope S_f is the longitudinal gradient of head loss due to friction: $S_f = - \partial h_f / \partial x$ where x is the curvilinear abscissa along the watercourse.

Problem to be solved

Whatever the model used, stability and numerical convergence criteria generally require discretization of the river reach between the upstream station (where the inflow hydrograph is known) and the downstream station (where the outflow hydrograph must be estimated) into elements of finite but possibly variable length Δx. The number of elements must be chosen according to the distance between the stations and the variability of the physical and hydraulic characteristics between the two stations. Simulation of streamflow routing between the upstream and downstream stations of a reach consists in estimating, for each time step, the variables selected to describe the flow at each of the watercourse sections delimiting these elements. When all these variables have been estimated for a given time t_0, the estimation is repeated for time $t_0 + \Delta t$ where Δt is the possibly variable time step separating successive estimations.

To solve the system of equations, it is necessary to define the initial conditions for each channel reach considered (i.e., the variables at each of the sections for $t=t_0$), the boundary conditions (i.e., inflow to the upstream station at $x=0$, a water level or hydraulic regime condition for the downstream station at $x=L$) and lateral conditions (i.e., lateral inflows or outflows $q(x,t)$). The problem to be solved and the typical spatial and temporal discretizations used for this purpose are illustrated in Figure 6.10.
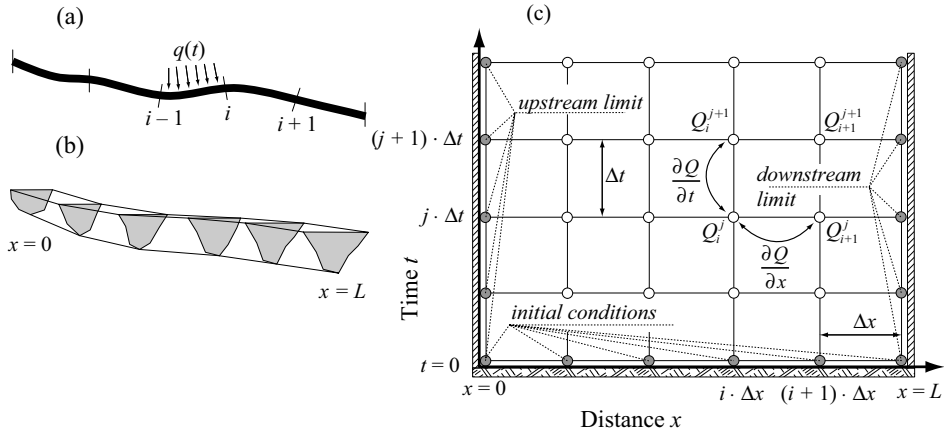
Fig. 6.10: Illustration of the problem of routing streamflows between the upstream station at x=0 and the downstream station at x=L. a) Division of the channel reach into different elements. b) Channel cross-sections for the estimation of the variables describing the flow. c) Typical spatial and temporal discretization scheme along with the variables to be estimated at each point of the grid, initial conditions and boundary conditions.

6.3.2 System of Equations of the Barré de Saint-Venant Model

State equations

Different variables are required to describe the flow cross-section. They are related to the flow geometry (Table 6.4 and Addendum 6.1). The state equations express the relationship between these different variables at every point M on the curvilinear abscissa x (e.g., the relationship between the flow area and the flow depth h).

For the general case, they can be obtained on the basis of topographic surveys of the selected flow cross-sections. For cross-sections with simple geometry, the state equations can be expressed analytically (Table 6.4).

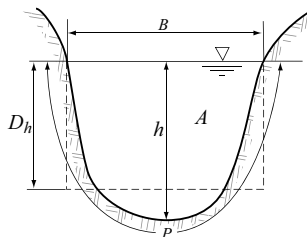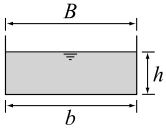**Addendum 6.1 Variables describing a flow cross-section**
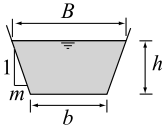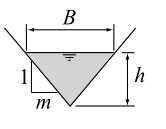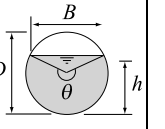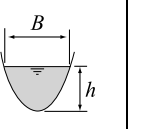
Fig. 6.11: Geometric characteristics of a flow section.

The following variables can be used to describe a given flow cross-section.

- Flow depth h: maximum depth of water across the cross-section.
- Flow area $A(h)$: area of the channel cross-section occupied by the flow.
- Wetted perimeter $P(h)$: length of the contact between the channel bed and the flowing water (the wetted perimeter does not include the surface of the water).
- Free surface width $B(h)$: width of the free water surface across the channel.
- Hydraulic radius $R_D(h)$: flow area divided by the wetted perimeter.
- Hydraulic depth $D(h)$: flow area divided by free surface width.

Table 6.4: State equations for cross-sections with simple geometry (adapted from Graf and Altinakar, 2000).

	Rectangle	Trapezoid	Triangle	Circle	Parabola
$A(h)$	$b \cdot h$	$(b+mh)h$	$m\,h^2$	$\frac{1}{8}(\theta - \sin\theta)\,D^2$	$\frac{2}{3}(Bh)$
$P(h)$	$b + 2h$	$b + 2h\sqrt{1+m^2}$	$2h\sqrt{1+m^2}$	$\frac{1}{2}(\theta \cdot D)$	$B + \frac{8}{3}\frac{h^2}{B}$ *
$Rh(h)$	$\dfrac{b\,h}{b+2h}$	$\dfrac{(b+m\,h)h}{b+2h\sqrt{1+m^2}}$	$\dfrac{m\,h}{2\sqrt{1+m^2}}$	$\frac{1}{4}\left[1 - \dfrac{\sin\theta}{\theta}\right]D$	$\dfrac{2\,B^2 h}{3B^2 + 8h^2}$ *
$B(h)$	b	$b + 2m\,h$	$2m\,h$	$(\sin\theta/2)\,D$ *or* $2\sqrt{h(D-h)}$	$\frac{3}{2}\frac{A}{h}$
$Dh(h)$	h	$\dfrac{(b+m\,h)h}{b+2m\,h}$	$\frac{1}{2}h$	$\left[\dfrac{\theta - \sin\theta}{\sin\theta/2}\right]\dfrac{D}{8}$	$\frac{2}{3}h$

* Valid for $0 < \xi \leq 1$, where $\xi = 4h/B$. If $\xi > 1$: $P = \left(\frac{B}{2}\right)\left[\sqrt{1+\xi^2} + \frac{1}{\xi}\ln(\xi + \sqrt{1+\xi^2})\right]$

Barré de Saint-Venant equations

The equations formulated on the basis of the assumptions of Barré de Saint-Venant (1871) express the laws of conservation of mass, momentum and energy in a finite control volume delimited by two cross-sections on a watercourse separated by a finite distance, the free surface and the channel bed (Addendum 5.2). When the flow variables and geometric characteristics of the channel bed are continuous and differentiable, the conservation of momentum and energy equations are equivalent (Cunge, 1995). The commonly used one-dimensional equations referred to as the Barré de Saint-Venant equations are expressed as follows:

$$\frac{\partial A}{\partial t} + \frac{\partial Q}{\partial x} = q \tag{6.15}$$

$$S_0 - S_f = \frac{\partial h}{\partial x} + \frac{1}{g}V\frac{\partial V}{\partial x} + \frac{1}{g}\frac{\partial V}{\partial t} - (k-1)\cdot\frac{q}{g}\cdot\frac{V}{A} \tag{6.16}$$

where A [m²] is the flow area of the cross-section; V [m/s] and Q [m³/s] are respectively the mean velocity and discharge across the cross-section, q [m³/s/m] represents any lateral inflows/outflows expressed per unit length, h is the flow depth [m], S_0 and S_f [m/m] are respectively the slope of the channel bed over the reach and the slope of the energy grade line (linear head losses) and k is the coefficient that depends on the direction of lateral flows ($k = 0$ for lateral inflows and $k = 1$ for lateral outflows).

The different terms of the equation for the conservation of momentum have different orders of magnitude depending on the characteristics of the input signal—in particular its speed—and on the characteristics of the reach (Section 6.6.2). For this reason, some of these terms can be neglected. The models generally used in hydrology are dominated by friction. The diffusion-wave model neglects inertia terms and the kinematic-wave model neglects in addition the pressure term (Table 6.5 and Addendum 5.2). The kinematic-wave model, and thus even more so the diffusion-wave model, therefore represent a reasonable simplification for most cases encountered in hydrology.

Table 6.5: Possible simplifications of the Barré de Saint-Venant equations (without the term related to possible lateral inflows and outflows).

Equation	Model
$S_0 - S_f = \dfrac{\partial h}{\partial x} + \dfrac{1}{g} V \dfrac{\partial V}{\partial x} + \dfrac{1}{g} \dfrac{\partial V}{\partial t}$	**Dynamic wave**
$0 = \dfrac{\partial h}{\partial x} + \dfrac{1}{g} V \dfrac{\partial V}{\partial x} + \dfrac{1}{g} \dfrac{\partial V}{\partial t}$	**Gravity wave**
$S_0 - S_f = \dfrac{\partial h}{\partial x} + \dfrac{1}{g} V \dfrac{\partial V}{\partial x}$	**Quasi-steady dynamic wave**
$S_0 - S_f = \dfrac{\partial h}{\partial x}$	**Diffusion wave**
$S_0 - S_f = 0$	**Kinematic wave**

Friction equation

The relationship between flow velocity V and friction slope S_f depends in particular on the dimensionless Reynolds number (Re) that expresses the ratio between the forces of friction and inertia. It is defined as:

$$\mathrm{Re} = \frac{\rho \cdot V \cdot h}{\mu} \tag{6.17}$$

where ρ is the fluid density [kg m^{-3}], μ the fluid viscosity [kg m^{-1} s^{-1}] and V and h the flow velocity [m s^{-1}] and depth [m] respectively.

When Re > 2000, which is generally the case for most hydrological applications, the flow is turbulent. The friction equation can then be expressed in the following form:

$$V = K \cdot \sqrt{S_f} \tag{6.18}$$

where the conductivity K is mainly a function of the cross-section dimensions and roughness and the irregularities of the channel bed.[2] The two equations employed are the empirical Manning-Strickler and Chézy equations:

---

[2]When Re < 500, the flow is laminar and the momentum equation of the flow can be expressed as a function of the conductivity K of the reach and the friction slope in the following form: $V = K \cdot grad(H)$ where H is the hydraulic head and K the conductivity that depends on the properties of the water (density viscosity) and the dimensions of the cross-section. Different expressions are possible for intermediate Reynolds numbers (Graf and Altinakar, 2000).

Chézy: $V(h) = C \cdot R_H(h)^{1/2} \cdot \sqrt{S_f}$ (6.19)

Manning: $V(h) = \dfrac{1}{n} \cdot R_H(h)^{2/3} \cdot \sqrt{S_f}$ (6.20)

where $V(h)$ is the mean flow velocity [m/s], $R_H(h)$ the hydraulic radius [m], S_f the slope of the head losses [dimensionless] and C and n are respectively the Chézy [m$^{1/2}$/s] and Manning [m$^{-1/3}$s] coefficients. n is known as the hydraulic roughness coefficient of the flow section. The Manning-Strickler equation is considered to provide a good approximation of reality for hydraulically rough flows.

Addendum 6.2 Assumptions and derivation of the Barré de Saint-Venant equations

Assumptions

The assumptions of the Barré de Saint-Venant equations are the following:

1) The water density is constant.
2) The pressure distribution is hydrostatic (i.e., the piezometric head defined by $p/\gamma + z_p$, where z_p is the elevation of the considered water particle and p the pressure applied to this particle, is constant in the vertical direction), i.e., vertical acceleration is negligible.
3) The flow is essentially horizontal (i.e., the longitudinal slope is low).
4) Within a given cross-section, each fluid element moves at mean velocity V and the free surface is horizontal.
5) The head losses can be expressed using the empirical formulas for steady flows.
6) All changes in the bed geometry are gradual and the boundaries of the river reach are fixed (i.e., erosion and deposition phenomena are neglected).

Continuity equation

The continuity equation expresses the fact that changes in storage (water volume) within an element of the watercourse of length dx are equal to the sum of the inflow volumes V_{in} minus the sum of the outflow volumes V_{out}. For the element of the watercourse described in Figure 6.12, this gives:

Inflow volume: $V_{in} = Q \cdot dt + q \cdot dx \cdot dt$ (6.21)

Outflow volume: $V_{out} = \left(Q + \dfrac{\partial Q}{\partial x} \cdot dx \right) \cdot dt$ (6.22)

Change in volume: $\Delta V = \dfrac{\partial A}{\partial t} \cdot dx \cdot dt$ (6.23)

where A is the flow area and q the lateral flows per unit length ($q<0$ for lateral outflows and $q>0$ for lateral inflows). The continuity equation is obtained by considering that $\Delta V = V_{in} - V_{out}$ and by simplifying the resulting equality. This gives:

$$\frac{\partial A}{\partial t} + \frac{\partial Q}{\partial x} = q$$ (6.24)

Energy conservation equation

The energy equation expresses the conservation of energy in the direction of flow. The total energy within a flow section, commonly expressed as the hydraulic head H in [m], can be written as the sum of three terms as follows:
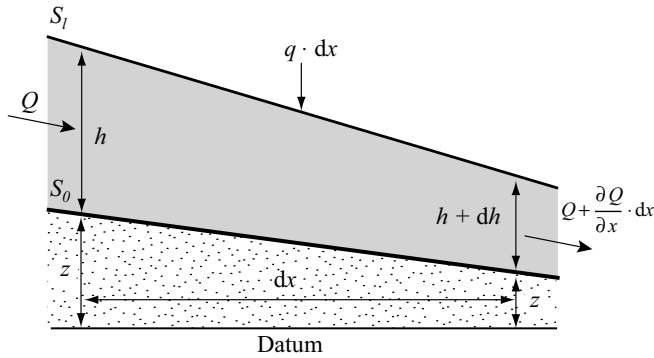
Fig. 6.12: The different terms of the continuity equation.

$$H = V^2/2g + h + z \tag{6.25}$$

where $V^2/2g$ is the velocity head [m] representing kinetic energy due to velocity V, h is the pressure head [m] (equal to the depth of the water) representing potential energy in the form of pressure and z is the position head [m] representing potential energy due to the elevation of the water above an arbitrary datum.

According to the first law of thermodynamics, the total energy must decrease from upstream to downstream due to energy dissipation by friction. For steady flow, this energy loss per unit length is the sum of the energy lost by the three energy components described above. In terms of head loss, this can be expressed as:

$$\frac{dh_f}{dx} = \frac{dH}{dx} = \frac{d}{dx}\left[\frac{V^2}{2 \cdot g} + h + z\right] = \frac{V}{g}\cdot\frac{dV}{dx} + \frac{dh}{dx} + \frac{dz}{dx} \tag{6.26}$$

For unsteady flow, the energy loss by friction is also influenced by velocity variations along the watercourse. These variations introduce another energy loss term that can be expressed as $1/g \cdot \partial V/\partial t$ (Figure 6.13). Energy can also be added by lateral inflows, if present, leading to the following energy equation:

$$\frac{\partial h_f}{\partial x} = \frac{\partial H}{\partial x} + \frac{1}{g}\frac{\partial V}{\partial t} - (k-1)\cdot\frac{q}{g}\cdot\frac{V}{A} \tag{6.27}$$

The definitions of friction slope and bed slope lead to the following final expression:

$$S_0 - S_f = \frac{\partial h}{\partial x} + \frac{1}{g}V\frac{\partial V}{\partial x} + \frac{1}{g}\frac{\partial V}{\partial t} - (k-1)\cdot\frac{q}{g}\cdot\frac{V}{A} \tag{6.28}$$

(a) (b)   (c)   (d)   (e)   (f)

The different terms of the equation are related to: a) gravity forces, b) friction forces, c) pressure forces, d) local acceleration, e) convective acceleration and f) lateral inflows.
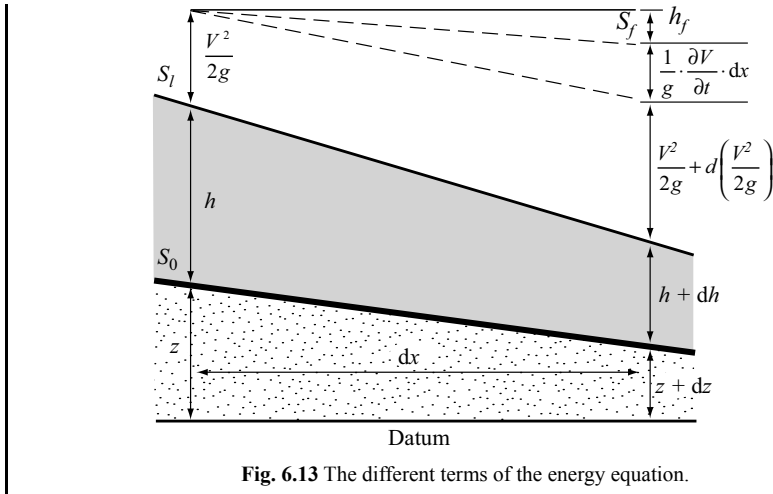
Fig. 6.13 The different terms of the energy equation.

6.3.3 Solving the Equations

The system of equations governing open-channel unidirectional gradually-varied flows does not have an exact solution for real physical systems. The equations are solved mainly using numerical methods that make it possible to linearize the initial non-linear system of equations. For one-dimensional flow, the most common numerical methods use implicit or explicit schemes involving finite differences (Addendum 6.3) or, more rarely, finite elements. These methods are based on the discretization of the considered channel reach into sections of finite lengths and on the discretization of the derivatives found in the partial derivative equations. They have been widely studied and described in the literature (Preissmann, 1965; Cunge *et al.*, 1980, Hervouet, 2003). Frequently used discretization schemes include for example the Lax scheme explicit scheme and the Preissmann (Preissmann, 1961; Preissmann and Cunge, 1961) and Abbott and Ionescu (1967) implicit schemes.

Addendum 6.3 Implicit and explicit finite difference schemes for the solution of streamflow equations

Explicit schemes

These methods can be used to calculate, at each calculation point, the flow variables at time $t+\Delta t$ as a function of the values known for these variables at time t for the neighboring calculation points. The values obtained with explicit methods are highly unstable if the calculation time step is to long. Suitable results are obtained if the time and space steps respect the Courant-Friedrichs-Lewy condition, i.e., if the Courant number Cr is less than 1 where $Cr = (c+|u|)\cdot\Delta t/\Delta x$ and where the shallow-wave speed c is equal to $(g\cdot A/B)^{1/2}$.

Although the explicit schemes are simpler and allow immediate calculations, they are not generally suitable for calculation of the propagation of flood waves in natural rivers because the time steps required for the calculation are far too small (Cunge, 1995).

Implicit schemes

Implicit methods consider that the values of the variables at time *i* are the weighted means of the values of the variables at time *t* (which are known) and their values at time *t+Δt* (that are the unknowns to be estimated). This method is not subject to the Courant-Friedrichs-Lewy numerical stability condition and can accept very high Courant numbers (often higher than 10). Too high a Courant number does however often lead to a calculation error referred to as numerical diffusion (behavior similar to an artificial viscosity).

The implicit schemes can be made unconditionally stable however they present the drawback of producing a large linear system that must be solved at each time step.

6.3.4 Kinematic-wave Model

When the pressure and inertia terms are negligible compared to the forces of gravity and friction, these last two forces balance and are therefore equal. The model obtained is referred to as the kinematic-wave model (Table 6.5). The friction slope S_f and bed slope S_0 being equal, the momentum equation can be approximated by assuming steady flow as described by the Manning or Chézy empirical friction equations. The system of equations is then reduced to the following continuity and friction equations:

$$\frac{\partial A}{\partial t} + \frac{\partial Q}{\partial x} = q \tag{6.29}$$

$$Q = Q(h) = \frac{1}{n} \cdot A(h) \cdot R_H(h)^{2/3} \cdot \sqrt{S_0} \tag{6.30}$$

The second equation above establishes an unequivocal relationship between the discharge Q and the flow area A and also between the discharge and flow depth h. These two equations can be combined to form an equation that depends on only one variable (e.g., h or Q or A). This equation, referred to as the kinematic-wave equation, has no analytical solution. It must be solved by a suitable numerical scheme which can nevertheless be relatively straightforward under certain simplifying assumptions concerning in particular the geometry of the flow cross-section (Appendix 6.2).

Given the unequivocal relationship between discharge and flow area, the discharge and flow depth propagated with this model appear to be constant to an observer moving along the watercourse at velocity c_k defined by the following equation:

$$c_k = \frac{dQ}{dA} \tag{6.31}$$

The velocity c_k, referred to as the *kinematic-wave speed*, expresses that any local change of discharge with time propagates downstream at a speed that is proportional to the rate of change of the discharge with flow area (Addendum 6.4). The wave speed is always greater than the mean flow velocity V (equal to Q/A). Moreover, for a stationary observer, the kinematic wave appears to be a uniform unsteady flow with the free surface parallel to the river bed and the energy grade line (Figure 6.14).

The kinematic-wave model propagates a flood without attenuating its peak discharge. Furthermore, given that the velocity of the flood wave increases with the considered

discharge, the flood hydrograph becomes steeper as it is propagated downstream. The time-to-peak of the hydrograph therefore decreases as the flood is propagated downstream (Figure 6.15).

The kinematic wave can be used both for the routing of streamflows and for the transformation of rainfall to runoff by sheet flow (Chapter 5).
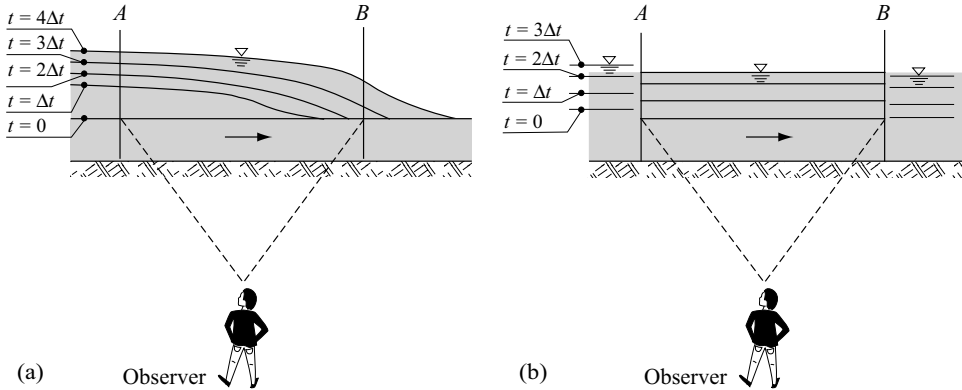
Fig. 6.14: Appearance of: a) a dynamic wave and b) a kinematic wave as seen by an observer standing on the river bank (adapted from Bedient and Huber, 2002).
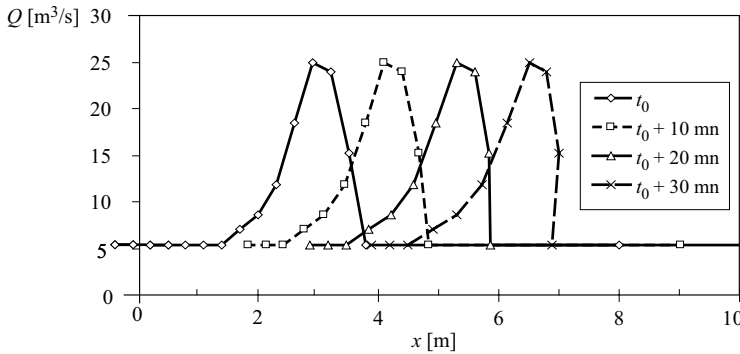
Fig. 6.15: Longitudinal variations of flood flows within a channel (slope 0.1%, roughness n=0.02, width B=3 m) obtained using the kinematic-wave model for different times t ($t=t_0$, $t=t_0+10$ min, $t=t_0+20$ min, $t=t_0+30$ min).

Addendum 6.4 Expression for the kinematic-wave speed for one-dimensional open-channel flow

For a unidirectional open-channel flow modeled by a kinematic wave, the unequivocal relationship between discharge and water depth makes it possible to write the differential equation of discharge as:

$$dQ = \frac{\partial Q}{\partial t}\, dt + \frac{\partial Q}{\partial x}\, dx \tag{6.32}$$

Consequently, for a streamline in which the discharge remains constant ($dQ=0$), the speed of propagation of this discharge is:

$$\left(\frac{dx}{dt}\right)_{Q=constant} = -\frac{\partial Q / \partial t}{\partial Q / \partial x}$$

For an observer moving along the watercourse at speed $c_k = -(\partial Q/\partial t)/(\partial Q/\partial x)$, the discharge and consequently the flow area and depth do not vary.

In the absence of lateral inflows, the continuity equation can also be written for any section with abscissa $x = x_0$, in the following form:

$$\frac{dA}{dQ} \cdot \frac{\partial Q}{\partial t} + \frac{\partial Q}{\partial x} = 0 \tag{6.33}$$

Consequently, the wave speed c_k can be expressed as:

$$c_k = -\frac{\partial Q / \partial t}{\partial Q / \partial x} = \frac{dQ}{dA} \tag{6.34}$$

Using the Manning-Strickler friction model, the flood wave speed for a rectangular channel of width B and a discharge corresponding to a flow depth h is therefore:

$$c_k = \frac{S_0^{1/2} \cdot B^{2/3}}{n} \cdot \left[\frac{h^{2/3} \cdot (5 \cdot B + 6 \cdot h)}{3 \cdot (B + 2 \cdot h)^{5/3}} \right] \tag{6.35}$$

The wave speed is not the same as the mean flow velocity. To simplify, let us assume that the flood wave has the profile illustrated in Figure 6.16 and that this profile remains constant as it is propagated in the downstream direction.
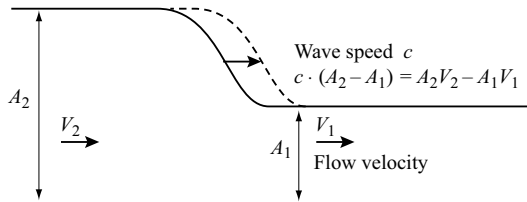
Fig. 6.16: Speed of a flood wave and flow velocities (adapted from Bedient and Huber, 2002).

The flood wave advances at speed c. Neglecting waveform modifications, applying the continuity equation between the upstream and downstream cross-sections of the considered reach leads to the following relationship:

$$c \cdot (A_2 - A_1) = A_2 \cdot v_2 - A_1 \cdot v_1 \tag{6.36}$$

where c and v are respectively the wave speed and flow velocity and where A is the flow area. Consequently:

$$c = \frac{A_2 \cdot v_2 - A_1 \cdot v_1}{A_2 - A_1} = v_2 + \frac{A_1 \cdot (v_2 - v_1)}{A_2 - A_1} = v_1 + \frac{A_2 \cdot (v_2 - v_1)}{A_2 - A_1} \tag{6.37}$$

Given that flow velocity is an increasing function of flow area, the term $(v_2-v_1)/(A_2-A_1)$ is positive. The wave speed is therefore greater than the flow velocity upstream and downstream of the wave propagation front. The ratio c/V can be determined analytically for different flow cross-section shapes (Table 6.6). For a natural rivers, and average ratio c/V of 1.5 is generally used.

Table 6.6: Ratio c/V for different flow cross-section shapes.

Cross-section shape	c/V
Wide rectangle	1.67
Wide parabola	1.44
Triangle	1.33

6.3.5 Wave-diffusion Model

When lateral inflows/outflows are zero and the inertia terms are negligible compared to the pressure, gravity and friction terms, the equation for the conservation of momentum can be expressed as follows:

$$S_0 - S_f = \frac{\partial h}{\partial x} \tag{6.38}$$

In this case, the relationship between discharge and flow depth is no longer unequivocal. Combining this equation with the continuity equation gives the diffusion-wave equation:[3]

$$\frac{\partial Q}{\partial t} + c \cdot \frac{\partial Q}{\partial x} - \mu \cdot \frac{\partial^2 Q}{\partial x^2} = c.q - \mu \cdot \frac{\partial q}{\partial x} \tag{6.39}$$

where c is the diffusion-wave speed and μ the diffusion coefficient. These coefficients can be approximated as (Roche, 1985):

$$c = -\frac{dQ}{dA} \quad \text{and} \quad \mu = \frac{Q}{2 \cdot B \cdot S_0} \tag{6.40}$$

where B is the surface width of the flow cross-section. The diffusion coefficient is responsible for the attenuation of the hydrograph. The coefficients c and μ depend on the discharge. The model is therefore non-linear.

Modeling of flood propagation using the diffusion wave makes it possible to simulate the attenuation of peak discharges (Figure 6.17). It is also possible to specify the downstream boundary conditions and consequently to take into account any backwater effects. Except under special conditions, this equation must be solved using the numerical methods already mentioned above (see also Cappeleare, 1997).

If upstream discharge variations are limited, constant average values can be used for the wave speed and the diffusion coefficient. The model becomes linear. The diffusion-wave equation then has an analytical solution and the outflow can be expressed in the form of a convolution product. The corresponding model is known as the Hayami model (1951). The downstream hydrograph is obtained directly from the upstream hydrograph. The model can no longer take into account backwater effects.

---

[3]This diffusion equation (origin of the name of the diffusion-wave model) is a sort of standard equation that also governs heat transfer by thermal conduction (Fourier's law), the conduction of electrical current (Ohm's law), gas diffusion (Fick's law) and the flow of water in saturated soil (Darcy's law).
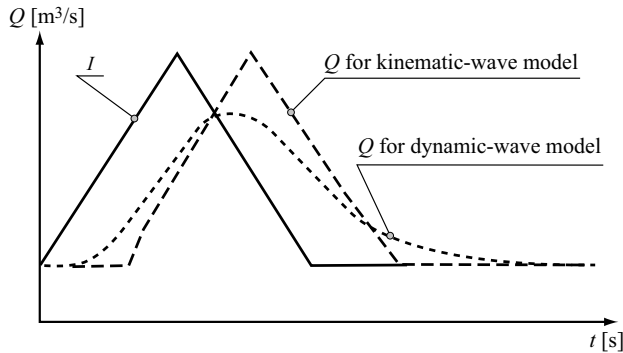
Fig. 6.17: Illustration of the influence of the selected model on the propagation of a simple triangular hydrograph between two stations S1 and S2.

6.3.6 Hydraulic Singularities

The Barré de Saint-Venant equations are not suitable if the different variables characterizing the flow are discontinuous or change abruptly. Such situations are generally observed in the neighborhood of singularities such as those associated with a weir, a confluence or a fork on the river, a narrowing or widening of the channel, a hydraulic jump, a waterfall or an abrupt change in direction of a river (Figure 6.18).

In this case, the flow is said to be rapidly-varied. Appropriate equations for these singularities, generally making it possible to take into account singular head losses, are required to estimate the flow variables. Each singularity is represented by an independent model that is either based on an empirical model calibrated on a series of observations of the behavior of the singularity or on assumptions designed to simplify the representation of the system. At each confluence or fork in a drainage network, it is often assumed that the water levels on the upstream and downstream side of a node are equal. For singularities such as weirs, orifices, gates, etc., different discharge models can be used to relate the

Fig. 6.18: Different types of flows including gradually-varied and rapidly-varied flows and uniform and non-uniform flows (adapted from Graf and Altinakar, 2000).

upstream and downstream hydraulic heads to the discharge flowing across the singularity. In practice, the free surface elevations are often used (Section 6.2.1).

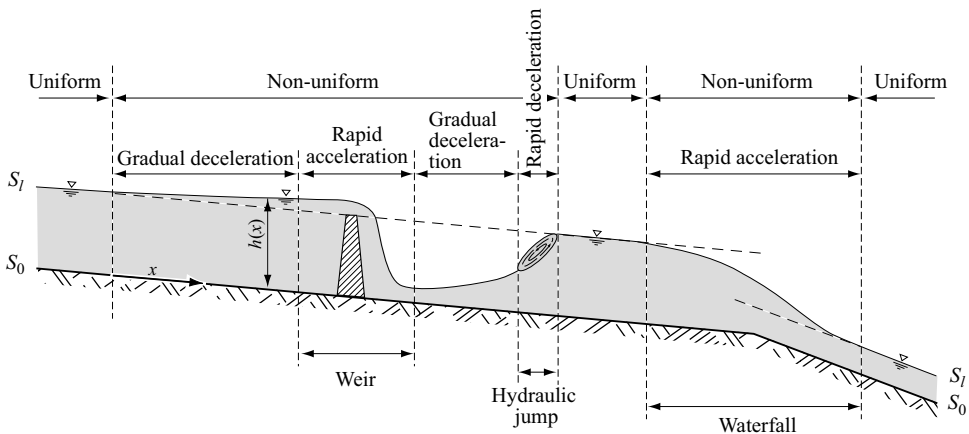The equations associated with singularities are added to the system of equations used to describe the flows on the overall reach of the river considered. For more information on this topic, the reader can refer to the works of Copeland *et al.* (2001), Chaudhry (1993) or Henderson (1966) in English or Carlier (1972), Lencastre (1999) or Sinniger and Hager (1989) in French.

6.3.7 Data Required

Whatever the hydraulic routing model used, data requirements are more or less the same. They include the: 1) cross-sections and lengths of the considered reaches, 2) roughness coefficients of the reaches and 3) initial and boundary conditions.

The cross-sections are necessary to determine the state relationships between flow depth and wetted perimeter and between flow depth and flow area. They are typically based on topographic surveys carried out orthogonally with respect to the channel bed. Key issues are the required accuracy of the surveys, the density of cross-sections to be surveyed and the way to estimate the cross-sections for all the calculation points taken into account in the hydraulic routing model. Spatial interpolation is often necessary between two surveyed cross-sections to obtain intermediate data (Beck, 2006).

The roughness coefficients are estimated either by calibration or by characteristics of the medium using empirical nomographs. The unidirectional hydraulic routing model does not see meanders in the river and cannot explicitly take into account the associated head losses. The roughness coefficients therefore depend in particular on the sinuosity of the watercourse. Various nomographs (see also Table 6.7) have been proposed by Chow

Table 6.7: Roughness coefficients *n* depending on the characteristics of the medium (adapted from Bedient and Huber, 2002).

Type of channel	n [m$^{-1/3}$s]
Closed conduits	
Smooth concrete	0.010–0.015
Masonry	0.018–0.030
Open channels	
Masonry	0.015–0.035
Earth, straight and uniform—short grass	0.022–0.033
Earth, winding, sluggish—dense weeds	0.030–0.040
Rivers	
Clean, straight, full stage, no brush	0.025–0.033
Clean, winding, some pools and shoals, sparse vegetation	0.033–0.045
Mountain stream with steep banks—gravels and cobbles	0.030–0.050
Mountain stream with steep banks—cobbles with large bolders	0.040–0.070
Floodways and flood plains	
Pasture—no brush, high grass	0.030–0.050
Brush, scattered brush, heavy weeds	0.035-0.070
Medium to dense brush in summer	0.070–0.160
Trees—heavy stand of timber	0.080–0.120

(1959) to estimate these characteristics. Various recommendations have also been made by the USACE (1986) and by Vidal (2005).

The initial conditions include the discharges at every point on the watercourse for the beginning of the simulation. The flow depths and corresponding velocities can be estimated on the basis of steady flow equations (e.g., normal depth estimated with the Manning equation). The upstream and lateral boundary conditions are respectively the upstream inflow hydrograph and lateral inflow/outflow hydrograph. The downstream boundary condition is a known or assumed relationship between the discharges and flow depths (e.g., normal depth, critical flow relationship).

6.4 HYDROLOGICAL STREAMFLOW ROUTING

Different streamflow routing methods referred to as hydrological can be used to propagate discharges through a river reach of finite length. They are based on a conceptual and lumped representation of the phenomenon. For this representation, the modified Puls method[4] uses a cascade of linear reservoirs of the type described in Chapter 5. Another method referred to as lag-and-route propagates flows using a combination of two operations: a temporal shift of the inflow hydrograph and attenuation by a conceptual reservoir. For more information on these methods, the reader can consult USACE (1994).

The Muskingum method, named after the river where McCarthy first applied this method in 1934, is without a doubt the most popular conceptual approach. It is based on the continuity and storage equations for the considered river reach. This method is widely used in common hydrological applications because the system of equations has an exact solution that can be easily obtained and for which the discretized expression is, under certain conditions, an approximation of the diffusion-wave model. The Muskingum model, its assumptions and application procedure are described in this section.

6.4.1 Equations of the Muskingum Model

The storage equation of the Muskingum model expresses the volume of water stored in a given channel reach as a function of upstream inflows and downstream outflows. This equation is based on the following simplifying assumptions: 1) a constant cross-sectional geometry over the entire reach and 2) a discharge Q that is an unequivocal function of the flow area A expressed in the form $Q = a \cdot A^n$.

For steady flow, the volume S stored in a reach of length Δx can therefore be expressed as a function of the discharge flowing through the reach:

$$S(t) = A(t) \cdot \Delta x = b \cdot \left(Q(t) / a \right)^{\frac{1}{n}} \cdot \Delta x \tag{6.41}$$

For unsteady flow, the stored volume is assumed to be a weighted average of the stored volume S_I due to inflows $I(t)$ and the stored volume S_Q due to outflows $Q(t)$ (Figure. 6.19).

---

[4]The reservoirs used in the Puls method are not linear. The difficulty with this method lies in the determination of the relationship between reservoir discharge and storage volume. It is based on the geometry of the reach and on different assumptions concerning the hydraulic regime within the reach.
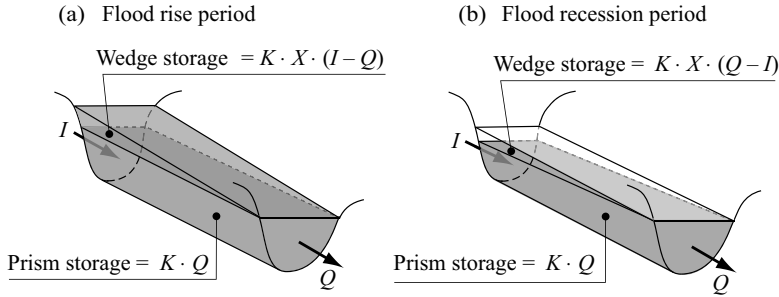
(a) Flood rise period   (b) Flood recession period

Wedge storage $= K \cdot X \cdot (I - Q)$

Wedge storage $= K \cdot X \cdot (Q - I)$

I

I

Prism storage $= K \cdot Q$

Prism storage $= K \cdot Q$

Q

Q

Fig. 6.19: Principle of the Muskingum model. Volume stored within a reach of finite length as a function of inflows and outflows.

$$S(t) = b \cdot \left[X \left(I(t)/a \right)^{\frac{1}{n}} + (1 - X) \left(Q(t)/a \right)^{\frac{1}{n}} \right] \cdot \Delta x \tag{6.42}$$

where X is a weighting factor. When the exponent n is equal to 1, the stored volume becomes a linear function of inflows and outflows. The Muskingum model is made up of the resulting storage and continuity equations for the studied reach:

$$S(t) = K \left[X \cdot I(t) + (1 - X) \cdot Q(t) \right] \tag{6.43}$$

$$\frac{dS(t)}{dt} = I(t) - Q(t) \tag{6.44}$$

where K is the proportionality constant of the storage equation. K and X are the two parameters of the model that must be estimated or calibrated.

6.4.2 Discrete Expression for the Muskingum Model

The exact expression for the outflow at time t_0 can be obtained as a function of the inflow for $t < t_0$ by integration (Brustaert, 2005). This expression, in the form of a convolution product, is however difficult to use operationally. The Muskingum model is in fact commonly used in a discretized form (at time step Δt). It is obtained by expressing the change in storage within the considered reach over the time interval $[j\Delta t, (j+1)\Delta t]$ based on the storage and continuity equations (Addendum 6.5).

The outflow over time step $(j+1)\Delta t$ is therefore expressed as a function of the outflow over the previous time step $j\Delta t$ and the inflows over these two time steps:

$$Q_{j+1} = C_1 \cdot I_{j+1} + C_2 \cdot I_j + C_3 \cdot Q_j \tag{6.45}$$

The coefficients C_1, C_2, and C_3 depend on the selected time step Δt, the length of the channel reach Δx and the parameters K and X (Addendum 6.5). The sum $C_1 + C_2 + C_3$ is equal to 1. If parameters K and X and the initial discharge Q_0 are known, these equations can be used to route the inflow hydrograph defined in a discrete manner by the values I_j, $j \geq 0$. The values I_j, $j \geq 0$ can include any lateral inflows and/or outflows that may be present. In this case, $I_j = Q_{in,j} + Q_{L,j}$, $j \geq 0$, where $Q_{in,i}$ is the upstream inflow and $Q_{L,j} = q_j \Delta x$, the lateral inflow or outflow.

Addendum 6.5 Derivation of the discretized Muskingum equation

Based on the storage equation of the model, the volumes S_j and S_{j+1} stored at times $t=j\Delta t$ and $t=(j+1)\Delta t$ can be expressed respectively as:

$$S_j = K \cdot \left[X \cdot I_j + (1 - X) \cdot Q_j \right] \tag{6.46}$$

$$S_{j+1} = K \cdot \left[X \cdot I_{j+1} + (1 - X) \cdot Q_{j+1} \right] \tag{6.47}$$

The change in storage over time interval $[j\Delta t, (j+1)\Delta t]$, estimated on the basis of the storage equation, is therefore:

$$\Delta S_{j,j+1} = K \cdot \left\{ \left[X \cdot I_{j+1} + (1 - X) \cdot Q_{j+1} \right] - \left[X \cdot I_j + (1 - X) \cdot Q_j \right] \right\} \tag{6.48}$$

Based on the continuity equation, the change in storage over this time interval, estimated by finite differences, can be also expressed as (Figure 6.7):

$$\Delta S_{j,j+1} = \frac{I_j + I_{j+1}}{2} \Delta t - \frac{Q_j + Q_{j+1}}{2} \Delta t \tag{6.49}$$

Combining equations 6.48 and 6.49 gives the recurrence relation expressing the outflow over time step $(j+1)\Delta t$ as a function of the outflow over the previous time step $j\Delta t$ and the inflows over these two time steps:

$$Q_{j+1} = C_1 \cdot I_{j+1} + C_2 \cdot I_j + C_3 \cdot Q_j \tag{6.50}$$

where: $C_1 = \dfrac{\Delta t / K - 2X}{2(1 - X) + \Delta t / K}$, $C_2 = \dfrac{\Delta t / K + 2X}{2(1 - X) + \Delta t / K}$, and

$$C_3 = \frac{2(1 - X) - \Delta t / K}{2(1 - X) + \Delta t / K} \tag{6.51}$$

6.4.3 Influence of Flood Routing Model Parameters

The two parameters K and X of the Muskingum model determine the time shift and attenuation of the routed flood.

The parameter K is expressed in units of time. The value of K is equal to the time shift between the centers of mass of the inflow and outflow hydrographs. This also represents the mean residence time of the discharges within the studied reach. Consequently, the flood wave speed obtained with the Muskingum model is:

$$c_m = \Delta x / K \tag{6.52}$$

where Δx is the length of the considered channel reach. The time shift of the flood peaks also increases with K.

The parameter X is a dimensionless. It is used to adjust the influence of the upstream and downstream cross-sections on the storage and thus to adjust the change in shape of the hydrograph over the reach. Calculation of a simple integral shows that the difference between the second-order moments of the outflow and inflow hydrographs, that reflect the changes in shape of the hydrographs, is equal to the product $K^2(1-2X)$ (Brutsaert, 2005).

The quantity (1-2X) defines the degree of attenuation between the inflow and outflow hydrograph.

- Values of $X > 0.5$ are physically impossible because they would lead to a maximum outflow greater than the maximum inflow.
- When $X = 0.5$, the hydrograph simply passes through the channel reach without changing shape.
- When $X \leq 0.5$, the inflow hydrograph is attenuated by its passage through the channel reach. The attenuation increases as X tends towards 0.
- When $X = 0$, attenuation is maximum. Storage is then independent of the inflow. This behavior can be assimilated to that of the linear reservoir controlled only by downstream conditions and independent of upstream conditions (Chapter 5).

Figure 6.20 shows the influence of parameters K and X on the change in shape of the inflow hydrograph.
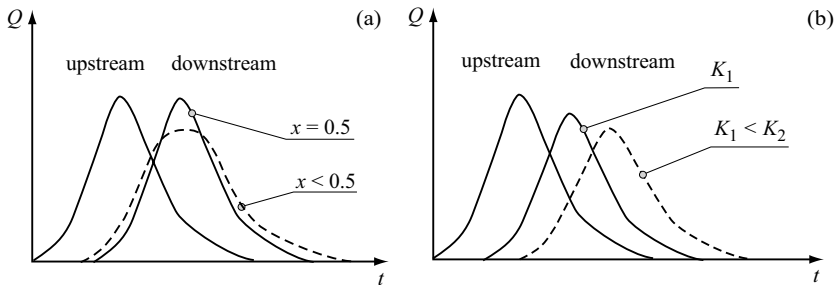
Fig. 6.20: Schematic influence of parameters X (Fig. a) and K (Fig. b) of the Muskingum model on the change of shape of the inflow hydrograph.

6.4.4 Muskingum-Cunge Model

When the parameters K and X are constants, Cunge (1969) demonstrated that the Muskingum recurrent equation is an approximation of the kinetic-wave equation (Section 6.3.4). Cunge also demonstrated that the Muskingum equation is an approximation of the diffusion-wave equation (Section 6.3.5) when the parameters K and X are estimated at each time step using the following two equations:

$$K = \Delta x / c \tag{6.53}$$

$$X = \frac{1}{2}\left(1 - \frac{Q}{B \cdot c \cdot S_0 \cdot \Delta x}\right) \tag{6.54}$$

where Δx is the length and B the water surface width of the channel reach, Q the discharge in the reach, S_0 the slope of the reach and c the wave speed of the flood wave corresponding to Q and B, estimated using the following equation:

$$c = \frac{1}{B} \cdot \frac{dQ}{dh} \tag{6.55}$$

The corresponding model, referred to as the Muskingum-Cunge model, is non-linear given that the variables Q, B and c and consequently the coefficients K, X, C_1, C_2 and C_3 must be evaluated for each reach for each time step.

6.4.5 Estimating the Parameters of the Muskingum Model

To simulate streamflow routing on a river reach of length L between two stations, it is generally necessary to divide the studied reach into sub-reaches The USACE (1994) suggests for example to divide up the reach so that the travel time within each sub-reach is approximately equal to the time step Δt. The number N of reaches to be taken into account is therefore:

$$N = \frac{L}{\Delta x} \geq \frac{T_t}{\Delta t} \text{ where } T_t = \frac{L}{c} \tag{6.56}$$

where c is the flood wave speed and T_t the time it takes for this wave to travel through the reach of length L. The wave speed c can be estimated using equation 6.55 for a discharge representative of the hydrograph. It is therefore necessary to know the relationships $B(h)$ and $Q(h)$ for the reach, where h is the depth the flow. The relationship $Q(h)$ given by the Manning friction model can be used for this (eq. 6.20). The ratio c/V can be determined analytically for different flow cross-section shapes (Table 6.6). The wave speed can also be estimated from the mean flow velocity V, which can in turn be obtained, for example using the Manning friction equation, on the basis of a flow area and discharge representative of the flow.

To estimate the parameters X and K of the model, several approaches may be followed, depending on the nature of available data. These approaches are described in Addendum 6.6. A graphical method to estimate the parameters of the Muskingum model is illustrated in Example 6.2. In all cases, the parameters of the Muskingum model must satisfy various constraints to provide satisfactory flood routing. These constraints are also described in Addendum 6.6.

It must be kept in mind that parameter K corresponds to the average travel time of the flood wave across the reach. X can vary from 0, leading to the maximum attenuation of the inflow hydrograph, to 0.5, corresponding to simple progression of the hydrograph without attenuation. Experience shows that X is generally close to 0 for river beds with flat slopes and for floods that overflow their banks. For well-channeled watercourses with steeper slopes, X approaches 0.5. In most cases, the value of X is generally between 0.2 and 0.3 (USACE, 1994).

6.4.6 Data Required

The advantage of a hydrological routing model is that it generally requires fewer data than a hydraulic routing model. However, for the Muskingum-Cunge model, data are required for a representative cross-section of the watercourse and for the reach length, average slope and roughness coefficient. For the Muskingum model, these data may also be required if the two parameters X and K of the model cannot be estimated on the basis of observed hydrographs.

Addendum 6.6 Muskingum parameter estimation and constraints

Estimation using the Muskingum-Cunge method

If the relationships $B(h)$ and $Q(h)$ are available, Muskingum-Cunge formulas (equations 6.53 and 6.54) can be applied to estimate parameters X and K. If, in addition, concomitant observed inflow and outflow hydrographs are available for the considered reach, the hydraulic roughness of the reaches can be adjusted to optimize a chosen performance criterion related to the differences between simulated and observed hydrographs.

Estimation by calibration

If only concomitant observed inflow and outflow hydrographs are available for the considered reach, the parameters X and K can be estimated using a classical calibration method. The estimation must explore all possible combinations of X and K to determine a pair (X, K) that maximizes the chosen performance criterion.

Estimation using a graphical method

If an observed hydrograph is available upstream of the considered reach along with the corresponding downstream hydrograph and if it is not necessary to divide the reach into sub-reaches, X and K can be determined by considering the following relationship $K = K(X)$, extracted from the storage and continuity equations of the model:

$$\frac{1}{K} = \frac{X \cdot \left(I_{j+1} - I_j\right) + (1 - X) \cdot \left(Q_{j+1} - Q_j\right)}{0.5 \cdot \Delta t \cdot \left[\left(I_j + I_{j+1}\right) - \left(Q_j + Q_{j+1}\right)\right]} = \frac{D_{j,j+1}(X)}{\Delta S_{j,j+1}} \tag{6.57}$$

The denominator of this equation is the change in storage over the time interval $[j\Delta t, (j+1)\Delta t]$, which depends on X. The numerator, referred to as the weighted flow, is also a function of X. If the routing of discharges through the considered reach can be modeled perfectly by the Muskingum model, the ratio between the change in storage $S_{j,j+1}$ and the weighted flow term $D_{j,j+1}(X)$ is constant and equal to the reciprocal of the model time constant K. In other words, the relationship between these two variables is linear for the value of X that is optimal for the considered reach of the watercourse. The slope of the line is $1/K$. In practice, the curves of the weighted flow $D_{j,j+1}(X)$ versus change in storage $S_{j,j+1}$ are determined for different values of X. The curve that is closest to a straight line corresponds to the correct value of X (Figure 6.21).
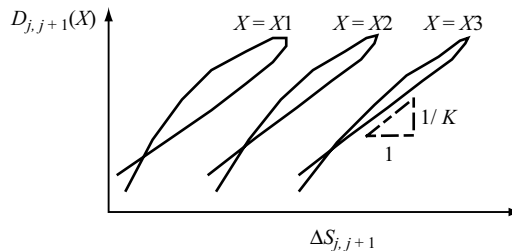

Fig. 6.21: Estimation of parameters X and K of the Muskingum model using the graphical method (weighted flow diagram).

Muskingum parameter constraints

For satisfactory streamflow routing, the parameters of the Muskingum model must satisfy a number of constraints.

1) For attenuation of the flood wave passing through a reach, X must be less than or equal to 0.5.

2) The coefficients C_1, C_2, C_3 must be greater than zero to prevent negative outflow values. This imposes the following two supplementary conditions:

$$\frac{\Delta x}{\Delta t} \leq \frac{c}{2X} \quad \text{and} \quad \frac{\Delta x}{\Delta t} \geq \frac{c}{2(1-X)}$$

(6.58)

where c is the flood wave speed to be estimated on the basis of the discharge that is characteristic of the considered flood. The criteria for valid Muskingum parameters are illustrated in Figure 6.22.
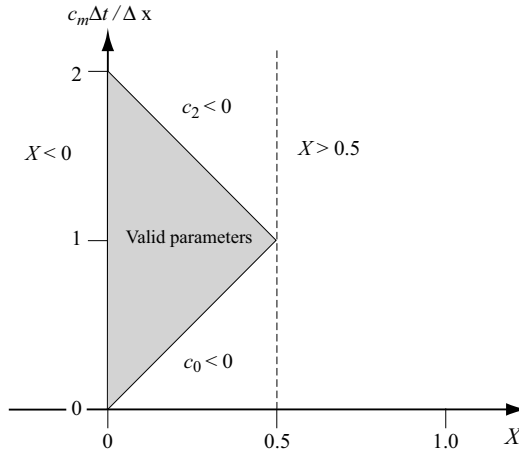
Fig. 6.22: Triangle defining valid Muskingum parameters.

3) The time step Δt must be small enough to provide a reasonable description of the rising limb of the inflow hydrograph. The USACE (1994) suggests the following empirical rule where t_p is the time-to-peak of the hydrograph:

$$\Delta t < t_p / 5$$

(6.59)

4) Finally, to route streamflows through a river reach of length L between two stations, the Muskingum model has often been applied in a global manner, i.e., considering a single storage element. It is in fact generally necessary to divide the studied reach into sub-reaches such that, for example, the travel time through each sub-reach is roughly equal to the time step Δt (USACE, 1994). The recommended number N of sub-reaches is:

$$N = \frac{L}{\Delta x} \geq \frac{T_t}{\Delta t} \quad \text{where} \quad T_t = \frac{L}{c}$$

(6.60)

and where c is the flood wave speed and T_t the travel time of this flood wave through the considered reach of length L.

Muskingum-Cunge parameter constraints

To ensure the validity of the Muskingum-Cunge method, the time step must be either the time-to-peak of the hydrograph divided by 20 or the travel time of the flood wave through the reach, whichever is smaller. The spatial step estimated by $\Delta x = c\Delta t$ must also satisfy the following condition (Ponce, 1983):

$$\Delta x < \frac{1}{2}\left(c - \frac{Q}{B \cdot S_0 \cdot \Delta x} \right)$$

(6.61)

Example 6.2

Estimating Muskingum parameters

The inflows and outflows of a reach on a natural river were measured during a flood. The values are given in columns 3 and 4 of Table 6.8 for a time step of $\Delta t = 10$ minutes. The objective here is to determine parameters K and X of the Muskingum method for this reach on the basis of these two hydrographs. The river reach has a length of $L = 4$ km and flows over a natural plain. It is relatively straight and free of trees. The slope of the channel reach is approximately 0.005 m/m and its cross-section is roughly trapezoidal with $B = 15$ m and $m = 2$ m/m (Table 6.4).

We must first check that the time step for which data are available is short enough to correctly represent the flood rise. Given that Δt (600 s) is less than $t_p/5$ (70/5 min = 840 s), this criterion is satisfied. We must then check that the river reach does not have to be divided into sub-reaches. For this, we must estimate the average travel time of the flood wave passing through the reach. The description provided for the watercourse can be used to estimate the velocity corresponding to the maximum inflow using an iterative procedure. The Manning-Strickler friction model is used for this with a Manning roughness coefficient of $n = 0.03$ m$^{-1/3}$ s (Table 6.7). The velocity to be estimated, corresponding to a flow depth of approximately 4.2 m, is $V = 4.7$ m/s. The speed and travel time of the flood wave are therefore respectively $c = 7.1$ m/s (based on the ratio $c/V = 1.5$) and $T_t = 560$ seconds. This is close to the value of the time step Δt, meaning that the river reach does not have to be divided into sub-reaches (Addendum 6.6).

For streamflow routing to be modeled by the Muskingum model, the relationship between the weighted flow term $D_{j,j+1}(X)$ and the change in storage $\Delta S_{j,j+1}$ must be linear for a value of X to be determined (eq. 6.57). The procedure for estimating parameters K and X is iterative, i.e., X is varied until the N-1 pairs ($\Delta S_{j,j+1}$, $D_{j,j+1}(X)$) obtained using the data fall as close as possible to a straight line. The slope of the line is then $1/K$. Different values of X between 0.1 and 0.5 are tested. For each value of X considered, the weighted flow terms $D_{j,j+1}(X)$ and the change in storage in the reach $\Delta S_{j,j+1}$ are calculated, for each time interval, on the basis of the instantaneous inflow and outflow values at time step j and $j+1$. We obtain N-1 pairs ($\Delta S_{j,j+1}$, $D_{j,j+1}(X)$) that can be plotted on a graph (Figure 6.23).

The calculations for the first time interval are given below for value of $X = 0.3$. At time step $j = 0$, this gives:

$Q_{in,0} = 30$ m^3/s, $Q_{in,1} = 45$ m^3/s,

$Q_{out,0} = 30$ m^3/s, $Q_{out,1} = 39$ m^3/s

$D_{0,1}(X=0.3)\ = 0.3(Q_{in,1} - Q_{in,0}) + (1-0.3)(Q_{out,1} - Q_{out,0})$

$\qquad\qquad = 0.3(45-30) + (1-0.3)(39-45) = 11$ m^3/s

$\Delta S_{0,1} \qquad\quad = (Q_{in,0} + Q_{in,1})/2\Delta t - (Q_{out,0} + Q_{out,1})/2\Delta t$

$\qquad\qquad = (30+45)/2\cdot600-(30+39)/2\cdot600= 1771$ m^3

The results for all the time steps are presented in Table 6.8.

Table 6.8: Inflow and outflow hydrograph values and $\Delta S_{j,j+1}$ and $D_{j,j+1}(X=0.3)$ values.

j	t_j [min]	$Q_{in,j}$ [m³/s]	$Q_{out,j}$ [m³/s]	$\Delta S_{j,j+1}$ [m³]	$D_{j,j+1}(X)$ [m³/s]
0	0	30	30	1771	11
1	10	45	39	6649	13
2	20	65	49	12891	17
3	30	89	62	22465	35
4	40	139	91	29292	47
5	50	187	138	34284	56
6	60	254	189	34766	49
7	70	293	242	9955	19
8	80	264	282	−20780	−29
9	90	212	263	−35523	−39
10	100	162	229	−36420	−50
11	110	121	175	−30157	−32
12	120	95	141	−22774	−24
13	130	82	112	−18144	−17
14	140	64	95	−14250	−19
15	150	55	72	−12398	−8
16	160	42	67	−13170	−11
17	170	35	54	−10499	−12
18	180	26	42		

After plotting the pairs $(\Delta S_{j,j+1}, D_{j,j+1}(X))$ on a graph (Figure 6.23), it is possible to assess the quality of fit and consequently the quality of the model and its parameter estimates. Apart from a visual assessment, the simplest method is to calculate the correlation coefficient R^2 between the plotted pairs $(\Delta S_{j,j+1}, D_{j,j+1}(X))$ and the associated regression line. The procedure is repeated for every value of X to determine the best possible fit. It is obtained here for $X = 0.29$.

We then calculate the parameter K, which is simply the reciprocal of the slope of the linear regression line fitted to the pairs of points $(\Delta S_{j,j+1}, D_{j,j+1}(X))$. For $X = 0.29$, we obtain $K = 737$ s. We finally check that the parameters X and K obtained satisfy the numerical stability constraints (Addendum 6.6). We obtain $X < 0.5$ and $C_1 = 0.105 > 0$, $C_2 = 0.624 > 0$ and $C_3 = 0.271 > 0$, satisfying all the constraints. The final hydrograph routed with the Muskingum model with parameters $X = 0.29$ and $K = 737$ s is shown in Figure 6.23.

6.5 TWO-DIMENSIONAL FLOW MODELS

When streamflows have a marked two-dimensional character, the hydraulic and hydrological routing models presented in the previous sections of this chapter are not well-suited. This is often the case, for example, when floods overflow the natural river banks into a wide floodway or natural flood plain. In this type of situation, two-dimensional flow models are required to provide a reasonable description of streamflow routing. The two most widely used approaches are presented below.
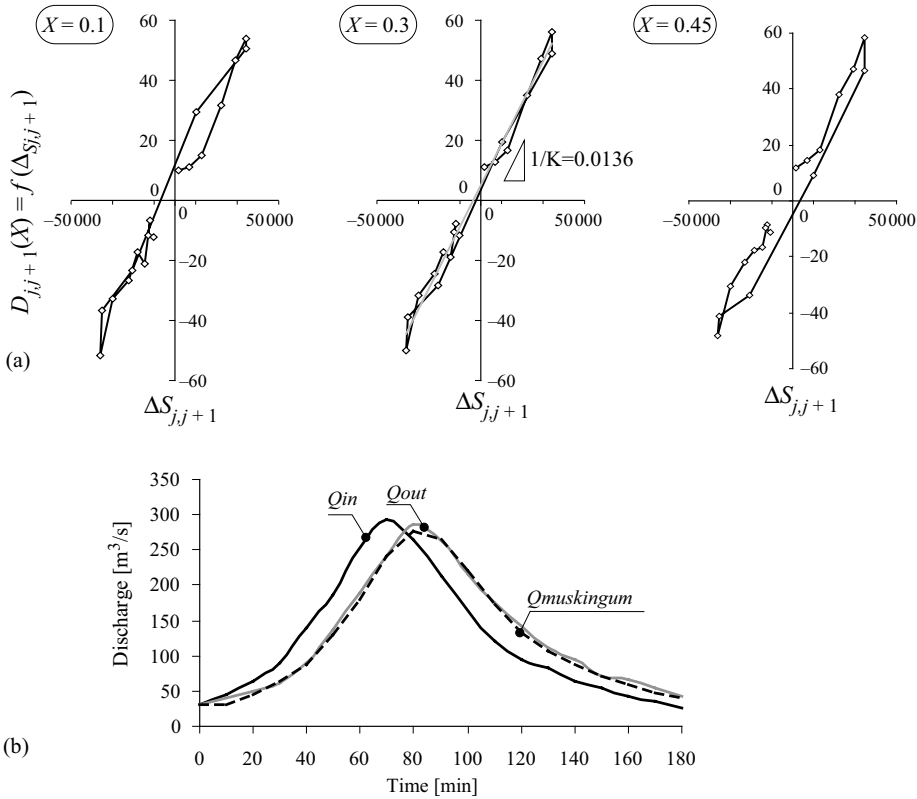
Fig. 6.23: Hydrological streamflow routing using the Muskingum method. a) Weighted flow $D_{j,j+1}(X)$ versus change in storage $\Delta S_{j,j+1}$ for different values of parameter X. b) Inflow and outflow hydrographs obtained by hydrological streamflow routing ($X = 0.29$, $K = 737$ s).

6.5.1 Two-dimensional Flow Equations

The various models that exist are generally based on the use of the Barré de Saint-Venant equations expressed on the two-dimensional (x,y) plane. At point M with coordinates (x,y), these equations can be expressed in vector form as follows (Pochat, 1994; Lane, 1998):

Continuity equation: $\dfrac{\partial h}{\partial t} + \text{div}(h \cdot \mathbf{V}) = q$ (6.62)

Momentum equation: $\dfrac{\partial \mathbf{V}}{\partial t} + (\nabla \mathbf{V}) \cdot \mathbf{V} = -g \cdot (\mathbf{grad}(Z) + \mathbf{J})$ (6.63)

where h is the depth of water [m], Z the elevation of the free surface of the flow [m], q any possible inflows or losses per square meter of area [m³/s/m² or m/s], g acceleration due to gravity [m/s²], $\mathbf{V}$ the velocity vector with components Vx and Vy [m/s] and $\mathbf{J}$ the hydraulic gradient with components Jx and Jy [m/m]. The velocity vector is assumed to have no vertical component. Its horizontal components Vx and Vy correspond to the mean velocity over the vertical direction in the directions x and y.

The schemes for solving the system of equations are numerical schemes that require a discretized representation in space, with a certain time step, of each of the variables describing the flow. One of the difficulties of two-dimensional modeling lies in the description of the topography. For this reason, finite difference methods are not well-suited and finite element methods such as the Galerkin method (Hervouet, 2003) are preferred. Their use is however limited by programming difficulties.

Whatever the type of numerical scheme used to solve the system of equations, two types of two-dimensional flow models exist: true 2D models and quasi-2D models. They are distinguished by their way of discretizing the medium, by the simplifying assumptions used for the description of the velocity vector field and by the resulting simplifications.

6.5.2 2D Flow Models

True two-dimensional models make no major assumptions concerning the velocity field, thereby allowing application of an arbitrary grid structure to the area to be described. The components Vx and Vy of the velocity vector are determined at every point of the grid by one of the previously mentioned solution methods, most often the finite element method.

These models often have a pre-processor designed to optimize the grid structure of the medium by matching the grid cell density to the degree of variability of the medium (topography, roughness, structures) (Figure 6.24).

In addition to classical problems related to the stability and convergence of numerical schemes for solving a system of non-linear equations, the Galerkin finite element method generally used to solve these systems first requires a reformulation of the different equations governing flow (i.e., integration of the equations over the different grid cells of the discretized area). This requirement can be hard to satisfy or even unmanageable when the system to be modeled includes many hydraulic singularities—such as weirs, orifices and other special hydraulic works—each requiring specific modeling that can in addition vary as a function of hydraulic conditions. Furthermore, the behavior of the different singularities present cannot necessarily be modeled, in particular when the streamlines above the singularity are not oriented in any specific direction and even more so if their orientation varies with time. Finally, partially wet/dry or dry zones observed on inundated areas are often a source of instability when using numerical methods to solve the equations (Hervouet, 2003).

For these reasons, the use of true 2D models is essentially restricted to currentology (e.g., estuaries, lakes), dike or dam failure simulations and streamflow studies not requiring the modeling of singularities.

6.5.3 Quasi-2D Flow Models

Quasi-2D flow models perform a discretization suited to the system to be modeled, making it possible to reduce the number of calculation points and variables to be calculated. For this, the size and shape of the grid cells are adjusted according to the relative orders of magnitude of the hydraulic gradients (elevations and velocities) and the main flow directions. It is essential to take into account any obstacles or axes that structure the flows (e.g., dikes, bridges, weirs, canals).

Elevation [masl]

■	45
	43.5
	42
	40.5
	39
	37.5
	36
	34.5
	33
	31.5
	30

1000 m

N

(a)

(b)

(c)
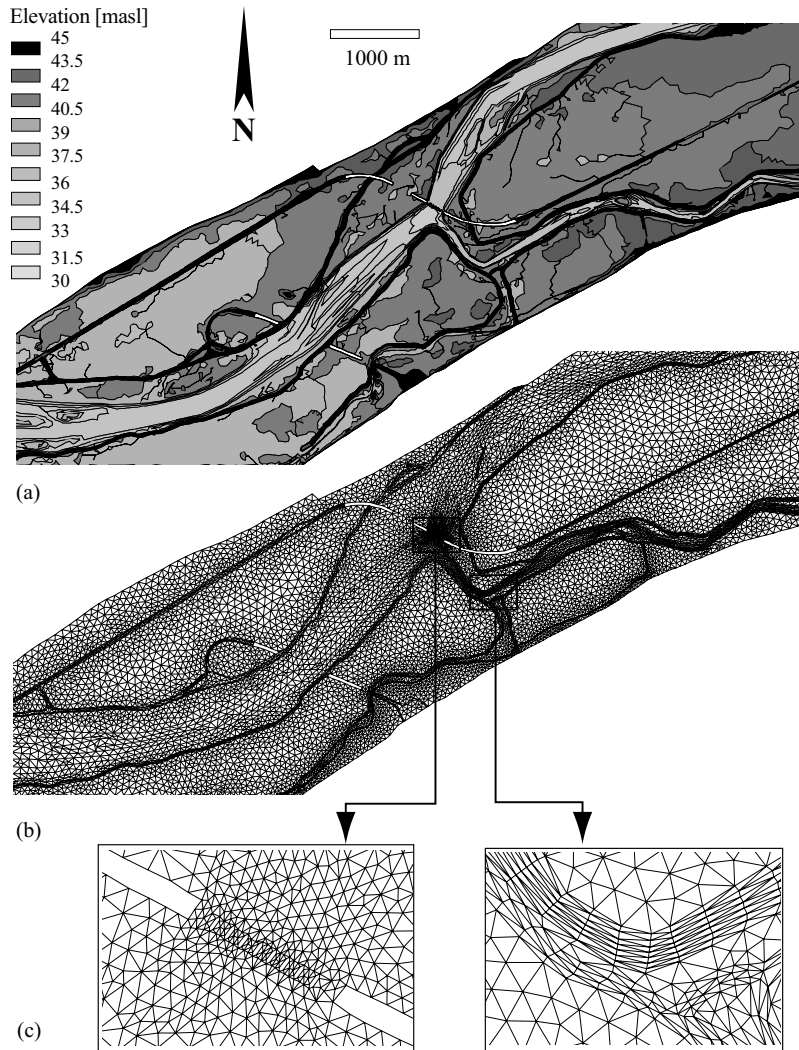
Fig. 6.24: Two-dimensional modeling of the main channel and floodway of a reach of the Loire river downstream of Tour. a) Elevation map of the river and the floodway. b) Discretization of the medium conditioned by its characteristics and the different structures and features present (dikes, roads, railways, bridge piles, confluence with the Cher river, river forks and weirs). c) Details of the discretization for the railway bridge upstream of Bec du Cher and for the last bend of the Cher river before its confluence with the Loire river (Sogreah, personal communication).

The advantage of such a discretization is that the two-dimensional formulation of the momentum equation can be integrated at each interface between adjacent grid cells. This is subject the condition that the discretization was carried out in such a way that variations of the hydraulic head and angle of flow remain low along the interface (Cappelaere, 1985). The flow through this interface can therefore be considered homogeneous. These grid cells correspond to the physical reality of the medium. The resulting two-dimensional models are often referred to as cell-based or cell-to-cell streamflow models (Figure 6.25b).

(a)

(b)

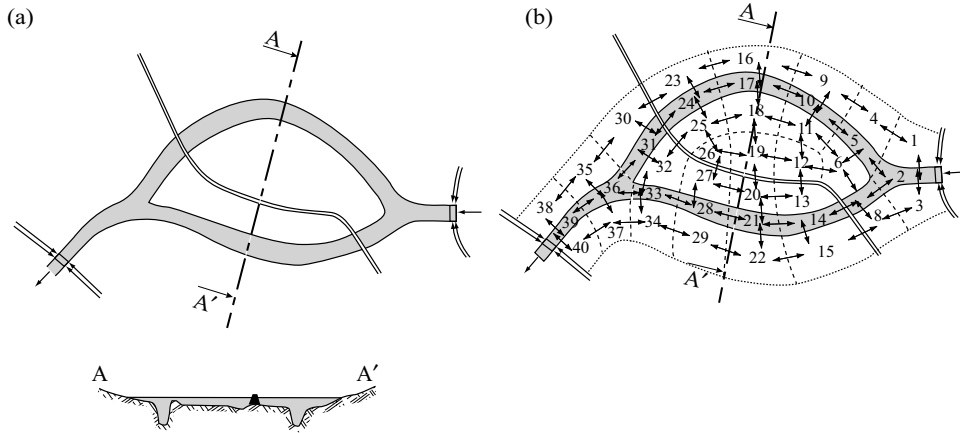**Fig. 6.25:** Spatial discretization for a quasi-2D model. The different cells are numbered (adapted from Cappelaere, 1985).

The system of equations of the two-dimensional formulation of the Barré de Saint-Venant equations initially involved three equations—a continuity equation and two momentum equations projected on x and y. With the quasi-2D model described above, it can be simplified at each interface by projecting the momentum equation on the normal to the interface. Furthermore, except in the main channel of the river, inertia forces are generally negligible in the flow with respect to friction forces. For this reason, the inertia terms of the momentum equation are often neglected (Bocquillon, 1978). Flow in a floodway or on the flood plain is in fact mainly influenced by the slope and geometry of the terrain, bed resistance and obstacles (Cunge, 1995).

The formulation of the system of equations is then simple and the only unknowns are the water depth at the center of the different cells. The system is reduced to writing the N continuity equations (eq. 6.62), corresponding to the N cells (Cunge, 1980), completed by the appropriate initial conditions and boundary conditions of the system (Figure 6.26):

$$A_{s_i} \cdot \frac{dz_i}{dt} = q_i(t) + \sum_k Q_{i,k}^j \left(z_i, z_k \right) \tag{6.64}$$

where z_i is the water depth at the center of the cell, A_{si} the area of the water surface in the cell, $q_i(t)$ the inflows/outflows per square meter within the cell—positive for inflows (e.g., precipitation) and negative for outflows (e.g., infiltration)—and where the discharge $Q_{i,k}$ between cell i and cell k is related at each time step $j\Delta t$ to the water depths z_i and z_k in the cells or to the hydraulic heads $z_i + \alpha_i V_i^2/2g$ and $z_k + \alpha_k V_k^2/2g$.[5]

The equations generally used to describe the flow $Q_{i,k}$ between two neighboring cells varies according to the types of links between the cells (Addendum 6.7).

---

[5]If all the inertia terms of the momentum equation must be retained, the discharge at a given point depends on the hydraulic head and on the discharge itself. The discharge can therefore not be eliminated from the equations, leading to a double set of variables (z and V or z and Q). The system to be solved is then much more complicated.
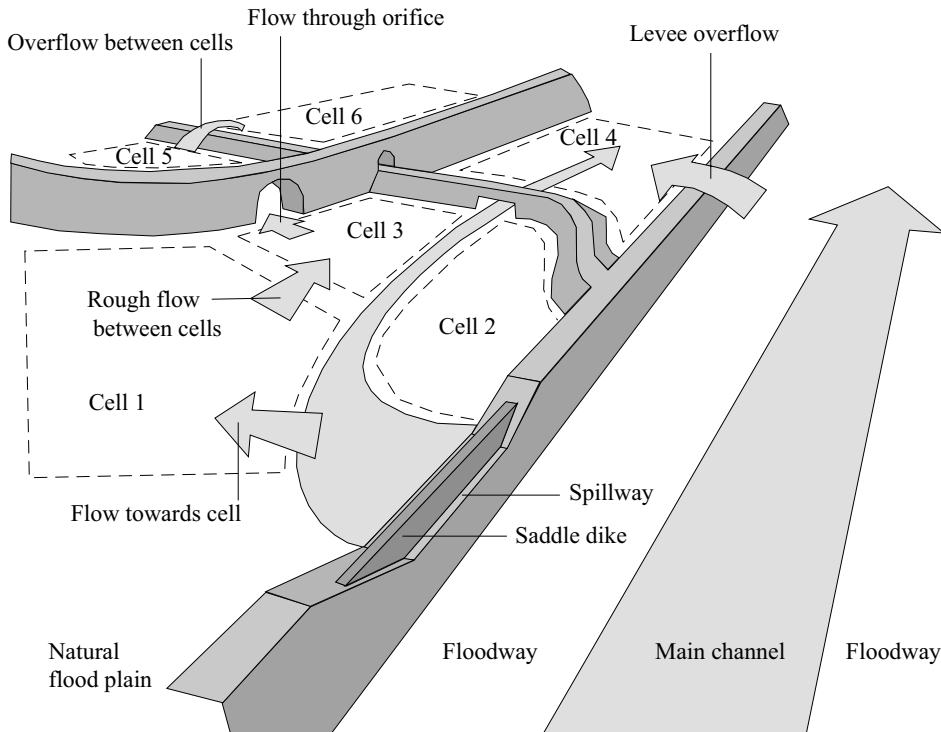
Fig. 6.26: Different types of links defined in a cell-based model (adapted from Marti, 1997).

Addendum 6.7 Different types of links defined in cell-based models.

The main links used in the so-called cell-based models are the following (Cunge, 1980; Riccardi, 1997).

River type links: This type of link is used when two neighboring cells form part of the main channel or the flood plain and are not separated by any particular topographic or hydraulic discontinuity. The situation induces a linear head loss between the centers of the cells. The expression for $Q_{i,k}$ is deduced from the discretization of the momentum equation, neglecting the inertia terms and using a head loss model of the Manning type:

$$Q_{i,k} = Sign(z_k - z_i) \; K \; \sqrt{\frac{|z_k - z_i|}{\Delta x}} \tag{6.65}$$

where z_i and z_k are the water levels in cells i and k, K the conveyance factor between the cells defined by $K = 1/n \cdot A \cdot R_H^{2/3}$ where n is the roughness coefficient, A the flow area, R_H the hydraulic radius of the interface and Δx the distance between the centers of the cells.

Weir type link: This type of link is used for cells separated by a structure representing a weir, including dikes, railway or road embankments, etc. For such cases, the broad-crested weir model is often used. A distinction must be made between submerged and free flow conditions.

Submerged weir: $Q_{i,k} = m \cdot L \cdot (h_{down} - h_{weir}) \cdot \sqrt{2g \cdot (h_{up} - h_{down})}$ (6.66)

Free flow weir: $Q_{i,k} = \dfrac{2}{3\sqrt{3}} \cdot m \cdot L \cdot \sqrt{2g} \cdot \left[h_{down} - h_{up} \right]^{3/2}$ (6.67)

where m is a discharge coefficient, L the length of the crest in the direction perpendicular to the flow, h_{weir} the elevation of the weir and h_{up} and h_{down} respectively the elevations z_i and z_k if $z_i > z_k$ and z_k and z_i if not.

Local energy loss type link: This type of link can be used for cells separated by singularities corresponding to rapid changes of the flow cross-section. The discharge is then determined by considering that the portion of kinetic energy lost in the flow contraction is k_i. The discharge can then be related to z_i and z_k in the following manner (Riccardi, 1997):

$$Q_{i,k} = \sqrt{2g} \; \sqrt{\dfrac{z_k - z_i}{\left(\dfrac{1+k_i}{A_i^2} - \dfrac{1}{A_k^2} \right)}}$$ (6.68)

Kinematic type link: This type of link is only used when hydrodynamic information is propagated downstream. This type of relationship can be determined for the upstream cells of the model and makes it possible to represent the hydrological inflows of upstream basins. The discharge is then a function of only the water level in the upstream cell (Riccardi, 1997):

$$Q_{i,k} = f(z_k)$$ (6.69)

Links between a cell *i* and a fictitious downstream cell (Cunge, 1980): These links can be used to determine the downstream boundary conditions of the system by defining a discharge model that can be for example of the type:

$$Q_{i,k} = a_0 + a_1 z_i + a_2 z_i^2 + ...$$ (6.70)

Another frequently used model is obtained by considering that the water level corresponding to the outflow from the system is the normal water level of the flow.

Other links that can be defined include for example links corresponding to flows through an orifice or conduit or links partially taking into account the inertia terms of the momentum equation (Riccardi, 1997). The exchange models used can therefore be chosen in a wide variety of ways and nothing prevents a software user from defining other exchange models corresponding to particular phenomena or mechanisms. This high level of flexibility is one of the main advantages of this type of model.

6.5.4 Data Required

The information required for these models concerns the topography and the hydraulic parameters of the flow zones (roughness) and any special structures or hydraulic singularities that may be present.

The topographic data required for quasi-2D models are the cross-sections for each interface and the topography inside each cell for the determination of the water elevation-volume relationship. For "true" 2-D models, the topography of the entire modeled zone must be described. Remote sensing, in particular the LIDAR technique, is well-suited for this (Chapter 2 or Metzger, 2002).

Hydraulic roughness values are often mapped by experts according to the characteristics of the medium. When observations of water elevations are available for one or more flood events, these values are often subsequently fine-tuned by calibration.

6.6 CHOOSING A ROUTING METHOD

To route flows through a reservoir, two methods were presented at the beginning of this chapter. These methods are roughly equivalent. The Runge-Kutta numerical method has the advantage of being explicit however its stability depends on the time step chosen for its resolution.

To route streamflows through rivers and canals, several methods are available. Identifying the best method is not always obvious. Several methods may often provide good results for a given situation. The main factors to be considered when choosing a method are presented below. The first concerns the information available for the watercourse that must satisfy the data requirements of the model to be used. Another key factor is the modeling context that must correspond to the field of application of the chosen model.

6.6.1 Available Information and Model Data Requirements

Sections 6.3.7, 6.4.6 and 6.5.4 indicate the data required to use the various one-dimensional and two-dimensional routing and flow propagation models.

As opposed to hydrological routing models—with the exception of the Muskingum-Cunge model—hydraulic routing models can in principle be applied even without observed hydrographs of the system inflows and outflows. Given that they are physically-based, they have no parameters to be calibrated other than the roughness of the different reaches that can be estimated on the basis of the characteristics of the medium using appropriate tables (Section 6.3.7). In practice, however, it is always a good idea to use any available observations (e.g., discharges, water levels, flood zone extent in the event of bank overflow) to adjust the roughness of the various reaches and/or flow sections to the studied medium.

On the other hand, hydraulic routing models—as well as the Muskingum-Cunge model—required detailed information on the geometry of the medium and on the flow cross-sections. The accuracy of simulations is highly dependent on the accuracy of available data. A number of authors consider that the availability and accuracy of this information (e.g., topography, roughness) has a greater influence on the quality of simulations than the type of model (Beven and Wood, 1993).

Current practice in hydrology consists in simulating the propagation of flows in a deterministic manner, i.e., floods are routed for a given bed topography and given hydraulic parameters. However, due to the uncertainty related to the estimation of roughness parameters and bed topography,[6] a probabilistic approach can be proposed, i.e., flood routing is carried out for different sets of roughness parameters and bed topographies. The results obtained for these different configurations are then combined to produce, for example, a probabilistic map of overbank flood zones with the corresponding extents and water depths (Aronica *et al.*, 1998; Metzger, 2002).

---

[6]The roughness parameters are often hard to estimate. Several parameter sets can generally produce the same simulation results. The accuracy of source topographic data can strongly affect the quality of simulation results, in particular for partitioned cells (Metzger, 2002).

6.6.2 Flow Modeling Context

The main contextual elements to be taken into account when choosing a routing model are the presence of backwater effects, the presence of overbank flooding and the associated type of flow, the channel slope and the intensity and rapidity of inflow variations that affect the rise time of the hydrograph. Table 6.9 summarizes the suitability of the different methods for the main situations discussed below.

Backwater effects

Backwater effects that can influence the propagation of streamflows include tidal fluctuations, major inflows from a downstream tributary, reservoirs and hydraulic singularities such as weirs or channel constrictions. These factors tend to attenuate and delay the flood wave.

Table 6.9: Streamflow routing methods that are suitable (●) or unsuitable (□) according to the flow modeling context (modified from USACE, 1994).

Criteria	High slope	Medium slope	Low slope	Bank overflow	Bank overflow	Backwater effects
Type of flow	Slow rise time[1]	Medium rise time[1]	Fast rise time[1]	1D	2D	
1D full Barré de Saint-Venant	●	●	●	●	□	●
Diffusion wave	●	●	□	●	□	●
Kinematic wave	●	□	□	●	□	□
Muskingum-Cunge	●	●	□	●	□	□
Muskingum	●	●/□[1]	□	□	□	□

[1]See the following pages for more details on these criteria.

Hydrological routing models cannot take into account backwater effects on flood wave propagation (except for the modified Puls model not described here—see USACE, 1994). On the other hand, backwater effects are taken into account by all hydraulic routing methods except for the kinematic-wave model.

Bank overflow

If the flood hydrograph exceeds the carrying capacity of the main channel, water will flow over the river banks where it is propagated in the floodway or on the natural flood plain before possibly returning to the main channel after a certain delay. Bank overflow can greatly affect the shape of the flood hydrograph between the upstream and downstream end of the overflow zone. The main factors that determine this are the storage capacity of the floodway or natural flood plain—determined by its topography and in particular its width and transversal slopes—and the resistance to flow due to vegetation or buildings.

The routing model must take into account these special conditions. If the flows have a marked two-dimensional character or if the flood plane is bounded by various topographic obstacles such as dikes or roadways, a 2D or quasi-2D model is required.

In the event of bank overflow, the flows can however remain predominantly one-dimensional. This can be the case for instance when the watercourse flows in a narrow valley, limiting the width of the floodway or natural flood plain. In this type of situation,

the one-dimensional Barré de Saint-Venant models and hydrological routing can be used, generally adapting one or more of their equations.

The flow cross-section can for example be considered as a composite section to take into account the possibly different roughness characteristics of different sub-sections (Figure 6.27). The friction equation is in this case often formulated as follows:

$$Q(h) = \sum_{i=1}^{N} K_i(h) \cdot \sqrt{S_f} \tag{6.71}$$

$$K_i(h) = \frac{1}{n_i} \cdot A_i(h) \cdot R_{H,i}(h_i)^{2/3} \tag{6.72}$$

where N is the number of sub-sections considered and $K_i(h)$ the conveyance factor of each sub-section, which depends on the roughness, flow area and hydraulic radius of each sub-section.

This formulation can be used in a more general manner if the flow velocity can no longer be considered as uniform within the flow section, in particular when the hydraulic properties and hydraulic roughness vary greatly over the section. This is often the case when flows reach levels for which the banks are covered by dense vegetation.

If certain parts of the floodway or natural flood plain contribute to storage but not to flow, the conveyance of the corresponding sub-sections is zero.

For the 1D Barré de Saint-Venant model, the corresponding adaptation of the continuity and momentum conservation equations is described for example by Cunge *et al.* (1980).

When water is stored on the floodway or natural flood plain but does not flow (due to vegetation on the flood plain that greatly increases the roughness and therefore obstructs flow), the wetted area to be considered in the continuity equation is for example the full wetted area while in the momentum conservation equation, only the area taking part in flow should be considered. The adaptation of the momentum equation consists mainly in introducing a correction factor applied to the convective acceleration term (taking into account the major non-uniformity of the velocity field).
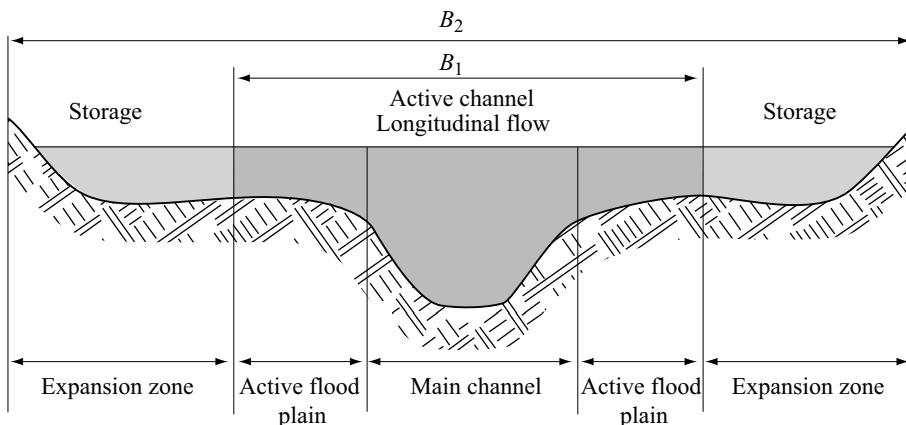

Fig. 6.27: Composite flow cross-section for a mainly one-dimensional flow. The different sub-sections include the main channel, the active part of the floodway or natural flood plain and the inactive part of the floodway or natural flood plain (pure storage).

Channel slope and inflow variations

Streamflow modeling is easier for low channel slopes and fast inflow variations. Of all the routing models presented in this chapter, the only one capable of correctly representing all situations for one-dimensional flows is the full Barré de Saint-Venant model.

The possibility of using one or more simplifications of the full model depends on the relative importance of the inertia, pressure and friction terms in the conservation of momentum equation. Moussa and Bocquillon (1996, 2000) have shown that the relative importance of these terms depends on three dimensionless quantities: the Froude number F_0 determined for conditions that are representative of the considered flow, the dimensionless period T_+ of the upstream disturbance and the ratio η between the width B_2 of the flood plain, assumed to contribute to storage but not to flow, and the width B_1 of the main channel and floodway, assumed to be active (Figure 6.27).[7] These quantities can be expressed as follows:

$$F_0^2 = \frac{V_0^2}{g \cdot h_0} \tag{6.73}$$

$$T_+ = \frac{T \cdot V_0 \cdot S_0}{h_0} \tag{6.74}$$

$$\eta = \frac{B_2}{B_1} \tag{6.75}$$

where V_0 and h_0 are respectively the flow velocity [m/s] and depth [m], S_0 the friction slope or channel bottom slope [m/m], g acceleration due to gravity [m s^{-2}], B_1 and B_2 the respective widths [m] of the main channel (including the floodway) and the flood plain and T the period [s] of the upstream disturbance. The disturbance is the inflow hydrograph and its period therefore corresponds roughly to its duration.

Each of the terms appearing in the dimensionless Barré de Saint-Venant equations is a function of the above three dimensionless quantities. The conditions under which various model simplifications can be applied can therefore be determined. They are indicated in Table 6.10 and Figure 6.28.

In the absence of storage on the flood plain, the diffusion wave provides a good approximation of the dynamic wave for most commonly encountered hydrological situations, even for rivers with very low bed slopes, as long as the hydrograph rises slowly. For rapidly rising hydrographs, the USACE (1994) recommends using the diffusion wave only for rivers with bed slopes $S_0 > 2 \cdot 10^{-4}$ m/m. The conditions for using the kinematic wave are more restrictive. According to the USACE (1994), its use should be restricted to rivers with relatively high slopes ($S_0 > 2 \cdot 10^{-3}$ m/m). The conditions under which these two models are valid become even more restrictive as the width of the inactive flood plain increases.

---

[7]To obtain these results, the authors used the Barré de Saint-Venant equations to determine the dimensionless differential equations governing the flows induced by the disturbance (assumed to be periodic) of the initial steady flow (velocity V_0 and depth h_0). The flow depth is assumed to be low compared to the width of the main channel and the friction model is assumed to be the Manning equation.

Given that the Muskingum-Cunge model can be used to approximate the diffusion wave, it can be applied to rivers with a similar range of slopes. The simple Muskingum method should not however be applied to rivers with slopes less than $4 \cdot 10^{-4}$ m/m.

Table 6.10: Criteria for the validity of different approximations of the Barré de Saint-Venant model for various ratios η between the widths of the inactive flood plain and the active channel. A term in the momentum equation is assumed to be negligible if its relative contribution in the equation is less than 10% (modified Moussa and Bocquillon, 2000).

	Gravity wave	**Dynamic wave**	**Diffusion wave**	**Kinematic wave**
$\eta = 1$	$\dfrac{F_0^2}{T_+} \geq 12.4$	*No restriction*	$0.0432 \geq \dfrac{F_0^2}{T_+}$	$0.0432 \geq \dfrac{F_0^2}{T_+}$ and $T_+ \geq 39$
$\eta = 8$	$\dfrac{F_0^2}{T_+} \geq 2.85$	*No restriction*	$0.0101 \geq \dfrac{F_0^2}{T_+}$	$0.0101 \geq \dfrac{F_0^2}{T_+}$ and $T_+ \geq 154$
$\eta = 20$	$\dfrac{F_0^2}{T_+} \geq 2.5$	*No restriction*	$0.0037 \geq \dfrac{F_0^2}{T_+}$	$0.0037 \geq \dfrac{F_0^2}{T_+}$ and $T_+ \geq 383$
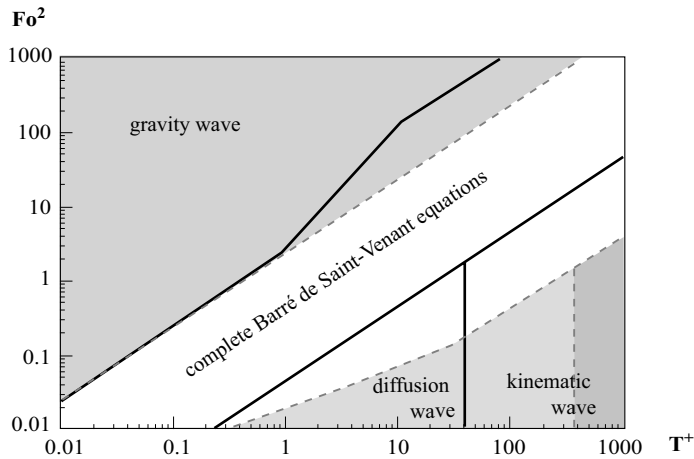
Fig. 6.28: Criteria for the validity of different approximations of the Barré de Saint-Venant model for various ratios η between the widths of the inactive flood plain and the active channel ($\eta=1$: zone delimited by the solid lines; $\eta=20$: white and gray zones delimited by broken lines) (modified from Moussa and Bocquillon, 2000).

Other factors to be considered

Various other criteria can be considered when choosing a routing model, for instance the nature and required accuracy of the data to be produced by the simulation, the possibility of controlling the flow regime transitions (e.g., sub-critical/super-critical/critical flow and laminar/turbulent flow), the possibility of reproducing the grid structure of the network if any (confluences and forks). The last point is crucial in particular in the event of bank overflow in a highly urbanized area. In this case, the overflows are propagated throughout

the complex drainage network made up in particular of the roadways that define its structure (Hingray, 1999; Mignot, 2005; Lhomme, 2006).

6.6.3 Hydrological or Hydraulic Routing

Hydrological routing models are typically used in rainfall-runoff modeling to calculate time series of streamflows at different stations of a given drainage basin. The representation of each reach of the watercourse is generally independent and flows are routed sequentially from upstream to downstream. Hydrological routing models are simpler and can be solved easily and quickly by numerical solution methods. For the majority of hydrological applications, they offer reasonable accuracy as long as flow is not greatly affected by backwater effects. However, they provide only the discharges. Hydrological routing is widely used for common hydrological applications.

The full Barré de Saint-Venant model can be used to represent a large number of hydraulic situations for a wide variety of watercourses. The system of equations associated with the full or simplified model has no analytical solution and must be solved using numerical schemes that are often relatively sophisticated. Many software packages including numerical solution modules well-suited to these equations have been developed to make it easier to apply the Barré de Saint-Venant model.[8] The use of the Barré de Saint-Venant model is therefore relatively widespread, especially for hydraulic-type studies requiring, in addition to discharges, the estimation of other flow characteristics such as flow depths and velocities. Finally, note that hydraulic routing models can if necessary be coupled with a model simulating the advection-diffusion of chemical and organic substances (e.g., pollution).

6.7 KEY POINTS OF THE CHAPTER

- Open-channel flow at any point M with coordinates x and y is characterized by the flow depth and the flow velocity components in the x, y and z directions.
- For common hydrological applications, flood routing can be modeled in a simplified manner. Often only the discharges are routed, corresponding to the change in the shape of the hydrograph from upstream to downstream (i.e., time shift and attenuation).
- Reservoir routing can be used to estimate the temporal variations of the volume of water stored in a reservoir and the outflows resulting from the inflows and operation of the known outlet and diversion works.
- Reservoir routing is relatively straightforward given that the outflow is either controlled or dependent only on the reservoir water level. It requires a storage equation combined with one or more discharge equations and a continuity equation. The system of equations is often solved using the Puls method or a numerical Runge-Kutta scheme.
- Streamflow routing methods are either of the hydrological or hydraulic type. They are used to estimate the temporal variations of streamflows (and possibly flow depths and

---

[8]The main European industrial institutes developing software for the simulation of open-channel flows are the Danish Hydraulic Institute, Delft Hydraulics, Hydraulic Research Ltd., Wallingford Software, Laboratoire Hydraulique de France and Laboratoire National d'Hydraulique of EDF.

velocities) at different cross-sections selected along the watercourse. The flows are considered to be one-dimensional.

- Hydraulic routing is based on the Barré de Saint-Venant model, which can be simplified in a number of ways. The associated system of equations includes in particular a continuity equation and a conservation of momentum equation. The system of equations can only be solved numerically. Hydraulic routing can be used to estimate different flow variables.
- The Barré de Saint-Venant model simplifications generally used in hydrology produce models that are dominated by friction.
- The diffusion-wave model neglects the inertia terms in the momentum equation of the Barré de Saint-Venant model. In most cases encountered in hydrology, this represents a reasonable simplification.
- The kinematic-wave model neglects, in addition, the pressure term. The momentum equation is then reduced to a friction equation (e.g., Manning equation). This model leads to flood routing without attenuation of the peak discharge. It can be suitable for channels with steep slopes.
- The Barré de Saint-Venant model is not suitable for rapidly varied flows induced for example by hydraulic singularities. Special additional models are required for such cases.
- Hydraulic routing models require estimation of only one parameter, i.e., the hydraulic roughness of the different flow sections. However, such models require a high-resolution description of the topography of the main channel and possibly the floodway or the natural flood plain in the event of bank overflow.
- Hydrological routing is based on a conceptual and lumped representation of the reaches of the considered watercourse.
- The Muskingum hydrological routing model is based on the continuity equation and an equation relating the volume of water stored in the reach to the inflows and outflows. It provides an explicit recurrence relation for the outflow to be determined. It includes two parameters that must be estimated on the basis of observed hydrographs.
- The Muskingum-Cunge model is a Muskingum model for which the two parameters are adjusted according to the flow conditions in each section of the watercourse and at each time step. It is an approximation of the diffusion-wave model.
- Only the diffusion-wave and dynamic-wave models can take into account the presence of backwater effects.
- When the flows have a marked two-dimensional character, streamflows must be routed using 2D or quasi-2D models referred to as cell-based or cell-to-cell models.

6.8 APPENDICES

6.8.1 Numerical Reservoir Routing Solution using the Runge-Kutta Scheme

Problem description

Assuming that reservoir outflow is an unequivocal function of outlet discharge and that the storage equation can be written in the following form:

$$dS = A_r(h) \cdot dh \tag{6.76}$$

then the continuity equation can be expressed on the basis of the first derivative of the reservoir surface elevation with respect to time:

$$\frac{dh}{dt} = \frac{I(t) - Q(h)}{A_r(h)} \text{ or alternatively } \frac{dh}{dt} = f(h_n, t_n) \tag{6.77}$$

The only variable to be estimated in the above equation is the reservoir elevation h. This differential equation is non-linear and therefore can only be solved using an appropriate numerical scheme.

An initial estimate of the reservoir elevation at time $t = (n+1)\Delta t$ can be obtained using the Euler numerical scheme:

$$h_{n+1} = h_n + \Delta h \text{ where } \Delta h = f(h_n, t_n) \cdot \Delta t \tag{6.78}$$

where Δh is the change of variable h over the time interval $[n\Delta t, (n+1)\Delta t]$. However, the value of the derivative f changes continually over the time interval $[n\Delta t, (n+1)\Delta t]$ since the variable h changes over this interval. The estimation obtained using the Euler scheme is therefore generally relatively inaccurate unless the considered time step is very small.

The Runge-Kutta numerical scheme is preferred over the Euler method because it estimates the function and its derivatives at several points over the interval $[n\Delta t, (n+1)\Delta]$. The estimation of h_{n+1} can for example be improved by estimating the value of the increment Δh at the beginning (estimate Δh_1) and end (estimate Δh_2) of the time interval using the elevation estimate h_{n+1} provided by equation 6.78. The estimate can be expressed as follows:

$$h_{n+1} = h_n + \Delta h \text{ where } \Delta h = \frac{\Delta h_1 + \Delta h_2}{2} \tag{6.79}$$

and where $\Delta h_1 = f(h_n, t_n) \cdot \Delta t$ and $\Delta h_2 = f(h_n + \Delta h_1, t_n + \Delta t) \cdot \Delta t \tag{6.80}$

This numerical scheme is known as the second-order Runge-Kutta scheme. The higher-order schemes are determined on the basis of a Taylor series expansion that can be expressed for example for the fourth-order scheme in the following form:

$$h_{n+1} = h_n + f(h_n, t_n) \cdot \frac{\Delta t}{1!} + f'(h_n, t_n) \cdot \frac{\Delta t^2}{2!} + f''(h_n, t_n) \cdot \frac{\Delta t^3}{3!} + f'''(h_n, t_n) \cdot \frac{\Delta t^4}{4!} + \varepsilon\left(\Delta t^5\right)$$

The estimates of the Runge-Kutta (RK) scheme improve with increasing order. The fourth-order schemes are the most widely used. One of them can be expressed as follows:

$$h_{n+1} = h_n + \Delta h \tag{6.81}$$

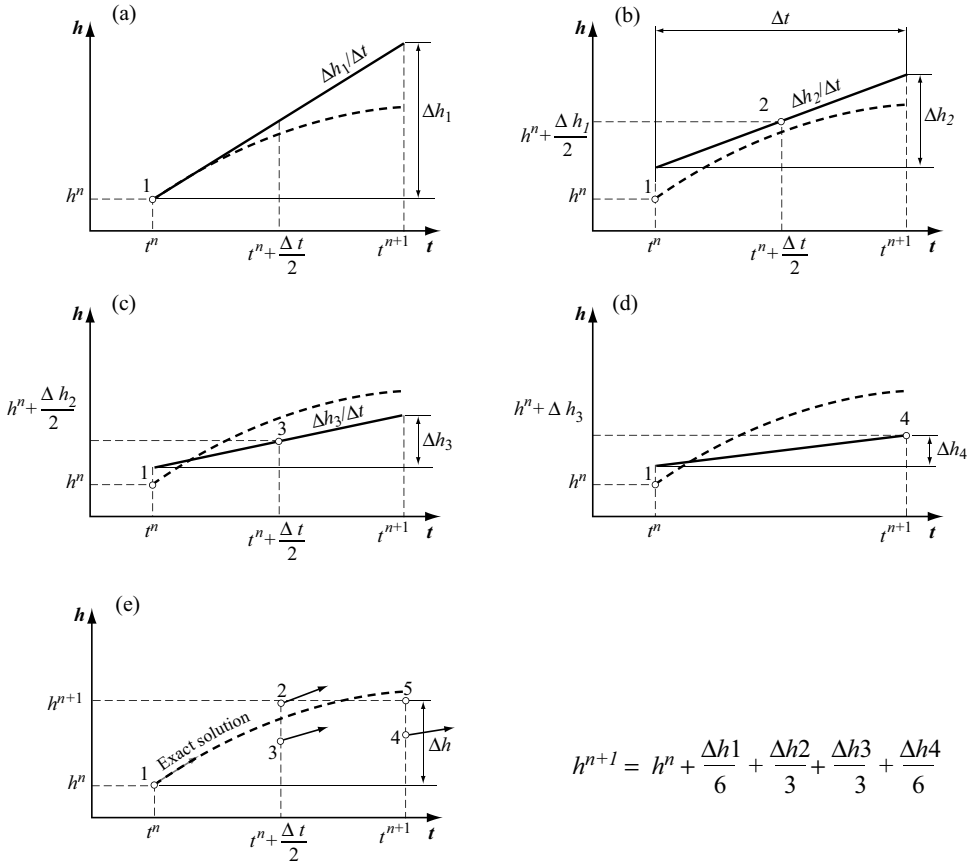$$\text{where } \Delta h = \frac{1}{6}(k_1 + 2k_2 + 2k_3 + k_4) \cdot \Delta t \tag{6.82}$$

$$k_1 = f(h_n, t_n) \tag{6.83}$$

$$k_2 = f(h_n + k_1 \cdot \Delta t / 2, t_n + \Delta t / 2) \tag{6.84}$$

$$k_3 = f(h_n + k_2 \cdot \Delta t / 2, t_n + \Delta t / 2) \tag{6.85}$$

$$k_4 = f(h_n + k_3 \cdot \Delta t, t_n + \Delta t) \tag{6.86}$$

The meaning of these different terms is illustrated in Figure 6.29.

Fig. 6.29: Illustration of estimates Δh_1, Δh_2, Δh_3 and Δh_4 made using a fourth-order Runge-Kutta scheme (RK4).

Example

The attenuation of the flood described in column 2 of Table 6.3 by the reservoir described in Figure 6.4 (Example 6.1) is estimated below using the RK4 method. The different calculation steps are detailed for the time interval $[t_0, t_0+\Delta t]$. The results for all the time intervals are summarized in Table 6.11. The reservoir outflow obtained using the RK4 scheme is given in Figure 6.9.

At $t_0 = 0$, $I_0 = 0$, $h_0 = 0$, $A_0 = 2000$ m², $Q_0 = 0$ (initial conditions of the problem).

$$k_1 = f(h_0, t_0) = \frac{I(t=0) - Q(h=0)}{A_r(h=0)} = \frac{0-0}{2000} = 0 \text{ [m/s]}$$

First estimate of reservoir elevation at time $t_0+\Delta t/2$: $h_{est1} = h_0 + k_1 \cdot \Delta t / 2 = 0$ [m]

$$k_2 = f(h_0 + k_1 \cdot \Delta t / 2, t_0 + \Delta t / 2) = \frac{I(t=5) - Q(h=0)}{A_r(h=0)} = \frac{2.98 - 0}{2000} = 0.0015 \text{ [m/s]}$$

Second estimate of reservoir elevation at time $t_0+\Delta t/2$: $h_{est2} = h_0 + k_2 \cdot \Delta t / 2 = 0.45$ [m]

$k_3 = f(h_0 + k_2 \cdot \Delta t / 2, t_0 + \Delta t / 2) = \dfrac{I(5) - Q(0.45)}{A_r(0.45)} = \dfrac{2.98 - 0.35}{2256} = 0.0012 \, [\text{m/s}]$

Third estimate of reservoir elevation at time $t_0 + \Delta t$: $h_{est3} = h_0 + k_3 \cdot \Delta t = 0.7 \, [\text{m}]$

$k_4 = f(h_0 + k_3 \cdot \Delta t, t_0 + \Delta t) = \dfrac{I(10) - Q(0.70)}{A_r(0.70)} = \dfrac{6 - 0.44}{2406} = 0{,}0023 \, [\text{m/s}]$

Final estimate h_1 of reservoir elevation at time $t_0 + \Delta t$:

$h_1 = h_0 + \Delta h = h_0 + \dfrac{1}{6}(k_1 + 2k_2 + 2k_3 + k_4) \cdot \Delta t = 0 + 0.76 = 0.76 \, [\text{m}]$

This gives the following estimate for the outlet discharge Q_1 corresponding to reservoir elevation h_1 at time $t_0 + \Delta t$:

$Q_1 = Q(h_1) = 0.46 \, [\text{m}^3/\text{s}]$

The calculation is then repeated over the entire time period [0, 120 min].

Table 6.11: Reservoir inflow and outflow hydrographs.

Step n	Time [min]	I_n [m³/s]	h_n [m]	$A(h_n)$ [m²]	Δh [m]	Q_n [m³/s]
0	0	0.00	0.00	2000	0.76	0.00
1	10	6.00	0.76	2443	2.22	0.46
2	20	18.80	2.99	3952	2.56	0.91
3	30	26.90	5.55	6089	1.19	3.53
4	40	19.80	6.74	7222	0.18	14.19
5	50	16.20	6.92	7405	-0.12	16.29
6	60	12.40	6.80	7283	-0.20	14.88
7	70	10.40	6.60	7091	-0.19	12.70
8	80	8.60	6.41	6907	-0.21	10.73
9	90	6.20	6.20	6706	-0.25	8.72
10	100	3.60	5.96	6468	-0.23	6.52
11	110	2.60	5.72	6253	-0.17	4.72
12	120	2.20	5.56	6104	-0.10	3.59

6.8.2 Numerical Solution of the Kinetic-wave Equations

For streamflows, it is often possible to represent the channel geometry in a simplified manner. In this case, the discharge can be expressed as a function of the flow area:

$$Q = \alpha \cdot A^m \tag{6.87}$$

where α and m are two constants that depend on the channel geometry used (Table 6.12).

Combining the above equation with the continuity equation gives the kinematic-wave equation for the following channeled flows:

$$\frac{\partial A}{\partial t} + \alpha \cdot m \cdot A^{m-1} \cdot \frac{\partial A}{\partial x} = q \tag{6.88}$$

This equation, similar to the kinetic-wave equation obtained for sheet flow, has no analytical solution. An approximate solution can be obtained using the explicit numerical finite difference scheme if the following Courant condition is satisfied:

$$c_k \Delta t / \Delta x \leq 1 \tag{6.89}$$

where Δt and Δx are the time and space steps used for the discretization and c_k is the previously defined wave speed. In this case, the discretization equation (eq. 6.88) can be used to estimate the flow area at point (x, t) of the discretization domain as a function of the known values of the flow area and previous points defined by x and t.

$$\frac{A_{i,j} - A_{i,j-1}}{\Delta t} + \alpha \cdot \beta \cdot \left[\frac{A_{i,j-1} + A_{i-1,j-1}}{2} \right]^{\beta-1} \frac{A_{i,j-1} - A_{i-1,j-1}}{\Delta x} = \frac{q_{i,j-1} + q_{i,j}}{2} \tag{6.90}$$

and $Q_{i,j} = \alpha \cdot \beta \cdot A_{i,j}^{\beta}$ (6.91)

Table 6.12: Coefficients α and β of the expression $Q = \alpha A^{\beta}$ for different channels with simple geometries.

Geometry	α	β
Rectangular channel with width $B \gg h$	$\dfrac{1}{n} \cdot \dfrac{\sqrt{S_0}}{B^{2/3}}$	5/3
Triangular channel with run-to-rise ratio m	$\dfrac{\sqrt{S_0}}{n} \cdot \left(\dfrac{m}{4(1+m^2)} \right)^{1/3}$	4/3

CHAPTER 7

SNOW HYDROLOGY IN MOUNTAINOUS REGIONS[1]

Mountains are the water towers of the world—the source of many major rivers and a key component in their hydrological systems. Often storing huge amounts of fresh water in snow and glaciers, their importance is twofold. First, many ecosystems in the mountains or plains depend on the hydrological processes of mountainous regions. Secondly, many populations around the world depend directly on these water resources either for direct consumption, agriculture or industry. Moreover, in many mountainous regions—for instance the European Alps—the tourist trade is also highly dependent on these resources.

In coming years, given the forecasted population growth in these areas and the changing climate, the international community is facing two major challenges concerning the management of water resources in mountainous regions. The first will be to ensure fair access to all users. The other challenge will be to protect these populations against hydrological risks related to heavy precipitation and snowmelt that can occur in mountains and catastrophes related to the sudden movement of water, snow and ice on their slopes.

For a wide range of hydrological applications (e.g., flood protection, hydropower generation, studies on the impact of climate change), it is therefore essential to understand and model the main hydrological processes at work.

Different mountainous regions around the world have different hydrological behaviors, depending on local climate and geology. This chapter focuses on mountainous regions where river regimes are largely influenced by snow, as in the European Alps. Section 7.1 reviews the main differences, from a hydrological viewpoint, between drainage basins in mountains and plains. Sections 7.2 and 7.3 then present the different methods and models that can be used to represent the main hydrological processes associated with snow and glaciers respectively. Section 7.4 deals with a number of factors required for successful hydrological modeling of snow-dominated mountainous regions.

For more information on any of the aspects dealt with in this chapter, the reader can refer for example to the works of Singh and Singh (2001), Willis (2005), Jong *et al*. (2005) and Anderson and McDonnell (2005).

---

[1]This chapter was written with the collaboration of Bettina Schaefli.

7.1 INTRODUCTION

7.1.1 Hydrological Features Specific to Mountain Drainage Basins

Mountain drainage basins exhibit higher annual discharges than drainage basins at lower elevations in the same climatic region. For example, the mean annual discharge of the Rhone river into Lake Geneva in the Alps is approximately half that of the Seine river where it enters Paris, even though its drainage basin is only one-eighth the size of the Seine drainage basin. This phenomenon is explained mainly by the fact that precipitation in mountainous regions is boosted by orographic effects. In addition, evapotranspiration rates are lower given the lower temperatures at high elevations and the comparatively sparse vegetal cover in the Alps.

Hydrological conditions in mountainous regions have a pronounced annual cycle with very low discharges in winter and very high discharges (up to a 100 times greater) in spring and summer. This cycle is a result of the temporary storage of precipitation on the surface of the drainage basins during cold periods in the form of snow or ice, leading to a delay between the falling of precipitation and its release by snowmelt processes (Figure 7.1). Depending on elevation, precipitation can be stored in this way for several days for individual snowfalls, several months for seasonal snowpacks, several years for high-elevation snowpacks and decades for glaciers.

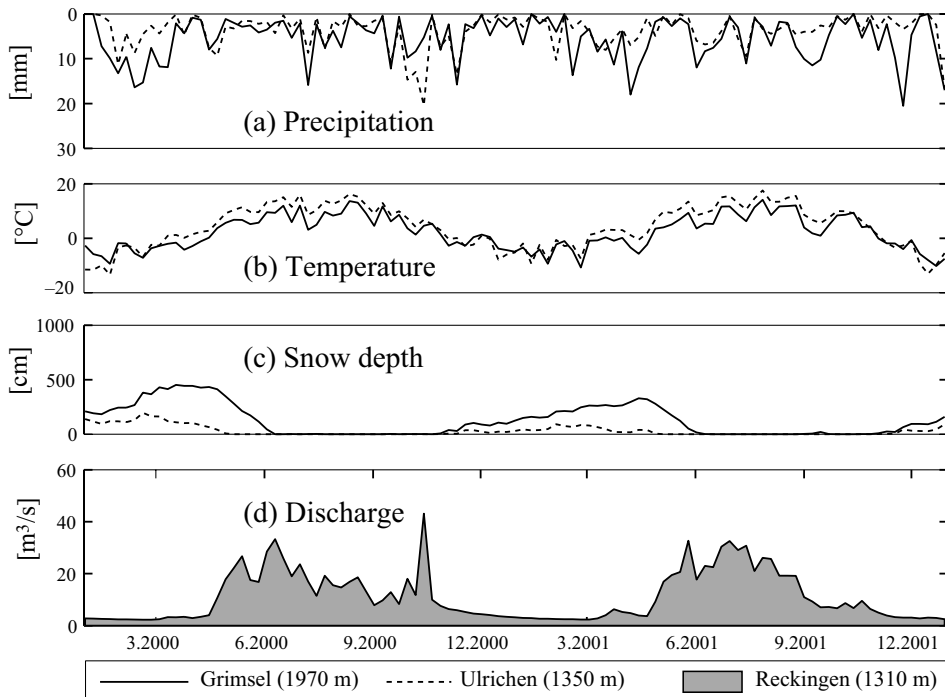**Fig. 7.1:** Hydrometeorological variables versus time (weekly time step) for the Rhone basin at Reckingen, Switzerland (years 2000–2001; basin area 233 km^2, mean elevation 2310 m, 19.6% of area covered by glaciers). a) Precipitation [mm/day] at Grimsel (1970 m) and Ulrichen (1350 m) stations. b) Temperatures [°C]. c) Snow depth [cm] at the same stations. d) Rhone river discharges at Reckingen [mm/day].

During the snowmelt period, a drainage basin with seasonal snow cover exhibits a daily discharge cycle of variable amplitude (Figure 7.2). This is the result of the diurnal temperature and radiation cycle and other factors. The cycle ends as soon as the snowpack has melted. If the snowpack remains all year round, the daily cycle can be observed throughout spring and summer.

If snow cover remains all year round, it gradually changes into firn. The possible transformation of this snow into ice leads to the formation of glaciers. Depending on the proportion of glacier cover, the effect of glaciers on discharges can been strong, both in terms of volume and seasonality. Glaciers temporarily store (over a number of years) a portion of the water falling on a drainage basin. Depending on the meteorological conditions of the considered year, the mass balance of the glacier can lead to an annual volume of runoff at the basin outlet that is significantly lower (accumulation on the glacier) or on the contrary higher (glacier melt) than the total volume of annual precipitation. In summer, streamflows from mountain drainage basins with a high proportion of glacier cover are produced largely by melt and runoff processes in glacierized zones. The magnitude of these discharges is determined mainly by the energy available for melting and is therefore generally high in summer, even if no precipitation falls over long periods.

In mountainous regions, the intensity of floods can be related to temperature and the resulting accumulation and melt processes. During a precipitation event, the elevation of the rain/snow limit can greatly increase or decrease the portion of precipitation that falls in liquid form. For example, an extreme precipitation event can lead to moderate floods if a large portion of the precipitation is stored on the slopes of the basin in the form of snow. On the other hand, the total runoff reaching the basin outlet can be greater than the amount of precipitation falling on a snowpack that is already near saturation—because the meltwater already accumulated within the snowpack is then rapidly released—or if meteorological conditions produce high volumes of meltwater.
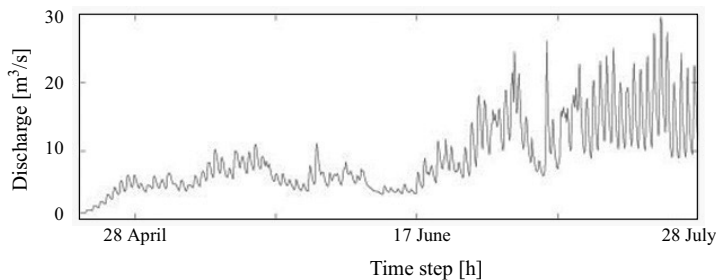
Fig. 7.2: Daily cycle of discharges observed during spring 1990 on the Lonza drainage basin at Blatten, Switzerland (area 78 km^2, mean elevation 2630 m).

7.1.2 Runoff Components and Hydrological Regimes

Streamflows observed at the outlet of a mountain drainage basin are made up of runoff from rain and from meltwater. This runoff may pass through snow, firn, glacier cover and/or the soil. Each component has its specific features in particular in terms of chemical composition, physical characteristics, residence time in the various compartments and temperature. The separation of total runoff into its various components is however difficult

to estimate. Environmental tracing studies have shown for example the predominant role of existing groundwater in snowmelt runoff events, even during spring snowmelt floods (Rodhe, 1998). This means that the flood volume cannot be directly determined from the snowmelt volume. It also depends on a number of other factors such as the initial soil moisture. Isotope tracing is however sometimes used to separate the fast and slow components of snowmelt hydrographs (Rodhe, 1998). This technique can also be used to determine the sources of glacier runoff (Sharp *et al.*, 1998).

Hydrological regimes in mountainous regions are generally classed according to the importance of the snow and glacier components. In Switzerland, mountain regimes are for example classified on the basis of dimensionless Pardé coefficients (1933) obtained by dividing the mean interannual monthly discharges by the annual discharge (Weingartner, 1986; Musy and Higy, 2011).

The glacier and snow regimes encountered in mountainous regions have the following characteristics:

- The glacier regime (Figure 7.3b) corresponds to basins that have at least 15 to 20% of their area covered by glaciers. The maximum monthly discharge occurs in summer (July and August) as a result of the melting of snow and ice. Streamflows are very low from the end of autumn to the beginning of spring. The ratio of maximum monthly to minimum monthly discharge is very high. Streamflows exhibit a pronounced daily cycle during the melt season. Year-to-year variations are relatively low for this regime and are essentially related to the interannual variation of the energy balance terms. Annual discharges tend to correlate positively with temperature and negatively with precipitation (Section 7.3.2).
- The mountain snow regime (Figure 7.3a) produces a more attenuated discharge curve than the glacier regime. The maximum monthly discharge occurs earlier (in June) and the corresponding flood rises rapidly in spring (May and June). Annual discharges tend to correlate positively with precipitation. Low flows are higher than for the glacier regime. Interannual variability is also greater, depending mainly on the variability of precipitation.
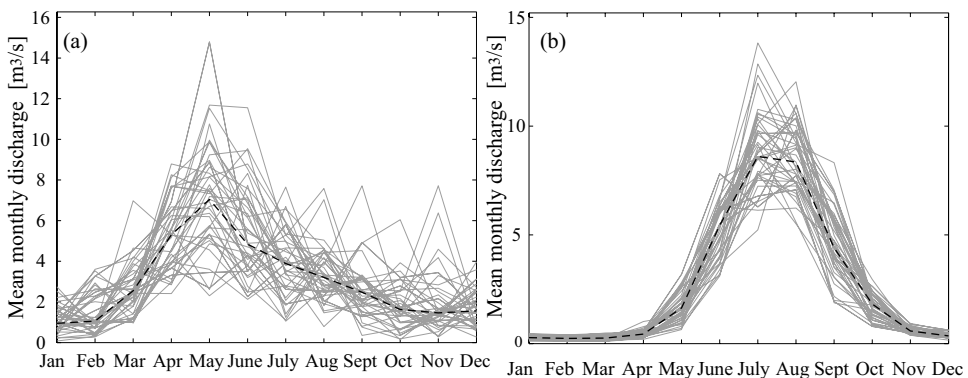
Fig. 7.3: Different types of hydrological regimes in mountainous regions (average discharges and interannual fluctuations). a) Mountain drainage basin with snow regime (Minster at Euthal, Rüti, Switzerland: median elevation 1351 m, area 59.2 km², period 1961-2000). b) Mountain drainage basin with glacier regime (Rhone at Gletsch, Switzerland: median elevation 2719 m, area 38.9 km², glacier cover 52.2%, period 1956–2000) (Horton *et al.,* 2006).

7.1.3 Objectives of Hydrological Modeling in Mountainous Regions

The modeling and prediction of hydrological processes in mountainous regions is intended to allow effective management of water resources both in the mountain areas and on the downstream plains. On the plains, meltwater from glacier-covered drainage basins is sometimes the only source of water during drought periods. The seasonality of streamflows, in particular discharges during long periods of low flows, in winter for example, often determines the water supply and/or hydroelectric potential of the considered basins. In this context, the seasonal forecasting of snowmelt (when carried out at the end of winter for summer) is very important, as well as the real-time forecasting of streamflows.

Another objective of hydrological modeling in mountainous regions is related to floods and associated hydrological risks. The estimation of low-frequency or extreme floods is indispensable for the management of hydraulic works (e.g., reservoirs, hydropower turbines, water supply facilities) and for the protection of life and property against natural risks (e.g., floods, debris flows).

Mountainous regions can also be major development zones, in particular for the tourist industry. In this context, it may be necessary to make quantitative estimates of the impacts of development projects on the water resources and associated natural risks or on the ecosystems.

Another important objective is the assessment of the possible impacts of potential climate change. Glaciers in the Alps are in general melting (e.g., Maisch, 2000; Vincent, 2002). They may be subject to significant retreat or even disappear if regional warming forecasts for the coming decades (IPCC, 2001, 2007) prove to be exact (Gerbaux, 2005; Horton *et al*., 2006). Such modifications will obviously have a direct impact on the hydrological regime of mountain watercourses, for instance in terms of streamflow volumes and seasonality, and also on human activities, natural risks and ecosystems (Appendix 7.6.1).

In this respect, understanding and predicting hydrological processes related to mountain drainage basins is a necessity both for present and future hydroclimatic contexts.

The following sections present the methods and models used to: 1) estimate meltwater runoff and 2) simulate the hydrological behavior of mountain drainage basins with or without glaciers. Approaches concerning seasonal snow cover are covered in Section 7.2 and those concerning glaciers in Section 7.3. Some of these approaches are used in the snowmelt modules of hydrological models (Chapter 3). Section 7.4 deals with a number of important factors for successful hydrological modeling of mountainous regions.

7.2 SNOW HYDROLOGY

This section presents the main factors governing the temporal and spatial evolution of the snowpack as well as the main methods and models used to estimate streamflows produced by snowmelt. For common hydrological applications, it is generally unnecessary to model the structure of the snowpack and its spatial and temporal evolution in detail. This may however be necessary for some special applications such as snowpack stability analysis for avalanche risk assessment. Detailed models have been developed for this purpose and can be used to monitor changes in the different layers of the snowpack and the transformation of the different types of crystals it is made of. Readers requiring more

information on these approaches can consult for example the review proposed by Lehning (2005) or publications describing the CROCUS model developed by the Snow Research Institute (CEN) of Météo-France (Brun *et al*., 1989, 1992) or the SNOWPACK model developed by the Swiss Federal Institute for Snow and Avalanche Research (Lehning *et al*., 1999).

7.2.1 Snowpack Properties and Dynamics

The snowpack can be characterized by a number of properties (Anderson, 1976). These include its albedo, structure, density, porosity, water equivalent, thermal conductivity and internal energy. The main characteristics among these are described in Addendum 7.1. Measurement techniques used to estimate some of them are presented in Appendix 7.6.2.

> **Addendum 7.1 Main properties of snowpacks**
>
> **Structure.** Snowpacks have characteristics similar to those of soil. Locally, they contain layers of different ages with structures that vary depending on the meteorological conditions prevailing during and between snowfalls. A snow layer is a porous medium made up of an ice matrix with interstices containing air and sometimes liquid water. The water content cannot exceed the maximum retention capacity of the snow layer, which depends on its structure. A water content of 3 to 10% is often used for hydrological applications. Ice layers are sometimes found between snow layers. They are formed during periods of successive melting and refreezing or when rain falls on a cold snowpack.
>
> **Density.** The density of fresh snow depends on the meteorological conditions prevailing when the snow falls (i.e., air temperature, cloud saturation, wind speed). Relative density values can be as low as 0.05 or as high as 0.30. Relative snow densities generally range between 0.07 and 0.15. Snow density is lower for snowfalls under cold conditions with little wind. An average value of 0.10 is often used for modeling.
>
> Fresh snow is subsequently compacted by its own weight (mechanical effect) and by the metamorphosis of snow crystals (grain rearrangement and shape changes). Certain external factors such as wind also favor densification. The density of snow cover generally varies from one snow layer to another. The average relative density is between 0.07 and 0.35 for seasonal snowpacks. In avalanche deposits, densities can reach values of 0.70. The relative density varies between 0.40 and 0.85 for firn and between 0.84 and 0.92 for ice.
>
> **Water equivalent.** The snow water equivalent (SWE), expressed in millimeters (mm w.e.), corresponds to the depth of water that would be obtained by melting the considered snow column. The snow water equivalent can be calculated from the thickness of the snow layer and its average density.
>
> **Albedo.** The albedo of the snow surface defines the proportion of solar radiation that is reflected. It therefore greatly affects the energy balance of the snow cover. The albedo depends on the wavelength of the radiation. It is between 0.7 and 0.95 for the ultraviolet and visible ranges, between 0.3 and 0.5 for the near infrared range and 0 for the infrared range. Snowpack warming is therefore mainly due to infrared radiation (Sergent *et al*., 1993). The radiation received at the Earth's surface is a function of elevation. Given that the thickness of the atmosphere decreases with elevation, so does infrared radiation. On the other hand, radiation in the visible range increases with elevation. This different elevation dependence results from the fact that the source of radiation is different depending on the considered wavelength. For example, radiation in the visible range comes from direct solar radiation

and radiation backscattered by the atmosphere, while infrared radiation comes from visible-range radiation absorbed and remitted by the atmosphere and by water vapor in particular (Chapter 2).

The albedo in the visible range varies greatly depending on the age, water content and thickness of the snowpack (Table 7.1). The albedo can drop 20 to 30% as snow ages. An equivalent decrease can also come from atmospheric pollution and the resulting deposits on the snow.

Table 7.1: Characteristic albedo values in the visible range (adapted from Maidment, 1993b).

Type of snow	Albedo [-]
Fresh snow	0.80–0.90
Old snow	0.60–0.80
Melting snow	0.40–0.60
Firn	0.43–0.69
Clean glacier	0.30–0.55
Dirty glacier	0.15–0.25
Debris-covered glacier	0.10–0.15

Snowpack internal energy and cold content. The internal energy of the snowpack depends on its temperature and the respective proportions of water in the form of vapor, liquid and solid. The internal energy E_s [J/m^2] can be expressed as:

$$E_n = \int_{h=0}^{h_n} \left(c_l\, \gamma_l\,(h)\, T(h) + c_s\, \gamma_s\,(h)\, T(h) \right) dh \tag{7.1}$$

where $\gamma_l(h)$ and $\gamma_s(h)$ [kg/m^3] are the specific weights of the liquid and solid phases respectively at depth h within the snowpack, c_l and c_s their respective specific heats [J/(kg°C)] and $T(h)$ [°C] the local temperature at depth h [m].

The internal energy required to raise the temperature of the snowpack to 0°C is sometimes referred to as the "cold content" of the snowpack.

Thermal conductivity.

Fresh snow is an excellent insulator (Table 7.2). The metamorphism of snow can increase its thermal conductivity by a factor of 10.

Table 7.2: Approximate thermal conductivities at 0°C (adapted from Hock, 2005).

Type of snow	Thermal conductivity [Wm^{-1}K^{-1}]
Fresh snow	0.08
Old snow	0.42
Water	0.55
Ice	2.1

Snowpack properties vary with time under the combined action of different processes directly related to local meteorological conditions (e.g., precipitation, temperature, radiation, wind, air humidity). These conditions can vary greatly with time. They are also highly dependent on elevation, orientation, slope and soil cover, in particular vegetation. Consequently, snowpack properties also vary greatly in space.

Temporal variability of the snowpack

The temporal variability of the different properties of snow cover depends on various processes related to snow accumulation, spatial redistribution (e.g., wind, avalanches), transformation (i.e., metamorphosis) and ablation (i.e., melting, evaporation and sublimation).

Accumulation corresponds to the gradual storage of solid precipitation at the surface of the drainage basin. At the end of the 20th century in the Swiss Alps, approximately 50% of precipitation at an elevation of 2000 m and 90% at 3000 m fell as snow. The state of aggregation or the form (liquid or solid) of precipitation reaching the ground depends mainly on the altitude of the 0°C isotherm. It rains if this freezing level in the atmosphere is sufficiently high above the ground to allow complete melting of the crystals formed in this medium. Outside the tropics, the majority of rain results from the melting of snow or ice crystals formed in the atmosphere (Dingman, 2002).

If the snow crystals that form in the atmosphere fall, they pass through increasingly warm air layers and start to sublimate (before melting). This process consumes energy and reduces the temperature at the surface of the crystals, which delays the melting process. Consequently, snow crystals continue to exist at temperatures above 0°C. The lower the humidity of the air, the lower the crystals can fall below the 0°C isotherm.

The elevation of the rain/snow limit is the elevation—or elevation band—where precipitation reaches the ground in the form of rain instead of snow. It is related to the 0°C isotherm altitude and to a lesser extent the temperature of the air mass above this isotherm. On the average, it is located approximately 300 m below the 0°C isotherm. For particular events and for short durations, it can however be located as far as 600 m below the freezing level.

As soon as snow is deposited on the surface, metamorphism processes begin, driven by the force of gravity (i.e., the weight of the snow) and energy exchanges. Energy exchanges are partly the result of the movement of meltwater and air within the snow cover due to local vapor pressure differences as well as vaporization and sublimation phenomena and solid or liquid condensation. The structure of the crystals is modified and consequently the snow crystals are redistributed. The result is a change in the density of the snow cover. For certain meteorological conditions, for example the first humidification or for fresh snow, this can take place very rapidly. The density of a snow layer can therefore for example increase greatly over a single day.

The existence of snow sublimation and melting processes depends on the energy state of the surface layer of the snowpack. The state in turn depends on energy exchanges between the snowpack and its neighboring environment. These energy exchanges take place mainly at the ground-snowpack and atmosphere-snowpack interfaces. Snowmelt takes place mainly at the surface (Section 7.2.3).

Snow crystals at the surface or bottom of the snowpack start to melt if the local temperature reaches 0°C and if the energy balance is locally positive. Ablation of the snow cover by melting processes generally largely exceeds ablation by sublimation. Snow sublimation requires between 2826 and 2847 kJ/kg of energy while melting requires only 335 kJ/kg. Snow suspended in the air can however be subject to major sublimation losses, especially in the presence of warm winds such as those related to foehn phenomena (Lehning, 2005).

The interception of snow by bushes and/or trees, as opposed to the interception of rain, often represents more a delay than a loss of precipitation reaching the ground. Estimation of this phenomenon is more difficult than for rain (Hedstrom and Pomeroy, 1998). The percentage of intercepted snow lost by sublimation is often considered to be low because most intercepted snow is returned to the ground either in solid form by gravity or liquid form (by melting or by the washing effect of rain). In coniferous forests, however, sublimation of intercepted snow can represent a major loss. For Canadian pine and spruce forests, Pomeroy *et al*. (1998a) observed sublimation losses amounting to as much as 30% of snowfalls.

Spatial variability of the snowpack

The high spatial variability of snow cover is the result of many factors affecting accumulation, redistribution by wind and ablation. The spatial variability of accumulation is particularly important in mountainous regions were precipitation depths and the form of precipitation (solid or liquid) depend highly on elevation.

The main cause of spatial redistribution of snow is wind, during or after snowfall events (Castelle, 1994). This redistribution takes place in particular in highly exposed mountainous regions or in forested zones where the vegetation disturbs the wind fields. Considerable quantities of snow can be moved by the wind. At high elevations, snow depths on mountain slopes exposed to the wind can be very low throughout the winter. On the other hand, the deep snow deposits on the opposite slopes can persist for long periods during the melt season.

Snow redistribution by avalanches can also influence the local spatial variability of snow cover. In the Alps, avalanches redistribute only very small quantities of snow.

Ablation processes can also cause significant spatial variability of the snow cover. This variability is related to the spatial variability of vegetal cover and the high spatial variability of incoming energy fluxes for different slope orientations and elevations. At a given time, it is possible to determine the basin melting limit, i.e., the geographic boundary separating the parts of the basin where snowmelt can occur from those where it cannot occur. By default, this limit is often considered to be the 0°C isotherm. During the snowmelt period, the snow cover ablation rate varies depending on the part of the basin considered. Some parts rapidly become snow free while in other parts, snow cover can persist late into the snowmelt season. For a given basin, snow cover therefore often presents a characteristic spatial distribution referred to as the snow pattern (Davison and Pietroniro, 2005).

If both the temporal evolution of the spatial extent and the water equivalent of the snowpack have been observed over a given period, snow depletion curves can be plotted. These curves relate the extent of snow cover (as a percentage of the area of the considered hydrological unit) to its water equivalent (as a percentage of the maximum water equivalent reached during accumulation). If the extent of snow cover can be obtained for a given date —for instance using remote imagery—such curves can be used to estimate the volume of water available on the drainage basin and/or to calibrate (or validate) snow accumulation and snowmelt models (Andreadis and Lettenmaier, 2006).

Balance equations

The volumes of water stored in solid and/or liquid form within the snowpack are the main variables used by hydrologists to characterize snow cover. Variations of the water

volumes stored in the snowpack at a given point in the drainage basin are governed by the mass balance equation:

$$\frac{dS_t(t)}{dt} = In(t) - Out(t) \tag{7.2}$$

where dS_t/dt represents instantaneous variations of storage $S_t(t)$ and $In(t)$ and $Out(t)$ are respectively the inflows and outflows. In practice, the various terms of this equation are expressed in millimeters of water equivalent [mm w.e.]. These terms, fully or partially related to the processes mentioned above, depend on whether the considered variable $S_t(t)$ refers to water present in solid and liquid form, in the form of snow only or in the form of liquid only. In the first case, the balance Equation (eq. 7.2) can be expressed as follows:

$$\frac{dW(t)}{dt} = P(t) - I(t) - E(t) - U(t) + \Omega(t) \tag{7.3}$$

where *dW(t)/dt* is the rate of change of the quantity of water stored in the snowpack in liquid and solid form, $P(t)$ total precipitation (solid + liquid) at time t, $I(t)$ interception of part of the total precipitation by vegetation, $E(t)$ losses or gains by evaporation and/or sublimation, $U(t)$ the intensity of meltwater losses at the base of the snowpack by infiltration and/or runoff (Section 7.2.2) and $\Omega(t)$ other possible inputs or losses (e.g., wind, avalanches).

If only water in the form of snow is considered within the snowpack, balance equation 7.2 becomes:

$$\frac{dH_s(t)}{dt} = S(t) - I_s(t) - M(t) - E_s(t) - \Gamma_s(t) + \Omega(t) \tag{7.4}$$

where *dH_s(t)/dt* is the rate of change of snow storage in the snowpack, $S(t)$ snowfall at time t, $I_s(t)$ interception of part of the precipitation falling as snow, $E_s(t)$ sublimation of part of the snow on the ground and *M(t)* the snowmelt flux, some of which remains trapped in the snowpack in liquid form. The term $\Gamma_s(t)$ represents all the processes transforming snow into firn and ice and the term $\Omega(t)$ represents any other possible inputs or losses (e.g., wind, avalanches).

In these equations, the terms corresponding to phase changes in the water stored within the snowpack in liquid or solid form are determined by the snowpack energy balance. The equation of the corresponding balance, detailed in Section 7.2.3, includes other snowpack state variables (e.g., internal energy).

7.2.2 Snowmelt Runoff: Processes and Explanatory Factors

Melting, percolation and infiltration

Meltwater produced at the surface of the snow cover percolates into the snowpack. It continues along its path as the local water retention capacity is reached, i.e., as the snowpack ripens.

In winter and early spring, most of the snow melting at the surface is stored in the snowpack. When the snowpack becomes saturated, any surplus meltwater produces runoff. Saturation of the snow cover can be increased during the snowmelt period by percolation of rain falling on the snow. If the temperature drops below 0°C within the snowpack, any water trapped by capillary retention will refreeze.

Under certain conditions, part of the meltwater flowing in the snowpack and/or on the ground surface under the force of gravity can infiltrate into the underlying soil. If the ground is not frozen, the fraction that infiltrates depends on the same factors as for rain falling on the soil (Chapter 4). If the ground is frozen, different situations must be considered.

- If the frozen ground is not saturated, the water infiltrates and inputs energy. Depending on the local energy balance, either the ground thaws—and the infiltration capacity gradually increases—or the infiltrating water freezes. In the latter case, the temperature of the soil increases and the soil becomes blocked by refreezing, reducing its infiltration capacity.
- If the frozen ground is saturated or if an impervious layer of ice is present on the soil surface, then runoff occurs at the soil-snow interface. In this case, there is no flow in the soil. As previously, the local energy balance can lead to thawing of part of the ice contained in the soil or at its surface.

Snow is an excellent thermal insulator. Consequently, the temperature at the soil-snow interface remains relatively constant throughout the accumulation season as soon as a closed and sufficiently thick snowpack has formed. This means in particular that the temperature at the soil-style interface will remain slightly above 0°C if the first snowfalls occur before the ground has frozen. On the other hand, if the ground is already frozen before the first snowfalls, it will remain frozen until it receives sufficient energy inputs to melt.

Meltwater runoff at the basin outlet

At the outlet of most mountain drainage basins, streamflows are the result of meltwater runoff and therefore exhibit strong seasonality. In the northern hemisphere, the time when a snowmelt flood occurs as well as its rate of rise and amplitude depend on the volume and spatial distribution of the snow cover and the temporal evolution of energy inputs to the basin.

If not limited by the amount of snow available for melting, snowmelt increases with energy input. Any increase in energy input leads to locally increased snowmelt volumes and, depending on the degree of snowpack saturation, increased snowmelt runoff. Furthermore, a higher energy input generally corresponds to an increase in the snowmelt elevation and thus an increase of the area that can potentially contribute to snowmelt.

For equal temperatures and energy inputs, snowmelt decreases with the amount of snow available for melting, i.e., with the area actually contributing to snowmelt. The time at which snow cover disappears varies throughout the basin. In particular, snow cover disappears later at high elevations (Figure 7.4).

The shape and intensity of a snowmelt flood therefore largely depends on the hypsometry of the drainage basin. For a drainage basin covering a large range of elevations, snowmelt is observed over a long period. Peak discharges are obtained roughly when the contributing area is maximum. For drainage basins covering a very low range of elevations, snowmelt takes place over a limited time interval.

Streamflows of course include glacier melt and rainfall components in addition to snowmelt. During the snowmelt season, the storage capacity of the basin gradually decreases with decreasing retention capacity of the snowpack and increasing saturation of the soil. Rainfall events can produce high peak discharges.
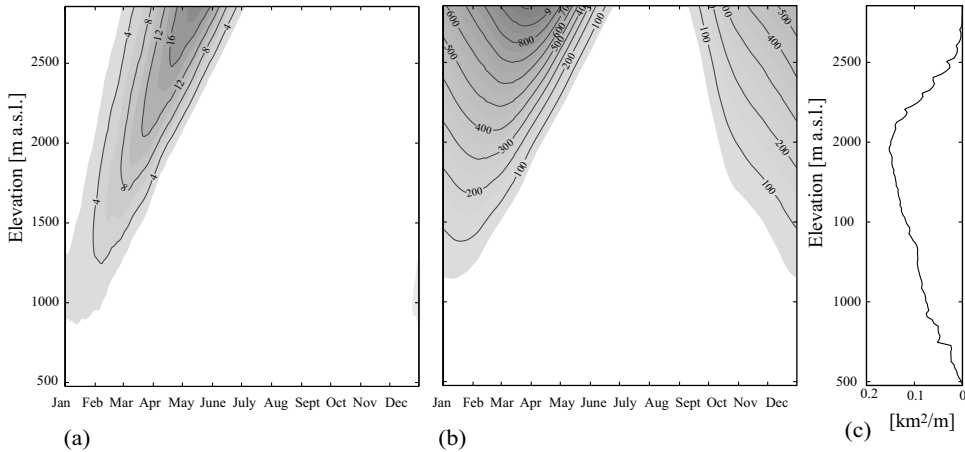
Fig. 7.4: Distribution of: a) mean interannual snowmelt runoff [mm/day] and b) mean interannual snowpack [mm w.e.] with elevation and time of year and c) distribution of basin area with elevation. The concerned basin is that of the Minster at Euthal, Rüti (Switzerland). Distributions (a) and (b) were simulated for the period 1981–2005 using the GSM-SOCONT hydrological model (Schaefli *et al.*, 2005).

7.2.3 Estimating and Modeling Snowmelt Runoff

Principle

Estimation of snowmelt runoff first requires estimation of the depth of the snowpack available for melting at every point in the basin and its level of maturity or ripeness. These estimates can be based on various measurements (Appendix 7.6.2), however the latter are rarely available or are often hard to use, mainly due to spatialization problems. These estimates can also be obtained by simulation, using an appropriate hydrological model. This type of simulation is described in Section 7.4.3.

Snowmelt runoff is subsequently estimated in two steps: 1) estimation of snowmelt at every point in the basin and 2) simulation of the transformation of snowmelt into runoff at the basin outlet.

Snowmelt can be estimated by two different approaches, i.e., either by quantifying the different energy exchanges that take place at the soil-snow and snow-atmosphere interfaces or by identifying empirical relationships between snowmelt and certain meteorological quantities or indices. The first approach requires physically-based models while the second approach uses mainly empirical models. Both approaches are presented below. Their expressions assume that the size of the snowpack is not a limiting factor. This can be easily modified if it is not the case as long as estimates of the snowpack are available.

The snowmelt volumes estimated using either of these approaches do not necessarily produce snowmelt runoff. For this, the snowpack must be ripe (Section 7.2.2). In various hydrological models, meltwater is in fact retained in the snowpack until the liquid water content exceeds the assumed retention capacity of the snowpack (Section 7.4.3). When this occurs, the surplus of liquid water produces the volumes available for the production of snowmelt runoff. The approaches used to simulate the transformation of the corresponding volumes into runoff are dealt with at the end of this section.

Estimating snowmelt using the energy balance

Energy exchanges take place mainly at the interface between the atmosphere and the snowpack. Other less important energy exchanges take place at the interface between the soil and the snowpack. They involve conduction and are therefore dependent on the temperature gradient at this interface. The principles of these exchanges and the methods that can be used to estimate them are described in detail in many specialized publications (Obled and Rossé, 1977; Boone and Etchevers, 2001).

At the snow-atmosphere interface, energy exchanges take place in a very thin surface layer that has very little mass and therefore very little thermal inertia (Obled and Rossé, 1977). Solar radiation can penetrate into the snowpack but is attenuated exponentially over a depth of a few centimeters, especially if the snow is old and dirty. The energy balance of the surface layer can be expressed in Joules per unit area and per unit time as:

$$R_n(T_s) + H_h(T_s) + H_{ph}(T_s) + H_p = \begin{cases} H_{cond}(T_s) & if\ T_s < 0°C \\ H_f & if\ T_s = 0°C \end{cases} \tag{7.5}$$

where T_s [°C] is the snow surface temperature, R_n [J/m²] the net solar radiation (longwave and shortwave), H_h [J/m²] the sensible heat flux due to convection between the snowpack and air (or water flowing on the surface of the snowpack), H_{ph} [J/m²] the quantity of heat associated with phase changes at the surface of the snowpack (condensation, melting, sublimation) and H_p [J/m²] the heat input by precipitation.

The temperature T_s at the snow surface is the explanatory variable for these exchanges. It directly influences certain terms of the balance, in particular: 1) infrared radiation re-emitted by the snow, 2) sensible heat exchanges that depend on the temperature difference between the air and the snow surface, 3) exchanges by conduction that depend on the temperature gradient between the surface and the inside of snowpack and 4) latent heat exchanges that depend on the difference between the water vapor pressure in the air and on the snow surface.

The surface temperature of the snowpack changes, sometimes within a few minutes, in such a way that the exchanges tend toward an equilibrium. If the energy balance is positive, the snow surface temperature increases until it reaches the critical melting temperature (0°C). Once the melting temperature has been reached, any excess input energy H_f [J/m²] is consumed by a change in phase (fusion), producing snowmelt. The amount of snowmelt M_s [m w.e.] can be expressed as:

$$M_s = \frac{H_f}{\gamma_l \cdot L_i} \tag{7.6}$$

where γ_l [kg/m³] is the specific weight of water and L_i [J/kg] the latent heat of fusion of ice. It is also possible to take into account the thermal quality of the snowpack χ (Appendix 7.6.3).

On the other hand, if the snow surface temperature is or becomes negative, the available energy H_{cd} [J/m²] is transmitted by conduction from the surface towards the rest of the snowpack. H_{cd} can be positive or negative depending on the temperature gradient between the surface and the rest of the snowpack. This changes the thermal profile of the snowpack and its internal energy $\Delta E_s = H_{cd}$ (Garen and Marks, 2005).

If a snowpack containing liquid water by capillary retention cools at the surface (i.e., the H_{cd} is negative), then some or all of this liquid water will first refreeze before the snowpack temperature decreases. The amount of liquid water M_r [m w.e.] that can be refrozen is:

$$M_r = -\frac{H_f}{\gamma_l \cdot L_i} \tag{7.7}$$

The terms of the energy balance can be quantified on the basis of different meteorological variables using empirical or physically-based equations, some of which are presented in Appendix 7.6.3. The relative importance of the different terms varies in time and in space, in particular according to meteorological conditions (Figure 7.5).
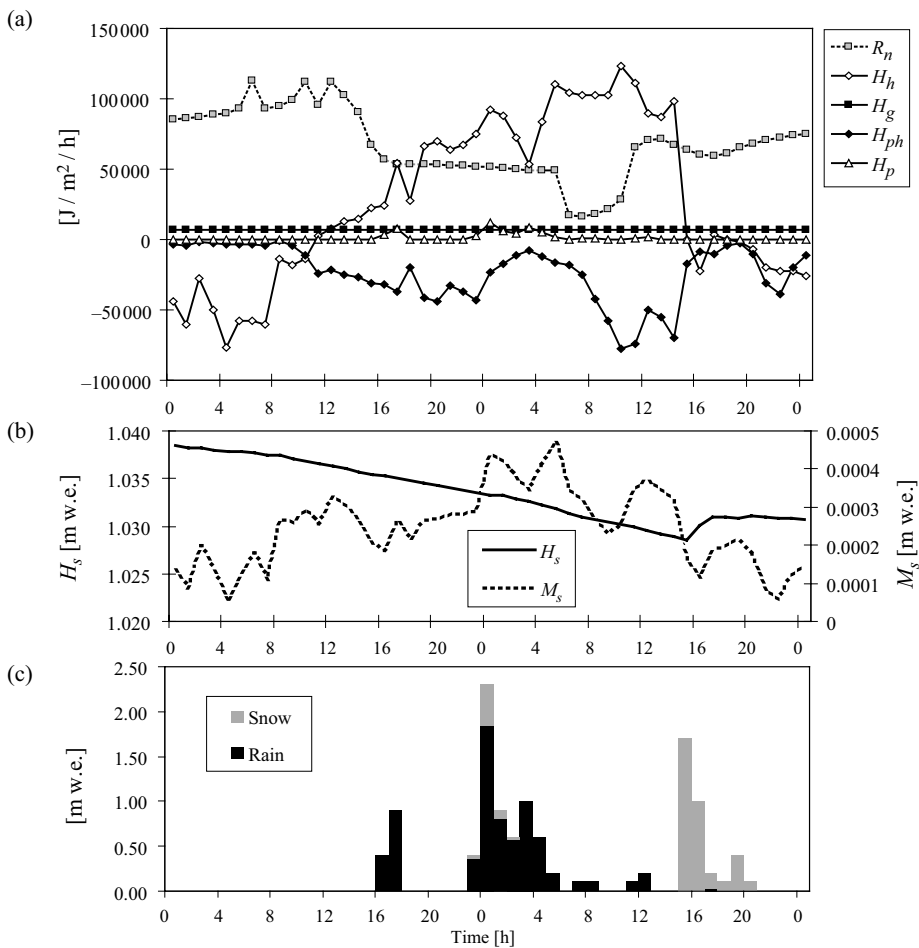

Fig. 7.5: a) Example of the variations of the different terms of the snowpack energy balance and of the resulting snowmelt with time (surface temperature T_s=0°C) (see Appendix 7.6.3 for details on the notation). b) Corresponding snowmelt M_s and variation of the snowpack depth H_s. c) Precipitation in the form of rain or snow.

Energy exchanges by conduction at the base of the snowpack can lead to melting at the soil-snow interface. In the Alps, this melting is mainly observed at the beginning of the season if snow falls on warm ground. In winter, however, there is generally no melting at the base of the snowpack. The heat flux re-emitted from the ground is in the order of 2 W/m² at an elevation of around 1500 m and is practically zero at 3000 m. When heat flux is non-zero, it is used to maintain the temperature at the base of the snowpack at 0°C.

Given the above considerations, the key variable required to estimate snowmelt is T_s, the temperature of the snow surface. One difficulty in this approach lies in solving equation 7.4 and particularly in estimating T_s, which determines most of the energy balance terms. Given that equation 7.4 is implicit with respect to T_s, it can only be solved by an iterative approach, which is possible numerically. Another difficulty lies in the estimation of the vertical temperature profile and its temporal evolution. A commonly used simplification consists in assuming a uniform temperature throughout the snowpack. Another possibility is to use a two-layer or multi-layer discretization of the snowpack (Brun *et al.*, 1992; Boone and Etchevers, 2001; Garen and Marks, 2005).

To estimate the different terms of the energy balance, measurements or estimates of the various meteorological variables such as solar radiation, wind, relative humidity and air temperature are required. These variables are however hard to measure and spatialize (Section 7.4.2).

Estimating snowmelt using empirical methods

Empirical approaches such as the degree-day method estimate snowmelt as a function of air temperature or, more precisely, as a function of the number of degrees above a certain temperature threshold for one day (i.e., the number of degree-days).

In its basic version, the snowmelt equation of the degree-day method can be written:

$$M_s(t) = \begin{cases} a_s(T_a(t) - T_0) & \text{if } T_0 > 0°C \\ 0 & \text{if not} \end{cases} \tag{7.8}$$

where $M_s(t)$ [mm w.e./day] is snowmelt over time step t (generally one day), $T_a(t)$ [°C] is the mean air temperature over time step t at the considered elevation (observed or estimated temperature), T_0 [°C] is the melting base temperature and a_s [mm/°C/day] the degree-day or melt-rate factor. The two parameters T_0 and a_s must be calibrated. The degree-day factor a_s is often chosen to represent the average behavior of the considered hydrological unit (e.g., basin, elevation band). Table 7.3 presents the range of values commonly used for the degree-day factor. The higher values obtained for ice are the result of lower albedo and higher roughness. The base temperature T_0 is often 0°C. It may be necessary to adjust this temperature if the measured or estimated temperature is not representative of the average temperature over the considered hydrological unit.

Table 7.3: Typical values of the degree-day factor (adapted from Hock, 2003).

Type of snow	a_s [mm/°C/day]
Snow	2.0–6.0
Ice	5.0–8.0

The degree-day factor a_s generally varies in space. For example, it is higher on a south-facing slope than on north-facing slope and higher on open ground than in a forested area.

It also depends on meteorological conditions that determine the dominant melting processes and consequently the snowmelt rate. On open ground and under clear-weather conditions, a_s depends highly on the snow albedo given that melting is in this case mainly due to solar radiation. The degree-day factor therefore varies significantly with time, first as a function of snow albedo and "aging", and also as a function of the angle of incidence of the sun and the type of weather (e.g., sunny, cloudy or rainy). For heavily forested areas, a_s varies less because the heat exchanges that determine the temperature (and therefore infrared radiation) under the trees take place mainly with the canopy.

One way of taking into account the spatial and temporal variations of the degree-day factor is to integrate meteorological variables other than temperature, if available, in the basic equation. Such variables could for example include wind or radiation. The basic equation must be adapted according to the context. One example is the equation incorporating radiation data, proposed by Kustas and Rango (1994):

$$M_s(t) = \frac{R_n(t)}{\rho_l L_i} + a_r(T_a(t) - T_0)\tag{7.9}$$

where a_r [mm/°C/day] is a restricted degree-day factor, ρ_l the specific weight of water and at 0°C, L_i the latent heat of fusion of ice and $R_n(t)$ the net radiation. Given that net radiation is a function of albedo (Chapter 2, Appendix 2.7.4), this relationship can also take into account the change of albedo over the snowmelt season.

A large number of case studies have shown that these simple empirical approaches give results that are comparable to more complex methods (WMO, 1986, Ohmura, 2001). This is mainly true when the melt processes are dominated by a particular process and occur under one weather type. For example, in semi-arid mountains—such as those in California, the Mediterranean, Central Asia, etc.—the heat input by solar radiation is well represented by the air temperature. On the other hand, when melting occurs under different types of weather (e.g., sunny, cloudy and rainy), the performance of this method is lower. This is because the air temperature should then be represented by different quantities depending on the prevailing weather type, i.e., solar radiation for sunny weather and infrared radiation and sensible heat exchanges for cloudy weather. Depending on the case, for the same positive degree-day value, the degree-day factor can vary by 30% or even 50% (Obled and Rossé, 1975).

Moreover, this method works well when the snow cover is "ripe" for melting and the temperature is around 0°C, even at night. However, when the temperature of the snow cover is well below freezing, this method gives relatively poor results. For this reason, it is important to represent, even in a very rough manner, the refreezing of some or all of the meltwater produced at the surface of the snowpack. Certain concepts such as those presented in Addendum 7.2 are sometimes proposed to improve the degree-day method. Furthermore, given that the temperature varies greatly with altitude, the method must not be applied to units of area covering too large an elevation band. For this reason, mountain basins require an appropriate discretization on the basis of elevation before applying the degree-day method to each of the discretization units (Section 7.4).

Addendum 7.2 Possible adaptations for the degree-day method

The following adaptations are sometimes proposed to improve the performance of the classical degree-day method (adapted from Singh and Singh, 2001).

- Estimation of snowmelt using: 1) a more general expression involving simplified versions of the main terms of the snowpack energy balance or 2) the basic expression but with different values for the parameter a_s depending on the meteorological situation observed on the considered basin.
- Separate management during the day (melting indexed by T_{max}) and during the night (refreezing indexed by T_{min}), with different coefficients for melting (positive degree-days) and cold accumulation (negative degree-days). Note that the cold content of the snowpack must first be overcome before melt can be produced.
- Refreezing of some of the liquid water contained in the snowpack when the degree-days of the considered day are negative.
- Use of a snowpack temperature index (or cold content variable) and a conceptual model to monitor its temporal evolution to estimate when snowmelt can occur. The following expression is often used for this:

$$T_s(t) = \beta \cdot T_s(t - \Delta t) + (1 - \beta) \cdot T_e(t) \tag{7.10}$$

where $T_e(t)$ is an "equivalent temperature" flux supplying the thermal reservoir of the snowpack and $\beta = \exp(-\Delta t / K_s)$ where K_s [h] is the responsiveness of the snowpack (in principle varying with time). The equivalent temperature flux $T_e(t)$ is sometimes assumed to be equal to the air temperature $T_a(t)$.

Meltwater modeling

The transfer of meltwater to the basin outlet involves different types of flows, i.e., within the snowpack and/or soil if not frozen and on the ground surface if the snow cover has disappeared.

Transfer of meltwater within the snowpack, in particular percolation, can be simulated using physically-based models. The factors that govern this transfer are however complex and models must include a number of major simplifications. One possible simplification consists in considering the snowpack as a homogeneous porous medium. Meltwater flow is then modeled as a Darcy flux in the same way as the flow of water in soil (Colbeck, 1978). Various other approaches are possible. Readers requiring more information on this topic can consult the review by Marsh (2005). Other than their complexity, the main limitation of physically-based models is related to the difficulty of estimating their parameters. Such models generally depend on various hydrodynamic properties of the snowpack, often unknown and always highly variable in space and time.

In operational hydrology, physically-based approaches are hardly ever used. The flow of meltwater within the snowpack is in fact generally not actually modeled. Only the retention of meltwater within the snowpack is dealt with (Section 7.4.3). Meltwater that flows, after retention, to the bottom of the snowpack is subsequently transferred as runoff to the basin outlet. It is therefore necessary to first estimate how it is distributed at the soil-snowpack interface.

If the ground is not frozen, this distribution process is usually modeled in the same way as for rainfall excess, described in Chapter 4. These models estimate the fraction of the fluxes that infiltrates and the fraction that produces surface runoff. The transfer of these fluxes to the basin outlet is then modeled. Once again, this is done using models

similar to those used for the transformation of excess rainfall into runoff at the basin outlet (Chapter 5). The models most often used are conceptual reservoir models. An example of a conceptual model of this type is presented in Appendix 7.6.4.

If the ground is frozen, the modeling of meltwater excess and its transfer to the basin outlet as runoff must in principle be adapted to the different situations that can be encountered (i.e., saturated and unsaturated frozen ground, see Section 7.2.2). In these situations, modeling should take into account energy exchanges at the soil-snowpack interface. In particular, this requires monitoring of the temporal and spatial evolution of the thermal profile in the ground. This is highly complex. Consequently, for common hydrological applications, most hydrological models take the state of the soil into account in a simplified manner or neglect it altogether (Zhao and Gray, 1999; Luo *et al.*, 2003).

7.3 GLACIER HYDROLOGY

Different types of glaciers exist and have varied and complex behaviors. This section summarizes the main aspects required to understand the workings of glaciers in temperate mountainous regions and the hydrological approaches that can be used to estimate runoff from glacier melt. Modeling methods to simulate the dynamic behavior of glaciers will not be dealt with here. Readers requiring more information on this topic can refer to specialized works (Lliboutry, 1964, 1965; Paterson, 1994; Fountain and Walder, 1998; Schneider, 2000).

7.3.1 Glacier Properties and Dynamics

A glacier is a large reservoir that stores water in solid and sometimes liquid form. Within a glacier, storage involves three main timescales. Medium- and long-term storage involves ice and/or firn. Long-term storage can cover periods of several years up to several centuries.[2] It affects the long-term balance of the glacier. Medium-term storage is mainly seasonal. It determines the hydrological regime of runoff from the glacier and the downstream basins. For shorter periods of time, storage concerns water present in the glacier in liquid form. It is associated with daily variations of melt and refreezing processes and with the flow of rainfall or meltwater through the snow, firn and ice via the corresponding drainage networks. It influences the daily fluctuations of glacier runoff (Jansson *et al.*, 2003).

A glacier is made up of an accumulation zone, where a permanent snowpack is formed, and an ablation zone characterized by a seasonal snowpack that disappears during the melt period (Figure 7.6). The different sources of accumulation include precipitation in the form of snow, frost or rime, along with snow that is redistributed by avalanches or wind. The term glacier ablation refers to the processes that decrease the ice mass, in particular melting and calving (i.e., blocks of ice that break off from a glacier front and fall into a water body).

In the accumulation zone, fresh snow is transformed into firn by metamorphosis mechanisms (Section 7.2.1). The firn layer of the current year is superimposed on older firn layers that become denser and transform into ice.

---

[2]In large glacier systems forming ice sheets (high-latitude continental glaciers) or in polar ice caps, water can be stored for 100,000 to 500,000 years or more.
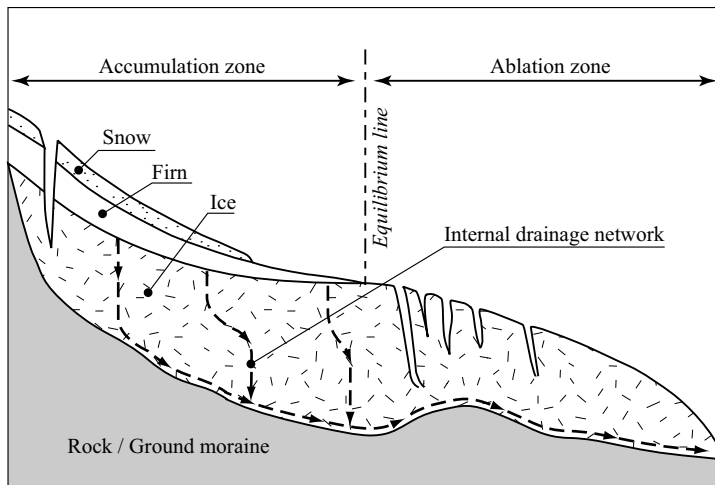
Fig. 7.6: Cross-section of the accumulation and ablation zones of a mountain glacier.

The ratio between the area of the accumulation zone and the total area of the glacier at the end of each melt season is referred to as the Accumulation Area Ratio (AAR). The mean elevation separating the ablation zone from the accumulation zone is called the Equilibrium Line Altitude (ELA). These two characteristics are frequently used in glaciology, for example to determine the mass balance of the glacier.

A glacier is generally a dynamic system. Under the force of gravity, many glaciers move continuously. The ice flows and slides along the bottom. During this movement, that results in an exchange of mass between the accumulation and ablation zones, rocky materials are transported and deposited by the glacier, forming lateral, terminal and ground moraines.

7.3.2 Glacier Runoff and Mass Balance

Glacier melt and drainage

The major variations of meteorological conditions over a 24-hour period produce a pronounced daily cycle of glacier meltwater runoff. Depending on the time within the melt season, glacier runoff is made up of water coming from the seasonal snowpack, firn or ice. The meltwater flows along pathways of varying length, through the different layers of the glacier before reaching the basin outlet. Runoff is therefore delayed with respect to melting.

Each type of snow and ice has its own melting characteristics. Fresh snow has the highest albedo and therefore absorbs less energy than firn or ice. Consequently, with equal energy inputs, glacier meltwater runoff observed after a snowfall is lower than the runoff observed before. For this reason, annual runoff tends to correlate negatively with precipitation, i.e., the amount of melting decreases with increasing amounts of snow due to the higher albedo of snow.

The albedo of the surface of the glacier can exhibit high spatial variability. This is due to the spatial variability of the state of metamorphosis of the snow and of the amount of

debris that may be concentrated locally for example on the sides of the glacier (rock debris). Given that snow is an excellent thermal insulator and that solar radiation is attenuated exponentially with depth, melting takes place generally only in the surface layer (i.e., the firn does not melt when covered by snow and no ice melts until the firn has disappeared).

At the beginning of the melt season, meltwater comes mainly from the bottom of the glacier and the resulting flows are relatively slow. Throughout the ablation period, the drainage system of the glacier develops to form an often complex system of conduits. Meltwater coming from the entire glacier enters these conduits via openings on the surface of the glacier (e.g., crevices, moulins) and flows very rapidly (Hubbard and Nienow, 1997; Hannah and Gurnell, 2001).

All these factors lead to high variability of the daily runoff cycle throughout the melt season at the outlet of a glacierized basin (Figure 7.2).

Glacier mass balance

The annual mass balance at a given point on the glacier is defined by the sum of the water accumulated at this point minus ablation:

$$b_a = a_a + c_a = \int_{t_0}^{t_1} [c(t) + a(t)] dt \tag{7.11}$$

where b_a [m] is the annual glacier balance at a given point, c_a [m] and a_a [m] respectively the annual accumulation and ablation, $c(t)$ [m/day] and $a(t)$ [m/day] respectively the accumulation and ablation rates at time t. Times t_o and t_1 are the beginning and end of the considered year.

Addendum 7.3 Glacier annual mass balance estimation methods

For hydrological applications in the Alps, the hydrological year generally begins on October 1. Mass balances are therefore often calculated over a year starting on this date. A number of annual mass balance estimation methods are described below. They can be used to estimate the balance over several years.

Direct glaciological method: The annual mass balances are measured locally at a number of points considered to be representative of the accumulation and ablation zones. The local estimates are generally obtained from boreholes thanks to visible accumulation horizons or by measuring the exposed heights of stakes inserted vertically in the ice. The total balance of the glacier is obtained by spatial interpolation of point estimates.

Photogrammetric/geodetic methods: Volume differences can be determined by superimposing aerial photos taken at the end of two ablation seasons. This method can in principle also be applied using topographic maps corresponding to different dates. However, the exact date corresponding to the updating of glacier zones on a topographic map is often hard to determine. The elevation accuracy of the data can also be a problem.

Estimation by the glacio-hydrological simulations: The annual balances are simulated for each spatial unit of the glacier using a snow and ice accumulation and melting model.

Hydrological estimation: Based on various hydrological measurements carried out on the glacierized basin, the various terms of the hydrologic balance are estimated and the change in the volume of stored water obtained over the considered period is assimilated to the glacier

balance. The variation of water stored in the ground is assumed to be negligible with respect to the variation of water stored in the glacier.

For glacier-covered basins, the glacier balance represents an important term in the hydrological balance. However, certain quantities of the hydrological balance are difficult to estimate (precipitation, evapotranspiration, evaporation and the sublimation of snow and ice in particular). Consequently, the resulting hydrological balance often represents a rough approximation of the real balance. The error present in the estimate of annual precipitation or evapotranspiration is for example generally considered to be of the same order of magnitude as that of the glacier balance, i.e., from a few centimeters to a few tens of centimeters. Glacier balance data calculated using the hydrological balance method are therefore often very uncertain.

Evolution of glaciers

The evolution of the surface elevation of a glacier is the result of complex dynamic processes driven mainly by the mass balance. If the balance is continuously negative over a long period, the surface elevation and volume of the glacier will decrease until the glacier reaches a new equilibrium. The corresponding release of storage is marked by an increase in the runoff volume at the basin outlet during an initial phase of glacier response (Figure 7.7).

Glaciers in mountainous regions have been continuously retreating—except for temporary reversals—since the Little Ice Age.[3] They therefore release more water than they receive.

It can take several decades for a glacier to visibly react (i.e., by a change in its surface area) to a change in climate. This delay depends on the type of glacier and is often referred to as the response time of the glacier. For the purposes of hydrological modeling, the climate is often assumed to be stationary and the glacier in equilibrium with the climate. Glacier surface areas are consequently also considered to be stationary. This approximation is invalid in a non-stationary context or when estimating the regime of a glacierized basin in a climate-change context (Schaefli, 2005).
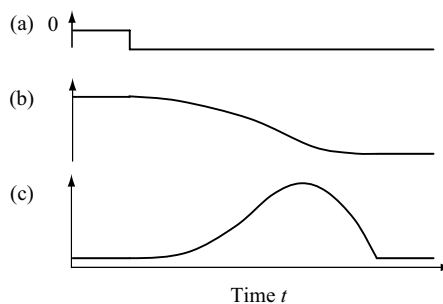

Fig. 7.7: Illustration of the effect of a long-term modification of: (a) the glacier mass balance on (b) glacier volume and (c) glacier runoff. Precipitation inputs are assumed to remain unchanged over the considered period (modified from Jansson *et al.*, 2003).

---

[3]The Little Ice Age ended in Europe around 1850 (e.g., Barry, 2006).

7.3.3 Estimating Glacier Runoff

Various glacier melt models were developed in the 1960s and 1970s for short-term and seasonal forecasting of glacier runoff, in particular for the purposes of hydroelectric power production. These models, often based on statistical analysis of observed data, relate glacier runoff directly to meteorological variables (e.g., temperature, wind speed, radiation).

The majority of recent models deal separately with: 1) the production of meltwater by the different glacierized parts of the basin and 2) the transformation of this meltwater into runoff at the outlet of the drainage basin. These models use empirical, conceptual and physically-based approaches.

Glacier melt models

The melting of firn or snow present on a glacier and the melting of the glacier ice itself are estimated using approaches similar to those used for seasonal snow cover (e.g., energy balance or empirical method, see Section 7.2.3). Hock (2005) for example has reviewed the various approaches.

For empirical approaches, the production of glacier meltwater $M_g(t)$ [mm w.e./day] is for example frequently calculated on the basis of a degree-day type expression such as:

$$M_g(t) = a_g(T(t)-T_c) \tag{7.12}$$

where a_g is the glacier melt degree-day factor [mm/°C/day] and T_c the critical melting temperature [°C]. In simulation models, ice is generally assumed to melt only if the considered spatial unit is no longer covered by snow or firn. If the spatial unit is covered, the same model can nevertheless be used however with a degree-day factor adapted to the type of cover (Table 7.3).

The volume of ice available for melting is difficult to quantify. It is generally assumed to be infinite. Hydrological modeling in the presence of glaciers then has the particularity of considering the drainage basin as an open system in which the glacier represents either a water source or sink.

Glacier melt runoff models

Models used to transform glacier meltwater into runoff consider this runoff either separately or together with the runoff from snow and firn meltwater. Whichever option is selected, different approaches are possible.

The first are physically-based methods designed to simulate the dynamics of runoff within the glacier (Arnold *et al.*, 1998; Flowers and Clarke, 2002). For this, they use open channel or closed conduit flow equations (Graf and Altinakar, 1998, 2000). The main difficulty is that they require a description of the meltwater drainage network. On a glacier, there are many possible pathways of different types that the water can take. The water can flow on the surface of the glacier or through different conduits in and under the glacier or even in the sub-glacial sediments. Moreover, the subsurface conduits form a complex grid network that is generally poorly known or totally unknown. Also, because ice can be deformed under moderate stresses, the conduits within the glacier can be modified, disappear or appear rapidly. Finally, the drainage network generally changes during the

melt season under the action of liquid flows. It is therefore highly non-stationary. Whatever the physically-based model used, it can only provide a very approximate or even conceptual representation of the real flows.

In practice, glacier meltwater runoff models are essentially conceptual (Hock and Jansson, 2005; Schaefli *et al.*, 2005). They use one or more linear reservoirs to simulate the transformation, sometimes in a differentiated manner, of snow, firn and ice meltwater into runoff. The GSM-SOCONT described in Appendix 7.6.4 is a model of this type.

7.4 HYDROLOGICAL MODELING IN MOUNTAINOUS REGIONS

The key issues of hydrological modeling in mountainous regions have been presented in the sections above. The objective of this section is to present the main factors to be considered for successful modeling in a given context. This section supplements the modeling concepts presented in Chapters 3 to 6 and in the previous sections of this chapter.

For illustration purposes, the concepts of a complete hydrological model developed for various drainage basins in the Swiss Alps are presented in Appendix 7.6.4 (GSM-SOCONT model, Schaefli, 2005 and Schaefli *et al.*, 2005).

7.4.1 Particular Modeling Difficulties in Mountainous Regions

When developing and using a hydrological model for a mountainous region, special attention must be paid to a number of points that are generally sources of major difficulties. Among them, it is important to consider the following.

- In a mountainous region, the spatial variability of meteorological variables is high and particularly hard to estimate and model. It must however be taken into account in so far as possible in the spatialization of meteorological variables.
- Highly variable in time and space, the form of precipitation is also hard to estimate. It does however determine the portion of precipitation that accumulates on the basin and the portion that can contribute to flood flows. Estimation of the form of precipitation at every point of the basin requires a specific model.
- Hydrological processes are highly variable in space. This high variability is related to topography and land use in addition to the spatial variability of meteorological variables. This must be taken into account by a suitable discretization of the drainage basin and possibly by different modeling for different parts of the basin.
- Meltwater runoff is highly dependent on the state of any snow cover present on the basin at the beginning of the considered simulation period. Runoff also depends greatly on the initial soil saturation conditions. Estimation of the initial state of water stored in solid and liquid form within the drainage basin is, particularly in this context, a hydrological modeling step in its own right.

These different points will be discussed in detail in the following sections.

7.4.2 Spatialization of Meteorological Variables

One of the main problems encountered when using a hydrological model at the scale of the drainage basin is how to take into account the spatial variability of meteorological quantities that are highly influenced by topographic relief. For example, the quantity of radiation received at a given point depends on solar inclination, the orientation of the slope and the surrounding topography. Wind also varies locally depending on the general direction of airflow and the topographic relief. Precipitation is influenced by orographic effects and can vary greatly from one valley to another or from one slope to another. It tends to be greater on slopes exposed to the wind and, on the average, increases with altitude. Temperatures are highly dependent on elevation but are also influenced by the topographic relief. Whatever the meteorological variable considered, spatialization is a difficult task in a mountain environment and represents a major source of uncertainty (Hingray *et al.*, 2012).

A promising way to obtain a useful description of the spatial variations of meteorological variables in a mountainous region is to use a physically-based spatialization approach based on simulations with a mechanistic meteorological model offering a high spatial and temporal resolution (Anquetin *et al.*, 2003; Kunstmann and Stadler, 2005). Unfortunately the complexity and presently modest performance of such models makes them relatively unsuitable for most hydrological applications.

In practice, simpler methods are used (Hock, 2005; Stahl *et al.*, 2006; Quintana-Segui *et al.*, 2008). They are designed to estimate the meteorological variables for each of the spatial discretization elements used to represent the drainage basin. Whatever the method chosen, the required and possible level of detail of the spatialization must be assessed for each variable as well as the errors that can result.

Current methods used to spatialize precipitation and temperature and their associated difficulties will be dealt with below. The possibility of estimating the form of precipitation to deduce rainfall depths and the equivalent water depths of fresh snow will then be discussed. For the spatialization of other variables, such as those required for the estimation of the different terms of the energy equation, readers are invited to consult for example Fierz *et al.* (2003) or Garen and Marks (2005). Whatever the variable considered, note that it is often worthwhile to condition the spatialization model parameters with respect to the season and/or weather type in order to reduce the associated errors (Paquet, 2004; Gottardi *et al.,* 2008).

Spatialization of precipitation data

The spatialization of precipitation and estimation of average precipitation over the basin (or a given spatial unit) is a difficult task in a mountain environment. The density of conventional measurement networks is often too low to properly capture the spatial variability of the observed variables. Moreover, the representativeness of measurements is limited by the scarcity or absence of stations at high elevations. This lack of stations is due to the extreme meteorological conditions that make measurements difficult and also to problems related to accessibility and equipment maintenance.

For practical reasons and often lacking a better method, most spatialization methods used for hydrological applications in mountain environments are simply modified versions of classical spatialization methods (Chapter 2). The adaptation of these methods to the

mountain context often consists simply in applying an assumed relationship between precipitation and elevation (Addendum 7.4). In the Swiss Alps, the increase of mean annual precipitation with elevation is roughly around 100 mm per 100 meters. Approaches based on such relationships offer however limited satisfaction because they often neglect the spatial heterogeneities of orographic effects such as those related to the exposure of slopes to wind. Moreover, the increase of precipitation with elevation that may be observed for average precipitation values over long periods is far less obvious for isolated events. The increase of precipitation volumes with elevation is related more to longer and more frequent precipitation events than to higher intensities. Note also that the spatial structure of precipitation is highly dependent on weather type.

Addendum 7.4 Spatialization with a forcing variable

One interpolation method frequently used for mountainous regions is based on the identification of a relationship between the variable to be interpolated and one or more external explanatory variables (often elevation or other topographic variables, e.g., Drogue *et al.*, 2002). This relationship can be identified for the considered time step using the *N* measurement stations available in the region. It is modeled by a suitable function (e.g., a linear, polynomial or piecewise linear function).
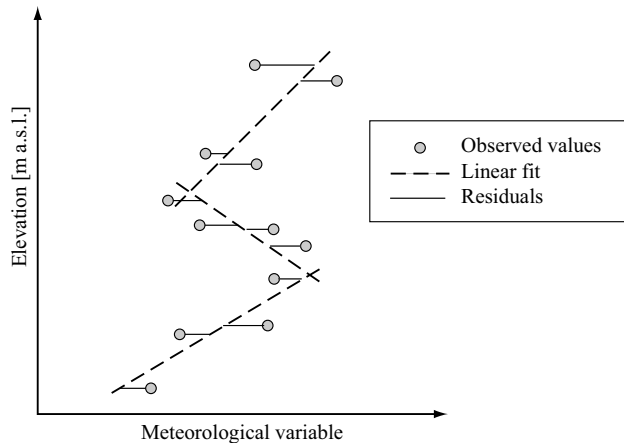

Fig. 7.8: Example of a discontinuous linear relationship between the meteorological variable to be interpolated and the external explanatory variable (i.e., elevation).

Modeling the variable to be interpolated on the basis of an exogenous explanatory variable does not produce an exact interpolation of the field given that the interpolated value at a point where an observation is available does not necessarily correspond to the measurement. On the other hand, the model supplies an initial rough estimate of the field that takes into account its shape at the regional scale. This rough estimate must then be refined by considering the residuals between the regression model estimates and the observed values. In practice, these residuals are spatialized by kriging techniques (e.g., kriging with external drift, see Appendix 2.7.2) or using another interpolation method (Chapter 2). For example, if the explanatory variable is elevation z, the variable Y at point $M(x_0, y_0, z_0)$ can be estimated using the following equation:

$$\hat{Y}_M(t) = f_t(z_0) + \sum\nolimits_{i=1}^{n} W_{M,i} \times \left(Y_i(t) - f_t(z_i) \right) \tag{7.13}$$

where $f_t(z)$ is the relationship determined between Y and elevation z at time t on the basis of the N considered measurement stations, $Y_i(t)$ is the observed value at the ith station and $W_{M,i}$ is the weighting coefficient assigned to the calculated error between this observation and the estimate $f_t(z_i)$ provided by the regression model for the same station. The interpolation obtained using this method is exact. The coefficient $W_{M,i}$ depends on the method used to interpolate the residuals.

Another approach consists in using a first guess estimate based on climatology. For example, if the spatial structure of the precipitation field is a function of weather type, the first guess estimate corresponding to the weather type observed for the time step over which interpolation is required can be used. The first guess estimate is in this case produced elsewhere on the basis of all the precipitation fields observed over the considered area for this weather type (Appendix 2.7.2).

Spatialization of temperature data

Temperature can potentially vary greatly with altitude. For a free air mass in the troposphere, the average decrease of temperature with altitude is –0.97°C per 100 m. For the standard atmosphere, this decrease is –0.65°C per 100 m of altitude. The relationship between temperature and altitude can vary greatly with time.

In mountainous regions, the average temperature gradient is generally lower, in terms of absolute value, for minimum temperatures (in winter) than for maximum temperatures (in summer) (Singh and Singh, 2001). Near the Earth's surface, the vertical temperature profile can also vary greatly over a 24-hour period due to thermal exchanges between the Earth and the atmosphere. The relationship between temperature and altitude is therefore not always linear. In winter, temperature inversions are frequently observed. They lead to a positive temperature gradient in the lowest layers of the atmosphere (Figure 7.9). Spatial variations of temperature can also be highly discontinuous due to topographical relief. For example, under foehn conditions, the temperature gradient depends on the exposure of slopes to the warm wind. Another example involves certain solid precipitation events, during which a local drop in temperature can be observed in certain deep valleys but not in neighboring valleys (Addendum 7.5).

Ideally, the relationship between temperature and altitude should be determined locally and for each considered time step on the basis of temperature measurements at different altitudes in the study zone. Due to a lack of measurement.
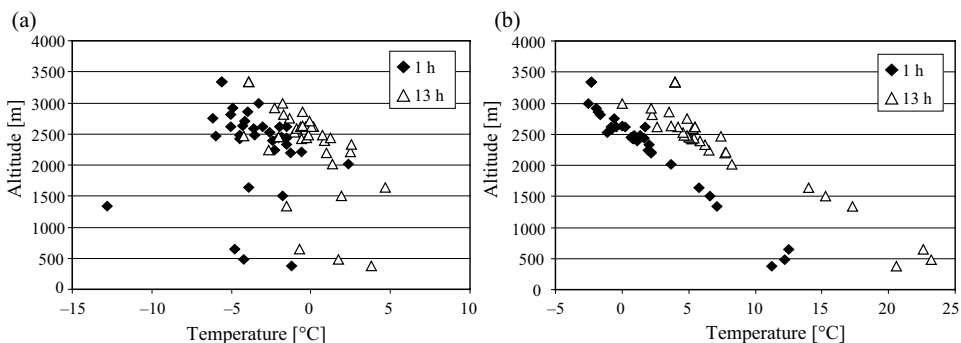

Fig. 7.9: Altitude versus temperature in the Rhone drainage basin upstream of Lake Geneva at 01:00 and 13:00 on: a) 09/12/2001 and b) 17/07/2001.

The relationship between temperature and altitude is often used to estimate the elevation of the isotherm corresponding to a critical temperature T_0 (e.g., the 0°C isotherm for melting). Together with the hypsometric curve of the drainage basin, this relationship can be used to determine the area of the basin for which the temperature is less than T_0. If the relationship is linear, the elevation $Z_M(T_0, t)$ of the T_0 isotherm at a given point M can be obtained easily on the basis of the temperature-elevation gradient $\nabla_T(t)$ estimated for the considered time step and the temperatures $T_i(t)$ observed at the N neighboring stations.

$$Z_M(T_0, t) = \sum_{k=1}^{N} W_{M,i} \cdot \left(Z_i + \frac{T_0 - T_i(t)}{\nabla_T(t)} \right) \tag{7.14}$$

where Z_i and $W_{M,i}$ are respectively the elevation of the ith temperature measurement station and the associated weighting factor of the station.

Note that the relationship between altitude and temperature must be estimated carefully for each time step considered. The quality of these estimates will determine the pertinence and quality of subsequent hydrological analyses (Example 7.1).

Example 7.1 Temperature-elevation relationship and the 0°C isotherm elevation

At Baltschieder (Upper Valais, Switzerland), the Rhone drainage basin is made up of two basins in parallel, that of the upper Rhone (913 km² at Brigue) and that of the Viège (789 km² at Viège). These basins cover a large range of elevations. Their hypsometric curves are shown in Figure 7.10b and the corresponding values are summarized in Table 7.4.

Table 7.4: Hypsometric data for the two basins.

Elevation Z [m]	Cumulative area $A(Z)$ [%]	
	Rhone at Brigue	*Viège at Viège*
600	0	0.0
700	0.1	0.2
800	0.5	0.7
1000	1.6	2.3
1200	3.1	4.9
1400	5.6	9.8
1600	9.5	15.4
1800	14.1	21.8
2000	19.3	29.3
2200	24.9	39.2
2400	32.4	51.3
2600	41.4	63.1
2800	53.8	73.6
3000	66.4	82.3
3200	77.5	88.8
3400	85.4	93.8
3600	92.0	97.6
3800	95.9	99.5
4000	98.2	99.9
4200	99.4	100.0
4400	99.8	100.0
4600	100.0	100.0

The problem here is to estimate the surface area on which precipitation fell in liquid form on each of the two basins at 13:00 on 17/07/2001. It is assumed that the rain/snow limit corresponds to the 0°C isotherm. The temperatures measured at different weather stations of the region are indicated in Table 7.5.

Table 7.5: Temperatures observed in the Valais region at 13:00 on 17/07/2001.

Station	Sion	Viège	Ulrichen	Montana	Zermatt	Gd St Bernard
Elevation [m]	482	640	1345	1508	1638	2472
Temperature [°C]	23.2	22.6	17.3	15.3	14	7.4

For the considered time, the relationship between temperature and elevation can be well represented by a decreasing linear relationship (coefficient of determination $R^2 = 0.99$). The temperature-elevation gradient estimated by the least squares method is $\nabla_0 = -0.836$°C/100 m. The corresponding linear regression line Δ_0 is shown in Figure 7.10a. The elevation of the 0°C isotherm is simply derived from this relationship and can be expressed as follows:

$$Z_0 = Z_R - \frac{T_R(t_0)}{\nabla T(t_0)} \tag{7.15}$$

where Z_R is the elevation of the reference station and $T_R(t_0)$ the temperature measured at this station at time t_0. Using the station of Zermatt, located within the Viège basin at Viège, the 0°C isotherm elevation is $Z_{0,0} = 3357$ m. It is then possible to calculate that the precipitation falling in liquid form covers 82.5% of the total area of the Viège basin at Viège and 92.5% of the total area of the Rhone basin at Brigue (Figure 7.10b). Given that the observed temperature gradient is very well represented by a linear relationship, these estimates depend little on the station used as the reference station.

The 0°C isotherm is often estimated not on the basis of the temperature-elevation relationship obtained from observations at the considered time but rather on the basis of the temperature-elevation gradient corresponding to the standard atmosphere: $\nabla_S = -0.65$°C/100 m.
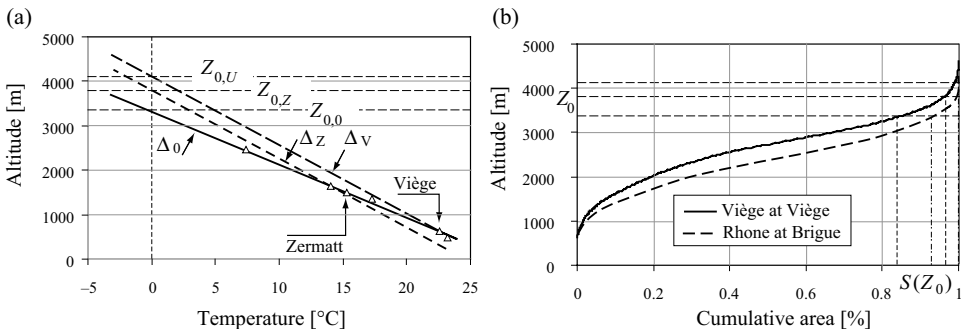

Fig. 7.10: Influence of the temperature-elevation relationship on the mountain drainage basin area receiving liquid precipitation. a) Temperature-elevation relationships and 0°C isotherm elevations obtained using: 1) the temperature gradient derived from observations (line Δ_0 fitted to the white triangles) and 2) the average gradient of the standard atmosphere and the temperature observed at a reference station (line Δ_V for Viège station and line Δ_Z for Zermatt station). b) Hypsometric curves for the basins and estimates of the area receiving liquid precipitation for different temperature-elevation relationships.

For the problem considered in this example, the estimate of Z_0 obtained with this gradient ∇_S is very different than the value obtained using the temperature-elevation relationship derived from observations. Furthermore, it depends greatly on the station considered as the reference station (Figure 7.10a). Using ∇_S, the elevation of the 0°C isotherm is overestimated by more than 435 m if the reference station is Zermatt ($Z_{0,Z}$ = 3792 m—estimate deduced from straight line Δ_Z; Figure 7.10a) and by more than 700 m if the reference station is Viège, located near Baltschieder ($Z_{0,V}$ = 4117 m—estimate deduced from straight Δ_Z). The estimation error in fact increases with the difference between the elevation of the reference station and the elevation of the required isotherm.

For the considered time, the use of ∇_S consequently leads to an overestimation of the basin areas on which precipitation is considered to fall in the form of liquid. For the Viège basin at Viège, using Zermatt as the reference station, this overestimation is 13.5% (i.e., 96% of the total basin area instead of 82.5% estimated using the observed temperature-elevation relationship). Using Viège as the reference station, the calculation indicates precipitation supposedly falling in the form of liquid over the entire basin (i.e., a 17.5% overestimation of the contributing area). For the Rhone basin at Brigue, the errors are lower. This is the result of the higher slope of the hypsometric curve around the elevation Z_0, corresponding to the 0°C isotherm for the considered time step. The errors remain however significant (Figure 7.10b).

In conclusion, for the present situation, errors on the estimation of liquid precipitation obtained using ∇_S add to the errors already resulting from the overestimation of meltwater runoff (coming both from glaciers and the remaining snow cover on the basin at this time). In other meteorological situations, the errors resulting from the use of the standard gradient can on the contrary lead to a significant underestimation of liquid precipitation and meltwater volumes. These errors in fact vary greatly from one season to another (in the Alps, they are on the average greater in summer than in other seasons) and from one time step to another (e.g., in Figure 7.9, they are greater at 13:00 than at 01:00 on the same day). In both cases, the estimation errors can strongly influence the quality of hydrological simulations (Hingray *et al*., 2010). The magnitude of the errors largely depends on the hypsometric curve of the considered basin. ∇_S should be used only when no local data are available to determine the temperature-elevation relationship.

Addendum 7.5 Difficulties concerning the spatialization of temperatures in mountain areas

This addendum presents the main difficulties encountered when spatializing temperature data in mountainous regions.

Temperature and basin orientation: South-facing slopes fully exposed to solar radiation are on the average warmer than north-facing slopes partially protected from solar radiation.

Temperature inversions: Air is normally warmer near the ground. A warm air mass can however sometimes be found above a colder layer of air. Warm air, lighter than cold air, traps the mass of cold air below and prevents it from being dispersed in the atmosphere. This situation is referred to as a temperature inversion. It can be observed for instance when a warm air layer coming from the tropics is transported above a colder air layer coming from the mid-latitudes. Temperature inversions are also observed during clear windless nights as a result of rapid cooling of the ground by infrared radiation losses, leading to cooling of the air near the surface. The altitude of the top of the inversion increases with the number of successive clear windless nights.

In the mountains, other typical inversion situations are frequently observed. For example, in the absence of wind, the air at the bottom of a deep valley is not moved out during the day and will be heated. At night, the cold air that forms along the slopes moves down into the valley bottom where it accumulates, pushing the warm air upwards and causing a stable inversion situation. Moreover, the presence of glaciers or snow cover can lead to continuous cooling of the air near the surface and the formation of a lasting intense inversion zone. During a temperature inversion, the relationship between temperature and elevation can change greatly and can take on a shape that cannot be represented by a simple function. The height of the inversion layer can vary from a few meters to several hundred meters (Singh and Singh, 2001). Temperature inversions generally end when there is sufficient wind to mix the air.

Deep valleys, snowmelt and local temperature drops: The high relief of mountainous regions can lead to major spatial discontinuities in temperature fields. The following phenomenon is for example often observed in deep, narrow valleys with very little wind. During a snowfall, sublimation and possible melting of snow crystals absorbs energy from the surrounding air. In the absence of wind, this air is not renewed and is therefore subject to cooling. Consequently, temperatures and the rain/snow limit drop. This phenomena is however very local, for example limited to a given valley. Such a situation was observed in October 2000 in the valley of the Viège river, one of the main tributaries of the Rhone river upstream of Lake Geneva. The sudden temperature drop in this valley greatly reduced the flood flows produced in the valley and alleviated the situation downstream in the Rhone Valley which experienced only 100-year flood for this extreme event.

Temperature gradients, humidity of air masses and slope exposure to wind: A dry air mass rises when it encounters a mountain range that it cannot circumvent. Given that atmospheric pressure decreases with altitude, the air temperature decreases by adiabatic expansion.

For dry air, the temperature decreases at a rate of 0.97°C per hundred meters. This is referred to as the dry adiabatic lapse rate. Downstream of the mountain range or ridge, the temperature increases at the same rate as the air mass descends. At the same elevation, the temperature is the same on both sides of the ridge.

If the air mass is humid, the water vapor it contains condenses as soon as the temperature reaches the dewpoint. This condensation releases heat (latent heat of vaporization) and consequently raises the temperature of the air. The resulting temperature gradient, referred to as the wet adiabatic lapse rate, is lower than the dry adiabatic lapse rate. It depends on the pressure and especially on the ambient temperature. The average wet adiabatic lapse rate is 0.6°C/100 m. If it does not rain on the windward slope when the water condenses, the air heats up as it descends on the leeward slope and the water drops evaporate once again. The heat released by condensation is reabsorbed by evaporation. At the end of this process, at the same elevation, the temperature is the same on both sides of the ridge.

If, on the other hand, it rains on the windward slope, the air mass loses some of the humidity it contains. When the air mass re-descends on the leeward slope, the energy required to evaporate the remaining humidity is less than the energy released by condensation. The air is therefore warmer on the leeward slope than on the windward slope. This produces the foehn effect.

Rain/snow separation

To estimate the phase of precipitation on each spatial discretization unit used for modeling, a rain/snow separation model is required. The most commonly used model is based on the estimated air temperature at the median elevation of the considered hydrological unit. Precipitation is then considered to be solid if the temperature is

below an estimated temperature threshold. It is difficult to determine this threshold on the basis of physical processes or observations. The instantaneous threshold is generally somewhere between 0°C in 2°C and is only rarely 0°C. The threshold varies in space and time. Moreover, the precipitation phase can vary greatly within a given time interval. Note also that in mountainous regions, the drainage basin is often discretized on the basis of elevation bands that, for the needs of modeling, generally cover a relatively large elevation range. The temperature difference between the top or bottom of an elevation band and its median elevation can be non-negligible. For instance, for a 500 m elevation band and a mean temperature gradient of –0.6°C/100 m, the temperature difference with respect to the median elevation temperature is respectively –1.5°C and +1.5°C at the top and bottom of the elevation band. It is therefore possible to have precipitation in different forms at the same time within a given elevation band. For this reason, it is often considered the precipitation can fall in the form of a rain/snow mixture within a given time step (Figure 7.11).

A distribution function is therefore often used to estimate the proportion of precipitation falling in liquid and solid form:

$$S(t) = \begin{cases} P(t) & \text{if } T(t) < T_a \\ \dfrac{(T_b - T(t))}{(T_b - T_a)} P(t) & \text{if } T_a < T(t) < T_b \\ 0 & \text{if } T(t) > T_b \end{cases} \tag{7.16}$$

$$R(t) = P(t) - S(t) \tag{7.17}$$

where $S(t)$ [mm] is precipitation falling as snow, $R(t)$ [mm] precipitation falling as rain, $T(t)$ [°C] the mean air temperature, $P(t)$ [mm] total precipitation, T_a [°C] the temperature
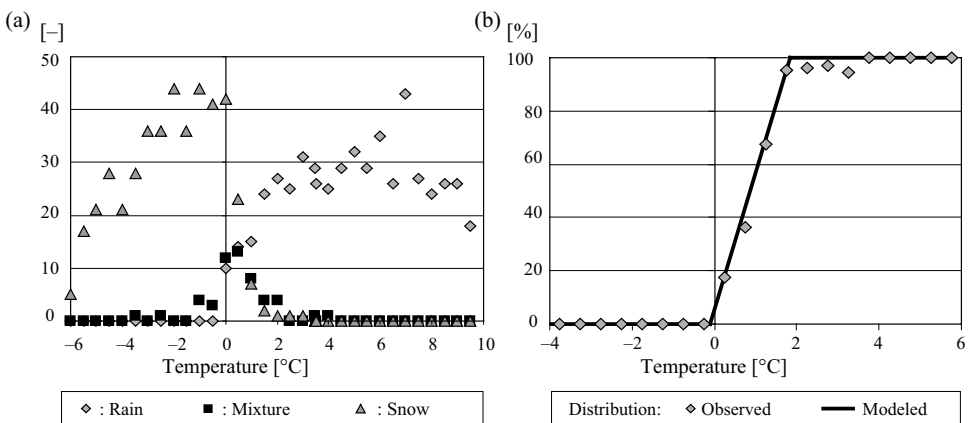
Fig. 7.11: Form of precipitation as a function of temperature. a) Number of events for which precipitation falls in liquid or solid form or as a mixture for the considered temperature interval. b) Relative frequency of precipitation falling in liquid form and the corresponding liquid precipitation distribution model. The distribution is based on the average of instantaneous observations obtained at 07:00, 13:30 and 19:30 at Zermatt station in Switzerland (elevation 1638 m, period 1982–2004).

threshold below which all precipitation falls in the form of snow and T_b [°C] the temperature threshold above which all precipitation falls as rain.

In principle, the width of the interval $T_b - T_a$ depends on the elevation resolution of the spatial discretization of the basin and the temporal resolution of the simulation. In the Swiss Alps, for 1-hour time step and 100 to 200 meter elevation bands, $T_a = 0°C$ and $T_b = 2°C$ provides a good approximation.

Temperature is obviously not the only factor affecting the form of precipitation. Relative humidity is another important factor as pointed out by Froidurot *et al*. (2013).

7.4.3 Simulation Aspects

Discretization of the drainage basin and homogeneous hydrological units

To account for the high variability of meteorological conditions in drainage basins covering a large range of elevations, the hydrological model requires a certain level of spatial discretization, as already discussed. The minimum level is:

- Elevation-based discretization to take into account the temperature and precipitation gradients.
- A terrain orientation-based discretization if solar radiation or wind variables are used.

Depending on the heterogeneity of the basin (i.e., soil cover, soil type, geology), a more detailed discretization may be necessary. In the presence of glaciers, the glacierized and non-glacierized parts must be separated. If the basin is divided into several sub-basins for the needs of modeling (Chapter 3), these discretizations must be carried out separately for each sub-basin.

The spatial discretization of a mountain drainage basin generally leads to the identification and modeling of relatively homogeneous hydrological units (RHHUs; e.g., Schaefli *et al*., 2005; Lafaysse *et al.*, 2011) or hydrologically similar response units (HRUs, e.g., Gurtz *et al*., 1999, see also Chapter 3). For many models, the RHHUs are the elevation bands obtained for each sub-basin used for modeling (Figure 7.12).

Note that the number of parameters to be estimated increases the degree of discretization of the basin and that a high level of discretization does not guarantee the quality of simulations. For a given parameter set, modeling performance however increases significantly with the accuracy of the elevation discretization of the basin (Etchevers *et al*., 2000; Schaefli *et al*., 2005). This performance generally reaches an upper bound at a certain level of discretization, partially depending on the density of the observation network. In the Swiss Alps, the limiting number of elevation bands for a given basin corresponds roughly to elevation intervals of 100 to 300 m (Schaefli *et al*., 2005). The number of RHHUs and elevation bands in particular can be reduced without sacrificing performance by using parameterizations based on appropriate grids (Addendum 3.2). For example, depletion curves (Section 7.2.1) can be used to take into account the grid-based variability of melting with elevation as well as various other parameters such as slope orientation or the presence of vegetal cover (WMO, 1986).

Finally, note that the hydrological behavior of mountain basins is often highly disturbed by hydraulic works such as dams and the associated intakes for hydropower production and/or water supply or diversions designed to convey some of the runoff produced by snow
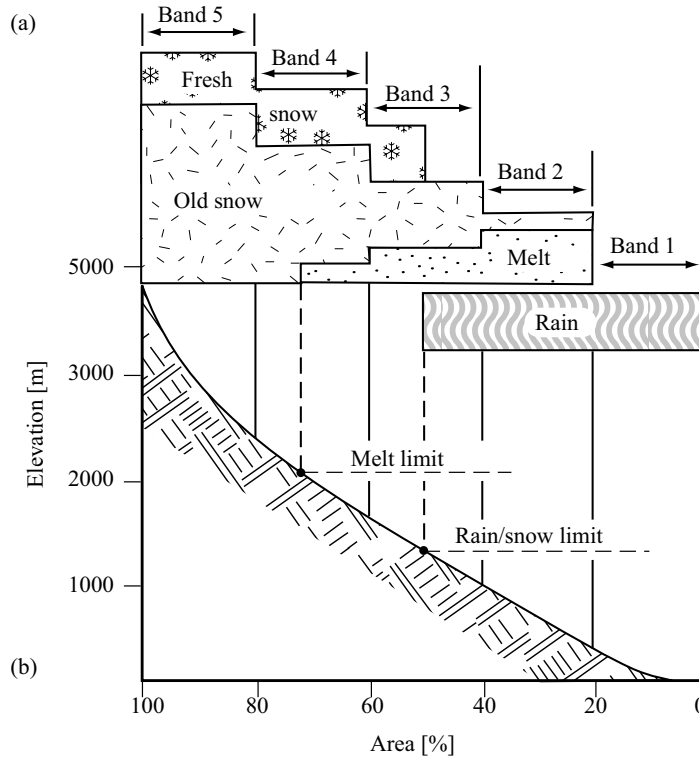
Fig. 7.12: Spatial discretization of a mountain drainage basin according to elevation. a) Schematic elevation distribution of snowpack water equivalent, liquid and solid precipitation and melt. b) Hypsometric curve of the drainage basin.

or glacier melt at high elevations to dryer slopes or valleys (e.g., the "Bisses" irrigation canals in the Swiss Valais). Hydrological modeling of these basins therefore often requires modeling of such hydraulic works and their operation (Schaefli, 2005). This means adapting the discretization to their layout in the basin.

Estimating the initial snowpack

The initial snowpack estimated and/or chosen for different elevation bands of the hydrological model is critical to the quality of simulated discharges. One approach consists in initializing the simulation model using measurements concerning the extent and water equivalent of the snow cover (Appendix 7.6.2). These measurements are however rarely available or difficult to use, mainly due to spatialization problems.

Another approach consists in estimating the initial snowpack using the hydrological model. The temporal evolution of water storage in the different compartments of the drainage basin is simulated over a period preceding the period of interest. This period is sufficiently long such that the state of storage at the end of this period is not influenced by the storage values at the beginning of the simulation period. This is referred to as the warm-up period, frequently used to initialize continuous simulation models (Chapter 3). For mountain drainage basins with seasonal snow cover, it is often necessary to use an initialization period extending over a full year.

Note that it is easier to initialize the model if the beginning of the simulation period is chosen within a period of the year in which snowpacks are small or inexistent. In the Alps, for example, snowpacks are the smallest in September and October, before the first snowfalls.

Simulating the evolution of the snowpack

Hydrological modeling can be used to simulate the spatial and temporal evolution of many variables describing the state of the snowpack, for instance the water equivalent [mm w.e.] of water stored in solid form as snow, the amount of liquid water [mm] stored in the snowpack and the internal energy [J/m²] of the snowpack.

For each element of the spatial discretization, the temporal evolution of the snowpack is often estimated using a reservoir-type accumulation and snowmelt model. The snowpack is assumed to have a certain retention capacity that allows it to store liquid water coming either from snowmelt or liquid precipitation (Kuchment and Gelfan, 1996; Boone and Etchevers, 2001).

Solid and liquid precipitation estimated using the rain/snow distribution model are respectively added to the snow and liquid water reservoirs of the snowpack. In the same way as the liquid water reservoir can be supplied by snowmelt coming from the snow reservoir, the snow reservoir can be supplied by the amount of liquid water transformed into solid water during negative temperatures. Runoff is produced by the snowpack if the quantity of liquid water present in the snowpack exceeds the retention capacity of the snowpack. Any release of liquid water from the snowpack produces an equivalent rainfall $P_{eq}(t)$ in the considered elevation band, which can then be transformed into infiltration and/or runoff. The mass balance equations governing the behavior of these two reservoirs are:

$$\frac{dH_s(t)}{dt} = S(t) - I_s(t) - M(t) - E_s(t) \tag{7.18}$$

$$\frac{dW(t)}{dt} = R(t) + M(t) - P_{eq}(t) \tag{7.19}$$

where $H_s(t)$ and $W(t)$ are respectively the amounts of solid and liquid water stored in the snowpack, $S(t)$ is snowfall, $R(t)$ rainfall, $I_s(t)$ the portion of solid precipitation that is intercepted, $E_s(t)$ the portion of the snow on the ground that is sublimated and $M(t)$ the flux of water exchanged between the two reservoirs. $M(t)$ is either the flux $M_s(t)$ of snowmelt in the event of a positive energy balance or the flux $M_r(t)$ of refrozen liquid water in the event of a negative energy balance.

In areas of dense vegetation, it is generally necessary to simulate interception of snow by the vegetation and the consequent sublimation (Pomeroy *et al*., 1998b). Few models are presently available for this. The approaches used are similar to those used for the interception of rain and the evaporation of intercepted liquid precipitation (Chapter 4). For example, one widely used approach is to attribute a certain snow storage capacity to the vegetation. Once this capacity is exceeded, the snow is either sublimated or transferred to the ground.
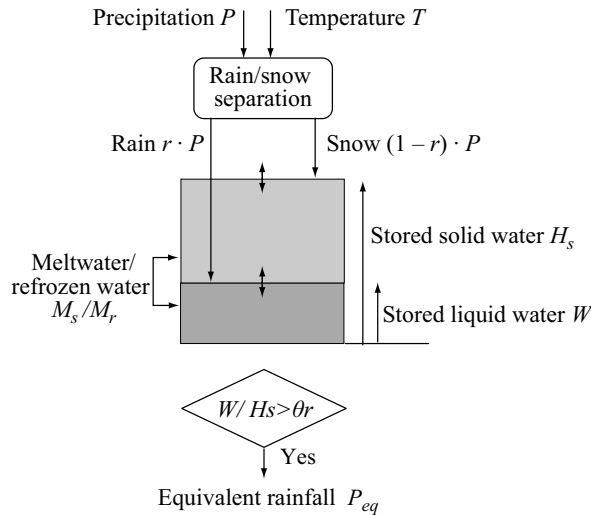
Fig. 7.13: Diagram of a typical snowmelt and snowpack monitoring model for a given elevation band. θ_r refers to snowpack saturation defined by a certain ratio of the volume of liquid water in the snowpack to the volume of solid water stored in the snowpack in the form of snow (adapted from Hamdi *et al*., 2005).

Choosing snowmelt and snowmelt runoff models

The right choice of a snowmelt and snowmelt runoff model must always depend on the modeling objectives and required results, the characteristics of the system and dominant processes, the simulation time step and available data.

In practice, most engineering applications use a degree-day type method for the snowmelt model (Paquet, 2004; Hamdi *et al*., 2005). This is generally due to the widespread availability of temperature data rather than to the characteristics of the system or modeling objectives. The numerous meteorological variables required to apply an energy balance method are rarely available. Moreover, even when the required measurements exist, their spatial interpolation or extrapolation is difficult given that they depend on topography (e.g., elevation, slope orientation) and the geographical location of the measurement stations (e.g., situated in different valleys) (Section 7.4.2).

Walter *et al*. (2005) however suggest that physically-based models using minimum and maximum daily temperatures can give highly satisfactory results, at least comparable to those of a simple degree-day type model. They estimated the different terms of the energy balance on the basis of simple relationships published in the literature, making their approach much more accessible than the detailed approach.

Whatever the model used, simulation of the seasonal snow accumulation/melt cycle is generally very satisfactory. Model performance can however vary greatly for infra-daily time steps, in particular when the retention capacity of the snowpack is neglected (Jin *et al*., 1999). The critical point is therefore the estimation of snowmelt volumes available for the production of runoff (after saturation of the snowpack and/or firn). Few studies have been devoted to this topic.

The model chosen to transform meltwater into runoff has less influence on the quality of results, even if it must take into account the evolution of the drainage system in the glacier

and firn over the season (Hock, 2005). In this respect, note that meltwater travel times can vary greatly depending on the medium. The transformation of glacier melt into runoff is for instance often considered to be much faster than the transformation of snowmelt into runoff. The travel time of snowmelt also depends on whether the meltwater comes from glacierized or non-glacierized areas. The quality of hydrological simulations therefore also depends on the meltwater runoff model used for these different inputs.

Many ongoing international initiatives are focused on comparing the performance of different snowmelt models (Slater *et al*., 2001; Luo *et al*., 2003; Etchevers *et al*., 2004). These comparisons concern the capacity of models to simulate both the state of the snowpack (e.g., snow depth, water equivalent, internal state) and its energy and hydrological balances. These initiatives should make it possible to identify the advantages and drawbacks of the different possible approaches.

7.4.4 Model Calibration

The calibration method to be used always depends on the modeling objectives, the type of model and available data (Chapter 3). The method should be of the semi-automatic type, i.e., combining automatic optimization methods and hydrological expertise. Three key aspects of rational semi-automatic calibration in mountainous regions will be discussed below. Examples of calibrations based on these concepts can be found in Schaefli *et al*. (2005) and Hingray *et al*. (2010).

Performance metrics

A hydrological model suitable for use in mountainous regions often has more than a dozen parameters that must be estimated (e.g., parameters of the models used to spatialize meteorological variables, critical rain/snow separation temperatures, melt parameters, parameters of the model used to determine the temporal evolution of albedo and snowmelt and snowmelt runoff parameters). Due to the equifinality problem discussed in Chapter 3, calibration is complex.

A sensitivity analysis can help identify how each of the parameters influences the simulated discharge series. For example, the date of the beginning of simulated melt discharges is often related to a critical melting temperature. The seasonality of simulated discharges often depends mainly on melt parameters (e.g., critical temperatures, degree-day factors). These parameters can typically be estimated in a first step so that the simulated mean interannual cycle corresponds to the observed mean interannual cycle. Similarly, the reproduction of high rainfall floods observed in fall, when the seasonal snow cover has in principle disappeared, is mainly related to direct runoff coming from non-glacierized parts of the basin. An in-depth sensitivity analysis is therefore strongly recommended since it will often make it possible to define a rational calibration strategy and the associated performance measurements.

Different metrics can be used to estimate the performance of a hydrological model (Chapter 3). The bias between simulated and observed discharges over the entire period available is a fundamental measure in the case of glacierized basins because the hydrological balance can be greatly influenced by the mass balance of the glaciers. The simulated hydrological balance must therefore be adjusted in particular by an appropriate calibration of glacier melt parameters.

Similarly, the mean error (absolute or quadratic) between observations and model estimates over the entire simulation period is also an essential measure of performance. In a mountainous region, the Nash-Sutcliffe criterion widely used by hydrologists is often greater than 0.80. This does not however necessarily guarantee pertinent modeling. Given the high annual seasonality of mountain regimes and their often limited interannual variability (for glacier and snow-glacier regimes), the mean interannual cycle already offers good performance in reproducing observed discharges. It is therefore important to assess the capacity of a hydrological model to provide better estimates than this minimal model (Schaefli and Gupta, 2007).

In the light of the above remarks, it can be worthwhile to calculate the classical quality metrics (e.g., bias, Nash coefficient, Nash coefficient calculated using the logarithms of the discharges) not on the complete year but rather on an appropriate selection of certain periods or events contained in the discharge series (e.g., one of the different seasonal periods of the hydrological regime or autumn rainfall floods).

Interdependent parameters

The parameters of most models are often interdependent with respect to a given criterion. This is typically the case for melt parameters defined for the snow, firn and ice compartments. Insufficient melt from one of these compartments can be compensated by a greater contribution of another without modifying the performance of the model in reproducing the mean interannual hydrological balance (Figure 7.14).

Similarly, if the spatialization of precipitation involves a model based on elevation dependence, the parameters of this model (e.g., the precipitation gradient) and the melt parameters will also be strongly dependent—both influencing the hydrological balance.
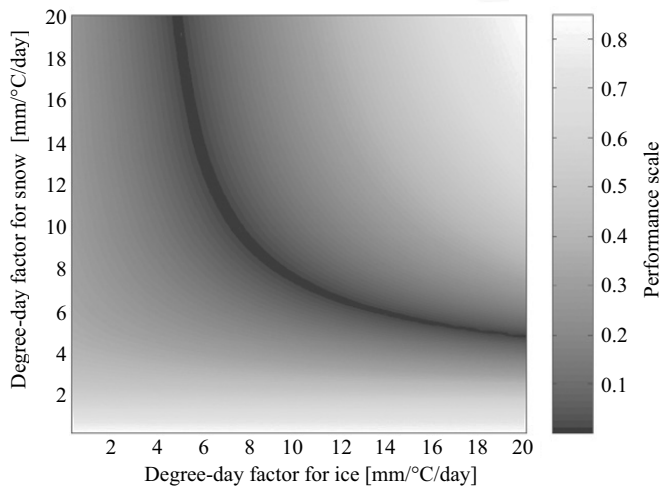

Fig. 7.14: Typical dependence between the degree-day factors for snow and ice. The considered quality criterion is the bias on the mean interannual hydrological balance (adapted from Schaefli *et al.*, 2005). The best performance corresponds to a zero bias.

Multi-signal calibration

Hydrological models are often calibrated using observations of the discharge at the outlet of the studied basin. In certain cases, observations are available for one or more other hydrological variables. If an observed quantity corresponds to a state variable simulated by the model, the corresponding data can be used for a multi-signal calibration of the model or for model validation (Chapter 3).

In mountain hydrology, certain state variables correspond relatively well to observable quantities, for example the spatialized water equivalent or extent of snow cover and the glacier balance. These data do not necessarily have to be available for the same time steps as used for the hydrological simulation. For this reason, series of annual glacier balances or snow cover spatial distributions obtained by remote sensing at different dates can provide highly informative additional signals. Such data can for example be used to calibrate snowmelt parameters. Two approaches can be followed. The first is to calibrate melt parameters on snow data and then validate and fine-tune them using discharge simulations. The second approach is to calibrate the parameters on the discharge and snow-ice data at the same time using a multi-objective optimization method.

The snowpack water equivalent variable simulated by a model is not the same as the snow depth variable generally observed. The performance of a hydrological model to reproduce the spatial distribution of snow cover and possibly its temporal evolution is often measured by comparing the spatial and/or temporal distributions of the binary variable representing the presence or absence of snow. These distributions are derived respectively from observations and the model. A certain snow depth is often chosen to determine the presence or absence of snow cover at a given point on the basin.

7.4.5 Perspectives for Hydrological Modeling in Mountainous Regions

The objectives of hydrological research today include improving the understanding and mathematical description of the spatio-temporal variability of the processes observed in the field and optimal integration of knowledge thus acquired in hydrological models. Present research in the field of mountain hydrology therefore focuses for example on improving our understanding of the accumulation and ablation processes in forested areas and the processes transforming meltwater into runoff and also on the quantification of sublimation and condensation. In mountainous regions, the acquisition of observations required to study these processes is however particularly difficult owing to limited accessibility and often extreme meteorological conditions. Another important research topic concerns the optimum use of all available sources of data (in particular those concerning the snowpack) to improve the real-time forecasting of discharges coming from mountain drainage basins (Clark *et al*., 2006). In this respect, note the existence of remote-sensing data that can be used to estimate the spatial extent and temporal evolution of the snowpack and glacierized areas (Berthier, 2005; López, 2007).

At present, hydrological modeling in mountainous regions (as in other types of drainage basins) is confronted with a paradox. In spite of the relatively poor quality of input data and highly simplified models, good or at least satisfactory simulation results are

generally obtained.[4] This paradox is linked to the marked seasonality of inflows, driven by the particularly strong accumulation/melt cycles observed at high mountain elevations. A good simulation of observed discharges does not therefore necessarily mean that a given model correctly represents the hydrological processes involved.

This point is particularly important when models are used for extrapolations, for instance to determine design floods based on rare meteorological scenarios or to simulate the effects of climate change on hydrological regimes.

Finally, hydrological models generally perform well in mountain drainage basins when simulating discharges on a daily time step. Model performance generally decreases significantly when attempting to reproduce infra-daily discharge variations. This is for example the case in the Alps when the objective of modeling is to forecast flood discharges.

7.5 KEY POINTS OF THE CHAPTER

- Understanding the underlying processes of snow and glacier hydrology is of great importance to the management of water resources and natural risks in mountain drainage basins and for the management of large rivers in plains for which the hydrological regime is greatly influenced by the storage and release processes of mountain snow and ice.
- The hydrological behavior of mountain drainage basins shows high seasonality. This behavior strongly depends on the spatial and temporal evolution of snow cover and, if applicable, glaciers, which can in particular modify significantly the hydrological balance.
- The processes driving the accumulation of snowmelt (and glacier melt if applicable) are very heterogeneous, in particular due to the heterogeneity of meteorological forcing.
- In mountainous regions, the spatial variability of meteorological variables is very high. This variability is partly induced by the topography. The spatialization of these variables is the source of many difficulties and the associated uncertainties are generally great. This is the case for temperatures and in particular precipitation.
- The form of precipitation (i.e., solid or liquid) is a key factor explaining the hydrological behavior of a mountain drainage basin. A rain/snow separation model is necessary to estimate the phase of precipitation at every point of the basin.
- Given the great spatial heterogeneity of meteorological variables and hydrological processes in a mountain environment, hydrological modeling always implies a suitable discretization of the drainage basin. Discretization based on elevation bands and the separation of glacierized and non-glacierized areas is essential.
- Snow and ice melt simulation methods that take into account only local temperature (degree-day method) often give good results. Methods based on the energy balance can be used to better take into account the explanatory processes and consequently the temporal variability of melting, however they require extensive data.

---

[4]This paradox refers to the principle of "*Garbage in, reasonable things out*" by analogy with the "*Garbage In—Garbage Out*" principle often cited in modeling.

- The strong seasonality and limited interannual variability of the hydrological cycle of mountain basins means that hydrological models can produce good simulation results. This performance should however be kept in perspective.
- The combined use and processing of various data sources (e.g., meteorological and snow measurements, areal photos and satellite images, field trips) is recommended in order to obtain a better understanding and improved modeling of the key hydrological processes.

7.6 APPENDICES

7.6.1 Potential Effects of Possible Climate Change on the Hydrology of Mountain Drainage Basins

Possible climate change and in particular global warming could have significant impacts on the hydrological characteristics of drainage basins subject to snow or glacier regimes, on the use of water resources and on hydrological risks. Quantification of these potential impacts is now an important field of research in hydrology. The value of such an analysis depends above all on the plausibility of the climatic scenarios used, in particular concerning future precipitation and temperatures (Chapter 12). It also depends on our understanding of the interaction between hydrological processes, meteorological quantities and biological and geomorphological processes (evolution of the drainage basin). This scientific domain is evolving rapidly. Only a few aspects based on available climate scenarios for the Alps will be dealt with below.

According to the Intergovernmental Panel on Climate Change (IPCC), observations show that the global temperature increased by 0.6°C over the 20th century (IPCC, 2001). In the Alps, temperatures increased by more than 1.0°C over the same period (Bader and Bantle, 2004). This trend is expected to continue over the 21st century and all the scenarios/models presently available predict continued stronger annual warming for the Alps with respect to global warming (IPCC, 2007). According to these forecasts and observed trends, this warming could be accompanied by stronger seasonality of temperatures and lower annual precipitation in spite of an increase in winter precipitation. Note that predictions of changes in most hydrometeorological variables are very uncertain. This is mainly a result of high uncertainty in precipitation change projections (e.g., Lafaysse *et al.*, 2013). Even the sign of changes may therefore be uncertain. Projected changes are however classically significant when the studied variable is mostly influenced by changes in temperature (temperature warming being very significant whatever the prediction lead time). In this light, the possible impacts of climate change are the following.

Modification of the hydrological regime and processes

- Modification of the accumulation and melting cycle, leading in particular to a shorter accumulation period, less accumulated snow and glacier retreat.
- A shift in the beginning of the snowmelt period and maximum monthly discharges towards the beginning of the year.
- Higher winter low flows.
- Increased evaporation resulting from higher temperatures and changes in vegetation and land use (glacier retreat).
- Lower mean annual discharges resulting from increased evaporation and decreased rainfall.
- Increased interannual variability of discharges resulting from a decrease in the snow/ice component of the hydrological cycle.

Impacts on water use and management

- Less reliability in estimated discharges due to increased variability.
- Less water available for hydropower production, irrigation, etc.

Greater hydrological/glaciological risks

- Higher autumn floods resulting from an increase in the area receiving precipitation in the form of rain (higher rain/snow limit).
- Higher spring floods resulting from the superimposition of snowmelt floods and heavy precipitation events.
- Glacier retreat leading to more frequent glacial outburst floods on the periphery of glaciers (e.g., formation of glacial lakes and subsequent outburst floods) and increased areas of very loose ground (moraines) presenting a higher risk of erosion.
- Melting of permafrost (permanently frozen ground) resulting in far less cohesion of the soil in the concerned areas (leading to mudslides, landslides, etc.).

In addition, there could be an intensification of extreme precipitation events (higher intensities and frequencies), a phenomenon that is presently hard to simulate.

7.6.2 Measurement Techniques in Mountainous Regions

Measuring solid precipitation

In the same way as liquid precipitation, solid precipitation is measured by recording precipitation gages (heated type). These measurements are subject to the same types of error, the most important being the disturbance of the wind fields by the presence of the measurement device. Measurements often underestimate the real precipitation. For solid precipitation, the corresponding losses can amount to 20% or even 50%. Measurement stations in mountainous regions are particularly subject to systematic errors given that the proportion of solid precipitation is greater and the station locations are often highly exposed to the wind (Gottardi *et al*., 2012). Note that precipitation measurements supplied by national meteorological institutes have often been corrected. Such corrections are always imperfect. They are generally global and cannot for example take into account errors that vary with time.

Solid precipitation can also be estimated by measuring the evolution of snow cover on the ground with, in addition, an estimation (by measurement) of its water equivalent. The form of precipitation (rain, snow, hail, mixture) is not actually measured. It is sometimes estimated qualitatively by an operator on the basis of direct observation. If this information exists, it is generally discontinuous over time. In each of the climatological stations located in the Swiss Alps, the form of precipitation is for example estimated three times a day (at 07:30, 13:30 and 19:30). In France, the snow meteorology network supplies two measurements per day (at 08:00 and 13:00).

Measuring various properties of the snowpack

It is important to distinguish between point measurement techniques carried out on the ground and measurements based on remote sensing.

On the ground, snow depth and its evolution can be measured by manual reading of snow stakes or by automatic measurement stations. The latter carry out optoelectronic measurements based on ultrasonics (Brown and Goodison, 2005). Another solution consists in fixing a set of thermometers on a vertical stake to deduce the snow/atmosphere limit from the observed temperature gradient.

The water equivalent of the snow cover can be measured directly using snow pillows placed on the surface of the ground before the first snowfalls. They are made of a circular or octagonal

membrane (with an area of 5 to 10 m^2) containing an antifreeze fluid. Each pillow is equipped with a pressure sensor that measures variations of the load applied to the membrane by the accumulated snow (Dingman, 2002). Another type of measurement quantifies the water equivalent of the snow based on the attenuation of gamma rays emitted by a radioactive source or by the attenuation of cosmic radiation. The water equivalent of the snowpack can also be measured on the basis of its dielectric properties, in particular its electrical impedance (Marco *et al*., 1998). These indirect methods are however the source of major uncertainties.

Remote-sensing methods include satellite imagery and airborne measurement methods (for a detailed discussion, see Rango *et al*., 2000; Hall *et al*., 2005; Berthier, 2005, 2007). The extent of snow cover can be quantified on the basis of images in the visible or near-infrared spectrum. Such satellite images are already used operationally in a number of regions of the world (in particular in North America). Landsat Thematic Mapper satellite images can also be used to estimate snow albedo.

Snow depth can be estimated using microwave sensors or radar. These images are not obstructed by clouds (the main problem of images in the visible spectrum) however a number of other factors make them hard to use. For instance, the waves emitted by the snow are influenced by the liquid water contact, the structure and density of the snow and by the vegetal cover (Durand and Margulis, 2006; Andreadis and Lettenmaier, 2006).

Microwave images combined with *in situ* measurements make it possible to relate the optical properties of snow to its water equivalent. The spatio-temporal extrapolation of this relationship can be used to estimate water equivalent over a wider area.

Finally, a high-resolution laser altimeter can be used to estimate snow depth. This method requires a reference measurement on snow-free ground. Its major drawback is its high price.

Measurements on the ground are more accurate but lack spatial representativeness. Such point measurements are consequently hard to generalize. Spatialization must always take elevation into account. Kriging with external drift is sometimes used in this context (Tapsoba *et al*., 2005). Data obtained by remote sensing are often highly uncertain. Furthermore, they can be expensive to acquire, require a great deal of post-processing and are often not continuous over time. Ideally, several sources of information should be used simultaneously for modeling.

Measuring snow ablation

The most direct measurement of snow ablation is based on snow lysimeters that collect, at the base of the snowpack, meltwater coming from the superimposed snow layers above and deliver it to flow measurement devices.

Snow ablation can also be monitored by snow pillow measurements. Snow sublimation can be measured using evaporation pans that are weighed on a regular basis. This type of device can be equipped to separately quantify losses by melting and sublimation. Note that these measurement instruments are placed under the snow layer and therefore modify its properties, creating discontinuities that can modify the radiation balance and separate the snow layer from the ground. The effect of interception can be estimated on the basis of snow depth measurements made in forested areas.

7.6.3 Estimating the Different Terms of the Snowpack and Snowmelt Energy Balance

This appendix presents the formulas often used to estimate the different terms of the energy balance of the snowpack. For more detailed information, the reader is invited to consult Lehning (2005) in English or Boone and Etchevers (2001) in French. Similar formulas are used to estimate the energy balance terms of glaciers. They are described by Hock (2005).

Net absorbed radiation (longwave and shortwave) R_n

The quantity of energy provided by radiation depends on the albedo α of the surface of the snowpack, shortwave solar radiation R_S and net longwave radiation R_b. The way to estimate these different quantities is described in Appendix 2.7.4. Longwave radiation emitted by the snowpack depends on the snowpack surface temperature T_s.

The albedo can change significantly over time as a result of snowpack aging and fresh snowfalls. Empirical models are sometimes used to simulate albedo. For periods between two snowfalls, the albedo is often assumed to decrease exponentially or linearly and the corresponding time constants are parameters that must be estimated (Boone and Etchevers, 2001). In the event of a snowfall, the albedo is often increased in proportion to the snowfall depth.

Heat exchanges at the snow-atmosphere interface

Sensible heat transfer H_h. Heat exchanged between the air and the snow due to a temperature difference between them is governed by turbulent exchange processes in the boundary layer of the atmosphere. The different variables required for its estimation are not often available. For this reason, the sensible heat H_h [J/m²/h] supplied by convection is often estimated using the following simplified equation:

$$H_h = D_h \cdot u_z (T_z - T_s) \tag{7.20}$$

where D_h is the coefficient of proportionality, known as the bulk transfer coefficient for sensible heat transfer and equal to approximately 3400 J/(km/h)/°C for surfaces without trees (see Singh and Singh, 2001, for other values). u_z is the wind speed [km/h] at altitude z above the ground ($z = 2$ m) and T_z and T_s [°C] are the air temperatures respectively at altitude z and at the surface of the snowpack.

Latent heat transfer H_{ph}. Depending on atmospheric conditions, condensation, melting and sublimation processes lead to an exchange of latent heat (phase change heat) between the air and the surface of the snow. Condensation takes place generally when the vapor pressure of the air exceeds that at the surface of the snow at 0°C. Assuming that the vapor pressure of the air above the surface of the snow is often equal to the saturated vapor pressure $e_0(T_s)$, the quantity of heat H_{ph} [J/m²/h] provided by condensation is:

$$H_{ph} = D_{ph} \cdot u_z (e_z - e_0) \tag{7.21}$$

where D_{ph} [J/(km/h)/mb] is an empirical coefficient (+/–2800 J/(km/h)/mb), u_z the wind speed [km/h] at altitude z above the ground and e_z the vapor pressure [mb] at altitude z. $e_0(T_s)$ is a function of surface temperature T_s ($e_0(T_s) = 6.11$mb at 0°C). The latent heat flux H_{ph} can be used to estimate the water flux E associated with phase change. This flux plays a role in the snowpack mass balance equation (eq. 7.2).

Conducted heat transfer H_g at the ground-snow interface. The quantity of heat H_g conducted between the ground and the snowpack depends in particular on the temperature gradient dT_g/dz normal to the ground surface.

$$H_g = k_g \cdot \frac{dT_g}{dz} \tag{7.22}$$

The dimensionless constant k_g depends on the properties and moisture content of the ground as well as the properties of the ground/snow interface. During the melting period, snow melt corresponding to this the term varies between 0.1 and 1.5 mm/day.

Conducted heat transfer H_p at the snow-rain interface

When liquid precipitation reaches the snowpack, its initial temperature T_p decreases and the temperature of the snow surface T_s increases to establish a thermal equilibrium at the final temperature

T_r. The quantity of heat transmitted by the rain water to the snowpack is the difference between the thermal energy in the rain before it reaches the snowpack and after it reaches thermal equilibrium with the snowpack. It is directly proportional to the quantity of rain and the rain/snow temperature difference.

Under melting conditions (initial temperature of the surface of the snowpack $T_s = 0°C$, positive energy balance), the quantity of heat H_p [J/m²/h] provided by the rain for melting is:

$$H_p = \rho_l \cdot c_l \cdot P / 1000 \cdot (T_p - T_s)$$

(7.23)

where T_p [°C] is the temperature of the rain, P the quantity of rain [mm/h], c_l the specific heat of liquid water [J/kg/°C] and ρ_l the mass density of liquid water [kg/m³].

When the snowpack temperature is negative, different situations can occur depending on the available energy. Either some or all of the precipitation freezes or the temperature of the entire snowpack is raised to 0°C and any surplus energy leads to partial melting of the snowpack.

Quantities

Specific heat of solid water (ice or snow): $c_s = 2.09 \cdot 10^3$ J/kg/°C

Specific heat of liquid water: $c_l = 4.185 \cdot 10^3$ J/kg/°C

Mass density of water at 0°C: $\rho_l = 1000$ kg/m³

Mass density of glacier ice at 0°C: $\rho_g = 917$ kg/m³

Latent heat of fusion of ice at 0°C: $L_i = 335 \cdot 10^3$ J/kg

Latent heat of vaporization of water at 0°C: $L_v = 2501 \cdot 10^3$ J/kg

Latent heat the sublimation of snow at 0°C: $L_s = 2834 \cdot 10^3$ J/kg

Latent heat of fusion of snow: L_s. Under standard atmospheric conditions and for snow at 0°C, the value for snow is near that of ice at 0°C. It varies slightly with the initial water content and temperature of the snowpack.

Thermal quality of the snow: χ. The ratio of the heat required to melt a unit weight [kg] of snow to that required to melt a unit weight [kg] of pure ice at 0°C. It depends on the water content and mean temperature of the snowpack. It is slightly higher than 1 when the temperature of the snowpack is negative. Its value is between 0.95 and 0.97 for snow with a water content of 3 to 5%. It can be expressed as: $\chi = (L_s + c_s T_s) / L_i$, where T_s [°C] is the temperature of the snowpack.

7.6.4 GSM-SOCONT—A Simple Glacio-hydrological Model

The GSM-SOCONT (Glacier and SnowMelt SOil CONTribution) model was developed by the former Hydrology and Land Improvement Laboratory (HYDRAM), now the Ecohydrology laboratory (ECHO), of the Ecole Polytechnique Fédérale of Lausanne for various applications in mountainous regions such as flood forecasting, design flood prediction or estimation of the potential hydrological impact of climate change (Schaefli *et al*., 2005; Hamdi *et al*., 2005; Horton *et al*., 2006; Mezghani and Hingray, 2009; Hingray *et al*., 2010). Only the basic version using a daily time step is presented below (Schaefli *et al*., 2005). Another version takes into account the saturation of the snowpack and the possibility of refreezing of meltwater before infiltration or runoff (Horton *et al*., 2006; Mezghani and Hingray, 2009).

This conceptual reservoir-based model is of the semi-distributed type. Each sub-basin is divided into glacierized and non-glacierized parts and each of these entities is subdivided into elevation bands. The same parameters apply to all elevation bands. The model includes four modules dedicated to: 1) spatial interpolation of the meteorological variables, 2) simulation of snow accumulation and the melting of snow and ice, 3) the transformation of meltwater and rainfall into runoff and 4) streamflow

routing. The model used to simulate discharges at the outlet of each sub-basin is described below. The routing of the contributions of the different sub-basins through the hydrographic network is, if applicable, carried out using a Muskingum model (Chapter 6).

Simulations are carried out separately for each elevation band j of each sub-basin. The total discharge Q [m³/s] of the sub-basin is calculated as follows:

$$Q(t) = \sum_{j=1}^{n} Q_j(t) \tag{7.24}$$

where $Q_j(t)$ [m³/s] is the mean daily discharge of the jth elevation band over time step t and n is the total number of elevation bands.

Spatial interpolation of meteorological series

Precipitation. Assuming that a precipitation gradient exists for each time step, the total precipitation $P_M(t)$ falling at point $M(x_0, y_0)$ over time interval $[t, t+\Delta t]$ can be estimated as a weighted mean of the point precipitation values $P_i(t)$ observed over Δt at the n nearest rain-gage stations. These point values are first multiplied by a factor $\Lambda_{M,i}$ to take into account their elevation differences with respect to point M:

$$P_M(t) = \sum_{i=1}^{n} W_{M,i} \times \Lambda_{M,i} \times P_i(t) \tag{7.25}$$

where $\Lambda_{M,i} = 1 + \dfrac{\alpha}{P_i} \left[Z_M - Z_i \right]$ \hfill (7.26)

and $W_{M,i}$ is the weighting factor associated with the ith rain-gage station for the considered spatialization method (e.g., Thiessen or inverse distance method), Z_M and Z_i are respectively the elevations [m] of point M and the ith rain-gage station, P_i is the mean interannual precipitation [mm] measured at the ith station and α is the local (or regional) precipitation gradient [mm/m/an]. Equation 7.25 can depend on the season and/or weather type, in which case it will be adapted accordingly.

Temperatures. For a drainage basin with a mean elevation Z_R, taken as the reference elevation, the temperature assumed to be representative of the temperature of elevation band j is calculated using the following formula:

$$T_j(t) = \sum_{k=1}^{NsT} W_k \cdot \left(T_k(t) + \nabla(t) \cdot \left(Z_j - Z_k \right) \right) \tag{7.27}$$

where $T_j(t)$ is the mean daily temperature of elevation band j, $T_k(t)$ the mean daily temperature of the kth temperature measurement station, W_k the weighting factor associated with the kth station and determined on the basis of the contour of elevation band j and the locations of the stations (Thiessen or inverse distance method) and $\nabla(t)$ is the regional daily temperature gradient.

Accumulation and melting of snow and ice

The following distribution function is used to estimate the proportion of total precipitation falling in liquid and solid form for each elevation band j (belonging to the glacierized part G and non-glacierized part NG):

$$S_j(t) = \begin{cases} P_j(t) & \text{if } T_j(t) < T_a \\ \dfrac{(T_b - T_j(t))}{(T_b - T_a)} P_j(t) & \text{if } T_a < T_j(t) < T_b \\ 0 & \text{if } T_j(t) > T_b \end{cases} \tag{7.28}$$

$$Pl_j(t) = P_{tot,j}(t) - S_j(t)$$ (7.29)

where $S_j(t)$ [mm] is snowfall, $Pl_j(t)$ [mm] rainfall, $T_j(t)$ [°C] the mean temperature of elevation band j, $P_j(t)$ [mm] total precipitation, T_a [°C] the threshold under which all precipitation falls in the form of snow and T_b [°C] the threshold above which all precipitation falls as rain.

The evolution of the snowpack depth $H_{s,j}$ [mm] can be calculated as:

$$\frac{H_{s,j}(t)}{dt} = S_j(t) - M_{s,j}(t)$$ (7.30)

where $M_{s,j}(t)$ [mm/day w.e.] is snowmelt calculated as follows:

$$M_{s,j}(t) = \begin{cases} 0 & \text{if } T_j(t) \leq T_m \\ a_s(T_j(t) - T_m) & \text{if } a_s(T_j(t) - T_m) \leq H_{s,j}(t) \\ H_{s,j}(t) & \text{if not} \end{cases}$$ (7.31)

where a_s [mm/°C/day] is the degree-day factor for the snow, T_m the melting threshold (0°C) and $H_{s,j}(t)$ [mm/day w.e.] the snow depth at the beginning of time step t.

For glacier-covered elevation bands ($\forall j \in G$), the same degree-day approach is used to simulate the amount of melted ice $M_{g,j}$ [mm/day w.e.]:

$$M_{g,j}(t) = \begin{cases} a_g(T_j(t) - T_m) & \forall j \in G \text{ if } H_{n,j}(t) = 0 \\ 0 & \text{if not} \end{cases}$$ (7.32)

where a_g [mm/°C/day] is the degree-day factor for the glacier ice. If the amount of ice stored on an elevation band is unknown, it is assumed to be infinite. For long simulation periods, the extent of glacier cover must be regularly updated.

The transformation of snow into firn and ice is not simulated. The same equations and parameters apply for the simulation of seasonal snow cover on non-glacierized elevation bands ($\forall j \in NG$) and for the simulation of permanent ice cover on glacierized bands ($\forall j \in G$).

Rainfall and meltwater transformation into runoff

For glacier-covered elevation bands ($\forall j \in G$), rainfall and meltwater are transformed into runoff using two linear reservoirs (see Chapter 5):

$$q_{s,j}(t_2) = q_{s,j}(t_1) \cdot e^{-\frac{t_2 - t_1}{k_s}} + [Pl_j(t_2) + M_{s,j}(t_2)] \cdot (1 - e^{-\frac{t_2 - t_1}{k_s}})$$ (7.33)

$$q_{g,j}(t_2) = q_{g,j}(t_1) \cdot e^{-\frac{t_2 - t_1}{k_g}} + M_{g,j}(t_2) \cdot (1 - e^{-\frac{t_2 - t_1}{k_g}})$$ (7.34)

where $q_{s,j}(t_i)$ [mm/day] and $q_{g,j}(t_i)$ [mm/day] are the runoff coming respectively from the snowpack and the glacier ice over time step t_i and Pl_j [mm/day] is the rainfall. k_s [1/day] and k_g [1/day] are the release constraints of the snow and ice reservoirs.

The total discharge $Q_{j,j \in G}(t)$ [m³/s] of a glacierized elevation band j corresponds to:

$$Q_{j,j \in G}(t) = c_u A_j[q_{s,j}(t) + q_{g,j}(t)] \qquad \forall j \in G$$ (7.35)

where c_u the unit conversion coefficient and A_j [km²] is the area of the elevation band.

For each non-glacierized elevation band ($\forall j \in NG$), the equivalent rainfall $P_{eq,j}(t) = Pl_j(t) + M_{s,j}(t)$ is transformed into runoff using the SOCONT model (Berod, 1995). This model is composed

of a linear reservoir that takes into account infiltration processes (slow reservoir) and a non-linear reservoir for the simulation of surface runoff (fast reservoir).

The equivalent rainfall is divided into net rainfall $P_{net,j}(t)$ [mm/day] supplying the fast reservoir and infiltration $P_{inf,j}(t)$ [mm/day] supplying the slow reservoir:

$$P_{net,j}(t) = P_{eq,j}(t) \cdot \left(\frac{S_{tj}(t)}{S_{t\,max}} \right)^2 \quad \forall j \in NG \tag{7.36}$$

$$P_{inf,j}(t) = P_{eq,j}(t) - P_{net,j}(t) \quad \forall j \in NG \tag{7.37}$$

where $S_{tj}(t)/S_{t\,max}$ is the fill fraction of the slow reservoir, $S_{t\,max}$ [mm] is the maximum storage capacity and $S_{tj}(t)$ is the storage at the beginning of time step t.

The slow reservoir has two outlets: 1) the base flow $q_{b,j}(t)$ [mm/day] that depends linearly on $S_{tj}(t)$ and the actual evapotranspiration $ET_j(t)$ [mm/day] that is a function of maximum evapotranspiration, expressed for the hydrologist community (see Chapter 4) as PET(t) [mm/day]:

$$ET_j(t) = PET(t) \cdot \left(\frac{S_{tj}(t)}{S_{t\,max}} \right)^{0.5} \quad \forall j \in NG \tag{7.38}$$

$$q_{b,j}(t) = k_l \cdot S_{tj}(t) \quad \forall j \in NG \tag{7.39}$$

where k_l [1/day] is the slow reservoir constant.

The first component of discharge is simulated by the following non-linear relationship:

$$q_{r,j}(t) = \beta \cdot J^{1/2} \cdot h_j(t)^{5/3} \quad \forall j \in NG \tag{7.40}$$

where $q_{r,j}(t)$ [mm/h] is the fast discharge, J [m/m] is the mean slope of the drainage basin, $h_j(t)$ [mm] represents the reservoir level at the beginning of time step t and β is a parameter to be calibrated.

The total discharge from a non-glacierized elevation band, $Q_{j,j\in NG}(t)$ [m³/s], therefore corresponds to:

$$Q_{j,j\in NG}(t) = c_u A_j(t)[q_{b,j}(t) + q_{r,j}(t)] \quad \forall j \in NG \tag{7.41}$$

where c_u is a unit conversion coefficient and A_j [km²] is the area of the elevation band. The GSM-SOCONT model has 7 parameters to be calibrated: a_g, a_s, A, k_g, k_s, k_l and β. A semi-automatic calibration method for these parameters and their possible range of variation can be found in Schaefli *et al.* (2005) or more recently in Hingray *et al.* (2010).
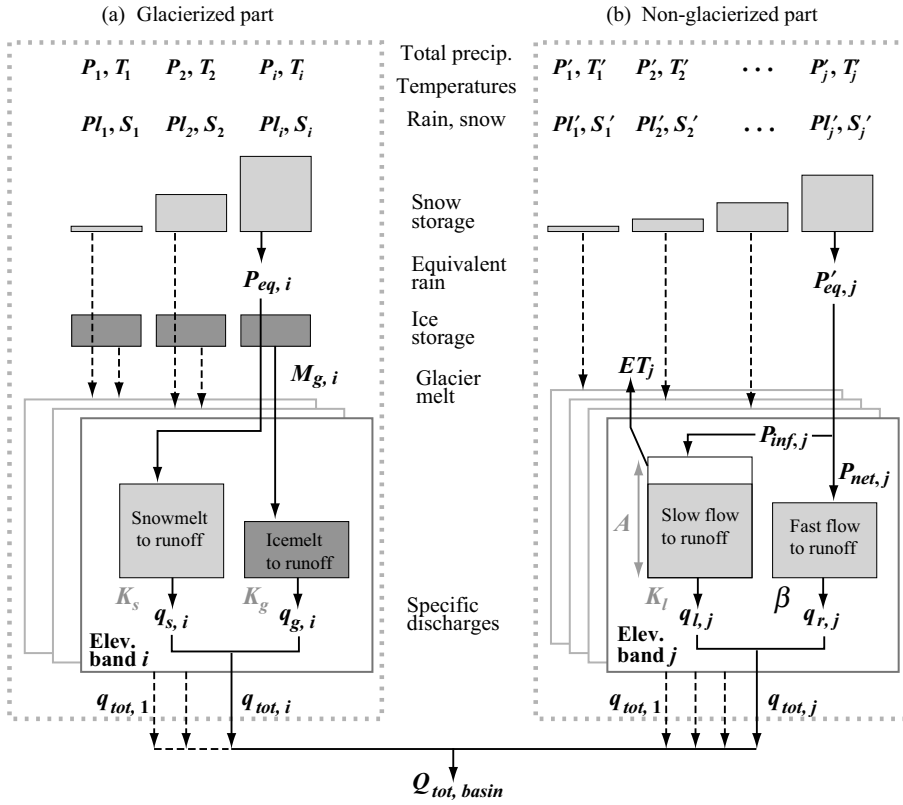
The model is illustrated schematically in Figure 7.15.

Fig. 7.15: Schematic illustration of the GSM-SOCONT conceptual model. See text for the notation.

CHAPTER 8

LOW-FLOW PREDICTION AND FORECASTING

Long overlooked, low flows—both in terms of discharges and water levels—are becoming increasingly important to hydrologists as well as public authorities and the overall population. This new awareness is the consequence of the ever-growing pressure placed on the water resources of streams and rivers. It also stems from the fact that water availability and needs rarely coincide due to the random nature of climate and its seasonal variability. Our society is therefore obliged to orient its activities according to available resources.

In this context, the estimation of water resources in rivers and in particular the minimum flows that can occur over a given period is an important input for water use planning (e.g., irrigation, water supply, hydropower, cooling water). In particular, it is important to set limits on controlled inflows and outflows so as to maintain suitable conditions in the watercourse during low-flow periods.

For example, a minimum discharge is often required to preserve aquatic life. One reason for this is to provide sufficient dilution of wastewater to attenuate the possible harmful effects of chemical and organic pollution. A minimum discharge may also be required to maintain a sufficient flow velocity to avoid the risk of sludge deposits near wastewater outlets or an increase in water temperature that could diminish the aeration capacity of the river

Understanding and/or estimating low flows is therefore essential to well-balanced and effective management of water resources taking into account the ecological requirements of streams and rivers.

This chapter presents information and methods required to analyze and estimate low flows. Section 8.1 first defines certain terms related to low flows and discusses various regulatory aspects. The main methods used to estimate low-flow discharges are also presented according to the objectives to be achieved. Section 8.2 deals with the methods used to predict characteristic low-flow discharges for design purposes, in the same way as flood discharges. Section 8.3 presents methods for forecasting low flows, as for floods, in order to improve the short-term management of water resources. For more information on low flows, the reader can refer to the extensive review published by Smakhtin (2001).

8.1 INTRODUCTION

8.1.1 Recession, Low Flows and Droughts

In the absence of precipitation, snowmelt and other inputs, the water stored in the hydrographic network of a basin and in the ground are drained by the network. Streamflows therefore decrease regularly. The curve representing this decrease of discharge with time at a given point of the network is referred to as the recession curve. The release of water stored in the network itself generally has a marginal effect on recession, the corresponding volumes being several orders of magnitude lower than groundwater volumes. Furthermore, water stored at the surface is generally transformed into runoff much faster than groundwater given the very low flow velocities of the latter.[1] The recession curve is therefore often considered to be the part of the hydrograph generated uniquely by groundwater flows after all surface flows have ceased.

To identify recession on a hydrograph, the different flow components must be separated. Different separation techniques are described in Appendix 8.5.1. Figure 8.1 shows two recession curves obtained after separating flows using the so-called graphical method. This widely used technique is based on a semi-logarithmic plot of discharge versus time. Such a representation is used to reveal discontinuities in the flood recession hydrograph and consequently the different flow components.

The term low flow is defined in a number of ways. According to the International Glossary of Hydrology (WMO, 1974), low flow is the "flow of water in a stream during prolonged dry weather". Low flow can also be obtained as a result of a long period of low temperatures that produce an accumulation of precipitation in the form of snow (no liquid precipitation) and prevent the melting of snow cover. A low-flow period refers to
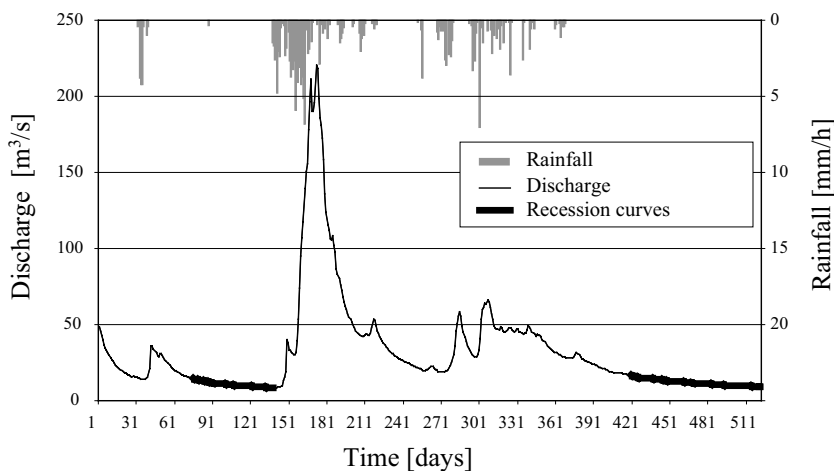

Fig. 8.1: Discharge versus time and empirical recession curves for the Emme drainage basin at Emenmatt station in Switzerland (recession not influenced by new rainfall supplying the reserves).

_____

[1]This is not necessarily the case for drainage basins with significant karst formations.

the period or periods of the years during which streamflows or water levels are the lowest. These periods are generally the same from one year to another. Snow-cover driven low flows are for instance observed in winter in Nordic countries. The term low flow also refers to the lowest value of discharge or water level observed in a stream during an average hydrological year.

A distinction must also be made between low flows and droughts. Low flows are regular seasonal phenomena that can take place in summer or winter (depending on the hydrological regime of the drainage basin), resulting from a prolonged recession of a watercourse. Low flows are an integral part of the hydrological regime of any watercourse. A drought, on the other hand, is an exceptional low flow sequence resulting from less than normal water inputs over an extended period. These lower inputs can be the result of a major precipitation deficit or an extended period of exceptionally low temperatures.

For more information on problems related to droughts, the reader is invited to refer to the many publications cited in Smakhtin (2001).

8.1.2 Factors Affecting Low Flows

Natural factors that influence low flows include the distribution and properties of soils, the hydraulic characteristics and extent of aquifers, the rate, frequency and amount of groundwater recharge, evaporation and evapotranspiration rates over the basin, the spatial distribution of vegetal cover, topography and climate.

Various anthropogenic factors can also significantly affect low flows. For example, the construction of dams and water withdrawn from or discharged into a watercourse for agricultural, industrial or municipal purposes have a direct impact on low flows. Other anthropogenic activities have an indirect impact, for example groundwater pumping, artificial drainage of soils for agriculture, land-use modifications related to urbanization and deforestation or reforestation. Figure 8.2 illustrates the typical effect of a water diversion project on the flow-duration curves of a watercourse (Section 8.2.2).
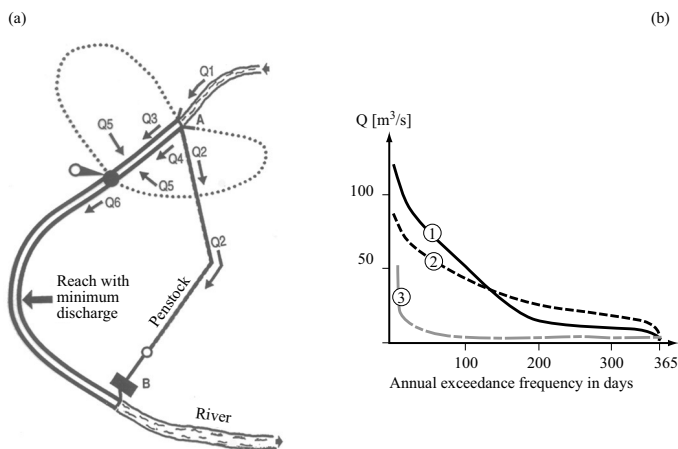
Fig. 8.2: Illustration of the influence of a water diversion project on the flow-duration curves of a watercourse. a) Basin configuration with diversion works at A and return of water (e.g., after turbining) at B. b) Flow-duration curves based on observations: (1) upstream of the diversion (corresponding to the "natural" flow), (2) downstream of the water return point and (3) between the diversion and water return points (reach with minimum discharge).

8.1.3 Characteristic Low-flow Discharges

Various characteristic low-flow discharges are generally defined to describe the low-flow regime of a watercourse. They can be divided into two types: 1) characteristic minimum discharges taken from chronological discharge times series and 2) discharges reached or exceeded *x* days per year on the average, determined from the annual flow-duration curves.

Characteristic minimum discharges

Various minimum discharges over a given period (hydrological or calendar year, season, month) can be determined on the basis of a chronological time series of mean daily discharges observed at a given measurement station (Figure 8.3). In this way, for a given year, it is possible to determine the annual minimum daily discharge, the minimum discharge for *n* consecutive days and the monthly minimum daily discharge (Table 8.1). Low-flow discharges are generally characterized by one of these characteristic discharges.

It is also possible to attribute, as for floods, a return period or a probability of non-occurrence to these characteristic flows. A frequency analysis of the different values of a characteristic flow over the *n* years of a given period can be used to attribute a return period to each of these values. For example, the quantity designated NM_7Q_5 corresponds to the lowest mean discharge over a period of 7 consecutive days with a 5-year return period, i.e., a 4 out of 5 probability of not being exceeded in a given year. $QMNA_5$ corresponds to the annual minimum monthly discharge with a 5-year return period (Joerin, 1995).

Table 8.1: Examples of characteristic low flows obtained from the chronological discharge time series of a watercourse. Different countries and/or institutions use different characteristic minimum discharge values (Joerin, 1995).

Characteristic discharge	Definition
Annual minimum daily discharge	The lowest daily discharge observed over the hydrological or calendar year.
Absolute minimum daily discharge	The lowest daily discharge over a long observation period (e.g., 20 years).
Q_n, NM_nQ, VCN_n	The lowest mean discharge value over *n* (1, 7, 14 or 30) consecutive days for the considered period (see graph below). This value is determined by identifying the lowest value of the series of sliding mean values over *n* consecutive measurement days.
QCN_n	The lowest maximum discharge value over *n* consecutive daily discharges, i.e., the minimum discharge which is not exceeded over *n* consecutive days (see graph below).
QMNA	The annual (A) minimum (N) monthly (M) discharge (Q) (i.e., the minimum value of the 12 mean monthly discharges of a calendar year).

Discharges reached or exceeded on the average x days per year

These characteristic discharges introduce the notion of a threshold, particularly useful when dealing with water uses. They are determined from flow-duration curves obtained for the considered measurement station. This curve represents the number of days for which the value of the mean daily discharge *Q*, plotted on the y-axis, was reached or exceeded during a year (Figure 8.4). Methods for constructing this curve are described in Section 8.2.2.
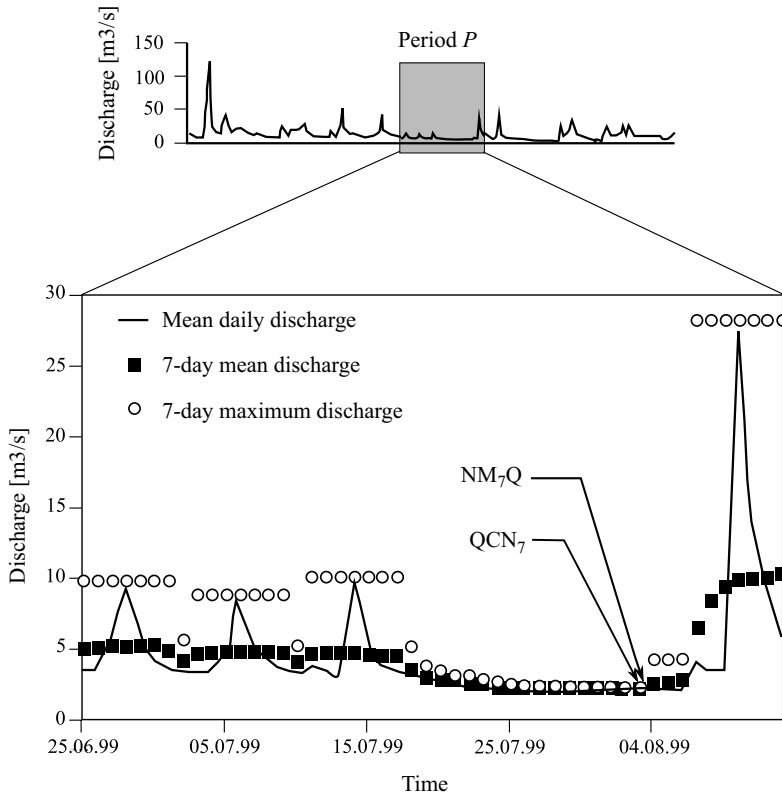
Fig. 8.3: Chronological discharge time series for the Broye river (Switzerland) for the year 1999 illustrating the determination of the QCN_7 and NM_7Q discharges (respectively the lowest mean and lowest maximum discharges over 7 consecutive days of the considered period P).

Table 8.2: Examples of characteristic low flows determined from the flow-duration curves (DC) of a watercourse (Joerin, 1995).

Characteristic discharges	Definition
DCE or *DC355*	Characteristic low-flow discharge, i.e., the daily discharge reached or exceeded on the average 355 days a year.
DC1, *DC3* and *DC6*	Discharge reached or exceeded during respectively 1, 3 and 6 months a year.
Q_{347} (or $Q_{95\%}$)	Discharge reached or exceeded on the average 347 days a year (i.e., 95% of the time).

8.1.4 Low-flow Regulations and Related Issues

As already pointed out in the beginning of this chapter, acceptable conditions must be maintained in rivers during critical low-flow periods. For this reason, special regulations, agreements and laws have been set up in recent years. They generally define minimum streamflows required to maintain water supply to communities and/or preserve aquatic life.
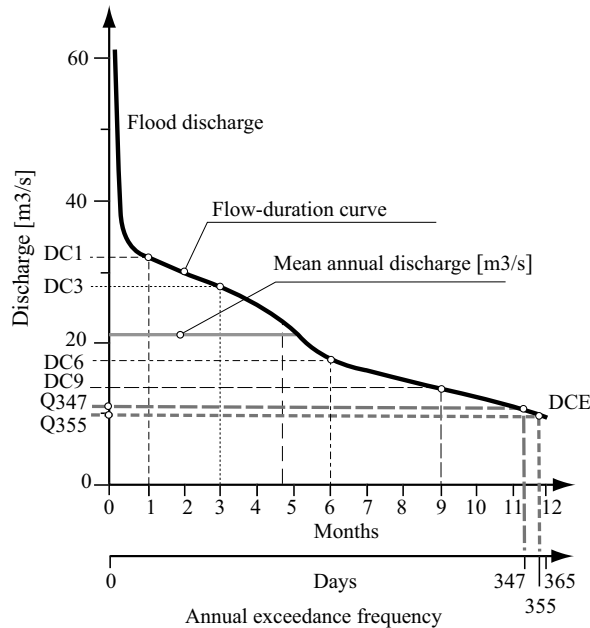
Fig. 8.4: Flow-duration curve and characteristic low-flow discharges.

For example, in Germany, more particularly in Baden-Württemberg, the authorities propose a certain minimum discharge NM_7Q_5 that must be respected by the different users of river water resources. In Switzerland, a law passed in 1992 imposes certain minimum discharges estimated on the basis of Q_{347} (Appendix 8.5.2). In France, the reference low-flow discharge for quality objectives and for regulations concerning effluent flows into rivers and diversions is the five-year minimum mean monthly discharge ($QMNA_5$).

8.2 PREDICTION METHODS

Prediction of low flows is an important problem that consists associating recurrence intervals or return periods with estimated low-flow discharges.

This provides the basis for determining the characteristic low-flow discharges required to establish regulations concerning the protection of water resources.

Low-flow prediction methods are based either on historical low-flow data or on a frequency analysis of discharges observed over a given period. Hydrological simulation models or regional methods are also often used when few or no observed discharges are available. These different approaches are described below.

8.2.1 Prediction based on Historical Data

The historical method is not really a prediction method given that it does not necessarily provide a recurrence interval for estimated low-flow discharges. It is based on the assumption that it is relatively unlikely to observe low flows as severe as those observed over a sufficiently long past and requires a careful and detailed study of local discharge

records (e.g., official archives of governmental organizations or local communities, hydrological yearbooks, historical studies).

Low flows are rarely well documented. Compared to floods, low flows are often far less spectacular and rarely leave identifiable physical evidence behind them. This historical method must therefore be applied with caution and the results compared with those of other prediction techniques.

8.2.2 Frequency Analysis of Low Flows

Frequency analysis can have one or two objectives presented below. In both cases, sufficient data are required.

One objective is to determine how many days per year, on the average, a given mean daily discharge Q is reached or exceeded. The other objective is to determine the value of the mean daily discharge Q that is, on the average, reached or exceeded n days per year. The flow-duration curve must be constructed to meet either of these objectives.

Frequency analysis can therefore be used to determine the return period of a characteristic low flow or inversely the value of the characteristic low flow corresponding to a given return period T (Addendum 8.1). This method uses classical frequency analysis techniques applied to a sample of N estimates of the characteristic low flow obtained over a long observation period (Meylan *et al*., 2012).

Addendum 8.1 Non-exceedance probability and return period

If the hydrological quantity of interest is a random variable designated X, the probability that a realization of this quantity will be less than or equal to a set value x is expressed by:

$$P(X \leq x) = F_X(x) \tag{8.1}$$

where $F_X(x)$ is the distribution function of the variable X. This probability is referred to as the non-exceedance frequency or probability. The return period T of an event is generally defined as the reciprocal of the frequency or probability of exceedance of the event p where $p = 1 - F_X(x)$. This gives:

$$T = \frac{1}{p} = \frac{1}{1 - F_X(x)} \tag{8.2}$$

Consequently, a maximum flood discharge with a return period T is the discharge that will be exceeded on the average once every T years (i.e., k times in kT years).

For low flows, the non-exceedance of x sometimes refers to the fact that the value of X remains greater than or equal to x. The non-exceedance frequency of X is then defined by $F_X(x) = P(X \geq x)$ The return period is once again expressed by equation 8.2.

If the number of discharge observations available is insufficient, frequency analysis of low-flow discharges can be based on reconstructed discharge data. The reconstruction of the discharge time series is generally based on long series of various relevant meteorological variables (precipitation and evapotranspiration in particular) using a deterministic continuous simulation hydrological model. The hydrological model must obviously represent the main processes producing the low flows, in particular losses related to evaporation losses (e.g., evapotranspiration).

Flow-duration curves estimation methods

Flow-duration curves have many possible applications both in engineering and water resources management (Vogel and Fennessey, 1995). Two main methods are used to estimate flow-duration curves:

- Global method over a long period. Using a classical statistical approach, the daily discharges observed over the *n* considered years are classed in decreasing order. For discharge *Q*, the annual exceedance frequency (in %) is then given by the ratio *x/N*, where *x* (the rank) is the number of days during the *n* years for which the discharge was greater than *Q* and *N* is the number of days in the *n* years considered. For example, the discharge Q_{347} corresponds to a 95% exceedance probability ($Q_{347} = Q_{95\%}$). Figure 8.4 illustrates such a flow-duration curve. The preferred units for the frequency expressed on the x-axis is the number of days ((x/N)×*365*).
- Method based on the mean or median of annual flow-duration curves. For each of the *n* years of observations, an annual flow-duration curve is determined. The curve for the entire period is then obtained by calculating the mean—or median—of the discharges of the *n* annual curves for each frequency (i.e., number of days of exceedance). For example, the value of Q_{347} read on such a curve corresponds to the arithmetic mean of the *n* annual Q_{347} values.

The median method is recommended by Vogel and Fennessey (1994). It is expected to be to be able to represent the distribution of discharges for a typical year of the considered period. The global method seems to be excessively dependent on the period considered. This is particularly a limiting factor when the flow-duration curve must be regionalized using the flow-duration curves of different basins for which data are not available over the same periods (Niadas, 2005). The construction of a flow-duration curve for each year of the observation period is also worthwhile in that it can provide the confidence intervals of the main curve as well as the return periods of certain characteristic low-flow discharges (Vogel and Fennessey, 1994).

Return period of a characteristic low-flow discharge

Low flows, as for most hydrological processes, can be considered to be a random process. The different values of a characteristic low-flow discharge (e.g., NM_nQ) over a given period can therefore be considered as different realizations of a random variable. Frequency analysis of these values can be used to determine the frequency model that best describes the statistical behavior of this variable.

For low flows, the theoretical distributions generally used are the Log-normal, Log-Pearson III, Weibull and Fréchet distributions (Abi-Zeid and Bobee, 1999; Meylan *et al.*, 2012). For convenience, frequency analysis is sometimes carried out on the logarithms of discharges. The distribution of low-flow discharges can also have an unusual shape not corresponding to any common theoretical distribution. In this case, a graphical fitting procedure can be used.

By fitting a theoretical distribution or an empirical model, the low-flow discharge for a given exceedance frequency can be determined or, on the contrary, the return period of an observed discharge (Example 7.1). For more information on distribution fitting techniques

for frequency analysis and in particular the various steps to be followed when fitting a frequency model, see Meylan *et al*. (2012). Some important aspects to be considered in this type of analysis are mentioned in Addendum 8.2.

Addendum 8.2 Overview of frequency analysis in hydrology (see Meylan *et al*. (2012) for more details)

A frequency model describes, in an analytical manner, the relationship between the value of the considered hydrological variable (e.g., the characteristic low-flow discharge or the characteristic flood discharge) and its exceedance probability—often expressed by its return period in years. The use of a frequency model makes it possible to estimate discharge values for events with different return periods and in particular return periods that are higher than those of the events represented in the sample.

Before statistically processing the acquired data, it is essential to make sure that they are representative, homogeneous, plausible, independent and stationary. These techniques are also an integral part of preliminary data processing. In this respect, note that discharge data are frequently non-stationary due to the modification of hydrosystems by human activities (e.g., Figure 2.4).

Sufficient data must be available to fit the model. If this condition is not satisfied, statistical procedures can be used to artificially increase the number of data values for fitting. For example, data can be truncated above a given threshold to produce a "peak over threshold" series or more data can be sampled for each year of the considered period by taking the k greatest annual values, producing a so-called "inflated" series (Lang *et al*., 1999; Meylan *et al*., 2012). Frequency corrections are necessary in this case.

The choice of the experimental frequency formula (e.g., Hazen, Hirsch, Gringorten) used for frequency analysis and the choice of a frequency model depends on the data and phenomena considered.

A model is the simplified representation of the real statistical behavior of the considered hydrological variable. It is therefore necessarily imperfect. It is essential to verify the statistical fit by appropriate tests—including a visual check—and to qualify the results obtained by considering their confidence intervals.

Use of a frequency model for extrapolation can lead to very different quantile estimates depending on the frequency model and parameter estimation technique used.

Use of a regional frequency model, constructed on the basis of all available and useful hydrological information for the considered region, generally increases the robustness of estimates (Chapter 11).

Example 8.1

The low-flow discharge data indicated in the table below (column 3) come from the Murg drainage basin at Murgenthal (Switzerland) for the 1981–2004 period. These data have been positioned on the Gumbel plot using the Hazen plotting position formula (Meylan *et al*., 2012). For this, the values of the sample are first classed in decreasing order. The number of the order within the classed series is the rank *r*. As opposed to the case for maximum flood discharges, rank 1 is assigned to the highest low-flow discharge (i.e., the most frequent) and rank *n* (*n* being the sample size) to the lowest value (i.e., the least frequent). If the value of the low-flow discharge corresponding to rank *r* is designated *x*[*r*], the empirical non-exceedance frequency of this value (in the sense used for low flows, see Addendum 8.1) estimated using the Hazen formula is: $\hat{F}\left(x_{[r]}\right) = \dfrac{r - 0.5}{n}$.

Frequency fitting was carried out on the logarithms of the discharges using the theoretical Gumbel distribution. Estimation of low-flow discharges for different return periods are indicated in the table below. They are obtained on the basis of the equations corresponding to the following Gumbel frequency model:

$$Log \; \hat{Q}_{14}(T) = \hat{a}_{14} + \hat{b}_{14} \cdot u(T) = \hat{a}_{14} - \hat{b}_{14} \cdot \ln\left(-\ln(1 - 1/T)\right) \tag{8.3}$$

where $u(T)$ is the reduced Gumbel variable for return period T and $\hat{a}_{14}$ and $\hat{b}_{14}$ are the parameters of the frequency estimation model estimated using the moments method.

Table 8.3: Annual minimum mean 14-day discharges.

| Rank	Non-exceedance frequency	Q_{14} [m³/s]	LogQ_{14}
1	0.02	2.43	0.386
2	0.06	2.39	0.378
3	0.10	2.29	0.359
4	0.15	2.25	0.353
5	0.19	2.20	0.342
6	0.23	2.17	0.336
7	0.27	2.16	0.334
8	0.31	2.11	0.324
9	0.35	2.08	0.318
10	0.40	2.06	0.313
11	0.44	1.86	0.269
12	0.48	1.79	0.254
13	0.52	1.77	0.248
14	0.56	1.69	0.227
15	0.60	1.63	0.211
16	0.65	1.62	0.210
17	0.69	1.59	0.200
18	0.73	1.52	0.183
19	0.77	1.52	0.181
20	0.81	1.35	0.130
21	0.85	1.27	0.103
22	0.90	1.15	0.061
23	0.94	1.12	0.050
24	0.98	0.98	−0.008
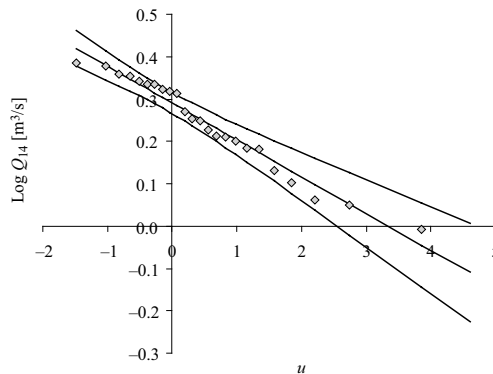
Fig. 8.5: Frequency analysis of annual low-flow discharges Q_{14} and Gumbel frequency estimation (with the 80% confidence interval according to the formula of Dick and Darwin, see Meylan *et al.*, 2012).

Table 8.4: Estimates of low flows for different return periods.

T [years]	F(T)	*u*(T)	LogQ_{14}	Q_{14} [m³/s]
2	0.50	0.37	0.26	1.30
5	0.80	1.50	0.16	1.17
10	0.90	2.25	0.09	1.10
20	0.95	2.97	0.03	1.03
50	0.98	3.90	−0.05	0.95
100	0.99	4.60	−0.11	0.90

8.2.3 Predicting Low Flows on Ungaged Basins

The basic principles for basins without data are detailed in Chapter 11. The methods used more specifically for low flows are covered briefly below.

Multiple regression

The advantage of regionalizing hydrological characteristics with multiple regression is the immediate and straightforward nature of the method. The regression model provides a relationship between the characteristic low-flow discharge *Y* and certain pertinent characteristics of the drainage basin. The model is of the type:

$$Y = b_0 + \sum_{i=1}^{N} b_i \cdot X_i + \varepsilon \tag{8.4}$$

where X_i is the ith of the *N* considered characteristics of the drainage basin, b_0 and b_i are the regression parameters and ε is the error of estimate of the regression line.

The objective of the regression analysis is to express as much of the discharge variance as possible with the least number of explanatory variables. It is therefore important to select, among available variables, only those that have a certain influence on the low-flow process. Demuth (1993) investigated 30 studies dealing with the regionalization of low-flow discharges by regression analysis. The 120 models of this investigation were constructed on the basis of 374 different explanatory variables. Certain variables, more frequently used than others, appear to have a determining influence on the low-flow process (Table 8.5). Physical variables (e.g., morphology, land use, geology and pedology) are the most frequently used (73% of the 374 variables). They are followed by various climatological (22%) and hydrological (5%) variables.

A regression model can also be determined for a characteristic low-flow discharge corresponding to a given return period. For example, the following equation is used for ungaged basins in Germany to estimate the lowest 7-day mean discharge [m³/s] with a 5-year return period (NM_7Q_5):

$$NM_7Q_5 = 7.296 \cdot 10^{-8} \cdot A^{0.966} \cdot P^{1.535} \tag{8.5}$$

where *A* is the area of the drainage basin [km²] and *P* the mean annual precipitation [mm].

Low-flow estimation models obtained by multiple regression are valid only in the region for which they were developed and for drainage basins respecting the application constraints (e.g., Example 8.2).

Table 8.5: The 10 most often used low-flow explanatory variables in the 120 models considered by Demuth (1993).

Drainage basin characteristics	Frequency of use
Drainage basin area [km^2]	66%
Mean annual precipitation [mm]	49%
Soil index*	22%
Mean elevation of the drainage basin [m]	15%
Proportion of lake to drainage basin area [%]	13%
Proportion of drainage basin above tree-line [%]	13%
Slope of the main river [m/km]	12%
Weighted lake proportion [%] **	11%
Low-flow index ***	10%
Drainage density [km/km^2]	10%

*   Index characterizing the soil of a region based on its potential infiltration capacity.

**   Lake proportion weighted by the area drained by each lake of the drainage basin.

*** Proportion of base flow with respect to the observed discharge.

Example 8.2

___

In Switzerland, the National Hydrological Survey used a direct regression method to estimate the Q_{347} discharges of drainage basins of the Swiss Alps region with mean elevations above 1550 m and areas between 10 and 500 km² (Aschwanden, 1993).

Northern Alps $\Rightarrow q_{347} = -6.59562 + 0.002391 \cdot mH + 1.0142 \cdot Mq_{\min}$

Southern Alps $\Rightarrow q_{347} = -4.73404 + 0.001915 \cdot mH + 0.8141 \cdot Mq_{\min}$

where q_{347} [l/s/km^2] is the specific discharge reached or exceeded, on the average, 347 days per year, mH [m] the mean elevation of the drainage basin and Mq_{min} [l/s/km^2] the lowest mean monthly specific discharge. Mq_{min} is also estimated using mathematical regressions based on the climatic and hydrological conditions as well as the physical parameters of the studied drainage basin. These parameters can be evaluated from topographic and thematic maps covering all of Switzerland and from data records and archives.

___

Analog method

In this context, the analog method is based on the postulate that two basins presenting very similar hydro-physiographic characteristics (e.g., shape, relief, area, geology, pedology, soil cover) and climatic characteristics (e.g., precipitation and temperature) will also have similar low-flow characteristics (Chapter 11).

The analog method can be used to evaluate the order of magnitude of low-flow discharges on the basis of better-known values from one or more hydrologically similar watercourses.

Because low flows depend directly on groundwater percolation and storage conditions, the nature of the subsoil can lead to major differences from one basin to another in spite of similar basin shape, relief, vegetation and meteorological regime. Therefore, before

using the analog method, it is important to make sure that the pedological and geological properties of the basins are similar, in addition to the hydrological properties. Addendum 8.3 illustrates two such methods.

Addendum 8.3 Two analog methods for the regionalization of characteristic low flows

Specific discharge method

This method is based on the assumption that the specific low-flow discharges of two hydrologically similar drainage basins are approximately equal:

$$\frac{Q_{x_u}}{A_u} = \frac{Q_{x_g}}{A_g} \tag{8.6}$$

The low-flow discharge Q_{xu} of the ungaged basin can be expressed as follows:

$$Q_{x_n} = \left(\frac{A_u}{A_g}\right) \cdot Q_{x_g} \tag{8.7}$$

where Q_{xg} is the low-flow discharge of the gaged basin, A_u the area of the ungaged basin and A_g the area of the gaged basin. In general, discharges determined using this method should be considered as rough estimates however the results can be satisfactory if the ratio of areas is between 0.5 and 2.0. Note that this method should not be used on very small basins due to the non-linearity of their response. The quality of the results obtained using this method improves with the size of the basin studied. By increasing the size of the drainage basins, local variability is in a certain manner attenuated. However, above a certain threshold, additional inter-basin variability of large-scale factors such as geology or climate can come into play and affect the quality of the results. For France, Larras (1972) proposes an upper limit of 10,000 km² for the basin area.

Quantile ratio method for the estimation of Q_{347}

This method consists in estimating the Q_{347} discharge of an ungaged basin on the basis of appropriate discharge measurements carried out simultaneously on this basin and a hydrologically similar gaged basin. It is based on two assumptions:

- During low-flow periods, the discharges observed simultaneously in two basins of the same region have the same exceedance probability.
- The ratio between the Q_{347} discharge and another low-flow discharge quantile Q_x of the same drainage basin (where x is the exceedance frequency) is the same for all basins of a given region, such that:

$$\frac{Q_{347}(basin \cdot 2)}{Q_x(basin \cdot 2)} = \frac{Q_{347}(basin \cdot 1)}{Q_x(basin \cdot 1)} = constant \tag{8.8}$$

To determine the Q_{347} discharge of an ungaged basin (here *basin*2), the streamflow must be measured during a low-flow period (i.e., a period during which the discharge is between Q_{300} and Q_{365}) while observing the discharge Q_R on a reference basin (here *basin*1). The discharge $Q_{347}(basin2)$ is then given by equation 8.8 on the basis of the gaged discharge Q_{gaged} ($=Q_x(basin2)$), the discharge Q_R ($=Q_x(basin1)$) observed simultaneously on the reference basin and the value of $Q_{347}(basin1)$ for the reference station (R) (Figure 8.6). This method of course requires knowledge of the value of Q_{347} for the reference basin.
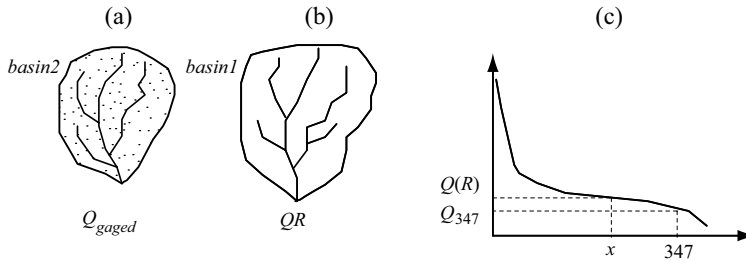
Q_{gaged} and QR must be determined on the same day during a low-flow period (exceedance frequency x).

Fig. 8.6: Illustration of the quantile ratio method designed to determine the Q_{347} discharge of an ungaged basin. a) Ungaged *basin*2. b) Gaged *basin*1. c) Flow-duration curves of the reference basin (*basin*1) based on at least 10 years of measurements.

The regionalization of Q_{347} is therefore in principle easy for a given region if the ratio Q_{347}/Q_x can be assumed constant for this region and is known for the reference station. Before applying this method, it is necessary to check the homogeneity of the considered region and the representativeness of the reference station chosen for the region.

Using the method described above, the Q_{347} discharge has for example been regionalized in Switzerland over the entire canton of Vaud. For this, streamflows were measured over the full length of the main rivers of the canton during a low-flow period. The Q_{347} discharges were then deduced for each measurement point. Finally, for each of the rivers, a relationship was established between the distance separating the measurement point from the basin outlet and the value of the Q_{347} discharge (Figure 8.7). This relationship can be used to determine the Q_{347} discharge at any point in the hydrographic network.
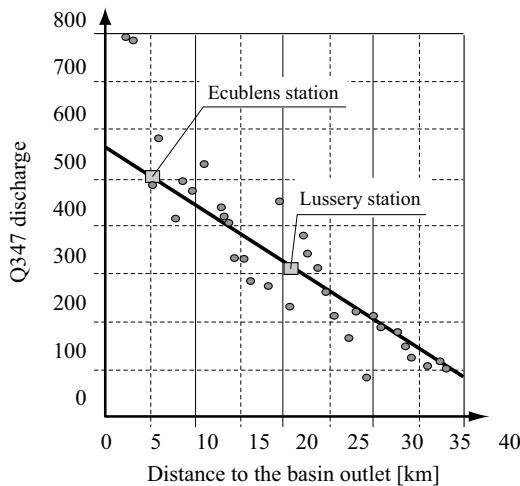

Fig. 8.7: Example of a relationship between the distance of a streamflow measurement point from the basin outlet and the Q_{347} discharge at that point (Venoge river, Switzerland).

Regional flow-duration curves

The two regional methods described above can only estimate a particular low-flow discharge. On the other hand, regional flow-duration curves can be used to estimate a full

range of characteristic low-flow discharges. A regional flow-duration curve is constructed using the flow-duration curves obtained for different gaged drainage basins belonging to a hydrologically homogeneous region (Chapter 11, Figure 11.7). These curves are normalized, superimposed and averaged—possibly with appropriate weighting—to produce the required regional curve (e.g., Niadas, 2005). The individual curves can be normalized with respect to the area of the drainage basin, the mean (or median) interannual discharge or any other appropriate flow index.

The flow-duration curve for an ungaged basin can then be obtained simply by multiplying the regional curve by the estimated normalization factor for this basin. The normalization factor (e.g., mean basin discharge) can also be estimated on the basis of an appropriate regional relationship (Niggli *et al.*, 1999).

Regionalized continuous simulation hydrological models

In ungaged basins, it is often possible to apply a regionalized hydrological model that can be used to reconstruct a discharge time series and deduce the flow-duration curves (Figure 11.10). In this case, the model parameters can be estimated from the different pertinent physical characteristics of the drainage basin. The basin must be hydrologically similar to the basins used to determine the relationships between model parameters and the physical characteristics of the basin. The reader can refer to Chapter 11 for more information on these regionalization techniques and to Perrin (2000) for an illustration of an application of such models.

8.3 FORECASTING METHODS

Low-flow forecasting is a key issue in the management of water resources. It consists in determining or evaluating the near-future evolution of low-flow discharges starting from a given date (initial time). By anticipating the moment when the discharge will drop below a critical level, it is possible for example to satisfy the requirements of regulations and optimize the use of water resources.

The most commonly used forecasting methods are based on recession curves, hydrological simulation models or on correlation analyses aimed at establishing relationships between the discharges to be forecasted and different pertinent explanatory variables.

8.3.1 Recession Curve Method

At the beginning of the 20th century, Boussinesq (1904) and Maillet (1905) proposed various mathematical relationships to describe the decrease of discharges in a watercourse in the absence of inputs (Perreira, 1977). For a given watercourse, a recession equation can be used to forecast the low-flow discharge at a given time in the future simply from the known initial discharge Q_0 (observed at time $t = t_0$).

Different recession equations exist. The choice of the one to use for a given case should be based on its ability to reproduce the observed recession curves. For more information on this subject, the reader can refer to the review by Tallasken (1995). In this section, only the most widely used equations will be presented.

Simple recession equations

The simple recession concept designates any recession of an aquifer, source or watercourse that takes place under conditions similar to those of release, in a hydrological regime not influenced by intermediate inflows and in the absence of groundwater losses,[2] from a confined or unconfined aquifer, whatever its depth. In other words, the simple recession process is equivalent to groundwater recession under conditions that can be assimilated to the emptying of a single aquifer. Under certain assumptions, solving the Boussinesq equation therefore gives different relationships of which the two most widely known are: 1) the simple exponential recession equation and 2) the simple hyperbolic recession equation (see expressions in Table 8.6).

Table 8.6: Simple exponential and simple hyperbolic recession equations.

Expression	Type of equation
$Q(t) = Q_0 \cdot e^{-\alpha \cdot (t - t_0)}$	Simple exponential
$Q(t) = \dfrac{Q_0}{\left(1 + \alpha \cdot (t - t_0)\right)^2}$	Simple hyperbolic

Where $Q(t)$ is the low-flow discharge at time t, α the recession coefficient and $Q_0 = Q(t_0)$ the initial discharge at time t_0.

Under certain assumptions (Addendum 8.4), the simple hyperbolic equation corresponds to the decrease of discharges from an unconfined aquifer above an impervious substratum located at a shallow depth. The simple exponential equation corresponds to the decrease of discharges from an unconfined aquifer above an impervious substratum located at a great depth below the bed of the river. The exponential equation can also be expressed in a discretized form as:

$$Q(t_0 + \Delta t) = c \cdot Q(t_0) \tag{8.9}$$

where c is the recession constant (less than 1) defined by:

$$c = e^{-\alpha \cdot \Delta t} \tag{8.10}$$

Consequently, the low-flow discharge at time $t_0 + n \cdot \Delta t$ can be expressed as:

$$Q(t_0 + n \cdot \Delta t) = c^n \cdot Q(t_0) \tag{8.11}$$

It can easily be demonstrated that the exponential recession equation corresponds to the discharge from a linear reservoir (Chapter 5), where groundwater storage S is related to streamflow Q by the following equation:

$$Q = \alpha\, S \tag{8.12}$$

---

[2]The water stored in the ground is assumed to be drained only by the hydrographic network of the considered basin, i.e., without any underground leakage to neighboring drainage basins.

Similarly, the hyperbolic recession equation corresponds to discharge from a reservoir with an outflow proportional to the square of the stored volume:

$$Q = \alpha \, S^2 \tag{8.13}$$

Coutagne (1948) proposed a more general recession equation corresponding to discharge from a non-linear reservoir with the following discharge equation:

$$Q = \alpha \, S^b \tag{8.14}$$

where b is a parameter corresponding to the degree of non-linearity of the recession discharge process. By combining equation 8.14 with the reservoir continuity equation, the following equation is obtained for the behavior of the reservoir:

$$\alpha \, S^b = -\frac{dS}{dt} \tag{8.15}$$

This expression is in fact valid for various other solutions of the Boussinesq equations (Rupp *et al.*, 2004).[3] When $b \neq 1$, the recession expression resulting from this representation is:

$$Q(t) = Q_0 \cdot \left[\; 1 + (b-1)\alpha^{1/b} Q_0^{(b-1)/b} \cdot \; (t - t_0) \right]^{-b/(b-1)} \tag{8.16}$$

It can also be written in the following form:

$$Q(t) = Q_0 \cdot \left[\; 1 + (b-1) \cdot (t - t_0) / \tau_0 \right]^{-b/(b-1)} \tag{8.17}$$

where $\tau_0 = S_0 / Q_0$ is the groundwater residence time at $t = t_0$. The exponential recession equation is a special case of equations 8.15 and 8.16 when $b = 1$. For the exponential equation, the residence time is the reciprocal of the recession coefficient α (α is therefore the reciprocal of a time and is expressed for example in s^{-1} if the unit of time is seconds).

Addendum 8.4 The Boussinesq equation

The Boussinesq equation describes the evolution of an aquifer draining into any type of groundwater catchment system (e.g., drain, well) under the following general assumptions (Soutter *et al.*, 2007):

- The soil is homogeneous and isotropic.
- The water and soil are incompressible and there is no other inflow or outflow within the flow domain.
- The substratum is horizontal and located at elevation $z = -D$, with the elevation datum taken as the free surface of the water in the groundwater catchment system.
- The aquifer is unconfined; therefore, when the water table level varies, the volume of water released or stored per unit volume of soil corresponds to the drainage porosity μ.

---

[3]Brutsaert and Nieber (1977) obtained a solution of this type for so-called short-term recession behavior (when the basin can be considered to be completely saturated and drainage is therefore not affected by the zero-flux condition at the drainage basin boundary) and for long-term recession behavior (when at every point of the basin, the soil is not saturated). Rupp *et al.* (2004) obtained an identical expression for an aquifer for which the hydraulic conductivity is assumed to vary with depth according to a logarithmic relationship.

- A zero-flux condition is imposed on the lateral boundaries of the flow domain and a zero-pressure condition is imposed at the entry point to the groundwater catchment system.
- In the saturated zone, the flow can be described by Darcy's law, the equipotential lines are assumed to be quasi-vertical and the same flow system is reproduced infinitely in the third dimension for linear catchment systems and by central symmetry in the case of point catchment systems. The flow is therefore mono-directional (direction *x*).

Under these conditions, the Boussinesq equation results from the combination of Darcy's law, integrated vertically, and the continuity equation. It represents the variation of the ordinate *h* of the water table surface as a function of the sole coordinate *x* (Figure 8.8).

$$\mu \cdot \frac{\partial h}{\partial t} = q_c(t) + \frac{\partial}{\partial x}\left[K \cdot (D + h) \cdot \frac{\partial h}{\partial x}\right] \tag{8.18}$$

where μ is the dimensionless soil drainage porosity, h [m] the height of the water table above the reference level z = 0, t [s] time, x [m] the distance along the x-axis, K [m/s] the hydraulic conductivity, D [m] the depth of the impervious substratum below the reference level and $q_c(t)$ [m³/m²] a uniform recharge term.
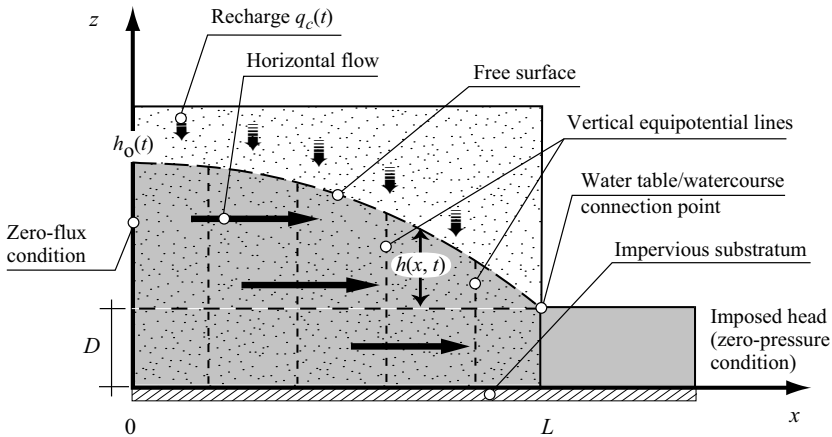

Fig. 8.8: Schematic representation of an unconfined aquifer with an initial non-horizontal profile under different assumptions concerning the application of the Boussinesq equations.

For a recession regime without recharge, i.e., $q_c(t)=0$, the Boussinesq equation can be solved by a classical variable separation method. For the special case of drains located either on the impervious substratum ($D=0$) or far above ($D \gg h$), the following two expressions are obtained:

$$(1) \quad q(t) = \frac{q_0}{\left(1 + a \cdot (t - t_0)\right)^2} \quad \text{where} \quad a = \frac{2 \cdot K \cdot h_0}{\mu N E^2} \tag{8.19}$$

$$(2) \quad q(t) = q_0 \cdot e^{-b \cdot (t - t_0)} \quad \text{where} \quad b = \frac{4 \cdot K \cdot d}{\mu N E^2} \tag{8.20}$$

and where $q(t)$ is the recession discharge per linear meter of the drain, h_0 the initial height of the water table (at $t=t_0$), N a water table shape coefficient, E the distance between drains, d the equivalent depth of the impervious substratum estimated on the basis of the Hooghoudt equations and q_0 the initial recession discharge that can also be expressed as a function of the initial conditions and the characteristics of the medium.

Compound recession equations

The recession cannot always be represented by the simple equations presented above. This is the case, for example, when recharge (in or out) must be taken into account or when the recession involves the draining of several aquifers. The latter case is referred to as compound recession. This can be dealt with in two ways. The first is to divide the recession curve of the watercourse into several segments, each corresponding to a simple recession equation. The second is to use a mathematical model with three or four parameters (Table 8.7).

Table 8.7: Example of complex recession equations with 3 or 4 parameters.

Expression	Type of equation
$Q(t) = \sum_{i=1}^{m} Q_{0_i} \cdot e^{-\alpha_i \cdot (t - t_0)}$	Compound exponential
$Q(t) = \sum_{i=1}^{m} \dfrac{Q_{0_i}}{\left(1 + \alpha_i \cdot (t - t_0)\right)^2}$	Compound hyperbolic
$Q(t) = \dfrac{Q_{0_1}}{\left(1 + \alpha_1 \cdot (t - t_0)\right)^2} + Q_{0_2} \cdot e^{-\alpha_{2i} \cdot (t - t_0)}$	Combined (exponential + hyperbolic)

The discharge at time *t* forecasted using any of the above recession equations is always strictly greater than zero. These equations are therefore not appropriate for hydrological contexts in which the streamflow can drop to zero. This is in particular the case for drainage basins in which the stored groundwater volume flows partly outside the basin boundaries. It is also the case for streamflows subject to major losses (e.g., by infiltration or evaporation) and for intermittent regimes (e.g., in arid regions). Other low-flow discharge forecasting approaches can be used for these cases (e.g., reservoir models proposed by Chapman, 1999).

Estimating the parameters

For simple recession equations, three parameters must be estimated: the initial discharge Q_0, the recession coefficient α and the non-linearity coefficient *b*. The recession coefficient α characterizes the draining rate, the coefficient *b* determines the shape of the recession curve and the initial discharge Q_0 indicates the volume of groundwater available at the time of the forecast. These three parameters depend on the properties of the soil and aquifers (e.g., depth, width, initial head, hydraulic conductivity, porosity). The initial depth Q_0 also depends on recent meteorological conditions affecting the drainage basin (e.g., precipitation and evapotranspiration).

During recession, the initial discharge Q_0 decreases with time, following more or less the recession equation identified for the watercourse. In operational mode, the value of the initial discharge can be updated as the forecast time t_0 advances (Chapter 10). This updating is often carried out on the basis of streamflow measurements at time $t = t_0$. It can also be deduced from discharge equations established on the basis of the boundary conditions of the considered aquifer. However, these boundary conditions are rarely known

at time t_0 and furthermore almost never correspond to the idealized framework required for the theoretical solution of the Boussinesq equations (Addendum 8.4).

As opposed to the initial discharge Q_0, the recession coefficient α and the non-linearity coefficient b are often considered to be constant for the considered basin and, in all cases, invariant over the forecast period (from t_0 to t_0+t). These two parameters must be known before a forecast can be made. They are estimated using recession curves identified within the discharge series available for the drainage basin (Appendix 8.5.3). To identify these curves, it is necessary to identify the time starting at which the observed discharge is supplied solely by groundwater recession. Often based on prior separation of the hydrograph, this identification is neither straightforward nor without uncertainty (Appendix 8.5.1).

Estimation of the parameters of complex recession equations is more difficult, in particular because several values of the initial discharge $Q_{0,i}$ must be estimated (Table 8.7). This estimation can be carried out by minimizing an objective function-based for instance on the least squares between the observed and simulated discharges. However, given the large number of degrees of freedom, different parameter sets are possible. The estimation is consequently not very robust and forecasting uncertainty can be high, increasing with the length of the forecasting period. For suitable management of discharges, this uncertainty must be characterized (Chapter 10).

8.3.2 Method based on Characteristic Recession Curves

For a given drainage basin, flood hydrographs and in particular their recession curves exhibit infinitely varied shapes. This is due to a number of factors including in particular the spatial distribution of initial soil moisture conditions and water table height as well as the spatial and temporal distribution of antecedent precipitation. Consequently, the recession of a watercourse can, depending on the event, follow the same equation with different parameter values or even different types of equations.

It is obviously difficult to account for all this variability. It can however be worthwhile to analyze and model the recession for different reasonably homogeneous configurations with respect to this phenomenon. For example, the year is often divided into periods or seasons during which losses and recharge are relatively uniform. In this way, a mean recession curve can be estimated for each of these periods. Different methods developed in this context are described in Addendum 8.5.

> **Addendum 8.5 Determining characteristic recession curves**
>
> Different ways of dividing up the year have been proposed to determine characteristic recession curves. For example, for an application in Switzerland, Pereira (1977) divided the year into two distinct periods in order to take into account the precipitation and evapotranspiration regime and their influence on the flow regimes. For the considered drainage basins, he therefore defined a summer season (from May to August) and an autumn season (from September to November). For each of these periods, he associated a characteristic recession curve representing the average discharge conditions of the basin.
>
> To obtain a characteristic recession curve, all observed recessions should be analyzed. These recessions are then divided up into several segments, corresponding to simple recession equations. The segments are then classed according to the value of their recession coefficient α, thereby forming groups of recession curves. Within each of these groups, the mean values of the recession coefficient α and discharges Q_0 are calculated, thereby defining the average

recession values (average segments). When a simple exponential type recession equation is chosen, different methods are available to estimate this mean recession coefficient α for each of the chosen periods (e.g., the graphical method of the master recession curve used by Sujono *et al.*, 2004). The characteristic recession curve is finally obtained by successively take into account these average segments.

Gloor and Walter (1986) propose a similar approach for dividing up the recession time into characteristic periods. They identify homogeneous recession periods according to mean reference evapotranspiration values MET_0, calculated as follows:

$$MET_0 = \frac{ET_{0i-4} + 3 \cdot ET_{0i-3} + 5 \cdot ET_{0i-2} + 7 \cdot ET_{0i-1} + 9 \cdot ET_{0i}}{25} \tag{8.21}$$

where ET_0 is the monthly reference evapotranspiration calculated using the Turc equation and MET_0 is the weighted mean monthly reference evapotranspiration from time step *i-4* to *i, i* varying from 1 to 12. It then becomes possible to distinguish three different hydrological and climatological periods, as shown in Figure 8.9. For each of these periods, a characteristic recession curve is defined. For each curve, it is possible to estimate the discharge at the given time simply knowing the mean evapotranspiration and initial discharge Q_0.
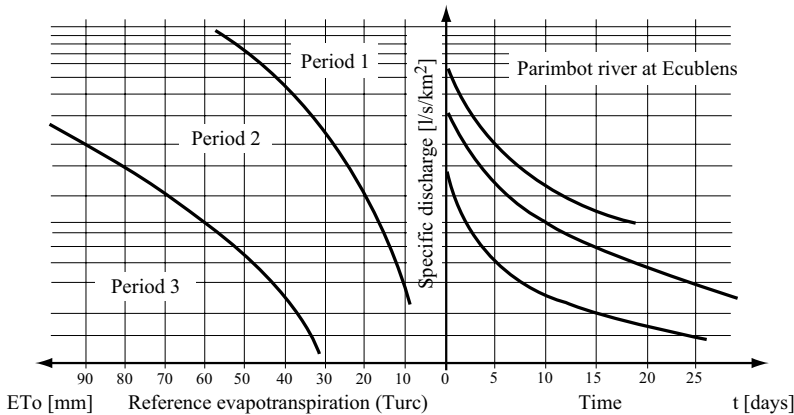

Fig. 8.9: Representation of the three hydrological periods and definition of the three characteristic recession curves for the Parimbot basin at Ecublens/Eschiens (Switzerland) according to Gloor and Walter (1986).

8.3.3 Correlation or Regression Model Method

The low-flow discharges of a watercourse depend on the state of water storage in the basin before the recession period. This in turn depends on climatic aspects such as precipitation, temperature and evaporation. For this reason, it is possible to look for correlations between low flows and local or even regional climatic parameters. Such relationships are of the type

$$Q_t = f(Q_0, P_i, T_i, ...) \tag{8.22}$$

where Q_t is the low-flow discharge at time *t*, Q_0 the discharge at the beginning of the recession curve, i.e., at forecast time t_0, P_i the precipitation that fell during the periods preceding time t_0 and T_i the temperatures observed during the periods preceding time t_0. The correlation relationship is often a simple multiple regression equation. Q_0 is naturally a key explanatory variable.

8.3.4 Hydrological Simulation Models

Most of today's hydrological models can carry out continuous simulations. If meteorological forecasts are available for the temporal horizon of interest or if it is possible to estimate the probable evolution of the key meteorological variables influencing low flows (in particular ET_0), it is in principle possible to use these models to forecast low-flow discharges over the hours to come.

For this, it is first necessary to check that the ability of the hydrological model to simulate low flows was included as a performance criterion for the development and calibration of the model. Furthermore, a module to update the model, its state variables and its parameters is often necessary to regularly bring the initial state simulated by the model for the present time in line with the real state observed in the field (see Chapter 10 for more information on this topic).

Note that the simple recession equations presented in Section 8.3.1 are often obtained implicitly with basin hydrological models since delayed flows are often simulated using reservoirs (linear or non-linear).

8.3.5 Water Volumes Stored Within the Drainage Basin

One application of recession equations is to determine the volume of water stored as groundwater at a given time.

If the pure recession (i.e., regime not influenced by intermediate inflows) equation $f(t)$ of the drainage basin is known, the volume of water stored in the basin can be evaluated by integrating this equation over the time interval $[t_0, +\infty]$ (Figure 8.10). The volume of water $V(t_0)$ present within the drainage basin at time t_0 is given by:

$$V(t_0) = \int_{t=t_0}^{\infty} f(t) \cdot dt = \int_{t=t_0}^{\infty} Q(t) \cdot dt \tag{8.23}$$

For a simple exponential recession equation and taking $t_0 = 0$, the equation becomes:

$$V(t_0) = \int_{t_0}^{\infty} Q_0 \cdot e^{-\alpha \cdot t} \cdot dt = Q_0 \cdot \left[-\frac{1}{\alpha} \cdot e^{-\alpha \cdot t} \right]_{t=0}^{\infty} = \frac{Q_0}{\alpha} \tag{8.24}$$
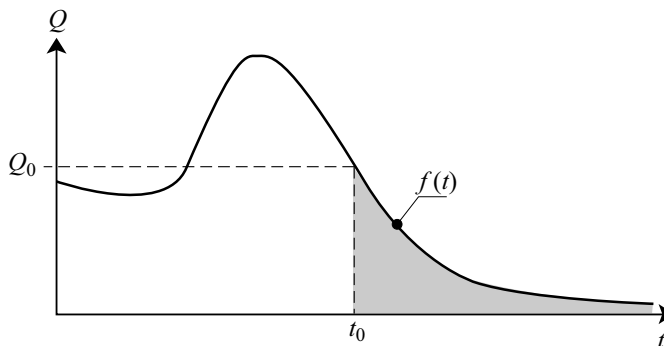

Fig. 8.10: Volume of water stored within a drainage basin (gray volume *V*).

The calculated volume of water can be used to evaluate the possibility of low-flow compensation during the dry period of a given region.

Note that the estimate of the volume stored within the basin depends on the recession model used and that this estimate remains an approximation.

8.3.6 Forecasting Low Flows on Ungaged Basins

After regionalization, low flows can be forecasted on an ungaged basin using any of the models presented above. Two types of data must be regionalized: 1) the parameter(s) used to describe the shape of the recession curve—for instance the recession coefficient α and the non-linearity coefficient b in the case of simple recession curves and 2) the value of the initial discharge Q_0 at time $t=t_0$. For the recession equation shape parameters, as for the value of the initial discharge, different regionalization methods can be used (Chapter 11). If the shape parameters can be estimated a priori for an ungaged basin, the same is not true for the initial discharge $Q(t_0)$. This value must be regularly re-estimated on the basis of continuous real-time measurements carried out for example on similar basins located near the ungaged basin and in particular subject to the same precipitation forcing.

8.4 KEY POINTS OF THE CHAPTER

- Knowledge of low flows is essential to the management of water resources for the estimation of available water and the preservation of the quality of the river habitat.
- Ideally, before any analysis of low flows on a given basin, the different processes or factors influencing the low-flow discharges should be identified
- Flow-duration curves can be used to determine different characteristic low-flow discharges including the Q_{347} discharge.
- The Q_{347} discharge is the mean daily discharge reached or exceeded, on the average, 347 days a year.
- Certain characteristic low-flow discharges, such as the Q_{347} discharge in Switzerland (or the $Q_{95\%}$ discharge in France), provide the basis of regulations setting the minimum residual discharges to be maintained in a watercourse.
- The return period of a characteristic low-flow discharge such as the NM_7Q discharge can be estimated on the basis of an appropriate frequency analysis.
- For an ungaged basin, characteristic low-flow discharges can be estimated by different regional methods (regression, analog method or simulation using a regionalized hydrological model).
- The most widely used methods to forecast low-flow discharges are based on the use of recession curves or hydrological models.
- For a given basin, the parameters of a given recession equation generally vary from one event to another. After separating the hydrograph, these parameters can be estimated on the basis of observed recession curves. For a simple exponential recession equation, the recession coefficient α can be estimated by graphical fitting of the observed data.
- Use of a continuous simulation hydrological model to reconstruct characteristic low-flow discharges or to forecast low flows requires prior verification of the suitability and performance of the model for the simulation of low flows.

• To compare certain low-flow characteristics over *n* basins, the pedological and geological properties of the basin must be similar. The same is true for characteristics related to the vegetal cover, topography or climatic context.

8.5 APPENDICES

8.5.1 Flow Separation Methods

The objective of separating flows is to identify the different components of the total flow observed at a given streamflow measurement station. The components to be separated depend on the purpose of the study. Generally, base flows (slow flows), observed more or less continuously on a given watercourse, are separated from direct flows (fast flows) observed irregularly on the occasion of precipitation events. Slow flows are often considered to be the result of draining from aquifers and fast flows are related to surface and sub-surface runoff resulting from recent precipitation on the basin. Several separation methods can be used.

• *Separation using environmental tracers.* Environmental tracers are often used to separate "old" water (water in the soil) from "new" water (rainwater) (Musy and Higy, 2011). This technique is however not well-suited to the identification of base flows given that base flows and "old" water are not necessarily related in a simple manner.

• *Graphical separation.* The separation of the base flow of the total hydrograph consists in identifying the times when direct flows starts and finishes. The beginning of fast flow simply corresponds to the time when the discharge starts to increase. The end of direct flow can be determined on the basis of the decreasing function of the logarithm of discharge versus time. This function is linear before and after the end of direct flow, but with different slopes. The end of direct flow corresponds to the point of intersection of the two lines (bottom graph in Figure 8.11). The base flows between these two critical points of the flood hydrograph are classically interpolated by one of two methods: 1) simple linear interpolation or 2) so-called concave interpolation (Figure 8.11). The major drawback of these techniques is that they are manual and therefore cannot be used to separate long discharge series.
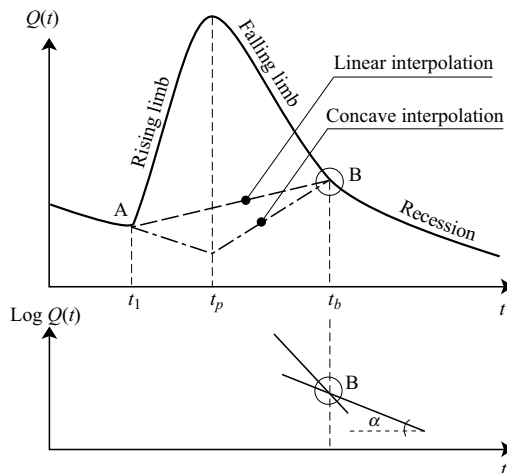

Fig. 8.11: Determining base flows by graphical separation.

• *Numerical separation*. Many numerical methods are available. Some are based on the identification of characteristic points in the total discharge series and on linear interpolation of base flows between these characteristic points. This is the case for the so-called BFI method presented below. Most of these methods are based on the use of numerical filters presenting varying degrees of sophistication. These filters use the values of total discharge over the previous two or three time steps to estimate the base flow at a given time.

Example 8.1

Separation using the base-flow index method.

The base-flow index (BFI) is an index that measures, over a given period, the proportion of base flow in the total discharge of a watercourse (ratio of the volume coming from base flow to the total measured volume). The so-called BFI flow separation method proposed by the British Institute of Hydrology (1980) is described below (Figure 8.12):

The discharge series is divided into successive periods of f_1 hours. For each of these periods, the minimum flow is identified. The series (Q_1, Q_2, ..., Q_n) of minimum discharge values over the *n* consecutive intervals of f_1 hours is thus obtained.

Blocks of three successive intervals (Q_1, Q_2, Q_3), (Q_2, Q_3, Q_4), ..., (Q_{n-1}, Q_n, Q_{n+1}), etc. are formed and, in each case, if the central value multiplied by a coefficient f_2 to be estimated is less than the two other values, it is retained as a turning-point of the base-flow line. Once all the data have been analyzed, a set of values QB_1, QB_2, ..., QB_i separated by variable time intervals is obtained.

The turning-points are finally joined together by linear interpolation to produce a base-flow line for an hourly time step. If any value Qb_i obtained in this way is greater than the value Q_i of the observed discharge, Qb_i is replaced by Q_i.
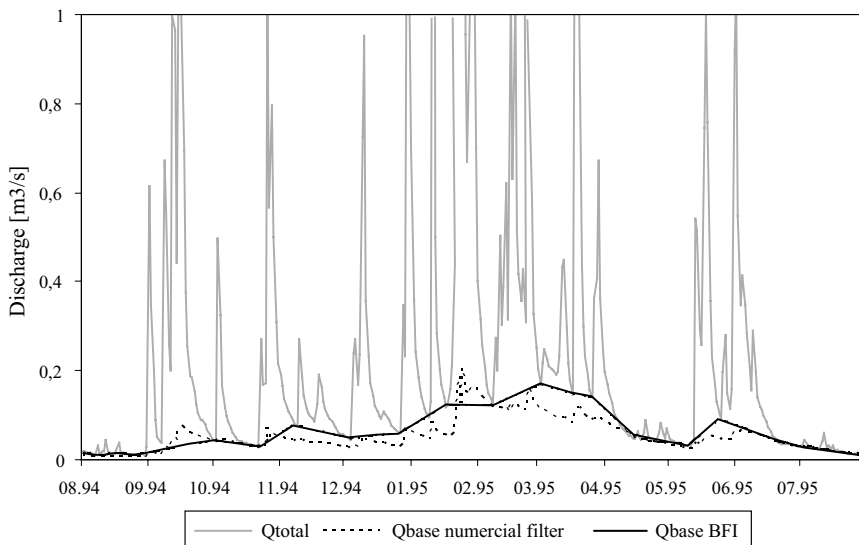

Fig. 8.12: Determination of the base flow of the Parimbot basin (Switzerland) for the period August 1994 to July 1995 using the so-called BFI method and a numerical filter. The BFI method separation parameters are: $f_1 = 120$ hours and $f_2 = 0.9$. The numerical filter proposed by Chapman (1999) has the following three parameters: $K = 0.984$, $C = 0.025$ and $\alpha_r = 0.67$.

The calculation window and the turning-point identification factor are often assigned the values f_1=120 hours and f_2=0.9 respectively. The series of base flows obtained using this separation is sensitive to both these parameters and in particular f_1. If f_1 is increased, the series of base flows tends to be smoother and the BFI lower. In practice, these parameters must be adjusted to the considered basin.

Example 8.2

Separation by numerical filtering.

Most numerical filters are empirical or conceptual. In the usual form of the linear module of the IHACRES model for example (Jakeman and Hornberger, 1993), the net rainfall $u(i)$ is assumed to produce a slow base flow $Q_b(i)$ and a rapid flow $Q_r(i)$ expressed as follows:

$$Q_b(i) = \alpha_b \cdot Q_b(i-1) + \beta_b \cdot u(i) \tag{8.25}$$

$$Q_r(i) = \alpha_r \cdot Q_r(i-1) + \beta_r \cdot u(i) \tag{8.26}$$

Eliminating the net rainfall from these two equations and expressing the rapid flow $Q_r(i)$ as the total flow $Q(i)$ minus the slow flow $Q_b(i)$, the following expression is obtained for the base flow:

$$Q_b(i) = \frac{k}{1+C} \cdot Q_b(i-1) + \frac{C}{1+C} \cdot \left[Q(i) - \alpha_r \cdot Q(i-1) \right] \tag{8.27}$$

where $C = \dfrac{\beta_b}{\beta_r}$ and $k = \alpha_s + \alpha_q \cdot \beta_s / \beta_q$ \hfill (8.28)

Equation 8.27 is the expression for the numerical filter used to estimate the base-flow series solely from the total discharge series. Note that the rate of variation of the base flow is positively correlated with the rate of variation of the total flow in the watercourse. Taking $\alpha_r = 0$, the two-parameter filter proposed by Boughton (1993) is obtained. The three parameters k, C and α_r of the filter (as for the parameters of any numerical filter) are calibrated to give a satisfactory signal. The satisfaction criteria for this estimation are in fact highly subjective and the estimation of the parameters is consequently delicate. When separation with this filter is carried out over a sufficiently long period, it is possible to obtain the following analytical expression of the BFI (Chapman, 1999):

$$BFI = \frac{C \cdot (1 - \alpha_r)}{1 + C - k} \tag{8.29}$$

Other numerical filters have for example been presented by Arnold and Allen (1999) and Eckhardt (2005).

8.5.2 Swiss Water Protection Act

The Swiss Water Protection Act was passed on 24 January 1991 in order to protect the quality of water resources, particularly in rivers. This law includes measures to protect water against pollution and to maintain suitable residual discharges in watercourses.

One new aspect of this law is the necessity of an authorization before diverting water from a permanently flowing watercourse. Articles 29 to 36 lay down the rules aimed at maintaining suitable residual discharges.

In particular, Article 31 of the law stipulates the minimum residual discharges to be maintained when diverting water. The limiting values are based on the Q_{347} discharge (Figure 8.13). Figure 8.13 expresses the empirical concept according to which a relatively small watercourse requires a residual

discharge greater than that of a large watercourse. The effective residual discharge, i.e., the discharge remaining after diversion, must never be less than the minimum residual discharge defined by this law.

The competent authorities are however free to set higher residual discharges (see Article 33 of this law). In this case, the authorities must take care to respect local interests that can be taken into account according to an impact study (Figure 8.14).

For each case, the competent authority sets the allocated flow and other measures necessary to protect watercourse downstream of the diversion. This allocated flow is defined as the discharge required to respect the residual discharge (minimum). The minimum flow can vary with time. These flows must not be less than the set minimum residual discharge.
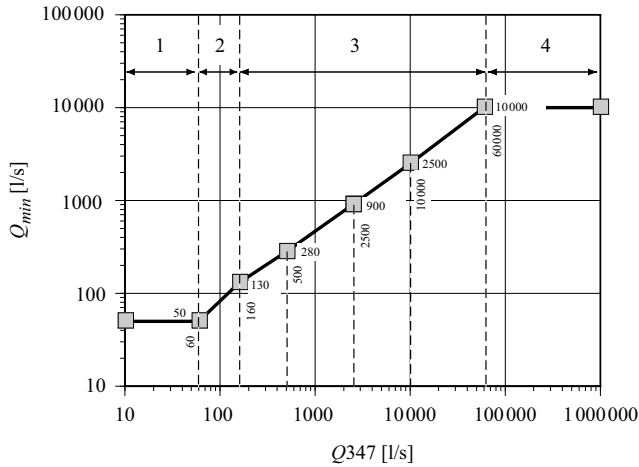

Fig. 8.13: Minimum residual discharge Q_{min} versus Q_{347}. Q_{min} is the minimum discharge to be conserved in a watercourse in accordance with Article 31 of the Swiss Water Protection Act.
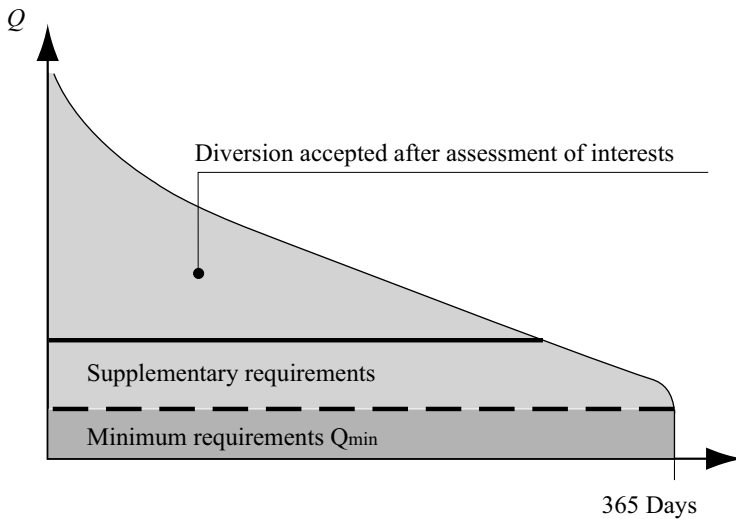

Fig. 8.14: Diversion of water from the river authorized in accordance with the Swiss Water Protection Act.

8.5.3 Estimating the Parameters of a Simple Recession Equation

In the particular case of a simple exponential recession equation, the recession coefficient α can be obtained by graphical methods. Using logarithms, the exponential recession equation can be written:

$$\ln Q(t) = \ln Q_0 - \alpha \cdot (t - t_0) \tag{8.30}$$

The logarithm of the discharge becomes a linear function of time. The slope of the line is the coefficient α and the ordinate at the origin is the initial discharge Q_0. The recession line can be fitted graphically to the observed points ($t, ln(Q(t))$) to determine the constants Q_0 and α (e.g., Figure 8.15).

For the general case of recession obtained on the basis of the non-linear reservoir model of equation 8.15, estimation of the two parameters α and b is less straightforward. For a chosen value of parameter b, one possible method consists in estimating the parameter α by considering the empirical expression and a theoretical expression (along the lines of eq. 8.14) of the base flow volume flowing over a given time step Δt:

Empirical expression: $Vobs_i \approx 0.5\left(Q_{i-1} + Q_i\right) \cdot \Delta t \tag{8.31}$

Theoretical expression: $Vsim_i \approx -\left(S_i - S_{i-1}\right) = 1/\alpha^{1/b}\left(-Q_i^{1/b} + Q_{i-1}^{1/b}\right) \tag{8.32}$

The equality of empirical and theoretical volumes flowing over the recession period lasting between t_0 and t leads to the following expression for the parameter α (Wittemberg, 1999):

$$\alpha \approx \left(\frac{2 \cdot \sum_i \left(Q_{i-1}^{1/b} - Q_i^{1/b}\right)}{\sum_i \left(Q_{i-1} + Q_i\right) \cdot \Delta t}\right)^b \tag{8.33}$$

The parameter b can be estimated using an iterative approach that compares the observed and simulated recession curves for the event considered for different parameter sets (α, b).
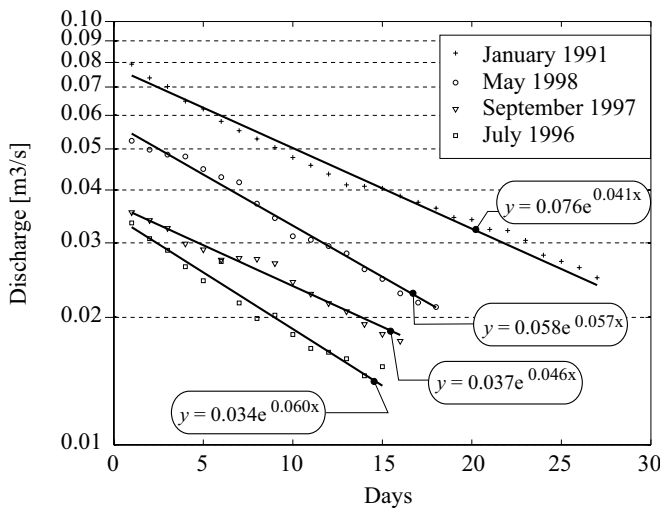

Fig. 8.15: Representation of simple exponential recession for two distinct events on a semi-log plot.

Instead of analyzing the hydrograph $Q(t)$ itself, another method consists in considering the slope of the hydrograph as a function of $Q(t)$. It can easily be demonstrated that equation 8.15 can also be written in the form:

$$-\frac{dQ}{dt} = f(Q) \text{ where } f(Q) = A\,Q^B \tag{8.34}$$

and where A and B are two parameters that are functions of α and b.

$$A = b \cdot \alpha^{1/b} \text{ and } B = 2 - 1/b \tag{8.35}$$

By taking the logarithm of equation 8.34, the two parameters A and B can be estimated graphically, giving the parameters α and b of equations 8.15 or 8.16. Practically speaking, the graph required for this estimation can be constructed from discharge measurements carried out during recession, on the basis of points with the following coordinates (Brutsaert and Nieber, 1977):

$$x_i = \left(\frac{Q_{i+1} + Q_i}{2}\right) \text{ and } y_i = \left(\frac{Q_{i+1} - Q_i}{\Delta t}\right) \tag{8.36}$$

where Δt is the time steps separating two successive measurements of discharges Q_i and Q_{i+1} (Figure 8.16). The advantage of this graphical method is that it allows simultaneous analysis of a large number of recessions by capturing the mean statistical behavior. According to Brutsaert (2005), it is possible to assume that low flows correspond to the points on the graph for which the value $|dQ/dt|$ is the lowest for a given value of Q (or for which the value of Q is the greatest for a given $|dQ/dt|$). Consequently, the relationship $f(Q)$ of equation 8.34 corresponds, for this type of representation, to the bottom line of the point swarm envelope.

This method is however not straightforward to apply. For example, the periods for which it is certain that the observed discharges come from slow flows and not from surface flows must first be extracted from the discharge series. Another difficulty is related to the accuracy of low-flow discharge measurements which, given the very nature of these discharges, is generally low. Estimation errors of the variable $-dQ/dt$ are therefore potentially high, in particular for small time steps (see also various other potential problems identified by Rupp and Selker, 2006). A pertinent estimation of the two parameters A and B for recession therefore requires preliminary data filtering.
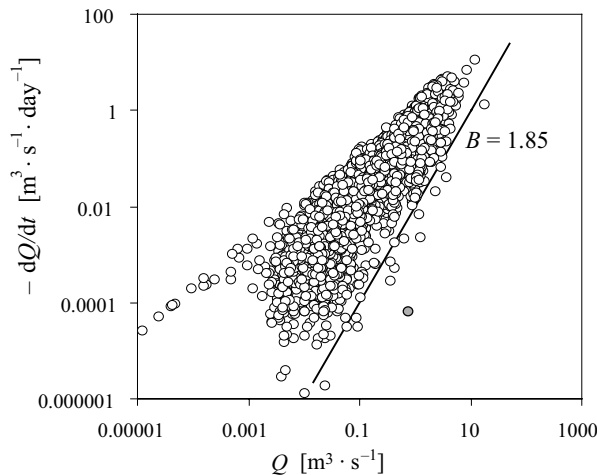

Fig. 8.16: Ratio $-dQ/dt$ as a function of Q for data from the Parimbot basin at Ecublens in Switzerland (area 6.75 km²) and the bottom line of the point swarm envelope with slope $B=1.85$ according to equation 8.34 (period 1978–1999).

CHAPTER 9

FLOOD PREDICTION

A flood represents a higher than usual quantity of water conveyed by a hydraulic system (i.e., lakes, reservoirs and watercourses), with or without bank overflow.

Concerns related to floods, in particular the rarest events, are many and go back to the origins of civilization. Estimating flood flows is essential both for water resources management (e.g., design of related projects) and for the protection of life and property (i.e., identification of flood hazards and implementation of adequate structural and non-structural flood control schemes). Today, in particular due to socio-economic changes in many regions where flood hazards exist, flood damage can have serious consequences, often generating very high social and financial costs. In Switzerland, for example, the six major floods observed between 1987 and 2007 had a financial cost estimated at more than 3 billion Swiss francs. To better control the often devastating and catastrophic effects of flooding, engineers must be able to understand and estimate flood discharges.

Over the years, many methods and models have been developed to determine either a peak discharge, a hydrograph or various scenarios for floods. In practice, the best method for particular case depends mainly on the data available for the studied drainage basin—in particular streamflow data, generally the limiting factor in hydrology—and on the time allowed for the hydrological study.

This chapter will provide the reader with the necessary understanding and methods for predicting flood flows. Section 9.1 presents a number of definitions and the origin of floods as well as the main methods currently used to determine the characteristics of a flood associated with a given return period. These methods are classed in particular according to their requirements in terms of discharge data available at the site. Section 9.2 focuses on methods used to estimate peak flood discharges and Section 9.3 on methods used to estimate design floods. Guidelines for choosing an appropriate method for a given case are provided in Section 9.4. For more information on related practices in Switzerland and France, the reader can refer respectively to the recommendations of the Swiss Federal Office for Water and Geology (OFEG, 2003) and the French Ministry of Ecology and Sustainable Development (Lang *et al.*, 2005). For the UK and the US, information can be found respectively in NERC (1975) and USACE, 1994.

9.1 INTRODUCTION

9.1.1 Origins and Characteristics of Floods

Definitions and characteristic variables

According to the international glossary of hydrology (WMO, 1974), a flood can be defined as "a rise, usually brief, in the water level in a stream to a peak from which the water level recedes at a slower rate". This definition restricts floods to the rising limb of the hydrograph. Here, the term flood will be used to designate the complete event including the fall of discharges until reaching a normal regime. Note that in a hydrological sense, floods must be distinguished from inundation, i.e., the flow of water over the banks of a normal river channel or lake. For our purposes here, a flood does not necessarily lead to bank overflow and inundation.

Variables generally used to characterize floods are (Figure 9.1) the peak discharge Q_p [m³/s] or specific flood discharge [m³/s/m²], the maximum mean discharge $Q_{max}(d)$ [m³/s] over a given duration d, the flood volume [m³], the time-to-peak t_p [hours], the time during which streamflow remains above a given discharge threshold (e.g., spillway capacity) and the flow velocity [m/s].

To characterize a flood, it is often necessary to determine its non-exceedance frequency—generally expressed as a return period in years. This is a key characteristic, in particular because it provides the probability of exceedance of an event over a period of n years corresponding for example to the lifetime of a given project (Appendix 9.6.1).

Only major floods will be considered here, i.e., floods for which the maximum discharge largely exceeds the mean annual discharge (i.e., return periods greater than 10 years).
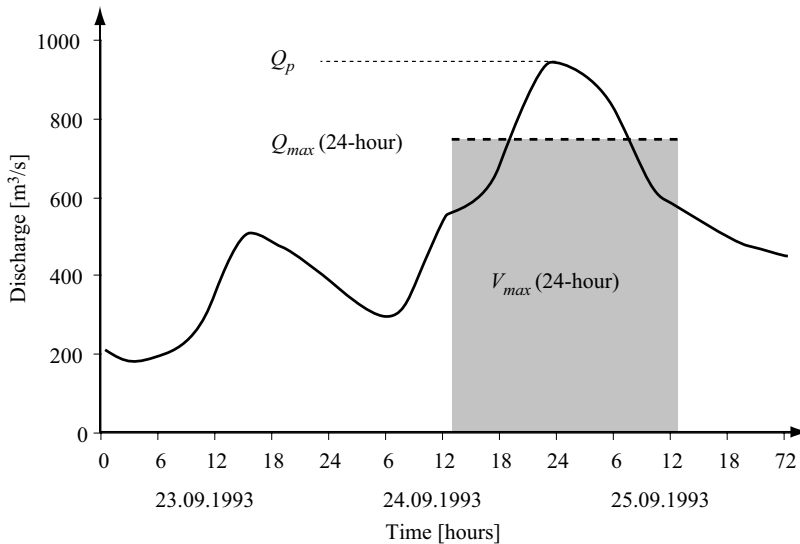

Fig. 9.1: Peak discharge and maximum 24-hour mean discharge for the 24/09/1993 flood on the Rhone river at Branson.

Origins of floods

Floods can be caused by different processes or phenomena, sometimes working together in a combined manner. The most common causes of floods are rainfalls with unusually high volumes, intensities and/or durations, unusually high melting of snow or ice or normal melting combined with other factors (e.g., rainfall). For a given precipitation depth or meltwater volume, flood flows will be higher if the initial state of water stored within the basin is near saturation (i.e., depression storage and surface reservoirs full and soil and/ or snowpack fully saturated). On a saturated basin (or a basin not subject to infiltration because the surface is frozen for instance), major floods can be produced by moderate rainfall or meltwater volumes.

Floods can also result from the formation and breaking of ice jams or other natural dams formed by floating debris (e.g., branches and logs). Ice-jam floods are caused by the blocks of ice released during thawing of frozen rivers in spring. The situation is characteristic of cold regions like Siberia or Canada but can also occur in more temperate regions. Spring thaw leads to a flow of floating blocks of ice that can pile up and become jammed when they encounter an obstacle. The water that backs up behind the resulting dam can lead to upstream flooding and inundation. In addition, flash floods can be caused by the sudden breaking of ice jams. For example, such a flood occurred on the Rhine river at Cologne in February 1784 and generated the highest flood ever recorded at the station.

Many other causes of floods exist. For example, flash floods can be caused by breaking of natural dams (e.g., Lake Silvolta at Simplon, Switzerland in 1891) or man-made dams (e.g., Malpasset dam upstream of Fréjus, France in 1959), overtopping of dams due to insufficient spillway capacity, sudden filling of reservoirs by landslides (e.g., Vajont, Italy in 1954), spillway plugging by floating debris (e.g., Palagnedra dam in Switzerland in 1978) or rockfalls in lakes (e.g., Lake Lucerne in Switzerland in 1991). Glacial outbursts (or jökulhaups) are another type of flash flood that can occur when water trapped within, on or behind a glacier is suddenly released (e.g., Summit lake outburst flood in British Columbia, Canada in 1967).

Other phenomena are often associated with floods. These include mainly debris flows (transport of water and debris), landslides (around a watercourse or on its path during bank overflow) and torrential erosion phenomena (within and around mountain torrents). The consequences of such phenomena are often as serious as the direct consequences of floods but are generally the subject of special studies and analyses.

9.1.2 Flood Estimation Objectives and Parameters of Interest

Flood estimation is essential for many operational applications such as:

- management of hydrological systems (e.g., watercourses and their tributaries and outlets, lakes and reservoirs, dams, wetlands),
- management of associated systems (e.g., water supply, groundwater recharge),
- management of drainage basins where floods originate (e.g., use of hillside reservoirs and appropriate agricultural practices to control runoff),

- management of flood-related hydrological risks to protect life and property and ensure the safety of hydraulic works (e.g., risk of inundation, erosion).

Depending on the objectives, the characteristics used to describe a flood may differ: peak discharge or flow, maximum water level, flood volume or the complete hydrograph. These characteristics must often be associated with a return period.

Peak discharge and flood hydrographs

It is generally sufficient to know the peak discharge of a flood if only the discharge capacity of the considered system is involved. This is the case for instance when designing diversion works, weirs or storm drains.

Knowledge of the entire flood hydrograph, in particular its total volume, is indispensable for many other applications such as the design of flood-control reservoirs or flood risk mapping.

Floods exhibit great diversity, as much from the viewpoint of maximum discharge as from that of flood volume or hydrograph shape. The most unfavorable flood for a given system is therefore not easy to identify or construct. Multi-event approaches involving an assessment of the performance of the considered system for different flood scenarios are therefore generally used. The scenarios can be extracted from a series of observations, calculated by simulations or taken from a flood catalog compiled elsewhere.

Associated return period

It is generally necessary to choose a return period to be associated with the design variable (Addendum 8.1). This criterion is often imposed by the project owner or applicable regulations. However, engineers are sometimes called on to make recommendations.

Note that an acceptable return period for the flood used to design a project can vary greatly from one country to another (e.g., Meylan *et al.*, 2012). In Germany, for example, storm sewers are sized for a return period of one year while in North America a 5-year return period is used. In Switzerland, a return period of 10 years is sometimes used for this type of calculation (Example 9.1). For flood protection in rural areas, a return period of around 30 years is recommended in Switzerland (Figure 9.2) while no protection at all is required in rural areas in Germany. Major differences can also exist within a given country. In Canada, for example, floodways in Manitoba attenuate floods with return periods greater than 100 years while in British Columbia, a 200-year return period is presently used.

Example 9.1

Flood protection requirements in Switzerland

For flood protection in Switzerland, design parameters vary depending on what is to be protected (e.g., towns, infrastructures, agricultural land). The admissible frequency of occurrence of inundation is related to the socio-economic value of the property to be protected. It is recommended to increase the degree of protection for vital areas and special property and reduce it for areas such as agricultural land (Figure 9.2).
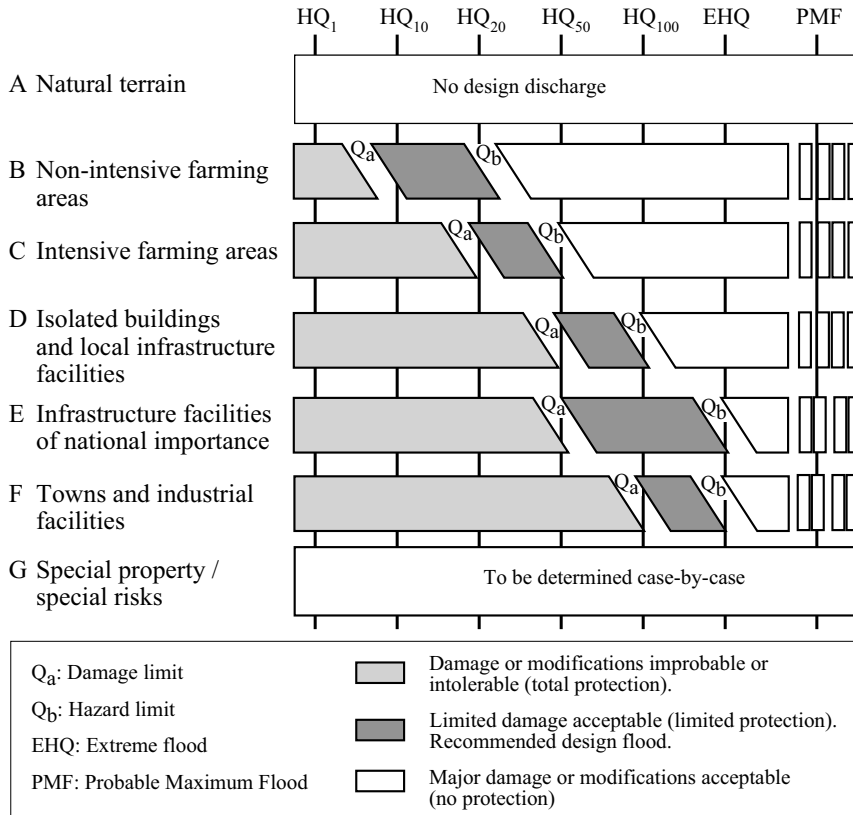
Fig. 9.2: Matrix of possible protection objectives published by the Swiss Federal Office for Water and Geology (adapted from OFEG, 2001).

9.1.3 Overview of Prediction Methods

Many flood prediction methods exist, the oldest dating back to the 19th century. Most of them are designed to estimate the characteristics of floods and associate them with return periods. The main factors determining the models that can be used in a given case are:

- the nature and quality of historical data available for the studied drainage basin (e.g., discharges, precipitation, temperature) as well as the length of any available time series for these variables,
- the availability of geographic data for the drainage basin (e.g., physiographic properties, characteristics of the hydrographic network, hydraulic works, etc.),
- the possibility of using a hydrological simulation model (e.g., rainfall-runoff model) for the considered basin,
- the availability of regional models for the studied area to fill in any missing data.

It is in particular possible to distinguish between the three following possible configurations:

- In the ideal case where a long homogeneous series of observed discharges exists (i.e., at least 50 years of measurements) and as long as the behavior of the basin has not been modified significantly over the observation period, the series can be processed statistically using an appropriate method (i.e., frequency analysis). This generally makes it possible to extract floods or pertinent flood characteristics that can be used to achieve the objectives of a given study—as long as the behavior of the basin is not modified significantly over the decades to come. This ideal situation concerns very few drainage basins.
- In another much more frequent situation, a long precipitation series exists however discharge data are insufficient for the considered basin. Under certain conditions, the statistical behavior of observed maximum precipitation on the basin can be used to extrapolate that of flood discharges. The precipitation series can also be used to reconstruct or generate a long discharge series by simulations carried out with a hydrological model suited to the basin. This series is then processed using an appropriate statistical technique.
- The most frequently encountered case is that of ungaged basins or basins with insufficient instrumentation (i.e., insufficient discharge and precipitation data). Various more or less approximate methods can be used. They vary greatly depending on the type of data and information available for the considered basin (e.g., rainfall data, physiographic characteristics) and region (e.g., IDF curves, regional models).

Flood prediction methods are many and varied. The main methods available for the estimation of peak flood discharges and flood hydrographs are respectively presented in Sections 9.2 in 9.3. Section 9.4 provides guidelines for choosing a suitable method for a given case.

9.2 ESTIMATION OF PEAK FLOWS

Prediction of peak flood discharges is common task for hydrologists. This section first presents methods for gaged basins and then for ungaged basins.

9.2.1 Statistical Methods used for Gaged Basins

Flood discharges, in particular annual flood discharges, are well suited to standard statistical techniques for the analysis of random variables. The different values of annual floods of a given series are generally considered to be independent. This is the result of the random nature of the meteorological phenomena at the origin of these events, in particular precipitation, as well as the random nature of the antecedent moisture conditions of the basin before each precipitation event. Note that the observations are not always independent. This can be the case if the considered floods come from an intra-annual series, i.e., a series made up of several floods per year (Meylan *et al.*, 2012).

The objective of the statistical analysis of flood discharges is generally to estimate the return period of observed events or to estimate the discharge corresponding to a given return period. Such analyses are carried out on the basis of series of maximum values

extracted from long series of observations. The data used are generally the series of annual maximums (e.g., maximum hourly discharges) or partial duration series (i.e., peak over threshold values).

In certain ideal cases with sufficiently long discharge series, a conventional frequency analysis can be carried out (e.g., Meylan *et al.*, 2012). Data from known historical floods are sometimes integrated in the series to improve the estimation. If the discharge series is too short, rainfall data can be included in the frequency analysis (GRADEX method). The methods corresponding to these different situations are presented below.

Frequency analysis of flood discharges

In practice, frequency analysis is based on frequency distribution fitting techniques. A theoretical statistical distribution function—the frequency model—is fitted to the empirical distribution deduced from the considered observation series (Figure 9.3). To represent the statistical behavior of flood discharges, it is therefore necessary to choose an appropriate frequency model and to estimate its parameters.

For flood discharges, the most widely used distribution functions are the generalized extreme-value (GEV) distributions (e.g., Gumbel, Weibull or Fréchet) and the Log-normal, Pearson type III and Log-Pearson type III distributions.

The frequency model describes the relationship between the intensity of a flood and its return period in an analytical manner. A frequency model therefore makes it possible to estimate the value of discharges for events with different return periods, in particular return periods that are higher than those of the events represented in the sample. Extrapolation of such a model can however lead to very different estimates of the required quantile depending on the frequency model and parameter estimation technique used.
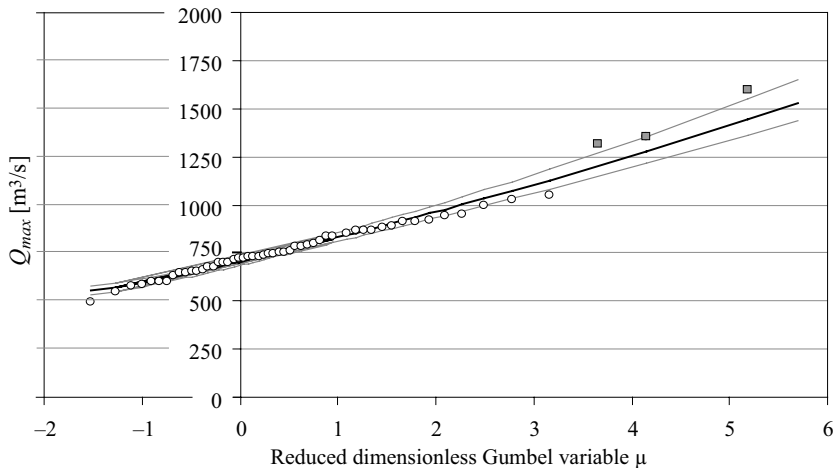

Fig. 9.3: Fitting of an LPIII (Log-Pearson III) frequency distribution with 80% confidence intervals to the annual maximum discharges of the Rhone river at Scex (Switzerland) observed before the construction of the main dams in the Canton of Valais (1905–1956 period). The discharge series is homogeneous over the 1905–1956 period. The maximum discharges of three floods in 1987, 1993 and 2000, reconstructed for natural conditions by the Swiss Federal Office for Water and Geology (OFEG, 2002) (see also Figure 2.4), are considered as historical floods and integrated in the analysis (Hingray *et al.*, 2006b).

For more information on frequency models and parameter estimation methods used in hydrology and on the estimation of the associated uncertainties, the reader can refer to Meylan *et al.* (2012). A number of precautions that are essential when using this type of analysis are presented in Addendum 8.2. It is particularly important to ensure that the available discharge series are homogeneous over the considered period (e.g., Renard, 2006). This is not the case for many drainage basins in which the hydrological behavior has been modified by the gradual transformation of the medium (e.g., urbanization) or by the construction of various projects at different times. In this case, frequency analysis must be adapted to take this into account (e.g., McGuen, 1979).

Frequency analysis of historical floods

Historical floods can represent a useful addition to available discharge records (Addendum 9.1). A frequency analysis on the complete sample of floods (continuous series of observations + historical floods) is always possible but the frequency distribution fitting techniques must be adapted to take into account missing information over the period covered by the data (Condie and Lee, 1982; Ouarda *et al.*, 1998; Naulet *et al.*, 2005; Payrastre, 2005).

> **Addendum 9.1 Usable historical floods**
>
> Historical floods often used to supplement observed floods are particularly heavy floods that occurred in the past before the installation of measurement stations. Historical floods can only be used if information based on souvenirs (for the most recent) or written personal accounts and public archives (for the oldest) is available to allow estimation of the corresponding discharges. In certain cases, estimation can be based on marks inscribed on buildings to record the magnitude of such events or on natural evidence left by the watercourse in its environment. Such estimations are often based on the techniques of paleoflood hydrology (Baker, 1987). The difficulty of estimating historical flood discharges obviously increases with the length of time that has passed since their occurrence.
>
> Another increasingly encountered factor may justify the use of historical floods. It is related to continuous modification of the hydrological behavior of an increasing number of drainage basins by various projects (e.g., hydraulic works). Flood discharge series available on such basins therefore become non-homogeneous and cannot be used for conventional frequency analysis. The estimation of flood discharges for a given return period becomes difficult. Note however that although such projects generally have a strong influence on common floods, this influence decreases and even becomes negligible for major events. To effectively manage floods, it is therefore important to be able to estimate flood discharges for a project-free basin situation. One solution consists in using, if available, all floods observed on the basin before project construction and the different major floods observed on the basin after project construction (the latter being a priori little influenced by the projects or reconstructed). The major post-project floods can be considered as historical floods and can be used to supplement the series of pre-project discharges for the required frequency analysis. The frequency analysis presented in Figure 9.3 is based on this principle.

QDF curves

Frequency analysis of flood discharges can be carried out on maximum mean discharges corresponding to different durations. This leads to the construction of so-called QDF curves.

Similar to the IDF curves used for precipitation (Chapter 12), QDF curves summarize the statistical relationships existing between the main characteristics of the flood hydrograph, i.e., the maximum mean discharge *Q*, duration *d* and frequency *F,* hence the name QDF. In other words, these curves indicate the maximum mean flood discharge estimated over a duration *d*, corresponding to a given return period *T* (Figure 9.4). The method for constructing QDF curves is summarized in Addendum 9.2.

Addendum 9.2 Construction of QDF curves

QDF curves are constructed in the same way as IDF curves. The method is based on the frequency analysis of one of the following two variables (Figure 9.5):

- *VCXd:* The characteristic mean discharge (equivalent to a volume) over continuous duration *d*, representing the maximum for a given period, generally a year.
- *QCXd:* the characteristic discharge threshold (*Q*) continuously exceeded over duration *d*, representing the maximum for a given period.

The variable *VCXd* corresponds to a volume flowing through a reach over a duration *d*. This quantity is obtained by dividing the volume of water flowing between times t_1 and t_2 by the duration $d = t_2 - t_1$. This gives:

$$VCXd = \frac{1}{d} \cdot \int_{t_1}^{t_2} Q(t) \cdot dt \tag{9.1}$$

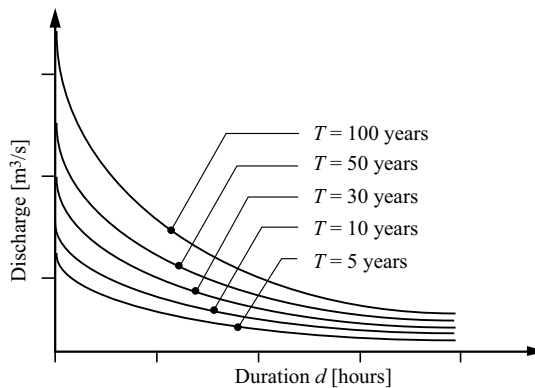where *Q(t)* represents the maximum mean discharge as a function of time. This variable is therefore a mean quantity.

Fig. 9.4: Principle of QDF curves for *VCXd* or *DCXd*.

QCXd is the value of the discharge continuously exceeded over the same duration *d*. The integral of the hydrograph above *QCXd* corresponds to the overflow volume of the watercourse if the considered discharge threshold is equal to the bank-full discharge capacity of the watercourse.

For each considered duration *d,* statistical analysis of the values of *QCXd* (or *VCXd*) extracted from the series of mean discharges over *d* can be used to determine the discharge quantiles corresponding to different return periods.
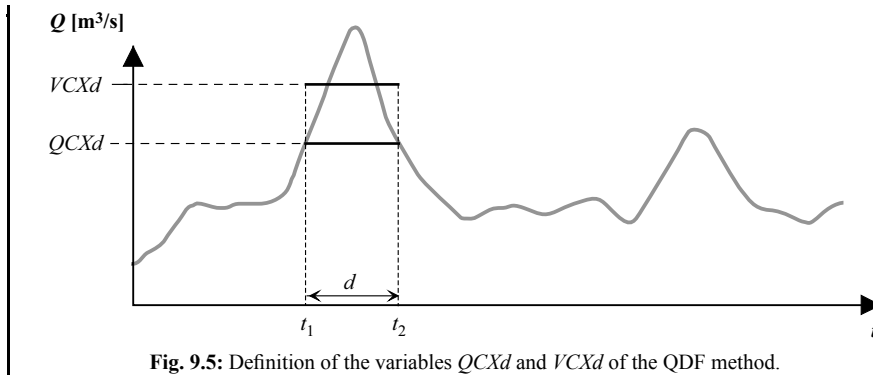
Fig. 9.5: Definition of the variables *QCXd* and *VCXd* of the QDF method.

Hydrometeorological frequency analysis

The length of the observed discharge series is generally insufficient to estimate the maximum discharges of floods corresponding to rare and very rare frequencies of occurrence, i.e., return periods greater than 100 years. On the other hand, a long series of precipitation measurements is often available for the basin. The GRADEX method, designed, tested and validated in France by the research division of EDF[1] (Guillot and Duband, 1967), was developed in this context to determine safe floods for large dams. The method uses the statistical behavior of maximum precipitation observed on the basin to extrapolate the behavior of flood discharges. It differs from conventional frequency analysis of flood discharges in that it uses precipitation data related to the production of floods. This method makes maximum use of all data available for the studied basin. For this reason, it is often classed as a hydro-meteorological flood estimation method.

Two series of data are required for the basin to apply the GRADEX method: a long series of maximum rainfalls (i.e., at least 30 years) and a series of maximum discharges covering at least 10 years. The method is based on the following assumptions:

- The maximum discharges to be estimated are caused uniquely by maximum rainfalls uniformly distributed over the basin.
- The soil retention capacity reaches an upper limit starting at a certain rainfall value. Once this threshold has been reached, maximum rainfalls in the corresponding discharges (maximum discharges) follow the same statistical distribution function, referred to as an extreme-value distribution given the nature of the considered phenomenon (i.e., rare floods). The runoff coefficient of the drainage basin is assumed to be near 1.
- The threshold, corresponding to a saturated drainage basin, is reached for a rainfall event producing a discharge with a 10-year (or sometimes 20-year) return period.

In other words, the asymptotic behavior of maximum flood discharges is assumed to be identical to that of maximum rainfalls on the basin. On an appropriate frequency diagram, e.g., a Gumbel plot with the reduced variable $u = -\ln(-\ln(F(T))$ on the x-axis, the distribution of discharges is a straight line parallel to that of rainfall starting from a threshold corresponding to return period of 10 years (Figure 9.6). The GRADient of

---

[1]Electricité De France, the main French electrical utility.

EXtremes values (GRADEX) is the same for both distributions. The statistical distribution used is generally the Gumbel distribution.

Application of the GRADEX method requires a duration of maximum mean rainfalls that corresponds exactly to that of the maximum mean discharges considered (generally 24 hours). This duration generally depends on the time of concentration of the basin at the point of interest. The units for rainfalls and discharges must be the same (e.g., mm/24h). Given that the results obtained are mean values over the chosen time steps, the peak flood discharges can be deduced by multiplying the mean discharges by a coefficient that is a characteristic of the basin. This coefficient can be estimated on the basis of real flood hydrographs observed on the basin.

The GRADEX method is valid only for relatively small basins—with concentration times less than four days and maximum areas of 5000 km²—on which maximum floods are produced by liquid precipitation. A document (CFGB, 1994) published by Comité Français des Grands Barrages provides full explanations on how to apply this method. Although the method poses certain difficulties specific to the context of the study (Lang *et al.*, 2005), it is still one of the most widely used methods for sizing the spillways of large dams. One of the numerous adaptations of the GRADEX approach is the AGREGEE method (Margoum *et al.*, 1994) that, in particular, allows a gradual transition of the statistical distribution of floods between the domain of observed floods and that of exceptional floods that follow the maximum rainfall distribution. The AGREGEE method also accepts an asymptotic exponential function for the maximum precipitation distribution.

Recent developments of the GRADEX method propose an analysis based on events observed during the season presenting the highest risk for extrapolation of the annual event or based on events during specific "weather types" inducing a high risk of floods (Paquet *et al.*, 2006) (see also Chapter12).
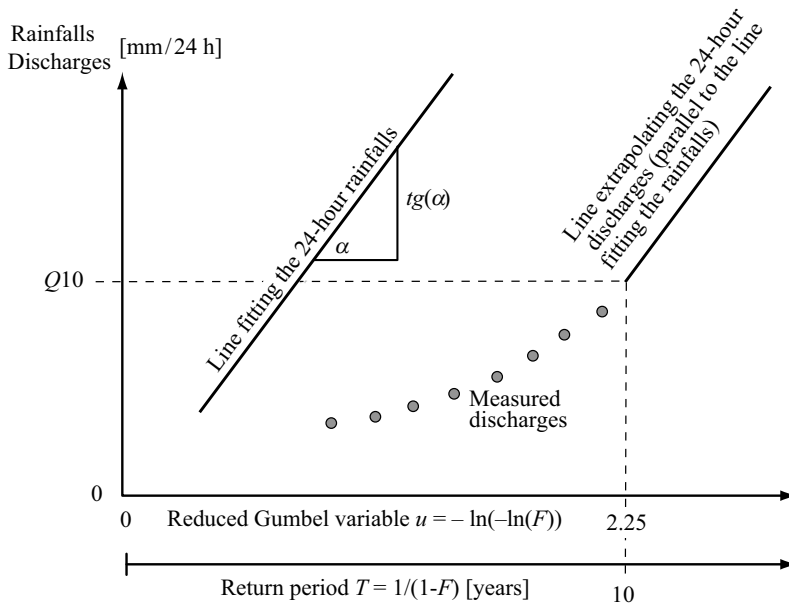

Fig. 9.6: Principle of the GRADEX method.

9.2.2 Regional Methods for Basins with Few or no Data

In most cases, the hydrometeorological data required for frequency analysis of flood discharges are not available for the studied basin. In such a case, so-called regional models can be used. They have varying degrees of complexity and require only a minimum quantity of local and/or regional data. Regional flood estimation models are constructed on the basis of experience acquired on gaged basins of a hydrologically homogeneous region (Chapter 11). If a model of this type is available for the region in which the basin of interest is located, it offers a simple way to estimate flood discharges for this basin. However, in many cases, no such regional model exists for the region of interest or no model is applicable to the basin in question. In this case, a regional model must be constructed on the basis of information available from gaged basins of the region. Chapter 11 describes in detail various aspects related to the development and application of regional models, including the delimitation of homogeneous regions and methods for estimating the hydrological variable of interest. The main regional methods for estimating flood discharges are presented below.

Empirical models

Empirical models make use of experimental knowledge of the relationships existing between maximum flood discharges and certain basin characteristics (e.g., Table 9.1). They often include a variable related to basin precipitation. These models are generally expressed as follows:

$$Q_{\max} = f_1(A) \cdot f_2(X_1, X_2, ..., X_n, P, t_c) \tag{9.2}$$

where Q_{max} is the maximum discharge of the drainage basin, A the area of the basin, X_1, X_2, … X_n various other basin characteristics, t_c time of concentration of the basin and P a precipitation variable.

The function f_1 is an increasing function of area. This function is however sub-linear, indicating that, all other factors being equal, the specific flood discharge decreases with the size of the drainage basin. In addition to the basin area and time of concentration, the most widely used basin characteristics include the slope (e.g., a power law with an exponent often around –0.5), land use and vegetation. These characteristics influence the productivity of the drainage basin (i.e., runoff coefficient) as well as the flow velocities of runoff over the basin and streamflows in the hydrographic network. The application of empirical models to ungaged basins therefore requires field investigations or cartographic analyses to estimate the necessary characteristics.

For information purposes, note that an envelope curve for maximum discharges has been proposed in the literature for all terrestrial systems based on various regional empirical expressions and various point observations of maximum discharges. This curve, derived from the Myers-Jarvis enveloping curve (Jarvis, 1942), is expressed as follows:

$$Q_{\max} = \frac{3009.2 \cdot A}{(41.31 + A)^{0.78}} \tag{9.3}$$

with A in km^2 and Q_{max} in m^3/s.

Empirical models provide a very rough estimate of floods but do not replace a true hydrological study. Moreover, such models, whatever the formulations, all make use of empirical coefficients that are valid only for the region in which they have been established. Note also that these models do not consider the return period of the event.

Table 9.1: Examples of empirical formulas used to estimate floods on small drainage basins (10 to 500 km²) in Switzerland. There are no other restrictions on basin characteristics, which means that the model may not always provides satisfactory results (adapted from OFEG, 2003).

Method	Expression
Kürsteiner *	$Q_{\max} = c \cdot A^{2/3}$ Q_{max}: Peak discharge [m³/s], c: Coefficient characterizing the drainage basin = f(slope, glacier-covered area), A: Drainage basin area [km²]
GIUB'96	$Q_{100} = a \cdot A^b$ Q_{100}: Peak discharge of 100-year flood [m³/s], a and b: Regional coefficients (15 regions identified for Switzerland), A: Drainage basin area [km²]

* Method based on the envelope curve encompassing all the highest floods observed in the region of interest.

Pseudo-empirical methods—the rational method

Pseudo-empirical methods can be distinguished from the models presented above by their degree of conceptualization. For example, they often express floods as a function of one or more variables related to the maximum precipitation that can affect the basin. Among these methods, the most widely known is without a doubt the rational method. Many versions of this method have been derived for use in different regions of the world. This is the case, for example, of the Caquot method widely used in France (Fouquet *et al.*, 1978).

The concept of the rational method was first proposed by Thomas Mulvaney, an Irish engineer in charge of agricultural drainage in the 19th century (1850). The principle of the method is that the peak discharge $Q_p(T)$ produced by a uniform rainfall with a given return period T is maximum when, all else being equal, the duration θ of this rainfall is equal to the time of concentration t_c of the drainage basin, i.e., when the entire area of the basin contributes to runoff (Addendum 9.3). This method assumes that the return periods of the precipitation and discharge calculated in this manner are equal, as expressed by:

$$Q_p(T) = u \cdot C_r \cdot i_{max}(t_c, T) \cdot A \tag{9.4}$$

where $i_{max}(t_c, T)$ is the maximum mean rainfall intensity with a return period T for a rainfall of duration θ equal to the time of concentration of the drainage basin ($\theta = t_c$), C_r is the dimensionless runoff coefficient of the basin, A the area of the drainage basin and u a unit conversion coefficient. With A in ha, i in mm/h and $u = 0.0028$, Q is in m³/s. With A in ha, i in l/s/ha and $u = 1$, Q is in l/s.

Application of the rational method therefore requires, in addition to the area of the drainage basin A, identification of the various coefficients that characterize the basin, i.e., the runoff coefficient C_r and time of concentration t_c of the drainage basin along with the maximum mean rainfall intensity i for the chosen return period T. They can be obtained from nomographs, regional models and IDF curves for the considered basin or region (Musy and Higy, 2011).

Mainly because of its simplicity, the rational method is by far the most widely known and widely used flood discharge estimation method. It has been adapted to allow estimation of flood hydrographs. The corresponding method is referred to as the isochrone method (e.g., Musy and Higy, 2011).

Addendum 9.3 Time of concentration and critical precipitation duration

Time of concentration t_c of a drainage basin

The time of concentration of runoff in a drainage basin is defined as the time it takes for a drop of water falling at the point from the basin outlet (from a hydrological viewpoint) to reach the basin outlet. The time of concentration is often evaluated using empirical formulas (e.g., Table 9.2) or using one of the two calculation methods presented below. These methods differ according to the type of runoff considered.

In the case of runoff corresponding mostly to concentrated flows, the L/V method, also referred to as the "velocity method", is generally suitable. It is widely used for road drainage projects. For the L/V method, the time of concentration of the basin is estimated as the maximum sum of a runoff initiation time t_i necessary for the soil to absorb water before surface runoff begins, a runoff time t_r corresponding to the time it takes the runoff to reach the hydrographic network and a channel routing time t_{ch} corresponding the time it takes for water that has reached channels to reach the basin outlet. The initiation time is generally fixed in an arbitrary manner, between 5 and 10 minutes. The runoff time is estimated on the basis of the flow length L_r on the basin slopes and a runoff velocity V_r estimated using appropriate nomographs taking into account the vegetal cover and slope of the drainage basin (Musy and Higy, 2011). The channel routing time t_{ch} is calculated from the length of the flow line in the hydrographic network L_{ch} and the velocity of flow in the channels V_{ch}. This velocity can be estimated using nomographs or an empirical head loss formula such as the Manning-Strickler or Chezy formulas.

When runoff can be assimilated to sheet flow, the time of concentration can be evaluated using the kinematic wave assumption (Appendix 5.7.1).

Critical rainfall intensity $i(t_c, T)$

Under the assumptions of the rational method, the critical duration of a rainfall event with a maximum mean intensity corresponding to a return period T is equal to the time of concentration t_c of the basin (Figure 9.7). The corresponding rainfall intensity is obtained from IDF curves constructed for the studied basin or the concerned region.

Table 9.2: Examples of regional formulas for the estimation of the time of concentration t_c [minutes].

Method	Expression
Kirpicher	$t_c = t_i + 0.0195 \cdot L^{0.77} I^{-0.385}$ where t_i [minutes] is the runoff initiation time, L [m] the length of the main flow line and I [m/m] the mean slope between the basin outlet and the furthest point upstream.
Swiss SNV standards**	$t_c = 5 + \dfrac{12 \cdot L}{C_r^{5/3} \cdot K^{2/3} \cdot I^{1/2}}$ where C_r is the dimensionless runoff coefficient, K a coefficient that depends on location and return period, L [m] the length of the main flow line and I [m/m] the slope.

** These standards were published by the Swiss Association for Standardization (SNV) for the calculation of road drainage discharges.
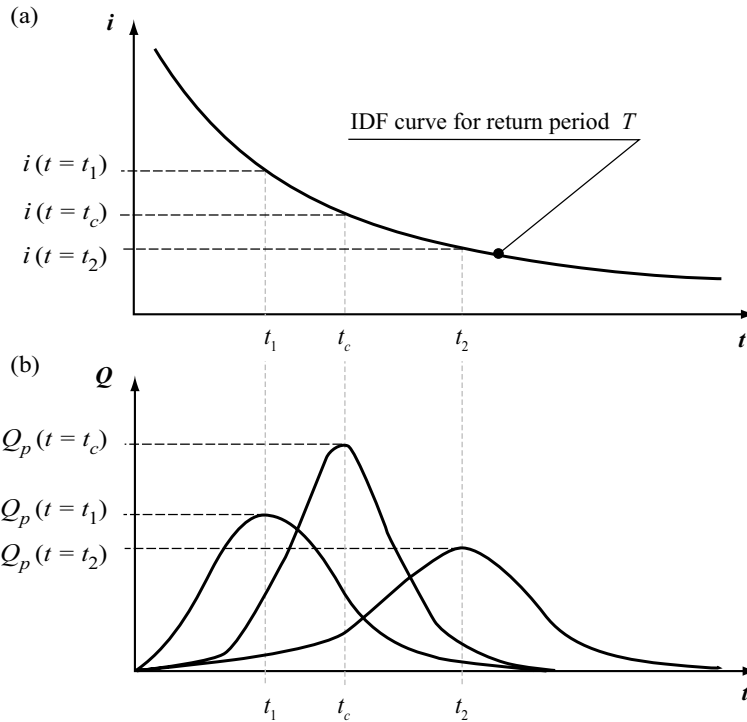
Fig. 9.7: Maximum flood discharges obtained for rainfalls of different durations t1, t2 and t3 and for which the respective mean intensities (i1, i2 and i3) all have the same return period T. a) IDF curve for return period T and corresponding maximum mean intensities. b) Schematic illustration of the hydrographs and the discharges resulting from block rainfalls having respectively these mean intensities over the corresponding durations. The maximum peak discharge among these 3 hydrographs is obtained for the rainfall with a duration equal to the time of concentration.

The rational method is based on a number of simplifying assumptions that cannot be checked (e.g., constant runoff coefficient in time and space, uniform and constant precipitation over the entire drainage basin). This restricts its use to small drainage basins (less than 20 km²). If the method is used in an abusive or uncontrolled manner, the results can be erroneous. A common error is to consider that the critical duration of the rainfall producing the maximum mean intensity corresponding to a return period *T* always corresponds to the time of concentration of the drainage basin. This major assumption is sometimes not checked and is often invalid in urban environments. Consider the two following examples: 1) a basin including a hydrological irregularity (Figure 9.8b) and 2) a basin with major spatial heterogeneities, for example in terms of size, runoff coefficients and/or response of the different sub-basins (Figure 9.8a) (adapted from Consuegra and Musy, 1989). An example for these situations is presented in Appendix 9.6.2.

Two verifications should be carried out to ensure the consistency of the estimates obtained by direct application of the rational method. They make use of the double-calculation method and the area-concentration time diagram. These two methods are presented in Appendix 9.6.2 and Appendix 9.6.3.

(a)   (b)

Fig. 9.8: Hydrological configurations for which the rational method cannot be applied without precautions (see Appendix 9.6.2). a) The case of a basin made up of a rural basin (B1) with a slow response producing little runoff and a small but highly productive urban basin (B2) with a fast response. b) The case of a basin with a hydrological irregularity.

Example 9.2

The objective is to determine a design flood with a return period T of 5 years at the basin outlet for the situation described in Figure 9.9.

The upstream (B1) and downstream (B2) parts of the drainage basin cover respectively 20 and 40 ha. Upstream flows concern surface runoff only while the downstream basin includes a 2000 m long open channel. The two parts of the basin have the same type of land use (crops). The crops are planted in the direction of the slope (roughly 2%).

For the considered region, the maximum mean intensity of the 5-year return period T can be expressed as follows:

$i(t, T) = a / (b+t)$ with i in mm/h, t in minutes, $a = 1980$ mm/h and $b = 12$ minutes.

The calculation procedure consists in determining successively the time of concentration of the drainage basin, the maximum mean intensity of the corresponding critical rainfall, the mean runoff coefficient of the entire basin and the required peak discharge.

The runoff coefficient and runoff and flow velocities are estimated for the two parts of the basin using appropriate nomographs (Musy and Higy, 2011). A single runoff coefficient
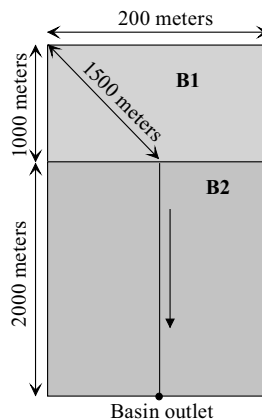

Fig. 9.9: Drainage basin configuration.

of 0.2 is used for the two sub-basins. The runoff velocity and the flow velocity in the canal are assigned the respective values of 1.2 m/s and 1.0 m/s. This gives:

Runoff initiation time: t_i = 10 minutes (arbitrary value)

Runoff time: $t_r = L_r / V_r$ = 1500 m / 1.2 m/s = 21 minutes

Channel routing time: $t_{ch} = L_{ch} / V_{ch}$ = 2000 m / 1 m/s = 33 minutes

Time of concentration: $t_c = t_i + t_r + t_{ch}$ = 64 minutes

Corresponding critical intensity: $i(t_c, T)$ = 1980/(12+64) = 26 mm/h

Design flood discharge: $Q_p(T)$=0.0028*0.2*26*(20+40) = 0.87 m³/s

An additional study was then carried out with a different land use in basin B1 resulting in a runoff coefficient of 0.4 instead of 0.2. The mean runoff coefficient for the entire basin was therefore updated. The new value was estimated by the weighted mean of the corresponding coefficients of the two sub-basins (the weights correspond to the respective surface areas).

Mean runoff coefficient: Cr_{mean}=(20*0.2+40*0.4)/(20+40) = 0.33

New design discharge: $Q_p(T)$=0.0028*0.33*26*(20+40) = 1.44 m³/s

Regional statistical models

To estimate flood discharges, regional statistical models are sometimes based on a statistical regression model representing the relationship between the characteristic flood discharge Y_T and certain pertinent characteristics of the basin. This relationship can be expressed as:

$$Y_{iT} = b_0 + \sum_{j=1}^{N} b_j \cdot X_{ij} + \varepsilon \tag{9.5}$$

where Y_{iT} is the required flood discharge quantile for the ith basin, X_{ij} is the magnitude of the jth characteristics of the N characteristics considered for the ith drainage basin. Coefficients b_0 and b_i are the regression coefficients and ε is the error of the regression line. The explanatory characteristics used are the same as those of empirical models.

A second approach consists in using a regional frequency model already determined from data available for the instrumented sites of the homogeneous region considered. The corresponding estimation method is the very popular "index flood method" described in detail in Chapter 11. Briefly, the regional frequency approach models the statistical behavior of the normalized flood discharges for all the basins of the region. The normalization factor is referred to as the index flood. The index flood for a given basin is often the value of the mean annual flood for the basin or the value of the annual flood discharge with a return period of 2.33 years. These two values are in fact often considered to be equal. The required flood quantile Y_{iT} can then be expressed as:

$$Y_{iT} = \mu_i \cdot Y_{RT} \tag{9.6}$$

where μ_i is the index flood for the considered basin and Y_{RT} the value of the regional frequency model for return period T. Y_{RT} is referred to as the growth factor corresponding to the selected non-exceedance frequency. If a series of hydrometric measurements is available for the drainage basin, the index flood is generally estimated on the basis of

observations. For an ungaged basin, it can be estimated by a direct regression model using the physiographic or climatic characteristics of the basin as explanatory variables.

The advantages and drawbacks of the different estimation methods for basins with few or no observations are discussed in Chapter 11.

9.3 ESTIMATION OF DESIGN FLOODS

The different methods presented above can be used to estimate a given flood flow, in general for a given return period. However, for many applications it is essential to estimate the complete flood hydrograph. The volume and shape of a flood can, for certain applications, be more critical than the simple conventional peak discharge. This is the case for example when designing dams and reservoirs or mapping flood hazards.

Most methods used to identify or produce one or more flood hydrographs associated with a given return period require relatively extensive data for the studied site. They are either based directly on observed discharge series or use meteorological scenarios transformed into flood hydrographs by a hydrological simulation model. A regional model can once again be used on poorly gaged or ungaged basins.

9.3.1 Floods based on Observed Discharges

When long series of observed discharges are available, the design flood can be chosen among the observed floods or estimated on the basis of derived QDF curves.

Historical floods

When the design flood is chosen among observed floods on the considered basin, it is difficult to assign a return period to the flood. This is because the flood is not characterized by its peak discharge alone. Its time-to-peak, duration and volume above various discharge thresholds represent other characteristics that can be of major importance in determining the effect of the flood on the system studied. However, for a given flood, these characteristics have different return periods.

A mean return period is often estimated by plotting a flood on the QDF curves of the studied basin (Figure 9.10). The principle is the same as for the plotting of observed precipitation on IDF curves of the considered region. Special importance must be placed on the return period obtained for the mean maximum discharge corresponding to the estimated critical duration for the studied system. Note that it is often not possible to identify an observed flood with a return period corresponding to return period defined for the design of the project. This is generally the case when looking for an extreme design flood. An observed flood that is artificially inflated so that its modified return period corresponds to the required return period is sometimes used in such a case.

Mono-frequency synthetic hydrographs

When represented as a function of the variable *QCXd* (Addendum 9.2), QDF curves can be used to construct a mono-frequency synthetic hydrograph (MFSH). Different MFSH shapes can be produced on the basis of a given QDF curve. The choice of the shape of the design MFSH should if possible be carried out in such a way that it is representative of

the shapes of observed floods on the studied basin. The procedure below, proposed by CEMAGREF,[2] makes it possible to partially satisfy this condition (Figure 9.11).

The time-to-peak t_p of the MFSH is deduced from statistical analysis of the values found for observed hydrographs. The peak discharge $QIX(T)$ corresponds to the maximum instantaneous discharge with a return period T (to be determined elsewhere). The rising limb of the hydrograph is assumed to be linear. Recession is determined from the threshold discharges ($QCXd$) with the same frequency but with increasing event durations. The point $QCXd1(T)$ is obtained by shifting the peak of the same discharge found on the rising limb of the MFSH by a duration *d1*. An interesting particularity of MFSHs is that the mean discharge for any duration (*d*) is equivalent to the *VCXd* of the same frequency and same duration.
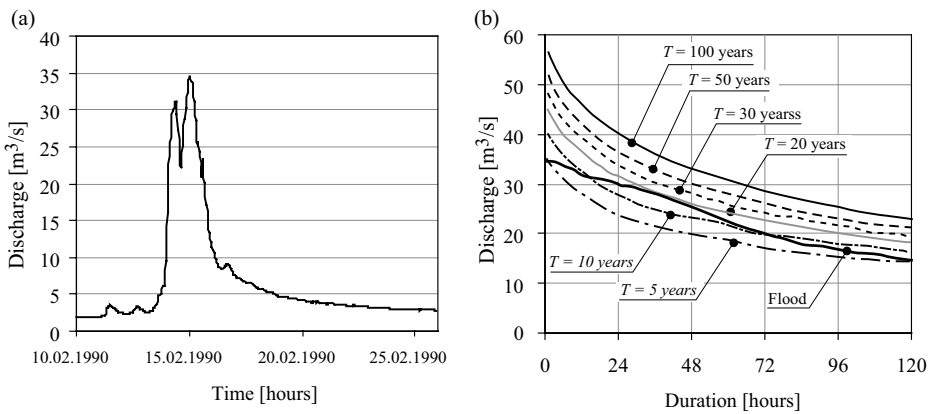
Fig. 9.10: Return period of maximum mean flood discharges over different durations. a) Hydrograph of the 15.02.1990 flood on the Murg river (Switzerland) at Murgenthal, Walliswil (207 km²). b) Plotting of the flood on QDF curves obtained for the basin (1981–2004 period). The return period of the maximum mean discharge for a duration of 1 to 2 days is roughly 30 years.

Fig. 9.11: Construction of a mono-frequency synthetic hydrograph (MFSH).

---

[2]In 2012, Cemagref became Irstea, the French institute for research in environmental and agricultural sciences and technologies.

The MFSH technique is contested by those that prefer working with realistic observed flood hydrographs. It is important to note that the hydraulic combination of differen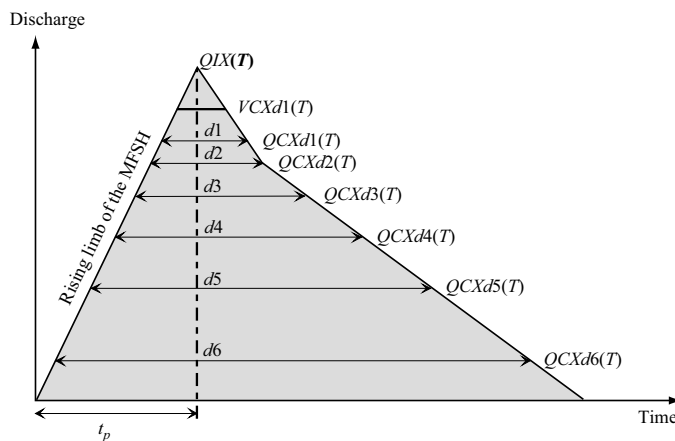t MFSHs at the confluence of a given watercourse leads to discharges with return periods that are in principle different from those of the original MFSHs. The resulting flood can become difficult to use. It can for example be difficult to assign a return period to the flood map constructed using these combined discharges. The use of an MFSH however makes it possible to construct a design hydrograph for which the return period is greater than that of the highest flood observed on the drainage basin. Moreover, the QDF and MFSH curves can be regionalized without major difficulties and in this way make it possible to estimate a design hydrograph for any non-instrumented basin of a given region (Javelle, 2001).

9.3.2 Design Floods Obtained by Hydrometeorological Simulations

Design floods can be obtained by simulations based on selected meteorological scenarios using an appropriate hydrological model. This approach is widely used, in particular when insufficient discharge data are available for the basin.

Many hydrological models can be used for simulations. They are generally conceptual or physically-based models representing the hydrological behavior of the basin with varying degrees of simplification (Chapter 3). Depending on the nature and quality of available data for the basin or more widely for the region of the considered basin, the model necessary for hydrological simulations can be obtained in various manners. If series of concurrent data for discharges and key meteorological variables (e.g., rainfall, temperature) are available for the basin, the model can be constructed, calibrated and validated using these data. If data for the basin is insufficient or inexistent, and if instrumented basins exist in the region that are similar to the basin of interest, a regionalized hydrological model can be used (Chapter 11). In all cases, it is necessary to make sure that the model can be used to simulate events corresponding to the required return period. In particular, this means that the discharge series used to develop the model must contain major floods.

When a hydrological model is available for the basin, it can be used to simulate floods corresponding to various meteorological scenarios observed or generated elsewhere (Chapter 12). In both cases, the approach can be based on single events (i.e., the estimated flood is produced by a particular meteorological event) or multiple events (i.e., with simulation of several meteorological events).

Single-event approach

The single-event approach consists first in defining a design meteorological scenario and then in choosing an initial state of the basin so as to obtain, by simulation, the required flood hydrograph. The meteorological and initial state scenarios then form a design hydrometeorological configuration.

The design meteorological scenario is in most cases restricted to the definition of the design rainfall for the basin. To identify or construct a design rainfall, several approaches can be followed. They are described in Chapter 12. The design rainfall, whether synthetic or corresponding to an observed event, will often be chosen according to the return period of its maximum mean intensity over the critical duration for the studied drainage basin. The meteorological scenario must in certain cases specify the values to be assigned to other

key meteorological variables. In mountainous regions, this concerns for example the 0°C isotherm elevation (Chapter 7).

The description of the initial state of the basin consists in specifying the main state variables of the medium. These variables condition the intensity and characteristics of the flood resulting from the design meteorological scenario (e.g., soil moisture, storage level of reservoirs, snowpack state). The choice of the initial state of the basin is often restricted to the main state variables of the model related to the rainfall-process (e.g., degree of saturation of the soil, see Chapter 4). In this way, the runoff coefficient obtained by simulation corresponds to a design runoff coefficient, chosen elsewhere.

This single-event approach is in fact highly questionable. The intensity of a flood resulting from a given rainfall is for example very dependent on the antecedent basin saturation conditions (Figure 9.12a). However, these conditions can also be considered to be a random variable. The intensity of the flood and its shape is also very dependent on the shape of the design rainfall (Figure 9.12b). The design flood estimated using a single-event approach therefore depends on a certain number of necessarily arbitrary choices.

Moreover, the single-event approach is most often used to produce a design flood hydrograph corresponding to a given return period *T*. Note however that it is a priori impossible to construct a design hydrometeorological configuration corresponding to a given return period or, conversely, to associate a return period to a given design hydrometeorological configuration. In particular, there is no reason why the return period of a design flood obtained by simulation should be equal to the return period of the project rainfall used to produce it. This is however all too often assumed to be the case for reasons of convenience.

Note that this approach is used especially in North America and Great Britain (NERC, 1975) to estimate the Probable Maximum Flood (PMF) produced by the Probable Maximum Precipitation (PMP) falling on the considered drainage basin (Chapter 12). This approach, referred to as the PMP-PMF method, provides one of the most conservative flood estimates given that it theoretically corresponds to a quasi-zero probability of exceedance. The PMF is generally used as a design flood for hydraulic projects such as large dams (e.g., Berod, 1994; Dumas, 2006).
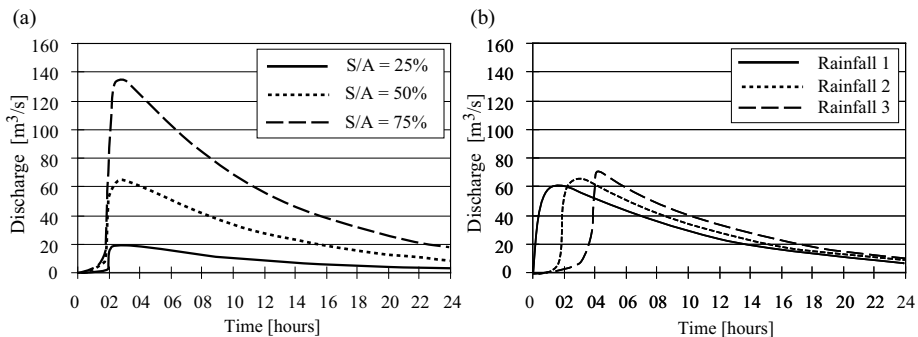
Fig. 9.12: Design floods obtained for the Murg river (Switzerland) at Murgenthal, Walliswil (207 km²) by simulations using the GSM-SOCONT hydrological model (Schaefli *et al.*, 2005) and a synthetic design rainfall with a return period *T* of 20 years. a) Influence of initial conditions for a centered synthetic rainfall (degree of saturation of the soil *S(t)/A*). b) Influence of the shape of the design rainfall (rainfalls 1, 2 and 3 corresponding respectively to a right-skewed (lagging), centered and left-skewed (leading) synthetic design rainfall as represented in Figure 12.14).

Multi-event approach

The multi-event approach avoids some of the limitations of the single-event approach. This method does not consider the notion of rainfall event return periods, but rather that of the return period of simulated floods.

The principle is to simulate floods for different hydrometeorological configurations that result from random combinations of different meteorological situations and different initial states of the drainage basin. This approach therefore eliminates the difficult choice of a single design hydrometeorological rainfall (i.e., the choice of the structure of the design rainfall as well as the choice of the initial state of the basin). It can be used to produce a catalog of floods. Appropriate statistical processing of the floods in this catalog makes it possible to extract floods or flood characteristics that are pertinent for a given study.[3]

Two methods can be used to build a flood catalog. The first consists in generating a catalog of meteorological situations. Different situations concerning the initial state of the basin must also be generated elsewhere. These two types of situations can be obtained either by re-sampling observed situations or by simulations using appropriate stochastic generators. The different random variables considered in this approach are generally assumed to be independent and can be used to construct as many hydrometeorological situations as required. Such an approach was used for example by Consuegra *et al.* (1998) to produce a catalog of floods at different stations on the Rhone river upstream of Branson, Switzerland (Figure 9.13 and Figure 9.14).

The second method is based on continuous simulation. Given the many advantages of this approach, it is tending to replace the single-event and multi-event approaches discussed above. Its principle will be described below.

Production of flood scenarios by continuous simulation

Continuous simulation based on time series of key meteorological variables for the basin (e.g., precipitation, reference evapotranspiration, temperature) can be used to reconstruct or generate discharge time series. The simulated discharge series are subsequently processed statistically to extract floods or flood characteristics that are pertinent to the concerned study. Note that the continuous simulation model monitors the state of the drainage basin (e.g., saturation, snowpack). As opposed to the multi-event approach presented above, continuous simulation eliminates the need to choose the initial state of the drainage basin.

The procedure to be implemented varies according to the length of the available series of observed meteorological variables, in particular precipitation. If a precipitation series exists for the basin, along with other meteorological variables, over a period at least equal to the required return period for the design flood, continuous simulation can then be used to reconstruct part of the discharge record and consequently extend the length of the "observed" discharge series.

If, on the other hand, the return period of the design flood is greater than the length of the precipitation series, values of precipitation and other key meteorological variables can be produced using an appropriate stochastic generator (Chapter 12). These series are then transformed into discharges using a deterministic hydrological model. Such an approach

---

[3]It is also possible to study hydrological system failures (e.g., overflows).
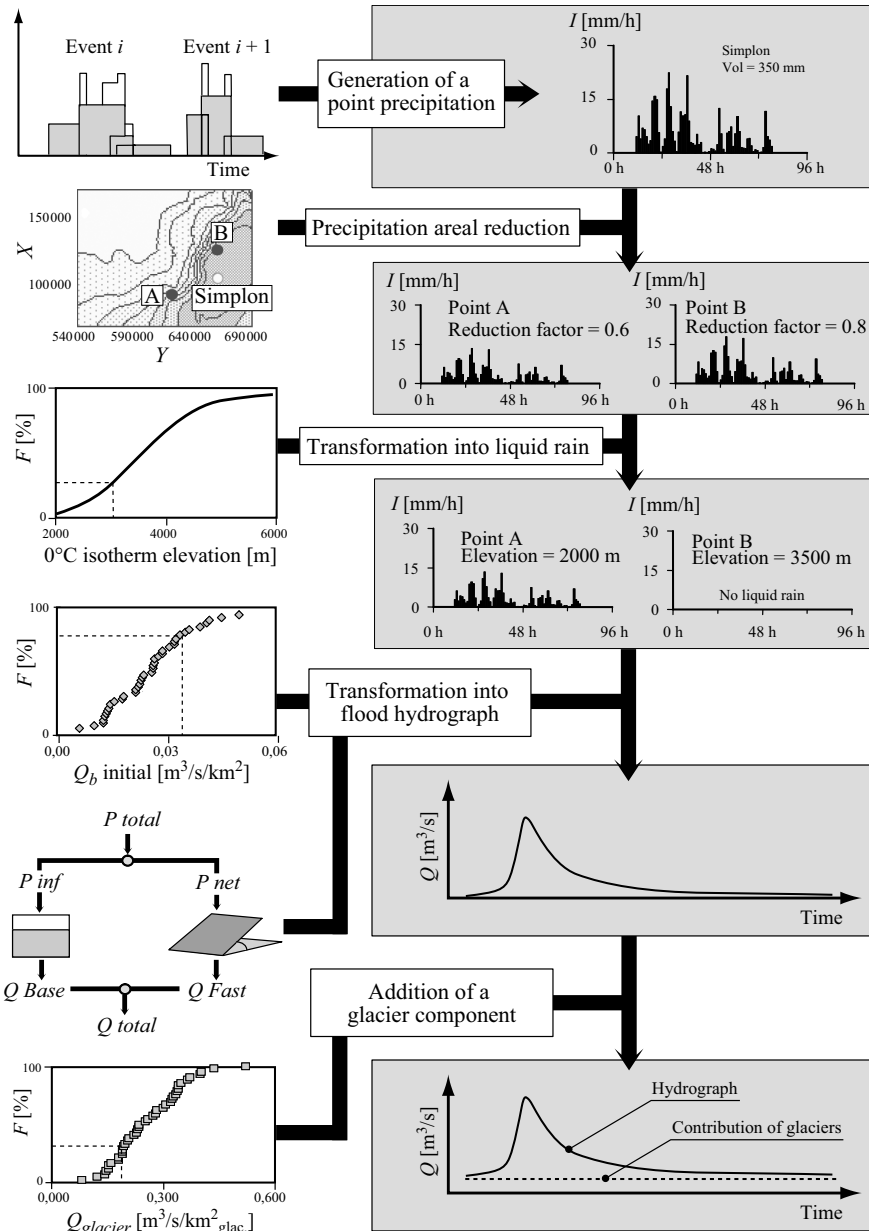
Fig. 9.13: Illustration of a multi-event approach for the generation of design flood scenarios (adapted from Consuegra *et al.*, 1998). The precipitation scenarios are extracted from a precipitation series generated using the NSRPM stochastic generator (Section 12.4.2 and Favre, 2001). The percentage of precipitation falling in liquid form is determined after randomly drawing the 0°C isotherm elevation from the empirical distribution corresponding to the considered season. The glacier and non-glacier base flows (that depend on the saturation state of the drainage basin) are drawn randomly from appropriate empirical distributions. The non-glacier base flow can be used to initialize the hydrological model (initialization of the ground storage fill fraction) used finally to simulate the basin response to the meteorological configuration obtained elsewhere.
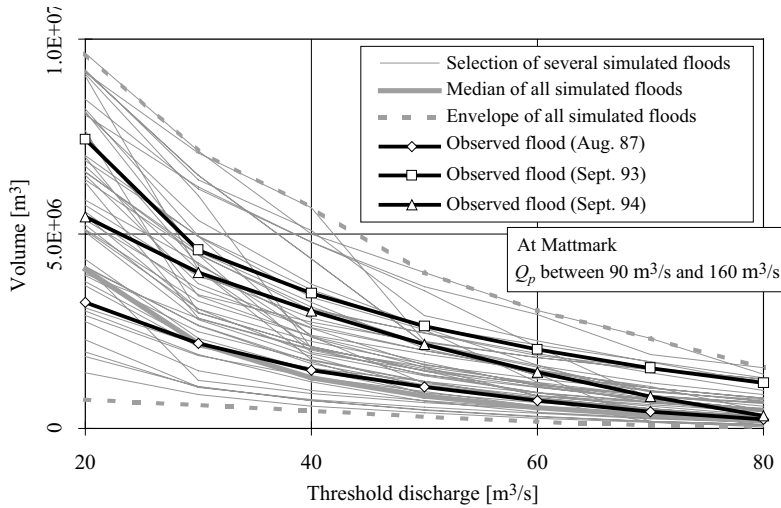
Fig. 9.14: Continued from Figure 9.13. Volumes greater than different threshold discharges for the *n* floods in the flood catalog obtained using the methodology proposed Consuegra *et al.* (1998).

has been used to generate discharge time series and produce a catalog of floods for different stations on the Rhone river upstream of Lake Geneva (Hingray *et al.*, 2006b). Figure 9.15 illustrates the principle of the corresponding method.

A stochastic generator can be used to create as many plausible meteorological scenarios as necessary for the present climatic context (Mezghani and Hingray, 2009). In particular, it is possible to produce precipitation with different shapes, spatial structures and intensities. The method also allows generation of inter-event durations of varying lengths and rapid successions of infrequent precipitation events leading to exceptional hydrological situations. In this way, continuous simulation can artificially reproduce a large number of plausible hydrological events induced by a wide variety of meteorological forcing conditions and initial drainage basin situations. Similarly, different flood configurations can be produced as well as "pulsed" floods corresponding to rapid successions of rainfalls.

When using this approach, it is recommended to generate *N* time series of meteorological variables to produce *N* discharge time series with a hydrological model. Then, *N* frequency distribution fits can be carried out on the annual maximum discharges and *N* estimates of peak discharge quantiles with return periods *T*. It is therefore possible to estimate the possible variation interval of a given quantile in addition to its conventional unique value. For example, the 90% confidence interval can be determined for the values of the obtained quantiles. For a given return period, is also possible to extract—from the generated discharge series—all events for which the maximum discharges are included in this likelihood interval. This catalog of events can then be used to carry out various sensitivity analyses. Examples include submersion impact analysis as a function of different overflow volumes. Figures 9.16 and 9.17 show examples of maximum hourly discharge statistics along with various design floods obtained using this methodology for two stations on the Rhone river upstream of Lake Geneva.
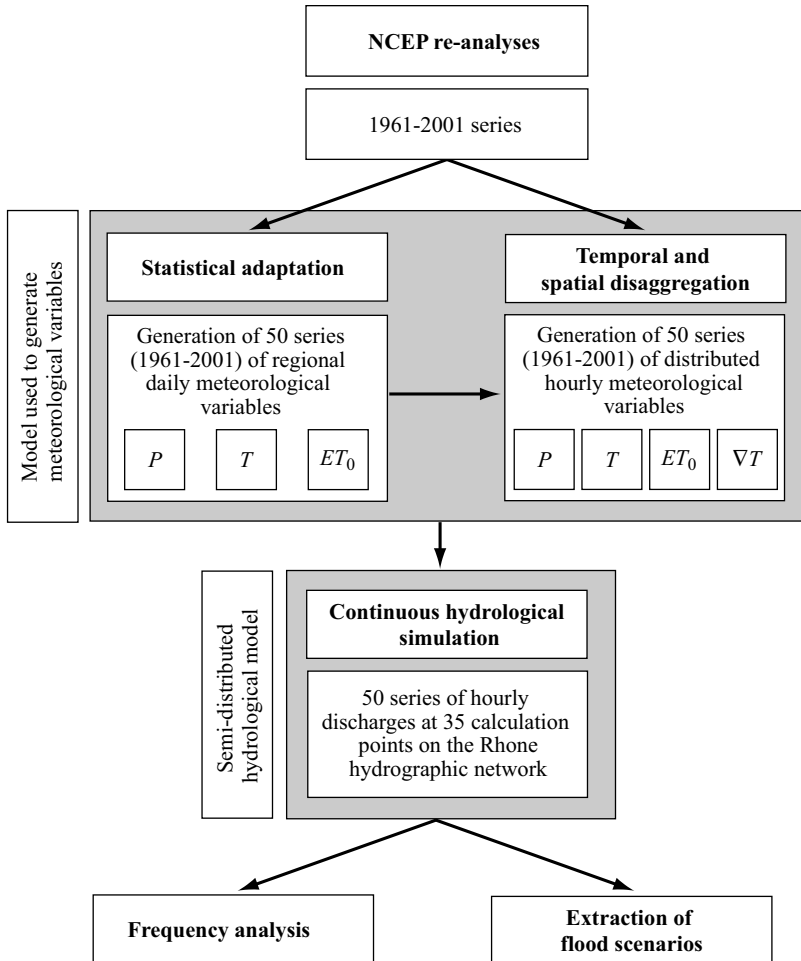
Fig. 9.15: Illustration of a continuous simulation approach for the generation of design flood scenarios on the basis of 50 meteorological scenarios produced by a stochastic generator of precipitation/temperature time series (adapted from Hingray *et al.*, 2006b) and methodology for the generation of discharge time series at 35 control sections of the Rhone river basin upstream of Lake Geneva. Note that: 1) the atmospheric re-analyses used are NCEP atmospheric re-analyses (Chapter 2), 2) the principle of the statistical downscaling method used to generate scenarios on the basis of re-analyses is presented in Section 12.4.4, 3) temporal and spatial disaggregation is used to adapt regional daily meteorological variables to the time and space scales required for the hydrological model by applying a plausible spatial and temporal structure (see also Section 12.4.4).

By producing a wide range of complete flood hydrographs, this methodology involving stochastic rainfall generation makes it unnecessary to make the difficult choice of a unique flood hydrograph. Although more complicated to use than classic flood prediction methods, it is increasingly used to generate flood scenarios. In addition to the method presented above, other examples include the SHYPRE method developed by CEMAGREF (Arnaud and Lavabre, 2002) or the SCHADEX method presented by EDF (Paquet *et al.*, 2006).
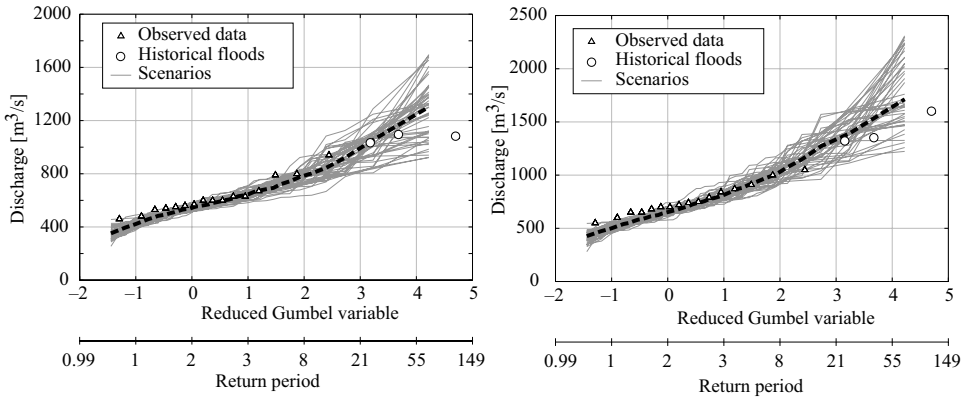
Fig. 9.16: Continued from Figure 9.15. Statistics of simulated maximum hourly discharges (solid curves) and observed discharges (triangles) for the Rhone river at Porte du Scex and Branson (u is the reduced Gumbel variable and the dashed curve joins the median values of the 50 quantiles obtained for non-exceedance frequencies).
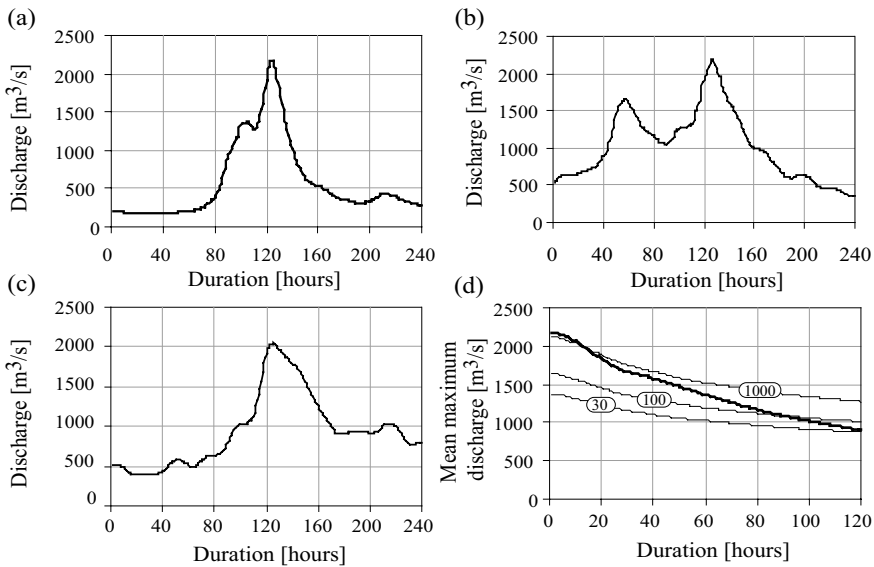
Fig. 9.17: Continued from Figure 9.16. Three design floods generated for Porte du Scex for a return period T of approximately 1000 years. d) Plot of one of the floods on the QDF curves obtained from the simulations.

9.4 CHOICE OF APPROPRIATE METHODS

A wide range of methods are available to estimate flood discharges, hydrographs and scenarios. Although a number of practical guides have been published (e.g., OFEG, 2003; Lang *et al.*, 2005), few criteria or recommendations are available to choose the best method for a given case. For a given project, this choice depends mainly on available data, technical criteria and the objectives. Other considerations should however be analyzed. The objective of this section is to point out the implications of certain choices. The final

decision will however often be guided to some extent by the intuition, subjectivity and consequently experience of the engineer in charge.

9.4.1 Importance of the Geographic Context

The physiographic characteristics of the drainage basin and the different projects constructed within it greatly influence the hydrological response of the basin to a given meteorological forcing (Musy and Higy, 2011). The geographic context of a project therefore generally influences the choice of an estimation method, which should be able to take into account key factors related to floods.

The tendency to omit certain key factors is particularly strong when the analysis is based mainly on a statistical method. On the other hand, when a simulation method is used, the engineer is often obliged to pay special attention to the characteristics of the drainage basin and its hydrographic network and take into account any projects that could affect flood discharges.

9.4.2 Importance of the Historical Context

When estimating flood flows, it is always important to take into account the effects of changes in land use or hydraulic modifications of the watercourse itself. A historical study can often identify the main processes generating floods as well as certain key factors related to basin development projects that may have modified these processes. These factors include deforestation, reforestation, land improvement projects, agricultural practices, urbanization, the construction of transportation infrastructures (e.g., railways, highways), the maintenance of watercourses, restoration of channel sections and the construction of dikes and any other hydraulic works intended to retain, capture, divert or discharge water.

Note that it is also necessary to take future basin development projects into account when estimating flood scenarios. Neglecting the planned evolution of the drainage basin can lead to premature obsolescence of development projects.

9.4.3 Importance of the Size of the Drainage Basin

The size of the drainage basin is often a limiting factor in the application of a flood prediction method. For instance, use of the rational method is limited to relatively small drainage basins due to the assumption of uniform precipitation over the basin. On the other hand, the index flood method is generally not recommended for small basins (Chapter 11). Simulation models in principle impose no limits on the size of the basin except possibly those related to the meteorological scenario generator—often limited to the generation of fields with little spatial variability (Chapter 12).

9.4.4 Importance of the Project Objective

As already emphasized throughout this chapter, the hydrological variable to be estimated as well as the level of complexity of the method generally depend on the objective of the project or study. For example, standard design work generally does not require the use of

complex methods. Simpler formulations should be preferred, as long as their parameters can be estimated using nomographs or regional models validated for the study zone.

Note that there is also a "cultural" factor affecting the choice of a method or the required accuracy of flood prediction. The methods used for the same objective can thus differ greatly from one region of the globe to another. The perception of flood risks and the way they are dealt with are for example not the same around the world.

Note also that design projects and studies increasingly impose the use of a hydrological simulation model that provides more information and that can eventually be used as continuous hydrologic model. Theoretically, any type of rainfall-runoff model could be used for this type of approach. The most suitable models are generally distributed conceptual models. They offer reasonable performance and are in particular parsimonious, thereby reducing computing time. Combined with adequate hydrometeorological scenarios, such models are a good alternative to frequency analysis which is often used for extrapolation. Such models can also sometimes take into account the effect of anthropogenic modifications on floods. These modifications may be the result of urbanization or the construction of hydraulic works such as reservoirs or diversion works. These models are however not always easy to use. The main problem remains their parameterization that, in the absence of data, must be based on the judgment of the engineer or on regionalized parameter values.

9.4.5 Summary

In summary, Figures 9.18 and 9.19 present the main methods that can be used to predict flood flows, depending on the nature of available hydrometric and meteorological data and the possibility of hydrological modeling on the basin. Note that these figures are not decision trees. For example, if a flood peak discharge must be estimated on a large drainage basin, the index flood method should be preferred over the rational method, even if IDF curves are available. The application of each method is obviously conditioned by the validity of its specific assumptions. For reasons of legibility, only the main constraints affecting the choice of a method are presented in these figures.

Note also that in certain contexts, several methods may be applicable. In such cases, if compatible with available time and financial resources, it is recommended to use all the methods to obtain different estimates of the variable of interest. In this way, it is possible to estimate inter-model consistency. It may also be possible to combine the estimates. An example of a combined estimate is presented in Chapter 11.

9.5 KEY POINTS OF THE CHAPTER

- Estimating flood flows is essential for the management of water resources and associated hydrological risks.
- Ideally, before any analysis of flood flows, the different processes or factors influencing flood discharges on the considered basin should be identified.
- If only the discharge capacity of the system is concerned (e.g., for the sizing of a spillway), estimation of the characteristic flood flow is sufficient. For other cases (e.g., sizing of a reservoir), a complete flood hydrograph is generally required.

Fig. 9.18: Estimation of peak discharges according to available data. Remarks: (1) The hydrological model can be calibrated using local data (concurrent precipitation and discharge series) or can use regionalized parameters. (2) Precipitation data can be either observed or generated stochastically. Other series of key meteorological variables are sometimes required (temperature, reference evaporation, net radiation, etc.). (3) The GRADEX method requires a series of maximum flood discharges of at least 10 years. (4) If the length of the available discharge series is sufficient, the index flood is estimated on the basis of observed annual maximum discharges. If not, it can be estimated on the basis of a regional statistical model.

- If sufficient discharge measurements are available, the return period of the characteristic flood flow can be estimated on the basis of an appropriate frequency analysis. It is often worthwhile to integrate information on historical floods if available.
- If a maximum precipitation series much longer than the maximum discharge series is available, these data can be used to estimate the asymptotic behavior of maximum discharges (GRADEX method).
- In the absence of sufficient hydrometric data, various regional methods can be used to estimate the required characteristic flood flow.
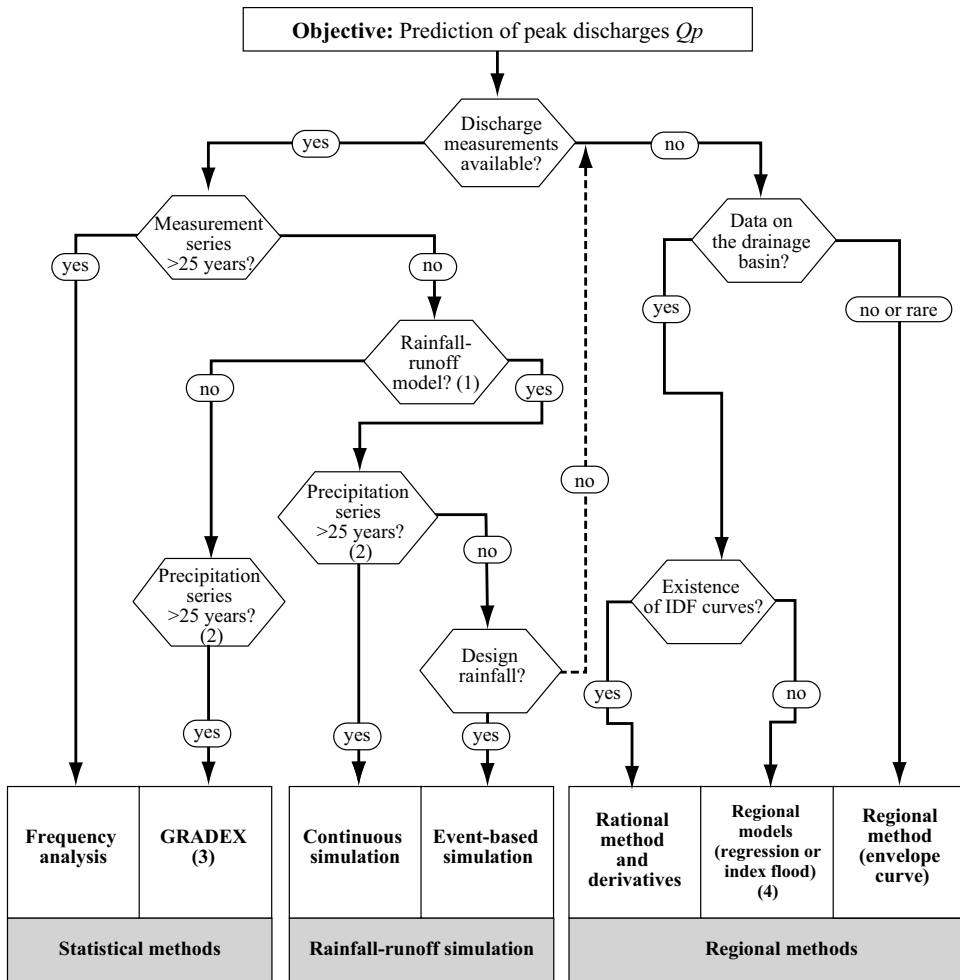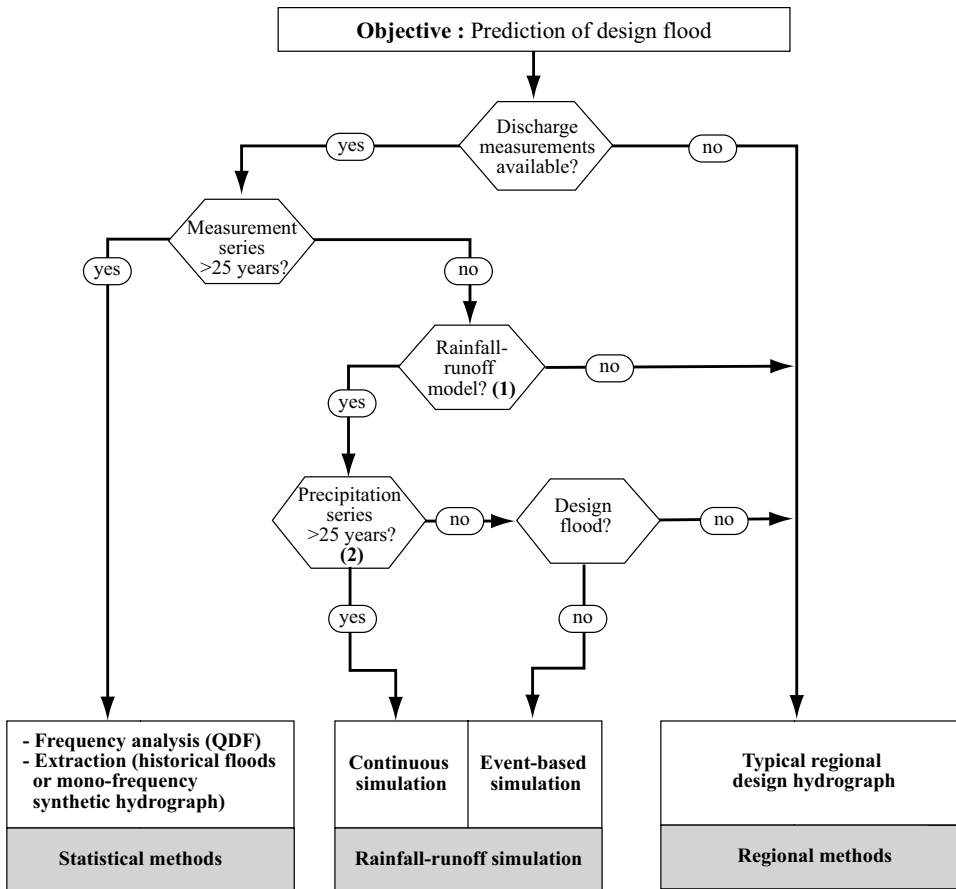
Fig. 9.19: Estimation of design floods according to available data. Remarks: (1) The hydrological model can be calibrated using local data (concurrent precipitation and discharge series) or can use regionalized parameters (if a regional model is available, discharge data is not required to apply rainfall-runoff simulation type methods. (2) Precipitation data can be either observed or generated stochastically. Other series of key meteorological variables are sometimes required (temperature, reference evaporation, net radiation, etc.).

- The most widely used regional methods are the statistical index flood method and pseudo-empirical approaches such as the rational method. The first is based on a regional frequency model estimated on instrumented basins of the region. The second uses in particular statistics on the maximum mean precipitation of the basin.
- The return period of a flood hydrograph is difficult to estimate.
- A hydrological study based on different flood scenarios is better than a study based on a single flood.
- If sufficient discharge measurements are available for the basin, different flood hydrographs can be extracted from the data (observed or mono-frequency synthetic hydrographs).

- If a hydrological model is available for the considered basin, it can be used to produce different flood scenarios on the basis of different hydrometeorological scenarios. This approach can be based on single or multiple events. The hydrometeorological scenarios can be either based on observations or produced by an appropriate stochastic generator.

9.6 APPENDICES

9.6.1 Questions Concerning the Return Period and the Probability of Occurrence Over a Period of *N* Years

The return period *T* of a given event is associated with the non-exceedance probability *F* of the corresponding quantile or its probability of exceedance *p* (Addendum 8.1). The estimated return period *T* of a given discharge indicates that the discharge will be exceeded on the average once every *T* years (*i.e., k* times in *k T* years). The notion of return period does not however provide answers to other pertinent questions that an engineer can pose such as:

- What is the probability that an event with a return period *T* will occur at least twice over the next 10 years?
- What is the return period of the flood that has a 1 in 3 chance of being exceeded over the next 50 years?

In order to answer such questions, it is necessary to use Bernoulli and binomial probability distributions (Meylan *et al.*, 2012).

Question 1: What is the probability *P* that a flood with a return period *T* will be reached or exceeded at least once during the *n* years of the project lifetime?

The probability *P* that the flood will occur at least once over the *n* next years can be expressed as:

$$P = p(X \geq 1) = 1 - p(X = 0) = 1 - (1 - p)^n = 1 - (1 - 1/T)^n \tag{9.7}$$

Question 2: What is the average return period *T* of discharges that will have a *P* percent chance of occurring at least once over the *n* next years.

The return period in question can be obtained directly from the equation above:

$$T = 1/p \text{ where } p = 1 - (1 - P)^{1/n} \tag{9.8}$$

The table below gives the values of return period *T* for different probabilities *P* of exceedance and different project lifetimes *n*.

P [%]	Number of years *n*						
	2	5	10	20	50	100	500
99	1.1	1.7	2.7	4.9	11	22	109
90	1.5	2.7	4.9	9.2	22	44	218
75	2.0	4.1	7.7	15	37	73	361
50	3.4	7.7	15	29	73	145	722
25	7.5	18	35	70	174	348	1739
10	19	48	95	190	475	950	4746
1	199	498	995	1990	4975	9950	49750

The following graph summarizes the relationship between the 3 quantities *T*, *n* and *P*.
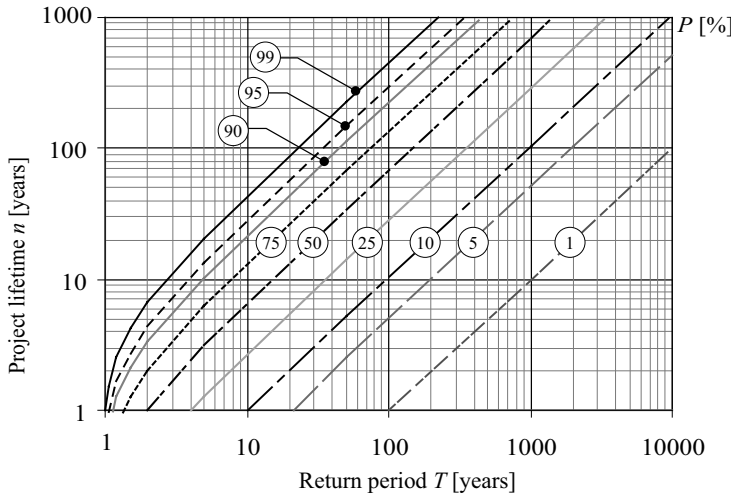
Fig. 9.20: Probability of exceeding the design flood for different return periods and project lifetimes.

Question 3: In how many years will the first project failure occur.

First determine the probability that the failure will occur in exactly *n* years. The probability distribution is the geometric function expressed by:

$$p\{X = n\} = (1 - p)^{n-1} \cdot p \tag{9.9}$$

From this, the probability that the first failure will occur only after at least *k* years is given by:

$$p\{X \geq k\} = (1 - p)^{k-1} \tag{9.10}$$

Note that the expected value of the random variable *X* according to a geometric distribution is equal to $1/p$, i.e., the quantity commonly referred to as the return period.

Question 4: What is the probability that a flood with a return period greater than *m* will occur at least once during the *m* next years.

Apply once again the binomial distribution B($m, 1/m$) which gives:

$$p(0) = 1 - (1 - 1/m)^m \tag{9.11}$$

For a sufficiently large value *m*, the probability is 63%. This value is important in that it leads to the following conclusion:

A project designed for a critical event with a return period of *T* years globally has 2 out of 3 chance (63%) of failing over the *T* years to come.

9.6.2 Double-calculation Verification of the Peak Discharge Estimated by the Rational Method

Let us assume that the rational method has been applied to estimate the peak discharge of return period *T* at the outlet of a given basin *B* (e.g., basin *B4* in the configuration presented in Figure 9.21). The objective of the double-calculation procedure is to identify a sub-basin configuration that could possibly produce a higher peak discharge at this outlet than the initial configuration (see Figure 9.21). It is assumed that the drainage basin is made up of sub-basins B_1, B_2, ...B_n with different

characteristics. For each sub-basin or group of sub-basins, the time of concentration through to the outlet of the complete basin B can be calculated. When the time of concentration tc_k of a given configuration C_k (a sub-basin B_i or a group of sub-basins GB_j) is less than the time of concentration tc_B of basin B, the rational formula is applied to this configuration C_k using tc_k. This procedure makes it possible to identify, in a simple and effective manner, the possible parts of the complete basin that produce a higher estimate of the required peak discharge.

In the event of a positive test result (i.e., when the discharge obtained with configuration C_k is greater than that obtained initially for basin $B4$), the peak discharge obtained initially for the complete basin B with time of concentration tc_B cannot be used for design. Note that the critical rainfall duration for basin B is therefore not equal to its time of concentration. Furthermore, the highest peak discharge obtained for a configuration C_k cannot be taken directly as the design flood discharge. It is first necessary to add the contribution of the rest of basin B (i.e., B-C_k) that also contributes with time of concentration tc_k to the discharge at the outlet of B. This contribution is only a portion of the contribution that could be calculated by applying the rational formula to this additional part since its time of concentration (tc_B) is higher than the critical duration (tc_k) of the obtained rainfall. Example 9.3 below illustrates the principle of this design flood verification method.
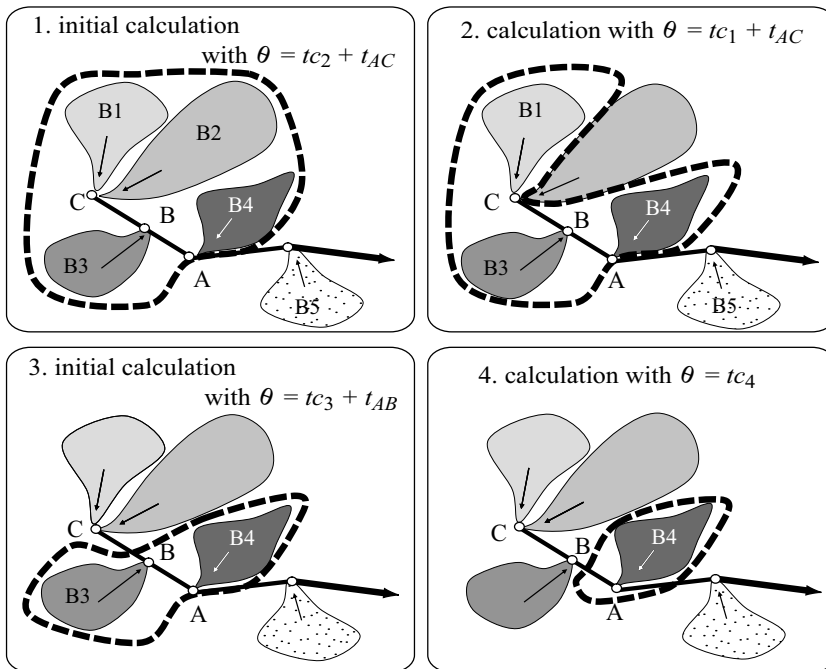
Fig. 9.21: Principle of the double-calculation method. The design discharge is to be determined at outlet A of basin B4. Three additional calculations will be carried out with the three parts of basin B4 for which the time of concentration is less than that of complete basin B4. The corresponding configurations are: C1 = B1 + B3 + B4, C2 = B3 +B4 and C3 =B4.

Example 9.3

The basin is made up of two sub-basins in parallel, one urbanized and the other a rural type peri-urban basin that is larger, far less responsive but also far less productive in terms of runoff. The configuration is illustrated on the left-hand side of Figure 9.8 (Figure 9.8a). The characteristics of the different sub-basins are indicated in the table below. For the studied region, the appropriate

IDF model is the following: $i(t) = a(T)/(b+t)$ where i is the rainfall intensity in mm/h, t the rainfall duration in minutes, $a(20 \text{ yrs})=2300$ and $b=12$ minutes.

	Rural zone (B1)	Urban zone (B2)
Area (A)	110 ha	40 ha
Runoff coefficient (C_r)	0.2	0.5
Time of concentration (t_c)	60 minutes	20 minutes
Reduced area (A_R)	22 ha	20 ha

1. The time of concentration tc_3 of basin $B3=B1+B2$ is: $tc_3=60$ minutes
2. The corresponding maximum mean intensity is: $i_3 = a/(b+tc_3) = 32$ mm/h
3. The mean runoff coefficient for the entire basin ($B3=B1+B2$) is:

$$Cr_3 = (A_1 Cr_1 + A_2 Cr_2)/(A_1 + A_2) \tag{9.12}$$

4. The peak discharge at the outlet of $B3$ for a return period $T = 20$ years is:

$$Q_{3\text{-}20}(tc_3) = A_3 Cr_3 i_3 = A_3 Cr_3 a/(b+tc_3) = 3.8 \text{ m}^3/\text{s} \tag{9.13}$$

5. Verification with the urban basin: The time of concentration of the urban basin ($B2$) is $tc_2=20$ minutes. The intensity of the rainfall of corresponding duration is $i_2 = a/(b+tc_2) = 72$ mm/h and the peak discharge at the outlet of $B3$ resulting from the sole contribution of $B2$ for this rainfall is:

$$Q_{2\text{-}20}(tc_2) = A_2 Cr_2 i_2 = 4.1 \text{ m}^3/\text{s} \tag{9.14}$$

Conclusion: The peak discharge coming from the urban zone alone, corresponding to a rainfall of duration tc_2, is greater than the total peak discharge corresponding to a rainfall of duration tc_3 obtained for the entire basin $B3$. The critical duration for basin $B3$ is therefore not tc_1, given that tc_2 produces a higher peak discharge than tc_1. The discharge that should be used to design the storm sewer at the outlet of basin $B3$ for a return period of $T=20$ years is therefore greater than 4.1 m³/s (it is in fact equal to $4.1+x$ m³/s where x is the contribution of rural sub-basin $B1$ for the same rainfall with intensity i_2 and duration tc_2).

9.6.3 Use of the Time-area Diagram to Verify Peak Discharges Calculated with the Rational Method

Definition of the time-area diagram

The time-area diagram (also referred to as the (A_R-t_c) diagram or the curve of area versus concentration time curve) can be used to evaluate the fraction of the total reduced area of the drainage basin effectively contributing to the discharge at the basin outlet at time t (t in minutes after the beginning of the rainfall). Note that the time-area curve of the basin is, after normalization with respect to the drainage basin area, equivalent to the S-curve of the drainage basin (Chapter 5).

Using the time-area diagram to check discharges calculated with the rational method

The time-area diagram can be used to check and correct discharges estimated with the rational formula. Assume that an IDF model of the Talbot type is available (the maximum mean intensity of a rainfall of duration t with a return period T has the following expression $i(T,t)=a(T)/(b+t)$). The time-area diagram can be used to check that the critical duration of a uniform rainfall over the considered basin (that leads to the maximum peak discharge) is strictly equal to the time of concentration of

the basin. If this is not the case, it can be used to graphically identify the critical duration for the basin and then calculate the corresponding peak discharge. For a given return period T, the peak discharge of the flood hydrograph resulting from a uniform rainfall of duration t less than the time of concentration of the basin can be expressed as follows:

$$Q_p(T,t) = A_R(t) \cdot i_{\max}(T,t) = a(T) \cdot \frac{A_R(t)}{b+t} \qquad (9.15)$$

where $A_R(t) = [C \cdot A](t)$, the fraction of the total reduced area of the basin effectively contributing to the discharge at the basin outlet at time t.

For a fixed return period, the peak discharge resulting from a rainfall of constant intensity is therefore, according to the above formulation, a function of the rainfall duration. The maximum peak discharge will be obtained for a maximum ratio $A_R(t)/(b+t)$. For a given rainfall duration t, this ratio is simply the slope of the line D passing through A($-b$,0) and M(t, $A_R(t)$) in the time-area diagram of the basin. To determine the critical rainfall duration for basin B, it is therefore sufficient to determine the straight line D tangent to the time-area diagram that has the steepest slope.

This corresponds to the line Dx for basin B3 presented in Example 9.3 of Appendix 9.6.2 (Figure 9.22). The corresponding critical duration for this basin is θ=20 minutes. The corresponding reduced surface is 27.3 ha and the corresponding critical discharge obtained using the above equation is Qp = 5.6 m³/s.
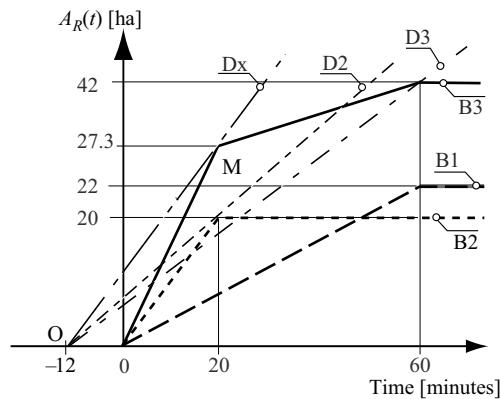
Fig. 9.22: Time-area diagrams for basins B1, B2 and B3 = B1 + B2 described in Example 9.3. The IDF model used is expressed by: $i(T,t)=a(T)/(b+t)$.

Constructing a time-area diagram

A time-area diagram can be constructed in a number of ways (choice of the default shape depending on the shape of the basin, choice of the default shape for each of the sub-basins followed by combination of the individual diagrams at the outlet of the complete basin, use of a simple transfer model derived for example from a digital elevation model). The simplest method assumes that the function $A_R(t)$ is an affine function of time for each sub-basin of the complete basin (method used to construct the diagram in Figure 9.22).

Advantages and limitations of this method

This method avoids the erroneous design discharges often produced by the rational method in various situations in which the assumptions of the method are not valid.

An important limitation of this method is related to the manual graphical approach used that can rapidly become tedious if the time of concentration of the basin is unknown. In a rural environment, the time of concentration can be estimated using regional models on the basis of the basin characteristics alone. In an urban environment, the behavior of the basins cannot usually be considered to be linear and the time of concentration of the basins, and consequently the time-area diagram itself, is generally dependent on the discharge in the considered network, which is unknown given that it is the quantity that must be estimated. The iterative procedure required in this case makes it difficult to use the time-area diagram.

CHAPTER 10

HYDROLOGICAL FORECASTING

The objective of hydrological forecasting is to provide a quantitative estimate of the future state of various hydrological variables (e.g., river discharge or stage, groundwater level) or their change over a given forthcoming time period. Forecasting provides information for the real-time management of water resources and associated hydrological risks. It is different from prediction (often referred to as "predetermination" in French-speaking countries), the objective of which is to associate a non-exceedance probability to these hydrological variables, but not for any predefined time in the future.

The environment, data and tools required for a forecasting system are specific to this task. In particular, a hydrological forecasting system requires:

- A system to collect and forward, most often in real time, the data required to define the state of the system at time t.
- A system to collect and process past or forecasted meteorological data.
- A hydrological forecasting model capable of processing all these data.
- A forecasting service, operational at all times, to monitor the forecasts and issue the associated reports and warnings.

Hydrological forecasts are useful in many applications such as flood and low-flow forecasting on through to longer term forecasting of water resources. Forecasting methods are also varied. They extend from simple statistical regression models on through to physically-based hydrological simulation models that represent the different inputs and outputs of energy and water within the considered drainage basins and hydrographic networks.

This chapter deals with the main questions related to hydrological forecasting. Section 10.1 will introduce the principles of forecasting, forecasting models and more generally forecasting systems. Section 10.2 will then present the components that can or must be used to develop and operate a forecasting model. Sections 10.3 and 10.4 will deal with uncertainties and the quality of a forecast. Section 10.5 will provide a few indications on how to choose the right forecasting method for a given context.

Readers looking for more information on existing forecasting methods and ways to implement them can refer to the many publications dedicated to this subject, for instance the Guide de Prévision des Crues published under the direction of P.A. Roche (Roche, 1987). This guide provides an overview of the work of the Flood Forecasting group of S.H.F. (Société Hydrotechnique de France) and is still today an authoritative reference in France.

10.1 INTRODUCTION

10.1.1 Forecasting Principles and Key Issues

Forecasting horizon, lead time and updating interval

The principle of forecasting is always associated with a given forecasting time horizon or lead time. The term forecasting horizon will be used here to designate the future time or date at which the value of the considered hydrological variable or its change with time must be estimated. The time interval between the forecast time, i.e., the time when the forecast is made, and the forecasting horizon is often referred to as the forecast period. This period also represents the lead time of the forecast. For a given forecasting horizon, the lead time decreases as the horizon approaches. For a fixed lead time, the forecasting horizon advances as time passes (Figure 10.1).

Whatever the forecasting model used, a forecast always reveals certain errors when subsequently compared with the observed values of the hydrological variable. If these errors are not used to correct future forecasts in real time, the quality of the forecast can decrease with time. To avoid this, the forecast is generally updated at regular intervals depending on the errors observed in the recent past. The forecast is updated as time advances and new observed or simulated data become available (e.g., observations on the state of the hydrological system, recently observed and newly forecasted meteorological data). The updating interval, i.e., the time between two successive forecast updates, is also an important time characteristic of a forecast. Regular updating of a forecast leads to a typical graphical representation of the forecast which can be referred to as a "spaghetti graph". Each "spaghetti string" corresponds to new forecast of the variable considered (Figure 10.1).
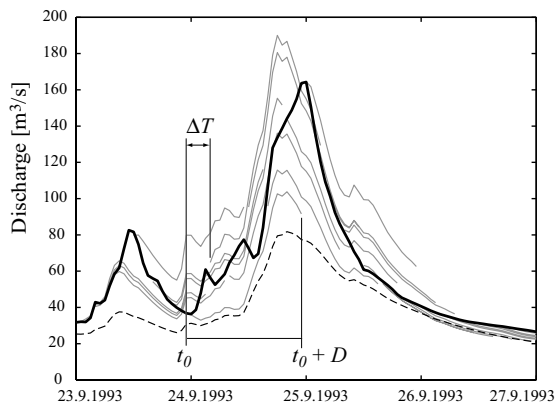
Fig. 10.1: Forecasting principles and time characteristics. Forecasting of discharges for the Rhone basin at Reckingen (215 km²) for a +24 h lead time with a forecast updating procedure. Bold curve: observed discharges (24–26/09/93). Dashed curve: forecast without updating procedure. Gray curves: successively updated forecasts. The meteorological forecast is assumed to be perfect. Each hydrological forecast (i.e., each "spaghetti string") covering a period equal to the selected lead time (D =24 h), is described by n values depending on the chosen sampling interval ($n=D/\Delta t$ =24). The horizon of a given forecast (t_0+D) depends on the time of issue of the forecast (t_0) and the forecast period D. Each update leads to a new forecast, shifted with respect to the previous forecast by a duration equal to the updating interval ΔT. For the sake of legibility, the forecast in the example was updated every 4 hours (ΔT = 4h) (adapted from Hamdi *et al.*, 2005).

Forecasting issues and variables

Hydrological forecasting brings up many issues. They concern the different aspects of water resource management, whether intended to optimize water use or to reduce the potential damage associated with major or extreme hydrological events (e.g., via warnings or the operation of hydraulic control works).

The variables that are generally forecasted are discharges and volumes (e.g., for the estimation of extreme events or inflows), water levels (e.g., for navigation, flood risks or recreational activities on lakes and reservoirs) or water-quality parameters (e.g., temperature and pollution levels). The objective of forecasting can be to estimate the mean value of a hydrological variable, its maximum or minimum value, the time at which or duration over which a given value is reached and/or exceeded or the change of the variable over the forecast period. For floods, the volume corresponding to a given water level or discharge threshold (e.g., overtopping threshold) is often forecasted as well.

Forecasts can also concern many other variables such as the melting of snow and ice and the associated volumes, the formation of drift ice, the freezing or breakup of river ice and the maximum drawdown of the water table.

Short-term, medium-term and long-term forecasts

In hydrology, as in meteorology, four types of forecasts are often distinguished: immediate (nowcasting), short-term, medium-term and seasonal. According to the definition of the WMO, the corresponding forecast lead-time ranges are respectively [0–6h] for nowcasting and [6h–72h] for short-term, [72h–12days] for medium term and [>12days] for seasonal forecasts.

Ideally, the choice of a forecast lead time depends on what the forecast is to be used for (Addendum 10.1). Short-term hydrologic forecasts can for instance be used to reduce potential flood damage (Example 10.1) while longer term forecasts are used to optimize the management of water resources.

> **Addendum 10.1 Immediate, short-term, medium-term and seasonal forecasts**
>
> **Immediate forecasts**, referred to as **nowcasts**, and **short-term forecasts** mainly concern instantaneous discharges or water levels. They are carried out for real-time management of extreme hydrological events (i.e., flood warnings) or for the day-to-day optimization of resource use (e.g., low-flow control).
>
> For floods, nowcasting or short-term forecasting makes it possible to minimize potential flood damage. If necessary, forecasts can be used to warn concerned people, authorities and services so that they can implement measures to protect life and property. Finally, through appropriate management of hydraulic structures installed in the system, they make it possible to reduce the intensity of floods, for example through precautionary drawdown of reservoirs to make use of their flood-mitigation storage capacity.
>
> Short-term forecasts are also necessary for lake or river navigation. They provide the necessary information to issue navigation warnings in the event of insufficient clearance under bridges, dangerous flow velocities or the displacement of shoals or islands in a river. They can also be used to optimize the day-to-day operation of hydroelectric power plants taking into account forecasts of the going price of kW-hours on the financial marketplace. Short-term forecasting is also very useful to ensure safety on construction sites involving hydraulic structures.

Medium-term forecasts are mainly carried out to estimate mean discharges, mean water levels, groundwater levels or flow volumes. They are generally used for the tactical management of water resources and their potential uses. They concern for example low flows for the management of intake and outlet works (quantity, quality, temperature), navigation channels (draft forecasts) and the cooling of thermal power plants. They are also important for the tactical management of water storage facilities whether they are used for the production of drinking water, irrigation water or the generation of electrical power. On very large river basins where flood characteristics are more related to flood routing in the river than on direct runoff, medium-term forecasts can be used for flood forecasting.

Seasonal forecasts are mainly used to estimate the inflows that can be expected to a given system over a given period. They are generally limited to estimating whether the mean inflows over a number of months n will be greater or less than the mean inflows for the corresponding season. They are used to determine the best water management strategy taking into account any eventual restrictions on use (precautionary or not), the constitution of precautionary storage strategies, priority attributions in the event of expected shortages and the availability of alternative resources (e.g., drinking water imports from other regions).

Example 10.1

Evaluation of precautionary drawdowns of hydroelectric reservoirs for flood control in the Swiss canton of Valais.

On the Rhone river basin upstream of Lake Geneva (5220 km²), 25% of the catchment area drains into various hydroelectric reservoirs located in this zone. The flood control potential of these reservoirs is however limited for several reasons. First of all, 75% of the area of the basin does not drain into the reservoirs. Secondly, the reservoirs must be filled by the end of September (i.e., at the end of the inflow season) for hydroelectric purposes, meaning that they are generally full or nearly so during the period when major floods usually occur in this region (September–October). A hydrometeorological forecasting system has been developed to allow precautionary drawdowns of the reservoirs in the event of a forecasted heavy flood (Hamdi *et al.*, 2005; Jordan *et al.*, 2006). Each reservoir can be drawn down by a maximum discharge equal to either the turbine capacity of the power plant alone or the combined discharge capacity of the turbines and low-level outlets, but obviously always below the capacity of the downstream system.

Figure 10.2 shows the effect of a hypothetical precautionary drawdown of hydroelectric reservoirs on the peak discharges at Lavey for the October 2000 Rhone river flood (estimated peak discharge of 1470 m³/s). The graph on the right shows that the reduction of the flood peak discharge and flood volume increases with the possible lead time, assuming a perfect meteorological forecast. For each lead time, the drawdown scenario followed is in fact identified on the basis of an expert system that minimizes hydropower losses. In particular, all the reservoirs that were initially full must be once again full at the end of the event (Jordan, 2006).

In this example, maximum possible peak discharge reduction is obtained for a lead time of 60 hours. With precautionary turbining and releases carried out during this lead time, the water level in the reservoir remains below the emergency level. Note that this is not the case if only precautionary turbining is carried out and even less so if no precautionary drawdown is carried out (Figure 10.2a).
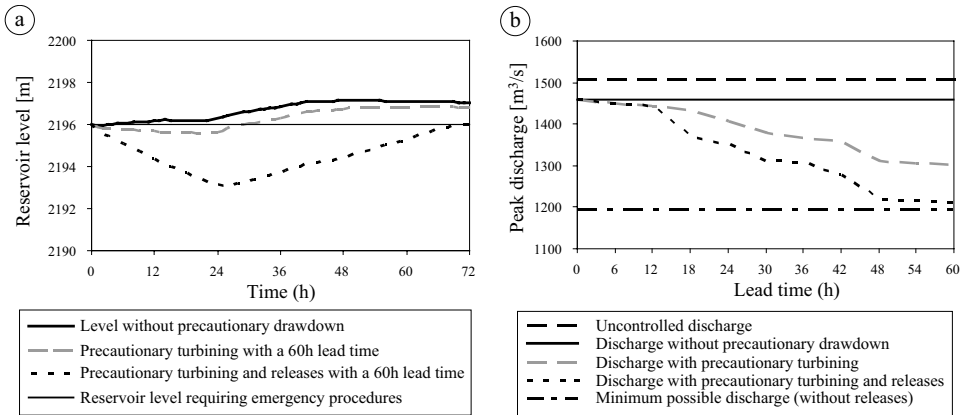
Fig. 10.2: The effect of a hypothetical precautionary drawdown of the Valais hydroelectric reservoirs on the October 2000 Rhone river flood at Lavey station. a) Reservoir levels versus time when the drawdown is carried out with a lead time of 60 hours. b) Reduction of peak discharge as a function of the lead time, assuming a perfect meteorological forecast (adapted from Jordan, personal communication).

10.1.2 Hydrological Forecasting Models

Over a given period, the changes in hydrological variables in a hydrological system depend partly on the system itself, in particular its state at the beginning of the period, and partly on meteorological forcing and other disturbances to which the system is subjected over the period. A hydrological forecast therefore in principle requires:

- An estimation of the initial state of the basin, in particular the soil moisture, river water levels, discharges and different forms of surface storage (e.g., depression storage, snowpack) at the time the forecast is made.
- An estimation of meteorological forcing observed up to the time the forecast is made and forecasted meteorological forcing for the future.
- An estimation of other past or future system disturbances related to the behavior of the hydrological systems and the management of upstream hydraulic works (e.g., diversions for irrigation or reservoir discharges for the generation of hydroelectric power).

A hydrological forecasting model is then required so as to estimate the variable of interest over the chosen forecasting period taking into account the estimated initial state and various past and future meteorological conditions and disturbances.

The forecasting model generally includes a hydrological simulation model, such as the ones presented in Chapters 3 to 7. The simulation model is however only one of the components of the forecasting model.

The forecasting model can also include an independent method designed to regularly estimate the current state of the considered hydrological system. This estimation, often referring to the initialization of the simulation model, can be obtained for instance by the assimilation of various observations. The forecasting model also always includes a method to regularly adjust the forecast. The adjustment procedure can concern the simulation model input variables, state variables, parameters or output variables.

A forecasting model must therefore, for various reasons, be distinguished from a simulation model (Figure 10.3). The main models and methods that frequently constitute the various components of a forecasting model (e.g., simulation models, initialization and adjustment methods) are presented in Section 10.2.
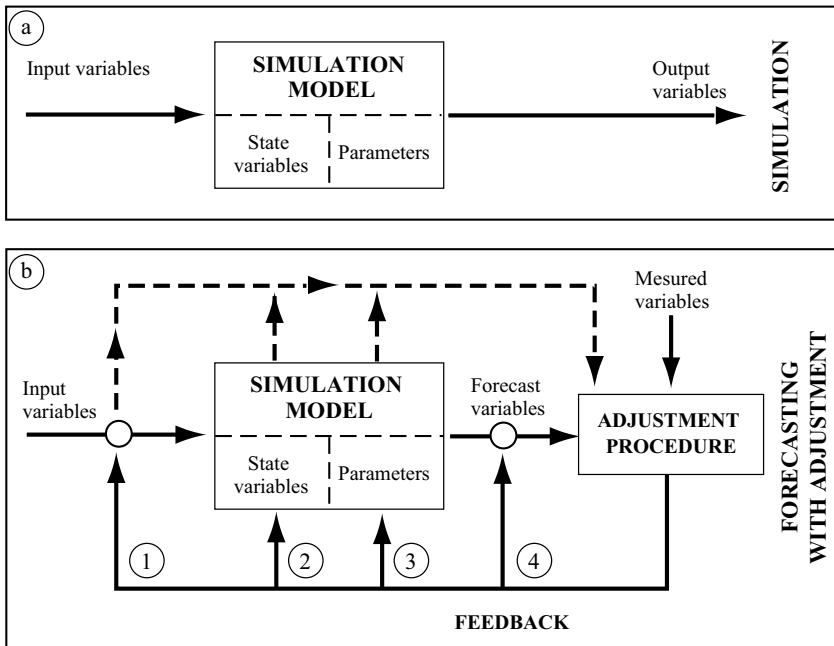
Fig. 10.3: Flow diagrams for a hydrological simulation model (a) and a hydrological forecasting model (b) (adapted from WMO, 1992).

10.1.3 Hydrologic Forecasting Systems

Hydrologic forecasting also requires the existence of an operational forecasting system, the overall aim of which is to produce and forward, in real time, information that can be used to manage resources and associated risks in an optimum manner. The flow diagram of a forecasting system is shown in Figure 10.4. Its components are presented below.

Main components of an operational system

The main components of an operational hydrological forecasting system are the following:

- A measurement network made up of instruments on the ground (e.g., stream gages, meteorological stations, piezometers and radars)—or on-board aircraft or satellites—to estimate the state of the system (e.g., soil moisture, depression storage, snow cover) and the forcing/disturbances to which it is subjected (i.e., meteorological or hydraulic).
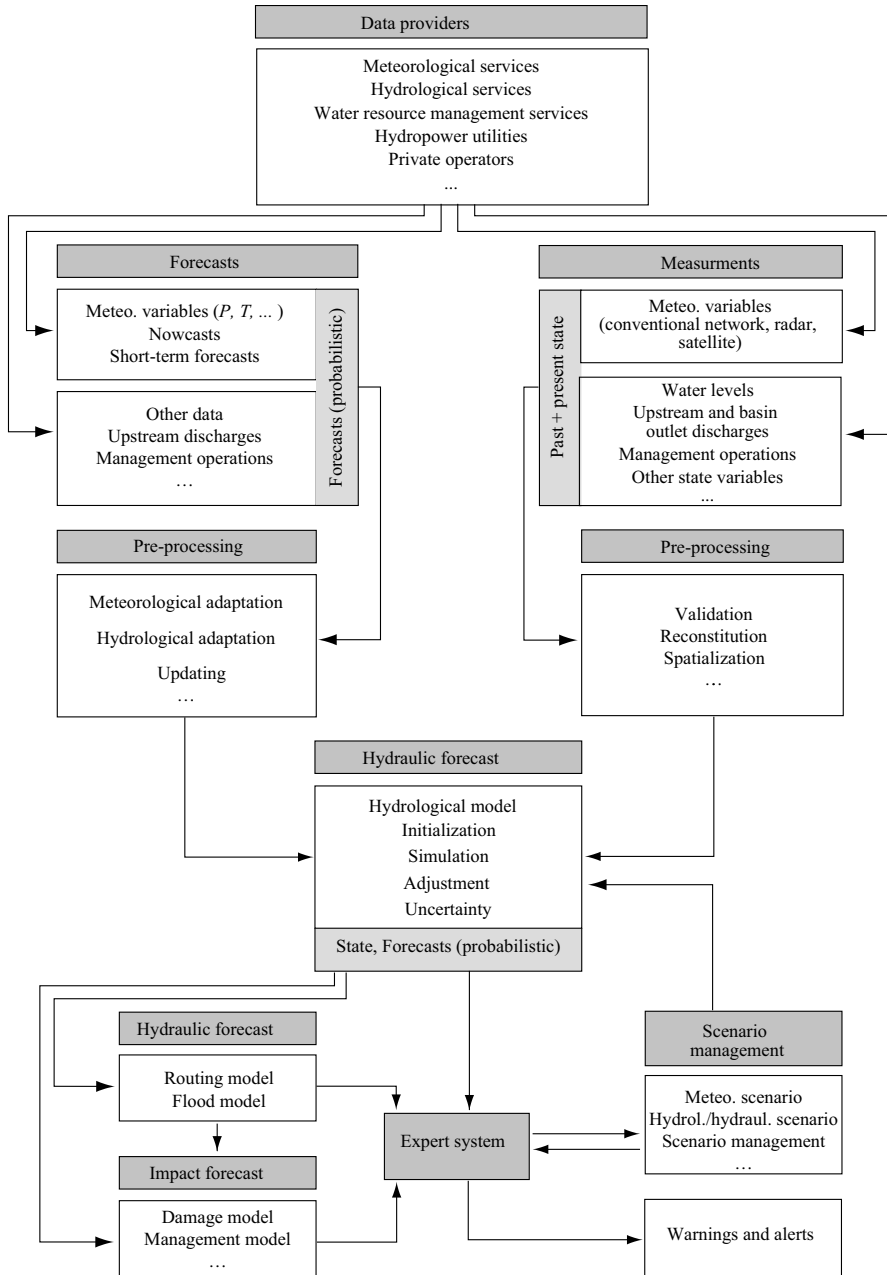
Fig. 10.4: Flow diagram of a hydrologic forecasting system, including an archiving system for the data used and produced by the system (not represented) and possibly a hydraulic model, a cost-benefit analysis model, a scenario management tool and an expert system. The forecasts can be deterministic (a unique value or series of values for the forecasted variable) or probabilistic (e.g., giving the statistical distribution of the variable) (Section 10.2.4).

- A real-time data collection system to continuously forward measurement data (for example via a telephone or optical-fiber network or a ground- or satellite-based radio communication) and store them at a central location where they can then be validated, pre-processed and reconstructed as necessary for their assimilation by the hydrological forecasting model.
- An acquisition and pre-processing system for meteorological forecasts produced elsewhere, if applicable. The pre-processing must in particular adapt the meteorological forecasts to the space and time scales required by the hydrological forecasting model. The principles behind these adaptations are discussed in Section 10.2.4.
- One or more hydrological forecasting models allowing optimal assimilation of the different types and sources of data, the simulation of the hydrological response of the system based on these data for the chosen time horizon and the regular updating of the forecast. Ideally, each of the forecasting models must also make it possible to characterize the forecasting uncertainty. The question of forecast uncertainty will be dealt with in Section 10.3.
- A forecasting center[1] with personnel trained to carry out the following main tasks: Quality control of input data, analysis of forecasting model outputs and the issuing of the corresponding warnings or alerts (Addendum 10.2).
- A group reporting to local or regional authorities and in charge of organizing any work that must be carried out (e.g., coordination of field staff).

Finally, the forecasting system ideally contains a data archiving system that can makes it possible to subsequently reanalyze source data, forecasts obtained by the hydrological forecasting model and the results of simulations carried out by other analysis models if applicable. The a posteriori evaluation of the performance of the forecasting system (e.g., reliability reports, event summaries) is an important task of the forecasting service. It is indispensable so that forecasters can build up their expertise and continuously improve forecasting performance. Evaluation of the performance of a forecasting model is dealt with in Section 10.4.

Other possible components of a forecasting system

Hydrologic forecasts are often used as inputs to hydraulic forecasting models to simulate future flows in hydraulic works or outside the hydrological network in case of failure of the latter (e.g., floods). Hydraulic forecasting is often the responsibility of another service.

To assist in making decisions related to forecasts, an expert system can also be used by the relevant services (e.g., Example 10.1). It can for instance be based on the outputs of socio-economic models used to assess, for the management options considered, the benefits and potential costs of the decision (e.g., operating benefits/losses). Given the high uncertainty generally associated with discharge forecasts, expert systems are often based on risk analysis.

---

[1]In Switzerland, for example, the Hydrology division of OFEV automatically transmits flood warnings for the Rhine river basin to central services as soon as certain water levels are reached. Other warning systems exist in Switzerland at the canton level, in particular in the canton of Valais. In France, twenty-two flood forecasting services are coordinated by SCHAPI, the central hydro-meteorology and flood forecasting support service. Many utilities and companies working with water resources have their own flood-warning systems (e.g., hydropower utilities such as EDF or CNR in France or HydroQuébec in Canada).

Addendum 10.2 Warnings and alerts

The objective of a forecasting system is to produce qualitative or quantitative information that can be used to implement measures capable of optimizing resource use or reducing damage related to a given hydrological event. For floods or low-flow forecasts, this information is often provided in the form of warnings or alerts.

- Warnings provide the public and relevant authorities with qualitative information on the existence and potential magnitude of a serious flood or low-flow event. Their objective is to attract the attention of the public and authorities to a potentially dangerous situation and give them the time to prepare for appropriate action if the risk persists. Warnings are also used to call in personnel in charge of forecasting and supervising and/or managing critical structures.

- Alerts are issued when the risk of the dangerous situation has been established. They can trigger local or regional action plans.

Warnings and alerts are addressed to technical services (e.g., other forecasting centers, reservoir operators), contractual users (e.g., water supply and hydropower providers) and local and regional authorities in charge of crisis management and emergencies (e.g., civil defense, army) that will in turn communicate the warnings and alerts to the concerned populations. These warnings and alerts are increasingly communicated to the public via the Internet, either directly or with restricted access. For example, the flood-warning system for the French hydrographic network—referred to as "Vigicrue"—supplies a flood-warning map twice a day, on which each section of the hydrographic network is assigned a color corresponding to the level of risk to be taken into account by authorities and the population. The four levels of risk are: Level 4: Risk of a major flood with high potential damage. Level 3: Risk of a flood leading to considerable inundations that could cause significant damage. Level 2: Risk of a flood or rapidly rising water levels not expected to cause serious damage. Level 1: No particular risk. The flood-warning map produced by SCHAPI can be accessed at http://www.vigicrues. ecologie.gouv.fr/.

Identification of the warning level does not necessarily require a sophisticated forecasting model as presented above. It is often based on a summary analysis of available data (Figure 10.5) and, in particular, on data concerning basin saturation and past and forecasted precipitation (amount, type, duration). Different approaches of this type have for example been presented by the WMO (1975) and Roche (1987). In this type of analysis, the main indicator used to estimate the state of basin saturation is often the river discharge. The diagnostic obtained is, if necessary, used to address a preliminary warning to public authorities and the population. It also indicates whether or not it is necessary to carry out more in-depth analyses using more sophisticated models to obtain quantitative forecasts.

Effectiveness and reliability of the hydrological forecasting system

The effectiveness of the hydrological forecasting system obviously depends firstly on the quality of the forecast (Section 10.4), especially in a crisis situation when various technical, human and/or organizational failures can take place. In this regard, the reliability of an automatic data acquisition system is critical. One way to improve this reliability is to add redundancy, however this has as an immediate effect on the cost of the system. The probability of a forecasting system failure is lower if the same task can be carried out at different locations by different equipment and/or models and if a reliable procedure is available to switch from one to another. The technical and scientific expertise of the forecasting service personnel, the maintenance of the equipment and the forecasting model used are also of primary importance to increase the reliability of the system (Roche, 1987).
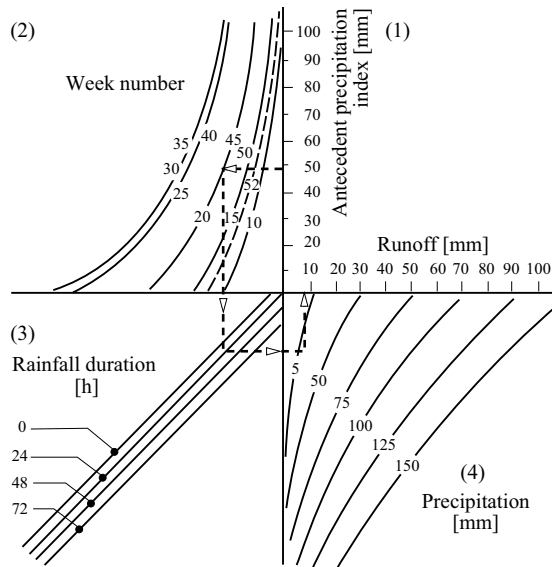
Fig. 10.5: Example of a diagram used to obtain a quick diagnostic of runoff volumes to be expected at the outlet of the considered basin. Factors considered: 1) antecedent precipitation index, 2) week of the year, 3) duration and 4) amount of forecasted precipitation (adapted from WMO, 1975).

10.2 FORECASTING MODEL COMPONENTS

Hydrological forecasting models are many and highly varied. Most of them are based on: 1) a hydrological simulation model, 2) a method designed to estimate the initial state of the hydrological system of interest and then use this estimate for simulation and 3) a simulation model adjustment scheme designed to take into account errors observed a posteriori between forecasted and observed values of the hydrological variable to be forecasted. These different components of forecasting models will be presented briefly in this section.

In certain contexts, hydrological forecasting also requires a forecast of various surface meteorological variables. In this case, the forecast is often referred to as a hydrometeorological forecast. To be used as input to hydrological forecasting models, output data from meteorological models must generally be adapted using an appropriate method. The underlying principles of such methods are presented at the end of this section.

10.2.1 Hydrological Simulation Models

Two approaches may be followed when developing hydrological simulation models. The first, based mainly on observed data, uses simple statistical models relating the hydrological variable to be forecasted to different explanatory variables that are measured and/or forecasted elsewhere. The second approach assumes that the processes explaining the hydrological variable of interest are either known or can be known and that this knowledge can be put to use when developing hydrological or hydraulic models. These

two approaches have been used to develop a multitude of models, many of which have been reviewed by Fortin *et al.* (1997).

Statistical models

Autoregressive models with exogenous variables (ARX) or autoregressive moving-average models with exogenous variables (ARMAX), formally introduced by Box and Jenkins (1970), have often performed well in hydrological forecasting applications (Clarke, 1973; Musy *et al.*, 2005). The exogenous variables used describe the main meteorological conditions on the basin (e.g., precipitation, temperature, reference evapotranspiration) and, when available, discharge observations at the station of interest and at stations located on the upstream hydrographic network (Figure 10.6). The structure and parameters of these models are estimated using available historical data. In some cases, these parameters are continuously updated on the basis of recent observations. These models are presented in greater detail in Appendix 10.7.1.
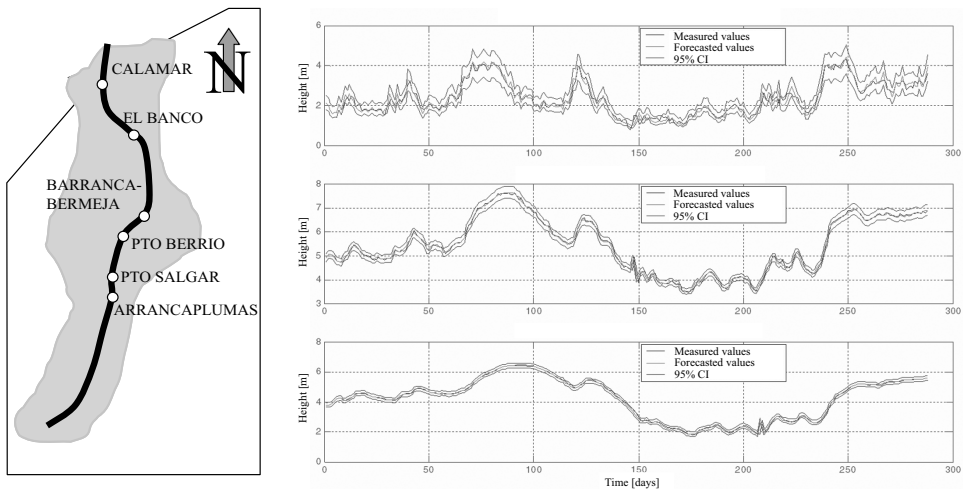
Fig. 10.6: One-day forecasts (with 95% confidence interval) of water levels at three stations on the Magdalena River, Columbia. The forecasts are for Barrancabermeja (upstream station, top graph), El Banco (middle graph) and Calamar (the basin outlet, bottom graph) and were made using an ARMAX statistical model in which the exogenous variables are the water levels observed at the upstream station. Model performance increases with the amplitude of the autoregressive component of the water levels, i.e., with the size of the drainage basin upstream of the station (adapted from Musy *et al.*, 2005).

Hydrological and hydraulic models

Hydrological and/or hydraulic models represent, with a varying degree of simplification, the geometry of the system in question (drainage basin or river respectively) and the hydrological or hydraulic processes that affect the hydrological variable to be forecasted. A priori knowledge of the relationships governing the behavior of the system is integrated in the model. This type of forecasting model includes the complete set of conceptual or physically-based models used to convert meteorological forcing data to discharges and route the latter through the hydrographic network (Chapter 3 to 7).

10.2.2 Initialization of the Simulation Model

For hydrological forecasting, simulation models must explicitly take into account, with a varying degree of simplification, the initial state of the drainage basins, i.e., the state of the drainage basins at the beginning of the hydrological event to be forecasted. In particular, this concerns the soil moisture content and/or areal extent of saturated zones, water levels in the rivers, degree of filling of depression storage and/or surface reservoirs (natural or artificial) and the state of the snowpack (volume, density and spatial distribution).

Estimating the initial state of the drainage basin and using it to initialize the hydrological simulation model is a difficult task that generally requires a specific procedure. The different approaches that can be followed will be discussed in detail below.

Note that the model initialization procedure must generally be distinguished from the model adjustment procedure. The first is essentially intended to estimate the initial state of the system on the basis of meteorological conditions that affected the basin in the previous days or months. The second is used to take into account forecasting errors observed a posteriori in the recent past. The model initialization procedure is often carried out only once at the beginning of the event to be forecasted but it can be updated as time goes on, especially when observations are available for this. The model adjustment procedure is always repeated continuously as time goes on. These two procedures are quite similar in certain aspects and are sometimes one and the same. They are however different in certain configurations, in particular when the drainage basin memory concerning meteorological conditions is long (e.g., seasonal snowpacks in mountainous drainage basins).

Initialization based on observations

For certain simulation models, the model state variables correspond to those of the physical system. In this case, the model state variables can be initialized with measurements carried out on the physical system. For snowpacks, for instance, the spatial extent of the snow cover can be initialized on the basis of satellite images and the water equivalent of the snowpack on the basis of measurements carried out on the ground (Andreadis and Lettenmaier, 2006; Clark *et al.*, 2006).

Initialization by continuous simulation

The model state variables can also be initialized by continuous simulation of the basin behavior (Chapter 3). For example, on the basis of meteorological conditions affecting the basin in the recent past, continuous simulation can be used to estimate the water entering and leaving the soil and thus the spatial and temporal evolution of its infiltration capacity (or saturated surface areas).

Initial conditions required for the various forecasts carried out with the European Flood Alert System (EFAS) are obtained in this way using the LISFLOOD continuous simulation model (Ramos *et al.*, 2006). One of the outputs of this model, specially developed to simulate floods on large European drainage basins, is a map of the state of soil moisture throughout Europe obtained from meteorological data measured on the ground.

In mountainous regions, continuous simulations can be used to estimate the state of snowpacks in the drainage basin when satellite data is not available (Hamdi *et al.*, 2005).

Initialization by assimilation of observations

A simulation model can be initialized using data assimilation techniques (Appendix 2.7.4). Assimilation methods estimate the state of the physical system at a given time by combining in an optimal manner: 1) the various observations and measurements provided by ground, airborne and satellite observation systems for all or some of the variables describing the state and 2) estimations of the same variables obtained from a model of the system behavior (Figure 10.7). Data assimilation reduces uncertainties in the estimated state of the system and maximizes the contribution of the different estimations to the modeling of its behavior. Data assimilation can also be used to correct model drift when a measurement is available. Data assimilation can be sequential, i.e., using only data observed and forecasted at the time of the forecast, or variational—using data observed and forecasted over the *n* time steps preceding the forecast time. For systems that are linear or that can be linearized at certain operating points, assimilation often uses extended Kalman filters (Appendix 10.7.2).
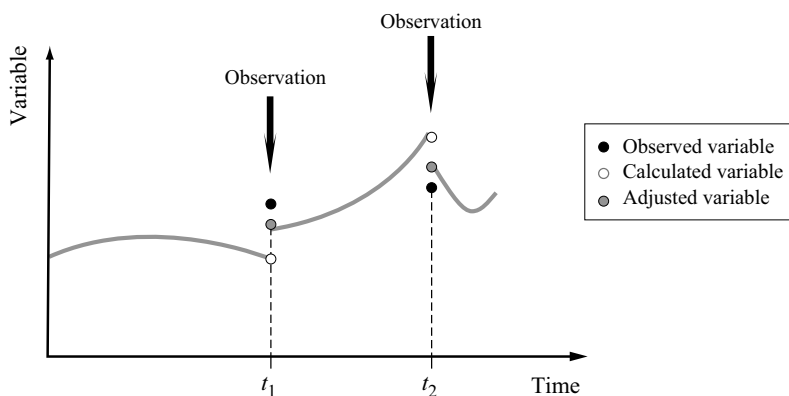
Fig. 10.7: Data assimilation principle for initialization and/or updating of the state variables of the simulation model. When an observation of the considered state variable is available (black dot), the corresponding value simulated by the model (white dot) is corrected using the method selected for the updating of the simulation model. The corresponding value (gray dot) is used for the forecast (adapted from Aubert *et al.*, 2003).

10.2.3 Simulation Model Adjustment and/or Error Processing

Whatever the simulation model used or data available, a hydrological forecast will always be imperfect, in particular due to the imperfections of the model itself and uncertainty concerning the input variables and the state of the modeled system (Section 10.1.1). Different errors come from the fact that the modeled system does not necessarily have a stationary behavior. Its behavior can change during a hydrological event (e.g., through scouring of the riverbed during a flood), during the year (e.g., due to seasonal vegetation cycles, or from one year to another (e.g., as a consequence of development projects affecting the river basin or the river itself).

Note that the error observed a posteriori by comparing the forecasted and observed values of the same variables can be used to reduce the potential forecasting error over future time steps. Different techniques have been developed for this purpose (O'Connell and Clarke, 1981; Refsgaard, 1997).

For ARMAX-type empirical simulation models, the structure of the simulation model is data-based and in principle not imposed a priori. The model is identified and its parameters estimated at the same time as an error model is identified. In this case, a recursive estimation of parameters, carried out with a Kalman filter on the basis of the most recent observations, is often adopted (Toth *et al.*, 2000). The water levels for the Magdalena River in Figure 10.6 of Section 10.2.1 were forecasted in this way.

For physically-based or conceptual simulation models, errors are managed using so-called simulation model adjustment methods. Four adjustment procedures are classically used for this purpose (Refsgaard, 1997). They are respectively based on the following principles:

- Adjustment of model input variables (i.e., meteorological and other).
- Adjustment of the values of some or all the model parameters (e.g., recalibration of the production and transfer parameters).
- Adjustment of model state variables—typically the degree of saturation of the unsaturated zone and the water table height.
- Correction of model outputs (e.g., forecasted discharges), superimposing on the forecasted signal a time series of residuals obtained from an error model calibrated using recent errors.

The principles underlying these different approaches are described in Addendum 10.3. The principles of the state variable adjustment method are illustrated in Example 10.2.

Application of a simulation model adjustment procedure requires availability of different system state observations (e.g., soil moisture, water table height, river discharges). In most cases, only the discharges at the basin outlet are available. Although this information alone is far from sufficient in all cases, it is important because it integrates all the hydrological processes present within the basin.

Addendum 10.3 Processing forecasting errors

The principles underlying the four classical procedures used to process forecasting errors in real time are described below.

Adjustment of model input variables

Adjustment of the forecasting model by correcting the input variables (i.e., meteorological forcing) is often justified because the uncertainty of these variables explains a significant part of the forecasting error. This is particularly the case for errors related to estimated depths of precipitation falling on the basin. This correction is sometimes based on the expert judgment of the hydrologist. It can also be carried out using a Kalman filter (or an extension of this filter) (O'Connell and Clarke, 1981).

This approach is not without limitations. The discharge observed at a given time is the result of meteorological conditions to which the environment has been subjected over a varying number of time steps. Note that the discharges do not necessarily depend on precipitation alone. For example, in mountainous regions, temperatures are often as important as precipitation (Chapter 7). Moreover, possible errors on the estimated initial state of the basin (soil moisture, state of the snowpack) have potentially as much influence on the quality of the forecast as errors concerning the estimated input data. For this reason, correction of input data is often risky.

Adjustment of model parameters

The adjustment of simulation model parameters consists in re-estimating at regular intervals, for instance at each time step, the values of some or all of the model parameters. This approach may be justified if the quality of the model input data is unsure. In this case, forecasting errors can come from parameters that are ill-adapted because conditions are temporarily different from those used for the calibration or because the conditions prevailing in the basin have gradually changed. The parameters may be adjusted using a Kalman filter (or an extension of this filter). The procedure consists in updating, on the basis of recent data, the parameter estimates obtained in a previous step (Roche, 1987).

The complete recalibration of the model on the basis of recent data may be warranted in some cases. The result of such an approach strongly depends on the complexity of the simulation model. Recent models, whether conceptual or physically-based, often involve more than a dozen parameters and estimation procedures are often long and tedious, in particular when the parameters must be estimated on ungaged basins (Chapter 11). In addition, they are difficult to automate because they often include manual input to make best use of the hydrologist's expertise.

Adjustment of model state variables

The model state variables are adjusted on the basis of the observation that the different fluxes simulated by the models depend on the state variables of the different model compartment states, typically the degree of saturation of the unsaturated zone and the water table height. Modification of the model state variables therefore modifies the associated fluxes.

State variables can be adjusted using a Kalman filter—or an extended form of this filter (Kitanidis and Bras, 1980; Georgakakos and Bras, 1982; Aubert *et al.*, 2003) or using a rational strategy based on the hydrologist's expertise (Hamdi *et al.*, 2005). When the model state variables correspond to the real system state variables—or when they can be related to them by a functional relationship, the model state variables can be adjusted using the data assimilation procedures discussed in Section 10.2.2. However, frequently the only state variable available is the basin outlet discharge, limiting the utility of this approach. Moreover, data assimilation is often quite difficult to carry out.

Adjustment of the variables (error modeling)

The errors obtained a posteriori by comparing the forecasts with observations are often strongly correlated over time. Consequently, errors are often managed by extrapolating into the future the errors observed in the near past on the basis of simple models such as autoregressive moving-average models (ARMA) (Box and Jenkins, 1970). As opposed to the previous methods, this is not an adjustment method, unless the parameters of the ARMA model are estimated in a recursive manner. The possibility of using neuron networks for error correction has also been explored in this context (Anctil *et al.*, 2003).

The advantage of this method is that it is easier to implement than the other approaches and does not necessarily require observation of the system. Consequently, the forecasting system can produce a forecast even if no discharge observations are available for the recent past, for instance as a result of a failure of a sensor or the remote transmission network. This was for a long time the method most widely used by hydrologists (WMO, 1992).

The main drawback of this approach is that it does not attempt to correct the possible error sources. Consequently, the error can take on values much greater than the actual signal to be forecasted. Moreover, the error model can only represent the autoregressive component of the error and therefore cannot capture future potential errors related to modifications of boundary conditions. Finally, this approach is hard to apply in situations where no observations are available because the spatial transposition of extrapolations for ungaged basins is difficult.

Example 10.2

The following recurrence equation simulates the change with time of 6-hour mean discharges at the outlet of a 2000 km² drainage basin:

$$Q_n^s = a Q_{n-1}^s + b Q_{n-2}^s + c \left(i_n^e + 2i_{n-1}^e + i_{n-2}^e \right) \qquad (10.1)$$

where Q_n^s and i_n^e are respectively the "simulated" mean discharge [m³/s] and the "estimated" net rainfall [mm/h], i.e., rainfall producing direct runoff (Section 4.1.2), falling on the basin over time step $[n\Delta t, (n+1)\Delta t]$, and where a, b and c are three parameters obtained by calibration using 10 years of observations; $a = 0.945$; $b = -0.223$; $c = 38.7$. This equation is the simplified expression of a Nash transfer model with two linear reservoirs in series and parameter K equal to 8 hours (Chapter 5). In this example, the simulation model is to be used to forecast the 6-hour mean discharges for the next four time steps starting from 00:00 on day D0 (31 May 2003). The net rainfall falling on the basin, estimated elsewhere from the gross rainfall (Section 4.1.2), and the discharges observed a posteriori at the base of outlet Q_n^o are indicated in the table below.

Table 10.1: Day D, time of issue of the forecast t_0, observed discharges Q_n^o and estimated net rainfall i_n^e over time step Δt.

t_0	[h]	18:00	00:00	06:00	12:00	18:00	00:00	06:00	12:00	18:00
D		D-1	D0	D0	D0	D0	D1	D1	D1	D1
Q_n^o	[m³/s]	2	1.5	9.5	44	225	497	616	553	435
i_n^e	[mm/h]	0	0	0.2	0.6	2.1	0.8	0.4	0.2	0.1
D			D2	D2	D2	D2	D3	D3	D3	D3
Q_n^o	[m³/s]		307	193	114	64	35	19	10	7
i_n^e	[mm/h]		0	0	0	0	0	0	0	0

For a given forecast time, the discharges $Q_{0+6}^f, Q_{0+12}^f, Q_{0+18}^f, Q_{0+24}^f$ for the 4 time steps to come can be forecasted on the basis of the recurrence equation. This gives:

$$
\begin{aligned}
Q_{0+6}^f &= a Q_0^e &&+ b Q_{0-6}^e &&+ c \left(i_{0+6}^f + 2i_0^e && + i_{0-6}^e \right) \\
Q_{0+12}^f &= a Q_{0+6}^f &&+ b Q_0^e &&+ c \left(i_{0+12}^f + 2i_{0+6}^f && + i_0^e \right) \\
Q_{0+18}^f &= a Q_{0+12}^f &&+ b Q_{0+6}^f &&+ c \left(i_{0+18}^f + 2i_{0+12}^f && + i_{0+6}^f \right) \\
Q_{0+24}^f &= a Q_{0+18}^f &&+ b Q_{0+12}^f &&+ c \left(i_{0+24}^f + 2i_{0+18}^f && + i_{0+12}^f \right)
\end{aligned}
\qquad (10.2)
$$

where $i_{0+6}^f, i_{0+12}^f, i_{0+18}^f, i_{0+24}^f$ are the net rainfalls [mm/h] forecasted for the 4 time steps to come and Q_0^e, Q_{0-6}^e and i_0^e, i_{0-6}^e are respectively the estimated discharges in the river [m³/s] and the net rainfalls [mm/h] for the current and previous time steps. In these equations and in those that follow, the exponents "o", "e", "s" and "f" refer respectively to the observed variables, the variables estimated elsewhere, the variables obtained from a simulation model without adjustment and the variables forecasted with the forecasting model considered (meteorological or hydrological). The index "$0+k$" refers to time step k that precedes or follows, depending on the sign, the current time step referred to by the index "0".

For each t_0, 4 types of forecasts are carried out using the above iterative model, i.e., with or without precipitation forecasts and with or without adjustment of the hydrological simulation model. In each case, the calculation steps are detailed below. The results are summarized in Table 10.2 and illustrated in Figures 10.8 and 10.9. The precipitation forecasts are assumed to be perfect, i.e., the forecasted values are equal to the values indicated in Table 10.1.

Case 1: Forecasting without adjustment and with precipitation forecast

Without adjusting the simulation model, Q_0^e, Q_{0-6}^e of the system of equations 10.2 are estimated to be equal to the discharges Q_0^s, Q_{0-6}^s obtained by continuous simulation for the current and previous time steps on the basis of the net rainfalls $i_0^e, i_{0-6}^e, i_{0-12}^e, ..., i_{0-m}^e$ estimated elsewhere for the m previous time steps. The corresponding values are $Q_0^s = 4$ m³/s and $Q_{0-6}^s = 1$ m³/s. The forecast carried out without adjustment at $t_0 = 00:00$ on day D0 gives (in m³/s):

$$Q_{0+6}^f = a \cdot 4.0 \quad + b \cdot 1.0 \quad + c \cdot (0.2 + 2 \cdot 0.0 + 0.0) = 11.3$$

$$Q_{0+12}^f = a \cdot 11.3 \quad + b \cdot 4.0 \quad + c \cdot (0.6 + 2 \cdot 0.2 + 0.0) = 48.4$$

$$Q_{0+18}^f = a \cdot 48.4 \quad + b \cdot 11.3 \quad + c \cdot (2.1 + 2 \cdot 0.6 + 0.2) = 178.6$$

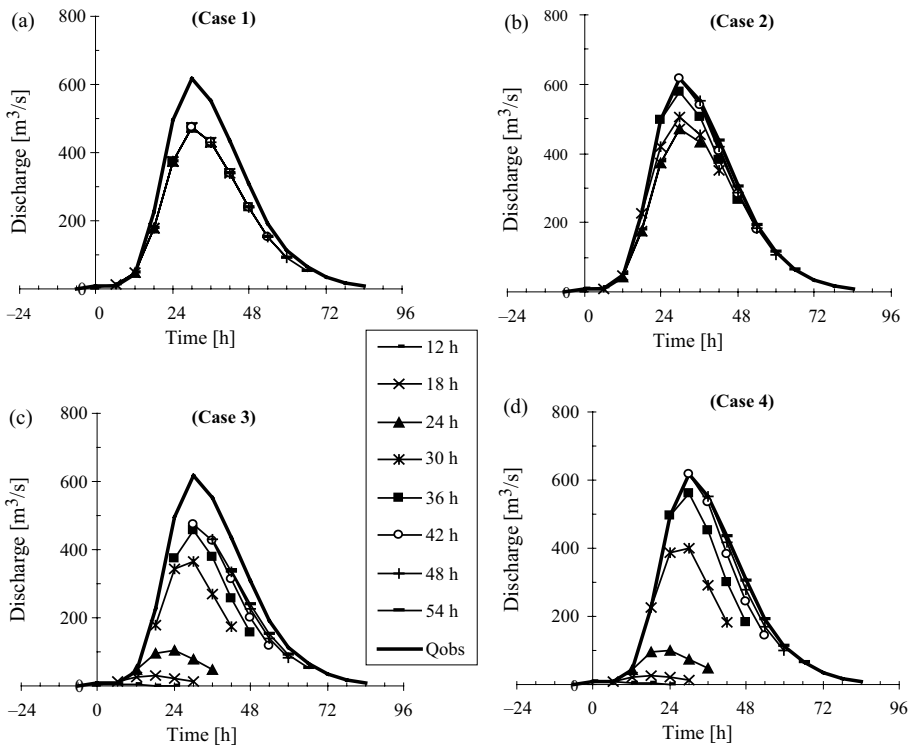$$Q_{0+24}^f = a \cdot 178.6 + b \cdot 48.4 \quad + c \cdot (0.8 + 2 \cdot 2.1 + 0.6) = 374.4$$

Fig. 10.8: Forecasts obtained every six hours for the 4 cases, i.e., with (top) and without (bottom) a precipitation forecast (assumed to be perfect) and with (right) and without (left) adjustment of the simulation model.

The next forecast carried out without adjustment at time t_0 = 06:00 gives (in m³/s):

$$Q^f_{6+6} = a \cdot 11.3 + b \cdot 4.0 + c \cdot (0.6 + 2 \cdot 0.2 + 0.0) = 48.4$$

$$Q^f_{6+12} = a \cdot 48.4 + b \cdot 11.3 + c \cdot (2.1 + 2 \cdot 0.6 + 0.2) = 178.6$$

and so on. Without adjustment, the discharges forecasted at t_0 = 06:00 for 12:00, 18:00 and 24:00 on day D0 are therefore the same as those forecasted 6 hours earlier. The same will be true for all the following time steps. The results are summarized in Table 10.2.

Case 2: Forecasting with adjustment and with precipitation forecast

The simulation model is adjusted simply by using the mean discharges Q^o_0, Q^o_{0-6} observed in the river over the current and previous time steps to estimate Q^e_0, Q^e_{0-6} in the system of equations 10.2. The first forecast carried out at t_0 = 00:00 on day D0 with adjustment and a precipitation forecast and with Q^o_0 = 1.5 m³/s and Q^o_{0-6} = 2.0 m³/s, gives (in m³/s):

$$Q^f_{0+6} = a \cdot 1.5 + b \cdot 2.0 + c \cdot (0.2 + 2 \cdot 0.0 + 0.0) = 8.7$$

$$Q^f_{0+12} = a \cdot 8.7 + b \cdot 1.5 + c \cdot (0.6 + 2 \cdot 0.2 + 0.0) = 46.6$$

$$Q^f_{0+18} = a \cdot 46.6 + b \cdot 8.7 + c \cdot (2.1 + 2 \cdot 0.6 + 0.2) = 177.4$$

$$Q^f_{0+24} = a \cdot 177.4 + b \cdot 46.6 + c \cdot (0.8 + 2 \cdot 2.1 + 0.6) = 373.7$$

The next forecast, carried out at t_0 = 06:00 with adjustment, gives (in m³/s):

$$Q^f_{6+6} = a \cdot 9.5 + b \cdot 1.5 + c \cdot (0.6 + 2 \cdot 0.2 + 0.0) = 47.3$$

$$Q^f_{6+12} = a \cdot 47.3 + b \cdot 9.5 + c \cdot (2.1 + 2 \cdot 0.6 + 0.2) = 177.9$$

and so on (Table 10.2). With adjustment and a precipitation forecast, the discharges forecasted at t_0 = 06:00 for 12:00, 18:00 and 24:00 on day D0 are therefore only slightly modified with respect to those forecasted six hours earlier (respectively 46.6, 177.4 and 373.7 compared to 47.3, 177.9 and 374.0 m³/s).

Case 3: Forecasting without adjustment and without precipitation forecast

If no precipitation forecast is available, the calculations of case 1 are repeated taking $i^f_{0+k} = 0$ for $k > 0$ in equations 10.2. The first forecast carried out without adjustment at t_0 = 00:00 on day D0 gives (in m³/s):

$$Q^f_{0+6} = a \cdot 4.0 + b \cdot 1.0 + c \cdot ("-" + 2 \cdot 0.0 + 0.0) = 3.6$$

$$Q^f_{0+12} = a \cdot 3.6 + b \cdot 4.0 + c \cdot ("-" + 2 \cdot "-" + 0.0) = 2.5$$

and so on (Table 10.2).

Case 4: Forecasting with adjustment and without precipitation forecast

In this case, the calculations of case 2 are repeated following the same principle and taking $i^f_{0+k} = 0$ for $k > 0$ in equations 10.2. The results are indicated in Table 10.2.

Remarks

Without adjustment but with a perfect precipitation forecast (case 1), the forecasting model is equivalent to a simulation model. The forecasted discharges are exactly those that would have been obtained by a continuous simulation (Figure 10.8a).

With or without a precipitation forecast: 1) the discharge forecasts are better if the simulation model is adjusted on the basis of the discharges observed a posteriori (Figure 10.8a and c) and 2) in both cases, forecasting performance decreases with increasing lead time. This drop in performance is however greater when future precipitation is not taken into account (Figure 10.9a and b).

Without adjustment and without a precipitation forecast (case 3), the discharge forecasts illustrate the portion of the discharge to come that can be explained solely by the precipitation that has already fallen. The explanatory capacity of past precipitation of course decreases with increasing forecast lead time (Figure 10.8c). This point is dealt with in detail in Section 10.4.3.
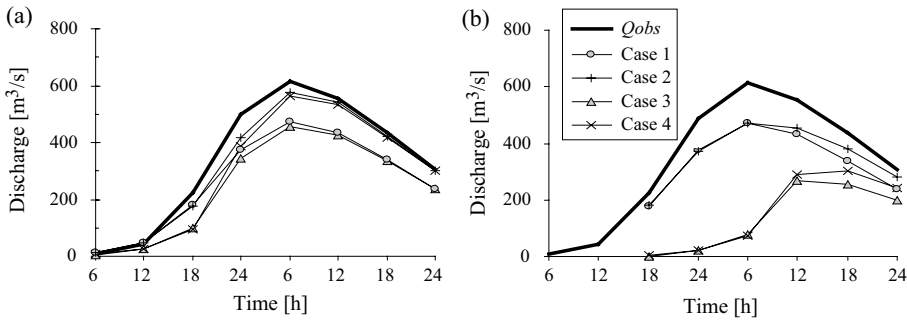
Fig. 10.9: Forecast performance for lead times of (a) 6 hours and (b) 18 hours.

Table 10.2: Summary of results for the 4 precipitation forecast cases. Discharges are in m³/s.

	D0	*D0*	*D0*	*D0*	*D1*	*D1*	*D1*	*D1*
$\Delta t \setminus t_0$	**00:00**	**06:00**	**12:00**	**18:00**	**00:00**	**06:00**	**12:00**	**18:00**

Case 1: Without adjustment but with perfect meteorological forecast

Q_{0-6}^{s}	1.0	4.0	11.3	48.4	178.6	374.4	472.4	432.4
Q_{0}^{s}	4.0	11.3	48.4	178.6	374.4	472.4	432.4	337.9
Q_{0+6}^{f}	11.3	48.4	178.6	374.4	472.4	432.4	337.9	238.2
Q_{0+12}^{f}	48.4	178.6	374.4	472.4	432.4	337.9	238.2	153.5
Q_{0+18}^{f}	178.6	374.4	472.4	432.4	337.9	238.2	153.5	91.9
Q_{0+24}^{f}	374.4	472.4	432.4	337.9	238.2	153.5	91.9	52.5

Case 2: With adjustment and perfect meteorological forecast

Q_{0-6}^s	2.0	1.5	9.5	44.0	225.0	497.0	616.0	553.0
Q_0^s	1.5	9.5	44.0	225.0	497.0	616.0	553.0	435.0
Q_{0+6}^f	8.7	47.3	174.8	419.3	577.9	540.7	419.8	303.0
Q_{0+12}^f	46.6	177.9	371.8	504.4	504.6	408.1	288.7	193.1
Q_{0+18}^f	177.4	374.0	470.8	452.6	382.6	280.4	182.9	114.8
Q_{0+24}^f	373.7	472.2	431.4	349.8	264.3	177.7	108.4	65.4

Case 3: Without adjustment or meteorological forecast

Q_{0-6}^s	1.0	4.0	11.3	48.4	178.6	374.4	472.4	432.4
Q_0^s	4.0	11.3	48.4	178.6	374.4	472.4	432.4	337.9
Q_{0+6}^f	3.6	25.2	97.4	343.5	457.0	424.6	334.0	238.2
Q_{0+12}^f	2.5	29.1	104.4	365.9	379.1	311.2	226.8	153.5
Q_{0+18}^f	1.5	21.8	76.9	269.0	256.2	199.3	139.7	91.9
Q_{0+24}^f	0.9	14.1	49.3	172.5	157.4	118.8	81.4	52.5

Case 4: With adjustment but without meteorological forecast

Q_{0-6}^s	2.0	1.5	9.5	44.0	225.0	497.0	616.0	553.0
Q_0^s	1.5	9.5	44.0	225.0	497.0	616.0	553.0	435.0
Q_{0+6}^f	1.0	24.1	93.6	388.3	562.4	532.9	415.9	303.0
Q_{0+12}^f	0.6	28.4	101.8	397.9	451.3	381.5	277.3	193.1
Q_{0+18}^f	0.3	21.4	75.3	289.2	300.9	241.5	169.1	114.8
Q_{0+24}^f	0.2	13.9	48.4	184.5	183.6	143.0	97.9	65.4

10.2.4 Hydrological Adaptation of Meteorological Forecasts

In certain contexts, hydrological forecasting requires a forecast of various surface meteorological variables—often precipitation. These meteorological variables are generally provided, for the considered forecast period, by output from meteorological forecasting models. However, for some of these variables, in particular precipitation, the corresponding forecasts often include significant errors and uncertainties (Chapter 12). Consequently, output from meteorological forecasting models must be adapted before it can be used for hydrological forecasting.

The output from meteorological models is often adapted using a statistical downscaling model. These downscaling models use forecasts of various meteorological variables related

to large-scale atmospheric circulation, generally better forecasted by the meteorological model, to estimate the future values of surface meteorological variables. Meteorological adaptation can be used to develop scenarios for precipitation forecasts as well as other surface meteorological variables (e.g., temperature, relative humidity, nebulosity). The main approaches used for this adaptation are described in Chapter 12.

The temporal and spatial scales of surface meteorological variables that can be reasonably explained by meteorological adaptation methods are not necessarily sufficient for a given hydrosystem. For example, meteorological adaptation cannot generally produce meteorological scenarios with an hourly temporal resolution. However this is the resolution required by forecasting models for small basins (typically less than 1000 km²) or basins with very fast response times (e.g., urban drainage areas). In such cases, the surface meteorological variables first produced using the selected meteorological adaptation method require hydrological adaptation. This consists in generating plausible meteorological scenarios at temporal and spatial scales that are relevant to the hydrological system considered.

Hydrological adaptation is commonly carried out using a spatial and temporal disaggregation model. The principles of these models are described in Chapter 12. They generally make use of stochastic generators. In this way, hydrological adaptation of a meteorological forecast often leads to the production of a set of meteorological scenarios (Kelly and Krzysztofowicz, 2000). Figure 10.10 illustrates such an adaptation.

As for meteorological adaptation, hydrological adaptation of meteorological parameters must be repeated after every update of the meteorological forecast (generally every 12 or 24 hours). The hydrological adaptation must also propose a temporal and spatial structure for the surface meteorological variables that is consistent with their past structure. Finally, if the precipitation forecast is probabilistic, the adaptation must produce different scenarios that respect the associated statistical distribution. A model satisfying these different constraints has been presented by Lardet and Obled (1994) and Marty *et al.* (2008).
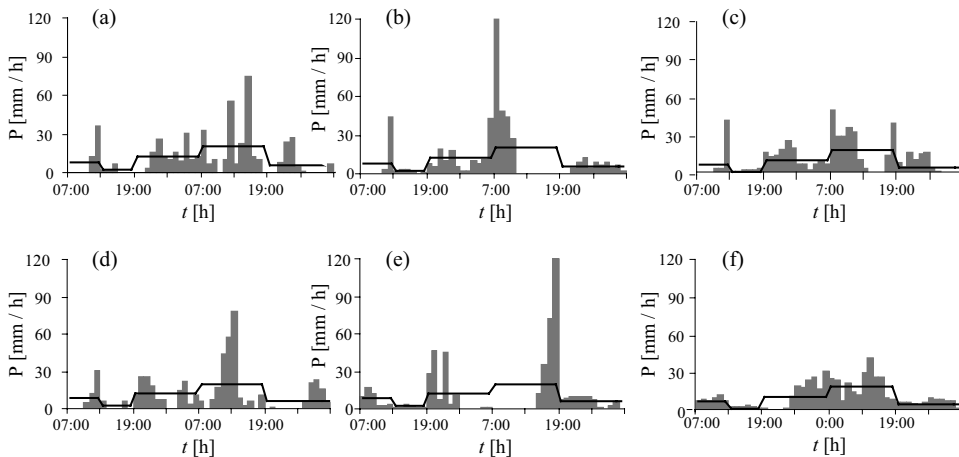
Fig. 10.10: Illustration of hydrological adaptation of a meteorological forecast. The six precipitation scenarios described at an hourly time step (gray histograms on graphs *a* to *f*) were produced by stochastic disaggregation of the meteorological scenario for 31 May 2003 at 07:00. The meteorological scenario defined at variable time steps (6 to 12 hours) was obtained for the next 48 hours by meteorological adaptation of the output of a given meteorological model (black line on each graph).

10.3 FORECAST UNCERTAINTIES

10.3.1 Deterministic Forecasting and Uncertainties

A hydrological forecast obviously cannot be perfect. It is by nature uncertain. For this reason, a deterministic forecast, i.e., a forecast that indicates only a single possible occurrence of the variable of interest for the required forecast horizon, is not sufficient. Even if sometimes accompanied by qualitative indications concerning the level of uncertainty, a deterministic forecast in fact gives an illusion of certainty and can lead to decisions that are non-optimal, inadequate or even dangerous (Houdant, 2004).

As shown in Figure 10.11 for the special case of flood level forecasting, knowledge of the forecast uncertainty allows users to take into account the associated risk in their decision process. Characterization of forecast uncertainty makes it possible to clearly separate the tasks of the forecaster and the user. Forecasting is a purely scientific field while the decisions made by the user require a socio-economic analysis of the consequences of the different scenarios.

The different sources of imperfections and uncertainties that contribute to the total uncertainty of the variable to be forecasted are mainly related to the data and tools required for the forecast including:

- the estimation of the initial state of the system (e.g., unavailability of the measurements required for this estimation and/or insufficient spatial representativeness of the available measurements),
- the estimation of the forcings/disturbances to which the hydrological system has been subjected to up to the forecast time (e.g., insufficient spatial representativeness of the measured meteorological variables),
- the forecasts concerning these forcings/disturbances over the forecast period (e.g., imperfection of meteorological models, lack of knowledge of operation of upstream hydraulic works),
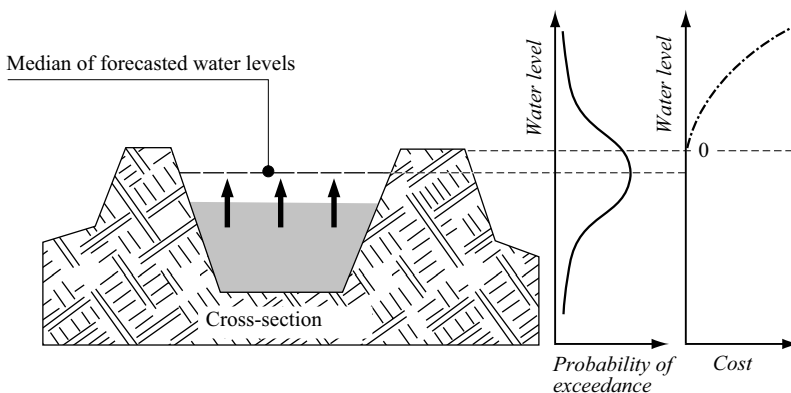
Fig. 10.11: Importance of a probabilistic forecast. The median value of the flood level distribution is less than the critical bank overflow level. A decision based solely on this estimation would result in no preventive action being taken to protect the surrounding areas as opposed to a decision based on a probabilistic forecast that includes the associated probability distribution, indicated in the middle graph. The cost of damage to be expected in the event of overflow depends on the height of the resulting flood (right-hand graph) (modified from Todini, 2005).

- the imperfection of the simulation model (e.g., simplifications made to simulate the process, parameterization),
- the imperfection of the forecasting model adjustment procedure (e.g., assumptions made, parameterization).

These different sources of uncertainty do not necessarily have the same importance. The most significant generally come from insufficient knowledge of the future meteorological forcings. If this information is necessary, a probabilistic quantitative precipitation forecast or a meteorological ensemble forecast is required (Chapter 12). If this is not the case, the main sources of uncertainty depend on the configuration considered and in particular on the complexity of the hydrological behavior of the basin, the quality of available data and the performance of the models. The most important of these sources of uncertainty are however often related to insufficient knowledge of the initial state of the system. The corresponding uncertainties are often considered to have a potential effect just as important as the effect of uncertainties in the precipitation forecasts.

Ideally, once identified and quantified, the main sources of uncertainty should be propagated and combined with the hydrological forecasting model to produce the total uncertainty of the forecast. This procedure is however seldom applied because it is relatively complicated to implement.

Generally speaking, the principal approaches that can be used to characterize the forecast uncertainty lead to the issuing of probabilistic hydrological forecasts or hydrological ensemble forecasts.

10.3.2 Probabilistic Forecasts

The objective of a probabilistic forecast is to describe the total forecast uncertainty by providing the probability distribution of the variable to be forecasted. The Bayesian forecasting system developed by Krzysztofowicz (1999, 2001a,b) offers a valuable mathematical and theoretical framework for the construction of such a forecast. In this approach, the uncertainty in the variable to be forecasted is generally divided into two parts. The first part is the uncertainty associated with the hydrological model inputs, i.e., the meteorological forecasts. The other part corresponds to all the other possible sources of error. These two types of uncertainty are quantified separately and then combined to produce the total uncertainty. This approach is presented in more detail in Appendix 10.7.3.

10.3.3 Hydrological Ensemble Forecasts

Hydrological ensemble forecasting is a method more widely used to estimate forecast uncertainty (Carpenter and Georgakakos, 2001; Pappenberger *et al.*, 2005; Wood *et al.*, 2006).

It consists in forecasting the hydrological variables of interest for an ensemble of probable hydrometeorological scenarios. In practice, it often involves simulating the hydrological response of the system to different meteorological forecast and initial system state scenarios.

In this way, the hydrological forecast produces an ensemble of future time trajectories for each hydrological variable to be forecasted (e.g., Figure 10.12).
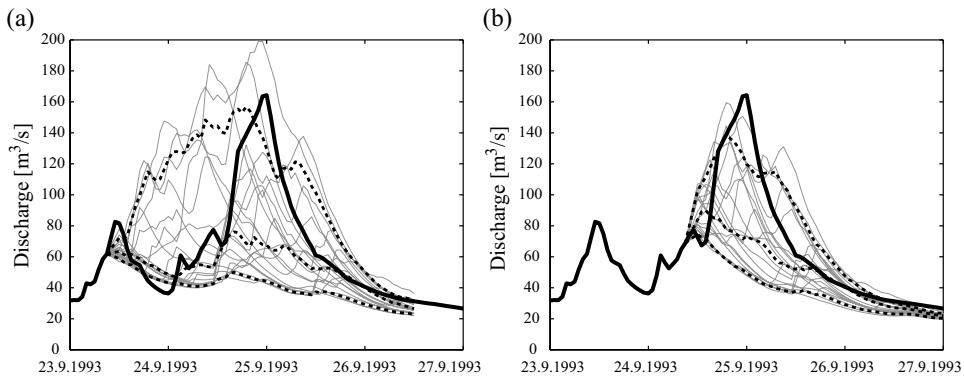
(a)

(b)

Fig. 10.12: Hydrological ensemble forecast for the Rhone River basin at Reckingen (215 km^2) based on a meteorological ensemble forecast. The meteorological scenarios considered have been obtained from meteorological forecasts using the so-called analogs meteorological adaptation method (Chapter 12). a) 23/09/1993 forecast at 12:00; b) 24/09/1993 forecast at 12:00. Bold curve: observed flood (24–26/09/1993). Gray curves: forecasts for the 20 scenarios. Dashed curves: 10, 50 and 90% quantiles.

The statistical distribution of the forecasted variable can be extracted from these different curves for each of the forecast horizons considered. Under certain conditions, linked in particular to the way in which the probability densities of the input variables are sampled, this distribution corresponds to a probabilistic forecast (e.g., Kelly and Krzysztofowicz, 2000). In general, a wide variety of meteorological scenarios can be used as input to the hydrological forecasting model. They come from:

- the different meteorological forecasting models available (Section 12.2.1 and 12.2.2),
- the different members of the ensemble forecast that may be produced by each meteorological model, each member depending on the initial conditions of the meteorological model (Section 12.2.4),
- the different meteorological adaptations possible for each member of the ensemble forecast (Section 12.2.2),
- the different hydrological adaptations possible for each meteorological adaptation (Section 10.2.4).

10.3.4 Multi-model Approach

In the same way as it can be of interest to consider the outputs of several meteorological models for forecasts of meteorological variables, it can be of interest to consider the outputs of several hydrological models for hydrological forecasts.

Various strategies can be used to combine the forecasts produced by different models (Shamseldin *et al.*, 1997; See and Openshaw, 2000; Georgakakos *et al.*, 2004; Fortin *et al.*, 2006). Some are simple (e.g., linear combination of estimations) while others are relatively complex (e.g., non-linear combination of estimations with a combination model that must also be calibrated). The best approaches are those that take into account the recent performance of each of the forecasting models. For example, the combination can be a weighted average of available estimations with weights for the contribution of each model that are inversely proportional to the residual variance obtained—in the recent past

– between forecasts and a posteriori observations of the forecasted variable. In this context, Bayesian combination methods offer a useful theoretical framework (Chapter 11).

To obtain meaningful combinations of estimations, it is important to make sure that the forecasting models used are not redundant in terms of the way they conceptualize the considered phenomena (nature, complexity), the input data they use (nature, pre-processing), the structure of their associated errors and the procedure used to take these errors into account (model adjustment).

10.4 FORECAST QUALITY

The quality of a forecast depends on whether the point of view of a forecaster or a user is considered. For a forecaster, the quality of a forecast is its statistical performance with respect to observations. For a user, forecast quality is assessed in terms of its utility, for instance the savings or losses that result from rational decisions based on the forecast. For a user, a forecast must therefore be informative.

10.4.1 Forecast Performance Criteria

Forecast performance criteria may be subjective or numerical. Subjective criteria are based on a graphical comparison of forecasted and a posteriori observed values. Numerical criteria are based on the differences between the forecasted and observed values. Certain numerical criteria are presented in Addendum 10.4 and in Chapter 3.

In operational mode, numerical criteria are calculated using recent data, for instance the differences between the discharges forecasted 48 hours before and the discharges observed over the last 48 hours. The calculation must be repeated each time the forecast is updated. This can be done for different times up to and including the maximum forecast horizon (e.g., for the discharge at t_0+6 h or at t_0+18 h where t_0 is the forecast time). It can consider the average value of the forecasted variable over a given forecast interval (e.g., mean daily discharge over [t_0+48 h; t_0+72 h]) or the evolution of this variable over a given period (e.g., hourly discharges over [t_0+6 h; t_0+18 h]).

For a probabilistic forecast, quality can also be assessed on the basis of its sharpness, which measures the forecast dispersion, and its accuracy, which measures the average degree of consistency between the forecast and observations (Bontron, 2004; Gneiting *et al.*, 2005). The sharpness of a forecast increases as the uncertainty of the variable decreases. Note that sharpness is independent of observations and that a deterministic forecast is always perfectly sharp. The accuracy of a forecast increases as the difference between the true value (observed a posteriori) and a characteristic value of the probabilistic forecast (e.g., the median) decreases (Figure 10.13).

In this context, it is often worthwhile to check whether the probabilistic forecast provides useful additional information with respect to the statistical distribution of the values of the variable to be forecasted over the entire period over which this variable has been observed. This statistical distribution provides an uninformative probabilistic forecast. It can be used as a forecast if the temporal horizon of forecastability of the considered hydrological variable has been exceeded. This distribution is called the "climatology" of the variable when the forecast concerns a meteorological variable.
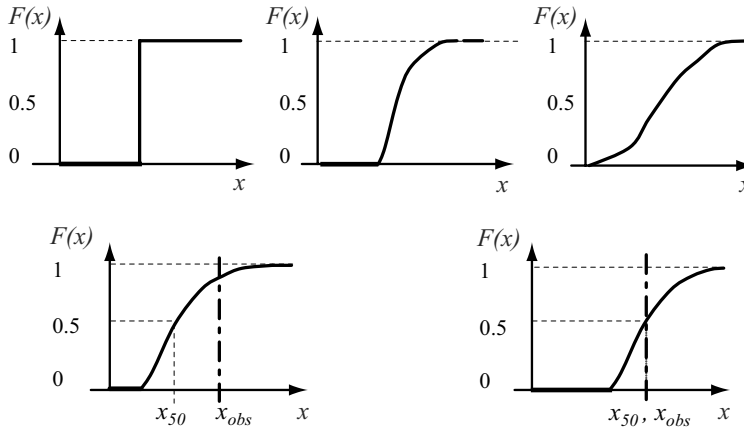
Fig. 10.13: Illustration of the quality of a hydrological forecast by comparing the value observed a posteriori and the initially forecasted distribution of the variable. The three graphs on top show a deterministic (left), sharp (middle) and less sharp (right) forecast. The two graphs on the bottom illustrate an accurate (right) and less accurate (left) forecast (adapted from Bontron, 2004).

When forecasting whether or not a given threshold will be exceeded (e.g., for flood warnings), the quality of the forecast is generally estimated on the basis of a contingency table that includes correctly forecasted events and non-events as well as missed events and false alerts. Different scores can be used to estimate the quality of a forecast in this context (Bontron, 2004).

Addendum 10.4 Quality of an operational forecast

The performance of a forecast made at present time t_0 for the n discharges to come at time steps Δt over the forecast period D (i.e., over $[t_0, t_0+n\Delta t]$ with $n\Delta t=D$) can be evaluated on the basis of different criteria, for instance the Nash criteria (Chapter 3) used for calibration of hydrological model parameters.

It is often worthwhile to check whether the forecasting model provides useful additional information with respect to a simpler reference model. A possible criteria for this is:

$$C(t_0) = 1 - \frac{\sum_{k=1}^{k=n}\left(Q_{obs}(t_0 + k \cdot \Delta t) - Q_{fore, t_0}(t_0 + k \cdot \Delta t)\right)^2}{\sum_{k=1}^{k=n}\left(Q_{obs}(t_0 + k \cdot \Delta t) - Q_{ref, t_0}(t_0 + k \cdot \Delta t)\right)^2} \tag{10.3}$$

where $Q_{fore}(t_0+k\Delta t)$ is the discharge observed at $t_0+k\Delta t$, $Q_{fore,t0}(t_0+k\Delta t)$ and $Q_{ref,t0}(t_0+k\Delta t)$ are respectively the discharge that was forecasted at t_0 for time $t_0+k\Delta t$ (i.e., with a lead time of $k\Delta t$) with the forecasting model to be evaluated and the discharge that would have been forecasted using the reference model.

A positive criterion indicates a performance gain and a negative criterion indicates a performance loss with respect to the reference forecasting model. Two reference models are generally considered:

• The simplest possible model ("naive" model) that consists in taking the observed discharge at the time of forecast as the forecasted discharge. In this case, $Q_{ref,t0}(t_0+k\Delta t) = Q_{obs}(t_0)$, $\forall k \in [1, n]$. The corresponding criterion can be referred to as a persistence criterion.

- The simulation model alone, i.e., the forecasting model without the adjustment procedure used to correct each forecast on the basis of recently observed errors. In this case, $Q_{ref,t0}$ $(t_0+k\Delta t) = Q_{sim}$ $(t_0+k\Delta t)$, $\forall k \in [1, n]$. The corresponding criterion measures the effectiveness of the forecasting model adjustment procedure.

Quality criteria for the development of a forecasting model

The numerical criteria already mentioned generally also provide the basis for the numerical criteria used to calibrate the various components (i.e., the simulation, initialization and adjustment models) of the forecasting model during its development phase. In this context, the criteria are calculated for all the values forecasted over a given time period (e.g., the *n* previous years) or for certain hydrological events that occurred during this period (e.g., the *p* floods over the previous *n* years with discharges exceeding $Q_{threshold}$ m³/s).

When a value is forecasted for a particular lead time (e.g., for $k\Delta t$ in the equation below), the following simple criterion is generally used to compare the performance of the forecasting model to that of a simple reference model:

$$C''(t_0) = 1 - \frac{\sum_{t_0}\left(Q_{obs}(t_0 + k \cdot \Delta t) - Q_{fore, t_0}(t_0 + k \cdot \Delta t)\right)^2}{\sum_{t_0}\left(Q_{obs}(t_0 + k \cdot \Delta t) - Q_{ref, t_0}(t_0 + k \cdot \Delta t)\right)^2} \qquad (10.4)$$

where $Q_{ref,t0}(t_0+k\Delta t)$ is the discharge obtained with a given reference model (e.g., the persistence model or the simulation model). The above criteria can of course be applied to hydrological variables other than discharges, for instance water levels, the slope of the rising front of a hydrograph, stage-discharge variations.

10.4.2 Forecast Utility Criteria

Utility criteria used to evaluate the quality of a forecast can be very different depending on the user and the nature of the forecast (Bontron, 2004). For example, in a flood-warning system, the utility of the forecast is related to the probability of detecting bank overflow and the number of false alerts. On the other hand, for a reservoir operator, utility is related to the accuracy of the forecasted inflow volumes.

Forecast utility is often evaluated in terms of social and financial benefits. These benefits must of course take into account the overall cost of the forecasting system including development, financing and operation of the system. Although these costs are generally substantial, they are often low or even very low compared to the benefits brought by the system or, in a flood control context, the cost of constructing flood mitigation works offering the same level of protection.

The utility of a forecast obviously increases with the robustness of the forecasting model. The model must be capable of producing good results for a wide variety of conditions that may be different from those encountered during calibration. Moreover, the forecasted values must show a certain consistency from one forecast update to another. For a hydrometeorological forecast, this will of course depend on the temporal consistency of the meteorological forecasts over their successive updates. From this point of view, the pertinence and robustness of the adjustment model are determining factors.

Finally, the utility of a forecast also increases with the possible event anticipation time, in particular the degree to which the anticipation time exceeds the time required to

carry out the actions required to meet the operational objectives set for the corresponding type of event (e.g., optimum safety of life and property in the case of flood forecasting). In the case of a flood forecast, the possible anticipation time extends from the issuing of a flood warning to the occurrence of the forecasted hydrological event. The anticipation time for a given event increases with the forecastability of the associated hydrological variables (Section 10.4.3). In practice, the possible anticipation time is limited by the forecast lead time of the forecasting system. It is in fact always less than this limit due to the time required to validate and analyze simulation results. Note that the forecast lead time is often determined by the time required for optimum control of the associated resource or hydrological risk, i.e., the time required for action as mentioned above.

A chronograph including action that must be taken and the possible anticipation time provided by meteorological and hydrological forecasts is illustrated in Figure 10.14 for a flood forecasting system.
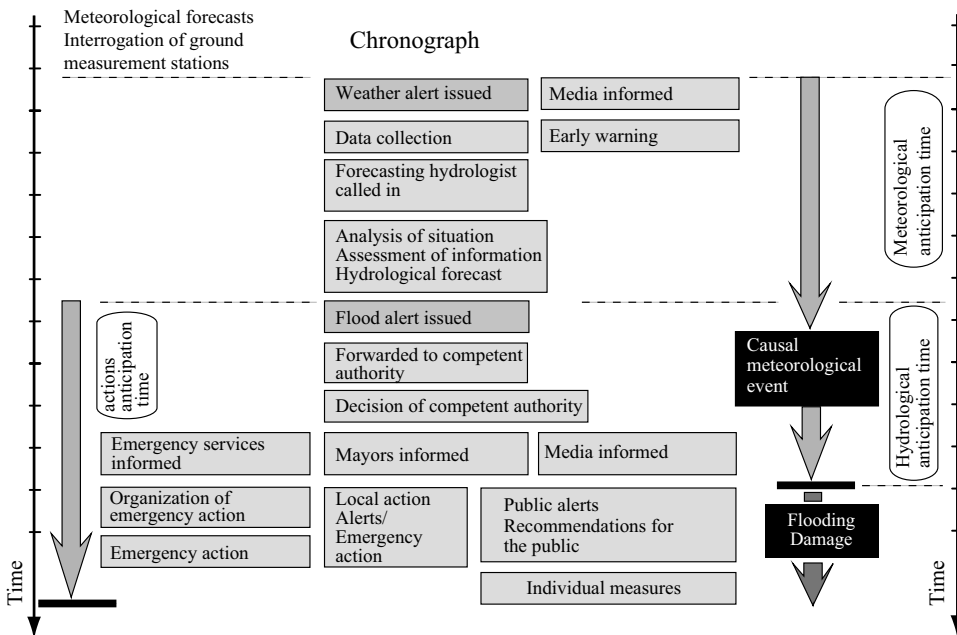
Fig. 10.14: A chronograph for a flood-warning system indicating the required action and the anticipation time provided by meteorological and hydrological forecasts.

10.4.3 Possible Anticipation Time and System Response Time

The uncertainty of the forecast of a given hydrological variable increases with the forecast lead time, thereby decreasing the quality of the forecast. For equivalent forecast uncertainties, the possible anticipation time of a given event depends on the response time of the hydrological system with respect to the main processes that affect the evolution of the considered variable with time.

For example, at a given basin outlet, the possible anticipation time of low-flow discharges can be several orders of magnitude greater than that of the flood discharges. This is because low flows are generated by relatively slow groundwater runoff while flood discharges are generated by much faster surface and sub-surface runoff. Note that in the first case, the memory of the hydrological system is longer than in the second case. The possible anticipation time also depends on the observations available for the state of the system and for the meteorological conditions it was subjected to in the recent past and will be subjected to in the future.

If the precipitation that has fallen on the basin in the recent past is known, the possible anticipation time for flood discharges is roughly between: 1) the rise time of the instantaneous unit hydrograph for the basin if the precipitation to come is of the same order of magnitude as the past precipitation and 2) the basin concentration time if the precipitation to come is much less than the past precipitation (Example 10.3). If all other factors are the same, the possible anticipation time of flood discharges increases with the size of the basin. If the discharges are measured at one or more upstream stations, the possible anticipation time depends on the propagation time of the flood wave between the measurement stations. The possible anticipation time also obviously increases if meteorological forecasts are available for the hours or days to come (Chapter 12).

On a given system, the possible anticipation time can also vary from one meteorological situation to another. It depends for instance on the change of the geographic origin of the inflows with time, i.e., it is shorter if they come from the downstream rather than the upstream part of the basin. It is also shorter if the future inflows are greater than the past inflows.

Example 10.3 Possible anticipation time for flood discharges

For a given basin without a hydrometric station upstream of the considered outlet, let us assume that the only precipitation falling in the recent past has fallen during the last time step. Let us also assume that the corresponding net rainfall p_1 is known and that the basin will receive the unknown net rainfalls $p_2, p_3, \ldots p_n$ in the following time steps.

The direct runoff at any time in the future can be estimated by convolution of the unit hydrograph of the basin and these net rainfalls. The relative contribution $\alpha_1(t_0+t)$ of net rainfall p_1 to the total discharge observed successively at times $t_0+\tau, t_0+2\tau, \ldots t_0+n\tau$ is:

$$\alpha_1(t_0 + \tau) = \frac{p_1 \cdot u(\tau)}{p_1 \cdot u(\tau) + p_2 \cdot u(0)} \tag{10.5}$$

$$\alpha_1(t_0 + 2\tau) = \frac{p_1 \cdot u(2\tau)}{p_1 \cdot u(2\tau) + p_2 \cdot u(\tau) + p_3 \cdot u(0)} \tag{10.6}$$

$$\alpha_1(t_0 + n\tau) = \frac{p_1 \cdot u(n\tau)}{p_1 \cdot u(n\tau) + p_2 \cdot u((n-1)\tau) + p_3 \cdot u((n-2)\tau) + \ldots + p_{n+1} \cdot u(0)} \tag{10.7}$$

where τ is the reference duration of the net rainfall that produced the basin unit hydrograph $u(t)$.

If the future net rainfall is non-zero, the above equations show that the percentage $\alpha_1(t_0+t)$ of the future discharge explained by net rainfall p_1 at time t_0+t decreases with the considered anticipation time $t = n\tau$. The rate of decrease depends on the relative size of

increment p_1 with respect to the other net rainfall increments p_2, p_3, ... p_n and its relative position within the rainfall event.

To illustrate this, consider a fictitious basin with the unit hydrograph (UH) plotted in Figure 10.15a and described in Table 10.3. The basin receives a uniform net rainfall (UR) as shown in Table 10.4. The hydrograph of the direct runoff obtained from the discrete convolution of the basin unit hydrograph and the uniform net rainfall (see Chapter 5 for the principles underlying this convolution) is shown in Figure 10.15b. For this simplified case, the percentage $\alpha_1(t_0+t)$ of the future discharge explained by the net precipitation p_1 drops to less than 50% after time $t_0+3\tau$. Note that $\alpha_1(t_0+t)$ decreases more rapidly after t_0+t_m where t_m is the rise time of the unit hydrograph, as illustrated on the discontinuous curve plotted between the open squares in Figure 10.15b.

Table 10.3: Unit hydrograph of the basin considered [0.01 mm/Δt] (see Chapter 5 for corresponding definitions and application principles).

Time	τ	2τ	3τ	4τ	5τ	6τ	7τ	8τ	9τ	10τ
$u(n\tau)$	2.1	4.2	6.3	8.4	11	13	10	8.4	6.9	5.7
Time	11τ	12τ	13τ	14τ	15τ	16τ	17τ	18τ	19τ	20τ
$u(n\tau)$	0.05	0.04	0.03	0.03	0.02	0.02	0.01	0.01	0.01	0.01

Table 10.4: Increments of net rainfall [mm/Δt] over time step Δt for two rainfall structures: uniform rainfall (UR) and rainfall with a concentrated peak (CP).

Increment	p_1	p_2	p_3	p_4	p_5	p_6	p_7	p_8	p_9	p_{10}	p_{11}	p_{12}	p_{13}	p_{14}	p_{15}	p_{16}	p_{17}	p_{18}	p_{19}	p_{20}	p_{21}	...	p_n
UR	1	1	1	1	1	1	1	1	1	1	1	1	1	1	1	1	1	1	1	1	0	0	0
CP	1	1	1	1	10	1	1	1	1	1	1	1	1	1	1	1	1	1	1	1	0	0	0

The evolution of the contribution of an increment of net rainfall to the total direct runoff at the basin outlet varies with the position of this increment within the event. For a uniform rainfall UR falling on the above basin, the percentage $\alpha_k(t_0+t)$ of the future discharge explained by the kth net rainfall increment (p_k) is however always maximum at time $t_0+ k\tau + t_m$, except for the first increments (p_1, p_2, ... p_4). It becomes zero at time $t_0+ k\tau + t_c$ where t_c is the basin concentration time. This is illustrated for example in Figure 10.15b by the curves plotted through open triangles and diamonds. They correspond respectively to the contributions $\alpha_5(t_0+t)$ and $\alpha_{15}(t_0+t)$ of net rainfalls p_5 and p_{15}.

Generally the percentage of future discharges explained by p_1 is higher when the relative values of future net rainfalls are low with respect to p_1. If all future net rainfalls are zero, the net rainfall increment p_1 alone explains the flood discharges up to time t_0+t_c. On the other hand, if a future net rainfall increment p_k is much higher than increment p_1, the contribution of p_1 to the total discharge will be negligible.

To illustrate this, let us consider the fictitious basin of the example above subjected to a rainfall with a concentrated peak (CP) as described in Table 10.4 (CP is a moderate and constant net rainfall of the same duration as that of uniform rainfall UR with a high net rainfall increment p_5 concentrated on the 5th time step). The direct runoff hydrograph resulting from the discrete convolution of the unit hydrograph of the basin and the net rainfall UR is shown in Figure 10.16. The relative contribution of the different net rainfall increments p_k, $k \neq 5$ is greatly reduced compared to the contribution for a uniform rainfall UR. On the other hand, the relative contribution of increment p_5 is predominant over a long time period. It is maximum at time $(t_0+ 5\tau) + t_m$.
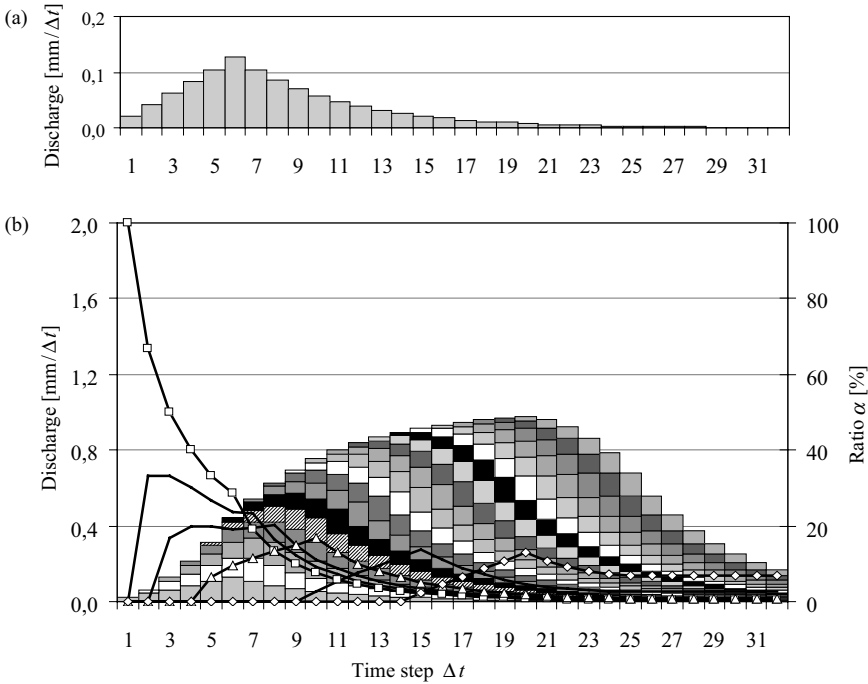
Fig. 10.15: Evolution of the contribution of an increment of net rainfall to the total direct runoff at the basin outlet. a) Unit hydrograph of the basin discretized over time steps $\Delta t = \tau$. The rise time is equal to $6\Delta t$. b) Hydrograph at the basin outlet resulting from a uniform rainfall UR and absolute and relative contributions of the different rainfall increments. The shaded rectangles represent the contribution of the ith net rainfall increment p_i to the total discharge that will be observed at $t_0 + n\Delta t$ (the rectangles containing the same shade of gray come from the same net rainfall increment; the cross-hatched rectangles come from the 5th net rainfall increment). The relative contribution (in %) of these net rainfall increments to the total discharge is represented by the discontinuous curves. The curves plotted through open squares, triangles and circles correspond respectively to the relative contributions $\alpha_i(t_0 + t)$ of net rainfalls p_1, p_5 and p_{15}.
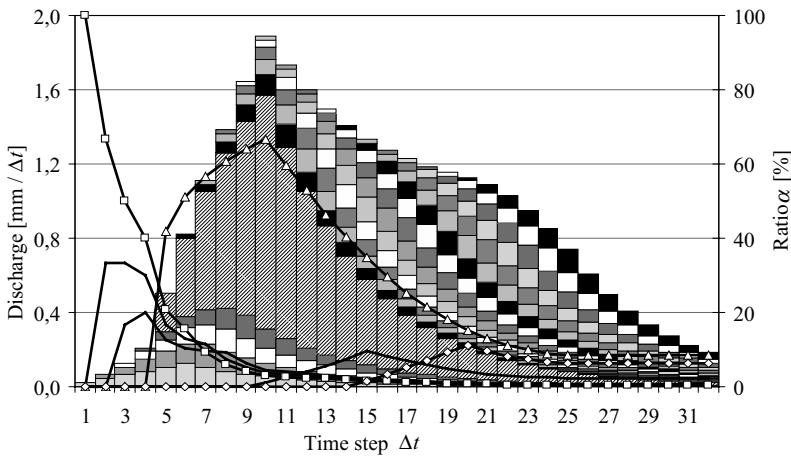

Fig. 10.16: Same as Figure 10.15 but with a net rainfall exhibiting a concentrated peak (CP) on the 5th time step. For indications concerning the symbols used in the different curves, see Figure 10.15.

10.5 CHOOSING A FORECASTING METHOD

As for the prediction (or "predetermination") of discharges, hydrological forecasting can be based on a wide variety of models and approaches that can provide similar levels of performance. The choice depends on the forecasting objectives (variable to be forecasted, required anticipation time, required accuracy, etc.) as well as the characteristics of the environment, the nature and response time of the main phenomena involved (that will determine the possible anticipation time of the events to be forecasted), the type and quality of available real-time data and finally the know-how and practices of the hydrologist. For example, low flows can be forecasted with limited data and relatively simple models (Chapter 8) compared to those required for flood forecasting. Similarly, the forecasting of flash floods in urban basins generally requires different data and a different approach than those required to forecast floods on large river basins such as the Rhine River at Cologne, the Niger at Mopti or the Mississippi at Baton Rouge.

Other aspects can be analyzed to fine tune the choice. In this respect, the following section will present several approaches regarding useful data and choices of a simulation model, model initialization method and error processing method.

10.5.1 Choosing a Simulation Model

As already mentioned, the simulation model can be statistical or behavioral. Statistical models of the ARX or ARMAX type are generally easy to develop and implement, however they have two major limitations for hydrological forecasting. First of all, the time series of the variable to be forecasted must be stationary. Secondly, the relationships between the explanatory variables and the variable to be explained must be linear or pseudo-linear. These two conditions are not satisfied for many hydrological systems. For example, flood discharges are not directly related to precipitation. The depend mainly on the net rainfall that takes into account the different runoff losses which are in turn related to the level of basin saturation. Moreover, in mountainous regions, a portion of the precipitation is stored in the snowpack and subsequently released via a process that is highly dependent on temperatures in the basin.

The limitations of empirical models of the ARX or ARMAX type can in some cases be partially relieved by appropriate preprocessing of the data. Conceptual models can for example be applied to precipitation data to determine the net precipitation (Young, 2002) or, in mountainous regions, to produce the "equivalent" precipitation (Mtir, 2004). Artificial neuron networks (ANN), which can be considered as a non-linear expression of the transfer functions, are sometimes also presented as a potential way of overcoming this limitation (Fortin *et al.*, 1997; Toth *et al.*, 2000). Moreover, to make time series stationary, a mathematical transformation of the considered variables is sometimes possible.[2] Finally, different models can be developed for different types of operation or different types of initial configurations of the basin leading under these conditions to pseudo-linear behaviors.

---

[2]To make time series stationary, the transformations $z_t = y_t - y_{t-1}$ or $z_t = y_t - 2y_{t-1} + y_{t-2}$, corresponding to the first- or second-order differential of the variable y_t, are sometimes sufficient. "Deseasonalization" of the variables can also be envisaged. One possible transformation consists for example in standardizing the observations: for each calendar period s, the deseasonalized variable is expressed as $z_{t,s} = (y_t - y_{m,s})/s_s$ where $y_{m,s}$ and s_s are respectively the mean and standard deviation of the observations over this period.

The most frequent criticism of statistical approaches is that they neglect decades of research and development focused on understanding and modeling hydrological processes. In particular, their empirical nature makes their application uncertain for the forecasting of events outside the area of observation. These approaches are therefore poorly suited for use on ungaged basins. In such cases, some of the parameters obtained by calibration ungaged basins have no physical or conceptual signification. Moreover, the structure of these models, optimized for the data of each of the sites where observations are available, can vary from one site to another. This is for example the case for the order of ARMAX models or the number of neurons of an ANN model. As a result, it is difficult or even impossible to spatially transpose such models and/or regionalize their parameters for ungaged basins.

Conceptual or physically-based models are often preferred over statistical models because they are expected to take into account, with varying degrees of simplification, both the non-linearity of the system considered and the non-stationarity of the processes. They should therefore better reproduce the determining processes outside the area in which they were observed. These models can also be adapted to take into account eventual modifications of the hydrological behavior of the system considered—for instance changes caused by hydraulic projects. In addition, they are principle more easily transposed to ungaged basins. Finally, forecasting uncertainties are generally reduced and possible anticipation times increased. Examples of hydrological models used for operational forecasting include the HBV semi-distributed conceptual model used in many countries of northern Europe (Lindstrom *et al.*, 1997), ARNO models of the variable contributing area type used in the framework of the European Flood Forecasting Operational Real-Time System (Todini, 1996) and, when considering physically-based distributed models, the tRIBS model used in the United States (Ivanov *et al.*, 2004).

10.5.2 Choosing an Initialization Method

Different methods can be used to initialize hydrological simulation models. The choice of a method depends mainly on the data available to estimate the initial state of a given hydrological system and the type of simulation model used for hydrological forecasting.

When various observations concerning the state of the system are available, assimilation techniques can be particularly useful. In principle, they make it possible to use the different types of information on the state, including observations and data from hydrological simulations, in an optimum manner. Data assimilation methods have been widely developed for oceanography and atmospheric science applications, in particular to improve meteorological forecasts (Heemink and Kloosterhuis, 1990; Ottle and Vidal-Majar, 1994). Various hydrological applications are beginning to see the day (Reichle *et al.*, 2002; Castaings *et al.*, 2006). Assimilation mainly concerns discharges observed in the hydrographic network and a number of other state variables related to the snowpack, soil moisture and groundwater storage (François *et al.*, 2003; Aubert *et al.*, 2003). This technique mainly applies to physically-based simulation models for which the state variables of the model correspond, with a specific mathematical transformation, to those of the physical system.

For conceptual models, on the other hand, initialization of the model state variables on the basis of measured system state variables is difficult or even impossible. This comes from the fact that simulation of the hydrological system behavior, for these models, is

based on the fluxes exchanged between different reservoirs that have, in some cases, no real link with the physical behavior of the real system. Moreover, most conceptual models neglect the spatial variability of state variables within the real system. When the measured variable does not explicitly correspond with the model variable, data assimilation can nevertheless be carried out if it is possible to identify an unequivocal relationship between these variables (Aubert *et al.*, 2003; Andreadis and Lettenmaier, 2006).

The complexity of assimilation techniques along with the complexity of the hydrological models to which they are applied often makes them hard to use. The simulation model state variables are for this reason more often initialized on the basis of a continuous simulation. This method offers the advantage of simplicity. Moreover, it often represents the only reasonable possibility for the initialization of many conceptual models.

10.5.3 Choosing an Adjustment Method

The question of choosing a real-time adjustment method for a simulation model applies only to physically-based or conceptual models (Section 10.2.3). The various advantages and disadvantages of the four main adjustment methods discussed in this chapter are presented in Addendum 10.3. The problem here is to know whether it is necessary to use an adjustment model or simply an error model to correct the model output.

Whatever the benefits of an adjustment model in terms of reducing forecasting errors, it is important to always first consider the possibility of improving the physical representation of the processes driving the hydrological variable to be forecasted. If the adjustment model is designed to correct significant modeling errors or to compensate for a major lack of data, the error processing used may not be appropriate with respect to the true cause of the difference and could subsequently increase instead of decrease the initial error (Roche, 1987). Along the same lines, it is always important to use the expertise of experienced forecasters who, knowing the limits of the forecasting systems they manage operationally, generally know how to interpret and adjust the forecasting model output subjectively.

Adjustment methods are generally most effective when dealing with regular, correlated or persistent errors corresponding to disturbances that are neither too long nor too short. Accidental errors are the most difficult to deal with, in particular when they have an exceptionally high amplitude. Finally, an adjustment method must be designed to handle crisis situations during which the observations used for adjustment (e.g., discharges) may no longer be available due to failure of measurement instruments (e.g., hydrometric sensors) or the data transmission system.

10.5.4 Data and Models used for Flood Forecasting

Data used for hydrological forecasting can be divided into two groups (WMO, 1994). The first includes all information that can be used to develop, calibrate and validate the forecasting model. This includes time series of the discharges and meteorological data along with physiographic data concerning the system. The second group concerns data required to produce the forecast itself, for example data on the state of the basin along with past and future meteorological data (Section 10.1.1).

Ideally, the data required for a forecast depends on the forecasting method used, the selected forecast lead time and the hydrological characteristics of the system considered.

This is illustrated below for a flood forecast case. Practically speaking, the availability of data is one of the main factors restricting the choice of a forecasting method.

For flood forecasting, two modeling approaches are widely used. One involves routing of flows through the hydrographic network (discharge-discharge approach) and the other simulates the transformation of rainfall to runoff (rainfall-runoff approach). The right choice between these two approaches essentially depends on the characteristics of the river basin (i.e., size, topography), available precipitation, discharge or water level data and the required anticipation time.

It is generally considered preferable to forecast discharges rather than water levels. Discharges are conservative while water levels are not. This is especially important if the forecast is of the discharge-discharge or rainfall-runoff type. Furthermore, discharge forecasts offer a wider choice of models (all models are capable of dealing with discharges). Finally, it is generally possible to estimate the water level on the basis of an estimated discharge.

If observations of discharges upstream of the point of interest are available, they are in principle sufficient to obtain a forecast of reasonable quality if: 1) the discharge propagation time between the upstream and downstream stations are greater than the required anticipation time and if 2) the flows measured by the gaging stations upstream of the point at which the forecast must be made are sufficient. This is generally the case on large water courses. In this case, the forecast is generally made using routing models (Chapter 6) or by simple regressions between two stations (statistical models).

In most cases, the discharges (or water levels) on the upstream network are unknown or insufficiently known to achieve the required accuracy. It is then necessary to use a hydrological rainfall-runoff model, possibly together with a hydraulic routing model, in particular if the discharges are mostly produced in the upstream parts of the basin. The important question is whether or not the required anticipation time is less than the sum of the rise time of the unit hydrograph and the time required for propagation.

If this is the case, observations of meteorological variables, in particular precipitation, may be sufficient to produce a reasonable discharge forecast. Upstream meteorological data from the past provides precious information. If this is not the case, meteorological forecasts are indispensable (Chapter 12).

These considerations that orient the choice of the type of approach to be used for flood forecasting are summed up in a simplified manner in Figure 10.17.
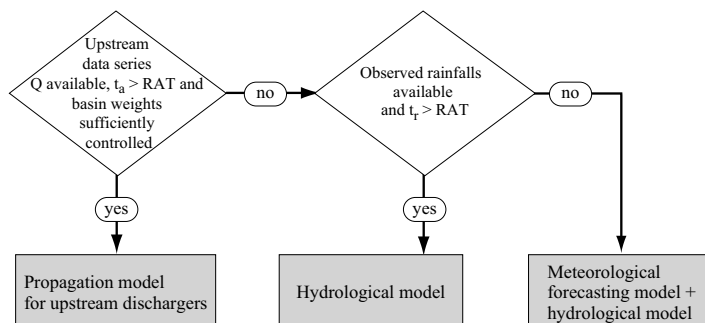

Fig. 10.17: Choosing a flood forecasting method according to available data and the characteristic times of the basin, including the required anticipation time (RAT), the discharge propagation time (t_a) between the downstream and upstream stations and the rise time (t_r) of the unit hydrograph of the basin.

Finally, the level of accuracy that can be expected of a flood forecast obviously depends on the configuration considered. For a given forecast lead time, forecast uncertainties will in principle be lower if it is possible to use a discharge-discharge model rather than a hydrological model. They will also be lower if recent meteorological observations are sufficient and meteorological forecasts are not required. If meteorological forecasts are used, the possibility of forecasting the spatial and temporal evolution of the meteorological variables on the system considered, the forecast lead time and the quality of the meteorological forecast are the key factors determining the quality of the hydrometeorological forecast (Chapter 12).

10.5.5 Probabilistic or Ensemble Forecasts

Hydrological forecasts are in fact rarely supplied in a probabilistic form. As already mentioned, a probabilistic forecast can be implemented using a Bayesian forecasting system. Although of interest from a formal viewpoint, the system is difficult to implement. In particular, this is a consequence of the relatively sophisticated formulation of the complete mathematical problem that requires analytical or numerical solution of successive integrals. This is only possible if certain conditions are satisfied by the statistical distributions used to characterize the different sources of uncertainty (normality/linearity), however this is not generally the case. The necessary conditions can however be created by first transforming the data (Kelly and Krzysztofowicz, 2000).

As opposed to a probabilistic approach, an ensemble forecast does not require complex mathematical and statistical developments. The main limitation of the approach stems from the difficulty of specifying scenarios other than those related to meteorological forecasts. The other scenarios to be considered concern past meteorological conditions to which the system was subjected, the initial conditions of the modeled hydrological system (i.e., soil saturation level for the different sub-basins of the system), the different parameters of the simulation model and the parameter settings used for the simulation or adjustment models. The associated variables are however often strongly interdependent and the corresponding statistical distributions are generally unknown. The approach is also limited by the required calculation time to simulate the hydrological response of the basin for all the considered scenarios.

Ensemble hydrological forecasts are sometimes criticized because the total forecast uncertainty can be greatly underestimated, in particular if the sources of uncertainty are not taken into account in the ensemble generator. However, this criticism also applies to the probabilistic approach. Considering the Bayesian forecasting system, the analytical complexity of the uncertainty integration processor increases very rapidly with the number of uncertainty sources considered. It is therefore only possible to consider the main source of forecast uncertainty, in practice the basin precipitation, in a probabilistic manner. Whatever the approach used, it is therefore always important to mention that the forecast issued depends on all the information and models used to create it.

10.6 KEY POINTS OF THE CHAPTER

- The forecasting of any hydrological variable requires an appropriate forecasting model and the real-time acquisition and processing of different data concerning the state of the hydrological system considered and the past and future conditions to which it will be subjected.
- A forecasting model is made up of a simulation model and various methods used to take into account the initial state of the system, adapt meteorological forecasts to the requirements of the simulation model and adjust the model on the basis of errors observed in the recent past between observed and forecasted values.
- Many different simulation models are available. The right choice for a given case depends on the objectives of the forecast and the context (e.g., characteristics of the system, required anticipation time, available data, know-how, etc.).
- The simulation model is initialized in such a way as to best represent the initial state of the physical system. This can be done by assimilation of observed data on the system or by a continuous simulation, in the recent past, of the behavior of the system.
- The simulation model can be adjusted to continuously manage the errors observed between forecasts and a posteriori observations of the considered hydrological variable. The objective is to reduce future errors.
- Forecasting uncertainties increase with the forecast lead time. To characterize these uncertainties, it is essential to know, characterize and propagate the uncertainties related to the estimation of input variables, the initial state of the system and the hydrological model.
- Characterization of the uncertainties leads to the issuing of a probabilistic forecast (described by the statistical distribution of the considered variable) or an ensemble forecast (made up of different scenarios).
- The quality of a forecast depends on its statistical performance, its utility and the possible anticipation time of the hydrological events to be forecasted.
- For a given level of uncertainty, the possible anticipation time depends on the data available and the response time of the analyzed hydrosystem.
- Hydrological forecasts generally require meteorological forecasts if the required anticipation time exceeds the rise time of the unit hydrograph of the considered basin. In this case, the required meteorological forecasting scenarios can be obtained by meteorological and then hydrological adaptation of the output from meteorological forecasting models.

10.7 APPENDICES

10.7.1 Autoregressive Moving-average Model with Exogenous Variables (ARMAX)

The expression of an ARMAX model is a special case of the general expression of linear transfer functions presented in Appendix 5.7.6. In this case, the parameters n_d and n_f of the general expression are equal to zero ($n_d = n_f = 0$).

The structure of a model of this type is defined by order p of the autoregressive component, order q of the moving average of the recent error values, the number of exogenous variables and, for each exogenous variable, the optimum order and lag.

With the formalism of Appendix 5.7.6, an ARMAX model with a single input (i.e., single exogenous variable) can be expressed as follows:

$$A(q)y(t) = B(q)u(t - n_k) + C(q)e(t) \tag{10.8}$$

where $A(q)$, $B(q)$ and $C(q)$ are the polynomials associated respectively with the variable to be explained $y(t)$, the explanatory variable $u(t)$ and the errors $e(t)$. This expression can be written more explicitly in the form:

$$y(t) = \quad -a_1 y(t-1) - ... - a_n y(t - n_a) + b_1 u(t - n_k) + ...$$
$$+ b_n u(t - n_b - n_k + 1) + e(t) + c_1 e(t-1) + ... + c_n e(t - n_c) \tag{10.9}$$

where n_a is the order of the autoregressive part, n_k and n_b are respectively the lag and order associated with the exogenous variable considered and n_c is the order of the moving average of the residuals. The predictor corresponding to this model is given by (Corriou, 1996):

$$\hat{y}(t,\theta) = [1 - A(q)] \cdot y(t) + B(q) \cdot u(t - n_k) + [C(q) - 1] \cdot e(t,\theta) \tag{10.10}$$

This can be expressed in condensed form:

$$\mathbf{\hat{y}(t,\theta) = \varphi(t,\theta) \ \theta^{T}} \tag{10.11}$$

where $\mathbf{\varphi(t,\theta)} = [y(t-1), ..., y(t - n_a), u(t - n_k), ..., u(t - n_k - n_b + 1), e(t-1,\theta), ..., e(t - n_c, \theta)]$ is the vector of the observations (water levels or discharges at the station considered or at upstream stations, meteorological data and recent errors), and $\mathbf{\theta} = [-a_1, ..., -a_{n_a}, b_1, ..., b_{n_b}, c_1, ..., c_{n_k}]^T$ is the vector of the parameters to be estimated.

With the same formalism, the predictor associated with an ARMAX model with multiple inputs (n_u exogenous variables) can be expressed as:

$$\hat{y}(t,\theta) = [1 - A(q)] \cdot y(t) + B_1(q) \cdot u_1(t - n_{k,1}) + ...$$
$$+ B_{nu}(q) \cdot u_{nu}(t - n_{k,nu}) + [C(q) - 1] \cdot e(t,\theta) \tag{10.12}$$

An ARMAX model is calibrated in several steps: 1) choice of the lag between the output and the inputs (increases with the required anticipation time), 2) identification of the minimum order required for each of the polynomials appearing in the model (one for the autoregressive part, one for each exogenous variable and one for moving average of the errors) and finally 3) estimation of the coefficients of the different polynomials. The parameters can be estimated using all available data or only the most recent data (recursive estimation). Recursive estimation is often used for forecasting applications (Delleur, 1991).

10.7.2 Kalman Filtering

Kalman filtering is an optimal sequential data assimilation technique when the dynamic system considered is governed by linear equations and the associated measurement errors are Gaussian. For a linear system, the behavior model can be expressed in a discrete manner in the following generic form:

$$\mathbf{x}_t = \mathbf{\Phi}_{t-1,t} \cdot \mathbf{x}_{t-1} + \mathbf{\Gamma}_t \cdot \mathbf{\varepsilon}_t^m \quad \text{(system equation)}$$

$\mathbf{x}_t[n,1]$ is the model state vector at time t, i.e., the vector containing all the state variables used to describe the behavior of the system, $\mathbf{\Phi}_{t-1,t}$ $[n,n]$ is the transition matrix, potentially variable from one time step to another, $\mathbf{\varepsilon}_t^m$ $[n,1]$ is the model error attributed to the structure and parameterization of the model and represented by a random Gaussian process with mean $\mathbf{\bar{\varepsilon}}_t^m$ and covariance matrix $\mathbf{Q}_t$ and $\mathbf{\Gamma}_t$ is an appropriate matrix with respect to the different dimensions of the variables.

Assume that the observations can be deduced from the state vector using a linear operator:

$\mathbf{z}_t = \mathbf{H}_t \cdot \mathbf{x}_t + \boldsymbol{\varepsilon}_t^o$ (measurement equation)

where $\mathbf{z}_t$ [m≤n,1] is the observation vector, $\mathbf{H}_t$[m,n] is the transformation matrix and $\boldsymbol{\varepsilon}_t^o$ [m,1] is the measurement error represented by a random Gaussian process with mean $\bar{\boldsymbol{\varepsilon}}_t^o$ and covariance matrix $\mathbf{R}_t$. It is assumed to be independent of the error model.

The Kalman filter is used to obtain an unbiased estimate $\hat{\mathbf{x}}_{t/t}$ of the unknown state $\mathbf{x}_t$ with minimum covariance along with its covariance matrix $\mathbf{P}_{t/t}$, subject to knowledge of the unbiased a priori estimate of this state $\hat{\mathbf{x}}_{t/t-1}$ and its covariance matrix $\mathbf{P}_{t/t-1}$ as well as the last observations $\mathbf{z}_t$.

At each time step, estimates of the states and their covariance matrix are obtained by extrapolating estimates from the previous time step:

$\hat{\mathbf{x}}_{t/t-1} = \boldsymbol{\Phi}_{t/t-1} \cdot \hat{\mathbf{x}}_{t-1/t-1} + \boldsymbol{\Gamma}_t \cdot \boldsymbol{\varepsilon}_t^m$ (extrapolation of the states)

$\mathbf{P}_{t/t-1} = \boldsymbol{\Phi}_{t/t-1} \cdot \mathbf{P}_{t-1/t-1} \cdot \boldsymbol{\Phi}_{t/t-1}^T + \boldsymbol{\Gamma}_t \cdot \mathbf{Q}_t \cdot \boldsymbol{\Gamma}_t^T$ (extrapolation of the error covariance)

The innovation matrix $\mathbf{v}_t$ and the Kalman gain matrix $\mathbf{K}_t$ are then estimated as:

$\mathbf{v}_t = \mathbf{z}_t - \bar{\boldsymbol{\varepsilon}}_t^m - \mathbf{H}_t \cdot \hat{\mathbf{x}}_{t/t-1}$ (innovation)

$\mathbf{K}_t = \mathbf{P}_{t/t-1} \cdot \mathbf{H}_t^T (\mathbf{H}_t \cdot \mathbf{P}_{t/t-1} \cdot \mathbf{H}_t^T + \mathbf{R}_t)^{-1}$ (Kalman gains)

Finally, the a priori estimates of the state vector and the covariance matrix can be updated using recent observations.

$\hat{\mathbf{x}}_t = \hat{\mathbf{x}}_{t/t-1} + \mathbf{K}_t \cdot \mathbf{v}_t$ (updating of states)

$\mathbf{P}_{t/t} = (\mathbf{I} - \mathbf{K}_t \cdot \mathbf{H}_t) \cdot \mathbf{P}_{t/t-1}$ (updating of error covariance)

The extended Kalman filter is a generalized version of the Kalman filter for systems that are not very non-linear (Kalman, 1960). The ensemble Kalman filter can be used to avoid limitations related to requirements pertaining to Gaussian errors and linearity of the simulation model equations.

10.7.3 The Bayesian Forecasting System (Krzysztofowicz, 1999, 2001a,b)

The Bayesian forecasting system proposed by Krzysztofowicz (1999, 2001a,b) is made up of three distinct operators: 1) the meteorological uncertainty processor, 2) the hydrological uncertainty processor and 3) the integrator of the two sources of uncertainty. To simplify the solution of the mathematical problem associated with this approach, the uncertainty of the meteorological forecasts takes into account only the uncertainty of the precipitation, more precisely the average precipitation on the basin. The spatial structure of precipitation, as for the other determining hydrometeorological variables such as temperature or initial basin saturation conditions, are taken into account in a deterministic manner by the processor.

The objective of the precipitation uncertainty processor is to produce by simulation (using the hydrological model conditioned for the forecast to be carried out) the probabilistic forecast of the hydrological variable of interest (e.g., discharge) corresponding to the available probabilistic forecast of precipitation (a probabilistic quantitative precipitation forecast (PQPF) is used for this (Chapter 12)). In this step, hydrological uncertainty is assumed to be non-existent. The probabilistic forecast depends on the values of all the deterministic inputs used by the hydrological model (Kelly and Krzysztofowicz, 2000).

The objective of the hydrological uncertainty processor is to quantify the hydrological uncertainty assuming that there is no uncertainty in the precipitation. This processor produces a

family of a posteriori distributions of the variable to be forecasted. Each distribution depends on the current observation of this variable and the forecast of this variable obtained from the hydrological model assuming that the precipitation depth to come is equal to a certain quantity v (Krzysztofowicz and Herr, 2001).

Under these conditions, the probability distribution of the variable to be forecasted obtained using the uncertainty integrator corresponds to the Bayesian revision of the a priori distribution of this variable.[3] Subsequently, the a posteriori distribution produced by the Bayesian forecasting system can only improve the information available a priori on the variable to be forecasted. Moreover, if the PQPF is perfect, the a posteriori distribution describes the hydrological uncertainty alone.

---

[3]If the a priori distribution of the variable to be forecasted is uninformative, it simply corresponds to the natural variability of the variable. A distribution that is a priori more useful (because informative) is the distribution obtained by analyzing the observed data of the relationship between the value of the variable at time t and its value at time t-Δt.

CHAPTER 11

REGIONALIZATION METHODS[1]

Drainage basins in many parts of the world are ungaged or poorly gaged. Moreover, some existing stream-gage networks are in a state of decline due to cost issues or maintenance difficulties. Note also that the behavior of drainage basins is often non-stationary, modified directly or indirectly by a wide range of human activities and/or development projects. Under such conditions, the estimation of hydrological variables is difficult and highly uncertain. Prediction of these variables is however essential for effective management and use of water resources, whether for the design of hydraulic works or the identification of hydrological risks related to extreme events (e.g., floods, low flows). Real-time forecasting of these hydrological variables is another equally crucial task in hydrology.

When the considered drainage basin is instrumented and the necessary measurements are available in sufficient quantity, the hydrological variable of interest can be estimated on the basis of observations. If an appropriate hydrological model of the basin is available along with the necessary meteorological input variables, discharges can also be reconstructed by simulations.

However, in most cases, hydrologists do not have all the data they need for hydrological analysis and/or modeling. In the absence of measurements (i.e., on ungaged drainage basins), the variable of interest must then be predicted or forecasted on the basis of all pertinent and information available in the region. This estimation method is referred to as regionalization.

Section 11.1 reviews the principles of such regionalization methods. Section 11.2 presents the main methods used to develop regional models and in particular to identify homogeneous hydrological regions. Section 11.3 deals with the estimation of a hydrological variable of interest within homogeneous hydrological regions. Section 11.4 discusses how various types of available information can be combined to estimate the variable of interest.

11.1 REGIONALIZATION PRINCIPLES

11.1.1 Hydrological Variables of Interest

In hydrology, regionalization methods were first developed to predict maximum flood discharges (Dalrymple, 1960; Benson, 1962; Bobée *et al.*, 1996a). The regionalization methods dealt with in this chapter often concern the estimation of this variable however

---

they can generally be adapted for use in predicting other hydrological variables. The reader is invited to refer to the works of Sauquet (2006) for the estimation of mean annual discharges, Weingartner and Aschwanden (1992) for hydrological regimes (monthly mean discharges), Durrans and Tomic (1996) and Laaha and Bloschl (2006) for the estimation of low flows and Mimikou and Kaemaki (1985), Fenessey and Vogel (1990) and Niadas (2005) for the estimation of flow-duration curves.

Most of the variables mentioned above can be reconstructed by simulations based on observed or generated meteorological scenarios using appropriate hydrological models (Chapter 12). For ungaged basins, such simulations require a regionalized hydrological model. Since the end of the 1990s, most work in the field of regionalization has therefore focused on the spatial transposition of hydrological models for the application on ungaged basins and in particular the estimation of their parameters for these basins (Sefton and Howarth, 1998; Andréassian *et al.*, 2006). This problem is also crucial for the real-time forecasting of flood discharges. It represents one of the highest research priorities of the hydrological scientific community today. It has led in particular to a number of international initiatives, the most important being the Decade on Predictions in Ungauged Basins (PUB), 2003–2014, initiated by the International Association of Hydrological Sciences (Sivapalan *et al.*, 2003). The main results of this important international research program have recently been published (Hrachowitz *et al.*, 2013; Parajka *et al.*, 2013; Salinas *et al.*, 2013; Viglione *et al.*, 2013).

Regionalization methods are also often used to propose a meteorological scenario at a site where there is no appropriate meteorological or climatological station. Regionalization is then used once again either for the estimation of the meteorological variable of interest (e.g., precipitation—Mora *et al.*, 2005; Mikkelsen *et al.*, 2005) or for the estimation of the parameters of a stochastic generator of this variable (Cowpertwait *et al.*, 1996).

In hydrology, regionalization can concern different types of variables, from characteristic discharges and meteorological variables to the parameters of a given model. In this chapter, all these will be referred to as hydrological variables. However, most of the methods and examples presented concern the regionalization of flood discharges.

11.1.2 Basic Principles of a Regionalization Method

Regionalization methods are used to extend information available at a limited number of points to an entire area. In hydrology, such methods are used to estimate a hydrological variable at a given site (the target site) by combining local information with regional information coming from instrumented sites similar to the target site.

Regionalization therefore requires development of a regional model capable of explaining the variable of interest. This model is then applied to the considered non-instrumented site.

Developing the regional model

A regional model can be developed in two main steps:

• Determination of regions that are homogeneous with respect to the hydrological variable of interest.

- Development of a method to estimate the hydrological variable of interest within each homogeneous region. For instance, this can involve identifying, on the basis of a number of gaged drainage basins, the statistical relationship between the hydrological variable and the various explanatory characteristics observed or estimated elsewhere in the basin (e.g., physiographic/climatic characteristics of the basin).

Development of a regional model requires sufficient data from a sufficient number of instrumented sites in the region. The variable to be regionalized must therefore first be estimated for each of the instrumented sites of the region. Regionalization of the 100-year flood discharge or the Q_{347} low-flow discharge, for example, requires an appropriate preliminary frequency analysis for each site. Regionalization of the parameters of a rainfall-runoff simulation model requires a procedure to calibrate/validate the parameters of the hydrological model for each instrumented site (Chapter 3).

Finalization of the regional model then requires, as for rainfall-runoff models, the two following steps:

- Calibration of the regional model, requiring selection of homogeneous regions, choice of the model structure and estimation of the parameters of the model used to estimate the hydrological variable of interest.
- Validation of the regional model.

Each of these two steps makes use of the data available on the instrumented sites. A sub-sample of the complete sample of instrumented sites is used to calibrate the regional model and the other instrumented sites are used to validate the model.

Applying the regional model

Once the regional model has been developed, calibrated and validated, the hydrological variable of interest can be estimated for the target site on the basis of few or even no measurements. This is carried out in two steps:

- Identification of the homogeneous region to which the site belongs.
- Application, for the site, of the regional estimation method developed for this region. For example, if a relationship has been identified between the physiographic/climatic characteristics of the gaged basins and the hydrological variable of interest, this relationship is used to derive the required variable from the physiographic/climatic characteristics of the considered ungaged basin.

11.1.3 Importance of Regionalization

For a basin without measurements, regionalization represents the most effective way to predict characteristic discharges or estimate the parameters of a simulation model. When a short series of measurements is available for the target site, regionalization can also be used to improve the estimation of hydrological variables (Cunnane, 1989; Laaha and Bloschl, 2005). This is referred to as a local/regional approach. As pointed out by Stedinger and Lu (1995), the missing temporal information is replaced by spatial information. In other words, regionalization in this case provides a tool to consolidate observations obtained at a certain site by taking into account observations at neighboring sites. For example, for the prediction of flood discharges, the sampling problems inherent to short measurement

series are attenuated, thereby facilitating the choice of a theoretical statistical distribution (in a parametric approach) and the estimation of the parameters of this distribution. It is also possible to use distributions involving a larger number of parameters (Cunnane, 1989; Mora *et al.*, 2005).

This chapter presents different methods used to develop regional models. Methods used to define homogeneous regions are described in Section 11.2 and those used to estimate the hydrological variable of interest are covered in Section 11.3. The last section of this chapter presents the advantages and ways of combining different regional estimates.

To illustrate the development principle of these methods, the so-called index flood method, frequently used to estimate flood discharges, is applied to the western part of Switzerland. Example 11.1 describes the study zone and presents a preliminary analysis of the flood regimes. This example is taken from Niggli (2004). The different steps in implementing this method for this region are then described in other examples throughout this chapter.

Example 11.1

Regionalization of flood discharges in western Switzerland: description of the study zone and preliminary analysis of the flood regimes

The study region includes the basin of the Aar river up to its junction with the Reuss river, the Swiss portion of the Rhone and Doubs rivers and the Swiss portion of the Rhine river downstream of the junction with the Aar river (Figure 11.1). Basins with hydrological regimes influenced by human activity, with areas greater than 500 km² or with mean elevations greater than 1500 meters (Bernese and Valais Alps for which the hydrological regime is strongly influenced by snow) were not included.

The hydrological data used are series of maximum annual discharges measured at the outlets of more than 100 gaged drainage basins. The lengths of theses series varies between 3 and 80 years. An initial qualitative evaluation of the overall study zone shows that, generally speaking, the hydrological behavior of each drainage basin can be explained by the geographical region to which it belongs, i.e., the Swiss Prealps, the Swiss Plateau (referred to hereafter as the Plateau) and the Jura region (referred to hereafter as the Jura). Figure 11.4 illustrates the different seasonality of floods in these three distinct regions.
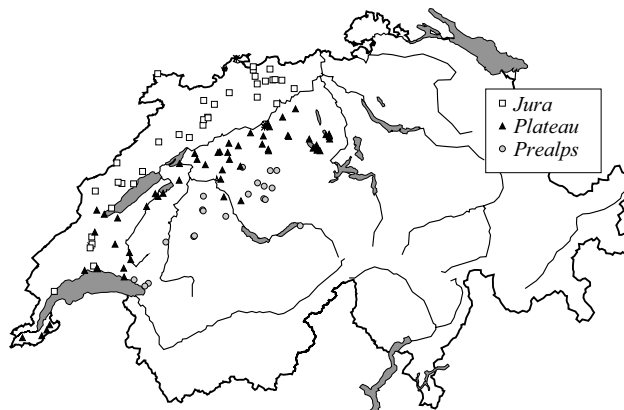

Fig. 11.1: Study zone and locations of the considered gaged drainage basins.

The Prealps include the sub-alpine sediment and molasse zones on the north-western border of the Alps. Given the high density of the hydrographic network, the quasi-impervious surfaces and the high slopes of this region, the drainage basins of the Prealps are characterized by a fast hydrological response and short concentration times. Given the relatively high mean elevation of the drainage basins (more than 800 meters), winter precipitation generally falls as snow, thereby limiting the frequency and intensity of winter floods. Summer floods produced by short-duration high-intensity convective precipitation are preponderant. The specific discharge values of such floods are particularly high, especially for small drainage basins.

The basins of the Plateau are mostly located in zones made up of molasse and alluvial or glacial deposits. The mean elevation of these basins is generally between 400 and 800 meters. They have lower slopes and higher concentration times than those of the Prealps. Annual floods mainly occur in winter as a result of long-duration, low-intensity frontal precipitation events. The specific discharge values of such floods are therefore lower than those in the Prealps and little affected by the size of the basin.

The sub-surface of the Jura basins is composed of karst and limestone, explaining the very high diversity and heterogeneity of their hydrological response. The hydrographic network generally has a low density, which increases the concentration times in spite of the high relief of the region (particularly in the south). Floods occur most frequently in winter. In the southern part of the region, i.e., the "Folded Jura" (Atlas de la Suisse, 1965–1978), the mean elevation of the drainage basins varies between 700 and 1500 meters. Winter precipitation can therefore fall in the form of snow. The annual floods are characterized by specific discharge values that are relatively low compared to the other two regions and relatively independent of the size of the basin.

11.2 DETERMINATION OF HOMOGENEOUS REGIONS

11.2.1 Homogeneity Criteria

A region is considered to be homogeneous from a hydrological viewpoint if it includes sites (e.g., drainage basins) with physiographic and climatic characteristics that produced a similar hydrological behavior (Gingras and Adamowski, 1993). From a statistical viewpoint, a region is considered to be homogeneous if it is made up of sites for which observations come from the same parent population (Hosking and Wallis, 1997). These two interpretations of homogeneity are complementary and form the basis for the homogeneity tests presented in Section 11.2.7.

The problem of identifying homogeneous regions has been a concern for a large number of hydrologists, explaining the abundant literature on this topic. A number of methods have been proposed to delineate homogeneous regions however there is no general consensus as to which method should be adopted in practice. Note however that the performance and even the pertinence of a regionalization method such as the index flood method (Section 11.3.4) depends largely on the homogeneity or non-homogeneity of the regions defined in the first step of the procedure. The main methods used in hydrology to define homogeneous regions will be presented below. These include methods based on geographic, physiographic and/or climatic or hydrological criteria as well as methods based on the notion of "neighborhoods".

11.2.2 Delineation based on Geographic Criteria

Geographic delineation is the simplest and most widely used approach to determine homogeneous regions. Examples include the delineation methods proposed by NERC (1975) for the UK, Matalas *et al.* (1975) for the USA, Gingras and Adamovski (1993) for part of Canada and Weingartner and Manser (1997) for Switzerland. The boundaries obtained are often related to marked geographic discontinuities (e.g., mountain ranges), but sometimes reflect simple administrative considerations (NERC, 1975). Regions obtained by geographic delineation are necessarily continuous in space (Figure 11.2a). The only criterion considered when assigning a given site to a given region is whether or not it belongs geographically to the region.

Geographic delineation, often used for the sake of convenience, is suitable if the factors that determine the hydrological response of the drainage basins (geology, relief, mean annual precipitation, type of soil) are spatially consistent. Certain characteristics of drainage basins can however be unrelated to geographic position. The size of the drainage basin is the most obvious example. If a characteristic that is clearly independent of geographic position is an important regional differentiation factor, this type of delineation is no longer suitable. Geographic proximity does not always ensure hydrological similarity and a number of authors have criticized this approach for this reason (Burn, 1990a; Cavadias, 1990).

Geographic delineation is sometimes reasoned and based on different considerations of a more hydrological nature. For instance, Weingartner and Manser (1997) identified geographic regions for the estimation of flood discharges on the basis of area and the residuals between observed 100-year discharges and those estimated by an initial global regression model (i.e., including all drainage basins and all regions). The shape of the empirical distribution of flood discharges (unimodal, bimodal and highly skewed), the nature of the mechanisms generating the floods or even certain climate characteristics can also be used to group the drainage basins and delineate homogeneous geographic units (Gingras and Adamovski, 1993). This type of geographic delineation is sometimes referred to a "subjective".
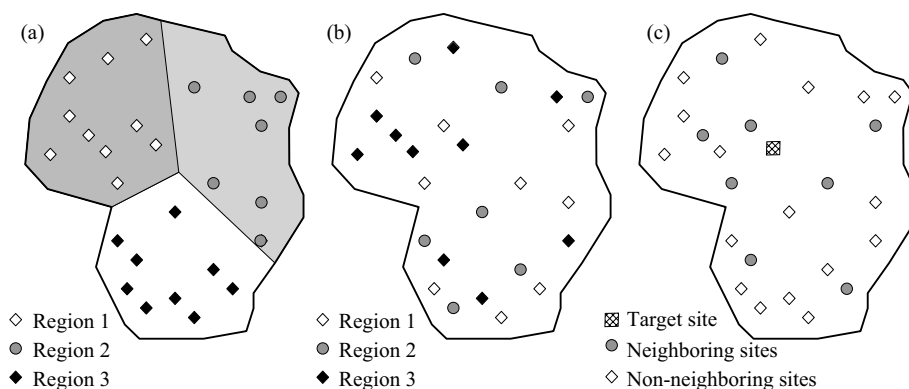

Fig. 11.2: Homogeneous regions based on: a) geographic criteria, b) physiographic/climatic or hydrological criteria and c) "neighborhood" type criteria.

11.2.3 Delineation based on Physiographic and/or Climatic Criteria

As opposed to regions delineated by a geographic approach, regions defined on the basis of physiographic and/or climatic criteria are not in principle spatially continuous (Figure 11.2b). The main physiographic and climatic characteristics used are indicated in Table 11.1. The most widely used are basin area, annual precipitation, land use and elevation (Bobée *et al.*, 1996a). Figure 11.3a illustrates the principle of this type of delineation.

Table 11.1: Explanatory characteristics most often used to delineate homogeneous hydrological regions.

Physiographic characteristics
Drainage basin area
Drainage network: length, density and mean slope
Drainage basin elevation: mean, variability and maximum elevation difference
Drainage basin slope: mean and variability
Topographic indices: mean and variability
Water cover indices (lakes and reservoirs)
Land use: type and area
Population density, percentage of impervious area, urbanization, road density
Percentage of area connected to storm sewer network
Pedological and geological characteristics
Main soil types: nature and percentage of area
Main geological formations: nature and percentage of area
Percentage of area of the basin covered by pervious substrates
Climatic characteristics
Mean annual and seasonal precipitation
Maximum mean precipitation
Precipitation seasonality and regularity
Mean annual evapotranspiration
Hydrological characteristics
Discharges: mean discharge, seasonality and variability, average yield
Flood discharges: mean, variability and frequency of discharges (> threshold)
Low-flow discharges: Base-flow index (BFI), duration and frequency (<threshold)

Once the physiographic and/or climatic criteria have been defined, various algorithms can be used to delineate the regions. Most of them are multivariate analysis techniques such as factor analysis, principal component analysis, correspondence analysis, cluster analysis or discriminant analysis. The reader can for example refer to Krzanowski (2000) for a description of these techniques and Obled (1979) or Nathan and McMahon (1990) for applications in hydrology.

Homogeneous regions are sometimes delineated sequentially. The principle consists in successively dividing in two the space of all the drainage basins of the study zone for example on the basis of threshold values of physiographic/climatic characteristics judged to be the most pertinent for regional differentiation. The principle of the sequential method proposed by Wiltshire (1986a) is presented in Addendum 11.1.
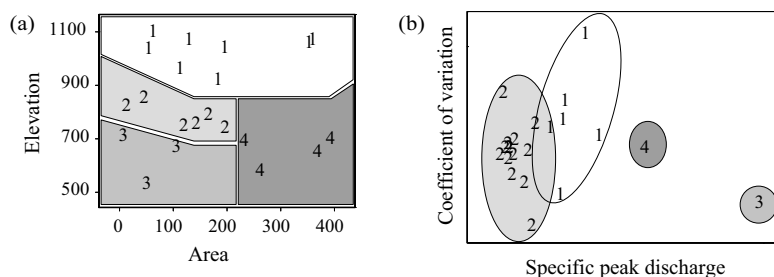
Fig. 11.3: Two hypothetical examples of delineating homogeneous regions. Left: Delineation based on physiographic criteria. Right: Delineation based on hydrological criteria. The drainage basins represented in these two diagrams are indicated by a number corresponding to the region to which they belong.

Addendum 11.1 Wiltshire sequential delineation method

The delineation method proposed by Wiltshire (1986a) consists in dividing the space including all the drainage basins into two sub-spaces depending on whether or not a physiographic or climatic characteristic considered to be the most important for regional differentiation exceeds a certain threshold value. The threshold value is chosen to maximize a criterion *F* that is the ratio between the variances of the inter-group and intra-group coefficients of variation. To obtain estimates of these two variances, Wiltshire (1986) used the jackknife numerical method (Parr, 1983).

The procedure used to subdivide (or group) the basins is then repeated with other physiographic and/or climatic characteristics and other threshold values. This approach is therefore a sequential method to delineate regions (or group together basins) by successively dividing the initial space into sub-spaces that continually decrease in size. Wiltshire (1986a) compared this method for delineating homogeneous regions with the geographic method proposed by NERC (1975) for the UK. On the basis of the homogeneity test presented in Addendum 11.3, he concluded that his method offered much higher performance for the identification of groups of homogeneous basins. A similar approach was used by Pearson (1991) for a regionalization study carried out in New Zealand. Hosking and Wallis (1997) referred to this method as objective partitioning as opposed to the so-called subjective partitioning method of Gingras and Adamovski (1993) discussed in Section 11.2.2.

11.2.4 Delineation based on Hydrological Criteria

Certain studies propose methods for the delineation of homogeneous regions on the basis of hydrological criteria (Düster, 1994; Bobée *et al.*, 1996a). The most widely used criteria are indicated in Table 11.1.

For the prediction of flood discharges, the empirical mean value of the annual peak specific discharges and the coefficient of variation of these discharges figure among the most widely used hydrological criteria (Figure 11.3b). Criteria related to flood seasonality are also used—for example the season of the year in which annual floods most frequently occur (Burn, 1997; Piock-Elena *et al.,* 2000)—as well as the inter-basin concomitance of maximum annual discharges (Burn, 1988).

The use of hydrological criteria to delineate homogeneous regions is however not highly recommended. The main criticism generally formulated is related to the fact that, as opposed to physiographic and climatic characteristics, hydrological characteristics include an estimation uncertainty that can lead to erroneous groupings. If, for example,

the delineation is based on the coefficients of variation of peak discharges, there is a tendency to group together basins for which exceptional floods have been recorded. The delineation method consequently lacks robustness in the presence of extreme values or outliers. Hydrological characteristics related to the seasonality of floods should be preferred because in principle they are less sensitive to sampling problems (Hosking and Wallis, 1997). Flood seasonality diagrams are a useful technique in this regard (Addendum 11.2). This is illustrated in Example 11.2.

Addendum 11.2 Flood seasonality diagram

In a flood seasonality diagram, each basin is represented by a point with the following coordinates:

$$x_i = \sum_{j=1}^{12} p_{ij} \cdot \sin\left(\pi/6 \cdot j\right) \tag{11.1}$$

$$y_i = \sum_{j=1}^{12} p_{ij} \cos\left(\pi/6 \cdot j\right) \tag{11.2}$$

where p_{ij} is the frequency of annual floods associated with basin i and month j. Therefore if all annual floods occur in the same month M, then $p_{ij} = 1$ if $j = M$. Similarly, $p_{ij} = 0$ if $j \neq M$. The angles in equations 11.1 and 11.2 are expressed in radians.

All the points are located within a circle of radius 1. The basins with points farthest from the origin are those for which the flood regime is highly dominated by a particular season or even a particular month. A point near the origin characterizes a mixed regime (e.g., made up of winter and summer floods) or a flood regime with no seasonal influence.

Example 11.2

Seasonality of floods for different drainage basins in Switzerland

Figure 11.4 illustrates the proximity, in terms of flood seasonality, of the drainage basins belonging to different hydrological regions considered to be homogeneous regarding flood discharges. The homogeneous regions were delineated on the basis of physiographic (elevation, geology) and geographic criteria (see examples below).
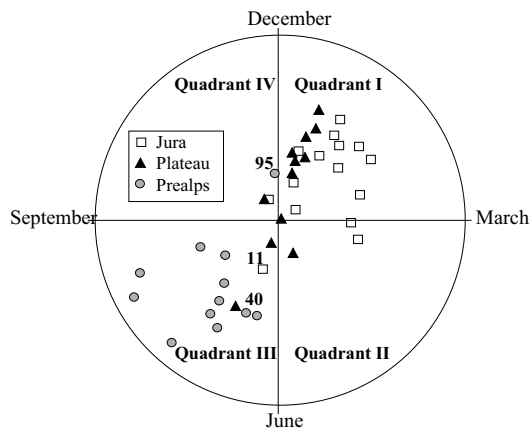

Fig. 11.4: Flood seasonality diagram for different gaged drainage basins in western Switzerland.

The basins represented are located north of the Alps in western Switzerland, in the Prealps, Plateau and Jura regions. This area has been subject to no major anthropogenic influences (urbanization, hydraulic projects, etc.).

Winter floods are preponderant in the basins of the Jura and Plateau regions (Quadrant I in Figure 11.4) while summer floods are preponderant in the Prealps region (Quadrant III in Figure 11.4). Certain basins, a priori in the Plateau region based on physiographic and geographic criteria, such as those of the Gürbe river at Belp (no. 40) and the Sionge river at Vuippens (no. 95), exhibit a flood regime that is different from that of the basins of the Plateau region. These are transition basins with a relatively high mean elevation, making it difficult to assign them to a single region (i.e., in this case, to the Plateau or Prealps region). In the Jura region, certain basins differ in terms of aspects other than their flood regime. Figure 11.4 shows for example the particular behavior of the Bied-du-Locle river basin (no. 11). In this case, it is not a question of a transition basin. This difference could possibly be explained by the heterogeneity of the region in relation to karst phenomena.

Another problem encountered when delineating homogeneous regions on the basis of hydrological criteria is the fact that hydrological characteristics are not generally known for ungaged basins. It is therefore difficult to assign an ungaged basin to a specific group and an additional estimation method is required before this can be done. For instance, a discriminant analysis based on physiographic and climatic criteria can be applied to make it possible to assign ungaged basins to identified groups (Wiltshire, 1986; Düster, 1994).[2]

11.2.5 Neighborhood-based Methods

To avoid the notion of a fixed limit between supposedly homogeneous regions, certain authors propose methods based on neighborhoods. With such a method, each site possesses its own homogeneous region made up of the drainage basins that are the closest in terms of certain geographic, physiographic, climatic and/or hydrological criteria (Figure 11.2c). From this viewpoint, the two most widely used approaches are canonical correlation analysis and the region-of-influence method.

Canonical analysis (Muirhead, 1982; Krzanowski, 2000) is a multivariate analysis technique that can be used to describe the dependence between two sets of random variables $X = \{X_1, X_2, \ldots X_p\}$ and $Y = \{Y_1, Y_2, \ldots Y_q\}$ with $p \geq q$. For example, X can contain various physiographic and climatic variables of the basin and Y can represent various peak discharge quantiles for the basin. On the basis of canonical variables associated with the variables X and Y, canonical analysis determines hydrological neighborhoods between the different sites considered in the region. This method has been used in many cases to predict flood discharges (Cavadias, 1990; Ouarda *et al.*, 2001). The corresponding studies often focused on two hydrological variables (set Y) representing respectively the median annual flood (e.g., specific discharge with a return period of 2 years) and the dispersion of flood values (e.g., ratio between 100-year and 2-year flood discharges). The advantage of using

---

[2]The principle of discriminant analysis is to find a combination (generally linear) of physiographic and climatic characteristics that minimizes the ratio of the mean variance of the means of the inter-group hydrological characteristics and the intra-group values.

only two hydrological variables is that this leads to only two pairs of canonical variables, making it easier to interpret the results (e.g., visually on bivariate graphs). This method can be used for both gaged and ungaged basins.

In the region-of-influence method, each site is considered to be the center of a region made up of similar sites. As for the clustering method, similarity is generally defined as the reciprocal of the Euclidean distance in the *p*-dimensional space formed by *p* characteristics chosen for the drainage basins (possibly weighted and/or standardized). All sites for which the "distance" to the target site is less than a given distance threshold are included in the region-of-influence of the target site (a region-of-influence is therefore not necessarily continuous). When estimating the hydrological variable at a given target site, the contribution of this estimation of each site of the region-of-influence is weighted according to its distance from the target site (Parajka *et al.*, 2005). For ungaged sites, only physiographic and climatic characteristics should be considered.

11.2.6 Choosing a Delineation Method

Supposedly homogeneous regions obtained by applying any of the methods presented in this section obviously depend on the method used and, for a given method, on the selected similarity criteria. Moreover, the performance of a regional estimation method increases with the degree of real homogeneity of the regions. Depending on the chosen delineation method, the real homogeneity of the regions referred to as homogeneous for the needs of regionalization can in fact be relatively low.

The choice of a delineation method and the choice of variables to be considered for delineation must always be based on available data, the experience of the hydrologist and a good physical understanding of the dominant processes related to the studied hydrological variable. A preliminary hydrological analysis of instrumented sites is therefore always necessary. Delineation should in general never be based on geographic, climatic and/or physiographic criteria alone.

For sites without measurements, homogeneous regions cannot be delineated on the basis of hydrological criteria alone. For this reason, delineation in such cases often combines, explicitly or implicitly, several of the methods presented above (Burn, 1989; Piock-Elena *et al.*, 2000). A hierarchical delineation based on successive application of different methods is also often used. In this case, an initial "subjective" geographic delineation based on different hydrological considerations is often carried out.

The choice of a method for delineating homogeneous regions is in principle based on metrics that can be used to assess performance, such as homogeneity statistics measuring the degree of homogeneity of regions with respect to the hydrological variable of interest (Section 11.2.1). Moreover, the performance of the complete regional hydrological model (homogeneous regions + estimation method) is highly dependent on the real homogeneity of the identified regions. The performance of the method used to delineate homogeneous regions can therefore also be estimated indirectly, for each of the different regions, by the performance of this regional model. To optimize the performance of the regional model, the implementation of a method for delineating homogeneous regions is therefore often an iterative process.

For the prediction of flood discharges, Bobée *et al.* (1996b) compared different methods used to identify homogeneous regions in two provinces of Canada. For these regions, they

showed that neighborhood-type methods (canonical correlation and region-of-influence) offered better performance than methods based on fixed delineation of regions. This was valid whatever the method subsequently used to estimate the hydrological variable in the region (e.g., index flood or direct regression). In this case, comparison showed that canonical correlation offered the best performance.

Example 11.3 illustrates the determination of homogeneous regions in western Switzerland on the basis of hydrological, physiographic and climatological criteria.

Example 11.3

Regionalization of flood discharges in western Switzerland: delineating homogeneous regions

The delineation of homogeneous regions is based on a preliminary analysis of annual floods observed on the considered drainage basins (Example 11.2). These floods can be partially explained by the geographic location of the basin however it is difficult to identify objective criteria based solely on geography. For this analysis, floods were better related by the mean elevation and sub-surface geology of the basin. Note that in this region, the mean elevation of the basin (*ELEV*) integrates to some degree the physiographic (slope) and climatic (precipitation and temperature) characteristics of the basin. This elevation was calculated using the DEM25 digital elevation model of the Swiss Federal Office of Topography. The variable used to characterize the sub-surface geology (*PROPJU*) is the proportion of the area of the considered basin included in the "Folded Jura" or "Tabular Jura" regions calculated using the Swiss Atlas (Atlas de la Suisse, 1965–1978).

The approach used to delineate homogeneous regions is therefore based on these two variables (*ELEV, PROPJU*). The criteria used to assign a drainage basin to one of the three regions are given in Table 11.2. This approach is similar to the method used by Wiltshire (1986a), described in Addendum 11.1. The 850 meter elevation threshold corresponds roughly to the limit above which summer floods are observed to occur more frequently than winter floods. The selected threshold value of 25% for the *PROPJU* variable is somewhat arbitrary but reflects the concern to avoid incorporating too many basins in the Plateau region, which could negatively affect the homogeneity. Other threshold values could be used that might lead to a different assignment of certain drainage basins located in the study area, in particular basins with "mixed" or "transition" flood regimes.

Table 11.2: Rules for assigning basins to one of the three regions (Jura, Plateau or Prealps). The criteria are based on the mean elevation of the drainage basin and the proportion of the area included in the "Folded Jura" or "Tabular Jura" regions calculated using the Swiss Atlas (Atlas de la Suisse, 1965–1978).

Region	Assignment criteria
Jura	*PROPJU* > 0.25
Plateau	0 < *PROPJU* < 0.25 OR (*ELEV* < 850 m AND *PROPJU* = 0)
Prealps	*PROPJU* = 0 AND *ELEV* > 850 m

11.2.7 Homogeneity Tests

The homogeneous regions obtained by applying any of the methods presented above are subject to a number of relatively important assumptions. In certain cases, the validity of these assumptions can be checked by statistical tests that will be presented briefly in Addendum 11.3 below.

Note that from a statistical viewpoint, a region is declared to be homogeneous when the observations at the sites making up the region are drawn from the same parent population.

Homogeneity can be situated at several levels. For the prediction of flood discharges, the homogeneity of the region can for example be analyzed solely on the basis of the coefficient of skewness of annual peak discharges (Rossi *et al.*, 1984). Inside the region characterized by a given coefficient of skewness, it is then possible to imagine sub-regions with a given coefficient of variation.

In general, tests proposed in the literature were developed for the index flood method described in Section 11.3.5 below. In this case, homogeneity can be checked using the "standardized" distribution of the maximum annual discharges, i.e., divided by a scaling parameter, generally the mean annual peak discharge. In other words, if the sites of the homogeneous region all have an infinitely long series of observations, they will all have, for the considered variable, the same coefficient of variation, skewness, kurtosis, etc. Similarly, their standardized discharge quantiles will all have the same value for a fixed return period. In practice, the authors proposing tests in the literature (Addendum 11.3) define a test statistic based on one or more variables of the flood distribution (standardized quantile with a fixed return period, coefficient of variation, etc.) and estimate the variance of the statistic (by an asymptotic or numerical method) under the hypothesis H_0 that the region is homogeneous.

Addendum 11.3 A few homogeneity tests used in hydrology

For the regionalization of flood discharges, Fill and Stedinger (1995) tested the homogeneity of a region on the basis of the 10-year quantile of the standard maximum annual discharges. Wiltshire (1986a,b) proposed an *S*-test based on the coefficient of variation (Wiltshire, 1986a) and an *R*-test based on the shape of the standardized distribution (Wiltshire, 1986b).

The tests proposed by Chowdhurry *et al.* (1991) and Hosking and Wallis (1997) are based on L-moment ratios (coefficients of L-variation and L-skewness). The advantage of L-moment ratios over the ratios of conventional statistical moments is that they are less biased and less sensitive to sampling variability (Hosking and Wallis, 1997). Calculation of the statistic under the H_0 hypothesis implies choosing a distribution for the maximum annual discharges. Fill and Stedinger (1995) propose a Gumbel distribution, Lu and Stedinger (1992a,b) and Chowdhurry *et al.* (1991) prefer a GEV distribution, while Hosking and Wallis (1997) recommend a 4-parameter Kappa distribution.

No overall comparison of statistical tests exists, however some tests have been compared. Fill and Stedinger (1995) demonstrated that, in most situations, tests based on L-moment ratios offer the best performance. Hosking and Wallis (1997) recommend the use of their own test, less restrictive regarding the assumed theoretical distribution of maximum annual discharges. Note that it can be shown that most 2-parameter and 3-parameter distributions are special cases of the Kappa distribution. This homogeneity test is described in Appendix 11.6.1.

Readers wishing to obtain more information on the different homogeneity tests used in hydrology can refer to Meylan *et al.* (2012).

Example 11.4

Regionalization of flood discharges in western Switzerland: testing the homogeneity of the regions

In a homogeneous region, all the basins will theoretically have the same coefficient of L-variation (t) and L-skewness (t_3). Within each of the three regions (Jura, Prealps and Plateau) already identified (Example 11.3), the L-moment ratios t and t_3 calculated for each of the basins are highly dispersed. The point swarms made up of the different basins of each of the three regions largely overlap (Figure 11.5). The dispersion of the points could have been related to a sampling problem alone, however this is not the case here.
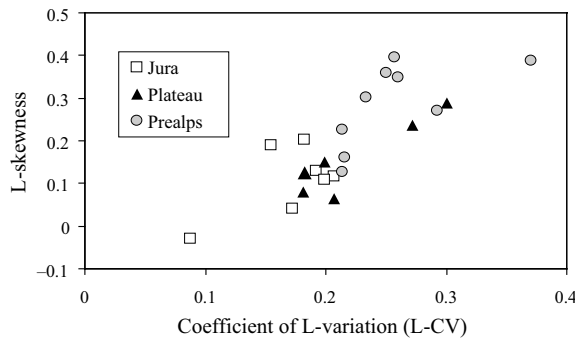

Fig. 11.5: L-moment ratio diagram of L-skewness (t_3) versus the coefficient of L-variation (t) for basins with annual flood series extending over 25 years or more.

The homogeneity of the three regions has been tested using the H statistic proposed by Hosking and Wallis (Hosking and Wallis, 1997) (for $N_{SIM} = 1000$) (Appendix 11.6.1). The results show that the three regions must be regarded as "definitely heterogeneous" (Table 11.3).

Table 11.3: Regional homogeneity test. N is the number of drainage basins in the region. If $H < 1$, the region can be regarded as "acceptably homogeneous", if $1 \leq H < 2$, it can be regarded as "possibly heterogeneous" and if $H > 2$, it can be regarded as "definitely heterogeneous".

Region	N	H	Diagnosis
Plateau	57	3.53	Definitely heterogeneous
Prealps	19	2.04	Definitely heterogeneous
Jura	37	8.00	Definitely heterogeneous

This result is not really surprising given that certain basins of the considered samples are very small. Consequently, their behavior during floods is very sensitive to local heterogeneities of the medium and can therefore be very different from the mean behavior of the basins of the region. The same test was therefore repeated after removing drainage basins with areas less than 10 km² from the sample (Table 11.4). The threshold of 10 km² corresponds to the arbitrary value used traditionally in Switzerland (Düster, 1994; BWG, 2003) to define small drainage basins.

Without the basins measuring less than 10 km², the Plateau and Prealps regions can be regarded as "acceptably homogeneous". The Jura region is however still diagnosed as "definitely heterogeneous". This heterogeneity can be attributed to the karst phenomena that strongly influence the hydrological behavior of the basins in this region.

Table 11.4: Regional homogeneity test without the small drainage basins (see the legend of Table 11.3 for a detailed explanation)

Region	N	H	Diagnosis
Plateau	42	0.85	Acceptably homogeneous
Prealps	14	0.50	Acceptably homogeneous
Jura	34	4.48	Definitely heterogeneous
All regions together	90	4.36	Definitely heterogeneous
Plateau+Prealps	56	1.87	Possibly heterogeneous

Note that the region containing all three regions (Jura, Plateau and Prealps) is diagnosed as "definitely heterogeneous". It is therefore worthwhile to analyze flood discharges separately for each of the regions. Note also that excluding the small drainage basins leads to a very small number of basins (N=14) for the Prealps region, which could adversely affect the robustness of the regional estimation method to be constructed for this region. It is however of no interest to construct a common estimation method for the Plateau and Prealps regions given that these two regions considered together are only "possibly heterogeneous" according to the *H* statistic.

For basins with areas greater than 10 km², a regional estimation method based on the L-moment ratios measuring regional L-variation and L-skewness can therefore be constructed separately for each of these two regions (Plateau and Prealps). For smaller basins, an estimation method capable of taking into account specific local features of the basins should be envisaged. It would otherwise appear to be difficult to develop a meaningful estimation method for the Jura region. If, in spite of this, an estimation method must be constructed for this region, it should be expected to offer only limited robustness and low performance.

11.3 ESTIMATION METHODS

Various methods can be used to estimate a hydrological variable. This section will present empirical, analog, geostatistical and regression methods as well as methods that make use of a regional frequency model.

11.3.1 Empirical Methods

As opposed to the statistical methods described below, empirical methods generally have an imposed structure resulting from acquired experience and a certain conceptualization of the hydrological behavior of the drainage basin. If the degree of conceptualization is high, the model is referred to as pseudo-empirical. This is the case for the rational method, the most widely used empirical model for the estimation of flood discharges (Chapter 9) and for many approaches derived from this method (Example 11.5).

The advantage of empirical methods is that fewer observations are required for their parameterization than for statistical models. In addition, they generally take better account of local particularities of the considered hydrological behavior. On the other hand, empirical methods are based on simplifying assumptions that are often invalid or valid for only some of the drainage basins. For example, the underlying assumptions of the rational method (constant runoff coefficient in time and space as well as uniform and constant precipitation over the entire drainage basin) restrict its use to small drainage basins. The maximum area recommended for application of the rational method varies from a few hundred hectares to a few tens of square kilometers, depending on the source (ASCE, 1996; ARR, 1998; BWG, 2003).

Example 11.5

Regionalization of flood discharges in western Switzerland: estimating a hydrological variable

The regional method for estimating maximum flood discharges proposed by Niggli *et al.* (2001), referred to as the HYDRAT method, is an adaptation of the rational method for small drainage basins in western Switzerland (areas less than 10 km²). Assuming that the time of concentration of the drainage basin is a power function of the ratio between its area *A* and its mean slope *p* and that the Intensity-Duration-Frequency (IDF) curves of maximum mean precipitation of the site follow a Montana relationship with parameters $\varepsilon_1(T)$ and $\varepsilon_2(T)$, the maximum discharge Q_T [m³/s] for return period *T* can be expressed as follows:

$$Q_T = u \cdot C_r \cdot \beta_R^{\varepsilon_2(T)} \cdot p^{-\alpha \cdot \varepsilon_2(T)} \cdot \varepsilon_1(T) \cdot A^{1+\alpha \cdot \varepsilon_2(T)} \tag{11.3}$$

where *u* is a unit conversion coefficient, C_r the runoff coefficient of the basin and β_R a parameter depending on the basin. Except for β_R, all the variables in this equation can be determined on the basis of physiographic and climatic data available for the region. The parameter β_R was estimated for each drainage basin of the region by minimizing the errors between the quantiles estimated using this equation and those obtained on the basis of a conventional frequency analysis of the observed discharges. The variability of β_R can be explained largely by the assignment of drainage basins to one of the three regions (Jura Plateau or Prealps) of western Switzerland. The regional values used (Prealps: $\beta_R=20$; Plateau: $\beta_R=30$; Jura: $\beta_R=75$) reproduce the peak discharge well, whatever the return period considered.

11.3.2 Analog Methods

Analog methods consist in transposing information obtained from one or more analogous gaged basins to a target drainage basin.

The analogous basin used is sometimes the gaged basin located just upstream or just downstream of the target basin (Chapter 8, Section 8.2.3). In Niggli *et al.* (2003), an analog approach based on instrumented basins located upstream or downstream of the target basin is used to estimate the flood quantile for a given return period. The quantile to be determined is obtained in this case by a weighted average of the "observed" quantiles of analogous basins. The weights assigned to the different gaged basins are estimated on the basis of proximity (i.e., the basins located directly upstream or downstream of the target

basin will therefore have the greatest influence) and the quantity of observed information available (e.g., length of the measurement series).

The information transposed to the target basin can also be the identified relationship between the variable to be estimated and various known explanatory variables or the various parameters of a model (e.g., a rainfall-runoff model). In this case, the complete set of parameters estimated for an analogous basin is assigned to the target basin. This approach presents the clear advantage of proposing a plausible parameter set and implicitly taking into account possible interdependencies between model parameters. This approach has in particular been used by Rojas-Serna (2005) and Parajka *et al.* (2005) who selected the analogous basin as the basin with the minimum similarity index φ defined as:

$$\phi = \sum_{i=1}^{k} \frac{\left| X_{G,i} - X_{U,i} \right|}{\Delta X_i} \tag{11.4}$$

where $X_{G,i}$ and $X_{U,i}$ are respectively the ith physiographic characteristic of the analogous basin (gaged) and target basin (ungaged) and where ΔX_i is a normalization factor. This factor is here the range of characteristic *i*.

11.3.3 Geostatistical Methods

Geostatistical methods such as kriging (Matheron, 1963) are used especially for the interpolation of certain climatic variables such as mean annual/seasonal precipitation and maximum mean precipitation. These methods are seldom used for the regionalization of other hydrological variables except sometimes for the parameters of certain models. Several studies have been carried out, in particular in Switzerland (Jordan and Meylan, 1986b; Meylan, 1986). English-speaking readers can refer to Pilgrim and McDermott (1982) for the runoff coefficient of the rational method, Parajka *et al.* (2005) for the parameters of a rainfall-runoff model and Soutter (2003) for the parameters of the Montana IDF model (Figure 11.6).

11.3.4 Regression Models

The so-called direct regression method consists in constructing a linear relationship between the variable to be explained and different variables capable of explaining a maximum amount of the variance. For instance, for a given homogeneous hydrological region, the variable Y_i to be explained for basin *i* is obtained on the basis of a multiple regression of the following type:

$$Y_i = \alpha_0 + \alpha_1 X_{1i} + ... + \alpha_p X_{pi} + \varepsilon_i \tag{11.5}$$

where $X_{1i},…,X_{pi}$ are physiographic and/or climatic characteristics that explain the variation of Y, $\alpha_0, \alpha_1, ..., \alpha_p$ are the regression parameters that must be estimated and ε_i is the error of the regression model. The parameters are often estimated using the ordinary least-squares method. This analytical method is based on the assumption that the variance of model errors ε_i does not depend on *i* (homoscedasticity condition) (Addendum 11.4).

The regression method can be used to estimate any hydrological variable such as the characteristic low-flow or flood discharge, annual discharge or annual/seasonal precipitation
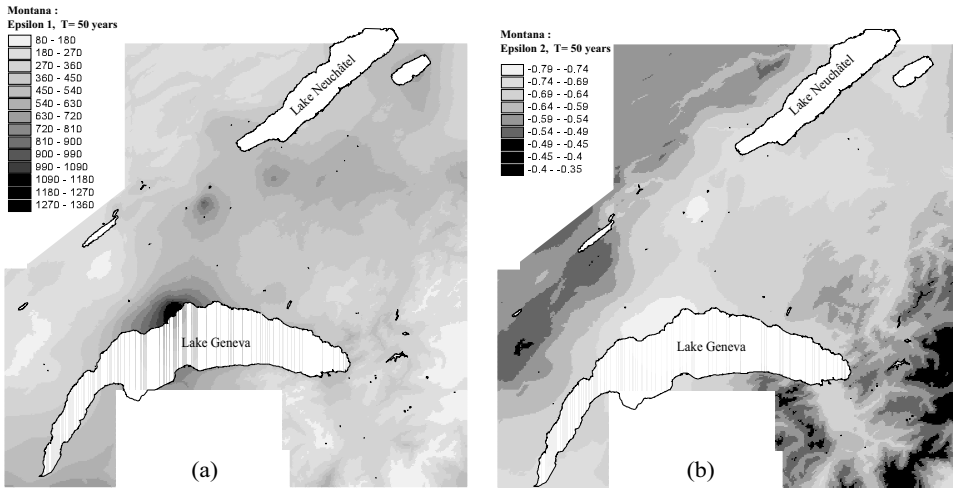
Fig. 11.6: Regionalization in western Switzerland of the parameters ε_1 and ε_2 of the Montana IDF model for maximum mean precipitation with a return period of 50 years. The regionalization is obtained for each variable after multiquadratic radial basis interpolation (according to Carlson and Foley, 1991a,b) of the residuals of a relationship established between the variable and elevation for all rain-gage stations of the region (from Soutter, 2003).

(Haberlandt *et al.*, 2001; Merz and Bloschl, 2005). It can also be used to estimate some or all of the parameters of a hydrological model (Abdulla and Lettenmaier, 1997; Perrin, 2000).

Addendum 11.4 Regionalization using a multiple regression model

A stepwise multiple regression procedure (Draper and Smith, 1981; Venables and Ripley, 1998) can be used to determine the variables for which the coefficients α_k are significantly different than zero. The explanatory characteristics generally used are the same as those potentially used to determine homogeneous regions (Table 11.1). Area and, to a lesser extent, annual rainfall are nearly always included in the model. The other explanatory characteristics included depend on the variable to be explained. For flood discharges, for example, or for the surface runoff parameters in a hydrological model, a descriptor of the morphology of the basin (area, perimeter, length of hydrographic network) and its slope, related to its time of concentration, are always included in the regression analysis.

A logarithmic transformation of the quantile of interest (Y_i) is often recommended before selecting the best regression model. In this way, the prediction provided by the regression model is always positive.

A similar transformation (logarithmic, power, etc.) can also be applied to the explanatory variables. The objective of this transformation (that can be different for each explanatory variable) is to linearize the relationship between the explanatory variable and the explained variables, while benefiting from the simplicity of the ordinary least-squares estimation method. When the physiographic and/or climatic characteristics included in the model are strictly positive (e.g., basin area, elevation, precipitation), the logarithmic transformation is often a natural choice. If the regression model includes basin area is an explanatory variable ($X_{1i} = A_i$), equation 2.1 becomes:

$$Y_i = \exp(\alpha_0) \cdot A_i^{\alpha_1} \cdot X_{2i}^{\alpha_2} \cdot \ldots \cdot X_{pi}^{\alpha_p} \cdot \exp(\varepsilon_i) \qquad (11.6)$$

> For flood discharges, equation 11.6 above, with parameter α_l roughly between 0.6 and 0.9, is widely accepted as a reasonable choice (Pitlick, 1994). It implies that the specific discharge decreases with increasing area (since $\alpha_l < 1$). Note that the model error, in the space of the real discharges (i.e., not in the space of the logarithms) is a multiplicative term.

When the direct regression method is applied to annual flood quantiles, the estimation of the regression model parameters must be repeated independently for each return period. To attenuate a certain number of potentially undesirable consequences of the use of this method (Section 11.3.6), Stedinger and Tasker (1985) propose to estimate the regression parameters using the weighted or generalized least-squares method. The weighted method takes into account the differences in the accuracy of the "observed" values between the sites considered (depending for example on the length of available observation series) and therefore provides more accurate and nearly unbiased parameter estimators. The generalized method takes into account the spatial correlation of the values of the quantiles for the studied region. In the presence of a strong inter-site correlation, the generalized method can provide better results than the weighted method (Madsen and Rjosberg, 1997).

The direct regression method is also often used to regionalize the M parameters θ_m of a given hydrological model. It is generally applied to the parameters obtained by calibration for the different instrumented sites. The performance of a hydrological model regionalized in this way is however sub-optimal, in particular due to the high uncertainties in the estimation of the model parameters and to the associated equifinality problem (Chapter 3). The determination of optimal regression models in fact consists in identifying: 1) the explanatory variables for the M regression models to be determined (corresponding to the M parameters θ_m), 2) the structure of the regression models and 3) the values of the corresponding parameters $\alpha_{m,k}$ that maximize a given discharge simulation performance criterion (e.g., minimization of the root mean square deviation between observed and simulated discharges for the N considered instrumented basins, e.g. (Perrin, 2000; Gotzinger and Bardossy, 2007).

In practice, the parameters θ_m of the hydrological model must first be calibrated independently for each of the N instrument sites. This makes it possible to identify potentially useful explanatory variables for each of the parameters and the corresponding dependence structure (i.e., the structure of the regression models intended for each parameter θ_m). Next, in a second step, the calibration of the hydrological model is reiterated by calibration of the parameters $\alpha_{m,k}$, this time carried out in a global and simultaneous manner on the N instrumented sites.

Example 11.6

Regionalization of flood discharges in western Switzerland: regionalizing the $Q_{2.33}$ index flood

Taking into account the results of the above homogeneity tests (Example 11.5), the $Q_{2.33}$ index flood is regionalized for all the drainage basins with areas greater than 10 km². Given the sparse data available for the Prealps region, the basins of this region were first combined with those of the Plateau region for this estimation. The regionalization approach used is based on multiple regression between the logarithm of the index flood and certain appropriate physiographic and meteorological characteristics of the basins (also transformed by the logarithmic function for those with values that are all strictly positive).

To implement the regression model, the $Q_{2.33}$ index flood was first estimated on the basis of available hydrometric data for the gaged basins of the study zone. Only basins with at least 5 years of measurements were used so as to ensure a certain estimation stability. The candidates for explanatory variables were extracted on the basis of available physiographic and climatic information.

The method used to determine the "best" regression model follows a forward stepwise type procedure (Draper and Smith, 1981). An initial model, relating the mean annual discharge to the area via a power function, is progressively refined by successively introducing 1 then 2 and then on through to n additional explanatory variables. When introducing the nth variable, it is important to check that: 1) it has a significant influence on the value of the explained variable (a 5% significance level was chosen) and 2) the obtained estimation of the linear regression coefficient associated with the variable has a physically plausible value (for example a positive and not a negative value for the basin slope variable). If none of the models with n explanatory variables satisfy these two conditions, the process is interrupted and the previous model with n-1 variables is selected. If not, the selected model is the one that maximizes the multiple correlation coefficient. The explanatory variables used must of course not be strongly inter-correlated.

The model obtained using this procedure includes 5 explanatory variables. It can be expressed as follows:

$$Q_{2.33} = 0.0053 \cdot A^{0.78} \cdot ALT^{0.68} \exp(0.58\,DRAIN - 0.025\,FOR + 0.023\,IMP) \tag{11.7}$$

The values of the regression parameters associated with the explanatory variables appear to be logical, i.e., an increase in the area, the drainage density, elevation and imperviousness (respectively the variables A, $DRAIN$, ALT and IMP) leads to an increase in $Q_{2.33}$, while an increase in the proportion of forested area (variable FOR) leads to a decrease in $Q_{2.33}$. Note that the value of the exponent associated with the area (0.78) is consistent with the results of many other similar studies. It reflects the fact that the mean annual specific flood discharge ($q_{2.33} = Q_{2.33}/A$) decreases with increasing area.

11.3.5 Regional Frequency Models

It is often necessary to estimate, for the considered hydrological variable, the quantile corresponding to a given frequency of exceedance or non-exceedance (return period for maximum flood discharges, minimum low-flow discharges or maximum mean precipitation and number of days exceeded per year for flow-duration curves). When the site of interest is instrumented and the number of observations sufficient, this quantile can be obtained by an appropriate frequency analysis (see Meylan *et al.* (2012) for methodologies and applications).

When the site is not instrumented, the required quantile can be estimated on the basis of a regional frequency model previously determined from data available on instrumented sites of the region and a scaling factor. The quantile to be determined then has the following expression:

$$Y_{iT} = \mu_i \cdot Y_{RT} \tag{11.8}$$

where Y_{RT} is the value of the regional frequency model for the required frequency of exceedance or non-exceedance (i.e., for the return period T or the number of days per year

N for which the value is exceeded). Y_{RT} is referred to as the growth factor corresponding to the selected frequency and is generally independent of the site. The scaling factor μ_i for the considered site is independent of the frequency.

Another frequent expression for a regional frequency model is $Y_{iT} = \mu_i + \sigma_Y \cdot K_T$ where μ_i is the scaling factor and σ_Y and K_T are respectively the standard deviation and growth factor of the standardized distribution. For the GEV distribution, for example, K_T is expressed as: $K_T = -\sqrt{6}/\pi \cdot \{0.577 + \ln[\ln(T/(1-T))]\}$.

This approach is based on the assumption that, within a homogeneous region, the hydrological variable has the same "standardized" statistical distribution for all sites of the region (Figure 11.7). "Standardization" here refers to division by a scaling factor that represents the inter-site variation of the real distribution of the variable. The "standardized" distribution is called the regional growth curve. The statistical distributions of different sites always show certain differences with respect to the regional distribution (Figure 11.7). An error model is therefore necessary to represent the associated uncertainty.

All the distributions commonly used for frequency analysis can be used to model the regional growth curve (GEV, Log-normal, Log-Pearson type III, etc.—see Meylan *et al.*, 2012). A single regional value is generally used for the shape parameters of the standardized frequency model (dispersion, skewness, kurtosis). If the inter-site variability of the dispersion parameter is high and if it can be explained, then it can be estimated using
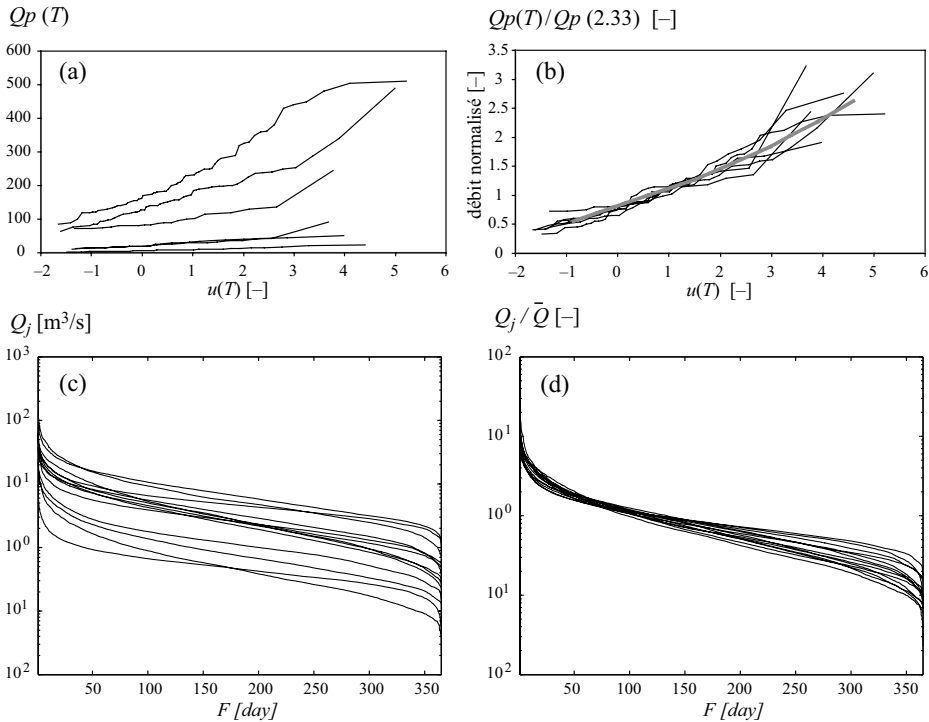

Fig. 11.7: Illustration of the statistical distribution "standardization" principle. Left: Non-standardized distributions. Right: Standardized distributions (the flood discharges have been divided by their mean and the daily discharges by the mean interannual discharge). Top: Annual flood discharges (*u* is the reduced Gumbel variable). Bottom: Flow-duration curves (*F* is the non-exceedance frequency).

a regional model. If a sufficient number of observations are available for the target basin, this parameter is sometimes also estimated on the basis of observations.

With this method, estimation of the required quantile for a given basin necessitates knowledge of the scaling factor μ_i for the basin. If a series of hydrometric measurements is available for drainage basin i, the scaling factor μ_i is customarily estimated on the basis of observations. If the basin is ungaged, μ_i is estimated using an appropriate regional model, e.g., a direct regression model using the physiographic or climatic characteristics of the basin as explanatory variables (Example 11.6).

Regional frequency models are for example used to regionalize flow-duration curves. The growth curve is often modeled using the Log-normal distribution (Fennessey and Vogel, 1990; Niadas, 2005). In this case, a single parameter is required to define it, i.e., the coefficient of variation of the data, often taken to be equal to its regional value. The scaling factor μ_i is generally the median annual discharge or mean annual discharge (Niadas *et al.*, 2005).

A regional frequency model is also often developed for the regionalization of IDF curves (Durrans and Kirby, 2004) or QDF curves (Javelle *et al.*, 2002).

The so-called index flood method is another widely-used application of regional frequency analysis. It is specific to the estimation of peak discharges for different return periods (Dalrymple, 1960). The term "index" refers in this case to the scaling factor μ_i mentioned above. The index flood is generally the mean of annual peak discharges of the basin.

The choice of a distribution can be guided by an L-moment ratio diagram (Hosking and Wallis, 1997), in particular the diagram of L-kurtosis versus L-skewness (Figure 11.8; see also Addendum 11.5).

The most commonly used distribution for the regional frequency analysis of flood discharges is the GEV distribution (Bobée *et al.*, 1996a; Piock-Elena *et al.*, 2000). When
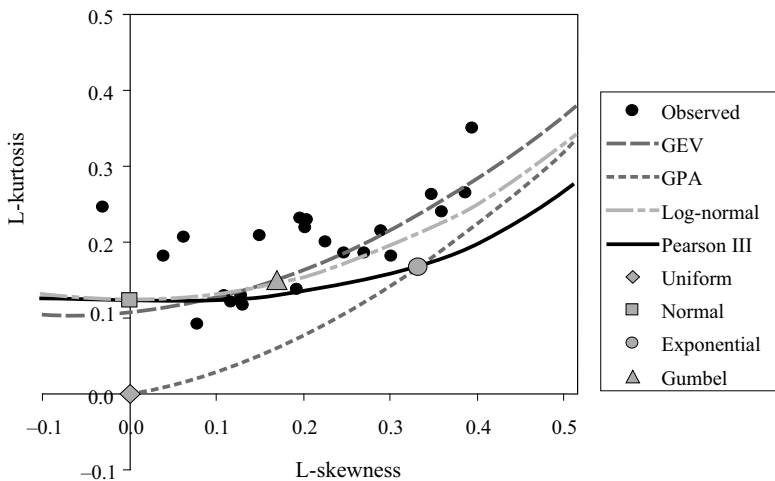

Fig. 11.8: L-moment ratio diagram (L-kurtosis versus L-skewness). The values corresponding to certain theoretical distributions are plotted (2-parameter distributions are represented by points and 3-parameter distributions are represented by curves) along with the values observed for the drainage basins of Example 11.1 that have at least 30 years of measurements.

associated with an estimation of parameters using the weighted moments method (GEV/PWM method) described by Hosking and Wallis (1997), this distribution offers the best compromise between the robustness and flexibility objectives required in regional frequency analysis (Cunnane, 1989; Potter and Lettenmaier, 1990). From a study on different drainage basins of Canada, the GEV/PWM index flood method once again proved to be the method giving the best results in the validation phase (Bobée *et al.*, 1996b). Note that the index flood method can be associated with the estimation procedure for peak-over-threshold series. In this case, the growth curve is the "standardized" distribution of discharges above a fixed threshold. It can be modeled by a generalized Pareto (GPA) distribution that, when "annualized" (Stedinger *et al.*, 1993), becomes a GEV distribution (Meylan *et al.*, 2012).

Addendum 11.5 Using the L-moments diagram to choose a regional frequency model

On a diagram such as the one shown in Figure 11.8, the mean regional values of the L-moments obtained for the considered homogeneous region on the basis of the L-moments estimated from the observations available at each of the *N* sites of the region can be compared to the theoretical L-moments of different distributions. Note that, although the term L-moment is used, it is in fact the L-moment ratios that are compared (Appendix 11.6.1). This comparison can be used to identify unsuitable distributions (Hosking and Wallis, 1997). Moreover, Vogel and Fenessey (1993) show that the use of L-moments improves the selection of the various candidate distributions compared to conventional statistical moments and also provides excellent robustness.

Identification of a regional frequency model is however not always possible. This is particularly the case if the points on the diagram characterizing the different sites are too dispersed around their regional mean value. This can indicate that the different sites do not share the same statistical distribution. It can also reflect problems concerning the representativeness of the considered sample for certain sites. Values obtained for sites for which only very short measurement series are available (for instance less than 10 years) are for example not sufficiently accurate to be positioned.

Furthermore, the theoretical L-moments of certain 3-parameter distributions commonly used in frequency analysis, such as the Log-Pearson III distribution, are unknown (at least from a theoretical viewpoint). Statistical goodness-of-fit tests must be used to supplement the diagram. Hosking and Wallis (1997) considered that the Chi-squared and Kolmogorov Smirnov tests (described in Meylan *et al.*, 2012) were not sufficiently powerful and therefore developed a test that also draws on the benefits of Monte Carlo type simulation techniques. This tested is described in Appendix 11.6.2.

Example 11.7

Regionalization of flood discharges in western Switzerland: constructing the growth curve (see Niggli *et al.*, (2001))

The growth curve was model for both the Prealps and Plateau regions by a generalized extreme value (GEV) distribution (Figure 11.9). The fitting method used is the procedure based on probability weighted moments (PWM) described by Hosking and Wallis (1997).

The growth curves obtained reflect the regional statistical properties of the annual peak discharge series. Note the particularly strong growth of the curve obtained for the Prealps region with increased curvature towards the top (a type II GEV distribution is used as proposed by Meylan *et al.*, 2012). The distribution obtained for the Plateau region shows no significant curvature, neither at the top nor at the bottom. A Gumbel distribution (type
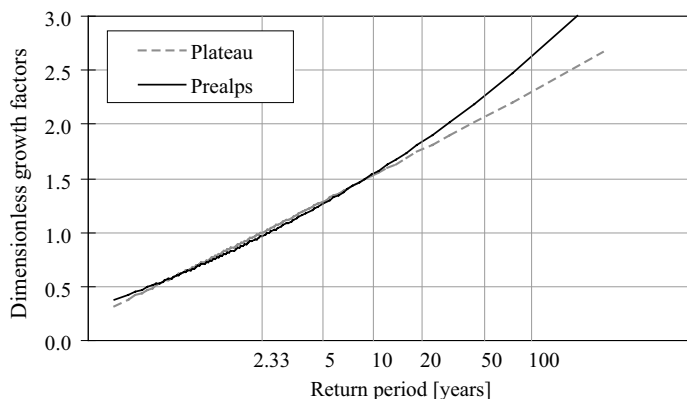
Fig. 11.9: Growth curves of the Plateau and Prealps regions.

I GEV distribution), although less flexible than the GEV distribution, could be suitable in this case. The index flood model for this region of western Switzerland (referred to hereafter as the HYDRIF model) is therefore made up of the regression model of Example 11.6 and the growth curves obtained in this example.

11.3.6 Choosing an Estimation Method

The methods available to estimate the variable of interest are highly varied. Furthermore, several methods are sometimes combined for the estimation. A linear regression model can for example be set up on the basis of the observations of N sites that are analogous to the considered target site (Merz and Bloschl, 2005).

No one method can be considered to be consistently better than the others. The choice of the best method for a given case depends mainly on the hydrological variable of interest and on the data available at the site and in the region. The following remarks can however help identify the method or methods that are the most promising with respect to certain criteria.

Estimation consistency

It is often necessary to ensure a certain consistency between various hydrological variables to be estimated.

Direct regression, the most widely used method—mainly due to easy implementation—is in this case relatively inappropriate. The main reason is that the regression models required for the estimation of the different variables are generally developed separately for each of the variables considering that they are independent. Consequently, certain inconsistencies are possible, for example non-monotony of the relationship between the discharges calculated by regression and the corresponding non-exceedance frequencies for a given basin. The estimated 10-year discharge can sometimes be greater than the estimated 100-year discharge. The same problem can be encountered when estimating different characteristic discharges of a flow-duration curve. The regional methods to be preferred in this context are those that are based on a regional frequency model (e.g., index

flood method, regional flow-duration curves), thereby ensuring hydrological consistency between the different estimated variables.

Similarly, the parameters of a given hydrological model are often highly inter-correlated, leading to the possibility of several parameter sets providing identical model performance. If the method used to calibrate the parameters of the hydrological model is not adapted in a reasoned manner to reduce such equifinality problems, applying the direct regression method to the calibrated parameters can lead to a regionalized hydrological model with mediocre or even poor performance (Tung *et al.*, 1997; Hingray *et al.*, 2006). A global estimation of the regression parameters on the basis of a hydrological performance criterion can partially solve this problem (Section 11.3.4). The analog method is in fact a much better alternative given that the optimal parameter set for the considered analogous basin or basins takes into account correlations between parameters (Rojas-Serna, 2005). This method however only works if it is possible to identify truly analogous gaged basins, which is not always the case. The potential for the success of the analog method increases with the number of gaged basins and their diversity.

Robustness of estimations

Development of a regional model mainly takes into account all observations available in the considered region, including those from sites with only short periods of measurements. The estimation method to be preferred in this case must be able to give more weight to estimations from sites with many measurements and be relatively insensitive to sampling problems. Methods based on a regional frequency model are once again preferred over the direct regression method because they are less sensitive to such problems when they are associated with a robust method to determine the regional growth curves (e.g., GEV/PWM method).

Taking into account heterogeneity within the region

Even if the first step in developing the regional model consists in identifying homogeneous regions, the homogeneity of the behavior of the hydrological variable within the region remains relative. If residual heterogeneity is significant, the estimation method must be able to take this into account. For this, methods based on a regional frequency model, where often only the scaling factor depends on the site,[3] generally offer limited performance (Gupta *et al.*, 1994). Empirical methods (e.g., the rational method), that conceptualize basin behavior to a certain degree, often prove better suited to taking this heterogeneity into account.

Use of information available at the site

When various observations (e.g., discharge) are available at the target site, an estimation method that uses this information is recommended. Geostatistical, analog and multiple regression models are in this case of less interest than empirical methods or methods based on a regional frequency model.

The rational method or derived empirical methods can for instance make use of local information regarding maximum mean precipitation, the time of concentration and the

---

[3]The coefficients of variation and skewness of the considered variable also in principle vary from one site to another.

runoff coefficient estimated for the target basin (estimated for example on the basis of various observed rainfall-runoff events). Moreover, a regional frequency model can make use of even a short series of hydrometric measurements at the studied site (local/regional estimation) since the scaling factor can then be estimated using discharge observations. For 3-parameter frequency models, the dispersion parameter of the model is sometimes also deduced from observations if they are sufficient in number (Anctil *et al.*, 2005).

If no information is available at the site, it may be very useful to set up a measurement program to obtain observations over a short period. Niadas *et al.* (2005) suggest that the median of around 30 estimates of instantaneous discharge made at regular intervals over a given hydrological year provides a sufficient estimate of the median annual discharge (i.e., the discharge required to estimate the scaling factor of a regional flow-duration curve). Similarly, a few instantaneous discharge measurements can be used to update some or all of the regional parameters of a hydrological model, possibly improving model performance significantly. The expected degree of improvement depends on the number of measurements required in the basin, the sampling program and the regional parameters updated. For a study carried out on 1111 gaged drainage basins located in the USA, Mexico, Brazil, France, Ivory Coast and Australia, Rojas-Cerna (2005) recommended measuring instantaneous discharges during flood periods and giving priority to the updating of the rainfall excess parameters. For many basins, performance was significantly improved by taking into account just two instantaneous discharge measurements.

11.3.7 Performance of an Estimation Method

Assessing the performance of a regional model used to estimate a given hydrological variable is the final step of a regionalization project. In particular, it is important to determine the uncertainties related to the use of the regional model. Comparison of estimates obtained with the regional model and observations from the sample of *N* estimated sites not used for the development of the model (validation sites) make it possible to propose an error model (e.g., bias, variance).

When regionalization concerns the parameters of a hydrological model, assessing the performance of the regional model requires: 1) comparison of the regional parameters with those obtained by a standard calibration procedure for the different validation sites (Figure 11.10a) and especially 2) estimation of the performance of the regionalized hydrological model for these same validation sites (Figure 11.10b). The second assessment can for instance involve comparing observed discharges and simulated discharges obtained with the regionalized hydrological model.

11.4 COMBINING AVAILABLE INFORMATION

In a regionalization project, estimation of the hydrological variable at a site with few or no measurements is always subject to uncertainty. This uncertainty can lie in the choice of the region to which the studied site belongs or in the choice of the model used to estimate the considered variable (e.g., empirical, regional frequency or multiple regression model). If a number of years of measurements are available for the site, the estimation can be based
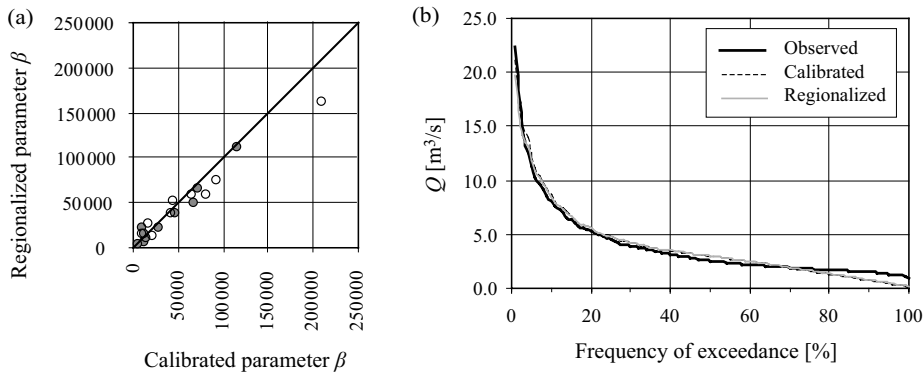
Fig. 11.10: Performance of a regional conceptual hydrological model applied to 19 nested basins of the Alzette river drainage basin in Luxembourg (Hingray *et al.*, 2006). a) Regionalized versus calibrated rainfall-runoff parameter β for the 10 calibration basins (filled circles) and the 9 validation basins (empty circles). b) Flow-duration curves derived from observed discharges and obtained by simulation with the calibrated hydrological model and with the regionalized model for a validation basin (Alzette river at Hesperange).

on a regional method or solely on observed data. Depending on the selected modeling options and estimation methods, different estimates of the variable of interest are therefore possible.

Among the different methods that make use of some or all available information, the Bayesian method is widely used. Rather than using only a single estimate and excluding all others considered a priori to be less likely, this method can combine the different possible estimates of the variable of interest, taking into account the associated uncertainties.

The Bayesian approach consists in using estimates from different models to update a prior distribution of the variable of interest. The prior distribution can be interpreted as the state of knowledge before information from the model is used. It can be uninformative if this knowledge is null. If several estimation models are available, this distribution is updated sequentially by successively using the information provided by the different models. The Bayesian estimate of the variable of interest is therefore a combination of the estimates obtained respectively on the basis of the prior distribution and the various models.

The Bayesian processor associated with this approach calculates not only the expected value of the variable, but also an estimate of its posterior distribution and variance. The posterior variance is always less than the prior variance, the variance reduction factor depending on the performance of each of the individual models (performance taken into account by the likelihood function) and the conditional interdependence on the true value of the variable of interest (in other words, on the correlation between the errors of the estimation models). The absence of conditional independence is automatically penalized by the Bayesian processor. In general, the chance of this problem occurring increases with the number of models considered (because there is not an infinite number of different independent models). If the posterior variance does not decrease significantly when a model is added, the Bayesian updating process can be considered to be exhausted and further updating is of no use.

The Bayesian approach is particularly useful when the models are complementary and fed by different information, e.g., local hydrometric information for frequency analysis, meteorological information for rainfall-runoff models and information on the relationship

between floods and the physiographic characteristics of the drainage basins for regional models. The sharing of regional information (Fill and Stedinger, 1998), historical information (Parent and Bernier, 2003) or, when available, site information is often of interest because it generally results in a more robust estimation of the considered variable (Kuczera, 1982b). In addition, this approach explicitly takes into account any heterogeneity in the considered region (Rasmussen *et al.*, 1994). Many studies have been carried out using this approach. Various examples can be found in Kuczera (1982a,b, 1983), Madsen and Rosbjerg (1997), Fill and Stedinger (1998), Kuczera (1999) or Parent and Bernier (2003).

The Bayesian approach has for example been used by Wood and Rodriguez-Iturbe (1975b) to produce a linear combination of the flood discharge distributions obtained on the basis of different frequency models. Model weighting can vary dependent on the considered field application. The Bayesian approach proposed by Niggli and Musy (2005) for the estimation of flood discharges takes for example into consideration the fact that the rational method is often better than the index flood regional method for small drainage basins (Example 11.8).

In conclusion, the Bayesian approach has the particular advantage of generalizing the different combination methods proposed in the literature. For instance, the simple arithmetic mean of model estimates, proposed for example by Weingartner and Manser (1997), can be obtained by considering that: 1) all the models are unbiased, 2) their estimates are conditionally independent of the true value of the variable of interest (in other words the errors of the flood estimation models can be inter-correlated), 3) the variance of the errors of models 1, 2, ..., *n* is the same for all and 4) the prior variance is infinite.

Example 11.8

Regionalization of flood discharges in western Switzerland: sequential Bayesian approach

Figures 11.11 and 11.12 illustrate the principle of the sequential Bayesian approach proposed by Niggli and Musy (2005) for the estimation of maximum flood discharges in the basins of the Swiss canton of Vaud. Each time the distribution of the variable of interest (the quantile for the return period *T* after logarithmic transformation) is updated, a new flood model is used to construct a new likelihood function. Implementation of
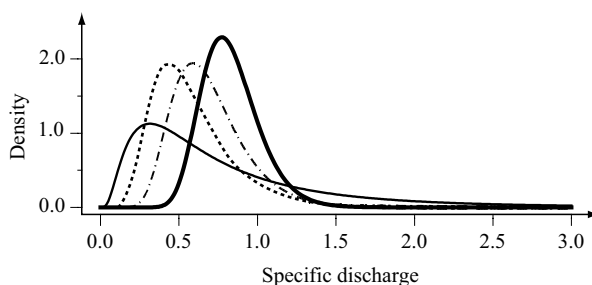

Fig. 11.11: Prior and posterior density functions of the specific flood discharge for the Mentue river at Dommartin (Switzerland) obtained by the Bayesian processor. The non-bold solid curve is the prior density function of the 30-year specific discharge. The dotted, dash-dotted and bold solid curves are respectively the first, second and third update of the prior distribution.
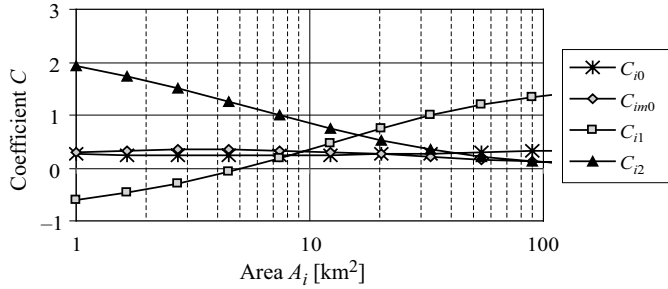
Fig. 11.12: Bayesian linear combination coefficients versus basin area for the case where the HYDRIF model was used to construct the first likelihood function and the HYDRAT model to construct the second likelihood function. All physiographic and climatic characteristics of the basin other than its area remain constant.

the methodology is most straightforward in the normal-linear case, i.e., when the prior distribution and the likelihood function are considered to be normal and when the "true" value of the variable of interest and the estimates of the flood models are interrelated by a linear combination. The posterior expected value of the parameter of interest is then given by a linear combination of the prior expected value of the variable and the quantiles, log-transformed, obtained with the *n* different flood estimation models (the semi-empirical HYDRAT method presented in Example 11.5, the HYDRIF index flood method presented in Example 11.5 and the HYPROX neighborhood-based method). If *n* = 3, the following expression is obtained:

$$m_p = C_0 + C_{m0}m_0 + C_{z1}z_1 + C_{z2}z_2 + C_{z3}z_3 \tag{11.9}$$

where z_1, z_2 and z_3 are estimates of the flood quantiles (log-transformed) obtained respectively for models 1, 2 and 3 and where m_p and m_0 are respectively the posterior and prior expected values of the variable of interest. C_0, Cm_0, Cz_1, Cz_2 and Cz_3 are the linear combination coefficients.

Figure 11.11 shows the effect of the successive use of the HYDRAT, HYDRIF and HYPROX models on the dispersion of the posterior distribution of the 30-year specific flood discharge for the Mentue river basin at Dommartin (Switzerland).

Figure 11.12 plots the weighting coefficients C_0, Cm_0, Cz_1 and Cz_2 of equation 11.9 versus basin area for the 30-year return period (in this case, only the HYDRIF and HYDRAT models were used).

Figure 11.11 shows that the coefficient associated with the HYDRIF model is greater than the coefficient associated with the HYDRAT model ($Cz_1 > Cz_2$) for drainage basins with areas greater than around 20 km² and smaller than the coefficient associated with the HYDRAT model ($Cz_1 < Cz_2$) for drainage basins with areas less than around 15 km². In other words, the HYDRIF model "dominates" the HYDRAT model for large basin areas and the HYDRAT model "dominates" the HYDRIF model for small basin areas. When the basin area is between 15 and 20 km², the models have roughly similar weights ($Cz_1 \approx Cz_2$). The Bayesian processor therefore leads to a linear combination of the HYDRIF and HYDRAT models with coefficients that are consistent with the logical recommendation for the use of the HYDRAT model for small basins and the HYDRIF model for large basins.

11.5 KEY POINTS OF THE CHAPTER

- Most sites requiring estimates of one or more hydrological variables for the management of water resources and associated risks have few or no measurements. In such cases, a regional model is required to estimate the variable or variables of interest.
- Regionalization can be applied to the parameters of hydrological models as well as to any meteorological variable or characteristic discharge (mean and maximum precipitation, characteristic flood or low-flow discharge, etc.). It can also be applied to the statistical distribution of a given hydrological variable (e.g., distribution of flood discharges, flow-duration curves).
- Implementation of a regionalization model requires the delineation of regions that are homogeneous with respect to the variable of interest and the development of a regional estimation method within each of the homogeneous regions.
- A regional model is developed on the basis of a sample of gaged basins (calibration basins). It must then be tested and validated on the basis of another sample of gaged basins (validation basins).
- The delineation of homogeneous regions can be based on different geographic considerations and on different criteria related to physiographic, climatic and hydrological characteristics of the drainage basins. Delineation is a process that always requires hydrological expertise. The identified regions are rarely continuous in space.
- It must be possible to estimate, with available data, the criteria used to assign a given non-instrumented site to one of the homogeneous regions. These criteria are not necessarily the same as those used to delineate the homogeneous regions.
- The probability of obtaining a regional model offering good performance increases with the real homogeneity of the region for the considered variable.
- The preferred methods to estimate the variable of interest are those that are the least sensitive to sampling problems, that take into account the residual heterogeneity within a given homogeneous region, that offer a certain consistency between the estimates made for different variables and that use the maximum amount of available information (in particular the observations available for the target site).
- Regional frequency models are a good approach for estimating many hydrological variables (e.g., characteristic flood and low-flow discharges, flow-duration curves, maximum mean precipitation).
- Instantaneous discharge measurements on the target site and estimates transposed to the target site from analogous basins often improve the performance of the selected regional model.
- When possible, combining prior knowledge and estimates from different estimation methods reduces the uncertainty associated with the estimation of the hydrological variable of interest. Bayesian theory provides a good framework for such combinations.

11.6 APPENDICES

11.6.1 Homogeneity Test Proposed by Hosking and Wallis (1997)

The objective of the *H*-test proposed by Hosking and Wallis (1997) is to check that the statistical distributions of the flood discharges of different sites can be considered to come from the same parent statistical distribution for the region.

The principle of the test is to compare the observed regional variance of L-moment ratios to the distribution of this regional variance under the hypothesis of regional homogeneity (H_0 hypothesis). This distribution of regional variance is obtained using a Monte Carlo method assuming that the maximum annual discharges of the region come from the same Kappa distribution. The use of a Kappa distribution is justified by the flexibility of this 4-parameter distribution. The Kappa distribution is in fact a generalized form of other distributions commonly used in frequency analysis (e.g., GEV, LN3, GPA).

The test is carried out in the following three steps:

1) On the basis of flood discharge observations at the *n* sites of the supposedly homogeneous region, the standard deviation between the regional mean value of the L-moment ratios and the values of these ratios is calculated for the *n* sites. For this:

- The L-moments up to the 4th order (l_1, l_2, l_3, l_4) are estimated for each site *j* on the basis of available observations of maximum discharges using the conventional expressions proposed for this (e.g., Meylan *et al.*, 2012).
- The L-moment ratios t (coefficient of L-variation), t_3 (L-skewness) and t_4 (L-kurtosis) are calculated for each site *j* using the following expressions:

$$t = l_2 / l_1 , \quad t_3 = l_3 / l_2 , \quad t_4 = l_4 / l_2 \tag{11.10}$$

- For each variable t, t_3 and t_4, the weighted mean values are calculated for the region using the following expressions:

$$t^R = \frac{1}{N} \sum_{j=1}^{n} n_j \, t^j , \quad t_3^R = \frac{1}{N} \sum_{j=1}^{n} n_j \, t_3^j , \quad t_4^R = \frac{1}{N} \sum_{j=1}^{n} n_j \, t_4^j \tag{11.11}$$

where the index *j* refers to the *j*[th] site of the tested region *R*, *n* is the number of sites, n_j a number of observations at site *j* and *N* the total number observations for all sites:

$$N = \sum_{j=1}^{n} n_j \tag{11.12}$$

- For each variable t, t_3 and t_4, the weighted standard deviation V_k between the regional mean value of the L-moment ratios and the values of these ratios for the *n* sites is calculated by:

$$V_k = \sqrt{\frac{1}{N} \cdot \sum_{j=1}^{n} n_j \left(t_k^j - t_k^R \right)^2} \tag{11.13}$$

where *k* refers to one of the three variables t, t_3 or t_4.

2) The mean and standard deviation of the variable V_k under the H_0 hypothesis are estimated by simulation. For this:

- Under the H_0 hypothesis, the parent statistical distribution of annual peak discharges is assumed to follow a Kappa distribution. The parameters of this distribution are estimated on the basis of observed regional L-moment ratios, i.e., on the basis of t^R, t_3^R, t_4^R.

- The Monte Carlo approach combined with this discharge distribution assumption is used to generate N_{SIM} sets of flood discharge data consistent with the data of the region under the H_0 hypothesis. Each dataset is composed of n_j values at the n sites of the region (where n_j is the number of observations for site j).

- For each of the N_{SIM} datasets (realization p), the values of ratios t, t_3 and t_4 are calculated for the n sites of the region on the basis of the generated flood discharge data. Their weighted regional values are calculated using an equation similar to equation 11.11. The weighted standard deviation $V_k(p)$ between the regional mean value of the L-moment ratios and the values of these variables for all the sites together is finally derived on the basis of an equation similar to equation 11.13.

- For each variable t, t_3 and t_4, the mean μ_{Vk} and the variance σ_{Vk} of the N_{SIM} values of $V_k(p)$ corresponding respectively to the N_{SIM} generated datasets are calculated.

3) Now the H_0 hypothesis concerning the homogeneity of the region is tested:

- For each variable t, t_3 and t_4, the homogeneity index H_{Vk} is calculated by:

$$H_{Vk} = \frac{V_k - \mu_{Vk}}{\sigma_{Vk}} \tag{11.14}$$

- If the three indices satisfy $H_{Vk} < 1$, the region is regarded as "acceptably homogeneous" and it is therefore not necessary to divide the region into sub-regions. Subdividing could even be counter-productive because it could lead to mini-regions with too few sites and for which the next step of the index flood procedure, i.e., the construction of a multiple regression model for the scaling factor, could be difficult or even impossible.

- If any one of the indices satisfies $1 \leq H_{Vk} < 2$, the region is regarded as "possibly heterogeneous" and further subdivision into sub-regions can be envisaged.

- Finally, if one of the indices satisfies $H_{Vk} > 2$, the region is regarded as "definitely heterogeneous" and subdivision into sub-regions is in principle necessary.

Hosking and Wallis (1997) recommend repeating the simulation for 500 or even 1000 replicates of the region (therefore $N_{SIM} \geq 500$) to obtain sufficiently stable values of the H_{Vk} statistics.

The mean values and standard deviations of the regional L-ratios are calculated in such a way as to give more weight to longer measurement series. Basins with short measurement series can therefore also be included in the analysis.

The choice of a theoretical frequency model capable of representing the statistical behavior of flood discharges for the different sites of the homogeneous region can be made on the basis of the Z statistic proposed by Hosking and Wallis (1997) (Appendix 11.6.2).

11.6.2 Choosing a Regional Frequency Model on the Basis of the Z Statistic Proposed by Hosking and Wallis (1997)

The Z statistic proposed by Hosking and Wallis (1997) can be used to test whether or not a given theoretical frequency model can represent the statistical behavior of flood discharges for the different sites of a region that is homogeneous with respect to these discharges. The region must first be delineated and tested for homogeneity possibly using the H statistic proposed by Hosking and Wallis (1997) (Appendix 11.6.1).

The principle of the Z-test proposed by Hosking and Wallis (1997) is to compare the theoretical L-kurtosis (τ_4) ratio of a candidate theoretical distribution (Gumbel, GEV, etc.) to a distribution of regional L-skewness ratios representing the "real" world, which are the values generated by the Monte Carlo simulation assuming that the maximum annual discharges of the region come from the same Kappa distribution.

The test is carried out in the following steps:

1) The empirical mean $\overline{t_4}$ of the N_{SIM} regional skewness ratios generated by the Kappa distribution are calculated along with the simulated standard deviation s_4 of regional skewness coefficients. For this:

- From the observed discharge data for the n sites of the supposedly homogeneous region, the regional values t^R, t_3^R, t_4^R of the L-moment ratios are calculated using expressions 11.10, 11.11 and 11.12 given in Appendix 11.6.1.
- The parameters of the Kappa distribution are estimated from the regional values t^R, t_3^R, t_4^R.
- Under the Kappa distribution assumption, N_{SIM} datasets consistent with the discharge data observed for the region are generated by a Monte Carlo simulation (Appendix 11.6.1)

$\overline{t_4}$ and s_4 are then calculated as follows:

$$\overline{t_4} = \frac{1}{N_{SIM}} \cdot \sum_{p=1}^{N_{SIM}} \overline{t_4}^{(p)} \tag{11.15}$$

$$s_4 = \frac{1}{N_{SIM} - 1} \sum_{p=1}^{N_{SIM}} \left(\overline{t_4}^{(p)} - \overline{t_4} \right)^2 \tag{11.16}$$

where $\overline{t_4}^{(p)}$ is the weighted regional mean of the individual values calculated at each of the n_j sites of the region on the basis of the data generated for the pth replicate of the region (eq. 12.11).

2) For each candidate theoretical distribution *DIST*, the 4th-order L-moment ratio τ_4^{DIST} is calculated from the regional values t^R, t_3^R.

3) This theoretical distribution *DIST* is now selected among the candidates and tested as follows:

- For each candidate theoretical distribution *DIST*, the test statistic Z^{DIST} is calculated. The statistic measures the difference, for the L-skewness ratios, between the theoretical value of the selected distribution and the mean value obtain on the basis of the N_{SIM} generations.

$$Z^{DIST} = \left(\tau_4^{DIST} - \overline{t_4} \right) / s_4. \tag{11.17}$$

- The candidate theoretical distribution for which Z^{DIST} is closest to zero is selected. It is accepted at the 90% confidence level if $| Z^{DIST} | < 1.64$.

The number N_{SIM} of replicates, chosen by the user, must be sufficiently high so that the test statistic is not subject to excessive sampling variability. Hosking and Wallis (1997) propose a value of 1000. They indicate that the Z statistic roughly follows a normal distribution.

METEOROLOGICAL SCENARIOS

To manage water resources and associated hydrological risks in an optimum manner, possible or probable hydrological scenarios must be determined for the considered hydro-climatic context. In practice, a hydrological model of the hydrosystem, developed to fulfill one or more objectives, is used to simulate these hydrological scenarios on the basis of appropriate meteorological scenarios that have been identified or generated elsewhere.

Management of water resources and associated hydrological risks also requires forecasting of the probable changes in hydrological variables in the near future. In most cases, the corresponding immediate, short-term, medium-term or seasonal hydrological forecasts are obtained by hydrological simulations based on appropriate meteorological forecasts.

The objective of this chapter is to present various approaches and models used to produce either the meteorological forecasts required for hydrological forecasting or the meteorological scenarios required for simulation of hydrological scenarios. This chapter focuses mainly on precipitation, the principal input variable of hydrological models. The possibility of generating other key meteorological variables such as temperature, wind and relative humidity is also discussed.

Section 12.1 reviews how precipitation is formed and presents certain explanatory factors. Section 12.2 discusses a few methods and models that can be used to forecast precipitation for different anticipation times. Section 12.3 describes various methods used in practice to identify or construct the design rainfall for a given project. Section 12.4 deals with several possible approaches to generate continuous precipitation time series. Section 12.5 presents the main methods used to generate scenarios in a climate-change climatic context. Finally, the last section provides guidelines for choosing a suitable method to produce meteorological scenarios among the different possibilities.

For details concerning some or all of the topics of this chapter dealing with meteorology or climatology, see Houze (1993); Holton (1992); McIlveen (1992). French-speaking readers can also consult for example Joussaume (2000); Chalon (2002); Malardel (2005).

12.1 INTRODUCTION

12.1.1 The Importance of Meteorological Forecasts

The importance of meteorological forecasts, in particular regarding precipitation, for hydrological forecasts has been discussed in detail in Chapter 10. In many cases, anticipation

of future changes in hydrological variables requires a quantitative precipitation forecast. For example, this is the case for flood forecasting when the required anticipation time is greater than the concentration time of the considered hydrosystem.

The required anticipation time for hydrological forecasts in fact determines the anticipation time required for meteorological forecasts. In the same way as for hydrological forecasts, meteorological forecasts can be distinguished by their lead times: nowcasts (lead time less than 6 hours) and short-term, medium-term and seasonal forecasts (lead times of respectively 6 to 72 hours, 72 hours to 12 days and greater). Forecasting models differ according to the anticipation time.

12.1.2 The Importance of Meteorological Scenarios

The type of hydrological scenario required for optimal medium-term or long-term management of water resources and associated hydrological risks obviously depends on the objectives. For instance, when designing or checking the size of diversion works, weirs or retention basins, only flood scenarios (i.e., the design flood) are necessary. On the other hand, when calculating the performance of a reservoir designed for low-flow compensation or when assessing the risk of river bank collapse due to progressive erosion, discharge time series over a number of years or decades are required.

Whatever the objective, the discharge series required by hydrologists to determine the necessary hydrological scenarios are often unavailable. Available discharge series are often too short or nonexistent. This is always the case for ungaged basins. Another problem is that the available discharge series may not correspond to the hydroclimatic configuration of interest. This is the case for two situations: 1) when analyzing a drainage basin where land use or the hydrological network will be subject to major changes in the future (e.g., urbanization, retention basins or diversion works) and 2) when estimating the hydrological behavior of a given system for a future or past climatic context that is different than today's.

For most of these situations, the usual approach is to simulate the required hydrological scenarios on the basis of appropriate meteorological scenarios. For this, a suitable hydrological model for the given context must be available (see Chapter 3). Meteorological scenarios are for example the design rainfall or time series of various meteorological variables (e.g., precipitation, temperatures). The type of meteorological scenario to be produced obviously depends on the objective of the analysis (e.g., design, diagnostics, assessment of the impact of climate change) and the type of hydrological model (e.g., global or spatialized) used to obtain the hydrological information required for the analysis (e.g., event based, multi-event based or continuous approach).

The methods used by hydrologists to produce these meteorological scenarios are many and varied. Some of them will be described in this chapter.

12.1.3 Precipitation Mechanism and Characteristics

Precipitation includes all meteoric water falling on the surface of the Earth, whether in the form of a liquid (e.g., drizzle, rain or storm) or solid (e.g., snow, sleet or hail).[1] It

---

[1]Deposited or hidden precipitation can also be included (dew, frost, rime, etc.).

results from the presence of water vapor in the air that, when in contact with cold air, rises and condenses around condensation nuclei (e.g., dust, pollen, aerosols) to form clouds. If condensation is substantial, the water drops become heavier and finally fall, resulting in rain or other forms of precipitation depending on temperature conditions. The formation of intense precipitation requires a continuous input of moist air in the considered region. These processes involve many different mechanisms (Chalon, 2002; Malardel, 2005).

The characteristics of precipitation (Addendum 12.1) depend largely on the current atmospheric circulation and air mass characteristics. For example, convective precipitation results from condensation of an unstable moist air mass that cools as it rises due to its instability. Such precipitation is generally of short duration, high intensity, limited extent and highly variable in time and space. It can lead to the formation of single rain cells or multiple rain cells grouped together in mesoscale systems. Frontal precipitation results from the collision of a cold air mass and a warm air mass (Figure 12.1). Precipitation produced by a cold front is often of short duration, high intensity, limited extent and stratiform if the warm air is stable. If the warm air is unstable, precipitation is convective and can lead to squall lines. Precipitation generated by a warm front is generally of long duration, wide extent, low intensity and limited spatial and temporal variability.

Precipitation is also highly dependent on the small-scale characteristics of the Earth's surface, e.g., orography, land/ocean contrast and cover. For example, orographic precipitation is linked to the presence of mountains that force air masses to rise and condense on windward slopes. Such precipitation events generally exhibit a relatively
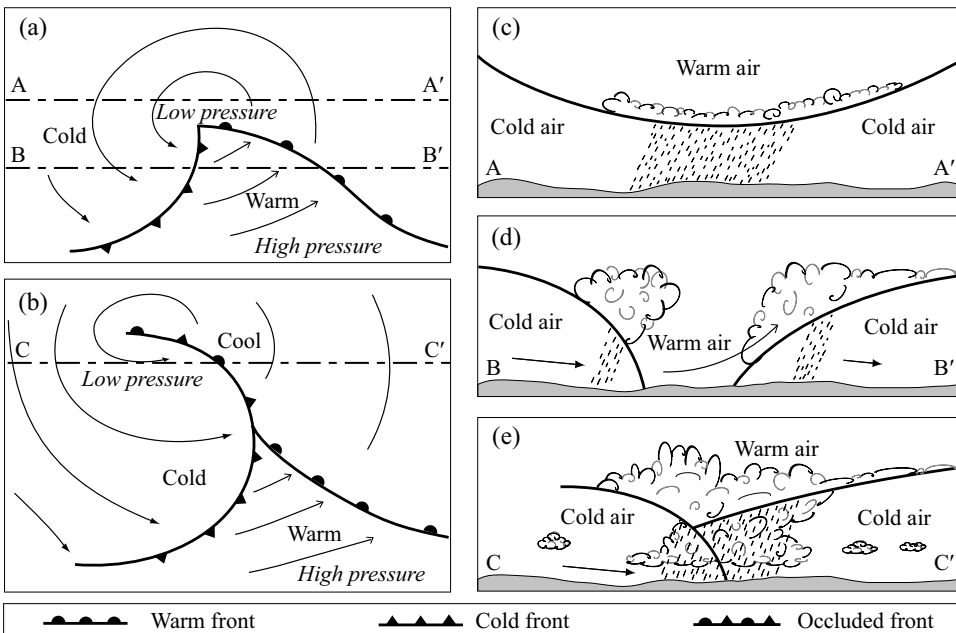

Fig. 12.1: Atmospheric circulation and precipitation. a) Plan view of typical air mass circulation within an extra-tropical cyclone associated with a disturbance and leading to frontal precipitation (northern hemisphere). b) Typical evolution of an extra-tropical cyclone with the appearance of an occluded front (the cold front overtakes the warm front), gradually filling the disturbance. c), d) and e) Cross-sections corresponding respectively to A-A', B-B' and C'C' indicated in Figures a) and b) (modified from Brutsaert, 2005).

regular intensity and frequency. Orographic events can lead to high amounts of precipitation over extended zones if air masses are blocked over long periods by the relief. Orographic precipitation is generally non-homogeneous, i.e., its spatial structure depends on the relief and wind direction.

Addendum 12.1 Characterization of precipitation

Whatever the temporal or spatial scale considered, precipitation is highly intermittent in space and time. At every point in space, precipitation intensity is zero most of the time. When it is non-zero, it can vary greatly and in an arbitrarily fast manner between two neighboring space-time points (Molini *et al.*, 2002). The stochastic or chaotic nature of precipitation has often been pointed out (Sivakumar, 2001). Non-zero values constitute a continuous random variable with a highly asymmetrical statistical distribution containing many low values and very few high values.

Within a given chronological series, wet periods presenting precipitation of variable intensity can be distinguished from dry periods with zero precipitation. For a given site, the duration of dry periods is also highly variable. Depending on the season and the region of the world considered, dry periods may last several hours, several weeks or even several years.

The spatial structure of precipitation is also highly variable over time. Precipitation is often organized in space and certain authors suggest that it is often possible to distinguish between different types of structures reflecting three different scales (Waymire and Gupta, 1981): 1) convective cells such as summer storms on a local scale (1 to 30 km^2), 2) rain bands and orographic precipitation on the mesoscale (5 to 50 km^2) and 3) stratiform precipitation on larger scales (Figure 12.2).
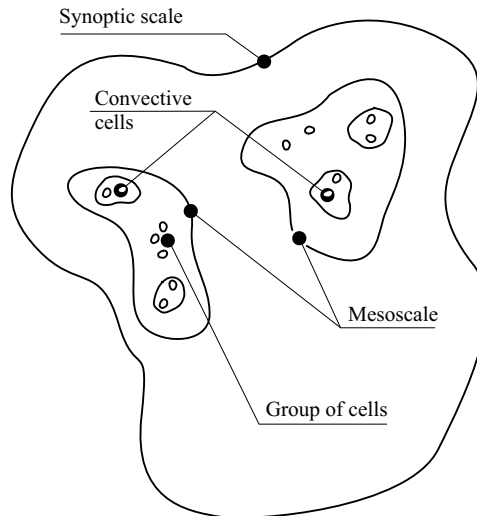

Fig. 12.2: Possible precipitation hierarchy as proposed by Waymire and Gupta (1981).

In certain situations, these structures tend to group together and may coexist. This hierarchy, initially proposed by Lecam (1961), has often been supported since by detailed analysis of certain rainfall fields derived from radar imagery.

The rainfall regime of a region, in terms of seasonality, variability and extremes in particular, is one of the main factors governing the hydrological variability of hydrosystems. Its characterization is necessarily of a composite nature and therefore imperfect. The following information is often used.

- Standard characteristics of a precipitation series. For example, for precipitation depths over a given time step Δt, these often include the probability of occurrence, the moments of order k of non-zero precipitation (in particular the mean, variance and asymmetry coefficient), auto-correlation coefficients, etc.
- The statistical distribution of certain key rainfall variables extracted from the series, for example duration of dry or wet periods, maximum mean precipitation over different durations (often described by the Intensity-Duration-Frequency (IDF) curves (Appendix 12.8.1).
- Certain scale invariance properties (Appendix 12.8.2).

Precipitation is ideally characterized for the amounts accumulated over different time steps (e.g., hourly, daily). Characterization can also concern the seasonal and inter-annual variability of certain quantities such as monthly volumes. If any information is available on the spatial variability of precipitation (e.g., multi-site time series, radar imagery), precipitation can be described statistically using similar composite variables (e.g., statistics concerning average precipitation depths of different areas).

All these statistical characteristics obviously provide only a simplified description of the spatial and temporal variability of the real precipitation. They do however provide useful information for the construction or generation of design rainfalls required for hydrological analyses.

12.1.4 Precipitation and Weather Types

As already mentioned, local or regional precipitation at a given time is strongly influenced by the state of the atmosphere and its circulation on the synoptic scale.[2] The same is true for other local meteorological variables (e.g., temperature, wind direction and speed). Although the relationship between local-scale and synoptic-scale meteorological variables is not unequivocal, it is generally sufficiently strong to consider that, from a statistical viewpoint, two atmospheric situations that are similar on a synoptic scale lead to meteorological situations that are similar on a local scale.

Synoptic-scale atmospheric situations observed for a given region are consequently often associated with typical atmospheric situations often referred to as weather types or patterns. A given weather type leads to certain types of local and/or regional meteorological situation, subject of course to the variability that exists within each type. Weather types have been identified for many regions of the world. They can be determined subjectively or objectively on the basis of all synoptic-scale atmospheric situations observed for the region (Addendum 12.2). They are generally described using the structures of the fields of sea-level pressure or certain geopotentials providing information on atmospheric circulation (Figure 12.3). In practice, the data used for this description are extracted from meteorological re-analyses (Chapter 2) or the output from meteorological/climate models (Section 12.2.2, 12.2.4 and 12.5.3).

As soon as the different weather types that can be observed in a given region have been identified, it is possible for a given day in the past or future to: 1) determine the weather type(s) corresponding to the atmospheric situation of the day and 2) estimate the main characteristics of the probable weather for this day. To take into account the associated

---

[2]In meteorology, the term synoptic applies to large-scale atmospheric systems, i.e., larger than several thousand kilometers horizontally, several kilometers vertically and several days in terms of duration.
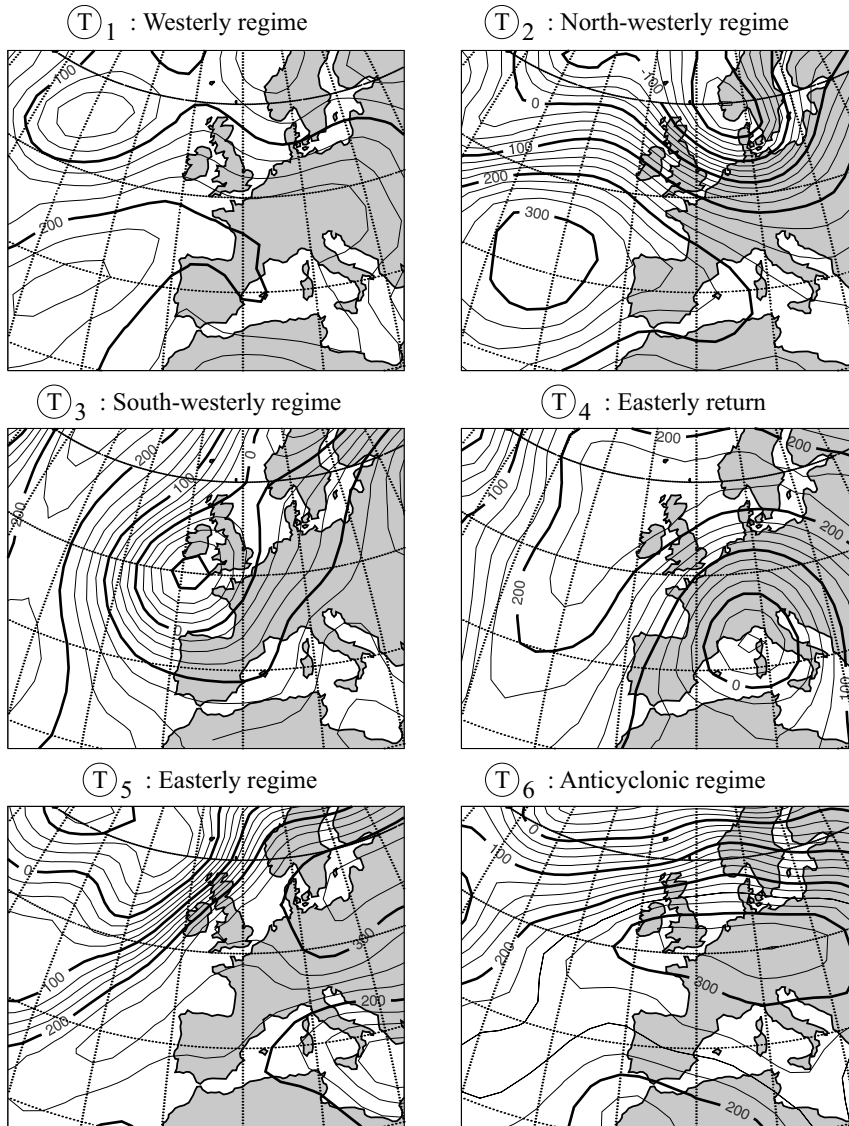
T₁ : Westerly regime — T₂ : North-westerly regime
T₃ : South-westerly regime — T₄ : Easterly return
T₅ : Easterly regime — T₆ : Anticyclonic regime

Fig. 12.3: Fields of 1000 hPa geopotential heights (i.e., altitudes above sea level at which an atmospheric pressure of 1000 hPa is reached) for situations characteristic of six different weather types selected by Bontron (2004) to explain precipitation in France and more particularly in the Alps (modified from Bontron, 2004).

uncertainty, the estimates are necessarily statistical. They are also necessarily imperfect given that the atmospheric variables used to define the weather types are not often the only variables affecting the regional weather.

The concept of weather types or, more generally, any information on the large-scale atmospheric situation that describes the local variable to be explained, is widely used both in meteorological forecasting (Section 12.2.2) and in the generation of meteorological scenarios (Section 12.4.4). The corresponding approaches, based on the relationship

between the synoptic-scale and local-scale atmospheric situations, are based on methods often referred to as statistical downscaling. The associated uncertainties vary greatly depending on the atmospheric variables to be explained (e.g., the type of variable and its spatial and temporal resolution) (Gangopadhay *et al.*, 2005; Mezghani and Hingray, 2009).

The seasonality, frequency and persistence of weather types and the characteristics of transitions from one weather type to another determine the seasonality and statistical characteristics of precipitation and other meteorological variables for a given region (Figure 12.4). Inter-annual variations of the frequency of weather types also partly explain inter-annual variations of local meteorological variables (Boé and Terray, 2008).
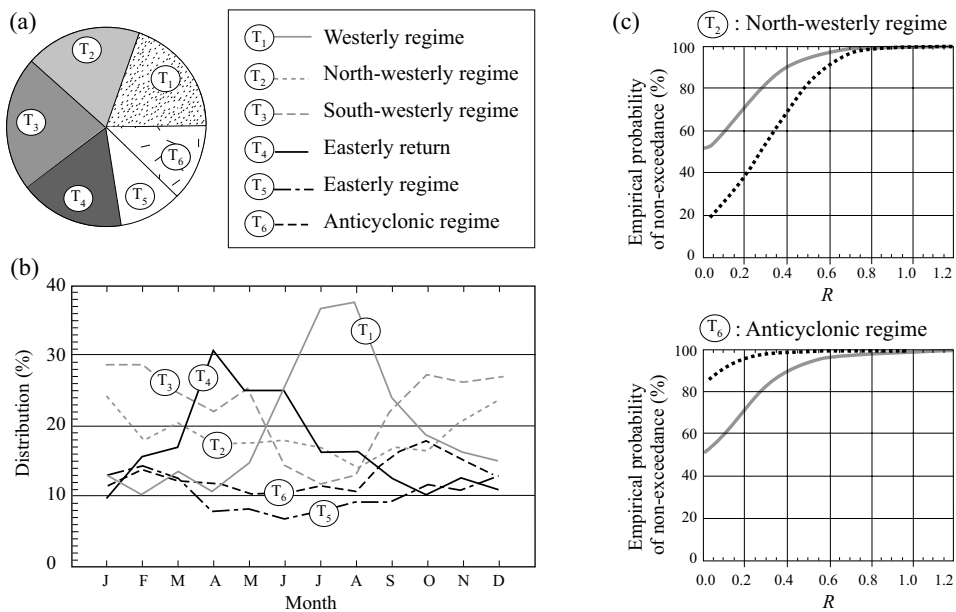

Fig. 12.4: Illustration of the relationship between precipitation and weather types. a) Annual and b) monthly frequencies of occurrence of the different weather types described in Figure 12.3. c) Statistical distribution of daily precipitation (*R*) observed for days with westerly (top) and anticyclonic regimes (bottom) (black dotted curves) and for all days (gray solid curves, representing the climatological statistical distribution). The distributions come from the Fier rain-gage station group (modified from Bontron, 2004).

Addendum 12.2 Classification of weather types and atmospheric circulation indices

Weather types can be classified by different techniques. They can be classified subjectively by competent meteorological services. This technique takes full advantage of the knowledge and experience acquired by the meteorologists over many years or even decades. Examples include classifications proposed by Baur *et al.* (1944) for Central Europe, Elliott (1949) for the USA, Lamb (1972) for the British Isles and Thillet (1997) for France and the French Alps in particular. The data used for these classifications are generally pressure fields and air mass trajectories.

Weather types can also be classified objectively by automatic classification algorithms using selected atmospheric data. Classification techniques are of many types. For example, they can be based on: 1) discriminant or principal component analysis of pressure fields (Stone,

1989; Corte-Real *et al.*, 1998), 2) analysis of these fields based on fuzzy logic (Bardossy *et al.*, 1995) or 3) various composite atmospheric circulation indices (Buishand and Brandsma, 1997, see also below). The k-means clustering algorithm or dynamic clustering algorithms are often used to identify classes.

The most useful weather type classification schemes are those that directly take into account the effects of large-scale circulation on local atmospheric variables (Buishand and Brandsma, 1997; Bates *et al.*, 1998; Bardossy *et al.*, 2002; Boé *et al.*, 2006).

Atmospheric Circulation Indices (ACIs) can be used to summarize some of the information contained in the fields of atmospheric variables (Conway *et al.*, 1996; Wilby and Wigley, 2000; Buishand and Brandsma, 2001). They vary continuously from one day to another. According to Jones *et al.* (1993), these indices correspond, for a given day, to the type of atmospheric circulation that would have been attributed subjectively by a meteorological expert.

The indices frequently used are mean sea-level pressure and various derived indices such as zonal and meridional air-flow components (i.e., the components in the west-east and south-north directions respectively), the resultant of the air-flow and its direction or vorticity. The vorticity provides information on the cyclonic intensity of the atmosphere. In the northern hemisphere, positive values indicate low-pressure conditions and negative values indicate anticyclonic conditions. These indices are often determined for different geopotential levels.

Other indices related to the state of the atmosphere and estimated for certain geopotential levels are often used, for example the temperature of the air and its relative or specific humidity (indicating respectively if the water vapor present in the atmosphere is near its condensation point and the absolute quantity of water present in the air at the considered level), baroclinicity (defined by the absolute value of the temperature gradient on the isobars, providing information on the capacity of the atmosphere to develop vertical movements) or precipitable water (corresponding to the integral of specific humidity over an air column and providing information on the quantity of water available for precipitation in this column).

12.1.5 Precipitation and Major Meteorological Phenomena

Local precipitation generally exhibits high seasonal and inter-annual variability. The temporal variability of atmospheric situations, which affect precipitation variability, may in part depend on major meteorological phenomena that can last several months or even years. The dependence of precipitation on these phenomena generally leads to low-frequency variations of seasonal precipitation. This is typically the case for precipitation in Indonesia, Polynesia and the western slopes of the Andean mountains strongly influenced by the Southern Oscillation, for which the warm phase is known as El Niño (Neelin *et al.*, 1988). This is also the case, to a lower extent, for precipitation in Western Europe and in south-eastern United States influenced by the North-Atlantic Oscillation (Cassou, 2004).

These major meteorological phenomena obviously influence more than precipitation alone (Addendum 12.3). Various composite indices have been proposed to describe the intensity of these phenomena, generally for monthly or seasonal time steps. For example, Rogers (1984) has proposed a possible North-Atlantic Oscillation Index (NAOI) based on the pressure difference between the Azores (at Ponta Delgada) and Iceland (Reykjavík). Trenberth (1984) has proposed a possible Southern Oscillation Index based on the pressure difference between Tahiti and Darwin. Other indices can be found on the web site of the United States Climate Prediction Center: http://www.cpc.noaa.gov/products/. These indices are sometimes used to condition the generation of meteorological scenarios, in particular those related to precipitation (Sections 12.2.2, 12.4.4 and 12.5.3).

Addendum 12.3 Southern and North Atlantic Oscillations

The El Niño phenomenon results from the modification of atmospheric and consequently oceanic circulation of the equatorial Pacific. Under normal conditions (Walker circulation), the western and eastern parts of this region are respectively in a low-pressure and high-pressure zone. The trade winds blow from east to west, inducing a warm current in the same direction at the ocean surface. This results in heavy precipitation over Indonesia and a compensating cold sub-surface current that flows in the opposite direction, thereby cooling ocean waters off the coast of Peru. During the El Niño phenomenon, observed every 3 to 7 years, the eastward shift of the low-pressure center from its usual location in the western region and the attenuation of high pressures in the eastern region weaken the trade winds, slowing both the warm surface current flowing in the direction of the trade winds and the compensating cold sub-surface current. This modification induces observable phenomena such as a decrease in precipitation over Indonesia and Australia and a modification of precipitation along the coast of South America. The El Niño phenomenon increases the temperature of the ocean surface during the warm phase of the Southern Oscillation, also referred to as ENSO, the El-Niño Southern Oscillation. La Niña is the opposite phenomenon corresponding to the ENSO cold phase.

The North-Atlantic Oscillation (NAO) is the result of a regular modification of atmospheric circulation over the North Atlantic (NA). Under normal conditions, the high latitudes of the NA are in a low-pressure zone while the center of the NA, western United States and eastern Europe are in a high-pressure zone. This results in a westerly jet stream over the NA. The positive phase of the NAO corresponds to above-normal pressures at low latitudes and below-normal pressures at high latitudes. The negative phase corresponds to the opposite pattern. Both phases are associated with changes in the intensity and location of the NA jet stream that modify moisture and heat transport over the region. Strong positive phases of the NAO are associated with above-average temperatures in the eastern United States and northern Europe and below-average temperatures in Greenland and often across southern Europe. They are also associated with above-average precipitation over northern Europe and Scandinavia in winter and below-average precipitation over southern and central Europe. Opposite patterns of temperature and precipitation anomalies are typically observed during strong negative phases of the NAO. The NAO presents high inter-seasonal and inter-annual variability. Extended periods (several months) of both positive and negative phases of the pattern are common.

12.2 METEOROLOGICAL FORECASTS

Different methods can be used to produce meteorological forecast scenarios. They can involve some or all of the meteorological variables required by hydrological forecasting models. The methods dealt with in this section mainly concern precipitation, the principal meteorological variable of hydrological models and also the most difficult to forecast. Meteorological forecasting methods use different data and models. They are essentially characterized by different possible anticipation times and are sometimes used in a complementary manner.

It should be kept in mind throughout this section that, whatever the meteorological forecasting model considered, the expertise of the meteorologist often leads to a modulation of the forecast produced by the model, generally improving its pertinence.

12.2.1 Meteorological Nowcasting

Forecasting over the next few hours is referred to as nowcasting. It is often associated with flood forecasting and mainly applies to the forecasting of precipitation alone. Present operational approaches are mostly based on radar imagery.

The use of meteorological radar for the estimation of precipitation has already been dealt with in Chapter 2. Estimates are based on the empirical relationship established between precipitation intensity and measured radar reflectivity. The latest available radar information is used to estimate the probable spatial and temporal evolution of the precipitation field observed over the considered forecasting lead time (Dolciné, 1997; Wilson *et al.*, 1998).

The most common approaches involve simple advection of the observed field. They assume that the trajectory, speed, activity and shape of the precipitation field—or the corresponding precipitating cells—are constant over the considered period (Addendum 12.4). This simple extrapolation method can be used to anticipate over the next few hours the movement of the squall lines within which the convective cells develop. The anticipation time can be up to six hours for stratiform precipitation systems. The performance of nowcasting based on simple advection however deteriorates very rapidly for individual convective cells for which lifetimes are often less than one hour.

More sophisticated approaches are sometimes used to estimate the way in which the shape and/or activity of precipitation fields are modified (Addendum 12.4). It is however not always possible to identify the main physical processes governing changes in precipitation activity on the basis of radar imagery. Consequently, these approaches often perform no better than extrapolation based on simple advection (Wilson *et al.*, 1998).

New nowcasting methods being developed tend to model the initiation and diffusion processes of the convective cells. For example, a number of approaches are based on the strong correlation observed between the development of these cells in the presence of an atmospheric convergence line in the boundary layer. This can be identified either by a ground anemometer network or by radar or satellite imagery (Wilson *et al.*, 1998). The use of physically-based atmospheric models is also being explored. The main difficulty in this case is the initialization of the model based on a limited number of observations and often without any direct relationship with the model state variables.

Given the many sources of uncertainty associated with radar estimates of precipitation (Chapter 2), forecasts are often qualitative. They are sometimes quantitative for very short lead times (e.g., 30 min.). Radar imagery is widely used by flood warning services, in particular for systems with very short response times, for example in highly urbanized areas or regions subject to flash floods (Boudevillain, 2003; Sharif *et al.*, 2006).

Addendum 12.4 Radar-based nowcasting

Estimates of trajectory and average speed, required for simple advection of the precipitation field, can be obtained from Doppler radar. Such radar can be used to estimate the direction and speed of the hydrometeors at any point in the explored region. The trajectory and speed can also be derived by comparing different radar images obtained successively in the recent past. In this context, the approach is based on a spatial cross-correlation analysis of successive images or on the identification and monitoring of anchor points (e.g., the centroid

of convective cells) within the precipitation field or characteristic precipitation structures. Monitoring is carried out manually or using appropriate image processing algorithms. For convective systems, the displacement of the squall line can be estimated on the basis of electric activity measured by storm detection systems.

Various approaches can be used to estimate the way in which the shape and/or activity of the precipitation field is modified. One approach consists in monitoring each convection cell in successive radar images. The probable evolution is then estimated on the basis of a simple advection-diffusion model (Jinno *et al.*, 1993; Willems, 2001). More sophisticated approaches, partially taking into account the internal dynamics of precipitation cells, are also possible. For example, French and Krajewski (1994) proposed a conceptual model in which the precipitating system is assimilated to an atmospheric column equivalent to a water reservoir present in different forms (see also Bell and Moore, 2000; Boudevillain *et al.*, 2006). Different assumptions can be used to define the equation governing the behavior of the liquid water contained in the column and in particular the estimated intensity of precipitation at the base of the column. Successive radar images may be used to estimate the various model parameters. Andrieu *et al.* (1996) adapted this approach to take into account the orographic component of precipitation in mountainous regions.

12.2.2 Short-term and Medium-term Meteorological Forecasts

Atmospheric models

Short-term and medium-term meteorological forecasting is classically performed using numerical models of the atmosphere, referred to as atmospheric models or weather models, which began to appear in the 1950s (Addendum 12.5).

Addendum 12.5 Numerical models of the atmosphere

Numerical models of the atmosphere are physically-based deterministic models. They are designed to solve the non-linear equations that describe the behavior of the atmosphere and in some cases the oceans, including equations for the conservation of mass, energy and momentum and the perfect gas equation (Coiffier, 2000). The techniques to solve these equations are necessarily numerical and based on a discrete representation of the system. For this, space is divided into grid boxes defined by a horizontal grid and different vertical levels (Figure 12.5). The atmosphere is assumed to be homogeneous within each grid box. Point estimates of the different meteorological variables of interest, such as air pressure, humidity and temperature or wind speed, are determined for each of these grid boxes.

The resolution used for the spatial and temporal discretization of a given model is generally imposed by computing time constraints. The spatial resolution is generally sufficient to represent large-scale processes concerning for example air mass circulation. It is however often greater than the characteristic length of many meteorological phenomena such as micro-physical and thermodynamic processes. The simulation of such sub-grid processes consequently requires a number of parameterizations. This is particularly the case for precipitation. The influence of these parameterizations on the accuracy of the results varies according to the resolution used.

When forecasting meteorological variables over several days, the behavior of the atmosphere must be modeled for the entire globe. This is classically carried out using planetary models. If the temporal resolution of the numerical scheme is several seconds, the spatial resolution of the grid is relatively coarse, from around 25×25 km to 50×50 km.
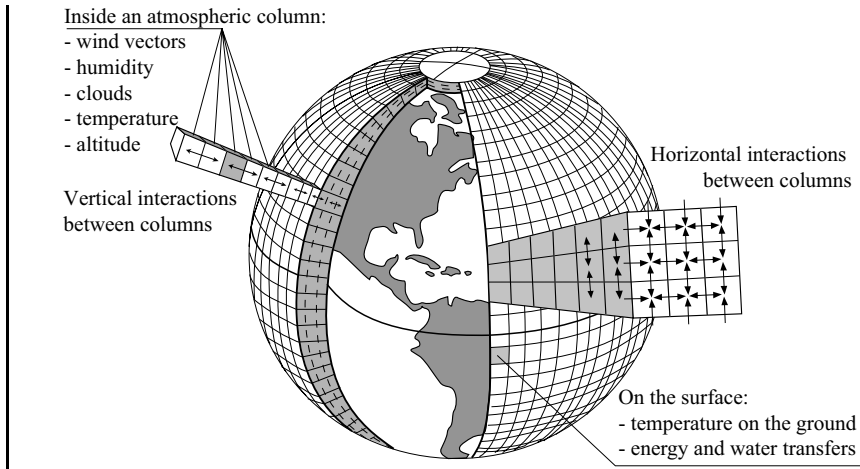
Inside an atmospheric column:
- wind vectors
- humidity
- clouds
- temperature
- altitude

Vertical interactions
between columns

Horizontal interactions
between columns

On the surface:
- temperature on the ground
- energy and water transfers

Fig. 12.5: Schematic representation of a planetary numerical model of the atmosphere. The atmosphere is divided into elementary grid boxes and the calculations are carried out at the center of each box (modified from NOAA, 2006).

This is insufficient to adequately describe the Earth's surface. Even marked relief such as the Alps is highly smoothed, leading to an uncertain forecast of regional or local meteorological variables.

Limited-Area Models (LAMs) have a higher resolution (as fine as 2.5×2.5 km) and therefore provide a more accurate description of the Earth's surface and atmospheric processes —for example the formation and evolution of clouds. LAMs have a limited spatial coverage extending from sub-regional (e.g., the Western Alps for the Italian BOLAM model—Buzzi and Foschini, 2000) to sub-continental (e.g., the European sub-continent for the French ALADIN model—Pailleux *et al.*, 2000). The initial conditions and boundary conditions of these models are generally determined by meteorological re-analysis (Chapter 2) for the near past and by forecasts from planetary models for the future. Nested models—combining LAMs and planetary models—provide a basis for operational meteorological forecasting. Although LAMs are not subject to some of the limitations associated with planetary models, their performance depends on that of the planetary models and on the quality of the parameterizations required for the simulation of sub-grid processes (Zorita and von Storch, 1999; Frei *et al.*, 2003).

An alternative to nested models is the use of variable-grid models offering finer spatial resolution in the zone of interest (e.g., ARPEGE-IFS developed by Météo-France and the European Center for Medium-Range Weather Forecasts—ECMWF; Pailleux *et al.*, 2000).

Existing atmospheric models provide forecasts of reasonable quality for lead times of 2 to 10 days, depending on the meteorological context and the considered variable (e.g., 5 to 10 days for pressure fields and 2 to 3 days for humidity fields). Certain variables are however often subject to major errors. This is particularly the case for the intensity and location of precipitation which are generally hard to predict. The associated errors increase with the anticipation time. They tend to decrease if the forecast variables are averaged or accumulated over a number of hours. Meteorological services therefore prefer to provide forecasts of total precipitation falling over time steps that are often greater than or equal to 6 hours.

Note that meteorological forecasts are almost always biased, i.e., they include systematic errors. Forecasts should therefore be subject to a meteorological adaptation whenever a reasonable quantitative estimate of future meteorological forcing is required.[3] The two main approaches used to adapt meteorological forecasts are described below. They are increasingly used by hydrologists in charge of producing hydrological forecasts. Adaptation methods are used to develop scenarios for forecasts of precipitation and other meteorological variables. Both approaches offer the advantage of forecasting variables not simulated by atmospheric models (e.g., fog). On the other hand, they require long time series of data for calibration (observations and forecasts from the atmospheric model for common periods of at least 30 to 40 years). The anticipation time for these methods is the same as that of forecasts produced by atmospheric models.

Statistical adaptation

The most common adaptation method uses appropriate statistical models to estimate the required local variable on the basis of meteorological forecasts produced by LAMs (Antolik, 2000; Gangopadhyay *et al.*, 2004). For each variable of interest, a regression model (often non-linear) must be identified to relate the observed values of the local variable to be forecasted and the various explanatory variables extracted from the output of the atmospheric model. This model can be identified on the basis of the history of past forecasts at each point where observations of the variable to be forecasted are available. The corresponding statistical relationship based on the past is assumed to be valid for the present. Particularly well-suited to the forecasting of local meteorological variables, this technique is often referred to as the Model Output Statistics (MOS) method.

The explanatory variables are meteorological variables that are pertinent with respect to the variable to be explained. When the variable of interest is simulated by the model, the relationship between the observed variable and the simulated variable is often determined directly. This relationship can be used in particular to remove the bias from model outputs. Explanatory variables can also be derived by the atmospheric model from simulated fields. This is for example the case for vorticity derived from geopotential or other Atmospheric Circulation Indices (Addendum 12.1). Note that all variables produced by atmospheric models do not have the same reliability. For this reason, the variables most commonly used are those related to the dynamic parts of models, for example the sea-level pressure field, various geopotential altitude fields (e.g., 500 hPa, 750 hPa, 1000 hPa) and relative or specific humidity fields at different levels. In this case, statistical adaptation of atmospheric model outputs therefore leads to downscaling approaches (Section 12.1.4).

Explanatory variables are sometimes constructed by combining different simulated variables. The product of the vertical component of wind and the relative humidity of the air layer is for example sometimes used as an explanatory variable of intense precipitation (Bontron, 2004). The statistical model may be established directly using the variables

---

[3]Meteorological adaptation must be distinguished from hydrological adaptation described in Chapter 10. The objective of meteorological adaptation is to produce plausible meteorological scenarios based on the output from meteorological models, independent of all hydrological constraints. Hydrological adaptation is superimposed on meteorological adaptation. Its objective is to produce meteorological scenarios that can be assimilated by hydrological forecasting models, i.e., scenarios satisfying various constraints linked in particular to the spatial and temporal resolution of the hydrological forecasting model and to the meteorological data that are continuously forwarded to the forecasting center.

of interest or using appropriate mathematical transformations of these variables (e.g., logarithmic transformations) that make it possible to take into account the non-linearity of certain relationships. Statistical models are sometimes estimated regionally when the meteorological behavior of the various stations is homogeneous. Several models can be developed for different typical meteorological situations or different seasons. The MOS technique generally used for local adaptation can be applied to estimate regional variables such as the average precipitation depth over a given drainage basin.

The drawback of this adaptation method is that the regression relationships often depend strongly on the version of the meteorological forecasting model used. They must therefore subsequently be updated whenever the atmospheric model is improved, a very long and tedious process.

Non-parametric adaptation using the analog method

Another atmospheric model output adaptation technique is the so-called analog method. It was initially proposed by Duband (1970) and has since been continuously refined (e.g., Obled *et al.*, 2002; Horton *et al.*, 2012). It is based on the "same cause, same effect" concept. The main assumption of this method, already mentioned in Section 12.1.4, is that the local meteorological situation is highly dependent on the synoptic-scale atmospheric situation. Consequently, two atmospheric situations that are very similar on the synoptic scale should lead to the same local meteorological situation, subject to some degree of uncertainty. Analog adaptation of atmospheric model outputs is therefore also a downscaling type approach (Section 12.1.4).

The local meteorological situation is generally characterized by variables such as temperature and precipitation. Application of the method requires a long history of both observed synoptic situations and the corresponding local situations. If a reliable estimate of upcoming synoptic situations is available, the closest historical synoptic situations can be identified and used to propose plausible local meteorological situations for the days to come (Figure 12.6).

The analog method requires determination of: 1) the atmospheric variables to be used to describe and compare synoptic situations, 2) the resemblance criteria to be used to identify similar synoptic situations that are optimal for the targeted local variable (e.g., precipitation) and 3) the spatial and temporal window over which this comparison must be made (Figure 12.7).

Data available to compare synoptic situations are different for the future and the past.

- For the future: outputs of the atmospheric models used for operational meteorological forecasting (e.g., forecasts of the ECMWF model).
- For the past: meteorological re-analysis data produced by the same models a posteriori and with more input data (e.g., ERA-40 re-analyses, see Chapter 2).

It is often preferable to use predictor variables from the dynamic parts of models, if informative, because they are better simulated than the variables from the physical parts of models.

Various resemblance criteria may be used to identify the situations closest to the forecasted synoptic situation. Some measure the similarity of the shape of the considered fields. This is the case for the criterion proposed by Teweless and Wobus (1954) and used by Bontron (2004) to compare the altitude fields of different geopotentials (Figure 12.8).
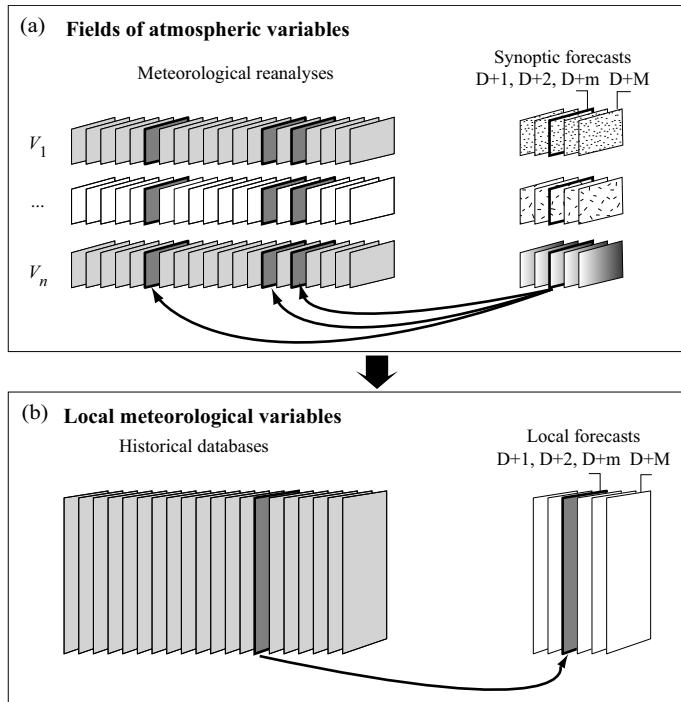
Fig. 12.6: Adaptation of numerical meteorological forecasts based on analogous situations observed in the past. a) Identification of k synoptic situations (daily) resembling the situation forecasted for day D+m. b) Use of observed local variables for one of the analogous situations as a meteorological scenario for day D+m.

When the synoptic situation on a given day is characterized on the basis of composite indices, the resemblance between the synoptic situation forecasted for day *t* and synoptic situation of any day *u* in the past is often measured by a simple Euclidean distance of the type:

$$d\left(D_u, D_t\right) = \left(\sum_{j=1}^{q} w_j \left(x_{t,j} - x_{u,j}\right)^2\right)^{1/2} \tag{12.1}$$

where state vectors D_t and D_u, composed of *q* composite indices, are used to characterize the respective synoptic situations for days *t* and *u*, where $x_{t,j}$ and $x_{u,j}$ are respectively the values of the jth index for these two days and where w_j is the corresponding weighting coefficient. The indices used are generally atmospheric circulation indices (Addendum 12.2). If a principal component analysis has been carried out on the explanatory synoptic atmospheric variables, for instance on the average sea-level pressure field, the indices for a given day may also correspond to the coordinates of the synoptic situation of the day in the space of the corresponding *q* first principal components.

Different precautions are often taken to avoid selecting analog situations that are incongruous or of limited pertinence. For example, the search for analogs in the past is often restricted to days within the same "season", where the season is for instance defined as a two-month period centered on the current day. The search can also be carried out among past situations that presented the same weather type according to appropriate local classifications.
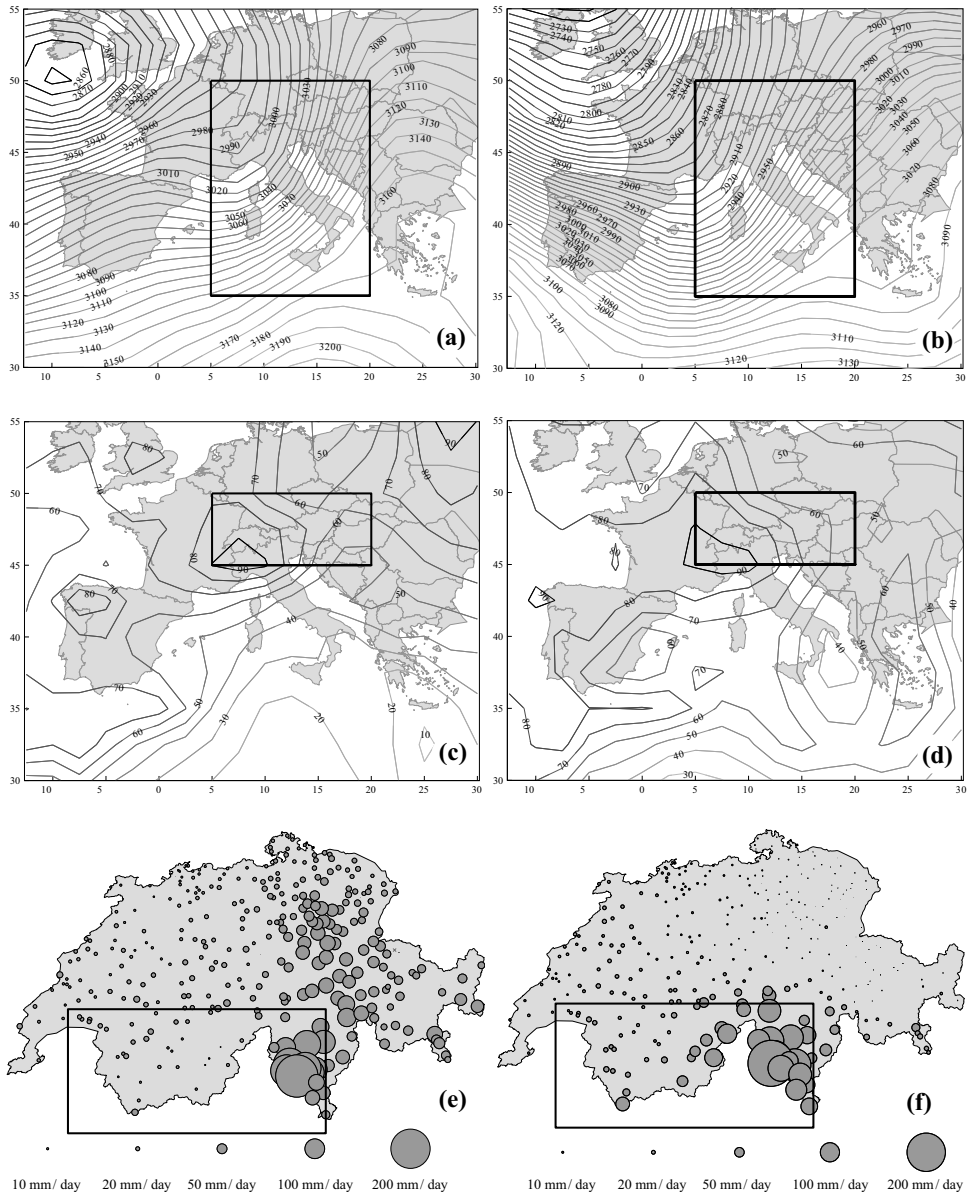
Fig. 12.7: Two analog synoptic situations (left for 08/10/1993 and right for 12/10/1976) with respect to precipitation on the Valais and Tessin regions of Switzerland. Top: Altitude of the 700 hPa geopotential field. Middle: Relative humidity field for the 850 hPa geopotential field. Bottom: Precipitation at each MeteoSwiss rain-gage station. Atmospheric data are from NCEP re-analysis. The spatial windows indicated in the figures are those used to compare synoptic situations.

For meteorological forecasts, the analog method is of interest for several reasons. First of all, it is based on synoptic atmospheric variables that are presently considered to be better forecasted by atmospheric models than local meteorological variables, in particular
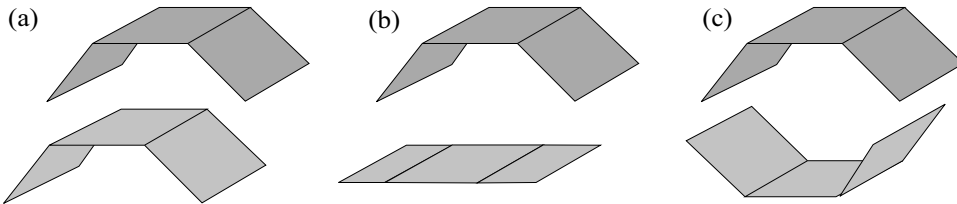
Fig. 12.8: The "distance" system proposed by Teweless and Wobus to measure the shape resemblance of two fields of a given atmospheric variable. For fields that are a) identical, b) totally independent or c) totally different, the distances are respectively 0, 100 and 200 (adapted from Bontron, 2004).

precipitation. The method can be used to forecast some or all of the local meteorological variables available in the past and to provide consistent local meteorological scenarios, i.e., preserving within a given day the spatial and temporal structures of these variables as well as the correlations between them (e.g., Chardon *et al*., 2013).

The possibility of identifying one or more situations that are truly analogous to the forecasted situation however depends on the size of the available historical database. For example, the ERA-40 re-analyses (Chapter 2), produced by the European Center for Medium-Range Weather Forecasts—ECMWF, are available only from 1957 and are not homogeneous throughout the whole period. Even when the database is long, it cannot be excluded that the forecasted situation may never have been observed in the past and that the closest analog is in fact very different. This point is especially important in a climate-change context. Note also that this method is relatively long to implement. It first requires a great deal of calibration work to identify pertinent analog variables and the optimal temporal and spatial windows over which they must be calculated. In addition, optimal parameterization of the model depends on the region for which local meteorological forecast is required and also in principle on the synoptic context. On the other hand, once calibrated, the analog method is very easy to use on a day-to-day basis.

12.2.3 Seasonal Meteorological Forecasts

In spite of continuous improvement of meteorological forecasts produced by numerical models, it is impossible to make an accurate forecast for lead times beyond around 15 days. This is due to a number of factors, in particular the imperfect representation of the atmosphere by models, the non-linear nature of equations governing the phenomena and uncertainties concerning the estimation of the initial state of the system. The high sensitivity of forecasts to initial conditions can lead to rapid divergence of two meteorological trajectories that are initially very similar. This is an example of the butterfly effect described by Lorenz in the 1960s. The objective of a seasonal forecast is therefore limited to estimating whether the monthly precipitation in *n* months will be greater or less than the climatological average.

The atmosphere can however be forecasted to some extent on a seasonal scale. This results from the persistence of certain initial conditions of the system, such as soil moisture, continental snow cover and especially the temperature of the ocean surface in tropical regions (Déqué, 2003). Atmospheric models can therefore provide a seasonal forecast if it is possible to predict the evolution of ocean surface temperatures. Statistical approaches mainly based on the persistence of tropical ocean temperature anomalies are sometimes used for this. Otherwise, atmospheric models are coupled with an ocean model. Forecasts

being highly dependent on the initial state of oceans and the atmosphere, different seasonal forecast scenarios are produced for different initial state scenarios (Hollingsworth, 1980). These scenarios constitute an ensemble forecast that increases forecastability with respect to individual forecasts (Déqué, 2003) and makes it possible to better assess the associated uncertainties. The forecastability of atmospheric models on a seasonal scale varies greatly for different regions. For a given region, forecasts may be impossible for certain seasons.

Other types of seasonal meteorological forecasts may be envisaged. For example, in certain contexts, seasonal anomalies of meteorological variables may be partly explained by major climatic phenomena affecting some parts of the entire globe. This is for example the case for the monsoons in Asia or for precipitation on the Pacific coast of South America, strongly influenced by the El Niño phenomenon (see Addendum 12.3). In such contexts, seasonal forecasting requires determination of a statistical relationship between one or more quantifiable indices of these phenomena and the given seasonal variable on the basis of observed historical data (Section 12.1.5 or Webster and Yang, 1992). The main drawback of this approach is the short length of time series generally available to establish the required relationships. The statistical significance of these relationships is therefore generally limited.

If the seasonal meteorological forecast is not sufficiently informative, the associated hydrological forecast is of little interest unless the temporal evolution of hydrological variables over the months to come is highly dependent on the initial state of the hydrological system (e.g., snowpack). In this context, a possible approach consists in using the observed climatology to establish different forecast scenarios. The *N* years of the past for which meteorological observations are available can be used to produce *N* scenarios for the future, thereby providing a seasonal meteorological (and subsequently hydrological) ensemble forecast (Figure 12.9) (Carpenter and Georgakakos 2001; Houdant, 2004).

The interest of this climatological approach increases with: 1) the dependence of future inflows on the initial state of the considered hydrological system and 2) the divergence of the initial state of the system from the average state of the system for the same period of the year. However it decreases with the divergence of the temporal evolution of the meteorological variables over the months to come from the typical temporal evolution. This approach is therefore of limited interest in a climate-change context.
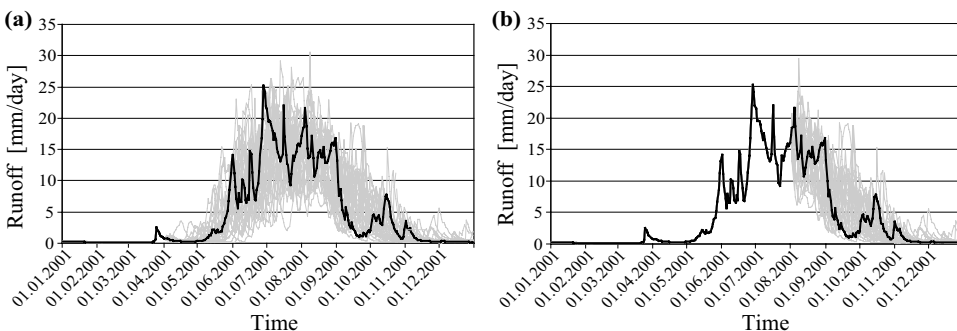

Fig. 12.9: Seasonal ensemble forecasts of discharges on the Dranse de Bagnes drainage basin in Switzerland for the year 2001 on the basis of 29 years of precipitation/temperature observations (1972 to 2000). Forecasting was carried out using the GSM-SOCONT model (Schaefli *et al.*, 2005) on two different dates: a) March 1 and b) May 1. The available snowpack on the basin was obtained for these two dates by simulations.

12.2.4 Uncertainties, Anticipation Time and Implications

As already mentioned, meteorological forecasts are subject to major uncertainties. For precipitation, these uncertainties concern the occurrence of events (rain vs. no rain) and their temporal distribution, spatial distribution (in particular their location and extent), intensity, volume and phase (rain vs. snow). Uncertainty concerning the phase results in part from the uncertainty associated with temperature forecasts. Although the uncertainty concerning the precipitation phase is often considered negligible, it can have a considerable influence on the estimation of potential flood volumes, in particular in mountainous regions (Chapter 7).

Whatever the method considered, uncertainties increase with the considered anticipation time. For nowcasts and short-term or medium-term forecasts, these uncertainties depend on the meteorological situation. For instance, precipitation forecastability is higher for frontal systems than for convective events.

Finally, uncertainties increase with the considered spatial and temporal resolution. It is therefore generally not advised to use the forecasted variable fields at their initial resolutions. Forecasted fields are consequently often averaged over spatial and temporal scales that increase with the considered anticipation time (Figure 12.10). Precipitation forecasts are therefore often provided for hourly or infra-hourly time steps for nowcasting, 6-hour to 12-hour periods for short-term forecasts, daily periods for medium-term forecasts and 10-day periods or even months for seasonal forecasts. The optimal scale for the description of meteorological forecasts also depends in principle on the type of meteorological event considered.
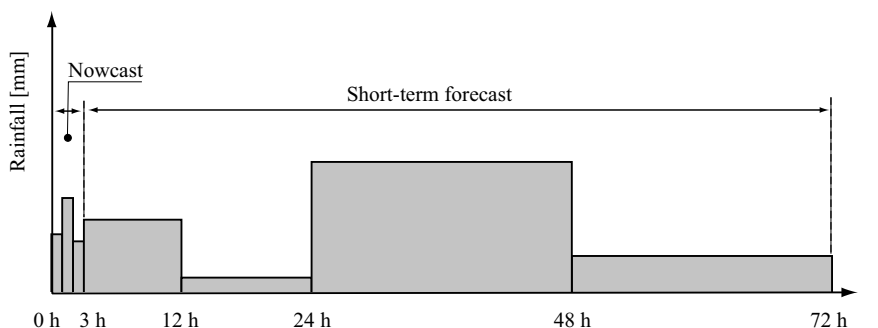

Fig. 12.10: Typical temporal discretization for precipitation forecasts.

12.2.5 Ensemble or Probabilistic Forecasts

To at least partially take into account the major uncertainties presented above, probabilistic or ensemble forecasts are necessary (Krzysztofowicz, 2001a, b; Palmer *et al.*, 2002).

Probabilistic forecasts provide the probability distribution for the different variables of interest over one or more selected forecast periods.

Meteorological ensemble forecasts provide a discrete number of possible future meteorological scenarios. Each of these scenarios corresponds to a possible temporal evolution of the different meteorological variables simulated by the forecasting model

over the selected forecast period. Ensemble forecasts are increasing used as a basis for probabilistic meteorological forecasting. The principles underlying these forecasts are presented below.

Meteorological ensemble forecasts

Meteorological ensemble forecasts are used primarily to characterize forecasting uncertainties related to uncertainties in the initial conditions of the meteorological forecasting model used (Section 12.2.3). This is the principle of the ensemble forecasting system proposed by the ECMWF that has been supplying 50+1 probable meteorological forecasting scenarios for 10-day forecasts since the year 2000 (Molteni *et al.*, 1996; Palmer *et al.*, 2002).

Ensemble forecasts can also take into account uncertainties related to imperfections in the atmospheric model used. These uncertainties concern: 1) the simplifications required to represent the environment—in particular topography and land use and 2) the solutions of differential equations. They also concern the parameterization selected for the modeling of sub-grid scale processes and the uncertainty in the values of the corresponding parameters —linked in particular to their spatial variability that is rarely taken into account (Risbey and Stone, 1996).

Consequently, different atmospheric models produce different forecasts for the same initial conditions (Hulme *et al.*, 2002; Frei *et al.*, 2003). It is therefore of interest to consider ensemble forecasts produced by several models, considering that the credibility of the results is reflected by the agreement between the respective forecasts. For this reason, the ECMWF produces seasonal forecasts that combine, in a super-ensemble with 63 members, the nine 6-month forecasts of seven recent European atmospheric models (DEMETER project; Palmer *et al.*, 2004; Gneiting and Raftery, 2005).

Probabilistic estimates using statistical adaptation

When the MOS technique (Section 12.2.2) is used to adapt forecasts produced by an atmospheric model, a probabilistic estimate of the variable of interest can be obtained. For this, the uncertainty present in the relationship between the variable to be forecasted and the explanatory variables must be characterized.

An appropriate MOS analysis can also be carried out to describe the probability distribution of the variable of interest. A MOS analysis for different classes of precipitation depth is often used to provide a Probabilistic Quantitative Precipitation Forecast (PQPF) (Antolik, 2000). A PQPF defines the probability of rain and, if rain occurs, the probability that the precipitation belongs to different predetermined classes of precipitation depths. PQPFs are generally produced for daily precipitation. A PQPF can also provide the probable temporal distribution of precipitation during the day (Krzysztofowicz, 1998).

Probabilistic estimates using analog adaptations

The analog method (Section 12.2.2) can also be used to produce an ensemble forecast since the *k* nearest analogs with respect to the forecasted synoptic situation can be extracted from historical data. Consequently, the *k* plausible meteorological situations for the days to come can be proposed as forecasting scenarios. These different analogous situations are not necessarily equiprobable and the probability of occurrence of each can be adapted according to its nearness to the forecasted situation. A probabilistic forecast can also be obtained by

fitting a frequency-based model to the different values of the variable of interest for these
k meteorological situations (PQPF—Bontron, 2004) (Figure 12.11).

The above approach, often referred to as the *k*-nearest neighbor method, is preferred
over the approach that uses only the nearest analog. The number *k* of analogs to be used is
a model parameter determined by calibration in order to optimize the forecasted value. It
increases with the considered anticipation time. For the sites considered by Bontron (2004),
for example, the optimal number of analogs varies from around 30 for a D+1 forecast
to around 500 for a D+5 forecast. This is related to the fact that the forecast provided
by the atmospheric model becomes less informative as the anticipation time increases.
The number of possible meteorological situations in fact tends rapidly to infinity and the
forecast then reflects the climatology.

As for the MOS technique, the analog method can obviously be used to adapt the
different members of an ensemble forecast provided by one or more atmospheric models.
This provides a better representation of the real uncertainty associated with meteorological
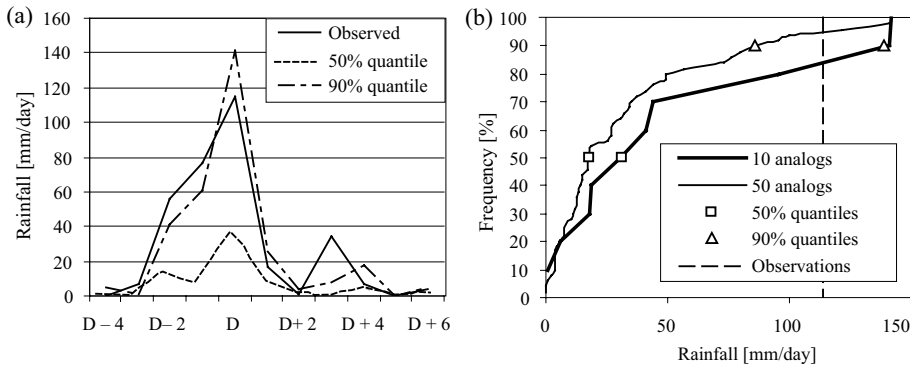forecasts.

Fig. 12.11: Probabilistic quantitative forecast of regional rainfall in the upper Valais region of Switzerland obtained
using the analog method (analog based on the 850 hPa geopotential altitude field). a) 50% and 90% quantiles as a
function of anticipation time considering the 50 closest analogs (from 20/09/1993 to 30/09/1993). b) Distribution
of forecasted precipitation for 24/09/1993 using the 10 or 50 closest analogs.

12.3 DESIGN RAINFALL

The most common and oldest meteorological scenario used by hydrologists is the
design rainfall. This is a rainfall hyetograph chosen or defined to produce, via rainfall-runoff
simulations, a design flood that can be used to design or assess hydraulic structures.

The design rainfall is often identified or determined on the basis of observations for
a selected return period corresponding to an acceptable risk for the studied system.[4] This
is the most common approach and results in the use of a historical design rainfall or a
design rainfall based on Intensity-Duration-Frequency curves (i.e., IDF curves). A second
approach considers the design rainfall to be the highest physically possible precipitation

---

[4]Rainfall information required, for example when dimensioning a project, can also be derived from the statistical
behavior of maximum precipitation. This information can be used directly, as in the Gradex method, to extrapolate
the behavior of maximum flood flows to rare frequencies (Chapter 9).

that can fall on a given area at a given site in a given climatic area. This is referred to as the probable maximum precipitation (PMP) (WMO, 1986). These different types of design rainfalls are presented below.

12.3.1 Observed Design Rainfall

The design rainfall can be chosen among rainfall events that have already occurred and that have been recorded at or near the site of interest. It may be a common event (short return period) or an extreme event that resulted in a major catastrophe in the region. In this case, the design rainfall is referred to as historical. The observed design rainfall is often chosen to satisfy two conditions. It must be: 1) representative of the spatial and temporal distribution of precipitation over the studied hydrological system and 2) have a return period roughly equal to the return period of the design flood to be calculated.

Estimating the return period of a real rainfall event is often a difficult task. The return period of the maximum mean intensity depends on the duration over which the mean intensity is estimated (Figure 12.12). The return period of a rainfall event is therefore not unique. An average return period is often estimated by considering preferentially the return period obtained for the maximum mean intensities corresponding to durations close to a given duration. This duration is often the critical duration for the hydrological system that may be exposed to the event.

Note that it is often impossible to identify an observed rainfall event with an average return period corresponding to that of the project. This is generally the case when an "extreme" design rainfall is to be determined. A major observed rainfall event is sometimes artificially boosted (i.e., each increment of the hyetograph is multiplied by a constant factor) so that the corresponding return period corresponds to the desired return period for the project.
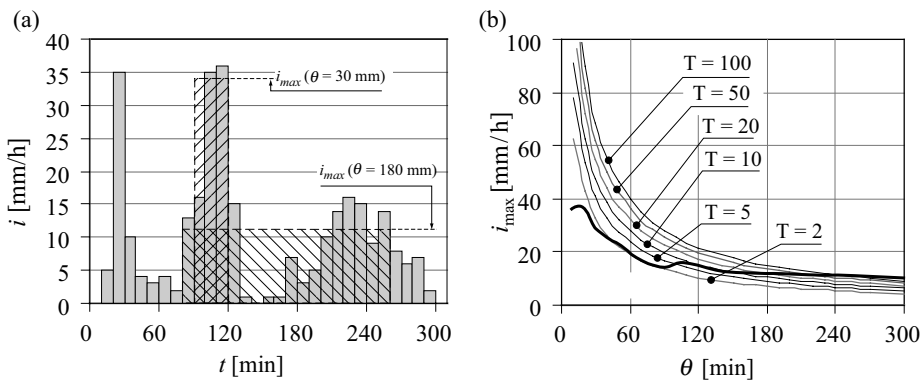

Fig. 12.12: Return periods of the maximum mean intensities of a given rainfall event for different durations. a) 10-minute time step hyetograph of precipitation observed on 21/08/2000 at Pully station (Switzerland) and maximum mean precipitation for two durations θ (30 and 180 minutes). b) Position of the rainfall event on the IDF curves obtained at Pully rain-gage station (1981–2004 period). Estimated return period for the event: 2 years or less if the critical duration to be considered is less than 90 minutes and 100 years or more if the critical duration is greater than 4 hours.

12.3.2 Synthetic Design Rainfall

Depending on the context of the required analysis, IDF curves (Appendix 12.8.1) are often used to construct a block design rainfall or a synthetic design hyetograph. A synthetic design rainfall can be constructed using various methods such as those of Desbordes (1984) or Cordery and Pilgrim (1984).

"Block" design rainfall

A "block rainfall" is a uniform rainfall defined by a rectangular pulse with a constant intensity equal to the mean intensity over the rainfall duration.

The duration used for this rainfall is the critical duration for the considered hydrosystem. When estimating flood discharge, this duration is often (but not always) equal to the concentration time of the corresponding drainage basin (Chapter 9). When sizing a storm retention basin, this critical duration depends among other factors on the possible release rate (Chocat, 1997).

The mean intensity used to determine the "block" design rainfall over this critical duration is the maximum mean intensity obtained for the return period of the project based on the pertinent IDF curve for the considered site (IDF curve of the site or region concerned).

Design hyetograph derived from IDF curves

Different methods have been proposed to derive a design hyetograph from pertinent IDF curves for the considered site.

The first method consists in applying a separately determined temporal distribution to a given "block rainfall". The mean intensity for the "block rainfall" is first obtained using the method described above. The temporal distribution is selected from different dimensionless rainfall curves established for the region (Appendix 12.8.3). These can be typical curves based on certain events observed in the region or curves simply based on particular observed events. They are generally in the form of a dimensionless curve of accumulated rainfall or a dimensionless hyetograph (Musy and Higy, 2011).

Knowing the "block rainfall" (duration and mean intensity), the intensity $i(t)$ of the design rainfall can be determined at time t using the following equation:

$$i(t) = i_{\max}(T,D) \cdot r(t/D) \tag{12.2}$$

where $i_{max}(T,D)$ is the maximum mean intensity of the design rainfall obtained using the IDF curve of the region for duration D and return period T where $r(t/D)$ is the value of the dimensionless distribution of dimensionless time t/D. Design rainfalls obtained with this method have been widely used in the past. The most widely known typical curves are the dimensionless distributions developed in the United States by the Soil Conservation Service for 6-hour and 24-hour rainfalls. Note that the dimensionless precipitation curves depend strongly on the type of precipitation considered (Figure 12.13). The curve used for the design rainfall must therefore be consistent with the curve of critical events for the considered hydrosystem.
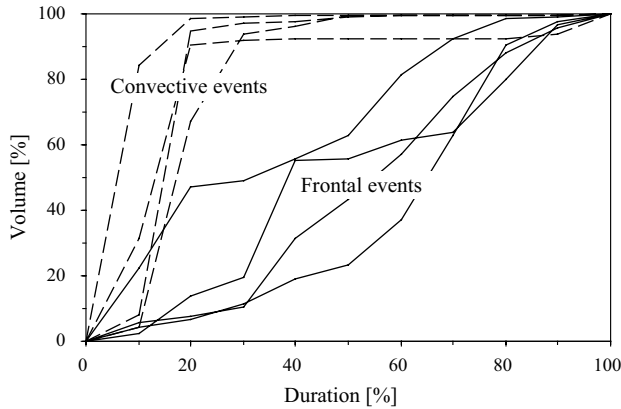
Fig. 12.13: Temporal distributions of various precipitation events observed at Payerne station (Switzerland). Dotted curves are for high-intensity, short duration convective events observed in summer. Solid curves are for very long duration frontal events observed in winter.

Another currently used method produces a single-frequency synthetic hyetograph (Addendum 12.6). Different single-frequency hyetograph distributions can be constructed however they may not all be plausible. The distribution selected for use should be plausible with respect to the typical distributions of the observed events of interest for the considered region.

Addendum 12.6. Construction of a mono-frequency synthetic hyetograph

The IDF curve for the selected return period can be used first to estimate the maximum mean intensities $i_1, i_2, \ldots i_k, \ldots i_n$ for different durations d_k where $d_k = k\Delta t$ and Δt is the selected time step for the description of the design rainfall. Precipitation depths $h_1, h_2, \ldots h_n$ for the first, second and n^{th} time step of the hyetograph are then estimated one after another in such a way that the maximum mean intensities of the hyetograph over k consecutive time steps are equal to intensities $i_1, i_2, \ldots i_k, \ldots i_n$. For this, the following equations are used successively:

$$h_1 = i_1 \cdot \Delta t \tag{12.3}$$

$$h_1 + h_2 = i_2 \cdot 2 \cdot \Delta t \qquad \text{therefore} \quad h_2 = i_2 \times 2 \cdot \Delta t - h_1 \tag{12.4}$$

$$h_1 + h_2 + h_3 = i_3 \times 3 \cdot \Delta t \quad \text{therefore} \quad h_3 = i_3 \times 3 \cdot \Delta t - (h_1 + h_2) \tag{12.5}$$

etc.

where h_k is the precipitation depth on the kth time step and i_k is the maximum mean intensity with a return period T for a duration $k\Delta t$ given by the appropriate IDF curve: $i_k = i_{max}(k\Delta t, T)$. The final distribution for the rainfall event is obtained by an appropriate temporal reorganization of rainfall depths $h_1, h_2, \ldots h_n$. For this, the depths are positioned successively in decreasing order around the rainfall body that is progressively constructed. For example, they can be positioned alternately to the right and left of the maximum depth h_1. Other arrangements are obviously possible, leading to asymmetrical rainfall distributions (Figure 12.14).

The so-called Chicago hyetograph (Keifer and Chu, 1957; Chow *et al.*, 1988) is a mono-frequency synthetic hyetograph. Its particularity is that it is described in a continuous manner rather than in a discrete manner as above. The intensity $i(t)$ is derived from a Talbot type analytical expression of the IDFs. It includes a parameter that expresses the degree of asymmetry of the design hyetograph. This parameter is assumed to depend on the region considered.
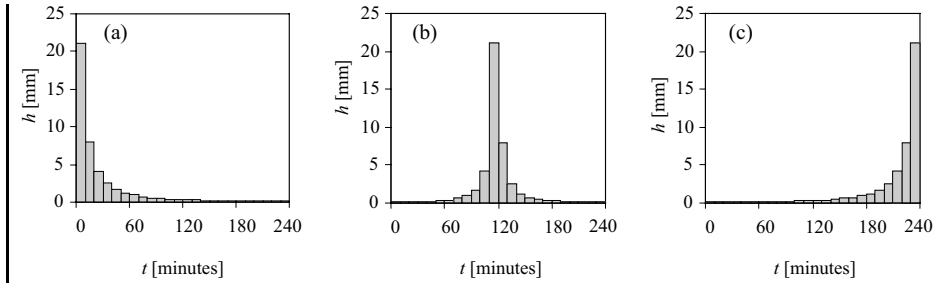
Fig. 12.14: Three mono-frequency synthetic rainfall distributions based on the same IDF curve. a) Right-skewed "lagging" distribution. b) Centered distribution. c) Left-skewed "leading" distribution.

12.3.3 Probable Maximum Precipitation

The probable maximum precipitation (PMP) is widely used to describe a quantity of precipitation approaching the upper physical limit of precipitation that can fall on a certain geographic area over a certain duration (WMO, 1986).

Given the complexity of the processes involved in the production of precipitation, current methods used to derive PMPs are based mainly on maximizing the key meteorological variables that govern precipitation (e.g., humidity, temperature, saturated vapor pressure of the air, wind speed and direction and convective or orographic phenomena). For a given region and duration, a PMP is generally estimated for each meteorological situation that can be potentially observed during the different seasons of the year (e.g., PMPs for air movements coming respectively from the eight quadrants). The greatest precipitation depth among the depths estimated for the different meteorological configurations is then selected as the PMP for the considered geographical area.

These methods are summarized in Chapter 29.4 of the Manual for Estimation of Probable Maximum precipitation published by the WMO (1986). The maximum local precipitation depths recorded on the surface of the Earth, also presented in the WMO publication, can prove useful to check the plausibility of estimated PMPs. These maximum depths are presented in Figure 12.15 as a function of the considered duration.

PMPs are especially used in Great Britain and North America (for dam design) where the national meteorological institutes publish PMP maps or atlases for different rainfall durations.
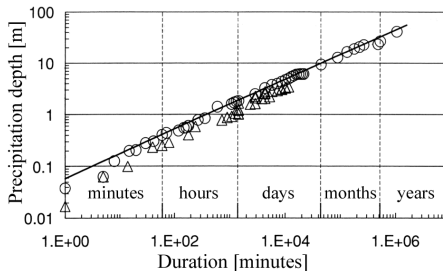

Fig. 12.15: Maximum precipitation depths observed for different durations. The equation of the upper envelope curve is: $P = 0.0584 \, D^{0.48}$ with P in meters and D in minutes (adapted from WMO, 1986).

Over and above the uncertainty of PMP estimates, their major drawback is that their exceedance probability is unknown. Finally, information relative to PMPs is often summarized on a regional scale in the form of maps expressing the PMP at each point. In practice, however, this information is unusable given that the PMP estimated at a given point does not necessarily come from the same meteorological situation as the PMP estimated at a point nearby. Note that every hydrological application requires a rainfall scenario that is consistent on the drainage basin scale. This limitation is particularly important in regions with marked orography.

12.3.4 Spatial Design Rainfall

For most hydrological applications, the drainage basin is too large to assume that the precipitation falling on the basin is equal to the point design rainfall estimated elsewhere. All other factors being equal, the maximum mean precipitation depths decrease with increasing area. In addition, on the scale of a drainage basin, critical rainfall events can have different typical spatial distributions. If this spatial dimension is taken into account, determination of the design rainfall becomes even more complex.

Different approaches can be used to estimate the spatial design rainfall. Their respective principles are similar to those of the methods used to attribute temporal distributions to a point design rainfall.

When the design rainfall is a historical event, the spatial distribution is simply the observed distribution. If IDF-area curves are available for the region (Appendix 12.8.1), the severity of the event can be estimated by positioning the observed rainfall on these curves, following the same principle as in Section 12.3.1. This severity can be represented in a summary manner using a diagram indicating the return period of the maximum mean intensity observed during the event as a function of the duration and area used to calculate this intensity (Figure 12.16). An average return period for the event can finally

Fig. 12.16: Return periods of maximum mean intensities of a rainfall event observed in the Marseille region (France) on 19 September 2000 (adapted from Ramos *et al.*, 2005). Left: Map obtained by kriging of the total precipitation depth falling over the duration of the event (the light line is the coastline). Right: Event severity diagram showing the return period of the maximum mean intensity observed during the event as a function of the duration and area used to calculate 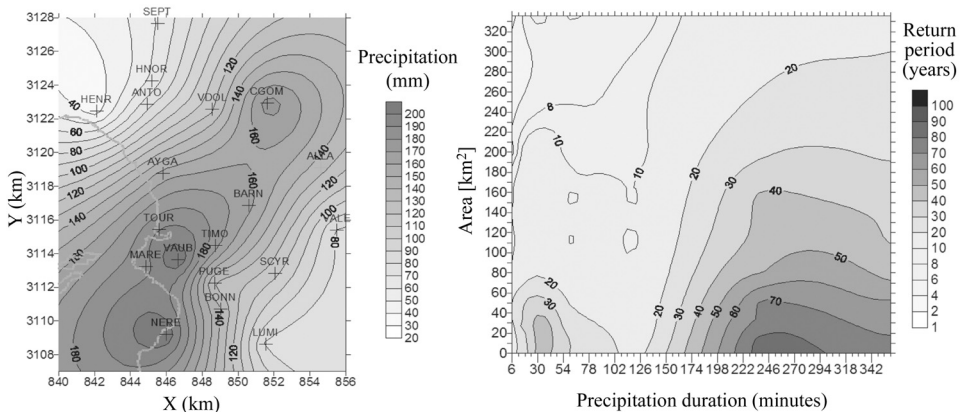this intensity. Estimated return periods for the event: 10 years for an area of 10×10 km^2 and a duration of one hour; 100 years for an area of 10 km^2 and a duration of 3 hours.

be roughly estimated by considering the return periods obtained for areas similar to that of the hydrological system of interest and for durations similar to the critical duration of precipitation for the system.

When a spatial block rainfall is sufficient (i.e., uniform rainfall in time and space for the considered duration and area), the maximum mean precipitation depth is obtained using the IDF-area curves of the region, if they exist, or by applying an areal reduction factor to the point intensity obtained on the basis of regional IDF curves. This factor can be expressed:

$$a(S) = 1/(a + S)^b \qquad\qquad (12.6)$$

where k is the reduction factor, A is the area of the drainage basin and a and b are two parameters estimated on the basis of rainfall observations available for the considered region.

A synthetic spatial rainfall can also be produced on the basis of IDF-area curves for the region. Different approaches are possible, all based on the same principles as those already presented for the construction of synthetic point hyetographs. The first approach consists in applying a typical spatial distribution and temporal distribution (deduced from observations) to a spatial block rainfall. Another approach leads to mono-frequency synthetic design rainfall. It consists in deducing the maximum mean precipitation depths for different areas from the IDF-area curves. The spatial distribution is then obtained by successive differences in the same way as already described for the construction of point mono-frequency synthetic hyetographs (Addendum 12.6). A simple typical shape, as close as possible the shape considered to be representative of critical precipitation for the considered basin, is generally used for this purpose (e.g., a circle or an ellipse with a chosen orientation).
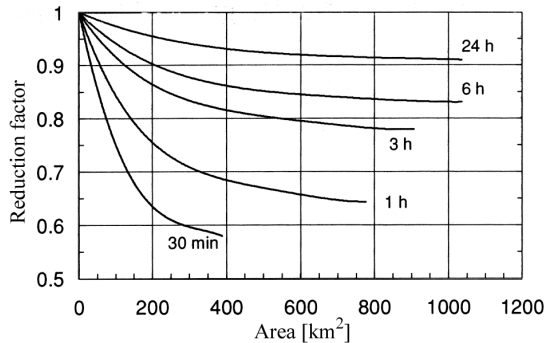
Fig. 12.17: Areal reduction factor used to transform point rainfall into spatial rainfall (adapted from Brutsaert, 2005).

12.4 GENERATING METEOROLOGICAL SCENARIOS

Hydrological studies increasingly rely on continuous simulations of the hydrological behavior of hydrosystems over long time periods that reflect the full variability of meteorological forcings. The reason for this is that optimal management of water resources must take into account both exceptional and ordinary hydrological events.

In addition to precipitation, the meteorological information required for these analyses includes meteorological variables related to water and energy transfers at the soil-vegetation-atmosphere interface (e.g., wind speed, net radiation, temperature, relative humidity). If available, time series observed for these different variables—in and/or near a given hydrosystem—represent a prime source of project design data. Such series may however be insufficiently long to fully portray the hydrological variability induced by the variability of meteorological forcings. In some cases, such data may not even exist for the considered hydrosystem.

The time series required for hydrological analysis are therefore increasingly generated by special models, often referred to as weather generators. The development of these models is presently an important field of research for hydrologists. Such models are many and varied. Most were developed for a specific hydrometeorological objective and context. Just like hydrological models, they have neither the intention nor the capacity to provide a universal solution.

12.4.1 Possible Approaches

Weather generators should be able to produce all the meteorological variables required for a given hydrological model (e.g., Richardson, 1981; Semenov *et al.*, 1998; Lafaysse *et al.*, 2013). Among these variables, precipitation is the most difficult to generate. Although other variables will be discussed, the objective of this section is primarily to present several approaches that can be used to generate rainfall scenarios. Three types of generators may be distinguished. In increasing order of complexity, these are:

- Mono-site generators designed to produce precipitation time series at a single rain-gage station.
- Multi-site generators designed to produce concurrent precipitation time series at two or more rain-gage stations.
- Spatio-temporal generators designed to produce precipitation at each point of a defined spatial and temporal domain.

The generation of rainfall scenarios does not necessarily require an in-depth understanding or detailed description of the mechanisms behind the formation and dynamics of precipitation events. Most the time, it is based on a simple empirical or conceptual description of the dynamics observed for these events. The ideal data for such modeling are those of observation networks combining conventional ground stations and meteorological radar (Chapter 2). BPSAT-Niger (Lebel *et al.*, 1992), OHMCV (Delrieu *et al.*, 2005) and HYDREX (Wheater *et al.*, 2000) are good examples of this type of network. These ideal networks, often set up in the framework of large national or international research projects, are obviously extremely rare and are not representative of typical data available for developing weather generators. Most weather generators are therefore based solely on observations from a discrete number of rain-gage stations. In such a context, the full spatial dynamics of precipitation remains unknown and therefore cannot be reproduced. The large majority of weather generators are therefore limited to mono-site or multi-site generation, i.e., the generation of precipitation time series at the station or stations where observations are available.

Weather generators are mostly of the stochastic type. They consider the observations of atmospheric variables of interest to be the result of a random process. The necessarily statistical and simplified description of this process can be used to generate different realizations of these variables by Monte Carlo simulation. The structure and parameterization of weather generators are optimized in such a way that the generated time series reproduce as accurately as possible certain key statistical characteristics of the observed variables (Addendum 12.1). Certain weather generators are sometimes used, after calibration on the current climate, to generate meteorological scenarios for climate-change studies (Section 12.5).

The following sections and the appendices of this chapter present the main approaches used to generate multi-site and spatio-temporal precipitation series. Since the end of the 20th century, a great deal of effort has been focused on developing such approaches. They differ greatly in terms of both concepts and complexity. Most multi-site generators tend to generalize mono-site approaches, some of which were developed as far back as the mid-1980s. Mono-site generators will therefore not be dealt with specifically here. For more information on these models, the reader can refer to publications by Wilks and Wilby (1999) and Hingray (2003). Recent reviews of key modeling issues for multi-site multi-variate weather generation have been proposed by Wilks (2012) and Hingray *et al.* (2013).

12.4.2 Multi-site Generation of Precipitation Series

Multi-site weather generators are either empirical or conceptual models. Generators requiring the estimation of various parameters are referred to as parametric and the others as non-parametric. The most recent multi-site generators take into account the synoptic-scale atmospheric circulation of the current day. They have been developed to generate precipitation time series with a selected time step (e.g., monthly, daily, infra-daily).

The main difficulties confronting multi-site generation are: 1) reproduction of the process that determines the occurrence or non-occurrence of precipitation at each station, i.e., the simulation of the succession of rain and no-rain sequences for which the statistical characteristics (e.g., durations) are the same as those of the observed sequences, 2) simulation of precipitation depths at each station that reproduce the statistical distributions of observed precipitation depths and, in particular, 3) reproduction of the spatial and temporal correlations between rainfall series observed at different stations (occurrence, precipitation depths).

Whatever the multi-site generator used, precipitation information is generated on a point basis at different sites of the considered area. For the targeted hydrological applications, this information must therefore always be spatialized in order to produce the spatial data required by hydrological models. The difficulties related to this spatialization process are the same as those already discussed for the spatial interpolation of data (Chapter 2).

Empirical parametric generators

Although many empirical parametric models have been developed for mono-site generation of precipitation time series (Richardson, 1981; Johnson *et al.*, 1996; Onof *et al.*, 2000), the case of multi-site generators is somewhat problematic. The main difficulty lies in the reproduction of correlations between stations.

Empirical parametric generators are mostly based on a two-step simulation process. The first step involves simulating the occurrence or non-occurrence of precipitation at each of the stations. Then, if precipitation occurs, the next step it is to generate the precipitation depth (Bardossy and Plate, 1992; Wilks, 1998; Hughes *et al.*, 1999). These models operate at time steps greater than or equal to a day. They are generally not suitable for shorter time steps.

For each station, occurrence is often generated on the basis of a uniform random variable for which the realization is compared to the probability of occurrence of rain or no rain for the day. This probability of occurrence depends on the state of the previous day (Wilks, 1998) and sometimes also on the state of a low-frequency circulation index, e.g., monthly indices such as the North-Atlantic Oscillation Index (NAOI) (Wilby, 1998; Katz *et al.*, 2003). This generation process produces an occurrence time series indicating wet and dry time steps for each station.

For wet time steps (i.e., with rain), the precipitation depth is generated by a random variable drawn from an appropriate statistical distribution (e.g., gamma or mixed exponential distribution). This generation process produces a time series indicating the precipitation depths for each station for the selected time step.

The inter-station correlation for both the occurrence and precipitation depths is often obtained using Gaussian random driving variables that are multi-variate and correlated (Wilks, 1998; Mezghani and Hingray, 2009). The underlying principles of such models are described in detail in 12.8.4.

Rectangular-pulse parametric generators

Rectangular-pulse parametric generators assume that rainfalls are made up of an agglomeration of superimposed rain cells (Figure 12.18). Well-known multi-site models of this type include those derived from Neyman-Scott and Bartlett-Lewis rectangular-pulse mono-site models, often referred to by their respective acronyms NSRPM and BLRPM.
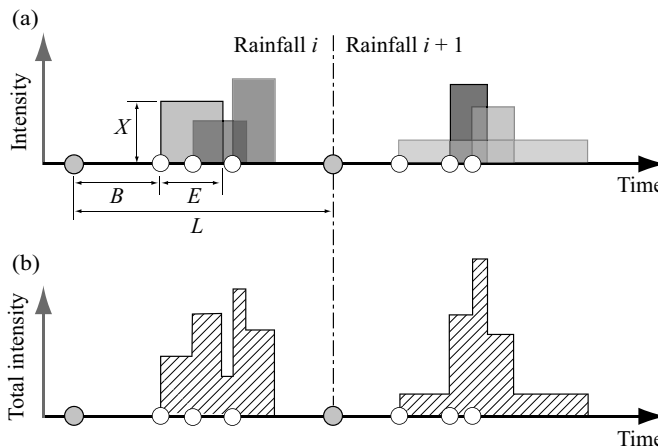
Fig. 12.18: Principle behind a rectangular-pulse mono-site generator designed to produce a precipitation series. a) Rainfall events and cells generated within the events. b) Rainfall intensities obtained by integrating the intensities of the different generated cells. The different random variables used for the generation of rainfall events and cells are the duration L of the rainfall event from the origin, the position B of each cell within the event, its duration E and intensity X and the number of cells C within the rainfall event.

For a given station, the occurrence of rainfalls as well as the occurrence and other characteristics (duration, depth) of the associated cells are generated on the basis of appropriate statistical distributions. The cells have rectangular pulse shapes, hence the name of the models.

With this approach, multi-site weather generation rapidly becomes complex, introducing a variety of difficult problems. The main difficulty consists in determining a rain-cell generation process that can reproduce the spatial correlations between stations. The various strategies presently used relate the generation of rain cells at each of the stations to a master process that describes rainfall occurrence for the considered region (Figure 12.19). The underlying principles of some of these strategies are discussed in Appendix 12.8.5. A complete review of the corresponding models and the methods used to estimate the associated parameters can be found in Onof *et al.* (2000).
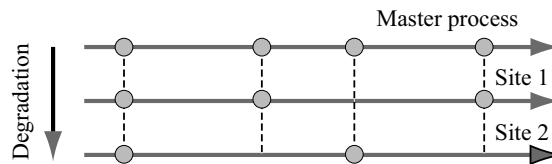

Fig. 12.19: Part of the principle of a rectangular-pulse multi-site generator. A stochastic master process is used to generate the occurrence of rainfalls on the region and a degradation process is used to generate the occurrence of rainfalls at two sites within the region.

Non-parametric generators

Two types of non-parametric generators exist. In both cases, the philosophy of the generation method is based on the "same cause, same effect" concept already presented (Section 12.2). If the cause is known for a given day, the corresponding effects can be estimated by identifying situations observed in the past that had similar causes.

In the present context, the "effects" to be determined are the precipitation depths at each of the stations for which observed data are available over the historical period considered. These effects can include other meteorological variables, such as temperature or sunshine duration, also observed at stations over the historical period (Wojcik *et al.*, 2000; Lafaysse *et al.*, 2013).

The "causes" taken into consideration to explain these effects are different depending on the model. Buishand and Brandsma (2001), for example, consider that the causes are related to the regional meteorological situation of day *D* that precedes day *D+1* for which the local variables must be generated. The situation of day *D* is described by the regional precipitation and temperature of the day—estimated on the basis of the local precipitation and temperatures generated in a previous step for this day. The causes can also be defined by the synoptic-scale atmospheric circulation of the current day (Wojcik *et al.*, 2000; Lafaysse *et al.*, 2013). In this case, the method assumes that two atmospheric situations that are similar on a synoptic scale lead to meteorological situations that are similar on a local scale (Section 12.1.4).

For this type of generator, it is always necessary to determine: 1) the variables to be used to describe and compare the causal situations (e.g., geopotential altitudes for a certain pressure level) and 2) the measurements to be used to identify the *k* nearest causal

situations with respect to the target local meteorological variable (e.g., precipitation at different stations within the basin).

Meteorological variables for the different days of a given period are generated progressively according to the following principle. First of all, it is assumed that the generation process has been applied in such a way as to produce, at a daily time step, a rainfall scenario for the N first days of a given generation period. It is also assumed that the data required to describe the causal situation of day $N+1$ are available. For day $N+1$, the generation process consists in: 1) identifying the k nearest causal situations in the past, 2) assigning a probability of occurrence to each of these situations, determined for example as a decreasing function of its similarity with respect to day $N+1$ and 3) randomly selecting one of the k situations. All the local variables of the causal situation selected in this way are finally used as the multi-site (and multi-variate if applicable) scenario for day $N+1$.

If the causal situation taken into account is the synoptic-scale atmospheric situation, different possible resemblance criteria and variables are indicated in Addendum 12.2 and Section 12.2.2. The data series required to determine the resemblance variables can be extracted from meteorological re-analysis data (Boé, 2007; Mezghani and Hingray, 2009). They can also be extracted from "climate experiment" output produced by a physical model of the atmosphere for some past or future climate (Zorita and von Storch, 1999).

If the causal situation is supposedly related to atmospheric circulation, weather generation can extend over the period covered by available meteorological re-analysis data or by the "climate experiment". If the causes are uniquely related to the variables generated for the days preceding the current day, weather generation can cover a period of infinite duration. In all cases, the stochastic nature of the generation process makes it possible to generate any number of time series (Lafaysse *et al.*, 2013). However, to avoid reproducing a time series that is identical to the observed series of the local meteorological variables, the number k of similar situations, at each time step, from which the analog situation is selected must be greater than or equal to 2.

Once the method has been set up and refined, scenarios can be easily generated. The main advantage of these methods is that it is possible to 1) simulate some or all of the local meteorological variables available from the past (e.g., precipitation, temperature, sunshine duration) and 2) produce consistent local meteorological scenarios, i.e., scenarios that conserve, for a given day, the spatial and temporal structures of the variables as well as the correlations between them (Chardon *et al.*, 2013). In addition, the generated local variables can have a temporal resolution less than that of the generation process (generation often being carried out for a daily time step).

The method also has a number of limitations. For example, it cannot be used to produce meteorological configurations other than those that have already been observed. It also requires that the causes and their effects have been observed simultaneously over a sufficiently long historical period.

12.4.3 Spatio-temporal Precipitation Generators

Spatio-temporal precipitation generators are far less popular than multi-site generators. First of all, they are complex both in terms of accessibility and implementation. Secondly, estimation of their many parameters is often a source of major difficulties given that the data required for the calibration (radar imagery and a precipitation series measured

at conventional stations) are rarely available. Some of these generators are presented for information purposes in Appendix 12.8.5 (parametric models based on cells clusters) and Appendix 12.8.6 (parametric models forced by Gaussian fields and physical models of the atmosphere).

12.4.4 Key Problems Related to the Generation of Scenarios

Temporal and/or spatial disaggregation

In many situations, the meteorological scenarios produced by a given model are not at the spatial and/or temporal scales required for the simulation of the hydrological behavior of the hydrosystems of interest. For example, hydrological analysis in urban environments generally requires time series with short time steps (10 minutes or less) while only hourly time series are available. This is also often the case when the time series of precipitation depths are generated at the drainage basin scale whereas the spatial variability of the precipitation is known to have a major effect on the hydrological response (Marty *et al.*, 2012).

Models used to produce high-resolution data from low-resolution data are referred to as disaggregation models. A further distinction can be made between temporal, spatial and spatio-temporal disaggregation models. For each type of disaggregation, many approaches are possible. First of all, let us consider the non-parametric approaches. They are based on the same principles as those of the analog and *k*-nearest neighbors models presented in Sections 12.2.2 and 12.4.2. A situation similar to the situation for which disaggregation is necessary is selected among the *k* nearest historical situations that have been identified on the basis of a selected similarity criterion. Disaggregation of the variable of interest then consists simply in applying the structure of the selected situation (spatial and/or temporal structure) on the variable. The *k* nearest situations are sometimes also identified among situations generated elsewhere using an appropriate stochastic generator (Segond *et al.*, 2006). Non-parametric disaggregation techniques are sometimes referred to as fragment methods (Wojcik and Buishand, 2003). Their field of application extends beyond the scope of precipitation disaggregation alone. A method of this type has for example been used by Mezghani and Hingray (2009) to produce multi-site precipitation and hourly temperature scenarios on the basis of regional precipitation and temperatures generated previously for a daily time step.

Disaggregation can also be carried out using certain multi-site or spatio-temporal models (e.g., disaggregation of precipitation depths using the modified turning bands method—Lebel *et al.*, 1998; Vischel, 2006 or temporal disaggregation of daily data using the NSRPM rectangular-pulse model—Wheater *et al.*, 2005).

Another disaggregation approach is based on certain scale invariance properties of precipitation. It has led to the development of parsimonious disaggregation models requiring for example the estimation of only two or three parameters. Among these models, multiplicative cascade fractal models can be used to generate series of data possessing these scale invariance properties (Over and Gupta, 1996; Deidda *et al.*, 1999; Mouhous, 2003). The volume of precipitation observed within a certain space-time domain is divided into *b* space-time sub-domains on the basis of a selected stochastic process. This operation is

repeated for each of the sub-domains until the final required spatial and temporal resolution is reached (Figure 12.20). These approaches are described in greater detail in Appendix 12.8.2.
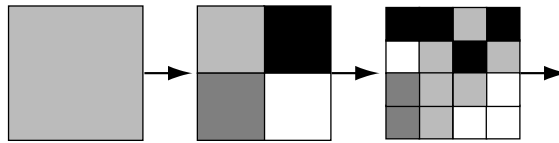

Fig. 12.20: Principle behind a disaggregation model based on discrete multiplicative cascades. The volume of precipitation falling on the initial spatial domain is divided into *b* sub-domains and so on.

Generators conditioned by atmospheric circulation

Many authors have mentioned the difficulty or even the impossibility of simulating precipitation series that reproduce the observed inter-annual variability (Wilks and Wilby, 1999; Srikanthan and McMahon, 2001; Wilby *et al.*, 2002). However, reproduction of this variability is essential for any meaningful hydrological analysis. For example, it is necessary to be able to generate long periods of dry years or wet years.

Weather generators conditioned by atmospheric circulation, also referred to as statistical downscaling models, can be used to partially solve this problem. Depending on the selected modeling options, this conditioning leads to the following types of generators:

- Parametric models (Section 12.4.2) for which the parameters are estimated differently for each of the *n* weather types previously identified for the region. For each day of the considered period, weather generation then consists in: 1) identifying the weather type closest to the atmospheric circulation pattern of the day and 2) generating the required local meteorological variables for the day using the generator parameterization optimized for this weather type. The weather generator proposed by Bardossy and Plate (1992) is an example of this type of model.
- Non-parametric *k*-nearest neighbor type models (Section 12.4.2) in which the similarity between the current day and days of the past is defined on the basis of the fields of various synoptic-scale atmospheric variables or on the basis of atmospheric circulation indices derived from these fields. The generator proposed by Wojcik *et al.* (2000) is a model of this type.
- Parametric models based on so-called transfer functions that express the variables to be explained (e.g., probability of occurrence of precipitation, expected value of precipitation depth if precipitation occurs, etc.) as a non-linear function of appropriate atmospheric circulation indices. The most widely used transfer functions are generalized linear models. The generator proposed by Bellone *et al.* (2000) is a model of this type (Appendix 12.8.4).

Note that many models are combined approaches for which the temporal information required to condition the generator (fields of atmospheric variables, atmospheric circulation indices) is extracted from meteorological re-analyses (e.g., NCEP or ERA40 re-analyses; see Chapter 2) or from climate experiments carried out using general circulation models (Section 12.5.3). Given that the scaling relationship between synoptic-scale atmospheric variables and local meteorological variables is not unequivocal, downscaling models are generally stochastic. For example, for transfer-function type models, a random disturbance

is often applied to the precipitation depth estimate obtained on the basis of synoptic explanatory variables (Mezghani and Hingray, 2009).

Downscaling models offer a number of advantages. Because their parameterizations do not necessarily require adaptation to the different types of rainfall events that can be observed in the region of interest, they are relatively parsimonious compared to non-conditioned approaches. They can be used: 1) to generate a certain seasonal and inter-annual variability—related to that of the considered synoptic-scale atmospheric variables and, in particular, 2) to induce a certain spatial and temporal correlation between the generated variables even if this correlation is not explicitly described in the simulation model (Qian *et al.*, 2002). Regarding these two important aspects of weather generation, the performance of downscaling models is always better than that of non-conditioned generators. Finally, they represent the best approach available today to generate meteorological scenarios in a climate-change context.

12.5 METEOROLOGICAL SCENARIOS IN A CLIMATE-CHANGE CONTEXT

Global climate change, related in part to the increase in greenhouse gases resulting from human activities, has already significantly modified regional climates and will continue to do so in the future. The resulting changes concerning the hydrological behavior of hydrosystems and consequently on water resources and hydrological risks must be assessed to prepare the inevitable adaptations that our society will have to undertake. Assessment of the hydrological impact of expected climate changes requires the availability of meteorological scenarios adapted to the spatial and temporal scales of the considered regions, drainage basins and hydrological systems.

Presently, most meteorological scenarios used for such impact assessments are developed from the output of climate models. The main aspects are presented below.

12.5.1 Background and Definitions

According to the Intergovernmental Panel on Climate Change (IPCC), a climate scenario is a "a plausible and often simplified representation of the future climate, based on an internally consistent set of climatological relationships, that has been constructed for explicit use in investigating the potential consequences of anthropogenic climate change, often serving as input to impact models". Similarly a climate-change scenario is "the difference between a climate scenario and the current climate" (IPCC, 2001).

12.5.2 Emission Scenarios and Climate Models

On a global scale, climate-change scenarios are produced using global climate models, often referred to as General Circulation Models (GCMs). These numerical models describe, with a varying degree of completeness and simplification, the processes that are known to affect climate such as atmospheric, oceanic and biogeochemical processes and the characteristics of the Earth's surface (e.g., sea ice and continental surfaces). They combine various sub-models that are often independent (e.g., atmospheric circulation, ocean

circulation, sea ice and carbon cycle models). Models that couple atmospheric and oceanic circulation are referred to as Atmosphere-Ocean General Circulation Models (AOGCMs). The IPCC provides a detailed description of these models (http://www.ipcc-data.org/).

For a given model, a climate-change scenario is obtained on the basis of datasets resulting from two types of numerical climate experiments that may be independent:

- "Control" experiments, that consist in simulating the climate for a historical period referred to as the control period. The standard control period used as the reference period in most impact studies often correspond to the 30 years 1961–1990 period but now most control experiments cover the entire post-industrial period (e.g., 1860–1999). The control experiment is in principle used to estimate the capacity of the model to reproduce the climate variability of this period. Model output for this period is compared to a wide range of data coming from observations. The reference data generally used for this comparison are typically meteorological re-analysis data that goes back to the 1950s (e.g., NCEP or ERA40 re-analyses) or to the 1860s for re-analysis delivered in recent years (e.g., 20CR and ERA-20C; see Chapter 2).

- "Future climate" experiments, that consist in simulating the future climate or future changes to the present climate related to the considered greenhouse gas emission scenario for the targeted period or time in the future. Several sets of scenarios have been commissioned and approved by the IPCC over the past two decades. New scenarios are created periodically to reflect advances in research, new data, and to support the increasing sophistication of integrated assessment and climate models. Standard scenarios commonly used in the recent years for climate research are described in Addendum 12.7. At the beginning of the 21st century, most future climate experiments were produced for the future period 2070–2099 or for different intermediate periods (e.g., 2020–2050). With the more powerful computing resources available today, future scenarios are mostly transient scenarios, now covering the entire 21st century.

The datasets (different atmospheric and surface meteorological variables) corresponding to these "control" and "future climate" experiments are often accessible on dedicated Internet sites such as that of the IPCC (see http://www.ipcc-data.org/ and other web sites indicated in Appendix 2.7.6).

Note that the data obtained with a specific climate model for given "control" or "future climate" experiment depends on the initial conditions of the simulation. Several simulations are therefore often carried out for the same climate experiment using different initial conditions. These are referred to as the "members" or "runs" of the simulation ensemble. Three such simulations are often carried out and considered separately to produce different climate-change scenarios (for the same emission scenario and the same climate model). In climate experiments for the pre-industrial control period (which fix the atmospheric composition prior to industrialization), such simulations can be run for several centuries with no atmospheric forcings to evaluate the internal variability of GCMs, i.e., their ability to simulate the natural variability of climate corresponding to the chaotic nature of meteorological phenomena.

For a given variable, the climate-change scenario that corresponds to the "control" and "future climate" experiments is often described in terms of variations between the control period and the future period (e.g., variation of mean precipitation depths, their variability or their probability of occurrence). To simulate the possible change of the Earth's climate

for a given emission scenario, climate models require relatively long computing times. This limits the spatial resolution of their discretization. For most of them, the horizontal grid of the atmospheric circulation model had a resolution at the Earth's surface of around 200 to 300 km at the beginning of the 21st century. This resolution is obviously not fine enough for impact assessments given that a country like France, for example, would be represented by only 5 to 10 grid cells depending on the model.

Addendum 12.7 IPCC greenhouse gas emission scenarios

The emission and accumulation of so-called greenhouse gases (GHGs) in the atmosphere has been identified as the main cause of present and future climate change (IPCC, 2007). The standard scenarios used in the beginning of the 21st century for numerical "climate experiments" describe the evolution of CO_2 emissions as well as emissions of other GHGs (IPCC, 2001).

The SRES scenarios,[5] as they are often called in reference to the IPCC Special Report on Emissions Scenarios, are described by Nakićenović and Swart (2000). Used in the early 2000s, they cover the entire 21st century and correspond to different socio-economic storylines for human activities. They were reviewed and revised as judged necessary for the IPCC Fourth Assessment Report (AR4) published in 2007. The SRES scenarios are grouped into four scenario families that explore alternative development pathways, covering a wide range of demographic, economic and technological driving forces and resulting GHG emissions.

- The A1 storyline assumes a world of very rapid economic growth, a global population that peaks in mid-century at 9 billion inhabitants, then decreases to 7 billion by the end of the century and a rapid introduction of new and more efficient technologies. The A1 scenario is divided into three groups that describe alternative directions of technological change aimed at eliminating energy dependence on fossil fuels: fossil intensive (A1FI), non-fossil energy resources (A1T) and a balance across all sources (A1B).
- B1 describes a convergent world, with the same global population as A1, but with more rapid changes in economic structures toward a service and information economy. This is the scenario that represents the lowest level of CO_2 emissions.
- B2 describes a world with intermediate population and economic growth, emphasizing local solutions to economic, social, and environmental sustainability.
- A2 describes a very heterogeneous world with high population growth (reaching 15 billion inhabitants at the end of this century), slow economic development and slow technological change.

Note that no likelihood has been attached to any of the SRES scenarios. Emission reductions that could result from a voluntary international agreement are not considered in any of these scenarios.

The Representative Concentration Pathways (RCPs) emission scenarios[6] were commissioned by the IPCC to underpin its 5th Assessment Report scheduled for completion in 2013/14. The development of these new scenarios follows a different process than previously. RCPs were not derived from specific socio-economic scenarios. They were chosen to represent a broad range of climate outcomes, based on a literature review. They are defined by their total radiative forcing (cumulative measure of human emissions of GHGs from all sources expressed in Watts per square meter) pathway and level by 2100. Each of the 4 RCPs retained by the IPCC is consistent with many socio-economic scenarios because different

---

[5]SRES scenarios: http://www.ipcc.ch/publications_and_data/ar4/syr/en/mains3.html
[6]RCP scenarios: http://sedac.ipcc-data.org/ddc/ar5_scenario_process/index.html

socio-economic futures could give rise to similar changes in atmospheric composition. They can therefore be used in parallel by:

- Earth System Models to explore future changes in physical and biogeochemical responses to changing atmospheric composition and radiative forcing
- Integrated Assessment Models (IA Model) to explore alternative socio-economic conditions that would result in such future atmospheric composition changes.

RCP description and citations (from http://www.ipcc-data.org)

	Description	IA Model	Publication – IA Model
RCP8.5	Rising radiative forcing pathway leading to 8.5 W/m^2 in 2100.	MESSAGE	Riahi *et al.* (2007) Rao and Riahi (2006)
RCP6	Stabilization without overshoot pathway to 6 W/m^2 at stabilization after 2100	AIM	Fujino *et al.* (2006) Hijioka *et al.* (2008)
RCP4.5	Stabilization without overshoot pathway to 4.5 W/m^2 at stabilization after 2100	GCAM (MiniCAM)	Smith and Wigley (2006) Clarke *et al.* (2007) Wise *et al.* (2009)
RCP2.6	Peak in radiative forcing at ~ 3 W/m^2 before 2100 and decline	IMAGE	van Vuuren *et al.* (2006; 2007)

For more and recent information, the reader can refer to the latest reports of the IPCC (http://www.ipcc-data.org) and to the following web-sites cited in footnotes 5 and 6.

12.5.3 Future Climate Scenarios Suitable for Impact Assessments

Different approaches have been developed to produce future climate scenarios from GCM output at the spatial and temporal resolutions required for impact assessments. The first are based on weather generators or downscaling models. Downscaling models can be of the dynamic or statistical type. Given that the climate experiment data required for these models is not always available, other methods have been proposed, often referred to as delta or perturbation methods.

The underlying principles of these different approaches are briefly presented below. For more information on this topic, the reader can refer to Wilby and Wigley (1997) Zorita and von Storch (1999), Xu (1999), Maraun *et al.* (2010).

These different approaches can be used independently or can be combined. The scenarios they produce are sometimes disaggregated by additional models to achieve sufficient spatial and temporal resolutions for the impact assessments to be carried out. A typical scenario production flow chart is illustrated in Figure 12.21.

Dynamic downscaling methods

Dynamic downscaling methods can be used to simulate the effects of global changes on selected regions of the globe with a finer spatial resolution than that provided by GCMs (Leung *et al.*, 2004; Christensen *et al.*, 2007). It is possible to distinguish between Regional Climate Models (RCMs) and Variable Resolution General Circulation Models (VR-GCMs). RCMs cover limited regions of the globe and are constrained on their lateral boundaries
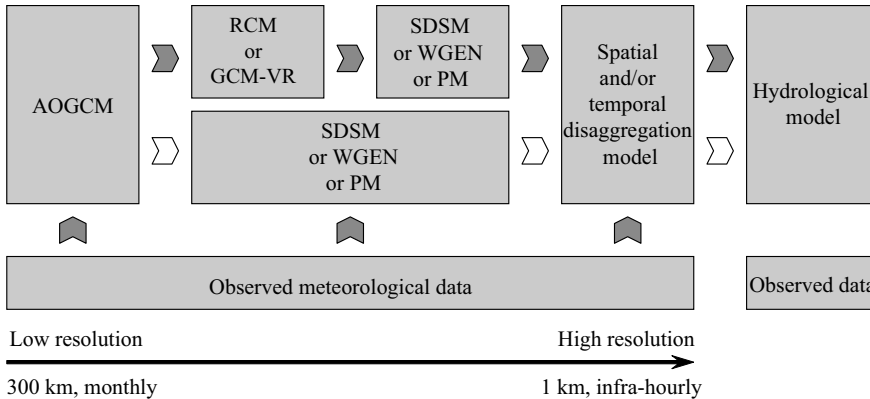
Fig. 12.21: Typical methodologies for the production of climate-change scenarios at the spatial and temporal resolutions required for impact assessments. AOGCM refers to GCMs combining atmospheric and oceanic circulation models. RCM and GCM-VR refer to dynamic downscaling models, SDSM to statistical downscaling models, WGEN to weather generators and PM to perturbation methods, all described in Section 12.5.3.

and for the ocean boundary conditions by AOGCMs (see the Swiss CHRM model—Vidale *et al.*, 2003 and the Swedish RCAO model—Räisänen *et al.*, 2004). VR-GCMs cover the entire globe but with a higher resolution for the region of interest, comparable to that of regional models (e.g., around 0.5°, corresponding to approximately 50 km in temperate regions). They are also constrained by AOGCMs for the ocean boundary conditions. This is the case for certain models developed by CNRM and IPSL (Dufresne *et al.*, 2006), for example the ARPEGE model in which the grid can be tilted and stretched by changing the position of the pole to increase the horizontal resolution over an area of interest.

Dynamic downscaling models offer a promising way of deriving the meteorological scenarios required for impact assessments. Direct use of the data for impact assessments is however still somewhat delicate. The performance of regional climate models first of all depends strongly on the biases inherited from global models, which can be considerable (van Ulden and van Oldenborgh, 2006). Moreover, their ability to represent forcing induced on a regional scale by topography or the heterogeneity of the Earth's surface (land/sea separation, vegetal cover) is still very limited (Section 12.6.2). Their outputs are therefore classically post-processed so that they can be applied to impact studies (e.g., bias correction, perturbation).

Statistical downscaling methods

As already discussed (Section 12.1.4), local atmospheric variables are strongly influenced by the synoptic-scale meteorological situation. Moreover, synoptic-scale atmospheric variables related to the dynamic parts of climate models are in principle better simulated by climate models than local meteorological variables, some of which are highly dependent on the parameterization selected for the associated physical processes (Section 12.2.2). Statistical downscaling methods therefore once again offer a promising alternative for the production of future meteorological scenarios suitable for impact assessments (Xu, 1999). They are based on various empirical relationships established, for the control period, between certain atmospheric variables (provided by meteorological re-analyses and simulated elsewhere by climate models) and the required local meteorological variables.

Statistical downscaling methods are many and varied. The different types of conditioned generators discussed in Section 12.4.4 belong to this category. These include analog methods (Zorita and Von Storch, 1999; Buishand and Brandsma, 2001), statistical transfer functions (Wilby *et al.*, 1998a,b) and weather generators conditioned by atmospheric circulation patterns (Stehlik and Bardossy, 2002, Xu *et al.*, 2007). These methods can also be combined (Bellone *et al.*, 2000; Vrac *et al.*, 2007; Mezghani and Hingray, 2009). They can also be used to generate various meteorological variables, for example precipitation and temperature (Wilby *et al.*, 1998a,b), wind speed (Yan *et al.*, 2006) or potential evaporation (Yang *et al.*, 2005). Addendum 12.8 describes how they can be used to generate future meteorological scenarios. This is also illustrated in Figure 12.22.
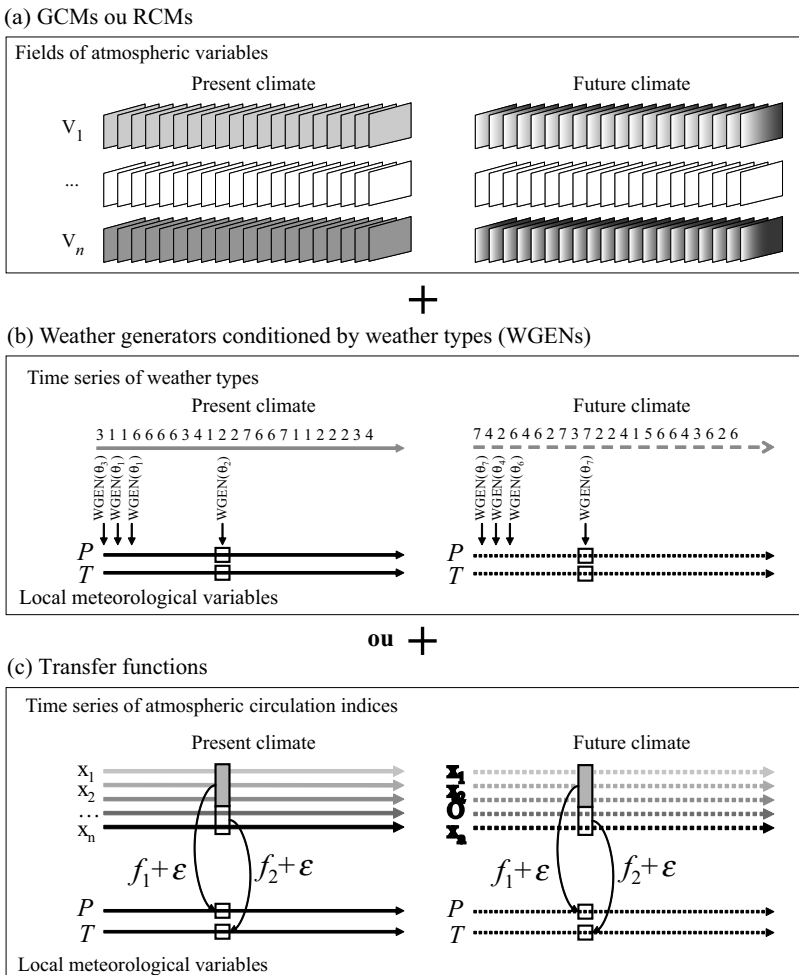
Fig. 12.22: The principle behind two statistical downscaling approaches for generating future scenarios. a) Synoptic-scale fields of atmospheric variables simulated by the climate model for the present and future climates. These fields provide the input variables for downscaling methods. b) Time series of weather types extracted from these fields and generation of local meteorological variables by a generator conditioned by weather types. c) Time series of different atmospheric circulation indices derived from the fields and generation of local meteorological variables by a statistical transfer function (ε refers to the residual of the relationship in this configuration).

This statistical characteristics of meteorological variables generated for a given period in the future using these methods are different than those of the variables observed for the control period. The cause and nature of the corresponding modifications depends on the type of statistical downscaling method used. If the method is for example the transfer function type, the modification will be the result of changes in the statistical characteristics of the indices used to describe the atmospheric circulation. If the method is based on the nearest-neighbors approach or if the generator is conditioned by the weather types, the modification will be the result of changes in the statistical characteristics of these weather types (frequency, persistence, probability of transitions between weather types).

Whatever the statistical downscaling method considered, the scaling relationships identified between the local and synoptic variables for the current climatic situation are assumed to remain unchanged for the targeted future period. This constitutes the main limitation of these methods. Other limitations are mentioned in Section 12.6.2.

> **Addendum 12.8 Implementing statistical downscaling methods**
>
> The development and use of statistical downscaling methods to produce future climate scenarios generally involves two steps.
>
> - In the first step, the conditioned generator is developed and parameterized on the basis of a historical dataset generally corresponding to (or including) the standard control period (1961–1990). Pertinent information on synoptic-scale atmospheric circulation is extracted from re-analyses available for the period (e.g., NCEP or ERA-40 re-analyses, see Chapter 2). The information on the required local meteorological variables (e.g., basin precipitation) is derived from time series of variables observed on or near the hydrosystem of interest (rain-gage stations, climatological stations).
> - In the second step, pertinent information on synoptic-scale atmospheric circulation is extracted from "climate experiments" supplied by climate models for the future period and the future climate-change scenario of interest. This information is then used as input to the generator developed in the first step in order to generate local meteorological variable scenarios for the future period. This information may be pre-processed to correct for any systematic bias that may have been identified between the observed values of the explanatory variables and the values obtained for the control period using the data simulated by the climate model.

Weather generators

Future scenarios are sometimes generated using weather generators that are not conditioned by atmospheric circulation. This approach is often classed as a statistical downscaling approach even though it is not really based on the same principles.

The generators used are parametric generators with parameters that can be estimated on the basis of certain key statistical characteristics of the local meteorological variables to be simulated (Section 12.4.2). For the control period, these characteristics are estimated on the basis of observations. For the future period of interest, they are estimated on the basis of observations and the outputs of "control" and "future climate" experiments produced by climate models. A commonly used method for this estimation is presented in Addendum 12.9.

Addendum 12.9 Estimating the future statistical characteristics of a local meteorological variable

Estimation of the statistical characteristics of a local meteorological variable corresponding to a given future climate scenario is a common problem.

When the variable of interest is an output variable of the climate model, these characteristics can in principle be extracted directly from time series produced by the model for the considered future scenario. However, this approach is not recommended given the present limitations of climate models with regard to simulating surface meteorological variables.

In practice, future statistical characteristics are estimated on the basis of: 1) the values of these characteristics estimated for the present climate on the basis of observations and 2) their changes between the control period and the considered period in the future. These changes are simply estimated here from the "control" and "future climate" experiments carried out using climate models (Overney *et al.*, 1997; Wilby *et al.*, 1998a,b; Wilks, 1999). This approach is based on the postulate that climate models better simulate the changes of the variables of interest than the absolute values of these variables. In other terms, for the "control" and observations, the bias of the models is assumed to be the same for the considered period in the future.

With regard to this, the following points must be emphasized.

- The changes considered depend on the variable of interest. For instance, changes in the variable can be considered in absolute terms (e.g., change of the mean temperature in °C) or relative terms (e.g., relative change of the seasonal precipitation in mm/mm). Another example concerns changes in the transformation of the variable of interest (e.g., log-odds transformation of the probability of occurrence of daily precipitation—Wilks, 1999). This type of change is often encountered in problems concerning the domain over which the variables are defined.
- Changes to the local variable required for impact assessments are assumed to be equal to the changes estimated at the regional scale on the basis of climate model outputs:

$$\Delta X_{site\ k} = \Delta X_{region} \tag{12.7}$$

- where $\Delta X_{site\ k}$ is the change of the statistical characteristic X at the local scale for site k (between the scenario to be constructed and observations) and where X_{region} is the change of this characteristic at the regional scale (between "future climate" and "control" experiments).
- Given the limitations of climate models, regional changes are often estimated using the output from the considered model over a region covering several calculation grid cells.
- For the same reason, changes estimated on the basis of model outputs generally concern statistical characteristics related to variables that have been averaged or accumulated over a long time step (e.g., monthly or seasonal totals). For example, changes in the mean and the coefficient of variation of monthly precipitation are often estimated.
- Changes over such time scales (e.g., monthly) are generally insufficient to estimate the parameters of weather generators that are often based on changes of the characteristics of the variable over a shorter time step (e.g., daily). Estimation of these characteristics is often based on theoretical or empirical models expressing these quantities as a function of quantities at longer time scales (Overney *et al.*, 1997; Wilks, 1999).
- The changes indicated by the models can strongly depend on the period of the year (e.g., less precipitation in summer and more precipitation in winter). The statistical characteristics of the variable of interest and consequently the parameters of the weather generator are therefore ideally modified differently for different periods of the year.

Delta or perturbation methods

These methods consists in producing future scenarios by applying simple perturbations on the time series observed for the control period (Etchevers *et al.*, 2002; Shabalova *et al.*, 2003). The series observed for the different sites of interest are simply shifted and/or expanded so as to reproduce the changes of the mean and variance obtained between the "control" and "future climate" simulations of a given climate experiment (Addendum 12.10).

> **Addendum 12.10 A temperature perturbation method**
>
> Perturbation of a daily temperature series observed at a given thermometer station over the period 1961–1990 is often carried out using the following equation:
>
> $$T_{scen,s}(t) = [T_{obs,s}(t) - MT_{obs,s}] \cdot (XSDT_s + 1) + MT_{obs,s} - XMT_s \qquad (12.8)$$
>
> where $T_{scen,s}(t)$ (°C) is the local temperature obtained by perturbation for the future scenario considered at day t for season s (s = 1: DJF; s = 2: MAM; s = 3: JJA; s = 4: SON). $T_{obs,s}(t)$ (°C) is the temperature observed at the station during the control period on day t of season s. $MT_{obs,s}$ (°C) is the mean temperature observed at the station for season s. XMT_s is the absolute change of the mean seasonal temperature. $XSDT_s$ are, for season s, the relative change of the standard deviation of daily temperatures. Both these changes are estimated at the regional scale and for the season s on the basis of climate model simulations for the future and control periods (Addendum 12.9).
>
> This type of perturbation is not necessarily suitable for other meteorological variables. For precipitation, for example, this method can lead to negative values and a multiplicative correction factor must be used to avoid this. The reader can refer to the method proposed by Prudhomme *et al.* (2002) or Shabalova *et al.* (2003) for this variable. The method proposed by Shabalova *et al.* (2003) can also be used to modify the statistical distribution of observed precipitation to match the modifications of this distribution indicated by the "control" and "future climate" experiments, while respecting for the future the statistical rank obtained for the present climate for each of the precipitation values of the observed series.

12.5.4 Climate Scenarios Produced by the Pattern Scaling Method

Future climate-change scenarios are also sometimes produced from climate experiments using the pattern scaling method initially introduced by Santer *et al.* (1990). This method is for instance well-suited when future climate experiments are available for a future period that is different than the one of interest. This method is based on the assumption that a scaling relationship exists between average warming on the global scale and the regional climate response simulated by the considered GCM or RCM. The regional climate response is defined here by the absolute or relative change of various regional climate variables used for impact assessments (e.g., regional warming and modification of the mean precipitation depth for each season, modification of the number of rainy days and the precipitation variability for each season) between the control period and the future period. The changes estimated by this method are generally applied as input to simple models used to produce future scenarios, for example the weather generators and perturbation methods described in Section 12.5.3.

In many studies, the scaling relationship is assumed to be linear. In this case, it is characterized for each climate variable considered by a scaling ratio that is simply the regional change expected per degree of global warming. In the studies of Jones (2000), Hulme *et al.* (2002) and Hingray *et al.* (2007a), for example, this scaling ratio is the seasonal regional warming or the change in seasonal precipitation depths per degree of global warming (expressed respectively in °C/°C and mm/mm/°C). Appendix 12.8.7 describes how this method can be used to generate future scenarios.

12.6 CHOOSING APPROPRIATE METHODS

The main objective of the previous sections was to present various methods designed to produce the meteorological forecasts and scenarios required for hydrological analysis. These methods are many and varied and a number of criteria can be used to choose the most appropriate for a given case. This choice will first of all depend on the type of meteorological information required, which in turn depends on the type of hydrological information required for the analysis to be carried out. The choice will also depend on the nature and availability of the input data required to use the different methods.

For meteorological forecasting methods, other selection criteria have been presented in Section 12.2. For precipitation scenarios, a few additional aspects will be dealt with in the following sections. The scenarios used for hydrological analysis will first be presented. Then the choice of appropriate methods to produce them will be dealt with, whether these scenarios are required for the present or future climate.

Note that it may be necessary to develop scenarios for key meteorological variables other than those related to rainfall. In mountainous regions, for example, estimation of snowmelt and the snowline require spatial knowledge of the elevation of the 0°C isotherm. In the same way as for rainfall, the required scenarios can be obtained on the basis of an appropriate statistical analysis of the corresponding variables (e.g., Lafaysse *et al.*, 2013). Scenarios for the 0°C isotherm elevation required for flood forecasting can for example be extracted from the statistical distribution of this variable for the season presenting the greatest risk of flooding. In all cases, if other meteorological variables must be considered, pertinent spatial and temporal structures must be proposed that are consistent with those proposed for precipitation. Such meteorological data can be used for hydrological studies carried out either for the present or future climate.

12.6.1 Useful Precipitation Scenarios

In the past, the design or assessment of hydraulic structures (e.g., retention basins, irrigation works, drainage networks) in a given drainage basin was based solely on a design rainfall, i.e., a unique rainfall event meeting certain statistical criteria (in particular a specific return period).

Today, the need to take hydrological variability between events, seasons or years into account in many hydrological studies has led hydrologists to consider the temporal variability of precipitation. For this, either a wide range of design rainfalls, referred to here as a catalog, can be used or one or several time series of the meteorological variables of interest.

The advantages and drawbacks of each of these three types of design rainfalls—single event, catalog of events and time series—are presented below.

Single-event design rainfall

In the past, the design "block rainfall" and hyetograph provided the key information on precipitation for most common hydrological analyses. The significant advantage of this approach is that once the design rainfall has been identified or constructed, hydrological analysis becomes a quick and easy task.

Block rainfalls are often used for the preliminary design of simple hydraulic works. Determination of the maximum mean intensity of the corresponding rainfall for a given rainfall duration and a desired return period is often sufficient in this context. This information is for example necessary when using pseudo-empirical flood estimation methods such as the well-known rational method (Chapter 9). It is also required for the so-called "rainfall" method proposed by Chocat (1997) for the design urban storm retention basins (Chocat, 2007).

Design hyetographs are generally used to produce a design rainfall that can be applied to size diversion works, weirs or, under certain conditions, retention basins. Among the different types of possible design hyetographs, those constructed on the basis of IDF curves have long been and are still widely used today. The design hyetograph can be obtained simply and quickly and, in addition, the hydrologist does not even have to construct the IDF curves given that they are the most widespread form of hydrometeorological information, readily accessible around the world.

Although the design rainfall can be used for the preliminary design of a hydraulic structure, it is not recommended for final design work (Chocat, 2007). One of the main criticisms concerns the climatological representativeness of the IDF curves used, which is often highly limited for a given basin (in particular if the IDF curves are regional). Furthermore, the event-based approach itself presents some major limitations already mentioned in Chapter 9. The main limitation is that a design hyetograph supplies only one scenario among a multitude of possible rainfall scenarios. The single event-based approach is therefore largely insufficient when it is necessary to analyze frequent hydrological phenomena (weir overflows on storm drainage networks, operation and fill levels of storm retention basins).

Catalog of design rainfall events

To take the diversity of rainfall forcing into account, while avoiding the generally heavy computational requirements of approaches based on the use of complete precipitation series, a limited number of varied observed rainfall events is sometimes used to provide multiple event-based design rainfalls.

The set of rainfalls is first identified in the observed time series. To limit their number, they are sometimes classed according to their key characteristics with respect to the project. One or more rainfalls are then selected to represent each class (a probability of occurrence is generally assigned to each representative rainfall on the basis of the number of individuals per class). A catalog of design floods corresponding to the rainfall events of this design rainfall catalog is then obtained by simulation. This is referred to as a multi-event approach (Section 9.3.2.). The hydrological analysis is then carried out for all the events in the flood catalog.

The first difficulty encountered in this context is how to attribute a return period to the hydrological events obtained in this way. Another difficulty lies in the impossibility of taking into account close successions of rainfall events. Such successions can have a major influence when storage capacity is the key characteristic of the hydrological response of the studied system (e.g., storm retention basins).

Design rainfall time series

To take into account the diversity of rainfall events—whether in terms of maximum mean intensities, precipitation depths or spatial and temporal structures—the ideal solution is to carry out the hydrological analysis for a series of discharges obtained by simulations based on a complete precipitation time series. Frequency analysis, which is difficult to carry out on precipitation, is based directly on the hydrological variable of interest (e.g., maximum discharges, fill levels, overflows).

If the precipitation series required for the hydrological simulation are not available for the basin of interest, rainfall series observed near the basin can be used for this purpose. It is also possible to produce the required time series using an appropriate precipitation generator (Section 12.4). The interest of generating long continuous time series has already been discussed in previous chapters. In this regard, one of the main advantages of stochastic generators is that they can be used to produce as many time series as required (Section 9.3.2). A number of constraints must however be satisfied in order to generate pertinent time series. Some of these are reviewed in Addendum 12.11.

The use of continuous simulation to produce long series of discharges is obviously recommended if the objective is to analyze a frequent hydrological phenomenon. However, the most common criticism of this method raised by the hydrology community concerns the heavy computational requirements and the necessity of having a hydrological model that is capable of carrying out the continuous simulation.

Addendum 12.11 Constraints concerning the generation of precipitation series

Among the characteristics that must be reproduced by a generator to construct pertinent precipitation series, four merit special attention.

- **The statistical characteristics of the precipitation.** Generators are generally parameterized to reproduce certain standard statistical characteristics of observed precipitation series (Addendum 12.1). It is often important to evaluate the capacity of the generator to reproduce the statistical distributions of rare events (e.g., durations of dry periods, maximum precipitation intensities). These characteristics must be reproduced at the various spatial and temporal scales that are important for the considered hydrosystem.
- **The variability of rainfall events.** Good performance when reproducing the statistical characteristics of observed precipitation does not in any way guarantee that the generator properly reproduces the high variability of the types of precipitation that can be observed in a given region. Different parameterizations, often conditioned by different weather types, are often used to make it possible to reproduce different types of precipitation (Over and Gupta, 1994; Cowpertwait, 1995; Bellone *et al.*, 2000).
- **The seasonal variability of precipitation.** For parametric models, a common approach used to reproduce the seasonality of precipitation (types, frequencies, intensities, durations, etc.) consists in estimating the parameters of the model for each season or each calendar month. For non-parametric models, it is often worthwhile to 1) de-seasonalize the explanatory and explained variables and 2) restrict the search for similar situations to the inside of a sliding

window of 2 or 3 months centered around the current day (Wojcik *et al.*, 2000). In any case, part of the seasonality can be simulated indirectly by conditioning the generator to atmospheric circulation.

• **The inter-annual variability of precipitation.** A frequently reported limitation of generators is the difficulty in reproducing low-frequency variations of precipitation. Similarly, a generator calibrated for a wet period often cannot be used to generate scenarios suitable for dry periods and vice versa. The only satisfactory solution to this difficult problem appears to be conditioning generation to low-frequency atmospheric circulation indices (e.g., NAOI; SOI) known to present a significant correlation with precipitation (e.g.,; Wilby, 1998; Katz *et al.*, 2003).

Design rainfalls for urban environments

The usefulness of the different types of precipitation data depends on the objective of the hydrological analysis to be carried out. For example, useful design rainfalls for various common hydrological applications related to stormwater drainage in an urban environment are presented in Figure 12.23. The constraints that precipitation data must satisfy for these hydrological analyses are also indicated in Figure 12.24 (Chocat, 1997; Butler and Davies (2000); Berne *et al.*, 2004).

Design/planning	Possible problem	Cause of failure	Possible design rainfalls	Return period considered
Sewers	Overflowt	Intensity	Block rainfall	5 to 10 yrs
SRB	Overflow Pollution	Volume	IDF (block rainfall) Rainfall series (volume method)	> 10 yrs
OW	Pollution	Intensity	Block rainfall for sewers + design nomographs	2 to 5 yrs

Checking/evaluation				
Sewers	Overflow Pressure flow	Intensity	Design rainfall(s)	5 to 20 yrs
SRB	Operating frequency Overflow	Volume	Rainfall series	Any
OW	Pollution	Intensity	Catalog of rainfall events Rainfall series	Any Any
		Volume	Rainfall series	Any

Analysis/operation				
Calibration Validation	Model adequacy	Discharges Runoff volumes	Observed rainfalls + hydrographs	Any
Real-time control	P1: overlflow P2: pollution	Intensity Volume	Observed rainfalls (rain gages or radar)	Any

Fig. 12.23: Possible or recommended precipitation data for different types of hydrological analyses commonly used for stormwater drainage management in urban environments (SRB = stormwater retention basin, OW = overflow weir) (adapted from Butler, 2000 and modified).

	Rainfall record duration	Rain-gage location with respect to drainage basin	Temporal resolution required	Spatial resolution required	Synchronization error between station
Design/planning					
Sewers	>10 years	Near vicinity	Block rainfall	None	<30 minutes
SRB	>20 years	Near vicinity	Block rainfall	None	<30 minutes
OW	>5 years	Near vicinity	<15 minutes	None	<30 minutes
Checking/evaluation					
Sewers	>20 years	Adjacent	1 minute	None	<10 minutes)
SRB	>20 years	Adjacent	5 minutes	None	<20 minutes
OW	>10 years	Nearby	5 minutes	$\leq 5 \text{ km}^2/\text{gage}$	≤ 5 minutes
Analysis/operation					
Calibration Validation	Several events	Within	2 minutes	$2 \text{ km}^2/\text{gage}$	0.25 minutes
Real-time control	On-line	Within	2 minutes	$2 \text{ km}^2/\text{gage}$	0.25 minutes

Fig. 12.24: Constraints that must be satisfied by precipitation data for different types of hydrological analyses commonly used for stormwater drainage management in urban environments (SRB = stormwater retention basin, OW = overflow weir) (adapted from Butler and Davies (2000) and modified).

12.6.2 Selecting a Method to Generate Future Scenarios

Each of the different methods that can be used to produce future scenarios has its advantages and disadvantages, summarized in Table 12.1. The limitations of the three types of methods currently used to generate future scenarios suitable for impact assessments are also indicated in Addendum 12.11.

Selection of the best method for a given case depends on a number of factors. First of all, it depends on the local meteorological variables required for the impact assessment that is to be carried out. It also depends on the accessibility of data from "control" and "future climate" experiments. In this respect, note that whatever the climate data used to produce a scenario, it will always be necessary to check their quality by comparing the control data to observations. If necessary, the data should be corrected to eliminate bias if it is not excessive. Note also that climate models do not all offer the same performance for simulating the observed atmospheric circulation and that some of them show considerable bias when reconstructing the fields of certain key variables such as pressure (van Ulden and van Oldenborgh, 2006).

Table 12.1: Advantages and disadvantages of the main methods used to produce future scenarios at the impact assessment scale (adapted from IPCC, 2001, modified and expanded).

	Advantages	Disadvantages
Dynamic downscaling	• Provides a better description of atmospheric processes and the Earth's surface than GCMs (2) • Provides information with a higher resolution than GCMs (2) • Produces physically plausible scenarios (2) • Considered to better represent extremes (2, 4) • Produces consistent scenarios for the different local atmospheric variables considered (2, 3) • Can account for feedback processes (1, 2) • Model calibration does not require observations from the region of interest (5)	• A climatologist is required to implement the models (5) • Number of scenarios limited by long computing times (4, 5) • Simulation quality strongly dependent on GCM forcing (2) • Very limited performance for precipitation and for fine spatial and temporal resolutions (2, 5) • Requires correction of bias observed on the variables of interest (2) • Simulated variables depend on the GCM and the RCM parameterizations used (1, 2)
Statistical downscaling	• Provides information at a higher resolution than GCMs and for non-uniform regions (3) • Relatively fast and easy to develop and implement (5) • Can address variables not simulated by RCMs and at various spatial resolutions (3) • Fast application to RCM or GCM outputs (4, 5) • Can supply a large number of scenarios for a single RCM (4, 5) • Uses input data that is better simulated by RCMs than local meteorological variables (2) • Suitable for sites with limited computational resources (5)	• Calibration/verification requires long concurrent series of explained and explanatory variables (5) • RCM and GCM data required for estimation of the explanatory variables are not always available (5) • Scaling relationship stationarity assumption does not hold (1, 2) • Limited explanatory capacity of scaling relationships for precipitation (2) • Requires correction of bias observed on the variables of interest (2) • Generated results depend on: —the downscaling model and predictors considered (2) —the GCM and the RCM parameterizations used (1, 2)
Perturbation	• Very easy to implement (5) • Provides easy access to climate change scenario data for the means and variability of main local meteorological variables (3)	• The temporal and spatial structures of the observed series cannot be modified (2) • Cannot consider changes in exceptional events (frequency, duration and intensity) (4) • Cannot consider inter-annual variability (1, 3)

[a]Numbers in parentheses under Advantages and Disadvantages indicate that they are relevant to one of the 5 following criteria: (1) Consistency at regional level with global projections; (2) Physical plausibility and realism; (3) Appropriateness of information for impact assessments; (4) Representativeness of the potential range of future regional climate change; (5) Accessibility for use in impact assessments.

12.6.3 Uncertainty in Future Projections and Internal Variability of Models

Whatever the methods used to produce them, future climate scenarios are always highly uncertain. The sources of uncertainty are many and often combined. They are in particular related to choices concerning the emission scenario, climate model (AOGCMs, RCMs) and statistical downscaling method. The contributions of these different sources of uncertainty vary depending on the considered region, season, spatial domain and

local meteorological variable. For temperature change in Great Britain, for example, the uncertainty induced by the regional climate model was found to be less than that induced by the emission scenario, while the opposite was found to be true for precipitation (Rowell, 2006). The uncertainty induced by GCMs was considered to be greater than that induced by RCMs. They can however be similar in certain cases, for instance for mean summer precipitation changes in continental Europe (Dequé *et al.*, 2005; Hingray *et al.*, 2007a). Note that recent studies have shown that both of these sources of uncertainty can be negligible compared to the uncertainty associated with the internal variability of the models[7] (e.g., Hawkins and Sutton, 2011; Lafaysse *et al.* 2014; Hingray and Saïd, 2014). In any case, an impact assessment should therefore not be based on a single future scenario. Although it is impossible to cover the full range of uncertainty related to the production of future scenarios, it is essential to construct future climate scenarios, for a given emission scenario, using different general circulation models (AOGCMs) and different models for different downscaling methods, i.e., dynamic and/or statistical (Christensen *et al.*, 2007; Terray and Braconnot, 2007; Lafaysse *et al.*, 2014).

Similarly, any impact assessment should account for the internal variability of the model to assess if the estimated changes are significant or not. Changes in regional precipitation are classically found to be much less significant (and sometimes not significant at all even for the end of the 21th century) than changes in temperature (e.g., Hawkins and Sutton, 2009, 2011; Lafaysse *et al.*, 2014; Hingray and Saïd, 2014).

Addendum 12.12 Limitations of methods used to generate future climate scenarios

Limitations of dynamic downscaling models

Like general circulation models, regional climate models are imperfect representations of reality. This is the result of incomplete knowledge of certain key atmospheric and oceanic processes and also the necessity of simplifying the description of the environment and complex meteorological phenomena. Consequently, large systematic errors may exist between observed and simulated fields of various atmospheric variables obtained for the standard control period (1961–1990). This is particularly the case for the main variables required for hydrological models and analysis, i.e., surface temperature and precipitation. For these variables, systematic errors between control and climatological data for continental Europe were on the average around 2°C and 1 mm/day in the beginning of the 2000s (Déqué *et al.*, 2005; Jacob *et al.*, 2007).

Note also that the quality of simulations of the present by regional models decreases with the temporal and spatial scales. Although such models can roughly reproduce the spatial distributions of mean variables on a continental or sub-continental scale, their performance diminishes significantly on the regional scale. Consequently, certain climatologists recommend that results produced at the grid scale should not be used, even though they correspond more or less to the scale required by hydrologists. Moreover, even if the simulation time step of GCMs and RCMs is in the order of several minutes, the reliability of the output from the model is very modest for time steps less than a month (Prudhomme *et al.*, 2002). This is particularly the case for precipitation, for which the statistical characteristics (frequency, intensity, distribution)

---

[7]The internal variability of a model is usually considered to provide good insight into the natural variability of climate. The internal variability of any simulation chain composed of a GCM and an SDSM can actually be partitioned into its large-scale and small-scale components. The first can be estimated for instance by the different runs of a given GCM. The second can be estimated from the different stochastic generations obtained with a given SDM from the outputs of a given GCM run (Hingray and Saïd, 2013).

are still relatively poorly reproduced and the bias on maximum daily precipitation is, for certain models, at best of the same order of magnitude as that of the mean precipitation (Frei *et al.*, 2006; Boroneant *et al.*, 2006). These problems are particularly important for seasons during which precipitation is produced mainly by local atmospheric processes that require parameterization for modeling (convection). Moreover, orographic precipitation being among the most difficult variables to simulate using climate models (Giorgi and Mearns, 1991), these problems are also particularly important in regions with marked relief as illustrated by Frei *et al.* (2003) for five regional models evaluated for different European regions including the Alps.

All this makes it difficult to directly use local meteorological variables produced by these models for the future climate scenarios required for impact assessments. This is reinforced by the fact that the differences between the results for future and control periods are lower, for certain variables, than the differences between control and climatological data.

Limitations of statistical downscaling methods

The use of statistical downscaling methods to generate future meteorological scenarios is based on four important assumptions:

- Assumption 1: The variables used to describe synoptic-scale atmospheric circulation are property simulated by the climate models.
- Assumption 2: These variables are physically pertinent for explanation of the local meteorological variables and have a strong explanatory capacity.
- Assumption 3: These variables can be used to fully describe the climate change simulated by the climate model.
- Assumption 4: The scaling relationships identified between the local and synoptic variables for the current climate situation will not be modified in the future.

These assumptions also concern the dynamic downscaling methods, however to a lesser extent. The first assumption greatly limits the choice of possible predictors and favors the use of synoptic variables related to the dynamic parts of models rather than certain thermodynamic variables that could be more pertinent. In particular, the predictor that appears to be unimportant for the present climate can become essential in a climate-change context. For example, it is probable that future surface temperature changes will be more related to changes in the radiative properties of the atmosphere than to changes in circulation. The assumption concerning temporal stationarity of the scaling relationships is in fact impossible to validate or invalidate given that available data that can be used for this purpose presently cover a wide range of atmospheric situations that are a priori little representative of those that could be observed in the future. The validity of this assumption can however be considered with respect to: 1) the capacity of the model to reproduce the low-frequency variability of the local meteorological variables as observed throughout past decades and 2) the consistency of the results produced by the considered method with respect to the results obtained using dynamic downscaling methods.

Over and above the problems related to validating these assumptions, each of the different types of statistical downscaling methods has its own specific limitations.

For the methods based on nearest neighbors or conditioned by weather types, it is assumed that the future synoptic-scale atmospheric situations have already been observed today, which is not likely the case. For example, the expected warming of the atmosphere will increase the capacity of the atmosphere to store water vapor and therefore increase the specific humidity of the air masses. In this light, possible changes to local meteorological variables, in particular precipitation, will not be solely related to modifications concerning the frequency of weather types observed today (Hewitson and Crane, 2002).

The main limitation of methods based on transfer functions is that the predictors used often described only part of the variability of local meteorological variables. The percentage of variance explained by a precipitation occurrence model (or respectively precipitation depth model) is for example often less than 50% (respectively 40%) (Mezghani *et al.*, 2013). Moreover, the scenarios generated for the future are highly dependent on the chosen predictors and transfer functions (Lafaysse *et al.*, 2013).

The main limitation of the method that consists in modifying the parameters of a weather generator according to changes indicated by climate experiments is finally related to the often arbitrary manner in which these parameters are modified.

Limitations of perturbation methods

Perturbation methods can immediately produce future scenarios. They are however greatly limited mainly because the temporal structure of the perturbed series (i.e., occurrence, persistence and internal structure of the different meteorological events) is the same as that of the observed series. These methods are therefore of very limited pertinence, in particular if the objective is to represent the change in frequency, intensity and duration of major phenomena, whether at the event or seasonal scale. The same limitations are true for aspects related to the spatial variability of the phenomena.

In spite of certain adaptations aimed at limiting the effects of the above problems (Prudhomme *et al.*, 2002), the use of perturbation methods should be limited to rough assessments of possible hydrological impacts resulting from a given climate-change scenario. It is also reasonable to use these methods when the objective is limited to estimating the modification of water resources, for example in terms of volumes and the seasonality of inflows. These methods cannot in any case be used to estimate modifications concerning extreme hydrological events.

12.7 KEY POINTS OF THE CHAPTER

Local meteorological variables and atmospheric circulation

- Local meteorological variables, in particular precipitation, are determined by synoptic-scale atmospheric circulation, the characteristics of the air masses present and the small-scale characteristics of the Earth's surface.
- The scaling relationship between local and synoptic-scale atmospheric variables is not unequivocal.

Meteorological forecasting

- Nowcasting of precipitation is mainly based on radar imagery.
- Short-term, medium-term and seasonal forecasts are generally based on the output of numerical models of the atmosphere. The performance of these models for the forecasting of local meteorological variables (in particular precipitation) is very limited.
- For impact assessments, meteorological forecasts must be adapted. Statistical and analog adaptation methods use the synoptic-scale meteorological information produced by the atmospheric model.

- Meteorological forecasts are highly uncertain. Such forecasts are only useful if the associated uncertainties are characterized. This involves carrying out either a probabilistic forecast (described by the distribution function of the variable of interest) or an ensemble forecast (consisting of different scenarios).

Meteorological scenarios for the present climate context

- Meteorological scenarios, in particular for precipitation, that are useful for hydrological analysis depend on the considered hydrosystem and the objective of the analysis.
- The use of traditional design rainfalls, whether historical, based on IDFs or derived from the probable maximum precipitation, is often limited to hydrological analysis and preliminary design.
- Today, hydrological studies increasingly require simulation of the hydrological response of hydrosystems to a wide variety of rainfall events or even continuous simulation of this response over a long period of time.
- Catalogs of design rainfalls required for these studies and the required time series are commonly simulated by weather generators. These generators are mostly of the stochastic and multi-site type. They consider the observations of the atmospheric variables of interest to be the result of a random process. They can be parametric or non-parametric.
- Statistical downscaling models are weather generators conditioned by atmospheric circulation. Some are based on various empirical scaling relationships established between synoptic-scale atmospheric variables and local meteorological variables. The so-called analog method is one of such method that can be used to generate spatially consistent multi-variate scenarios.
- A spatial and/or temporal disaggregation model is often added to weather generators to produce local meteorological variables at spatial and temporal resolutions that are appropriate for the hydrosystem.

Meteorological scenarios for climate-change studies

- The outputs of climate experiments produced by global (GCMs) or regional (RCMs) climate models are not well-suited to impact assessments and must be adapted.
- Statistical downscaling methods are often used for this adaptation. The scaling relationships identified between the local and synoptic-scale atmospheric variables for the control period are assumed to be identical for the future changed-climate context. This assumption represents a strong limitation for these methods.
- Here again, a spatial and/or temporal disaggregation model is often added to weather generators to produce local meteorological variables at appropriate spatial and temporal resolutions for the hydrosystem.
- The uncertainty associated with the development of future climate scenarios for a given hydrosystem is high. Ideally it must be estimated by taking into account emission scenarios, climate models, adaptation models and multiple parameterizations.
- The significance of estimated changes for future periods must be estimated with respect to the internal variability of the models. It is likely to be low for changes in precipitation and related hydrometeorological variables.

12.8 APPENDICES

12.8.1 Statistical Characteristics of Precipitation and IDF Curves

Given the random nature of precipitation and its high spatial and temporal variability, it can only be described in a synthetic manner for a given site or region, i.e., by a statistical distribution of certain variables that are characteristic of rainfall.

If the series of precipitation data recorded at the station is sufficiently long, a classical frequency analysis can be used to determine the statistical distribution of some or all of the characteristic variables (e.g., maximum mean intensity over a given duration, duration of dry periods). This analysis often leads to the construction of Intensity-Duration-Frequency (IDF) curves. This point will be discussed in detail below.

Precipitation can also be characterized by its scale invariance properties, if applicable. This point is discussed in Appendix 12.8.2.

Rainfall frequency analysis

A theoretical probability distribution function can be fitted to the empirical distribution deduced from a series of observations of the variable of interest. The procedure can be divided into three steps: 1) compilation of the series of values of the variable to be analyzed, 2) choice of the frequency model and 3) fitting of the frequency model (referred to Addendum 8.1 or Meylan *et al.* (2012) for more information on this topic). The frequency model can be used to estimate the return period of a particular value or inversely the quantiles corresponding to a given return period.

Intensity-Duration-Frequency curves

For a given rain-gage station, frequency analysis can be carried out on the maximum mean intensities corresponding to different rainfall durations. This leads to the plotting of Intensity-Duration-Frequency (IDF) curves for the station. These curves sum up the statistical relationships that exist between the maximum mean intensity *I*, the duration *D* and the frequency *F* (Figure 12.12). The procedure for creating IDF curves is described in detail by Musy and Higy (2011).

IDF curves can be represented in graphical form and/or in a mathematical form by analytical models. Classical formulations (Talbot, Montana) have the following general form:

$$\bar{i}_{\max}(T,\theta) = \frac{a \cdot T^b}{(c+\theta)^d} \tag{12.9}$$

where *T* is the return period in years, *θ* the duration of the mean intensity and *a*, *b*, *c* and *d* are parameters that depend on the considered site or region. The classical Talbot and Montana formulas are sometimes combined (Meylan *et al.*, 2012).

Regional IDF curves

To estimate maximum mean intensities at any point of a given territory, the parameters of IDF curves are often regionalized. Two types of regionalization are classically used:

- The first leads to constant regional parameters within the different regions of the considered territory. The IDF curves are therefore assumed to be invariant within a given region.
- The second is based on the creation of estimation models for each region. These models are used to estimate the various parameters of the IDF model (e.g., geostatistical regional model) at a given site within the corresponding region. In this way, the IDF curves can vary within a region (Figure 11.6).

The term "region" refers to an area in which the statistical behavior of maximum precipitation has been identified as being homogeneous. Possible regionalization techniques for the identification of homogeneous regions and creation of regional models are presented in Chapter 11.

Intensity - Duration - Frequency - Area curves

IDF curves are classically obtained on the basis of point precipitation data observed at a given rain-gage station. However, point rainfall is often little representative of the precipitation falling on a given area, particularly in geographic areas exhibiting high spatial variability of maximum precipitation. All other factors being equal, the maximum mean precipitation depth falling on a given area is inversely proportional to the size of the area.

The maximum precipitation falling on different areas can be analyzed in the same way as the maximum mean intensities for different durations (Koutsoyiannis *et al.*, 1998; Neppel *et al.*, 2006). This analysis leads to Depth-Area-Frequency curves. For a given duration, the structure of these curves is generally similar to that of the IDF curves (Figure 12.25). It is generally assumed that precipitation distributions are the same for different areas, meaning that a simple scaling factor can be applied, often referred to as an areal reduction factor. One possible expression for an Depth-Area-Frequency model is the following:

$$\overline{i}_{\max}(T,\theta,A) = \frac{1}{(e+A)^f} \frac{a \cdot T^b}{(c+\theta)^d} \tag{12.10}$$

where T is the return period in years, θ the duration of the mean intensity falling on area A and a, b, c, d, e and f are parameters that depend on the region. If the area is zero, the expression is the same as equation 12.9 that expresses point maximum.

The construction of Depth-Area-Frequency curves is non-trivial. The main difficulty lies in estimating the precipitation depths that can fall on different areas on the basis of point information provided by the rain-gage stations of the region. This estimation can make use of various spatialization techniques and is the source of major uncertainty (Chapter 2).
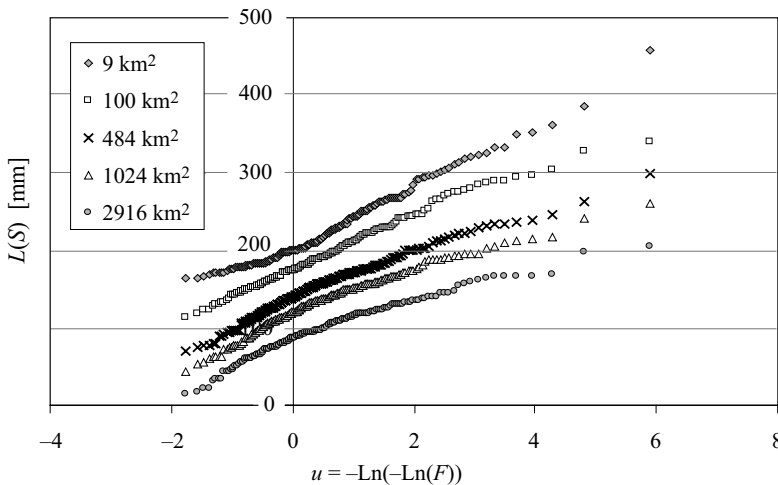

Fig. 12.25: Frequency analysis of the daily maximum precipitation [mm] for different surface areas [km²] within the region of France covered by the OMHCV observation system (adapted from Neppel *et al.*, 2006).

12.8.2 Scale Invariance Properties of Precipitation and Multiplicative Cascade Models for the Disaggregation of Precipitation Time Series

Scale invariance properties of precipitation

Scale invariance means that the variability of precipitation, or its fluctuations, has a similar statistical structure after appropriate normalization of the spatial and/or temporal coordinates.

The scale invariance properties on which precipitation generators are generally based is that of the qth order statistical moment of rainfall intensities (moments calculated on precipitation aggregated over different time steps and/or on spatial grids of different spatial resolutions r).

Consider for example the random field of point precipitation intensity $Z(x_1,x_2)$ in a two-dimensional planar space. Let $S_q(r)$ be the structure function of order q of this field defined by the expression:

$$S_q(r) = E\left[\left(\mu_r(x_1,x_2) \right)^q_{r=const} \right] \tag{12.11}$$

where $\mu_r(x_1,x_2)$ is the integral of this field on the grid cell of dimensions $r \times r$:

$$\mu_r(x_1,x_2) = \int_{x_1}^{x_1+r} \int_{x_2}^{x_2+r} Z(x_1,x_2) \cdot dx_1 \cdot dx_2 \tag{12.12}$$

$Z(x_1,x_2)$ is then considered to exhibit a scale invariance property (or the field is said to be multifractal or exhibiting a multiple scale invariance property) if the structure function $S_q(r)$ is such that:

$$S_q(r) \sim r^{\zeta(q)} \tag{12.13}$$

where $\zeta(q)$ is a non-linear function of order q. '$\sim$' indicates equality at the limit as r tends towards 0. The exponent $\zeta(q)$ is referred to as the scaling exponent function (Gupta and Waymire, 1990).

Evidence of the multifractal nature of precipitation has been reported many times, both for its temporal and spatial behavior (Lovejoy, 1981; Lovejoy and Mandelbrot, 1985; Gupta and Waymire, 1990). This is illustrated in Figure 12.26 for the temporal behavior of point precipitation at Pully station (Switzerland).
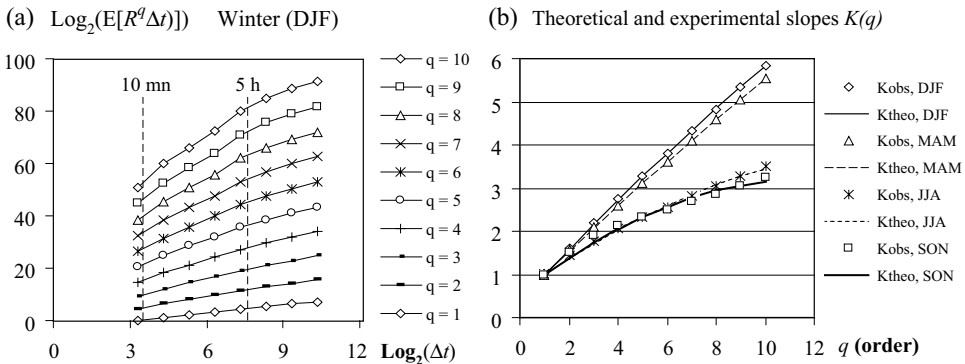

Fig. 12.26: Scale invariance properties of the qth order statistical moments for precipitation at Pully rain-gage station (Switzerland) for the period 1980–2001. a) The qth order statistical moment as a function of time step Δt (winter). b) Scaling exponents $\zeta(q)$ as a function of q estimated for all four seasons based on observations and fitting of the so-called beta-lognormal theoretical fractal model (adapted from Hingray and Ben Haha, 2005).

Multiplicative cascade models

Multiplicative cascade models are designed to distribute the rainfall volume observed within a certain space-time domain between b space-time sub-domains. If for example, on a two-dimensional domain, the mean precipitation intensity on the initial grid is W_0, this distribution leads to the following mean intensity on each of the b sub-grids: $W_0W_1(1)$, $W_0W_1(2)$, …, $W_0W_1(b)$, where the W's are appropriate random variables. This operation is repeated for each of the sub-domains until the required final resolution is reached. The key to the cascades is clearly the way that this distribution is carried out at each change in scale. Two types of multiplicative cascades can be distinguished.

- Canonical cascades: They first assume that the W's are independent and belong to the same statistical distribution. They then operate in such a way that the rainfall volume is conserved, on the average, between two successive scales, i.e., such that $E[W]=1$.
- Micro-canonical cascades: They assume that the W's are dependent and their respective values are such that the rainfall volume is fully conserved between two scales.

Canonical cascades are more attractive than micro-canonical cascades as they are well-suited to the exploration of statistical properties. These properties depend on the statistical distribution of W (Gupta and Waymire, 1993; Over and Gupta, 1996). Consequently, calibration of the parameters of a canonical cascade (i.e., the parameters of the statistical distribution W) is generally carried out by minimizing the differences between certain observed statistical characteristics and those of the theoretical model. The characteristics generally used for this purpose are the exponents $\zeta(q)$ estimated for the different values of q (see the example below). The fact that canonical cascades are non-conservative can be a major drawback for hydrological applications (Hingray and Ben Haha, 2005).

Examples of cascades for the temporal disaggregation of rainfalls

Two multiplicative cascades, one canonical and the other micro-canonical, are described below. They are presented in the framework of temporal disaggregation of precipitation series to shift from an hourly time step two a finer time step of 5 or 10 minutes. At each change in scale, these cascades distribute the volume of a given time step $[t, t+\Delta t]$ on two time sub-intervals $[t, t+\Delta t/2]$ and $[t+\Delta t/2, t+\Delta t]$. The principle is illustrated in Figure 12.27. The cascades are applied for the disaggregation of the time series of Pully station (Switzerland) extending over 22 years with an hourly time step.
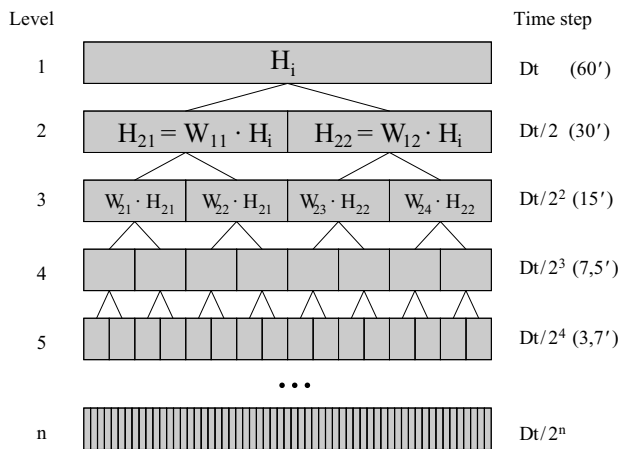

Fig. 12.27: Illustration of the principle behind a multiplicative cascade for the disaggregation of the time series. The W's are independent and identically distributed (i.i.d.) if the cascade is canonical. If the cascade is micro-canonical: $W_{12} = 1 - W_{11}$; $W_{22} = 1 - W_{21}$; $W_{24} = 1 - W_{23}$; etc.

Canonical cascade

The beta-lognormal generator (Over and Gupta, 1996) is a canonical cascade for which the random variable W is defined by the following distribution functions:

$$P(W = b^{\beta - \sigma^2 \frac{\log(b)}{2} + \sigma X}) = b^{-\beta} \text{ and } P(W = 0) = 1 - b^{-\beta} \tag{12.14}$$

where b, the number of sub-domains, is equal to 2, β and σ^2 are the two parameters of the model and X is a standard normal random variable. The generated precipitation depth $R(\Delta t)$ over a given time step Δt is a random variable for which the statistical moments present a scale invariance property the can be described by the theoretical scaling exponent function $\zeta_{theo}(q)$. For a log-distribution, $\zeta_{theo}(q)$ is a non-linear function of q:

$$\zeta_{theo}(q) = q - \log_b \left(E\left[W^q \right] \right) = 1 - \left[(\beta - 1)(q - 1) + \frac{\sigma^2 \cdot \log b}{2} \left(q^2 - q \right) \right] \tag{12.15}$$

An empirical scaling component function $\hat{\zeta}(q)$ can be estimated from the observed precipitation series by calculating the structure function $S_q(\Delta t)$ for different levels of temporal aggregation Δt and for different values of q (Figure 12.26b). The values of the parameters of the log-normal model can be estimated for each season k by minimizing the mean quadratic error between the theoretical and experimental values of the scaling exponent function. The criterion to be minimized is the following:

$$f_k = \sum_{q=1}^{n} \left(\zeta_{theo,k}(q) - \hat{\zeta}_k(q) \right)^2 \tag{12.16}$$

where n is the number of moments taken into consideration. Figure 12.26b shows the function $\zeta_{theo}(q)$ obtained by calibrating the parameters β and σ^2 of the model on the basis of this criterion (with $n=4$) for the precipitation observed at Pully station for each of the four seasons.

Micro-canonical cascade

A possible micro-canonical cascade can be based on the scale invariance properties of the empirical statistical distribution of the variable $x = R_{i,1}(\Delta t/2)/R_i(\Delta t)$ where $R_i(\Delta t)$ and $R_{i,1}(\Delta t/2)$ are the precipitation volumes falling over time intervals $[t_i, t_i + \Delta t]$ and $[t_i, t_i + \Delta t/2]$. The probability distribution $p(x/1-x)$ of this variable x is illustrated in Figure 12.28 for different changes of scale and for two classes of precipitation rainfall structures (increasing precipitation over three consecutive
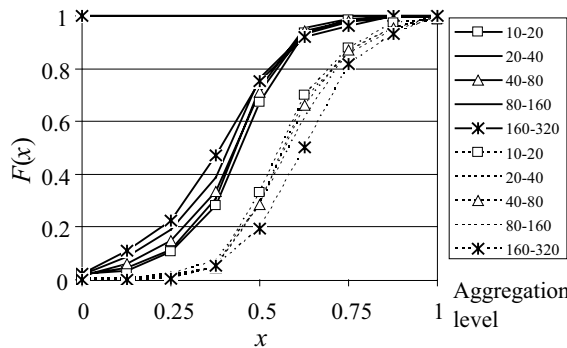

Fig. 12.28: Cumulative distribution $F(x)$ of the fraction x corresponding to the empirical distribution $p(x/1-x)$ for: a) precipitation increasing over the three time steps surrounding the time step to be disaggregated (solid curves; $R_{i+1} > R_i > R_{i-1}$) and b) decreasing precipitation (dotted curves; $R_{i-1} > R_i > R_{i+1}$). The data are for the winter season at Pully station (adapted from Hingray and Ben Haha, 2005).

time steps and decreasing precipitation). The cascade is completely defined by the mean distribution of this variable x for the different changes of scale considered. For each time interval $[t_i, t_i+\Delta t]$, the generating principle with this cascade then consists in: 1) drawing a value of x from the appropriate distribution $p(x/1-x)$ and 2) distributing rainfall volume R_i corresponding to this time step into two fractions (xR_i and $(1-x)R_i$) for the two corresponding time sub-steps.

12.8.3 Construction of Synthetic Rainfall Profiles

The typical approach used to produce synthetic dimensionless rainfall profiles consists in: 1) grouping the rainfall events of interest into homogeneous families on the basis of various criteria to be chosen and 2) identifying a typical structure for each of these families.

The grouping of rainfall events is often based on the key precipitation characteristics: duration, depth and frequency. For a given region, it can be based on rainfall types, weather types, season or even the type of impact considered.

Identification of a typical structure for each of the families is difficult given that such a structure does not necessarily exist. This identification is often based on curves expressing the precipitation volume that has accumulated since the beginning of the rainfall event as a function of the time elapsed since the beginning of the rainfall event. When the curves corresponding to the different rainfall events of the considered family are normalized (normalization of the x-axis using the total duration of the rainfall event and of the y-axis using the total precipitation volume), the corresponding dimensionless curves can be compared at the same scale. The compared rainfall events must have durations and volumes that are similar to the duration and volume of the design rainfall to be determined.

If the mean deviation between curves of a given family remains low, the simplest method to identify a typical structure is to average all the dimensionless curves. Another approach consists in dividing the dimensionless time axis into n intervals and to calculate for each interval the kth percentile of the p values of the normalized cumulative volume corresponding to the p events selected for the considered family. A profile can then be proposed by relating the kth percentiles of the n intervals considered. The profiles corresponding to the different quantiles (e.g., 10%, 50% (median) or 90%) can be constructed in this way. Note that they do not necessarily correspond to the observed structures and that the probability of occurrence of one of these profiles or another is difficult to estimate. This approach, initially proposed by Huff (1967), has recently been used in the United States to construct a design rainfall atlas for different durations and return periods (Bonnin *et al.*, 2004).

Note: A typical structure must never be produced by averaging very dissimilar rainfall structures. This would smooth the hyetograph in space and/or time and consequently lead to an underestimation of the intensity of the hydrological response of the considered hydrosystem (which is generally a highly non-linear function of meteorological forcing).

12.8.4 "Occurrence + Depth" Daily Precipitation Generators

This appendix describes the main mono- and multi-site generators used one after the other for precipitation occurrence and depth.

Mono-site generation

Precipitation occurrence models. Most occurrence models distinguish between two states corresponding to "wet" and "dry" days. A wet day is generally defined as a day for which the mean precipitation depth over the region is greater than a given threshold (e.g., 0.1 mm). To determine the state for day t at station k, the generating process uses the following expression to calculate the value of 2-state variable $X_t(k)$:

$$X_t(k) = \begin{cases} 1 & \text{(wet day)} \quad \text{if} \quad e_t(k) \le p_t(k) \\ 0 & \text{(dry day)} \quad \text{if not} \end{cases} \tag{12.17}$$

where $e_t(k)$ is a uniform random variable defined on interval $[0, 1]$ and $p_t(k)$ is the marginal probability that $X_t(k)$ corresponds to a wet state. $p_t(k)$ is often simply obtained for a given day by the coefficients of the transition matrix of a first-order Markov chain (the probability of occurrence on a given day is then assumed to depend only on the state of the previous day):

$$p_t(k) = \begin{cases} p_{01}(k) & \text{if} \quad X_{t-1}(k) = 0 \\ p_{11}(k) & \text{if} \quad X_{t-1}(k) = 1 \end{cases} \tag{12.18}$$

The values of the transition probabilities $p_{01}(k)$ and $p_{11}(k)$ are obtained on the basis of observed series. When these probabilities are assumed constant, it is often more convenient (in particular when estimating these parameters in a climate-change context—see Wilks, 1999) to define the Markov chain using the following two parameters:

$$\pi = \frac{p_{01}}{1 + p_{01} - p_{11}} \tag{12.19}$$

$$r = p_{11} - p_{01} \tag{12.20}$$

which are respectively the unconditional probability of daily precipitation and the lag-1 auto-correlation of the daily precipitation occurrence series (Wilks, 1999).

The transition probabilities $p_{01}(k)$ and $p_{11}(k)$ are not necessarily constant with time. They can depend on the season (Jimoh and Webster, 1999) or on appropriate information related to atmospheric circulation. The latter case involves non-homogeneous hidden Markov models (Hughes *et al.*, 1999; Bellone *et al.*, 2000; Mezghani *et al.*, 2013). For mono-site models, the probability of occurrence of a wet day is for example frequently estimated on the basis of an expression like:

$$p_k(t) = \left(1 + \exp\left[-\beta_0 - \sum_{i=1}^{m} \beta_i \, x_{i,d}(t)\right]\right)^{-1} \tag{12.21}$$

where $x_{i,d}$ are the values of the atmospheric circulation indices for considered day d (Addendum 12.2) and where model parameter β_i, which depends on whether the previous day was dry or wet, can be estimated on the basis of appropriate techniques for the estimation of generalized linear models (Brandsma and Buishand, 1997).

Precipitation depth models. A number of probability distributions are widely used to model daily precipitation depths at a given point. The most common are the Gamma, exponential, mixed exponential and truncated normal distributions (Srikanthan and McMahon, 2001). The precipitation depth at time t is generally generated independently with respect to the precipitation depths at previous time steps.

$$R_d = r_d \cdot E(R_d) \quad \text{[mm]} \tag{12.22}$$

where r_d is a positive random variable with a mean of 1 defined by $r_d = 1/\kappa \, Gam(\kappa,1)$, where $Gam(\kappa,1)$ is a random variable taken from the standard Gamma distribution $G(\kappa,1)$ with shape parameter κ and a dispersion parameter equal to 1, and where $E(R_d)$ is the expected value of precipitation depth for day d calculated using the following generalized linear model:

$$E(R_d) = \exp\left[\lambda_0 + \sum_{i=1}^{m} \lambda_i x_{i,d}\right] \tag{12.23}$$

where λ_i are the parameters the model and $x_{i,d}$ the values of the atmospheric circulation indices for considered day d. The parameters can also be estimated on the basis of appropriate techniques for the estimation of generalized linear models (Brandsma and Buishand, 1997).

Multi-site generation

When the probability of occurrence of precipitation at each of the sites depends on atmospheric circulation, an inter-station correlation between occurrences is generated indirectly. If not, the inter-station correlation can be forced using a Gaussian multivariate random driving variable $w_t = (w_t(1), w_t(2), \dots w_t(n))$ (Wilks, 1998). In this case, occurrence at station k is expressed by:

$$X_t(k) \;=\; \begin{cases} 0 & \text{if} \quad w_t(k) \le \Phi^{-1}\big[p_t(k)\big] \\ 1 & \text{if not} \end{cases} \tag{12.24}$$

where $w_t(k) = N(0,1)$ is the kth component of random variable w_t and where $\Phi[\,\cdot\,]$ represents the cumulative distribution function of the standard normal variable. The advantage of this formulation is that it facilitates generation of a multivariate Gaussian variable for which the statistical properties are known. The correlation between precipitation occurrences is induced by the correlation between the components of this random variable w_t. Wilks (1998) proposes a method that can be used to identify the variance-covariance matrix of this variable. In this type of approach, the spatial correlation can also be modeled as a function of the distance between stations (Stehlik and Bardossy, 2002).

For multi-site generation of precipitation depths, the spatial correlation of precipitation depths between stations can be obtained, as for the occurrence, using a correlated driving variable $s_t = (s_t(1), s_t(2), \dots s_t(n))$ that can once again be obtained on the basis of a correlated multivariate Gaussian variable. For example, in the multi-site version proposed by Wilks (1998), generation of precipitation depth $z_t(k)$ at station k is obtained using the following equation:

$$z_t(k) = z_{min} - \beta_t(k) \ln [s_t(k)] \tag{12.25}$$

where z_{min} is the precipitation threshold below which a day is considered to be dry and $\beta_t(k)$ is chosen appropriately as one of the two values $\beta_1(k)$ or $\beta_2(k)$ corresponding respectively to the median of each exponential distribution composing the mixed distribution used to describe the precipitation depth distribution.

12.8.5 Precipitation Generators based on Poisson Point Processes or Rectangular Pulses

This appendix describes the main models based on Poisson point processes or rectangular pulses.

Mono-site generators

The model structure is derived from the assumed hierarchical organization of precipitation structures and in particular the assumed rainfall cell temporal grouping process within independent rainfall events. The Neyman-Scott and Bartlett-Lewis rectangular-pulse models (respectively NSRPM and BLRPM) differ in the way they generate cells within a rainfall event. Whatever the model, the intensity $Z(t)$ of a given site at time t is the sum of the intensities of the cells that are active at time t:

$$Z(t) = \int_{\theta=0}^{\infty} Y_{t-\theta}(\theta) \cdot dN(t-\theta) \tag{12.26}$$

where $Y_\tau(\theta)$ is the precipitation depth at time θ for the cell that starts at time τ and $N(t)$ is the number of cells.

The temporal series generated by this process are continuous in time. To estimate the model parameters, they are aggregated at different time steps so they can be compared to the observed series.

For the NSRPM model, the variables to be generated randomly and the associated distributions generally used are:

- The time origin of the rainfall events (according to a Poisson process).
- The number of cells in a rainfall event (Poisson or geometric distribution).
- The position of each cell within the rainfall event (exponential distribution).
- The duration of each cell (exponential distribution).
- The intensity of each cell (exponential distribution).

The distributions used to generate rainfall events and cells within rainfall events are in fact chosen so that it is possible to determine in an analytical manner expressions for various key statistical characteristics of the generation precipitation series (e.g., probability of occurrence of daily precipitation, mean rainfall duration, 2nd and 3rd order moments of daily or hourly precipitation). These expressions depend on the parameters of the statistical distributions used for generation. Model calibration therefore consists simply in determining the distribution parameters that minimize the differences between the observed and "modeled" values of the q characteristics for which analytical expressions have been determined. A function with the following form is generally minimized for each considered calendar period k (e.g., month or season):

$$f_k = \sum_{q=1}^{n} \left(m_{model,k}(q) - m_{emp,k}(q) \right)^2 \tag{12.27}$$

where q refers to the qth considered characteristic, its model and empirical values for the month k being respectively $m_{model,k}(q)$ and $m_{emp,k}(q)$.

Multi-site generators

Multi-site generators are generally based on a master Poisson process to generate rainfall occurrence. This process is then modified to determine in a simpler although less accurate manner the rainfall occurrence at each site within the region. Each of the rainfalls of the master process has a probability p_i of being observed at the ith site of the region. If the master Poisson process has λ for a parameter, the arrival of rainfalls at each site also follows a Poisson process with parameter $p_i \cdot \lambda$.

Multi-site models differ in the way they take into account the dependence of individual cells between the sites. Many approaches, although offering an attractive conceptualization of the processes, are unfortunately of no practical interest given that it is impossible to derive the analytical expressions of the statistical characteristics required to estimate the model parameters. Drastic simplifications are therefore necessary for multi-site models. The following are examples of two extreme strategies.

1. The cells generated at a given station are reproduced identically at all stations, subject only to a homothety for the intensities. This generation process obviously leads to unrealistic scenarios. It is nevertheless sometimes used on small drainage basins for the sake of convenience.
2. The cells are generated independently at each of the stations. The correlations between stations induced by the process are however largely insufficient to reproduce the observed correlations.

Various intermediate strategies have been discussed by Kakou (1997). They are based on important assumptions. For the model proposed by Cox and Isham (1994), for example, the assumptions are: identical occurrences of cells at every site and independent cell depths and cell durations at site i derived from the cells of the master site using a constant multiplicative coefficient.

Another strategy consists in generating the correlation between stations on the basis of the generation of correlated driving variables. This is the case for the model proposed by Favre *et al*. (2002) (Figure 12.29). The duration (and similarly the intensity) of the cells at different stations
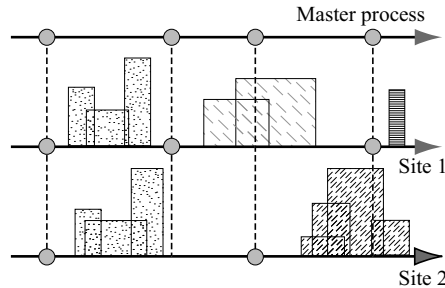
Fig. 12.29: Principle behind a multi-site model based on a point Poisson process with correlated random variables. The duration and intensity of the cells as well as their number within the rainfalls are dependent random variables (adapted from Favre, 2001).

are assumed to follow a bivariate exponential distribution as proposed by Lawrence and Lewis (1983). The number of cells within the rainfalls is similarly assumed to follow a bivariate geometric distribution. This approach is attractive in that it is less constraining for the generation process than the other approaches. Its main limitation is related to the impossibility of generating correlated variables, other than Gaussian variables, at more than two sites.

Spatio-temporal generators

The hierarchical organization of precipitation systems proposed by Lecam (1961) led to the development of cellular spatio-temporal models. These models are a two-dimensional generalization of the Bartlett-Lewis and Neyman-Scott rectangular-pulse mono-site models based on the grouped generation of cells within rainfalls generated elsewhere. Many models of this type have been proposed, the first version being that of Amorocho and Wu (1977). The generation process is hierarchical and generally leads to successive generation of: 1) precipitation bands, 2) rainfall events grouped within these bands and 3) rainfall cells grouped within the rainfall events. The appearance of bands, rainfall events and cells as well as their different characteristics (lifetime, size, number) are all generated according to a specific stochastic process. The rainfall field results from the summing of the intensities of the different cells. Cells with a given shape (e.g., paraboloid of revolution) have a certain trajectory, speed of displacement and life cycle (Figure 12.30). The main difficulty with these models is the estimation of their numerous parameters (Cowpertwait, 2006).
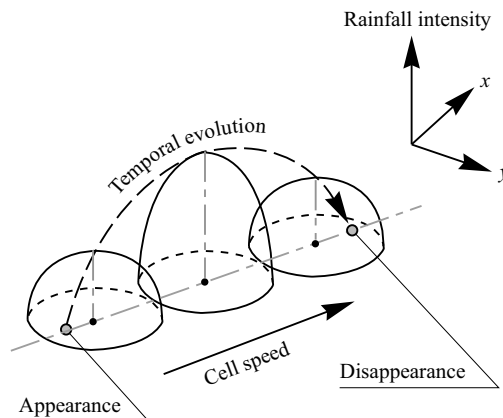

Fig. 12.30: Schematic representation of the typical life cycle of the rainfall cell simulated by a parametric spatio-temporal precipitation model based on the grouping of cells.

12.8.6 Other Spatio-temporal Precipitation Generators

Parametric models based on Poisson processes

The principle behind these generators was presented in Appendix 12.8.4.

Parametric models forced by Gaussian fields

Second-order stationary Gaussian fields have a number of important properties. One of these is that they are easy to generate, for example using the turning bands method introduced by Matheron (1973).

Precipitation fields are of course not Gaussian. Gaussian fields can however be used to force a rain-cell generation process (Mellor and Metcalfe (1996); Pegram and Clothier, 2001a,b). For example, using a modified turning bands method, Mellor and Metcalfe (1996) generate two trains of parallel rain bands that move in fixed directions at fixed speeds (Figure 12.31-1). The superpositioning of these bands, modulated by an appropriate function (Figure 12.31-2), determines a local precipitation potential (Figure 12.31-3). This potential defines the input variable of a non-homogeneous Poisson process that is then used to generate rain-cell occurrence (Figure 12.31-4). The sum of these identical cells, described by a given paraboloid of revolution and life cycle gives the required precipitation field (Figure 12.31-5). This field is progressively deformed with the appearance and disappearance of cells and the displacement of wave trains. The main difficulty of this method is to estimate the model parameters. Mellor and O'Connell (1996) proposed an estimation method based on radar images.
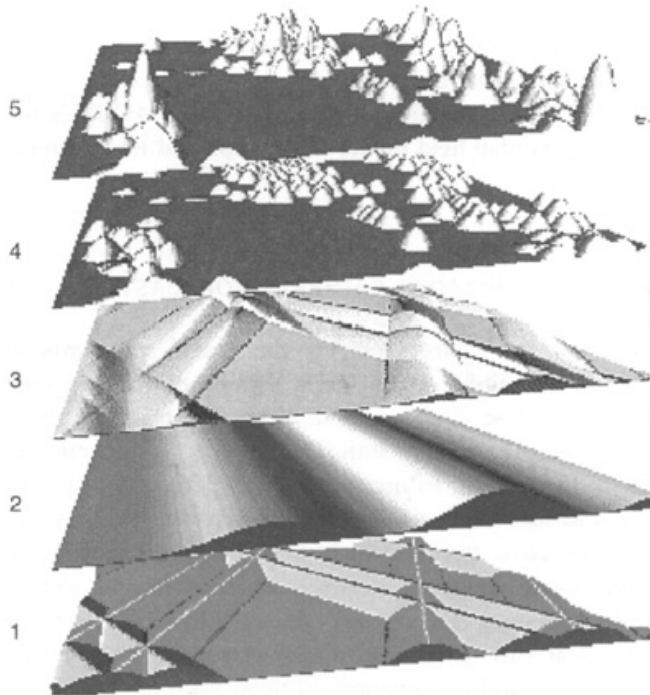

Fig. 12.31: The modified turning bands method for the generation of precipitation fields (adapted from Mellor *et al.*, 2000.

Physical models

Physical models of the atmosphere, already discussed in the section dealing with meteorological forecasts, can be used to simulate spatio-temporal meteorological scenarios for a given climatic context. The limitations of these models for the generation of sensitive meteorological variables such as precipitation have already been presented in Section 12.2.2. Before the output from such models can be used as scenarios for hydrological applications, it must be adapted. This can be done using analog or statistical adaptation methods developed for quantitative precipitation forecasting and subject to certain modifications. The multi-site models discussed in Section 12.4.2 can also be used for this adaptation as long as they are conditioned by atmospheric circulation variables that are properly simulated by atmospheric models. The use of these adaptation methods (also called downscaling methods) however leads to the loss of some of the spatial information given that the adapted meteorological scenarios become multi-site scenarios.

12.8.7 The use of a Linear Scaling Relationship to Produce Scenarios for Future Periods other than 2070–2099

This method, introduced by Santer *et al.* (1990), is based on the assumption that there exists a scaling relationship (also referred to as a scaling factor) between mean global warming and the regional climatic response simulated by the considered GCM or RCM.

In many studies, the scaling relationship is assumed to be linear. If this is the case, it is characterized for each climate variable considered by a scaling ratio that is simply the regional change expected per degree of global warming. In the work of Jones (2000) or Hulme *et al.* (2002), for example, the scaling ratio is the seasonal regional warming or the seasonal modification of precipitation depths per degree of global warming (respectively in °C/°C and mm/mm/°C). The linearity assumption would appear to be reasonable for many regional climate variables. It is illustrated in Figure 12.32 for winter warming and precipitation increase simulated for western Switzerland by different climate models considered in the framework of the PRUDENCE project (Hingray *et al.*, 2007b).
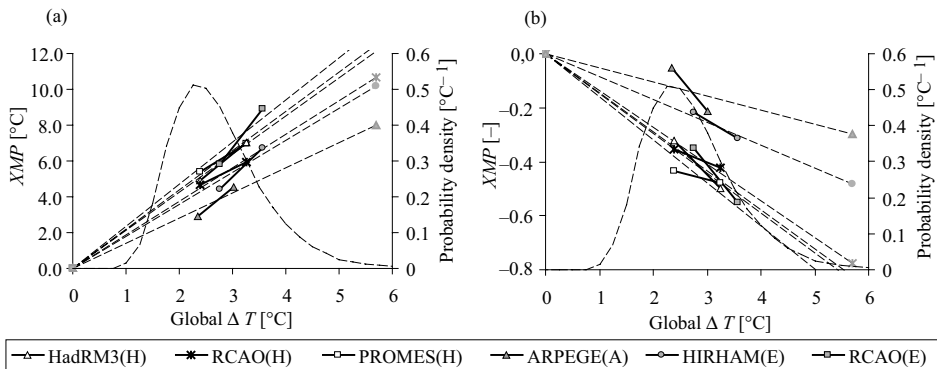

Fig. 12.32: Scaling relationships between summer climate changes for the Swiss plateau region and mean annual global warming (ΔT) as simulated for the period 2070–2099 by different climate models (AOGCM+RCM) considered in the framework of the European PRUDENCE project. a) Regional warming (*XMT* in °C). b) Relative change of mean precipitation (*XMP* in mm/mm). Each symbol corresponds to one of the two climate experiments (for scenarios A2 and B2 respectively) produced by each climate model. For each model, the slope of the dotted lines gives the scaling ratio of the scaling relationship between regional changes and global warming. Note that ΔT is specific to each model. The dotted curve is the probability density function of global warming between 1990 and the period 2070–2099 extracted from the data of Wigley and Raper (2001).

If several climate experiments for a given climate model are available, the scaling ratios can be obtained by linear regression. If not, they can be estimated for a given regional climate model r using the following simplified expression:

$$Y_{v,s,r} = X_{v,s,r}(t_f) / \Delta T_r(t_f) \tag{12.28}$$

where $X_{v,s,r}(t_f)$ is the absolute or relative change of the variable v for season s as simulated by the considered regional climate model between the control period and the future reference period t_f (e.g., $T_f = 2070$–2099), where $Y_{v,s,r}$ is the scaling ratio associated with this change and $\Delta T_r(t_f)$ the value of global warming obtained by the AOGCM used to drive RCM r. The vector $\mathbf{Y_r}$ of the scaling ratios for the different regional climate variables considered defines the sensitivity of the regional climate to global warming as estimated by climate model r (i.e., the regional climate response per degree of global warming).

$$\mathbf{Y_r} = [Y_{v,s,r}]_{v:1..n,\ s:1..m} \tag{12.29}$$

where n is the number of regional climate variables (e.g., temperature and precipitation changes in terms of mean values and/or variability) and m is the number of seasons considered ($m = 4$ for summer, fall, winter and spring and $m = 12$ if the 12 months of the year are considered).

A regional climate-change scenario $\mathbf{X_r}(t)$ between the control period and the future period t other than the future period t_f can be deduced from the climatic sensitivity $\mathbf{Y_r}$ as follows:

$$\mathbf{X_r}(t) = \mathbf{Y_r} \cdot \Delta T(t) \text{ with } \mathbf{X_r}(t) = [X_{v,s,r}(t)]_{v:1..n,\ s:1..m} \tag{12.30}$$

where $\Delta T(t)$ is an estimation of global warming for future period t. The absolute or relative change of variable v for season s can therefore be expressed for each variable and each season by: $X_{v,s,r}(t) = Y_{v,s,r} \times \Delta T(t)$.

The scaling factor, i.e., the global warming $\Delta T(t)$ for future period t of interest, can be simply extracted from one of the many distribution functions produced to characterize the uncertainty.[8] For example, Figure 12.33 shows the distribution functions proposed by Wigley and Raper (2001) for global warming between 1990 and three future periods.
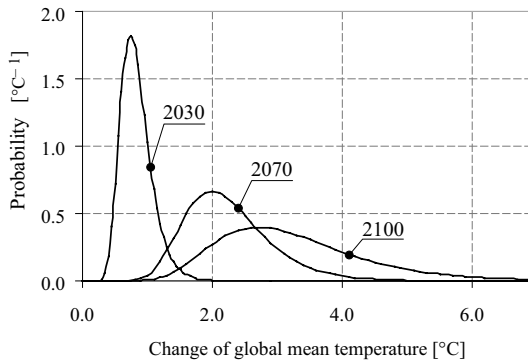

Fig. 12.33: Example of a probability density function for global warming between 1990 and various future periods (adapted from Wigley and Raper, 2001).

---

[8]These distribution functions are generally produced using so-called Simplified Climate Models (SCMs) requiring significantly less computing power than GCMs (Wigley *et al*., 2000). These SCMs can therefore be used to estimate the global warming associated with a multitude of scenarios, thereby making it possible to cover the uncertainties linked to the main factors conditioning climate change (e.g., greenhouse gas emission scenarios for the 21st century, the sensitivity of the Earth's climate to a doubling of the CO_2 content, vertical diffusivity of the oceans, the carbon cycle, etc.) (New and Hulme, 2000; Huntingford and Cox, 2000).

The regional climate sensitivity as defined above can also consider the spatial structure of the regional changes (the spatial structure simulated by the model and therefore also assumed to be conservative for any future periods other than the reference period t_f). The advantage of this scaling method, in addition to its extreme simplicity, is that it conserves the consistency of changes simulated for the future reference period t_f by the considered RCM (spatial and seasonal consistency and partial consistency between variables).

Regional climate sensitivity to global warming is highly uncertain in the same way as global warming. This sensitivity depends for example on the climate model considered (Figure 12.32). Ideally, the associated uncertainty should be taken into account in impact assessments. The different sensitivities that can be estimated by different climate models could be for example used to produce different regional scenarios (Hingray *et al.*, 2007a,b).

REFERENCES

Abbott, M.B. and Ionescu, F., 1967. On the numerical computation of nearly-horizontal flows. Journal of Hydraulic Research, 5(2): 97–117.

Abbott, M.B., Bathurst, J.C., Cunge, J.A., Oconnell, P.E. and Rasmussen, J., 1986a. An Introduction to the European Hydrological System—Systeme Hydrologique Europeen, SHE. 1. History and Philosophy of a Physically-Based, Distributed Modeling System. Journal of Hydrology, 87(1-2): 45–59.

Abbott, M.B., Bathurst, J.C., Cunge, J.A., Oconnell, P.E. and Rasmussen, J., 1986b. An Introduction to the European Hydrological System—Systeme Hydrologique Europeen, SHE. 2. Structure of a Physically-Based, Distributed Modeling System. Journal of Hydrology, 87(1-2): 61–77.

Abdulla, F.A. and Lettenmaier, D.P., 1997. Development of regional parameter estimation equations for a macroscale hydrologic model. Journal of Hydrology, 197(1-4): 230–257.

Abi-Zeid, I. and Bobee, B., 1999. The stochastic modeling of low flows: a literature review. Revue des Sciences de l'Eau, 12(3): 459–484.

Ambroise, B., 1999. Génèse des débits dans les petits bassins versants ruraux en milieu tempéré: 2-Modélisation systémique et dynamique. Revues des sciences de l'eau, 12(1): 123–153.

Ambroise, B., Beven, K. and Freer, J., 1996. Toward a generalization of the TOPMODEL concepts: Topographic indices of hydrological similarity. Water Resources Research, 32(7): 2135–2145.

Amerman, C.R., 1965. Use of Unit-Source Watershed Data for Runoff Prediction. Water Resources Research, 1(4): 499–507.

Amorocho, J. and Wu, B., 1977. Mathematical-Models for Simulation of Cyclonic Storm Sequences and Precipitation Fields. Journal of Hydrology, 32(3-4): 329–345.

Anctil, F., Perrin, C. and Andreassian, V., 2003. An output updating of lumped conceptual rainfall/runoff forecasting models. Journal of the American Water Resources Association, 39(5): 1269–1279.

Anctil, F., Rousselle, J. and Lauzon, N., 2005. Hydrologie. Cheminement de l'eau, 320 pp.

Anderson, E.A., 1976. A Point Energy and Mass Balance Model of Snow Cover, US Department of Commerce, Silver Spring, MD.

Anderson, M.G. and McDonnell, J.J., 2005. Encyclopedia of Hydrological Sciences—Part 14: Snow and Glacier Hydrology. Wiley, Chichester.

Andreadis, K.M. and Lettenmaier, D.P., 2006. Assimilating remotely sensed snow observations into a macroscale hydrology model. Advances in Water Resources, 29(6): 872–886.

Andréassian, V., Hall, A., Chahinian, N. and Schaake, J., 2006. Large sample basin experiments for hydrological model parameterisation, IAHS Red Books Series n°307.

Andreassian, V., Oddos, A. Michel, C. *et al.,* 2004. Impact of spatial aggregation of inputs and parameters on the efficiency of rainfall-runoff models: A theoretical study using chimera watersheds. Water Resources Research, 40(5).

Andréassian, V., Sarkissian, V., Chełmicki, W., Stănescu, V.A. and Moussa, R., 2001. Lexique Hydrologique pour l'Ingénieur: Anglais-Français-Arménien-Russe-Polonais-Roumain-Arabe Cemagref, Antony, 210 pp.

Andrieu, H., Delrieu, G. and Creutin, J.-D., 1995. Identification of vertical profiles of radar reflectivities for hydrological applications using an inverse method. Part 2: Sensitivity analysis and case study. J. Appl. Meteor., 34: 240–259.

Andrieu, H., French, M.N., Thauvin, V. and Krajewski, W.F., 1996. Adaptation and application of a quantitative rainfall forecasting model in a mountainous region. Journal of Hydrology, 184(3-4): 243–259.

Anquetin, S., F., Minsicloux, J.M.F., Creutin, J.-D. and Cosma, S., 2003. Numerical simulation of orographic rainbands. Journal of Geophysical Research, 108(D8): 8386, doi:10.1029/2002JD001593.

Antolik, M.S. 2000. An overview of the National Weather Service's centralized statistical quantitative precipitation forecasts. Journal of Hydrology, 239(1-4): 306–337.

Arnaud, P. and Lavabre, J., 2002. Coupled rainfall model and discharge model for flood frequency estimation. Water Resources Research, 38(6).

Arnaud, P., Bouvier, C., Cisneros, L. and Dominguez, R., 2002. Influence of rainfall spatial variability on flood prediction. Journal of Hydrology, 260(1-4): 216–230.

Arnold, J.G. and Allen, P.M., 1999. Automated methods for estimating baseflow and ground water recharge from streamflow records. Journal of the American Water Resources Association, 35(2): 411–424.

Arnold, N., Richards, K., Willis, I. and Sharp, M., 1998. Initial results from a distributed, physically based model of glacier hydrology. Hydrological Processes, 12(2): 191–219.

Aronica, G., Hankin, B. and Beven, K., 1998. Uncertainty and equifinality in calibrating distributed roughness coefficients in a flood propagation model with limited data. Advances in Water Resources, 22(4): 349–365.

ARR. 1998. Australian Rainfall and Runoff: A Guide to Flood Estimation , Vol. 1, Institution of Engineers, Australia, Editor-in-chief D.H. Pilgrim, Revised Edition 1987 (reprinted edition), Barton, ACT.

ASCE, 1992. Design & Construction of Urban Stormwater Management Systems. ASCE Manuals and Reports on Engineering Practice No. 77, New York, NY.

ASCE, 1996. Hydrology Handbook. ASCE Manuals and Reports of Engineering Practice N°28, 2nd Ed., New York.

ASCE, 2005. The ASCE Standardized Reference Evapotranspiration Equation. American Society of Civil Engineers, 173 pp.

Aschwanden, H., 1993. Le débit d'étiage Q347: détermination et estimation pour les bassins versants alpins de Suisse: une méthode pratique, Office fédéral de l'environnement, des forêts et du paysage, Service hydrologique et géologique national, Berne.

Atlas de la Suisse, 1965–1978. Atlas de la Suisse. Edition du Service topographique fédéral, Berne.

Atlas, D. and Ulbrich, C.W., 1977. Path-Integrated and Area-Integrated Rainfall Measurement by Microwave Attenuation in 1–3 Cm Band. Journal of Applied Meteorology, 16(12): 1322–1331.

Aubert, D., Loumagne, C. and Oudin, L., 2003. Sequential assimilation of soil moisture and streamflow data in a conceptual rainfall-runoff model. Journal of Hydrology, 280(1-4): 145–161.

Avissar, R. and Pielke, R.A., 1989. A Parameterization of Heterogeneous Land Surfaces for Atmospheric Numerical-Models and Its Impact on Regional Meteorology. Monthly Weather Review, 117(10): 2113–2136.

Bach, H. and Mauser, W., 2003. Methods and examples for remote sensing data assimilation in land surface process modeling. Ieee Transactions on Geoscience and Remote Sensing, 41(7): 1629–1637.

Bader, S. and Bantle, H., 2004. Das Schweizer Klima im Trend—Temperatur und Niederschlagsentwicklung 1864–2001. MétéoSuisse, 48 pp.

Baillargon, S., 2005. Le krigeage: revue de la théorie et application à l'interpolation spatiale des données de précipitation. Master Thesis, Université Laval, Québec.

Baker, V.R., 1987. Paleoflood Hydrology and Extraordinary Flood Events. Journal of Hydrology, 96(1-4): 79–99.

Bardossy, A. and Plate, E.J., 1992. Space-Time Model for Daily Rainfall Using Atmospheric Circulation Patterns. Water Resources Research, 28(5): 1247–1259.

Bardossy, A., Duckstein, L. and Bogardi, I., 1995. Fuzzy Rule-Based Classification of Atmospheric Circulation Patterns. International Journal of Climatology, 15(10): 1087–1097.

Bardossy, A., Stehlik, J. and Caspary, H.J., 2002. Automated objective classification of daily circulation patterns for precipitation and temperature downscaling based on optimized fuzzy rules. Climate Research, 23(1): 11–22.

Barré de Saint Venant, A.J.C., 1871. Théorie du mouvement non permanent des eaux. Comptes Rendus des séances de l'Académie des Sciences, 73: 147–154 et 237–240.

Barry, R.G. and Richard J.C., 1998. Atmosphere, Weather and Climate, Routledge, Seventh Edition.

Barry, R.G., 2006. The status of research on glaciers and global glacier recession: a review. Progress in Physical Geography, 30(3): 285–306.

Bastiaanssen, W.G.M., Molden, D.J. and Makin, I.W., 2000. Remote sensing for irrigated agriculture: examples from research and possible applications. Agricultural Water Management, 46(2): 137–155.

Bates, B.C., Charles, S.P. and Hughes, J.P., 1998. Stochastic downscaling of numerical climate model simulations. Environmental Modelling & Software, 13(3-4): 325–331.

Bates, P.D., 2004. Remote sensing and flood inundation modelling. Hydrological Processes, 18(13): 2593–2597.

Baudez, J.C., Loumagne, C., Michel, C., Palagos, B., Gomendy, V. and Bartoli, F. 1999. Modélisation hydrologique et hétérogénéité spatiale des bassins. Vers une comparaison de l'approche globale et de l'approche distribuée, Etude et Gestion des Sols, 6: 165–184.

Baur, F., Hess, P. and Nagel, H., 1944. Kalender der Großwetterlagen Europas 1881–1939, Bad Homburg v. d. H.

Baxter, B.E. and Rifai, H., 2002. Chapitre 10: GIS Applicaions in hydrology. pp. 633–658. In: P.B. Bedient and W.C. Huber (Editors), Hydrology and Floodplain Analysis. Prentice-Hall Publishing Co., 3rd Ed., Upper Saddle River.

Beck, J., 2006. Streambank erosion hazard mapping: concepts, methodology and application on the Venoge River (Switzerland). PhD Thesis, EPFL, Lausanne, 228 pp.

Becker, F. and Li, Z.L., 1990. Temperature-Independent Spectral Indexes in Thermal Infrared Bands. Remote Sensing of Environment, 32(1): 17–33.

Becker, L. and Yeh, W.W.-G., 1974. Optimization of Real-Time Operation of a Multiple Reservoir System. Water Resources Research, 10(6): 1107–1112.

Bedient, P.B. and Huber, W.C., 2002. Hydrology and Floodplain Analysis, 3rd Ed. Prentice-Hall Publishing Co., Upper Saddle River, 763 pp.

Bell, V.A. and Moore, R.J., 2000. Short period forecasting of catchment-scale precipitation. Part II: a water-balance storm model for short-term rainfall and flood forecasting. Hydrology and Earth System Sciences, 4(4): 635–651.

Bellone, E., Hughes, J.P. and Guttorp, P., 2000. A hidden Markov model for downscaling synoptic atmospheric patterns to precipitation amounts. Climate Research, 15(1): 1–12.

Benito, G. *et al.,* 2004. Use of systematic, palaeoflood and historical data for the improvement of flood risk estimation. Review of scientific methods. Natural Hazards, 31(3): 623–643.

Benson, M.A., 1962. Evolution of Methods for Evaluating the Occurence of Floods. U.S., Ecological Survey, Water Supply Paper, 1580-A.

Bergström, S. and Forsman, A., 1973. Development of a conceptual deterministic rainfall-runoff model. Nordic Hydrology, 4: 147–170.

Bergström, S., 1976. Development and application of a conceptual runoff model for Scandinavian catchments. SMHI report RH07, Sweedish Meteorological and Hydrological Institute, Norrköping, Sweden.

Bergström, S., 1992. The HBV model—its structure and applications. SMHI Reports RH, No. 4, Sweedish Meteorological and Hydrological Institute, Norrköping, Sweden.

Berne, A., Delrieu, G., Creutin, J.D. and Obled, C., 2004. Temporal and spatial resolution of rainfall measurements required for urban hydrology. Journal of Hydrology, 299(3-4): 166–179.

Bérod, D., 1994. Contribution à l'estimation des crues rares à l'aide de méthodes déterministes: apport de la description géomorphologique pour la simulation des processus d'écoulement. Thèse de doctorat, EPFL, Lausanne, 191 pp.

Bérod, D.D., Singh, V.P., Devred, D. and Musy, A., 1995. A Geomorphologic Nonlinear Cascade (Gnc) Model for Estimation of Floods from Small Alpine Watersheds. Journal of Hydrology, 166(1-2): 147–170.

Berthier, E., 2005. Dynamique et bilan de masse des glaciers de montagne (Alpes, Islande, Himalaya). Contribution de l'imagerie satellitaire. Thèse de doctorat, Université Paul Sabatier, Toulouse.

Berthier, E., 2007. Dynamique et bilan de masse des glaciers de montagne (Alpes, Islande, Himalaya). Contribution de l'imagerie satellitaire. La Houille Blanche, 2: 116–121.

Beven, K.J., 2012. Rainfall-Runoff modeling. The Primer, 2nd edition, Wiley-Blackwell, Chichester UK.

Beven, K., 1977. Hillslope Hydrographs by Finite-Element Method. Earth Surface Processes and Landforms, 2(1): 13–28.

Beven, K., 1989. Changing ideas in hydrology. The case of physically-based models. Journal of hydrology, 105(1-2): 157–172.

Beven, K., Kirby, M., Schofield, N. and Tagg, A., 1984. Testing a physically-based flood forecasting model (TOPMODEL) for three U.K. catchments. J. Hydrol., 69: 119–143.

Beven, K.J. and Binley, A., 1992. The Future of Distributed Models: Model Calibration and Uncertainty Prediction. Hydrological Processes, 6(3): 279–298.

Beven, K.J. and Kirby, M.J., 1979. A physically-based variable contributing area model of basin hydrology. Hydrologic Sciences Bulletin, 24: 43–69.

Beven, K.J. and Wood, E.F., 1993. Flow routing and the hydrological response of channel networks. pp. 99–128. In: K.J. Beven and M.J. Kirkby (Editors), Channel Networks. Wiley, Chichester, UK.

Beven, K.J., 1996. Equifinality and Uncertainty in Geomorphological Modelling. pp. 289–313. In: B.L. Rhoads and C.E. Thorn (Editors), The Scientific Nature of Geomorphology. Wiley, Chichester, UK.

Beven, K.J., 2000. Rainfall runoff modelling. The primer. Wiley, Chichester, UK, 372 pp.

Beven, K.J., Kirkby, M.J., Schofield, N. and Tagg, A.F., 1984. Testing a Physically-based Flood Forecasting-Model (Topmodel) for 3 Uk Catchments. Journal of Hydrology, 69(1-4): 119–143.

Blosch, G. and Sivapalan, M., 1995. Scale issues in hydrological modelling: a review. Hydrological Processes, 9(3-4): 251–290.

Bobee, B. *et al.,* 1996a. Presentation and review of some methods for regional flood frequency analysis. Journal of Hydrology, 186(1-4): 63–84.

Bobee, B. *et al.,* 1996b. Inter-comparison of regional flood frequency procedures for Canadian rivers. Journal of Hydrology, 186(1-4): 85–103.

Bocquillon, C., 1978. Propagation des écoulements transitoires intermittents dans les systèmes hydrauliques à surface libre, Note 44/78. Laboratoire d'Hydrologie Mathématique, USTL, Montpellier, 85 pp.

Boé, J. and Terray, T., 2008. Régimes de temps et désagrégation d'échelle. La Houille Blanche, 2: 45–51.

Boé, J., 2007. Changement global et cycle hydrologique: Une étude de régionalisation sur la France. Thèse de doctorat, Université Paul Sabatier, Toulouse, 256 pp.

Boé, J., Terray, L., Habets, F. and Martin, E., 2006. A simple statistical-dynamical downscaling scheme based on weather types and conditional resampling. Journal of Geophysical Research-Atmosphères, 111(D23).

Bonnin, G.M. *et al.,* 2004. NOAA Atlas 14—Precipitation—Frequency Atlas of the United States, Volume 2. National Oceanic and Atmospheric Administration (NOAA), National Weather Service, Silver Spring, Maryland.

Bontron, G., 2004. Prévision quantitative des précipitations: adaptation probabiliste par recherche d'analogues. Utilisation des Réanalyses NCEP/NCAR et application aux précipitations du Sud-Est de la France. Thèse de doctorat, INPG, Grenoble, 262 pp.

Boone, A. and Etchevers, P., 2001. An intercomparison of three snow schemes of varying complexity coupled to the same land surface model: Local-scale evaluation at an Alpine site. Journal of Hydrometeorology, 2(4): 374–394.

Boroneant, C., Plaut, G., Giorgi, F. and Bi, X., 2006. Extreme precipitation over the Maritime Alps and associated weather regimes simulated by a regional climate model: Present-day and future climate scenarios. Theoretical and Applied Climatology, 86(1-4): 81–99.

Bouchet, R.J., 1963. Evapotranspiration réelle et potentielle, signification climatique, IAHS General Assembly of Berkeley. IAHS Publ., No. 62, pp. 134–142.

Boudevillain, B., 2003. Contribution à la définition des caractéristiques d'un radar hydrologique urbain. Prévision de la pluie à très courte échéance. Thèse de doctorat, Université Blaise-Pascal, Clermont-Ferrand, 151 pp.

Boudevillain, B., Andrieu, H. and Chaumerliac, N., 2006. Evaluation of RadVil, a radar based very-short term rainfall forecasting model. J. Hydrometeor., 7(1): 178–189.

Boughton, W. and Chiew, F., 2007. Estimating runoff in ungauged catchments from rainfall, PET and the AWBM model. Environmental Modelling & Software, 22(4): 476–487.

Boughton, W. and Droop, O., 2003. Continuous simulation for design flood estimation—a review. Environmental Modelling and Software, 18(3-4): 309–318.

Boughton, W.C., 1993. A hydrograph-based model for estimating water yield of ungauged catchments. Institute of Engineers Australia National Conference, Publ. 93/14, pp. 317–324.

Boussinesq, J., 1904. Recherches théoriques sur l'écoulement des nappes d'eau infiltrées dans le sol. Journal de mathématiques pures et appliquées, 10(1 & 4): 5–78 & 63–394.

Box, G.E.P. and Jenkins, G.M., 1970. Time series analysis: forecasting and control. Holden-Day series in time series analysis and digital processing. CA: Holden-Day, San Francisco, 575 pp.

Braga, B.P.F., Yeh, W.W.G., Becker, L. and Barros, M.T.L., 1991. Stochastic Optimization of Multiple-Reservoir-System Operation. Journal of Water Resources Planning and Management-Asce, 117(4): 471–481.

Braud, I., Dantasantonino, A.C., Vauclin, M., Thony, J.L. and Ruelle, P., 1995. A Simple Soil-Plant-Atmosphere Transfer Model (Sispat) Development and Field Verification. Journal of Hydrology, 166(3-4): 213–250.

Bringi, V.N. and Chandrasekar, V., 2001. Polarimetric Doppler Weather Radar. Principles and Applications. Cambridge University Press, 629 pp.

Brown, R. and Goodison, B.E., 2005. Snow cover. pp. 2464–2474. In: M.G. Anderson and J.J. McDonnell (Editors), Encyclopedia of Hydrological Sciences—Part 14: Snow and Glacier Hydrology. Wiley, Chichester.

Brun, E., David, P., Sudul, M. and Brunot, G., 1992. A numerical model to simulate snow-cover stratigraphy for operational avalanche forecasting. Journal of Glaciology, 38(128): 13–22.

Brun, E., Martin, E., Simon, V., Gendre, C. and Coleou, C., 1989. An Energy and Mass Model of Snow Cover Suitable for Operational Avalanche Forecasting. Journal of Glaciology, 35(121): 333–342.

Brutsaert, W. and Nieber, J.L., 1977. Regionalized Drought Flow Hydrographs from a Mature Glaciated Plateau. Water Resources Research, 13(3): 637–644.

Brutsaert, W. and Stricker, H., 1979. Advection-Aridity Approach to Estimate Actual Regional Evapotranspiration. Water Resources Research, 15(2): 443–450.

Brutsaert, W., 2005. Hydrology—An introduction. Cambridge University Press, New York, NY, 605 pp.

Buishand, T.A. and Brandsma, T., 1997. Comparison of circulation classification schemes for predicting temperature and precipitation in the Netherlands. International Journal of Climatology, 17(8): 875–889.

Buishand, T.A. and Brandsma, T., 2001. Multisite simulation of daily precipitation and temperature in the Rhine basin by nearest-neighbor resampling. Water Resources Research, 37(11): 2761–2776.

Bulter, D. and Davies, J.W., 2000. Urban Drainage. Ed. E&FN Spon, London, 490 pp.

Burn, D.H., 1988. Delineation of Groups for Regional Flood Frequency-Analysis. Journal of Hydrology, 104(1-4): 345–361.

Burn, D.H., 1989. Cluster-Analysis as Applied to Regional Flood Frequency. Journal of Water Resources Planning and Management-Asce, 115(5): 567–582.

Burn, D.H., 1990. Evaluation of Regional Flood Frequency-Analysis with a Region of Influence Approach. Water Resources Research, 26(10): 2257–2265.

Burn, D.H., 1997. Catchment similarity for regional flood frequency analysis using seasonality measures. Journal of Hydrology, 202(1-4): 212–230.

Butler, D. and Davies, J.W., 2000. Urban drainage. E & FN Spon, London.

Butts, M.B., Payne, J.T., Kristensen, M. and Madsen, H., 2004. An evaluation of the impact of model structure on hydrological modelling uncertainty for streamflow simulation. Journal of hydrology, 298(1-4): 242–266.

Buzzi, A. and Foschini, L., 2000. Mesoscale meteorological features associated with heavy precipitation in the southern Alpine region. Meteorology and Atmospheric Physics, 72(2-4): 131–146.

BWG. 2003. Hochwasserabschätzung in schweizerische Einzugsgebieten, Praxishilfe, Bericht des BWG (Bundesamt fur Wasser und Geologie), Serie Wasser No 4, Berne, Switzerland

Calver, A., 1988. Calibration, Sensitivity and Validation of a Physically-Based Rainfall Runoff Model. Journal of Hydrology, 103(1-2): 103–115.

Cappelaere, B., 1985. Le modèle STREAM—Application à l'aménagement de la vallée du TARN à Montauban. BCEOM, 16 pp.

Cappelaere, B., 1997. Accurate diffusive wave routing. Journal of Hydraulic Engineering-Asce, 123(3): 174–181.

Cappus, P., 1960. Etude des lois de l'écoulement. Application au calcul et à la prévision des débits. Bassin expérimental de l'Alrance. La Houille Blanche, July–August, 1960, no. A: 493–520.

Carlier, M., 1972. Hydraulique Générale et Appliquée, 14. Editions Eyrolles, 566 pp.

Carlson, R.E. and Foley, T.A., 1991a. Radial Basis Interpolation Methods on Track Data, Lawrence Livermore National Laboratory, UCRL-JC-1074238.

Carlson, R.E. and Foley, T.A., 1991b. The Parameter R2 in Multiquadric Interpolation. Computers & Mathematics with Applications, 21(9): 29–42.

Carpenter, T.M. and Georgakakos, K.P., 2001. Assessment of Folsom lake response to historical and potential future climate scenarios: 1. Forecasting. Journal of Hydrology, 249(1-4): 148–175.

Carpenter, T.M. and Georgakakos, K.P., 2006. Intercomparison of lumped versus distributed hydrologic model ensemble simulations on operational forecast scales. Journal of Hydrology, 329(1-2): 174–185.

Cassou, C., 2004. Du changement climatique aux régimes de temps: l'oscillation nord-atlantique. La Météorologie, 45: 21–32.

Castaings, W., Le Dimet, F.-X. and Dartus, D., 2003. Assimilation de données *in situ* et télédétection pour la modélisation hydrologique. Bulletin—Société française de photogrammétrie et de télédétection, 172: 50–60.

Castaings, W., Le Dimet, F.-X., Dartus, D. and Saulnier, G.M., 2006. Potentiel et limitations des méthodes variationnelles pour la modélisation hydrologique, Colloque national sur l'assimilation de données, Toulouse.

Castany, G., 1998. Hydrogéologie: principes et méthodes. Ed. Dunod, Paris, 236 pp.

Castelle, T., 1994. Transport de la neige par le vent en montagne: approche expérimentale du site du Col du Lac Blanc. Thèse de doctorat, EPFL, Lausanne.

Cavadias, G.S., 1990. The canonical correlation approach to regional flood estimation, Regionalisation in hydrology. IAHS, Wallingford, Ljubljana, pp. 171–178.

CFGB, 1994. Les crues de projet des barrages: méthode du GRADEX. Design Flood Determination by the Gradex Method. Bulletin du Comité Français des Grands Barrages N°2, 18° Congrès CIGB-ICOLD, 96 pp.

Chadwick, A. and Morfett, J., 1998. Hydraulics in Civil and Environmental Engineering. 3rd edition, Spon, 600 pp.

Chahinian, N., Moussa, R., Andrieux, P. and Voltz, M., 2006. Accounting for temporal variation in soil hydrological properties when simulating surface runoff on tilled plots. Journal of Hydrology, 326(1-4): 135–152.

Chalon, J.-P., 2002. Combien pèse un nuage? Ou pourquoi les nuages ne tombent pas? EDP Sciences, Les Ulis, France, 187 pp.

Chapman, T., 1999. A comparison of algorithms for stream flow recession and baseflow separation. Hydrological Processes, 13(5): 701–714.

Chapon, B., 2006. Étude des pluies intenses dans la région Cévennes-Vivarais à l'aide du radar météorologique. Régionalisation des traitements radar et analyse granulométrique de la pluie au sol. Thèse de doctorat, INPG, Grenoble, 197 pp.

Chardon, J. *et al.,* 2013. Spatial similarity and transferability of analog dates for precipitation downscaling over France. J. Climate (in press).

Charleux-Demargne, J., 2001. Qualité des modèles numériques de terrain pour l'hydrologie. Application à la caractérisation du régime de crues des bassins versants. Thèse de doctorat, Univ. Marne la vallée, 350 pp.

Chastan, B., Gilard, O., Givone, P. and Oberlin, G., 1994. Le modèle Inondabilité, présent et avenir. Crues et Inondations, 23èmes Journées de l'Hydraulique, Congrès de la SHF, pp. 741–744.

Chaudhry, M.H. 1993. Open-Channel Flow. Prentice Hall, Englewood Cliffs, NJ, USA.

Chauvet, P., 1999. Aide-mémoire de géostatistique linéaire. Presses de l'Ecole des Mines de Paris, Paris, 370 pp.

Chiew, F.H.S. and McMahon, T.A., 1991. The Applicability of Morton and Penman Evapotranspiration Estimates in Rainfall-Runoff Modeling. Water Resources Bulletin, 27(4): 611–620.

Chin, D.A., 2000. Water Resources Engineering. Ed. Prentice Hall, New Jersey, US, 750 pp.

Chocat, B., (éd.), 1997. Encyclopédie de l'Hydrologie Urbaine et de l'Assainissement. Ed. Lavoisier, Paris, 1124 pp.

Chow, V.T., 1959. Open Channel Hydraulics. Mc Graw Hill, New York, 197 pp.

Chow, V.T., Maidment, D.R. and Mays, L.W., 1988. Applied Hydrology. Civil Engineering Series. McGraw-Hill International Editions, 572 pp.

Chowdhury, J.U., Stedinger, J.R. and Lu, L.H., 1991. Goodness-of-Fit Tests for Regional Generalized Extreme Value Flood Distributions. Water Resources Research, 27(7): 1765–1776.

Christensen, J.H., Carter, T.R., Rummukainen, M., Georgios, A. *et al.* 2007. Evaluating the performance and utility of regional climate models: the PRUDENCE project. Climatic Change, 81(1): 1–6.

Clabor, B. and Moore, W., 1970. Numerical simulation of watershed hydrology, University of Texas.

Clark, M.P. *et al.,* 2006. Assimilation of snow covered area information into hydrologic and land-surface models. Advances in Water Resources, 29(8): 1209–1221.

Clarke, L. *et al.* 2007. Scenarios of Greenhouse Gas Emissions and Atmospheric Concentrations. Sub-report 2.1A of Synthesis and Assessment Product 2.1 by the U.S. Climate Change Science Program and the Subcommittee on Global Change Research. Department of Energy, Office of Biological & Environmental Research, Washington, 7 DC., USA, 154 pp.

Clarke, R.T., 1973. Mathematical models in hydrology. Irrigation and Drainage paper N°19. FAO, Rome.

Coiffier, J., 2000. Un demi-siècle de prévision numérique du temps. La Météorologie, 30: 11–31.

Colbeck, S.C., 1978. The physical aspects of water flow through snow. Advances in Hydroscience, 11: 165–206.

Condie, R. and Lee, K.A., 1982. Flood Frequency-Analysis with Historic Information. Journal of Hydrology, 58(1-2): 47–61.

Consuegra, D. and Musy, A., 1989. La méthode rationnelle. Teaching notes for Bs hydrological courses, EPFL, Lausanne, 28 pp.

Consuegra, D., Niggli, M. and Musy, A., 1998. Concepts méthodologiques pour le calcul des crues. Application au bassin versant supérieur du Rhône. Wasser Energie Luft - Eau Energie Air, 9/10: 223–231.

Conway, D., Wilby, R.L. and Jones, P.D., 1996. Precipitation and air flow indices over the British Isles. Climate Research, 7(2): 169–183.

Copeland *et al.* 2001. Hydraulic Design of Stream Restoration Projects, US Army Corps of Engineers, Washington, DC 20314-1000, 110 p + Appendix.

Cordery, I. and Pilgrim, D.M. 1984. Time Patterns of Rainfall for Estimating Design Floods on a Frequency Basis. Wat. Sci. Tech. 16: 155–165.

Corradini, C., Morbidelli, R. and Melone, F., 1998. On the interaction between infiltration and Hortonian runoff. Journal of Hydrology, 204(1-4): 52–67.

Corriou, J.P., 1996. Commande des procédés. Génie des procédés de l'Ecole de Nancy, TEC&DOC. Ed. Lavoisier.

Corte-Real, J., Qian, B.D. and Xu, H., 1998. Regional climate change in Portugal: Precipitation variability associated with large-scale atmospheric circulation. International Journal of Climatology, 18(6): 619–635.

Cosenday, C. and Robinson, M., 2000. Hydrologie continentale. Ed. Armand Colin, Paris, 360 pp.

Courault, D., Seguin, B. and Olioso, A., 2005. Review on estimation of evapotranspiration from remote sensing data: From empirical to numerical modeling approaches. Irrigation and Drainage Systems, 19(3-4): 223–249.

Coutagne, A., 1948. Météorologie et hydrologie. Étude générale des débits et des facteurs qui les conditionnent. 2eme partie: les variations de débit en période non influencée par les précipitations. Le débit d'infiltration (corrélations fluviales internes). La Houille Blanche, pp. 416–436.

Cowpertwait, P.S.P., 1995. A Generalized Spatial-Temporal Model of Rainfall Based on a Clustered Point Process. Proceedings of the Royal Society of London Series a-Mathematical and Physical Sciences, 450(1938): 163–175.

Cowpertwait, P.S.P., 2006. A spatial-temporal point process model of rainfall for the Thames catchment, UK. Journal of Hydrology, 330(3-4): 586–595.

Cowpertwait, P.S.P., Oconnell, P.E., Metcalfe, A.V. and Mawdsley, J.A., 1996. Stochastic point process modelling of rainfall. 2. Regionalisation and disaggregation. Journal of Hydrology, 175(1-4): 47–65.

Cox, D.R. and Isham, V., 1994. Stochastic models of precipitation. pp. 3–18. In: V.D. Barnett and K.F. Turkman (Editors), Statistics for the Environment, 2: Water related issues. Wiley, Chichester.

Crawford, N.H. and Linsley, R.K., 1966. Digital simulation in hydrology: Stanford Watershed Model IV. Stanford Univ., Palo Alto, Calif., Tech. Rep. No. 39.

Creutin, J.D. and Obled, C., 1982. Objective analyses and mapping techniques for rainfall fields. An objective comparison. Water Resources Research, 18(2): 413–431.

Crockford, R.H. and Richardson, D.P., 2000. Partitioning of rainfall into throughfall, stemflow and interception: effect of forest type, ground cover and climate. Hydrological Processes, 14(16-17): 2903–2920.

Cunge, J.A., 1995. Modèles mathématiques en hydraulique et en hydrologie (Mathematical models in hydraulics and in hydrology). Techniques de l'ingénieur. Construction, CB1(C180): C180.1–C180.17.

Cunge, J.A., Holly, F.M. and Verwey, A., 1980. Practical Aspects of Computational River Hydraulics. Monographs and surveys. Water Ressources Engineering, 3. Pitman Publishing, London, 420 pp.

Cunge, J.A., 1969. Au sujet d'une méthode de propagation de crue. Journal of Hydraulics Research, 7: 205–230.

Cunnane, C., 1988. Methods and Merits of Regional Flood Frequency-Analysis. Journal of Hydrology, 100(1-3): 269–290.

Cunnane, C., 1989. Statistical distributions for flood frequency analysis. Operational Hydrology Report No. 33. World Meteorological Organization, Geneva.

D'Almeida, C. *et al.,* 2006. A water balance model to study the hydrological response to different scenarios of deforestation in Amazonia. Journal of Hydrology, 331(1-2): 125–136.

Dalrymple, T., 1960. Flood-Frequency Analyses. Manual of Hydrology: Part 3, Flood-Flow Techniques. Geological Survey Water-Supply Paper: 1543-A. US Geological Survey, Washington, 80 pp.

Dalton, J., 1802a. Experiments and observations to determine whether the quantity of rain and dew is equal to the quantity of water carried off by the rivers and raised by evaporation; with an enquiry into the origin of springs. Mem. Lit. Philos. Soc. Manchester, V, II, pp. 346–372.

Dalton, J., 1802b. Experimental essays on the constitution of mixed gases; on the force of steam or vapour from water and other liquids in different temperatures, both in a Torricellian vacuum and in air; on evaporation expansion of gases by heat. Mem. Lit. Philos. Soc. Manchester, V, II, pp. 535–602.

Darcy, H., 1856. Les fontaines publiques de la ville de Dijon: exposition et application des principes à suivre et des formules à employer dans les questions de distribution d'eau. Victor Dalmont, Paris.

Davison, B. and Pietroniro, A., 2005. Hydrology of Snowcovered Basins, Encyclopedia of Hydrological Sciences —Part 14: Snow and Glacier Hydrology. Wiley, Chichester, pp. 2506–2524.

De Roo, A.P.J., Wesseling, C.G. and Ritsema, C.J., 1996. LISEM: a single event physically-based hydrologic and soil erosion model for drainage basins. I: Theory, input and output. Hydrological Processes, 10(8): 1107–1117.

Deguchi, A., Hattori, S. and Park, H.T., 2006. The influence of seasonal changes in canopy structure on interception loss: Application of the revised Gash model. Journal of Hydrology, 318(1-4): 80–102.

Deidda, R., Benzi, R. and Siccardi, F., 1999. Multifractal modeling of anomalous scaling laws in rainfall. Water Resources Research, 35(6): 1853–1867.

Delleur, J.W., 1991. Time series analysis applied to hydrology, V.U.B.-Hydrologie, Brussels, 290 pp.

Delrieu, G. *et al.,* 2005. The catastrophic flash-flood event of 8–9 September 2002 in the Gard region, France: A first case study for the Cevennes-Vivarais Mediterranean Hydrometeorological Observatory. Journal of Hydrometeorology, 6(1): 34–52.

Delrieu, G., Andrieu, H. and Creutin, J.D., 2000. Quantification of path-integrated attenuation for X- and C-band weather radar systems operating in heavy rainfall. J. Appl. Meteor., 39(6): 840–850.

Demuth, S., 1993. Untersuchungen zum Niedrigwasser in West-Europa. Band/volume 1. Universität Freiburg, Freiburg.

Deque, M. *et al.,* 2005. Global high resolution versus Limited Area Model climate change projections over Europe: quantifying confidence level from PRUDENCE results. Climate Dynamics, 25(6): 653–670.

Déqué, M., 2003. La Prévision numérique à l'échelle saisonnière: que sait-on faire et que peut-on espérer? La Météorologie, 41: 20–29.

Desbordes, M., 1984. Modélisation en hydrologie urbaine. Recherches et applications. Université Montpellier II, Laboratoire d'hydrologie mathématique STU, 183 pp.

Dingman, S.L., 2002. Physical Hydrology. Prentice-Hall, New Jersey, 646 pp.

Dolciné, L., 1997. Prévision quantitative à très courte échéance de la pluie. Modèle global adapté à l'information radar. Thèse de doctorat, Université Joseph Fourier 1, Grenoble, 183 pp.

Douville, H., Royer, J.F. and Mahfouf, J.F., 1995. A New Snow Parameterization for the Meteo-France Climate Model. 1. Validation in Stand-Alone Experiments. Climate Dynamics, 12(1): 21–35.

Downer, C.W., Ogden, F.L., Martin, W.D. and Harmon, R.S., 2002. Theory, development, and applicability of the surface water hydrologic model CASC2D. Hydrological Processes, 16(2): 255–275.

Draper, N.R. and Smith, H., 1981. Applied regression analysis. Second edition, John Wiley & Sons, New York, 736 pp.

Drogue, G., Humbert, J., Deraisme, J., Mahr, N. and Freslon, N., 2002. A statistical-topographic model using an omnidirectional parameterization of the relief for mapping orographic rainfall. International Journal of Climatology, 22(5): 599–613.

Duan, Q. *et al.,* 2006. Model Parameter Estimation Experiment (MOPEX): An overview of science strategy and major results from the second and third workshops. Journal of Hydrology, 320(1-2): 3–17.

Duan, Q.Y., Gupta, H., Sorooshian, S., Rousseau, A.N. and Turcotte, R., 2003. Calibration of watershed models. Water Science and Application 6. American Geophysical Union, Washington, DC, 345 pp.

Duan, Q., Gupta, V.K. and Sorooshian, S. 1992. Effective and efficient global optimization for conceptual rainfall-runoff models, Water Resour. Res., 28: 1015–1031.

Duband, D., 1970. Reconnaissance dynamique de la forme des situations météorologiques. Application à la prévision quantitative des précipitations. Thèse de doctorat, Faculté des sciences de Paris.

Duband, D., 2002. Imagerie satellitaire et radar au service de l'eau. La Houille Blanche, 1: 29–30.

Duband, D., Obled, C. and Rodriguez, J.Y., 1993. Unit-Hydrograph Revisited—an Alternate Iterative Approach to Uh and Effective Precipitation Identification. Journal of Hydrology, 150(1): 115–149.

Dufresne, J.-L. *et al.,* 2006. Simulation du climat récent et futur par les modèles du CNRM et de l'IPSL. La Météorologie, 55(45-59).

Dumas, A., 2006. Méthode de maximisation: estimation des crues maximales probables (CMP). La Houille Blanche, 5: 74–79.

Dunkerley, D., 2000. Measuring interception loss and canopy storage in dryland vegetation: a brief review and evaluation of available research strategies. Hydrological Processes, 14(4): 669–678.

Dunne, T. and Black, R.D., 1970. An experimental investigation of runoff production in permeable soils. Wat. Resour. Res., 6: 478–480.

Dunne, T., Price, A.G. and Colbeck, S.C., 1976. Generation of Runoff from Subarctic Snowpacks. Water Resources Research, 12(4): 677–685.

Dupont, S., Demargne, L. and Durand, P., 1998. Production de MNT à partir de données SAR RADARSAT. Rapport Final, Programme AvalSAR, CNES, Toulouse.

Durand, M. and Margulis, S.A., 2006. Feasibility test of multifrequency radiometric data assimilation to estimate snow water equivalent. Journal of Hydrometeorology, 7(3): 443–457.

Durrans, S.R. and Kirby, J.T., 2004. Regionalization of extreme precipitation estimates for the Alabama rainfall atlas. Journal of Hydrology, 295(1-4): 101–107.

Durrans, S.R. and Tomic, S., 1996. Regionalization of low-flow frequency estimates: An Alabama case study. Water Resources Bulletin, 32(1): 23–37.

Düster, H., 1994. Modellierung der räumlichen Variabilität seltener Hochwasser in der Schweiz, Geographica Bernesia G44, Geographisches Institut der Universität Bern.

Eagleson, P.S., 1970. Dynamic Hydrology. McGraw-Hill, New York, pp. 337–366.

Eckhardt, K., 2005. How to construct recursive digital filters for baseflow separation. Hydrological Processes, 19(2): 507–515.

Edijatno, N. and Michel, C., 1989. Un modèle pluie-débit à trois paramètres. La Houille Blanche, 2: 113–121.

Edijatno, Nascimento, N.D., Yang, X.L., Makhlouf, Z. and Michel, C., 1999. GR3J: a daily watershed model with three free parameters. Hydrological Sciences Journal-Journal Des Sciences Hydrologiques, 44(2): 263–277.

El-Awar, F.A., Labadie, J.W. and Ouarda, T., 1998. Stochastic differential dynamic programming for multi-reservoir system control. Stochastic Hydrology and Hydraulics, 12(4): 247–266.

Elliott, R.D., 1949. The weather types of N. America. Weatherwise, 2: 15–18, 40–43, 64–67, 86–88, 110–113, 136–138.

Etchevers, P. *et al.,* 2004. Validation of the energy budget of an alpine snowpack simulated by several snow models (SnowMIP project). Annals of Glaciology, 38(1): 150–158.

Etchevers, P., Durand, Y., Habets, F., Martin, E. and Noilhan, J., 2000. Impact of spatial resolution on the hydrological simulation of the Durance high Alpine catchment. Annals of Glaciology, 32: 87–92.

Etchevers, P., Golaz, C., Habets, F. and Noilhan, J., 2002. Impact of a climate change on the Rhone river catchment hydrology. Journal of Geophysical Research-Atmospheres, 107(D16).

Evin, G. and Favre, A.-C., 2008. A new rainfall model based on the Neyman-Scott process using cubic copulas. Wat. Resour. Res., 44: W03433, doi:10.1029/2007WR006054.

Ewen, J. and Parkin, G., 1996. Validation of catchment models for predicting land-use and climate change impacts. 1. Method. Journal of hydrology, 175(1-4): 583–594.

FAO, 1998. Crop evapotranspiration. Guidelines for computing crop water requirements. FAO Irrigation and drainage paper 56. FAO, Rome, 300 pp.

Favre, A.C., 2001. Single and Multi-Site Modelling of Rainfall based on the Neyman-Scott Process. Thèse de doctorat, EPFL, Lausanne, 133 pp.

Favre, A.C., Musy, A. and Morgenthaler, S., 2002. Two-site modeling of rainfall based on the Neyman-Scott process. Water Resources Research, 38(12).

Favre, A.-C., Musy, A. and Morgenthaler, S., 2004. Unbiased parameter estimation of the Neyman-Scott model for rainfall simulation with related confidence interval. J. Hydrol., 286(1-4): 168–178.

Fenicia, F., Savenije, H.H.G., Matgen, P. and Pfister, L., 2007. A comparison of alternative multiobjective calibration strategies for hydrological modeling. Water Resources Research, 43(3).

Fenicia, F., Savenije, H.H.G., Matgen, P. and Pfister, L., 2008. Understanding catchment behavior through stepwise model concept improvement. Water Resources Research, 44.

Fennessey, N. and Vogel, R.M., 1990. Regional Flow-Duration Curves for Ungauged Sites in Massachusetts. Journal of Water Resources Planning and Management-Asce, 116(4): 530–549.

Fierz, C. and Lehning, M., 2001. Assessment of the microstructure-based snow-cover model SNOWPACK: thermal and mechanical properties. Cold regions science and technology, 33: 123–131.

Fill, H.D. and Stedinger, J.R., 1995. Homogeneity Tests Based Upon Gumbel Distribution and a Critical-Appraisal of Dalrymple Test. Journal of Hydrology, 166(1-2): 81–105.

Fill, H.D. and Stedinger, J.R., 1998. Using regional regression within index flood procedures and an empirical Bayesian estimator. Journal of Hydrology, 210(1-4): 128–145.

Flowers, G.E. and Clarke, G.K.C., 2002. A multicomponent coupled model of glacier hydrology, 1, Theory and synthetic examples. Journal of Geophysical Research, 107(B11): 2287, doi:10.1029/2001JB001122.

Fortin, J.P., Moussa, R., Bocquillon, C. and Villeneuve, J.P., 1995. Hydrotel, un modèle hydrologique distribué pouvant bénéficier des données fournies par la télédétection et les systèmes d'information géographique. Revue des Sciences de l' Eau, 8(1): 97–124.

Fortin, V., Favre, A.-C. and Said, M., 2006. Probabilistic forecasting from ensemble prediction systems: Improving upon the best-member method by using a different weight and dressing kernel for each member. Quarterly Journal of the Royal Meteorological Society, 132(B) (617): 1349–1369.

Fortin, V., Ouarda, T.B.M.J., Rasmussen, P.F. and Bobée, B., 1997. Revue bibliographique des méthodes de prévision des débits. Revue des Sciences de l' Eau, 10(4): 461–487.

Fountain, A.G. and Walder, J.S., 1998. Water flow through temperate glaciers. Reviews of Geophysics, 36(3): 299–328.

Fouquet, P. *et al.* 1978. Evacuation des eaux pluviales urbaines. Rapport de l'Amicale des Elèves de l'ENPC, 166 p. In Harms R.W., Verworn H.R. (1984).

Fowler, H.J., Blenkinshop, S. and Tebaldi, C., 2007. Linking climate change modelling to impacts studies: recent advances in downscaling techniques for hydrological modelling. International Journal of Climatology, 27: 1547–1578.

Franchini, M., 1996. Use of a genetic algorithm combined with a local search method for the automatic calibration of conceptual rainfall-runoff models. Hydrological Sciences Journal, 41(1): 21–39.

François, B., Hingray, B., Hendrickx, F. and Creutin, J.D. 2013. Storage water value as a signature of the climatological balance between resource and uses. Hydrol. Earth Syst. Sci. Discuss., 10: 8993–9025.

Frei, C. *et al.,* 2003. Daily precipitation statistics in regional climate models: Evaluation and intercomparison for the European Alps. Journal of Geophysical Research-Atmospheres, 108(D3).

Frei, C., Scholl, R., Fukutome, S., Schmidli, R. and Vidale, P.L., 2006. Future change of precipitation extremes in Europe: Intercomparison of scenarios from regional climate models. Journal of Geophysical Research-Atmospheres, 111(D6).

French, M.N. and Krajewski, W.F., 1994. A Model for Real-Time Quantitative Rainfall Forecasting Using Remote-Sensing. 1. Formulation. Water Resources Research, 30(4): 1075–1083.

Froidurot, S., Zin, I., Hingray, B. and Gautheron, A., 2013. On the precipitation phase discrimination over the Swiss Alps. The explanatory power of different near-surface and atmospheric variables. J. Hydromet. (in press).

Fujino, J. *et al.* 2006. Multi-gas mitigation analysis on stabilization scenarios using AIM global model. Multigas Mitigation and Climate Policy. The Energy Journal, 3 (Special Issue).

Gangopadhyay, S., Clark, M. and Rajagopalan, B., 2005. Statistical downscaling using K-nearest neighbors. Water Resources Research, 41(2).

Gangopadhyay, S., Clark, M., Werner, K., Brandon, D. and Rajagopalan, B., 2004. Effects of spatial and temporal aggregation on the accuracy of statistically downscaled precipitation estimates in the upper Colorado River basin. Journal of Hydrometeorology, 5(6): 1192–1206.

Gao, X.G., Sorooshian, S. and Gupta, H.V., 1996. Sensitivity analysis of the biosphere-atmosphere transfer scheme. Journal of Geophysical Research-Atmospheres, 101(D3): 7279–7289.

Garen, D.C. and Marks, D., 2005. Spatially distributed energy balance snowmelt modelling in a mountainous river basin: estimation of meteorological inputs and verification of model results. Journal of Hydrology, 315(1-4): 126–153.

Gash, J.H.C. and Morton, A.J., 1978. Application of Rutter Model to Estimation of Interception Loss from Thetford Forest. Journal of Hydrology, 38(1-2): 49–58.

Gash, J.H.C., 1979. Analytical Model of Rainfall Interception by Forests. Quarterly Journal of the Royal Meteorological Society, 105(443): 43–55.

Gash, J.H.C., Lloyd, C.R. and Lachaud, G., 1995. Estimating Sparse Forest Rainfall Interception with an Analytical Model. Journal of Hydrology, 170(1-4): 79–86.

Gash, J.H.C., Wright, I.R. and C.R., L., 1980. Comparative Estimates of Interception Loss from Three Coniferous Forests in Great Britain. Journal of Hydrology, 48(1-2): 89–105.

Gaume, E., 2007. Un parcours dans l'étude des phénomènes extrêmes en hydrologie. HDR, ENPC, Marne la vallée, 269 pp.

Gaume, E., Livet, M. and Desbordes, M., 2003. Study of the hydrological processes during the Avene river extraordinary flood (south of France): 6–7 October 1997. Physics and Chemistry of the Earth, 28: 263–267.

Gelman, A., Canlin, J., Stein, H. and Rubin, D., 1995. Bayesian Data Analysis. Chapman and Hall, London, UK, 552 pp.

Gendreau, N. and Puech, C., 2002. L'hydrologie et l'information issue du spatial. La Houille Blanche, 1: 31–34.

Georgakakos, K.P. and Bras, R.L., 1982. Real-Time, Statistically Linearized, Adaptive Flood Routing. Water Resources Research, 18(3): 513–524.

Georgakakos, K.P., Seo, D.J., Gupta, H., Schaake, J. and Butts, M.B., 2004. Towards the characterization of streamflow simulation uncertainty through multimodel ensembles. Journal of Hydrology, 298(1-4): 222–241.

Gerbaux, M., 2005. Reconstruction du bilan de masse des glaciers alpins et impact d'un changement climatique. Thèse de doctorat, LGGE, Université Joseph Fourier, Grenoble, 132 pp.

Gilli, E., Mangan, C. and Mudry, J.-N., 2004. Hydrogéologie: objets, méthodes, applications. Cours (Coll. Sciences Sup). Ed. Lavoisier, Paris, 302 pp.

Gingras, D. and Adamowski, K., 1993. Homogeneous Region Delineation Based on Annual Flood Generation Mechanisms. Hydrological Sciences Journal-Journal Des Sciences Hydrologiques, 38(2): 103–121.

Girard, G., 1975. Application du modèle à discrétisation spatiale à un bassin semi-désertique, Application des modèles mathématiques à l'hydrologie et aux systèmes des ressources en eau. IAHS Publication N°115, Bratislava, pp. 104–114.

Girard, G., Charbonneau, R. and Morin, G., 1972. Modèle hydro-physiographique, Comptes rendus Symposium international sur les techniques de modèles mathématiques appliquées aux systèmes de ressources en eau. Environnement Canada, Ottawa, pp. 190–205.

Gloor, R. and Walter, M., 1986. Estimation des débits d'étiage sur des cours d'eau sans mesures directe. Beitrage zur Geologie der Schweiz - Hydrologie nr. 33, pp. 37–100.

Gneiting, T. and Raftery, A.E., 2005. Atmospheric science—Weather forecasting with ensemble methods. Science, 310(5746): 248–249.

Gneiting, T., Raftery, A.E., Westveld, A.H. and Goldman, T., 2005. Calibrated probabilistic forecasting using ensemble model output statistics and minimum CRPS estimation. Monthly Weather Review, 133(5): 1098–1118.

Gottardi, F., Obled, C., Gailhard, J. and Paquet, E., 2012. Statistical reanalysis of precipitation fields based on ground network data and weather patterns: Application over French mountains. J. Hydrol., 432: 154–167.

Gottardi, F., Obled, C., Paquet, E. and Gailhard, J., 2008. Régionalisation des précipitations sur les massifs montagneux français à l'aide de regressions locales et par type de temps. Climatologie, 5 pp.

Gotzinger, J. and Bardossy, A., 2007. Comparison of four regionalisation methods for a distributed hydrological model. Journal of Hydrology, 333(2-4): 374–384.

Graf, W.H. and Altinakar, M., 1998. Hydrodynamique: une introduction. Traité de Génie Civil N°14, 492. Ed. PPUR, Lausanne.

Graf, W.H. and Altinakar, M., 2000. Hydraulique fluviale. Ecoulement et phénomènes de transport dans les canaux à géométrie simple. Traité de Génie Civil N°16. Ed. PPUR, Lausanne, 627 pp.

Graf, W.H., 1998. Fluvial Hydraulics: Flow and Transport Processes in Channels of Simple Geometry. In collaboration with M.S. Altinakar, John Wiley and Sons, England, 681 pp.

Grayson, R.B. and Bloschl, G., 2000. Spatial patterns in catchment hydrology: observations and modeling. Cambridge University Press, UK.

Grayson, R.B., Blöschl, G. and Moore, I.D., 1995. Distributed parameter hydrologic modeling using vector elevation data: THALES and TAPES-C. pp. 1130–78. In: V.P. Singh (Editor), Computer Models of Watershed Hydrology. CO, Water Resour. Publications, Fort Collins.

Grayson, R.B., Moore, I.D. and McMahon, T.A., 1992. Physically-based Hydrologic Modeling II: Is the Concept Realistic? Water Resources Research, 28(10): 2659–66.

Guilbaud, S. and Obled, C., 1998. L'approche par analogues en prévision météorologique. La Météorologie, 8(24): 21–35.

Guillevic, P. *et al.*, 2002. Influence of the interannual variability of vegetation on the surface energy balance—A global sensitivity study. Journal of Hydrometeorology, 3(6): 617–629.

Guillot, P. and Duband, P., 1967. La méthode du GRADEX pour le calcul des probabilités de crue à partir des pluies. Journal des sciences hydrologiques, 84: 560–569.

Gupta, V.K. and Waymire, E., 1990. Multiscaling Properties of Spatial Rainfall and River Flow Distributions. Journal of Geophysical Research-Atmospheres, 95(D3): 1999–2009.

Gupta, V.K. and Waymire, E.C., 1993. A Statistical-Analysis of Mesoscale Rainfall as a Random Cascade. Journal of Applied Meteorology, 32(2): 251–267.

Gupta, V.K., Mesa, O.J. and Dawdy, D.R., 1994. Multiscaling Theory of Flood Peaks—Regional Quantile Analysis. Water Resources Research, 30(12): 3405–3421.

Gurtz, J., Baltensweiler, A. and Lang, H., 1999. Spatially distributed hydrotope-based modelling of evapotranspiration and runoff in mountainous basins. Hydrological Processes, 13(17): 2751–2768.

Guswa, A.J., Celia, M.A. and Rodriguez-Iturbe, I., 2002. Models of soil-moisture dynamics in ecohydrology: A comparative study. Water Resources Research, 38(9): 5.1–5.15.

Haberlandt, U., Klocking, B., Krysanova, V. and Becker, A., 2001. Regionalisation of the base flow index from dynamically simulated flow components—a case study in the Elbe River Basin. Journal of Hydrology, 248(1-4): 35–53.

Habets, F. *et al.*, 2008. The SAFRAN-ISBA-MODCOU hydrometeorological model applied over France. J. Geophys. Res.-Atmos., 113 pp.

Hall, D.K., Kelly, R.E.J., Foster, J.L. and Chang, A.T.C., 2005. Estimation of Snow Extent and Snow Properties. pp. 811–830. In: M.G. Anderson and J.J. McDonnell (Editors), Encyclopaedia of Hydrological Sciences—Part 14: Snow and Glacier Hydrology. Wiley, Chichester.

Hamdi, Y., Hingray, B. and Musy, A., 2005. Un modèle de prévision hydro-météorologique pour les crues du Rhône supérieur en Suisse. Wasser, Energie and Luft, 11–12: 325–332.

Hannah, D. and Gurnell, A.M., 2001. A conceptual, linear reservoir runoff model to investigate melt season changes in cirque glacier hydrology. Journal of Hydrology, 246(1-4): 123–141.

Hansen, B., 2000. Estimation of surface runoff and water-covered area during filling of surface microrelief depressions. Hydrological Processes, 14(7): 1235–1243.

Hansen, J.R., Refsgaard, J.C., Hansen, S. and Ernstsen, V., 2007. Problems with heterogeneity in physically based agricultural catchment models. Journal of Hydrology, 342(1-2): 1–16.

Hastings, W.K. 1970. Monte Carlo Sampling Methods Using Markov Chains and Their Applications. Biometrika, 57(1): 97–109.

Hawkins, E. and Sutton, R., 2009. The Potential to Narrow Uncertainty in Regional Climate Predictions. Bull. Amer. Meteorol. Soc., 90: 1095–+.

Hawkins, E. and Sutton, R., 2011. The potential to narrow uncertainty in projections of regional precipitation change. Clim. Dyn., 37: 407–418.

Hayami, S., 1951. On the propagation of flood waves. Bulletin of the Disaster Prevention Research Institute, Kyoto University, 1: 1–16.

Hedstrom, N.R. and Pomeroy, J.W., 1998. Measurements and modelling of snow interception in the boreal forest. Hydrological Processes, 12(10-11): 1611–1625.

Heemink, A.W. and Kloosterhuis, H., 1990. Data assimilation for non-linear tidal models. Internat. J. Num. Methods in Fluids, 11(8): 1097–1112.

Henderson, F.M. 1966. Open channel flow MacMillan Publishing Company, 522 p.

Hervouet, J.-M., 2003. Hydrodynamique des écoulements à surface libre: Modélisation numérique avec la méthode des éléments finis. Presses de l'ENPC, Paris, 312 pp.

Hewitson, B.C. and Crane, R.G., 2002. Self-organizing maps: applications to synoptic climatology. Climate Research, 22(1): 13–26.

Hewlett, J.D., 1961. Soil moisture as a source of base flow from steep mountain watershed. US forest Service, Southeastern Forest Experiment Station, Asheville, North Carolina.

Hewlett, J.D. and Hibbert, A.R., 1967. Factors affecting the response of small watershed to precipitation in humid areas, International Symposium on Forest Hydrology. Pergamon, New York.

Hicks, W.I., 1944. A Method of Computing Urban Runoff. Transactions of the American Society of Civil Engineers, 109: 1217–1253.

Higy, C., 2000. Modélisation conceptuelle et à base physique des processus hydrologiques: application au bassin versant de la Haute-Mentue. Thèse de doctorat, EPFL, Lausanne, 338 pp.

Hijioka, Y. *et al.* 2008. Global GHG emissions scenarios under GHG concentration stabilization targets. Journal of Global Environmental Engineering, 13: 97–108.

Hillel, D., 1982. Introduction to Soil Physics. Academic Press, New York, 392 pp.

Hingray, B. and Ben Haha, M., 2005. Statistical performances of various deterministic and stochastic models for rainfall series disaggregation. Atmospheric Research, 77(1-4): 152–175.

Hingray, B. and Mezghani, A., 2007. Utilisation des réanalyses NCEP pour la génération de scénarios météorologiques. Application pour la génération de scénarios de crues pour le Rhône à l'amont du Leman. La Houille Blanche, 6: 104–110.

Hingray, B. *et al.,* 2006a. Simulation of streamflow by a regionalized lumped rainfall–runoff model over Luxembourg. IAHS Publ., No. 307, pp. 256–263.

Hingray, B. *et al.,* 2006b. Estimation des débits de crue du Rhône à Porte du Scex et autres points amont caractéristiques. Projet CONSECRU 2. Rapport final. HYDRAM, EPFL, Lausanne, 190 pp.

Hingray, B., Mezghani, A. and Buishand, A., 2007a. Development of regional climate change pdf's from uncertain global mean warming and an uncertain scaling relationship. Hydrology and Earth System Sciences, 11(3): 1097–1114.

Hingray, B. *et al.,* 2007b. Accounting for global warming and scaling uncertainties in climate change impact studies: application to a regulated lakes system. Hydrology and Earth System Sciences, 11(3): 1207–1226.

Hingray, B., 1999. Comportement et modélisation hydraulique des zones bâties en situation d'inondation: le cas des zones cloisonnées d'habitat individuel de Ouagadougou. Thèse de doctorat, Université de Montpellier 2, 389 pp.

Hingray, B., 2003. Multisite and spatial-temporal models for the generation of space-time rainfall fields: a review. Technical Report. HYDRAM, EPFL, Lausanne, 50 pp.

Hingray, B. *et al.,* 2012. Etat des lieux et opportunités pour une politique d'observation hydrométéorologique de long terme en zone de montagne. Hydrometeorological observations in mountainous areas. Constraints, limits and perspectives. La Houille Blanche., 2: 5–11.

Hingray, B. *et al.,* 2013. Downscaling of climate model outputs for Climate Related Energies estimation. Scoping Report. COMPLEX "Knowledge based climate mitigation systems for a low carbon economy" EU FP7 research project. Grant 308601, 70 pp.

Hingray, B., Picouet, C. and Musy, A., 2009. Hydrologie 2. Une science de l'ingénieur. 12 Chapitres. 650 p. Ed. Presses Polytechniques Universitaires Romandes, Lausanne.

Hingray, B. and Saïd, M., 2013. Partitioning internal variability and model uncertainty components in a multimodel multireplicate ensemble of hydro-meteorological climate projections. J. Climate (in revision).

Hingray, B., Schaefli, B., Mezghani, A. and Hamdi, Y., 2010. Signature-based model calibration for hydrologic prediction in mesoscale Alpine catchments. Hydrol. Sc. Journal, 55(6): 1002–1016.

Hobbins, M.T., Ramirez, J.A., Brown, T.C. and Claessens, L., 2001. The complementary relationship in estimation of regional evapotranspiration: The Complementary Relationship Areal Evapotranspiration and Advection-Aridity models. Water Resources Research, 37(5): 1367–1387.

Hock, R. and Jansson, P., 2005. Modelling glacier hydrology. pp. 2647–2655. In: M.G. Anderson and J.J. McDonnell (Editors), Encyclopedia of Hydrological Sciences—Part 14: Snow and Glacier Hydrology. Wiley, Chichester.

Hock, R., 2003. Temperature index melt modelling in mountain areas. Journal of Hydrology, 282(1-4): 104–115.

Hock, R., 2005. Glacier melt: a review of processes and their modelling. Progress in Physical Geography, 29(3): 362–391.

Hoffmann, L. *et al.,* 2004. Development of regionalized hydrological models in an area with short hydrological observation series. River Research and Applications, 20(3): 243–254.

Holland, J.H., 1975. Adaptation in Natural and Artificial Systems. University of Michigan Press, Ann Arbor.

Hollingsworth, A., 1980. An experiment in Monte-Carlo forecasting procedure, ECMWF workshop on stochastic dynamic forecasting. ECMWF, UK, pp. 65–97.

Holtan, H.N., 1961. A concept for infiltration estimates in watershed engineering. ARS-41-51. Agricultural Research Service, USDA., Washington, DC.

Holton, J.R., 1992. An Introduction to Dynamic Meteorology, Academic Press, San Diego, 511 pp.

Holwerda, F., Scatena, F.N. and Bruijnzeel, L.A., 2006. Throughfall in a Puerto Rican lower mountain rain forest: A comparison of sampling strategies. Journal of Hydrology, 327(3-4): 592–602.

Hooke, R. and Jeeves, T.A., 1961. Directed search solutions of numerical and statidal problems. Journal of the ACM, 8: 212–229.

Horton, P., Jaboyedoff, M., Metzger, R., Obled, C. and Marty, R., 2012. Spatial relationship between the atmospheric circulation and the precipitation measured in the western Swiss Alps by means of the analogue method. Nat. Hazards and Earth Syst. Sc., 12: 777–784.

Horton, P., Schaefli, B., Mezghani, A., Hingray, B. and Musy, A., 2006. Assessment of climate-change impacts on alpine discharge regimes with climate model uncertainty. Hydrological Processes, 20(10): 2091–2109.

Horton, R.E., 1940. An approach towards a physical interpretation of infiltration capacity. Soil Science Society of America Proceedings, 5: 399–417.

Hosking, J.R.M. and Wallis, J.R., 1997. Regional frequency analysis: an approach based on L-moments. Cambridge University Press, 224 pp.

Houdant, B., 2004. Contribution à l'amélioration de la prévision hydrométéorologique opérationnelle. Pour l'usage des probabilités dans la communication entre acteurs. Thèse de doctorat, ENGREF, Paris, 209 pp.

Houze, R.A., 1993. Clouds Dynamics, Academic Press, San Diego, 573 pp.

Hrachowitz, M. *et al.,* 2013. A decade of Predictions in Ungauged Basins (PUB) a review. Hydrol. Sci. J.-J. Sci. Hydrol., 58: 1198–1255.

Huang, X.M., Lyons, T.J., Smith, R.C.G. and Hacker, J.M., 1995. Estimation of Land-Surface Parameters Using Satellite Data. Hydrological Processes, 9(5-6): 631–643.

Hubbard, B. and Nienow, P., 1997. Alpine subglacial hydrology. Quaternary Science Reviews, 16(9): 939–955.

Huff, F.A., 1967. Time Distribution of Rainfall in Heavy Storms. Water Resources Research, 3(4): 1007–1019.

Hughes, J.P., Guttorp, P. and Charles, S.P., 1999. A non-homogeneous hidden Markov chain model for precipitation occurrence. Applied Statistics, 48(1): 15–30.

Hulme, M., Jenkins, G.J., Lu, X., Turnpenny, J.R., Mitchell, T.D., Jones, R.G., Lowe, J., Murphy, J.M., Hassell, D., Boorman, P., McDonald, R. and Hill, S., 2002. Climate change scenarios for the United Kingdom:

the UKCIP02 Scientific report. Tyndall Centre for Climate Change Research, School of Environmental Sciences, University of East Anglia, Norwich, 120 pp.

Huntingford, C. and Cox, P.M., 2000. An analogue model to derive additional climate change scenarios from existing GCM simulations. Climate Dynamics, 16(8): 575–586.

IEAust, 1987. A Guide to flood estimation, Chap.14: Urban Stormwater Drainage. Australian Rainfall and Runoff, 1. The Institution of Engineers, Australia, Barton, Australia.

Indarto, K., 2002. Découpages spatiaux et conséquences sur le bilan hydrologique—Application au bassin de l'Orb à travers une démarche de modélisation hydrologique distribuée. Thèse de doctorat, ENGREF, Montpellier, 258 pp.

Institute of Hydrology, 1980. Low Flow Studies Report 1–4, Institute of Hydrology, Wallingford, UK.

IPCC, 2001. Climate Change 2001: The Scientific Basis. Contribution of Working Group I to the Third Assessment Report of the Intergovernmental Panel on Climate Change. Cambridge University Press, Cambridge, UK, 881 pp.

IPCC, 2007. Fourth Assessment Report: Climate Change 2007, Cambridge, UK.

Ishidaira, H., Ishikawa, Y., Funada, S. and Takeuchi, K., 2008. Estimating the evolution of vegetation cover and its hydrological impact in the Mekong River basin in the 21st century. Hydrological Processes, 22(9): 1395–1405.

Ivanov, V.Y., Vivoni, E.R., Bras, R.L. and Entekhabi, D., 2004. Preserving high-resolution surface and rainfall data in operational-scale basin hydrology: a fully-distributed physically-based approach. Journal of Hydrology, 298(1-4): 80–111.

Jacob, D., Barring, L. and Christensen, O.B., 2007. An inter-comparison of regional climate models for Europe: model performance in present-day climate. Climatic Change, 81: 31–52.

Jain, S.C., 2001. Open-Channel Flow. John Wiley and Sons, New York, 328 pp.

Jakeman, A.J., Littlewood, I.G. and Whitehead, P.G., 1990. Computation of the Instantaneous Unit-Hydrograph and Identifiable Component Flows with Application to 2 Small Upland Catchments. Journal of Hydrology, 117(1-4): 275–300.

Jansson, P., Hock, R. and Schneider, T., 2003. The concept of glacier storage: a review. Journal of Hydrology, 282(1-4): 116–129.

Jarvis, C.S., 1942. Floods, in Hydrology, edited by O.E. Meinzer, pp. 531–560, McGraw-Hill, New York.

Javelle, P., 2001. Caractérisation du régime des crues: le modèle débit-durée-fréquence convergent. Approche locale et régionale. Thèse de doctorat, INPG, Grenoble, 277 pp. + annexes.

Javelle, P. *et al.* 2002. Development of regional flood-duration-frequency curves based on the index-flood method. J. Hydrol., 258: 249–259.

Jiang, T. *et al.,* 2007. Comparison of hydrological impacts of climate change simulated by six hydrological models in the Dongjiang Basin, South China. Journal of Hydrology, 336(3-4): 316–333.

Jimoh, O.D. and Webster, P., 1999. Stochastic modelling of daily rainfall in Nigeria: intra-annual variation of model parameters. Journal of Hydrology, 222(1-4): 1–17.

Jin, J. *et al.,* 1999. Comparative analyses of physically based snowmelt models for climate simulations. Journal of Climate, 12(8): 2643–2657.

Jinno, K., Kawamura, A., Berndtsson, R., Larson, M. and Niemczynowicz, J., 1993. Real-Time Rainfall Prediction at Small Space-Time Scales Using a 2-Dimensional Stochastic Advection-Diffusion Model. Water Resources Research, 29(5): 1489–1504.

Joerin, C., 1995. Méthodes de détermination des débits d'étiage, Diploma thesis at University of Freiburg in Breisgau (Allemagne), Publication IATE/HYDRAM – EPFL, 120 pp.

Joerin, C., 2000. Etude des processus hydrologiques par l'application du traçage environnemental: association à des mesures effectuées à l'échelle locale et analyse d'incertitude. Thèse de doctorat, EPFL, Lausanne, 289 pp.

Johnson, G.L., Hanson, C.L., Hardegree, S.P. and Ballard, E.B., 1996. Stochastic weather simulation: Overview and analysis of two commonly used models. Journal of Applied Meteorology, 35(10): 1878–1896.

Jones, P.D., Hulme, M. and Briffa, K.R., 1993. A Comparison of Lamb Circulation Types with an Objective Classification Scheme. International Journal of Climatology, 13(6): 655–663.

Jones, R.N., 2000. Analysing the risk of climate change using an irrigation demand model. Climate Research, 14(2): 89–100.

Jong, C., Collins, D.N. and Ranzi, R., 2005. Climate and Hydrology of Mountain Areas. Wiley, 338 pp.

Jordan, J.P., P., 1986. Estimation spatiale des précipitations de l'Ouest de la Suisse par la méthode du krigeage IAS, 13: 187–180, 1986b.

Jordan, F., 2006. Modèle de gestion des crues par opérations préventives sur les aménagements hydroélectriques à accumulation. Thèse de doctorat, EPFL, Lausanne, 270 pp.

Jordan, J.-P., 1992. Identification et modélisation des processus de génération des crues. Application au bassin versant de la Haute Mentue. Thèse de doctorat, EPFL, Lausanne, 370 pp.

Joussaume, S., 2000. Climat d'hier à demain. Centre National de la Recherche Scientifique, Paris, 143 pp.

Kakou, A., 1997. Point Process based models for rainfall. PhD Thesis, University College, London. UK.

Kalman, R.E. 1960. A New Approach to Linear Filtering and Prediction Problems. Transactions of the ASME—Journal of Basic Engineering, 82: 35–45.

Kalnay, E. and Coauthors, 1996. The NCEP/NCAR 40-year Reanalysis Project. Bulletin of the American Meteorological Society, 77: 437–471.

Kamphorst, E.C. *et al.,* 2000. Predicting depressional storage from soil surface roughness. Soil Science Society of America Journal, 64(5): 1749–1758.

Katz, R.W., Parlange, M.B. and Tebaldi, C., 2003. Stochastic modeling of the effects of large-scale circulation on daily weather in the southeastern US. Climatic Change, 60(1-2): 189–216.

Kavetski, D., Kuczera, G. and Franks, S.W., 2003. Semidistributed hydrological modeling: A "saturation path" perspective on TOPMODEL and VIC. Water Resources Research, 39(9).

Keifer, J.-C. and Chu, H.H., 1957. Synthetic storm patterns for drainage design. Journal of Hydraulic Division, 83(4).

Keim, R.F. and Skaugset, A.E., 2004. A linear system model of dynamic throughfall rates beneath forest canopies. Water Resources Research, 40(5).

Kelly, K.S. and Krzysztofowicz, R., 2000. Precipitation uncertainty processor for probabilistic river stage forecasting. Water Resources Research, 36(9): 2643–2653.

Kidd, C., 1978. Rainfall-runoff processes over urban surfaces. Proceedings of an International Workshop, Report No. 53. Institute of Hydrology, Wallingford, UK.

Kitanidis, P.K. and Bras, R.L., 1980. Real-Time Forecasting with a Conceptual Hydrologic Model. 2. Applications and Results. Water Resources Research, 16(6): 1034–1044.

Klaassen, W., Bosveld, F. and de Water, E., 1998. Water storage and evaporation as constituents of rainfall interception. Journal of Hydrology, 212–213(1-4): 36–50.

Klemes, V., 1986. Operational testing of hydrological simulation models. Hydrological Sciences Journal, 31(1): 13–24.

Koren, V., Smith, M. and Duan, Q., 2003. Use of a-priori parameter estimates in the derivation of spatially consistent parameter sets of rainfall-runoff models. pp. 239–254. In: Q. Duan, H.V. Gupta, S. Sorooshian, A.N. Rousseau and R. Turcotte (Editors), Calibration of Watershed Models. Water Science and Application 6. American Geophysical Union, Washington, DC.

Koren, V.I. *et al.,* 1999. Scale dependencies of hydrologic models to spatial variability of precipitation. Journal of Hydrology, 217(3-4): 285–302.

Koutsoyiannis, D., Kozonis, D. and Manetas, A., 1998. A mathematical framework for studying rainfall intensity-duration-frequency relationships. Journal of Hydrology, 206(1-2): 118–135.

Kozak, J.A., Ahuja, L.R., Green, T.R. and Ma, L.W., 2007. Modelling crop canopy and residue rainfall interception effects on soil hydrological components for semi-arid agriculture. Hydrological Processes, 21(2): 229–241.

Krajewski, W.F. and Smith, J.A., 2002. Radar hydrology: rainfall estimation. Advances in Water Resources, 25(8-12): 1387–1394.

Krzanowski, W.J., 2000. Principles of multivariate analysis: a user's perspective. Oxford University Press, Inc., New York, USA.

Krzysztofowicz, R. and Herr, H.D., 2001. Hydrologic uncertainty processor for probabilistic river stage forecasting: precipitation-dependent model. Journal of Hydrology, 249(1-4): 46–68.

Krzysztofowicz, R., 1998. Probabilistic hydrometeorological forecasts: Toward a new era in operational forecasting. Bulletin of the American Meteorological Society, 79(2): 243–251.

Krzysztofowicz, R., 1999. Bayesian forecasting via deterministic model. Risk Analysis, 19(4): 739–749.

Krzysztofowicz, R., 2001a. Integrator of uncertainties for probabilistic river stage forecasting: precipitation-dependent model. Journal of Hydrology, 249(1-4): 69–85.

Krzysztofowicz, R., 2001b. The special issue; Quantitative precipitation forecasting (vol 239, pg 1, 2000). Journal of Hydrology, 248(1-4): 224–224.

Kuchment, L.S. and Gelfan, A.N., 1996. The determination of the snowmelt rate and the meltwater outflow from a snowpack for modeling river runoff generation. Journal of Hydrology, 179(1-4): 23–36.

Kuczera, G. and Parent, E., 1998. Monte Carlo assessment of parameter uncertainty in conceptual catchment models: The Metropolis algorithm. Journal of Hydrology, 211(1-4): 69–85.

Kuczera, G., 1982a. Combining Site-Specific and Regional Information—an Empirical Bayes Approach. Water Resources Research, 18(2): 306–314.

Kuczera, G., 1982b. Robust Flood Frequency Models. Water Resources Research, 18(2): 315–324.

Kuczera, G., 1983. Effect of Sampling Uncertainty and Spatial Correlation on an Empirical Bayes Procedure for Combining Site and Regional Information. Journal of Hydrology, 65(4): 373–398.

Kuczera, G., 1999. Comprehensive at-site flood frequency analysis using Monte Carlo Bayesian inference. Water Resources Research, 35(5): 1551–1557.

Kunstmann, H. and Stadler, C., 2005. High resolution distributed atmospheric-hydrological modelling for Alpine catchments. Journal of Hydrology, 314(1-4): 105–124.

Kustas, W.P., Rango, A. and Uijlenhoet, R., 1994. A Simple Energy Budget Algorithm for the Snowmelt Runoff Model. Water Resources Research, 30(5): 1515–1527.

Laaha, G. and Bloschl, G., 2005. Low flow estimates from short stream flow records—a comparison of methods. Journal of Hydrology, 306(1-4): 264–286.

Laaha, G. and Bloschl, G., 2006. A comparison of low flow regionalisation methods—catchment grouping. Journal of Hydrology, 323(1-4): 193–214.

Labadie, J.W., 2004. Optimal operation of multireservoir systems: State-of-the-art review. Journal of Water Resources Planning and Management-Asce, 130(2): 93–111.

Lafaysse, M., Hingray, B., Etchevers, P., Martin, E. and Obled, C., 2011. Influence of spatial discretization, underground water storage and glacier melt on a physically-based hydrological model of the Upper Durance River basin. J. Hydrol. 403: 116–129.

Lafaysse, M., Hingray, B., Gailhard, J. and Mezghani, A., 2013. Internal variability and model uncertainty components in a multimodel multireplicate ensemble of hydrometeorological predictions. Wat. Resour. Res. (in press).

Laio, F., Porporato, A., Ridolfi, L. and Rodriguez-Iturbe, I., 2001. Plants in water controlled ecosystems: Active role in hydrological processes and response to water stress. II. Probabilistic soil moisture dynamics. Advances in Water Research, 24: 707–723.

Lamb, H.H., 1972. British Isles weather types and a register of daily sequence of circulation patterns, 1861–1971. Geophys Mem 110. Meteor. Office, London, UK.

Lane, L.J. and Nearing, M.A., 1989. USDA-Water Erosion Predictioo Project: Hillslope Profile Model Documentation. National Soil Erosion Research Laboratory, USDA-ARS-MWA, Report N° 2 W, Lafayette, 300 pp.

Lane, S.N., 1998. Hydraulic modelling in hydrology and geomorphology: A review of high resolution approaches. Hydrological Processes, 12(8): 1131–1150.

Lang, M., Lavabre, J., Sauquet, E. and Renard, B., 2005. Recommandations pour le calcul des aléas hydrologiques dans le cadre des plans de prévention des risques d'inondations. Ministère de l'Ecologie et du Développement Durable, Paris, 134 pp. + annexes.

Lang, M., Ouarda, T. and Bobee, B., 1999. Towards operational guidelines for over-threshold modeling. Journal of Hydrology, 225(3-4): 103–117.

Lang, M., Perret, C., Renouf, E., Sauqueta, E. and Paquier, A., 2006. Incertitudes sur les débits de crue. La Houille Blanche, 6: 33–41.

Lardet, P. and Obled, C., 1994. Real-Time Flood Forecasting Using a Stochastic Rainfall Generator. Journal of Hydrology, 162(3-4): 391–408.

Larras, J., 1972. Hydraulique et granulats, 1. Eyrolles, Paris, 254 pp.

Larry, M., 2001. Stormwater Collection Systems Design Handbook, McGraw-Hill, 1008 pp.

Lawrance, A.J. and Lewis, P.A.W., 1983. Simple Dependent Pairs of Exponential and Uniform Random-Variables. Operations Research, 31(6): 1179–1197.

Lebel, T. *et al.,* 1992. Rainfall Estimation in the Sahel—the Epsat-Niger Experiment. Hydrological Sciences Journal-Journal Des Sciences Hydrologiques, 37(3): 201–215.

Lebel, T., 1997. Variabilité des pluies au Sahel: observation, estimation et modélisation. HDR, INPG, Grenoble, 95 pp. + annexes.

Lebel, T., Braud, I. and Creutin, J.D., 1998. A space-time rainfall disaggregation model adapted to Sahelian mesoscale convective complexes. Water Resources Research, 34(7): 1711–1726.

LeCam, L., 1961. A stochastic description of precipitation, Proc. Of the 4th Berkeley Symposium on Mathematical Statistics and Probability. Neyman, Berkeley, US, pp. 165–186.

Ledoux, E., Girard, G., De Marsily, G. and Deschenes, J., 1989. Spatially distributed modelling: conceptual approach, coupling surface water and ground-water. pp. 435–454. In: H.J.M. Seytoux (Editor), Unsaturated Flow Hydrologic Modelling—Theory and Practice. Kluwer Academic NATO, ASI Series C.

Lehning, M. *et al.,* 1999. SNOWPACK model calculations for avalanche warning based upon a new network of weather and snow stations. Cold Regions Science and Technology, 30(1-3): 145–157.

Lehning, M., 2005. Energy balance and thermophysical processes in snowpack, Encyclopedia of Hydrological Sciences—Part 14: Snow and Glacier Hydrology. Wiley, Chichester, pp. 2475–2490.

Lehning, M., 2005. Energy balance and thermophysical processes in snowpacks. pp. 2475–2490. In: M.G. Anderson and J.J. McDonnell (Editors), Encyclopedia of Hydrological Sciences—Part 14: Snow and Glacier Hydrology. Wiley, Chichester.

Leij, F.J., Alves, W.J., van Genuchten, M.T. and Williams, J.R., 1996. The UNSODA unsaturated soil hydraulic database. User's Manual Version 1.0. National Risk Management Research Laboratory. Office of Research and Development, U.S. EPA, Cincinnati, US.

Lencastre, A., 1999. Hydraulique générale. Eyrolles, Paris, 633 pp.

Leung, L.R. *et al.,* 2004. Mid-century ensemble regional climate change scenarios for the western United States. Climatic Change, 62(1-3): 75–113.

Lhomme, J., 2006. Modélisation des inondations en milieu urbain: approches unidimensionnelle, bidimensionnelle et macroscopique, Université de Montpellier II, 224 pp. + annexes.

Lhomme, J., Bouvier, C. and Perrin, J.L., 2004. Applying a GIS-based geomorphological routing model in urban catchments. Journal of Hydrology, 299(3-4): 203–216.

L'Hote, Y., Chevallier, P., Coudrain, A., Lejeune, Y. and Etchevers, P., 2005. Relationship between precipitation phase and air temperature: comparison between the Bolivian Andes and the Swiss Alps. Hydrological Sciences Journal-Journal Des Sciences Hydrologiques, 50(6): 989–997.

Liang, X. and Xie, Z.H., 2001. A new surface runoff parameterization with subgrid-scale soil heterogeneity for land surface models. Advances in Water Resources, 24(9-10): 1173–1193.

Liang, X., Lettenmaier, D.P., Wood, E.F. and Burges, S.J., 1994. A Simple Hydrologically Based Model of Land-Surface Water and Energy Fluxes for General-Circulation Models. Journal of Geophysical Research-Atmospheres, 99(D7): 14415–14428.

Lindstrom, G., Johansson, B., Persson, M., Gardelin, M. and Bergstrom, S., 1997. Development and test of the distributed HBV-96 hydrological model. Journal of Hydrology, 201(1-4): 272–288.

Linsley, R.K., Kohler, M.A. and Paulhus, J.L.H., 1975. Hydrology for engineers. McGraw-Hill Education, 416 pp.

Litrico, X., 1999. Modélisation, identification et commande robuste de systèmes hydrauliques à surface libre. Thèse de doctorat, ENGREF, Paris, 204 pp.

Liu, S., 1997. A new model for the prediction of rainfall interception in forest canopies. Ecological Modelling, 99: 151–159.

Ljung, L., 1999. System Identification Theory for the User. 2nd edition. Prentice Hall, Upper Saddle River, N.J, 609 pp.

Lliboutry, L., 1964. Traité de glaciologie. Tome 1: Glace, neige, hydrologie nivale. Eds. Dunod, Paris, 428 pp.

Lliboutry, L., 1965. Traité de glaciologie. Tome 2: Glaciers, variations du climat, sols gelés. Eds. Dunod, Paris, 616 pp.

Lloyd, C.R., Gash, J.H.C., Shuttleworth, W.J. and Marques, A.D.O., 1988. The Measurement and Modeling of Rainfall Interception by Amazonian Rain Forest. Agricultural and Forest Meteorology, 43(3-4): 277–294.

Lohmann, D., Raschke, E., Nijssen, B. and Lettenmaier, D.P., 1998. Regional scale hydrology: I. Formulation of the VIC-2L model coupled to a routing model. Hydrological Sciences Journal-Journal Des Sciences Hydrologiques, 43(1): 131–141.

Longchamp, R., 2006. Commande numérique de systèmes dynamiques: Cours d'automatique. PPUR, Lausanne, 765 pp.

López, P., 2007. Impact de la variabilité cimatique sur le cryosphere du Campo de Hielo Norte: Apport de la télédétection. Thèse de doctorat, IRD, Université de Montpellier 2, Montpellier.

Lovejoy, S. and Mandelbrot, B.B., 1985. Fractal Properties of Rain, and a Fractal Model. Tellus Series a-Dynamic Meteorology and Oceanography, 37(3): 209–232.

Lovejoy, S., 1981. Analysis of rain areas in terms of fractals. 20th conf. on radar Meteorology. Bulletin of the American Meteorological Society, 476–484.

Lu, L.H. and Stedinger, J.R., 1992. Sampling Variance of Normalized Gev Pwm Quantile Estimators and a Regional Homogeneity Test. Journal of Hydrology, 138(1-2): 223–245.

Lu, L.H. and Stedinger, J.R., 1992. Variance of 2-Parameter and 3-Parameter Gev Pwm Quantile Estimators - Formulas, Confidence-Intervals, and a Comparison. Journal of Hydrology, 138(1-2): 247–267.

Luo, L.F. *et al.,* 2003. Effects of frozen soil on soil temperature, spring infiltration, and runoff: Results from the PILPS 2(d) experiment at Valdai, Russia. Journal of Hydrometeorology, 4(2): 334–351.

Madsen, H. and Rosbjerg, D., 1997. Generalized least squares and empirical Bayes estimation in regional partial duration series index-flood modeling. Water Resources Research, 33(4): 771–781.

Maidment, D.R., 1993a. GIS and Hydrologic Modeling. pp. 147–167. In: M.J. Goodchild, B.O. Parks, and L.T. Steyaert (Editor), Environmental Modeling with GIS. Oxford University Press.

Maidment, D.R., 1993b. Handbook of hydrology. McGraw- Hill, Inc., 1424 pp.

Maillet, E., 1905. Sur les solutions de certains systèmes d'équations différentielles; applications à un système hydraulique de n réservoirs. Bulletin de la Société Mathématique de France, 33: 129–145.

Maisch, M., 2000. The long-term signal of climate change in the Swiss Alps: glacier retreat since the end of the Little Ice Age and future ice decay scenarios. Geografia Fisica e Dinamica Quaternaria, 23: 139–151.

Malardel, S., 2005. Fondamentaux de météorologie: A l'école du temps. Cépaduès, Toulouse, 724 pp.

Manzi, A.O. and Planton, S., 1994. Implementation of the Isba Parametrization Scheme for Land-Surface Processes in a Gcm—an Annual Cycle Experiment. Journal of Hydrology, 155(3-4): 353–387.

Maraun, D. *et al.,* 2010. Precipitation Downscaling Under Climate Change: Recent Developments to Bridge the Gap Between Dynamical Models and the End User. Rev. Geophys., 48 pp.

Marco, O., Villemain, P. and Touvier, E., 1998. Snow density measurement using acoustic properties. La Houille Blanche, 53(5-6): 117–123.

Margoum, M., 1992. Estimation des crues rares et extrêmes: le modèle Agregee. Conceptions et premières validations. Thèse de doctorat, ENSMP, Paris, 252 pp.

Marsh, P., 2005. Water Flow Through Snow and Firn, Encyclopedia of Hydrological Sciences—Part 14: Snow and Glacier Hydrology. Wiley, Chichester, pp. 2492–2504.

Marshall, J.S. and Palmer, W.M., 1948. The Distribution of Raindrops with Size. Journal of Meteorology, 5(4): 165–166.

Marshall, L.A., Sharma, D. and Nott, J., 2006. Modelling the catchment via mixtures: issues of model specification and validation. Water Resources Research, 42, W11409, doi:10.1029/2005WR004613.

Marti, R., Le Pelletier, T. and Chatellier, V., 1997. Le modèle MRIF: Simulations des crues du bassin de la Seine en région Ile-de-France. La Houille Blanche, 8: 64–70.

Martin, E., Brun, E. and Durand, Y., 1994. Sensitivity of the French Alps Snow Cover to the Variation of Climatic Variables. Annales Geophysicae-Atmospheres Hydrospheres and Space Sciences, 12(5): 469–477.

Marty, R., Zin, I. and Obled, C., 2008. On adapting PQPFs to fit hydrological needs: the case of flash flood forecasting. Atmospheric Science Letters, 9(2): 73–79.

Marty, R., Zin, I., Obled, C., Bontron, G. and Djerboua, A., 2012. Toward Real-Time Daily PQPF by an Analog Sorting Approach: Application to Flash-Flood Catchments. J. Applied Met. and Climatol., 51: 505–520.

Massman, W.J., 1983. The derivation and validation of a new model for the interception of rainfall by forests. Agricultural Meteorology, 28: 261–286.

Matalas, N.C., Slack, J.R. and Wallis, J.R., 1975. Regional Skew in Search of a Parent. Water Resources Research, 11(6): 815–826.

Matgen, P. *et al.,* 2006. Patterns of remotely sensed floodplain saturation and its use in runoff predictions. Hydrological Processes, 20(8): 1805–1825.

Matheron, G., 1963. Principles of Geostatistics. Economic Geol., 58: 1246–1268.

Matheron, G., 1973. The intrinsic random functions and their applications. Advances in Applied Probability, 5: 439–468.

McCuen, R.H., 1979. Downstream Effects of Stormwater Management Basins. Journal of Hydraulics Division, ASCE, 1(1): 21–42.

McIlveen, R., 1992. Fundamentals of Weather and Climate, Chapman and Hall, London, 497 pp.

McKerchar, A.I. and Pearson, C.P., 1990. Maps of Flood Statistics for Regional Flood Frequency-Analysis in New-Zealand. Hydrological Sciences Journal-Journal Des Sciences Hydrologiques, 35(6): 609–621.

McMahon, T.A., Peel, M.C., Lowe, L., Srikanthan, R. and McVicar, T.R., 2012. Estimating actual, potential, reference crop and pan evaporation using standard meteorological data: a pragmatic synthesis. Hydrol. and Earth Syst. Sci. Disc., 9: 11829–11910.

Meischner, P., 2003. Weather radar. Principles and advanced applications. Springer Verlag, Berlin, 337 pp.

Mellor, D. and Metcalfe, A.V., 1996. The Modified Turning Bands (MTB) model for space-time rainfall. 3. Estimation of the storm rainband profile and a discussion of future model prospects. Journal of Hydrology, 175(1-4): 161–180.

Mellor, D. and Oconnell, P.E., 1996. The Modified Turning Bands (MTB) model for space-time rainfall. 2. Estimation of raincell parameters. Journal of Hydrology, 175(1-4): 129–159.

Mellor, D., 1996. The Modified Turning Bands (MTB) model for space-time rainfall. 1. Model definition and properties. Journal of Hydrology, 175(1-4): 113–127.

Mellor, D., Sheffield, J., O'Connell, P.E. and Metcalfe, A.V., 2000. A stochastic space-time rainfall forecasting system for real time flow forecasting I: Development of MTB conditional rainfall scenario generator. Hydrology and Earth System Sciences, 4(4): 603–615.

Merriam, R.A., 1960. A Note on the Interception Loss Equation. Journal of Geophysical Research, 65(11): 3850–3851.

Merriam, R.A., 1961. Surface water storage on annual ryegrass. Journal of Geophysics Research, 66: 1833–1838.

Merz, B. and Plate, E.J., 1997. An analysis of the effects of spatial variability of soil and soil moisture on runoff. Water Resources Research, 33(12): 2909–2922.

Merz, R. and Bloschl, G., 2005. Flood frequency regionalisation-spatial proximity vs. catchment attributes. Journal of Hydrology, 302(1-4): 283–306.

Messer, H., Zinevich, A. and Alpert, P., 2006. Environmental monitoring by wireless communication networks. Science, 312(5774): 713–713.

Metropolis, N., Rosenbluth, A.W., Rosenbluth, M.N., Teller, A.H. and Teller, E., 1953. Equation of state calculation by fast computing machines. Journal of Chemical Physics, 21(6): 1087–1092.

Metzger, R., 2002. Modélisation des inondations par approches déterministe et stochastique avec prise en compte des incertitudes topographiques pour la gestion des risques liés aux crues. Thèse de doctorat, EPFL, Lausanne, 177 pp.

Meylan, P., 1986. Régionalisation de données entachées d'erreurs de mesure par krigeage structural - Application à la pluviométrie. Hydrologie Continentale, 1: 25–34.

Meylan, P., Favre, A.-C. and Musy, A., 2008. Hydrologie fréquentielle : une science prédictive. PPUR, Lausanne, 191 pp.

Meylan, P., Favre, A.-C. and Musy, A., 2012. Predictive hydrology: a frequency analysis approach. CRC Press, Boca Raton, FL. 212 p.

Mezghani, A., 2003. Modélisation des précipitations journalières à partir d'indices de circulation atmosphérique. Application au bassin versant de Mauvoisin. Master Thesis, EPFL, Lausanne.

Mezghani, A., 2008. Génération multisite de variables météorologiques horaires pour la simulation de scénarios de crues en zone alpine. Application au bassin du Rhône–Suisse. Thèse de Doctorat, EPFL, Lausanne.

Mezghani, A. and Hingray, B., 2009. A combined downscaling-disaggregation weather generator for stochastic generation of multisite hourly weather variables in complex terrain. Development and multi-scale validation for the Upper Rhone River Basin. J. Hydrology., 377(3-4): 245–260.

Mezghani, A., Hingray, B. and Lafaysse, M. 2014. Predictive power of atmospheric predictors for daily precipitation over France. JGR-Atm. (submited).

Mignot, E., 2005. Etude expérimentale et numérique de l'inondation d'une zone urbanisée: cas des écoulements dans les carrefours en croix. Thèse de doctorat, Ecole Centrale de Lyon, Lyon, 320 pp.

Mikkelsen, P.S., Madsen, H., Arnbjerg-Nielsen, K., Rosbjerg, D. and Harremoes, P., 2005. Selection of regional historical rainfall time series as input to urban drainage simulations at ungauged locations. Atmospheric Research, 77(1-4): 4–17.

Milly, P.C.D. *et al.,* 2008. Climate change—Stationarity is dead: Whither water management? Science, 319: 573–574.

Mimikou, M. and Kaemaki, S., 1985. Regionalization of Flow Duration Characteristics. Journal of Hydrology, 82(1-2): 77–91.

Ministère de l'Environnement, 1985. Guide de prévision des crues. Ministère de l'Environnement, Paris, France.

Minshall, N.E., 1960. Predicting Storm Runoff on Small Experimental Watersheds. Journal of the Hydraulics Division ASCE 86, 86(HY8): 17–38.

Mitchell, J.K. and Jones, B.A., 1978. Micro-Relief Surface Depression Storage—Changes During Rainfall Events and Their Application to Rainfall-Runoff Models. Water Resources Bulletin, 14(4): 777–802.

Molini, A., La Barbera, P. and Lanza, L.G., 2002. On the properties of stochastic intermittency in rainfall processes. Water Science and Technology, 45(2): 35–40.

Molteni, F., Buizza, R., Palmer, T.N. and Petroliagis, T., 1996. The ECMWF ensemble prediction system: Methodology and validation. Quarterly Journal of the Royal Meteorological Society, 122(529): 73–119.

Moore, R.J. and Clarke, R.T., 1981. A Distribution Function-Approach to Rainfall Runoff Modeling. Water Resources Research, 17(5): 1367–1382.

Mora, R.D., Bouvier, C., Neppel, L. and Niel, H., 2005. Regional approach for the estimation of low-frequency distribution of daily rainfall in the Languedoc-Roussillon region, France. Hydrological Sciences Journal-Journal Des Sciences Hydrologiques, 50(1): 17–29.

Morgan, R.P.C. *et al.,* 1998. The European Soil Erosion Model (EUROSEM): A dynamic approach for predicting sediment transport from fields and small catchments. Earth Surface Processes and Landforms, 23(6): 527–544.

Morin, G., Paquet, P. and W., S., 1995. Le Modèle de Simulation de Quantité et de Qualité CEQUEAU. INRS-Eau Rapport de Recherche, No. 433, 341 pp.

Morton, F.I., 1969. Potential Evaporation as a Manifestation of Regional Evaporation. Water Resources Research, 5(6): 1244-&.

Mouhous, N., 2003. Intérêt des modèles de cascades multiplicatives pour la simulation de séries chronologiques de pluies ponctuelles adaptées à l'hydrologie urbaine. Thèse de doctorat, ENPC, Paris, 170 pp.

Moussa, R. and Bocquillon, C., 1996. Criteria for the choice of flood-routing methods in natural channels. Journal of Hydrology, 186(1-4): 1–30.

Moussa, R. and Bocquillon, C., 2000. Approximation zones of the Saint-Venant equations for flood routing with overbank flow. Hydrology and Earth System Sciences, 4(2): 251–261.

Moussa, R., 1997. Geomorphological transfer function calculated from digital elevation models for distributed hydrological modelling. Hydrological Processes, 11(5): 429–449.

Mtir, A., 2004. Modélisation d'un système de prévision de crues pour les différents affluents du Rhône en amont du Léman. Master Thesis, EPFL, Lausanne.

Muirhead, R.J., 1982. Aspects of multivariate statistical theory. Wiley, New York, 704 pp.

Musy, A. and Higy, C., 2011. Hydrology: a Science of Nature, CRC Press, 386 pp.

Musy, A. and Higy, C., 2004. Hydrologie - Une science de la nature. PPUR, Lausanne, 326 pp.

Musy, A. and Soutter, M., 1991. Physique du sol. PPUR, Lausanne, 335 pp.

Musy, A., Daynou, M., Hingray, B., Schaefli, B. and Metzger, R., 2005. Short-term hydrological forecasting in Colombia: application to the Magdalena River. FORAC/IDEAM project. HYDRAM, EPFL, Lausanne, 60 pp. + annexes.

Muzik, I., 1996. Flood modelling with GIS-derived distributed unit hydrographs. Hydrol. Process., 10: 1401–1409.

Nakicenovic, N. and Swart, R., Eds, 2000. Special Report on Emissions Scenarios. Cambridge University Press, Cambridge.

Nascimento, N.O., 1995. Appréciation à l'aide d'un modèle empirique des effets d'action anthropiques sur la relation pluie-débit à l'échelle du bassin versant. Thèse de doctorat, ENPC, Paris, 550 pp.

Nash, J.E. and Sutcliffe, J.V., 1970. River flow forecasting through conceptual models part I—A discussion of principles. Journal of Hydrology, 10(3): 282–290.

Nash, J.E., 1957. The form of the instantaneous unit hydrograph, Comptes Rendus et rapport. General Assembly Toronto. IAHS, Publ., N°45, 3, pp. 114–121.

Natale, L. and Todini, E., 1977. A constrained parameter estimation technique for linear models in hydrology. pp. 109–147. In: T.A. Ciriani, U. Maione and J.R. Wallis (Editors), Mathematical models of surface water hydrology. Wiley, London.

Nathan, R.J. and McMahon, T.A., 1990. Identification of Homogeneous Regions for the Purposes of Regionalisation. Journal of Hydrology, 121(1-4): 217–238.

Naulet, R. *et al.,* 2005. Flood frequency analysis on the Ardeche river using French documentary sources from the last two centuries. Journal of Hydrology, 313(1-2): 58–78.

Neelin, J.D. *et al.,* 1998. ENSO theory. Journal of Geophysical Research-Oceans, 103(C7): 14261–14290.

Nelder, J.A. and Mead, R., 1965. A simplex method for function minimization. Computer Journal, 7: 308–313.

Neppel, L., Bouvier, C. and Niel, H., 2006. Quelques illustrations des sources d'incertitudes dans l'analyse de l'aléa pluvieux. La Houille Blanche, 6: 22–26.

NERC, 1975. Flood Studies Reports. Department of the Environment. National Environmental Research Council, London.

New, M. and Hulme, M., 2000. Representing Uncertainty in Climate Change Scenarios: a Monte Carlo approach. Integrated Assessment, 1: 203–213.

Niadas, I.A. 2005. Regional flow duration curve estimation in small ungauged catchments using instantaneous flow measurements and a censored data approach. Journal of Hydrology, 314(1): 48–66.

Niggli, M., 2004. Combinaison bayésienne des estimations régionales des crues: concepts, développements, et validation, thèse de doctorat 2895, EPFL, Lausanne, 220 pp.

Niggli, M. and Musy, A., 2005. A Bayesian combination method of flood models: Principles and application results. Agricultural Water Management, 77(1-3): 110–127.

Niggli, M., Consuegra, D., Crausaz, P.A. and Vez, E., 1999. Régionalisation des courbes de débits classés du canton de Vaud. Projet Gesreau. Rapport d'étude., HYDRAM, EPFL., Lausanne.

Niggli, M., Talamba, D., Hingray, B. and Musy, A., 2001. Estimation des débits de pointe pour des bassins versants non jaugés: Application a la Suisse Occidentale. Wasser, Energie and Luft, 9–10.

Noilhan, J. and Planton, S., 1989. A Simple Parameterization of Land Surface Processes for Meteorological Models. Monthly Weather Review, 117: 536–549.

O'Connell, P.E. and Clarke, R.T. 1981. Adaptive hydrological forecasting—a review/Revue des méthodes de prévision hydrologique ajustables, 26(2): 179–205.

Obled, C. and Rossé, B., 1975. Modèles mathématiques de la fusion nivale en un point. Cahiers ORSTOM. Série Hydrologie, 12(4): 235–258.

Obled, C. and Rossé, B., 1977. Mathematical-Models of a Melting Snowpack at an Index Plot. Journal of Hydrology, 32(1-2): 139–163.

Obled, C. and Zin, I., 2004. TOPMODEL: principes de fonctionnement et application. La Houille Blanche, 1: 65–77.

Obled, C., 1979. Contribution à l'analyse des données en hydrométéorologie. Thèse de doctorat, Institut de Mécanique des Fluides, Université de Grenoble, Grenoble.

Obled, C., Bontron, G. and Garcon, R., 2002. Quantitative precipitation forecasts: a statistical adaptation of model outputs through an analogues sorting approach. Atmospheric Research, 63(3-4): 303–324.

Obled, C., Wendling, J. and Beven, K., 1994. The Sensitivity of Hydrological Models to Spatial Rainfall Patterns —an Evaluation Using Observed Data. Journal of Hydrology, 159(1-4): 305–333.

Obled, C., Zin, I. and Hingray, B., 2009. Choix des pas de temps et d'espace pour des modélisations parcimonieuses en hydrologie des crues. La Houille Blanche., 5: 81–87.

Oconnell, P.E. and Clarke, R.T., 1981. Adaptive Hydrological Forecasting—a Review. Hydrological Sciences Bulletin-Bulletin Des Sciences Hydrologiques, 26(2): 179–205.

OFEG, 2001. Protection contre les crues des cours d'eau. Directives 2001. Office fédéral des eaux et de la géologie, Berne, 72 pp.

OFEG, 2002. Les crues 2000. Analyse des événements, cas exemplaires. Rapports de l'OFEG, Série Eaux, Nr. 2. Office fédéral des eaux et de la géologie, Berne.

OFEG, 2003. Evaluation des crues dans les bassins versants de Suisse. Guide pratique—Rapports de l'OFEG, Série eaux n°4. Office fédéral des eaux et de la géologie, Berne, 114 pp.

Ogden, F.L. and Saghafian, B., 1997. Green and Ampt infiltration with redistribution. Journal of Irrigation and Drainage Engineering-Asce, 123(5): 386–393.

Ohmura, A., 2001. Physical basis for the temperature-based melt-index method. Journal of Applied Meteorology, 40(4): 753–761.

Olioso, A. and Jacob, F., 2002. Estimation de l'évapotranspiration à partir de mesures de télédétection. La Houille Blanche, 1: 62–67.

Olioso, A., Chauki, H., Courault, D. and Wigneron, J.P., 1999. Estimation of evapotranspiration and photosynthesis by assimilation of remote sensing data into SVAT models. Remote Sensing of Environment, 68(3): 341–356.

Onof, C. *et al.,* 2000. Rainfall modelling using Poison-cluster processes: a review of developments. Stochastic Environmental Research and Risk Assessment, 14(6): 384–411.

Onstad, C.A., 1984. Depressional Storage on Tilled Soil Surfaces. Transactions of the Asae, 27(3): 729–732.

Ottlé, C. and Vidalmadjar, D., 1994. Assimilation of Soil-Moisture Inferred from Infrared Remote-Sensing in a Hydrological Model over the Hapex-Mobilhy Region. Journal of Hydrology, 158(3-4): 241–264.

Ottlé, C., Le Hégarat, S. and Zribi, M., 2003. Applications de la télédétection spatiale en hydrologie. Revue du Palais de la Découverte, 304(37-47): 37–47.

Ouarda, T., Girard, C., Cavadias, G.S. and Bobee, B., 2001. Regional flood frequency estimation with canonical correlation analysis. Journal of Hydrology, 254(1-4): 157–173.

Ouarda, T., Rasmussen, P.F., Bobée, B. and Bernier, J., 1998. Utilisation de l'information historique en analyse hydrologique fréquentielle. Revue des sciences de l'eau, 11(1): 41–49.

Oudin, L. *et al.,* 2005. Which potential evapotranspiration input for a lumped rainfall-runoff model? Part 2 - Towards a simple and efficient potential evapotranspiration model for rainfall-runoff modelling. Journal of Hydrology, 303(1-4): 290–306.

Oudin, L., 2006a. Recherche d'un modèle d'évapotranspiration potentielle pertinent pour un modèle pluie-débit global. Thèse de doctorat, ENGREF, Paris, 496 pp.

Oudin, L., 2006b. Une formule simple d'évapotranspiration potentielle pour la modélisation pluie-débit à l'échelle du bassin versant. La Houille Blanche, 6: 113–120.

Over, T.M. and Gupta, V.K., 1994. Statistical-Analysis of Mesoscale Rainfall—Dependence of a Random Cascade Generator on Large-Scale Forcing. Journal of Applied Meteorology, 33(12): 1526–1542.

Over, T.M. and Gupta, V.K., 1996. A space-time theory of mesoscale rainfall using random cascades. Journal of Geophysical Research-Atmospheres, 101(D21): 26319–26331.

Overney, O. *et al.,* 1997. Influence des changements climatiques sur le régime hydrologique des cours d'eau. Rapport final PNR31., Hochschule Verlag ETHZ, Zurich.

Overney, O., 1997. Prédiction des crues par modélisation couplée stochastique et déterministe: méthode et analyse des incertitudes. Thèse de doctorat, EPFL, Lausanne, 174 pp.

Owe, M., de Jeu, R. and Walker, J., 2001. A methodology for surface soil moisture and vegetation optical depth retrieval using the microwave polarization difference index. Ieee Transactions on Geoscience and Remote Sensing, 39(8): 1643–1654.

Pailleux, J., Geleyn, J.-F. and Legrand. E., 2000. La prévision numérique du temps avec les modèles Arpège et Aladin; bilan et perspectives. La Météorologie, 30: 32–60.

Palmer, T.N., Barkmeijer, J., Buizza, R., Klinker, E. and Richardson, D., 2002. L'avenir de la prévision d'ensemble. La Météorologie, 36: 22–30.

Palmer, T.N. and Coauthors. 2004. Development of a European Multimodel Ensemble System for Seasonal-To Prediction (demeter). Bull. Amer. Meteor. Soc., 85: 853–872.

Pappenberger, F. and Beven, K.J., 2006. Ignorance is bliss: Or seven reasons not to use uncertainty analysis. Water Resources Research, 42(5).

Pappenberger, F. *et al.,* 2005. Cascading model uncertainty from medium range weather forecasts (10 days) through a rainfall-runoff model to flood inundation predictions within the European Flood Forecasting System (EFFS). Hydrology and Earth System Sciences, 9(4): 381–393.

Paquet, E., 2004. A new version of the hydrological model MORDOR: snowpack model at different elevations. Houille Blanche-Revue internationale de l'eau, 2: 75–82.

Paquet, E., Gailhard, J. and Garcon, R., 2006. Evolution of the GRADEX method: improvement by atmospheric circulation classification and hydrological modelling. La Houille Blanche, 5: 80–90.

Parajka, J. *et al.,* 2013. Comparative assessment of predictions in ungauged basins—Part 1: Runoff-hydrograph studies. Hydrol. and Earth Syst. Sci., 17: 1783–1795.

Parajka, J., Merz, R. and Bloschl, G., 2005. A comparison of regionalisation methods for catchment model parameters. Hydrology and Earth System Sciences, 9(3): 157–171.

Pardé, M., 1933. Fleuves et Rivières. Colin, Paris, 224 pp.

Parent du Chatelet, J., 2003. Aramis, le réseau français de radars pour la surveillance des précipitations = Aramis, the French weather radar network. La Météorologie, 40: 44–52.

Parent du Châtelet, J., Tabary, P. and Lamarque, P., 2005. Evolution du réseau radar opérationnel de Météo-France pour une meilleure estimation de la lame d'eau, Ateliers d'Expérimentation et d'Instrumentation (AEI), Toulouse, 4 pp.

Parent, E. and Bernier, J., 2003. Bayesian POT modeling for historical data. Journal of Hydrology, 274(1-4): 95–108.

Parlange, M.B. and Katul, G.G., 1992. An Advection-Aridity Evaporation Model. Water Resources Research, 28(1): 127–132.

Parr, W.C., 1983. A Note on the Jackknife, the Bootstrap and the Delta Method Estimators of Bias and Variance. Biometrika, 70(3): 719–722.

Parriaux, A., 2006. Géologie. Bases pour l'ingénieur. PPUR, Lausanne, 514 pp.

Paterson, W.S.B., 1994. The Physics of Glaciers. Pergamon, Oxford, 480 pp.

Payrastre, O., 2005. Faisabilité et utilité du recueil de données historiques pour l'étude des crues extrêmes de petits cours d'eau—Etude du cas de quatre bassins versants affluents de l'Aude. Thèse de doctorat, ENPC, Paris, 392 pp.

Payraudeau, S., 2002. Modélisation distribuée des flux d'azote sur des petits bassins versants méditerranéens. Thèse de doctorat, ENGREF, Montpellier, 436 pp.

Pegram, G.G.S. and Clothier, A.N., 2001a. Downscaling rainfields in space and time, using the String of Beads model in time series mode. Hydrology and Earth System Sciences, 5(2): 175–186.

Pegram, G.G.S. and Clothier, A.N., 2001b. High resolution space-time modelling of rainfall: the "String of Beads" model. Journal of Hydrology, 241(1-2): 26–41.

Pellarin, T. *et al.,* 2002. Hydrologic visibility of weather radar systems operating in mountainous regions: Case study for the Ardeche Catchment (France). Journal of Hydrometeorology, 3(5): 539–555.

Penman, H.L., 1948. Natural evaporation from open water, bare soil and grass, Proc. of the Royal Society of London. A (194), pp. 120–145.

Penman, H.L., 1963. Vegetation and Hydrology. Tech. Comm. 53. Commonwealth Bureau of soils, Harpenden, England.

Pereira, L.A.S., 1977. Etudes de tarissement sur des petits bassins versants de montagne, ETHZ, Zürich.

Perrin, C., 2000. Vers une amélioration d'un modèle global pluie-débit au travers d'une approche comparative. Thèse de doctorat, INPG, Grenoble, 287 pp. + annexes.

Perrin, C., 2002. Vers une amélioration d'un modèle global pluie-débit au travers d'une approche comparative. La Houille Blanche, 6/7: 84–91.

Perrin, C., Michel, C. and Andréassian, V., 2003. Improvement of a parsimonious model for streamflow simulation. Journal of Hydrology, 279: 275–289.

Perrin, C., Michel, C. and Andréassian, V., 2003. Improvement of a parsimonious model for streamflow simulation. J. Hydrol., 279: 275–289.

Peugeot, C., Cappelaere, B., Vieux, B.E., Seguis, L. and Maia, A., 2003. Hydrologic process simulation of a semiarid, endoreic catchment in Sahelian West Niger. 1. Model-aided data analysis and screening. Journal of Hydrology, 279(1-4): 224–243.

Pfister, L., Drogue, G., Poirier, C. and Hoffmann, L., 2005. Spatial variability of trends in hydrological extremes induced by orographically enhanced rainfall events due to westerly atmospheric circulations. Water Science and Technology, 51(5): 15–21.

Pfister, L., Humbert, J. and Hoffmann, L., 2000. Recent trends in rainfall-runoff characteristics in the Alzette River basin, Luxembourg. Climatic Change, 45(2): 323–337.

Picouet, C. 1999. Géodynamique d'un hydrosystème tropical peu anthropisé, le bassin supérieur du Niger et son delta intérieur. Thèse de Doctorat de l'université de Montpellier II (France), 350 p. + annexes. http://tel. archives-ouvertes.fr/tel-00006189/.

Pilgrim, D.H. and Mc Dermott, G.E., 1982. Design floods for small rural catchments in eastern New South Wales. Civil Engineering Trans. Inst. Engrs. Aust., CE24(3): 226–234.

Piock-Ellena, U., Pfaundler, M., Blöschl, G., Burlando, P. and Merz, R., 2000. Saisonalitätsanalyse als Basis für die Regionalisierung von Hochwässern. Wasser, Energie and Luft, 1–2: 13–21.

Pitlick, J., 1994. Relation between Peak Flows, Precipitation, and Physiography for 5 Mountainous Regions in the Western USA. Journal of Hydrology, 158(3-4): 219–240.

Planchon, O. and Darboux, F., 2002. A fast, simple and versatile algorithm to fill the depressions of digital elevation models. Catena, 46(2-3): 159–176.

Pochat, R., 1994. Cours d'hydraulique générale. ENGREF, Département Maîtrise de l'Eau, 128 pp.

Pomeroy, J.W. and Gray, D.M., 1995. Snowcover-accumulations, relocation and management. Report No. 7, National Hydrology Research Institute Science, Saskatoon.

Pomeroy, J.W. *et al.,* 1998a. An evaluation of snow accumulation and ablation processes for land surface modeling. Hydrological Processes, 12(15): 2339–2367.

Pomeroy, J.W., Parviainen, J., Hedstrom, N. and Gray, D.M., 1998b. Coupled modelling of forest snow interception and sublimation. Hydrological Processes, 12(15): 2317–2337.

Ponce, V.M., 1983. Development of Physically Based Coefficients for the Diffusion Method of Flood Routing, USDA, Soil Conservation Service, Report No. 83110.

Potter, K.W. and Lettenmaier, D.P., 1990. A Comparison of Regional Flood Frequency Estimation Methods Using a Resampling Method. Water Resources Research, 26(3): 415–424.

Preissmann, A. and Cunge, J.A., 1961. Calcul des intumescences sur machines électroniques, Proceedings of 9th Congress, Dubrovnik, pp. 656–64.

Preissmann, A., 1961. Propagation des intumescences dans les canaux et rivières, Proceedings of the First Congress of the French Association for Computation, Grenoble, France, pp. 433–442.

Preissmann, A., 1965. Difficultés rencontrées dans le calcul des ondes de translation à front raide, 11ème Congrès IAHR, Leningrade, pp. 3–52.

Prudhomme, C., Reynard, N. and Crooks, S., 2002. Downscaling of global climate models for flood frequency analysis: where are we now? Hydrological Processes, 16(6): 1137–1150.

Puech, C., 2000. Utilisation de la télédétection et des Modèles Numériques de Terrain pour la connaissance du fonctionnement des hydrosystèmes. HDR, Université Joseph Fourier, Grenoble, 83 pp. + annexes.

Qian, B., Corte-Real, J. and Xu, H., 2002. Multisite stochastic weather model for impact studies. International Journal of Climatology, 22: 1377–1397.

Quinn, P., Beven, K. and Culf, A., 1995. The Introduction of Macroscale Hydrological Complexity into Land Surface-Atmosphere Transfer Models and the Effect on Planetary Boundary-Layer Development. Journal of Hydrology, 166(3-4): 421–444.

Quintana-Segui, P. *et al.,* 2008. Analysis of near-surface atmospheric variables: Validation of the SAFRAN analysis over France. Journal of Applied Meteorology and Climatology, 47(1): 92–107.

Raisanen, J. *et al.,* 2004. European climate in the late twenty-first century: regional simulations with two driving global models and two forcing scenarios. Climate Dynamics, 22(1): 13–31.

Ramirez, J.A., Hobbins, M.T. and Brown, T.C., 2005. Observational evidence of the complementary relationship in regional evaporation lends strong support for Bouchet's hypothesis. Geophysical Research Letters, 32(15).

Ramos, M.H., Bartholmes, J., Thielen, J., Kalas, M. and de Roo, A., 2006. The additional value of ensemble weather forecasts to flood forecasting: first results on EFAS forecasts for the Danube river basin, Proc. 23rd Conf. Danube Countries on the Hydrological Forecasting and Hydrological Bases of Water Management, Belgrade.

Ramos, M.H., Creutin, J.D. and Leblois, E., 2005. Visualization of storm severity. Journal of Hydrology, 315(1-4): 295–307.

Rango, A., 1996. Spaceborne remote sensing for snow hydrology applications. Hydrological Sciences Journal-Journal Des Sciences Hydrologiques, 41(4): 477–494.

Rango, A., Walker, A.E. and Goodison, B.E., 2000. Snow and Ice. pp. 231–270. In: G.A. Schultz and T. Engman Edwin (Editors), Remote sensing in hydrology and water management. Springer, Berlin.

Rao, S. and Riahi, K. 2006. The role of non-CO2 greenhouse gases in climate change mitigation: Long-term scenarios for the 21st century. Multigas mitigation and climate policy. The Energy Journal, 3(Special Issue): 177–200.

Ravi, V. and Williams, J.R., 1998. Estimation of infiltration rate in the vadose zone: compilation of simple mathematical models, 1. USEPA, EPA/600/R-97-128a, 26 pp.

Rawls, W.J., Ahuja, L.R., Brakensiek, D.L. and Shirmohammadi, A., 1992. Chapter 5. Soil water movement and infiltration. In: D.R. Maidment (Editor), Handbook of Hydrology. McGraw Hill.

Refsgaard, J.C. and Knudsen, J., 1996. Operational validation and intercomparison of different types of. hydrological models. Water Resources Research, 32(7): 2189–2202.

Refsgaard, J.C. and Storm, B., 1995. Mike She. pp. 809–846. In: V.P. Singh (Editor), Computer models of watershed hydrology. Wat. Resour. Publications, Colorado, USA.

Refsgaard, J.C., 1997. Validation and intercomparison of different updating procedures for real-time forecasting. Nordic Hydrology, 28(2): 65–84.

Reichle, R.H. and Koster, R.D., 2005. Global assimilation of satellite surface soil moisture retrievals into the NASA Catchment land surface model. Geophysical Research Letters, 32(2).

Reichle, R.H., 2006. Data Assimilation Methods in the Earth Sciences. In: U. Aswathanarayana and R. Balaji (Editors), Research and Economic Applications of Remote Sensing Data Products. American Geophysical Union, Washington, D.C.

Reichle, R.H., McLaughlin, D.B. and Entekhabi, D., 2002. Hydrologic data assimilation with the ensemble Kalman filter. Monthly Weather Review, 130(1): 103–114.

Renard, B., 2006. Détection et prise en compte d'éventuels impacts du changement climatique sur les extrêmes hydrologiques en France. Thèse de doctorat, INPG, Grenoble, 364 pp.

Renault, D., 2004. Satellites météorologiques. La Météorologie, 45: 33–47.

Riahi, K., Gruebler, A. and Nakicenovic, N. 2007. Scenarios of long-term socio-economic and environmental development under climate stabilization. Technological Forecasting and Social Change, 74(7): 887–935. Available at http://dx.doi.org/10.1016/j.techfore.2006.05.026.

Ribeiro, J., Lauzon, N., Rousselle, J., Trung, H.T. and Salas, J.D., 1998. Comparaison de deux modèles pour la prévision journalière en temps réel des apports naturels. Canadian Journal of Civil Engineering, 25(2): 291–304.

Riccardi, G., 1997. The mathematical modelling of flood propagation for the delineation of flood risk zones, Sustainability of Water Resources under Increasing Uncertainty. IAHS Publ., N° 240, pp. 355–364.

Richardson, C.W., 1981. Stochastic Simulation of Daily Precipitation, Temperature, and Solar-Radiation. Water Resources Research, 17(1): 182–190.

Risbey, J.S. and Stone, P.H., 1996. A case study of the adequacy of GCM simulations for input to regional climate change assessments. Journal of Climate, 9(7): 1441–1467.

Roche, P.A., 1987. Guide de prévision des crues. Ministère de l'Environnement, Société Hydrotechnique de France, Paris, France.

Rodhe, A., 1998. Snowmelt-Dominated Systems. pp. 391–433. In: C. Kendall and J.J. McDonnell (Editors), Isotope Traces in Catchment Hydrology. Elsevier, Amsterdam.

Rodriguez Iturbe, I. and Valdes, J.B., 1979. Geomorphologic Structure of Hydrologic Response. Water Resources Research, 15(6): 1409–1420.

Rodriguez, F., Andrieu, H. and Creutin, J.D., 2003. Surface runoff in urban catchments: morphological identification of unit hydrographs from urban databanks. Journal of Hydrology, 283(1-4): 146–168.

Rodriguez-Iturbe, I. and Rinaldo, A., 1997. Fractal river basins: chance and self-organization. Cambridge Univ. Press New York, 547 pp.

Rogers, J.C., 1984. The Association between the North-Atlantic Oscillation and the Southern Oscillation in the Northern Hemisphere. Monthly Weather Review, 112(10): 1999–2015.

Rojas-Serna, C., 2005. Quelle connaissance hydrométrique minimale pour définir les paramètres d'un modèle pluie-débit? Thèse de doctorat, ENGREF, Paris, 225 pp.

Rosenbrock, H.H., 1960. An Automatic Method for Finding the Greatest or Least Value of a Function. The Computer Journal, 3(3): 175–184.

Rosnoblet, J., 2002. Dynamique du bilan hydrique parcellaire au sein de l'espace rural, et conséquences sur les transferts hydrologiques. Thèse de doctorat, INAPG, Paris-Grignon, 145 pp. + annexes.

Rossi, F., Fiorentino, M. and Versace, P., 1984. 2-Component Extreme Value Distribution for Flood Frequency-Analysis. Water Resources Research, 20(7): 847–856.

Rossman, L.A., 2005. Storm water management model, version 5: user's manual. U.S. Environmental Protection Agency (EPA) EPA/600/R-05/040, 249 pp.

Rowell, D.P., 2006. A demonstration of the uncertainty in projections of UK climate change resulting from regional model formulation. Climatic Change, 79(3-4): 243–257.

Rupp, D.E. and Selker, J.S., 2006. Information, artifacts, and noise in dQ/dt-Q recession analysis. Advances in Water Resources, 29(2): 154–160.

Rupp, D.E., Owens, J.M., Warren, K.L. and Selker, J.S., 2004. Analytical methods for estimating saturated hydraulic conductivity in a tile-drained field. Journal of Hydrology, 289(1-4): 111–127.

Rutter, A.J. and Morton, A.J., 1977. Predictive Model of Rainfall Interception in Forests. 3. Sensitivity of Model to Stand Parameters and Meteorological Variables. Journal of Applied Ecology, 14(2): 567–588.

Rutter, A.J., Morton, A.J. and Robins, P.C., 1975. Predictive Model of Rainfall Interception in Forests. 2. Generalization of Model and Comparison with Observations in Some Coniferous and Hardwood Stands. Journal of Applied Ecology, 12(1): 367–380.

Rutter, A.J., Robins, P.C., Morton, A.J. and Kershaw, K.A., 1972. Predictive Model of Rainfall Interception in Forests. 1. Derivation of Model from Observations in a Plantation of Corsican Pine. Agricultural Meteorology, 9(5-6): 367-&.

Salinas, J.L. *et al.,* 2013. Comparative assessment of predictions in ungauged basins—Part 2: Flood and low flow studies. Hydrol. and Earth Syst. Sci., 17: 2637–2652.

Saltelli, A., Chan, K. and Scott, E.M., 2000. Sensitivity Analysis. Wiley, Chichester, 475 pp.

Santer, B.D., Wigley, T.M.L., Schlesinger, M.E. and Mitchell, J.F.B., 1990. Developing climate scenarios for equilibrium GCM results, MPI report 47, Hamburg.

Sauquet, E., 2006. Mapping mean annual river discharges: Geostatistical developments for incorporating river network dependencies. Journal of Hydrology, 331(1-2): 300–314.

Sauvageot, H., 2000. Le radar polarimétrique, une nouvelle approche pour l'observation des champs de précipitations. La Météorologie, 31: 25–41.

Savenije, H.H.G., 2004. The importance of interception and why we should delete the term evapotranspiration from our vocabulary. Hydrological Processes, 18(8): 1507–1511.

Schaap, M.G., Leij, F.J. and van Genuchten, M.T., 2001. ROSETTA: a computer program for estimating soil hydraulic parameters with hierarchical pedotransfer functions. Journal of Hydrology, 251(3-4): 163–176.

Schaefli, B., 2005. Quantification of modelling uncertainties in climate change impact studies on water resources: Application to a glacier-fed hydropower production system in the Swiss Alps. PhD Thesis, EPFL, Lausanne, 209 pp.

Schaefli, B. and Gupta, H.V., 2007. Do Nash values have value? Hydrol. Process, 21: 2075–2080.

Schaefli, B., Hingray, B. and Musy, A., 2007. Climate change and hydropower production in the Swiss Alps: quantification of potential impacts and related modelling uncertainties. Hydrology and Earth System Sciences, 11(3): 1191–1205.

Schaefli, B., Hingray, B., Niggli, M. and Musy, A., 2005. A conceptual glacio-hydrological model for high mountainous catchments. Hydrology and Earth System Sciences, 9(1-2): 95–109.

Schmugge, T.J., Kustas, W.P., Ritchie, J.C., Jackson, T.J. and Rango, A., 2002. Remote sensing in hydrology. Advances in Water Resources, 25(8-12): 1367–1385.

Schneider, T., 2000. Hydrological processes in the wet-snow zone of glacier: a review. Zeitschrift für Gletscherkunde und Glazialgeologie, 36(1): 89–105.

Schumann, G. *et al.,* 2007. Deriving distributed roughness values from satellite radar data for flood inundation modelling. Journal of Hydrology, 344: 96–111.

See, L. and Openshaw, S., 2000. A hybrid multi-model approach to river level forecasting. Hydrological Sciences Journal-Journal Des Sciences Hydrologiques, 45(4): 523–536.

Sefton, C.E.M. and Howarth, S.M., 1998. Relationships between dynamic response characteristics and physical descriptors of catchments in England and Wales. Journal of Hydrology, 211(1-4): 1–16.

Segond, M.L., Onof, C. and Wheater, H.S., 2006. Spatiat-temporal disaggregation of daily rainfall from a generalized linear model. Journal of Hydrology, 331(3-4): 674–689.

Sellers, P.J. *et al.,* 1996. A revised land surface parameterization (SiB2) for atmospheric GCMs. 1. Model formulation. Journal of Climate, 9(4): 676–705.

Semenov, M.A., Brooks, R.J., Barrow, E.M. and Richardson, C.W., 1998. Comparison of the WGEN and LARS-WG stochastic weather generators for diverse climates. Climate Research, 10(2): 95–107.

Sergent, C., Pougatch, E., Sudul, M. and Bourdelles, B., 1993. Experimental investigation of optical snow properties. Annal of Glaciology, 17: 281–287.

Servat, E. and Dezetter, A., 1991. Selection of Calibration Objective Functions in the Context of Rainfall-Runoff Modeling in a Sudanese Savannah Area. Hydrological Sciences Journal-Journal Des Sciences Hydrologiques, 36(4): 307–330.

Shabalova, M.V., van Deursen, W.P.A. and Buishand, T.A., 2003. Assessing future discharge of the river Rhine using regional climate model integrations and a hydrological model. Climate Research, 23(3): 233–246.

Shamseldin, A.Y. and Nash, J.E., 1998. The geomorphological unit hydrograph—a critical review. Hydrology and Earth System Sciences, 2(1): 1–8.

Shamseldin, A.Y., Oconnor, K.M. and Liang, G.C., 1997. Methods for combining the outputs of different rainfall-runoff models. Journal of Hydrology, 197(1-4): 203–229.

Sharif, H.O., Yates, D., Roberts, R. and Mueller, C., 2006. The use of an automated nowcasting system to forecast flash floods in an urban watershed. Journal of Hydrometeorology, 7(1): 190–202.

Sharp, M., Richards, K.S. and Tranter, M., 1998. Glacier Hydrology and Hydrochemistry. Wiley, 350 pp.

Sherman, L.K., 1932. Stream flow from rainfall by the unit graph method. Engineering News-Record, 108: 501–205.

Singh, P. and Singh, V.P., 2001. Snow and glacier hydrology. Kluwer Academic Publishers, Dordrecht, 742 pp.

Singh, V.P. and Woolhiser, D.A., 2002. Mathematical modeling of watershed hydrology. Journal of Hydrologic Engineering, 7: 270–292.

Singh, V.P., 1995. Computer Models of Watershed Hydrology. Water Resource Publications, Highlands Ranch, CO, 1144 pp.

Sinniger, R.O. and Hager, W.H., 1989. Constructions hydrauliques: écoulements stationnaires, Vol. 15. PPUR, Lausanne, 456 pp.

Sivakumar, B., 2001. Is a chaotic multi-fractal approach for rainfall possible? Hydrological Processes, 15(6): 943–955.

Sivapalan, M. *et al.,* 2003. IAHS decade on Predictions in Ungauged Basins (PUB), 2003–2012: Shaping an exciting future for the hydrological sciences. Hydrological Sciences Journal-Journal Des Sciences Hydrologiques, 48(6): 857–880.

Slater, A.G. *et al.,* 2001. The representation of snow in land surface schemes: Results from PILPS 2(d). Journal of Hydrometeorology, 2(1): 7–25.

Smakhtin, V.U., 2001. Low flow hydrology: a review. Journal of Hydrology, 240(3-4): 147–186.

Smith, M. *et al.,* 1991. Report on the expert consultation on procedures for revision of FAO guidelines for prediction of crop water requirements. Land and Water Development Division, FAO, Rome, Italy.

Smith, M.B. *et al.,* 2004. The distributed model intercomparison project (DMIP): motivation and experiment design. Journal of Hydrology, 298(1-4): 4–26.

Smith, R.E., Goodrich, D.C., Woolhiser, D.A. and Unkrich, C.L., 1995. KINEROS: A KINematic. Runoff and EROSion model. pp. 697–732. In: V.J. Singh (Editor), Computer Models of Watershed Hydrology. Water Resource Publications, Highlands Ranch, CO.

Smith, S.J. and T.M.L. Wigley, 2006. Multi-Gas Forcing Stabilization with the MiniCAM. The Energy Journal, (Special Issue #3): 373–391.

Sommerfeld, R.A. and Rocchio, J.E., 1993. Permeability Measurements on New and Equitemperature Snow. Water Resources Research, 29(8): 2485–2490.

Soutter, M., 2003. Mise en oeuvre de la formule rationnelle synthétique pour l'estimation des débits de pointe des bassins versants du canton de Vaud, Projet Gesreau, Rapport Hydram/EPFL, Lausanne.

Soutter, M., Mermoud, A. and Musy, A., 2007. Ingénierie des sols et des eaux, processus et aménagements. PPUR, Lausanne.

Srikanthan, R. and McMahon, T.A., 2001. Stochastic generation of annual, monthly and daily climate data: A review. Hydrology and Earth System Sciences, 5(4): 653–670.

Stahl, K., Moore, R.D., Floyer, J.A., Asplin, M.G. and McKendry, I.G., 2006. Comparison of approaches for spatial interpolation of daily air temperature in a large region with complex topography and highly variable station density. Agricultural and Forest Meteorology, 139(3-4): 224–236.

Stedinger, J.R. and Lu, L.H., 1995. Appraisal of Regional and Index Flood Quantile Estimators. Stochastic Hydrology and Hydraulics, 9(1): 49–75.

Stedinger, J.R. and Tasker, G.D., 1985. Regional Hydrologic Analysis. 1. Ordinary, Weighted, and Generalized Least-Squares Compared. Water Resources Research, 21(9): 1421–1432.

Stedinger, J.R., Vogel, R M. and Foufoula-Georgiou, E. 1993. Frequency Analysis of Extreme Events. In Handbook of Hydrology, edited by D. Maidment, New York McGraw. Hill, Inc.

Stehlik, J. and Bardossy, A., 2002. Multivariate stochastic downscaling model for generating daily precipitation series based on atmospheric circulation. Journal of Hydrology, 256(1-2): 120–141.

Sterl, A., 2004. On the (in)homogeneity of reanalysis products. Journal of Climate, 17(19): 3866–3873.

Stone, R.C., 1989. Weather Types at Brisbane, Queensland—an Example of the Use of Principal Components and Cluster-Analysis. International Journal of Climatology, 9(1): 3–32.

Sturaro, G., 2003. A closer look at the climatological discontinuities present in the NCEP/NCAR reanalysis temperature due to the introduction of satellite data. Climate Dynamics, 21(3-4): 309–316.

Sturm, T. 2001. Open Channel Hydraulics, McGraw-Hill Science/Engineering/Math, 512 p.

Sugawara, M. and Maruyama, F., 1956. A method of prevision of the river. discharge by means of a rainfall model, Symposia Darcy, Dijon, pp. 71–76.

Sujono, J., Shikasho, S. and Hiramatsu, K., 2004. A comparison of techniques for hydrograph recession analysis. Hydrological Processes, 18(3): 403–413.

Szilagyi, J. and Parlange, M.B., 1999. A geomorphologically-based semi-distributed watershed model. Advances in Water Resources, 23: 177–187.

Tabary, P., Scialom, G. and Protat, A., 2002. Un radar météorologique Doppler: pour quoi faire? La Météorologie, 38(30-44).

Talamba-Balin, D., 2004. Hydrological behaviour through experimental and modelling approaches: application to the Haute-Mentue catchment. PhD Thesis, EPFL, Lausanne, 193 pp.

Tallaksen, L.M., 1995. A Review of Baseflow Recession Analysis. Journal of Hydrology, 165(1-4): 349–370.

Tapsoba, D., Fortin, V., Anctil, F. and Haché, M., 2005. Apport de la technique du krigeage avec dérive externe pour une cartographie raisonnée de l'équivalent en eau de la neige: aplication aux bassins de la rivière Gatineau. Revue canadienne de génie civil, 32(1): 289–297.

Tarboton, D.G., 1997. A new method for the determination of flow directions and upslope areas in grid digital elevation models. Water Resources Research, 33(2): 309–319.

Tardy, Y., 1986. Le cycle de l'eau : Climats, Paléoclimats et Géochimie globale. Masson.

Tardy, Y., 1986. Le cycle de l'eau, climats, paléoclimats et chimie globale. Masson, Paris.

Terray, L. and Braconnot, P., 2007. Livre blanc ESCRIME. Étude des Simulations Climatiques. IPSL & Météo-France, Paris, 70 pp.

Testud, J., 2002. Le radar météorologique à diversité de polarisation: un outil prêt à entrer dans l'application opérationnelle (The polarimetric weather radar: a tool ready for operational application). La Houille Blanche, 2: 46–49.

Teweless, S. and Wobus, H., 1954. Erification of prognostic charts. Bulletin of the. American Meteorological Society, 35: 286–296.

Thillet, J.J., 1997. La météo de montagne. Collection les guides du Club alpin français. Seuil, 189 pp.

Tholin, A.L. and Keifer, C.J., 1960. The hydrology of urban runoff. Transactions of the American Society of Civil Engineers, 125: 1308–1379.

Thomas, H.A., 1981. Improved methods for rational water assessment, Washington, Report, Contrat WR. 15249270 US Water Ressources Council, USA.

Todini, E., 1996. The ARNO rainfall-runoff model. Journal of Hydrology, 175(1-4): 339–382.

Todini, E., 2007. A mass conservative and water storage consistent variable parameter Muskingum-Cunge approach. Hydrology and Earth System Sciences, 11: 1645–1659.

Toma, A.C., 1996. Variabilité spatio-temporelle des champs précipitants et application aux méthodes d'estimation. Thèse de doctorat, ENSMP, Paris, 153 pp.

Toth, E., Brath, A. and Montanari, A., 2000. Comparison of short-term rainfall prediction models for real-time flood forecasting. Journal of Hydrology, 239(1-4): 132–147.

Trenberth, K.E., 1984. Signal Versus Noise in the Southern Oscillation. Monthly Weather Review, 112(2): 326–332.

Tung, Y.K., Yeh, K.C. and Yang, J.C., 1997. Regionalization of unit hydrograph parameters .1. Comparison of regression analysis techniques. Stochastic Hydrology and Hydraulics, 11(2): 145–171.

Turcotte, R., Rousseau, A.N., Fortin, J.P. and Villeneuve, J.P., 2003. Development of a process-oriented, multiple-objective, hydrological calibration strategy accounting for model structure. pp. 153–163. In: Q.Y. Duan, H. Gupta, S. Sorooshian, A.N. Rousseau and R. Turcotte (Editors), Calibration of watershed models. Water Science and Application 6. American Geophysical Union, Washington, DC.

Uppala, S.M. *et al.,* 2005. The ERA-40 re-analysis. Quarterly Journal of the Royal Meteorological Society, 131(612): 2961–3012.

USACE, 1986. Accuracy of Computed Water Surface Profiles, US Army Corps of Engineers.

USACE, 1994. Engineering and Design—Flood-Runoff Analysis. Publication Number: EM 1110-2-1417. US Army Corps of Engineers, 213 pp.

USDA-SCS, 1972. Section 4: Hydrology, National Engineering Handbook. United States Department of Agriculture, Soil Conservation Service, Washington DC.

Valente, F., David, J.S. and Gash, J.H.C., 1997. Modelling interception loss for two sparse eucalypt and pine forests in central Portugal using reformulated Rutter and Gash analytical models. Journal of Hydrology, 190(1-2): 141–162.

Valiantzas, J.D., 2006. Simplified versions for the Penman evaporation equation using routine weather data. Journal of Hydrology, 331(3-4): 690–702.

van Dam, J.C. and Feddes, R.A., 2000. Numerical simulation of infiltration, evaporation and shallow groundwater levels with the Richards equation. Journal of Hydrology, 233(1-4): 72–85.

van Dijk, A.I.J.M. and Bruijnzeel, L.A., 2001. Modelling rainfall interception by vegetation of variable density using an adapted analytical model. Part 1. Model description. Journal of hydrology, 247(3-4): 230–238.

van Genuchten, M.T., 1980. A Closed-Form Equation for Predicting the Hydraulic Conductivity of Unsaturated Soils. Soil Science Society of America Journal, 44(5): 892–898.

van Straten, G. and Keesman, J., 1991. Uncertainty propagation and speculation in projective forecasts of environmental change: a lake eutrophication example. Journal of Forecasting, 10: 163–190.

van Ulden, A.P. and van Oldenborgh, G.J., 2006. Large-scale atmospheric circulation biases and changes in global climate model simulations and their importance for climate change in Central Europe. Atmospheric Chemistry and Physics, 6: 863–881.

van Vuuren, D.P. *et al.* 2006. Long-term multi-gas scenarios to stabilise radiative forcing—Exploring costs and benefits within an integrated assessment framework. Multigas mitigation and climate policy. The Energy Journal. 3(Special Issue): 201–234.

van Vuuren, D. *et al.* 2007. Stabilizing greenhouse gas concentrations at low levels: an assessment of reduction strategies and costs. Climatic Change. Available at http://dx.doi.org/10.1007/s10584-006-9172-9.

VAW, 1996. Régularisation optimale de la IIe correction des eaux du Jura (IIe CEJ). 3941 F, Versuchsanstalt für Wasserbau, Hydrologie und Glaziologie der Eidgenössischen Technischen Hochschule, Zürich.

Venables, W.N. and Ripley, B.D., 1998. Modern applied statistics with S-Plus. Springer-Verlag, New York, 501 pp.

Verseghy, D.L., 1991. CLASS—A Canadian Land Surface Scheme for GCMS. I. Soil Model. International Journal of Climatology, 11(2): 111–133.

Verseghy, D.L., McFarlane, N.A. and Lazare, M., 1993. A Canadian Land Surface Scheme for GCMs: II. Vegetation model and coupled runs. International Journal of Climatology, 13(4): 347–370.

Vertessy, R.A., Hatton, T.J., O'Shaughnessy, P.J. and Jayasuriya, M.D.A., 1993. Predicting water yield from a mountain ash forest catchment using a terrain analysis-based catchment model. Journal of hydrology, 150(2-4): 665–700.

Vidal, J.P., 2005. Assistance au calage de modèles numériques en hydraulique fluviale—Apports de l'intelligence artificielle. Thèse de doctorat, INPT, Toulouse.

Vidale, P.L., Luthi, D., Frei, C., Seneviratne, S.I. and Schar, C., 2003. Predictability and uncertainty in a regional climate model. Journal of Geophysical Research-Atmosphères, 108(D18).

Viessman, W., Jr., Knapp, J.W., Lewis, G.L. and Harbaugh, T.R., 1977. Introduction to Hydrology, Second Edition. Harper & Row, New York.

Vieux, B.E., 2001a. Radar Rainfall Applications in Hydrology. Chapter 11. pp. 648–681. In: P.B. Bedient and W.C. Huber (Editors), Hydrology and Floodplain Analysis. Addison-Wesley Publishing Co., Reading, Massachusetts.

Vieux, B.E., 2001b. Distributed hydrologic modeling using GIS. Water Science Technology Series, 38. Kluwer Academic Publishers, Norwell, Massachusetts, 293 pp.

Viglione, A. *et al.,* 2013. Comparative assessment of predictions in ungauged basins—Part 3: Runoff signatures in Austria. Hydrol. and Earth Syst. Sci., 17: 2263–2279.

Vincent, C., 2002. Influence of climate change on French glaciers mass balance over the 20th century. La Houille Blanche, 8: 20–24.

Vischel, T. and Lebel, T., 2007. Assessing the water balance in the Sahel: Impact of small scale rainfall variability on runoff. Part 2: Idealized modeling of runoff sensitivity. Journal of Hydrology, 333(2-4): 340–355.

Vischel, T., 2006. Impact de la variabilité pluviométrique de méso-échelle sur la réponse des systèmes hydrologiques sahéliens: modélisation, simulation et désagrégation. Thèse de doctorat, INPG, Grenoble, 289 pp.

Vivoni, E.R., Ivanov, V.Y., Bras, R.L. and Entekhabi, D., 2004. Generation of triangulated irregular networks based on hydrological similarity. Journal of Hydrologic Engineering, 9(4): 288–302.

Vogel, R.M. and Fennessey, N.M., 1993. L-Moment Diagrams Should Replace Product Moment Diagrams. Water Resources Research, 29(6): 1745–1752.

Vogel, R.M. and Fennessey, N.M., 1994. Flow-Duration Curves. 2. New Interpretation and Confidence-Intervals. Journal of Water Resources Planning and Management-Asce, 120(4): 485–504.

Vogel, R.M. and Fennessey, N.M., 1995. Flow Duration Curves. 2. A Review of Applications in Water-Resources Planning. Water Resources Bulletin, 31(6): 1029–1039.

Vrac, M., Stein, M. and Hayhoe, K., 2007. Statistical downscaling of precipitation through nonhomogeneous stochastic weather typing. Climate Research, 34: 169–184.

Vrac, M., Stein, M.L., Hayhoe, K. and Liang, X.Z., 2007. A general method for validating statistical downscaling methods under future climate change. Geophysical Research Letters, 34 pp.

Walker, W.E. *et al.,* 2003. Defining Uncertainty: A Conceptual Basis for Uncertainty Management in Model-Based Decision Support. Integrated Assessment, 4(1): 5–17

Walter, M.T. *et al.,* 2005. Process-based snowmelt modeling: does it require more input data than temperature-index modeling? Journal of Hydrology, 300(1-4): 65–75.

Waymire, E. and V.K. Gupta. 1981. The mathematical structure of rainfall representations: 1. A review of the stochastic rainfall models, Water Resour. Res., 17(5): 1261–1272.

Webster, P.J. and Yang, S., 1992. Monsoon and Enso—Selectively Interactive Systems. Quarterly Journal of the Royal Meteorological Society, 118(507): 877–926.

Weingartner, R. and Aschwanden, H., 1986. Die Abflussregimes der Schweiz. Geographisches Institut der Universität Bern, Bern.

Weingartner, R. and Aschwanden, R., 1992. Abflussregimes als Grundlage zur Abschätzung von Mittelwerten des Abflusses. Tafel 5.2. hydrologischen Atlas der Schweiz, Bern.

Weingartner, R. and Manser, S., 1997. Möglichkeiten und Grenzen des Hochwasserabschätzung in kleineren schweizerischen Einzugsgebieten ohne Abflussmessungen. Wasser, Energie and Luft, 5/6: 131–138.

Wheater, H.S. *et al.,* 2000. Spatial-temporal rainfall fields: modelling and statistical aspects. Hydrology and Earth System Sciences, 4(4): 581–601.

Wheater, H.S. *et al.,* 2005. Spatial-temporal rainfall modelling for flood risk estimation. Stochastic Environmental Research and Risk Assessment, 19(6): 403–416.

Wigley, T.M.L. and Raper, S.C.B., 2001. Interpretation of high projections for global-mean warming. Science, 293(5529): 451–454.

Wigley, T.M.L., Raper, S.C.B., Smith, S. and Hulme, M., 2000. The Magicc/ScenGen Climate Scenario Generator: version 2.4: Technical Manual, CRU, UEA, Norwich, U.K.

Wigmosta, M.S., Nijssen, B, and Storck, P., 2002. The Distributed Hydrology Soil Vegetation Model. Chapter 2. pp. 7–42. In: V.S.D. Frevert (Editor), Mathematical Models of Small Watershed Hydrology and Applications. Water Resources Publications, Highlands Ranch, CO.

Wilby, R.L. and Wigley, T.M.L., 1997. Downscaling general circulation model output: a review of methods and limitations. Progress in Physical Geography, 21(4): 530–548.

Wilby, R.L. and Wigley, T.M.L., 2000. Precipitation predictors for downscaling: Observed and general circulation model relationships. International Journal of Climatology, 20(6): 641–661.

Wilby, R.L. *et al.,* 1998. Statistical downscaling of general circulation model output: A comparison of methods. Water Resources Research, 34(11): 2995–3008.

Wilby, R.L., 1998. Statistical downscaling of daily precipitation using daily airflow and seasonal teleconnection indices. Climate Research, 10(3): 163–178.

Wilby, R.L., Conway, D. and Jones, P.D., 2002. Prospects for downscaling seasonal precipitation variability using conditioned weather generator parameters. Hydrological Processes, 16(6): 1215–1234.

Wilby, R.L., Hassan, H. and Hanaki, K., 1998. Statistical downscaling of hydrometeorological variables using general circulation model output. Journal of Hydrology, 205(1-2): 1–19.

Wilks, D.S. and Wilby, R.L., 1999. The weather generation game: a review of stochastic weather models. Progress in Physical Geography, 23(3): 329–357.

Wilks, D.S., 1998. Multisite generalization of a daily stochastic precipitation generation model. Journal of Hydrology, 210(1-4): 178–191.

Wilks, D.S., 1999. Multisite downscaling of daily precipitation with a stochastic weather generator. Climate Research, 11(2): 125–136.

Wilks, D.S., 2012. Stochastic weather generators for climate-change downscaling, part II: multivariable and spatially coherent multisite downscaling. Wiley Interdisc. Rev.-Clim. Chang., 3: 267–278.

Willems, P., 2001. A spatial rainfall generator for small spatial scales. Journal of Hydrology, 252(1-4): 126–144.

Williams, J.R., Ouyang, Y., Chen, J.-S. and Ravi, V., 1998. Estimation of infiltration rate in the vadose zone: application of selected mathematical models, volume II. EPA/600/R-97-128b. USEPA, 44 pp.

Willis, I., 2005. Hydrology of glacierized basins. pp. 2601–2631. In: M.G. Anderson and J.J. McDonnell (Editors), Encyclopedia of Hydrological Sciences—Part 14: Snow and Glacier Hydrology. Wiley, Chichester.

Wilson, J.W., Crook, N.A., Mueller, C.K., Sun, J.Z. and Dixon, M., 1998. Nowcasting thunderstorms: A status report. Bulletin of the American Meteorological Society, 79(10): 2079–2099.

Wiltshire, S.E., 1985. Grouping Basins for Regional Flood Frequency-Analysis. Hydrological Sciences Journal-Journal Des Sciences Hydrologiques, 30(1): 151–159.

Wiltshire, S.E., 1986. Regional Flood Frequency-Analysis. 1. Homogeneity Statistics. Hydrological Sciences Journal-Journal Des Sciences Hydrologiques, 31(3): 321–333.

Wise, MA *et al.* 2009. Implications of Limiting CO2 Concentrations for Land Use and Energy. Science. 324: 1183–1186.

Wiltshire, S.E., 1986. Regional Flood Frequency-Analysis. 2. Multivariate Classification of Drainage Basins in Britain. Hydrological Sciences Journal-Journal Des Sciences Hydrologiques, 31(3): 335–346.

Wisner, P. and P'ng, J.C., 1983. OTTHYMO. A Model for Master Drainage Plans, IMPSWM Urban Drainage Modelling Procedures, Department of Civil Engineering, University of Ottawa, Ottawa, Ontario.

Wittenberg, H., 1999. Baseflow recession and recharge as nonlinear storage processes. Hydrological Processes, 13(5): 715–726.

WMO, 1974. International Glossary of Hydrology. World Meteorological Organisation, Genève.

WMO, 1975. Hydrological forecasting practices. Operational Hydrology. Report N°6, WMO N°425. World Meteorological Organisation, Genève.

WMO, 1986. Intercomparison of models of snowmelt runoff. Report No. 23. World Meteorological Organisation, Genève.

WMO, 1986. Manual for Estimation of Probable Maximum Precipitation, 2nd edition. Operational Hydrology Report No. 1, WMO - No. 332. World Meteorological Organisation, Genève.

WMO, 1992. Simulated real-time intercomparison of hydrological models. Operational Hydrology. Report N°38. WMO N°779. World Meteorological Organisation, Genève.

WMO, 1994. Guide to hydrological practices. Fifth edition. No. 168. World Meteorological Organisation, Genève, 735 pp.

Wojcik, R. and Buishand, T.A., 2003. Simulation of 6-hourly rainfall and temperature by two resampling schemes. Journal of Hydrology, 273(1-4): 69–80.

Wojcik, R., Beersma, J.J. and Buishand, T.A., 2000. Rainfall generator for the Rhine basin. Multisite generation of weather variables for the entire drainage area. KNMI Publication; 186 IV. De Bilt, Netherlands.

Wood, E. *et al.,* 2006. Implementation Plan for The Hydrological Ensemble Prediction Experiment (HEPEX), http://hydis8.eng.uci.edu/hepex/ (02.07.2007). HEPEX.

Wood, E., Lettenmaier, D. and Zartarian, V., 1992. A Land-Surface Hydrology Parameterization with Subgrid Variability for General-Circulation Models. J. Geophys. Res.-Atmos., 97: 2717–2728.

Wood, E.F. and Rodrigueziturbe, I., 1975. Bayesian Approach to Analyzing Uncertainty among Flood Frequency Models. Water Resources Research, 11(6): 839–843.

Wosten, J.H.M., Pachepsky, Y.A. and Rawls, W.J., 2001. Pedotransfer functions: bridging the gap between available basic soil data and missing soil hydraulic characteristics. Journal of Hydrology, 251(3-4): 123–150.

Xu, C.Y. and Chen, D., 2005. Comparison of seven models for estimation of evapotranspiration and groundwater recharge using lysimeter measurement data in Germany. Hydrological Processes, 19(18): 3717–3734.

Xu, C.Y. and Singh, V.P., 2005. Evaluation of three complementary relationship evapotranspiration models by water balance approach to estimate actual regional evapotranspiration in different climatic regions. Journal of Hydrology, 308(1-4): 105–121.

Xu, C.Y., 1999. From GCMs to river flow: a review of downscaling methods and hydrologic modelling approaches. Progress in Physical Geography, 23(2): 229–249.

Xu, C.Y., 2003. Chap. 4 Evapotranspiration in Hydrologic Models, Hydrological Models. Uppsala University, Uppsala, Sweden.

Xu, H., Corte-Real, J. and Qian, B., 2007. Developing daily precipitation scenarios for climate change impact studies in the Guadiana and the Tejo basins. Hydrology and Earth System Sciences, 11: 1161–1173.

Yan, Z., Bate, S., Chandler, R.E., Isham, V. and Wheater, H., 2006. Changes in extreme wind speeds in NW Europe simulated by generalized linear models. Theoretical and Applied Climatology, 83(1-4): 121–137.

Yang, C., Chandler, R.E., Isham, V.S., Annoni, C. and Wheater, H.S., 2005. Simulation and downscaling models for potential evaporation. Journal of Hydrology, 302(1-4): 239–254.

Yang, D., Herath, S. and Musiake, K. 2000. Comparison of different distributed hydrological models for characterization of catchment spatial variability, Hydrological Processes 14(3): 403–416.

Young, P.C., 2002. Advances in real-time flood forecasting. Philosophical Transactions of the Royal Society of London Series a-Mathematical Physical and Engineering Sciences, 360(1796): 1433–1450.

Zappa, M., 1999. Untersuchungen zur Aufbereitung unterschiedlicher Rauminformationen für die flächendifferezierte Einzugsgebietsmodellierung. Diploma Thesis, Geographisches Institut der ETH, Zürich, 106 pp.

Zech, Y., Sillen, X., Djenfa, S. and Pahaut, T., 1993. Rainfall Runoff modelling of partly urbanised watershed/Comparison between a distributed model using GIS and an other model, 6th Inter. Conf. on Urban Storm Drainage, Niagara Falls, Ontario, Canada, pp. 1452–1457.

Zhao, L. and Gray, D.M., 1999. Estimating snowmelt infiltration into frozen soils. Hydrological Processes, 13(12): 1827–1842.

Zhao, R.J., 1992. The Xinanjiang Model Applied in China. Journal of Hydrology, 135(1-4): 371–381.

Zin, I., 2002. Incertitudes et ambiguïté dans la modélisation hydrologique. Discussion, développements méthodologiques et application à l'hydrologie de crue en Ardèche. Thèse de doctorat, INPG, Grenoble, 200 pp.

Zorita, E. and von Storch, H., 1999. The analog method as a simple statistical downscaling technique: Comparison with more complicated methods. Journal of Climate, 12(8): 2474–2489.

LIST OF ACRONYMS

AAR	Accumulation Area Ratio (glacier)
AMSR-E	Advanced Microwave Scanning Radiometer for the Earth Observing System
ANN	Artificial neuron networks
AOGCM	Atmosphere-Ocean General Circulation Models
AR4	IPCC Fourth Assessment Report
ARMAX	Autoregressive moving-average models with exogenous variables
ARX	Autoregressive statistical models with exogenous variables
ASCE	American Association of Civil Engineering
CEN	Centre d'étude de la neige (Snow Research Institute of Météo-France)
CNRS	Centre National de la Recherche Scientifique (French National Center for Scientific Research)
CNR	Compagnie Nationale du Rhône (independent electricity producer in France)
CRP-Gabriel Lippmann	Centre de Recherche Public-Gabriel Lippmann (a public research center in Luxembourg)
DHI	Danish Hydraulic Institute
DMIP	Distributed Model Intercomparison Project
DSD	Drop size distribution
DSM	Digital Surface Model
DTM	Digital Terrain Model
DEM	Digital Elevation Model
ECHO	Ecohydrology laboratory of EPFL
ECMWF	European Center for Medium-Range Weather Forecasts
EDF	Electricité de France (the main French electrical utility)
EFAS	European Flood Alert System
ELA	Equilibrium Line Altitude (of a glacier)
ENAC	School of Architecture, Civil and Environmental Engineering of EPFL, Switzerland
ENSO	El-Niño Southern Oscillation
EPFL	Ecole Polytechnique Fédérale de Lausanne (Swiss Federal Institute of Technology in Lausanne)
ET	Evapotranspiration
ET_0	Reference Evapotranspiration

ETM	Maximum evapotranspiration
FAO	Food and Agriculture Organization of the United Nations
FOEN/OFEN	Swiss Federal Office for the Environment
GCM	General Circulation Models
GEV	General Extreme Value Distribution
GHG	Greenhouse gases
GIS	Geographical Information System
GLUE	Generalized Likelihood Uncertainty Estimation
GPA	Generalized Pareto distribution
GRADEX	Gradient of extremes values
Grenoble INP	Grenoble Institute of Technology, France
GUH	Geomorphological unit hydrograph
HRU	Hydrological Response Unit
HYDRAM	Hydrology and Land Improvement laboratory of EPFL (now ECHO), Switzerland
IDF	Intensity–Duration–Frequency curve
IEAust	Institution of Engineers of Australia
IGUL	Institute of Geography of the University of Lausanne, Switzerland
INRS	Institut National de la Recherche Scientifique (the research-oriented branch of the Université de Québec, Canada)
IPCC	Intergovernmental Panel on Climate Change
IRSTEA	Institute for research in environmental and agricultural sciences and technologies in France (former CEMAGREF)
IUH	Instantaneous unit hydrograph
KED	Kriging with external drift
LAI	Leaf area index
LAM	Limited-Area Models
LIDAR	Light Detection And Ranging
LTHE	Laboratoire d'Etude des Transfers en Hydrologie et Environnement (hydrology laboratory of OSUG, France)
MeteoSwiss	Federal Office of Meteorology and Climatology, Switzerland
MODIS	Moderate Resolution Imaging Spectroradiometer
MOS	Model Output Statistics method
NAO	North-Atlantic Oscillation
NAOI	North-Atlantic Oscillation Index
NCAR	National Center for Atmospheric Research, USA
NCEP	National Center for Environmental Prediction, USA
OFEG	Swiss Federal Office for Water and Geology
OHMCV	Cévennes-Vivarais Mediterranean Hydrometeorological Observation System, France
OSUG	Observatoire des Sciences de l'Univers de Grenoble (Earth Sciences Observatory of Grenoble, France)
PET	Potential evapotranspiration
PMF	Probable Maximum Flood
PMP	Probable Maximum Precipitation

PPUR	Presses Polytechniques Universitaires Romandes (official publisher of the EPFL Press, Switzerland)
PDF	Probability Density Function
PQPF	Probabilistic quantitative precipitation forecast
PTF	Pedotransfer functions
PUB	Decade on Predictions in Ungauged Basins (2003–2014), initiative of the International Association of Hydrological Sciences (IAHS)
PWM	Probability Weighted Moments
QDF	Discharge-Intensity-Frequency curve
RADAR	Radio detection and ranging
RCM	Regional Climate Models
RCP	Representative Concentration Pathways
RHHU	Relatively Homogeneous Hydrological Units
SHF	Société Hydrotechnique de France (French organization set up to encourage progress in and development of scientific culture and knowledge in all the fields relating to water resources and hydrotechnical sciences)
SCHAPI	Central hydro-meteorology and flood forecasting support service, France
SCS	US Soil Conservation Service
SCS-CN	US Soil Conservation Service Curve Number method for determining net rainfall excess
SDSM	Statistical downscaling models
SIGE	Service intercommunal de gestion des eaux (Intercommunal Management Service of Vevey, Switzerland
SRES	Representative Emission Scenarios
SOGREAH	International water resources engineering firm, now ARTELIA, France
SRTM	Shuttle Radar Topography Mission
SVAT	Soil-Vegetation-Atmosphere Transfer model
SWE	Snow Water Equivalent
TIN	Triangular Irregular Network
UH	Unit hydrograph
VR-GCM	Variable Resolution General Circulation Models
WGEN	Weather Generators
WMO	World Meteorological Organization

COPYRIGHT AUTHORIZATION LIST

Figure 5.19 on p. 203 reproduced from Minshall (1960) with the permission of the ASCE.

Figure 6.18 on p. 246 reproduced from Graf and Altinakar (2000) with the permission of PPUR (Presses Polytechniques et Universitaires Romandes), publisher of the EPFL Press.

Figure 10.3 on p. 392 reproduced from WMO (1992), Figure 10.5 on p. 396 reproduced from WMO (1975), figure 12.15 on p. 484 reproduced from WMO (1986) and Figure 12.17 on p. 486 reproduced from WMO (1994) with the permission of the WMO.

Figure 10.13 on p. 412, 12.3 on p. 465, 12.4 on p. 466 and 12.8 on p. 476 reproduced from Bontron (2004) with the permission of the author.

Figure 12.1 on p. 462 reproduced from Figures 3.3 and 3.5 of Brutsaert (2005) with the permission of the author and Cambridge University Press.

Figure 12.16 on p. 485 reproduced from Ramos *et al*. (2005) with the permission of Elsevier.

Figure 12.25 on p. 514 reproduced from Neppel *et al*. (2006) with the permission of la Houille Blanche—Revue Internationale de l'Eau.

Figures 12.26 on p. 515 and 12.28 on p. 517 reproduced from Hingray and Ben Haha (2005) with the permission of Elsevier.

Figure 12.31 on p. 523 reproduced from Mellor *et al*. (2000) with the permission of Copernicus Publications on behalf of the European Geosciences Union (EGU).

This book presents the main hydrological methods and techniques used in the design and operation of hydraulic projects and in the management of water resources and associated natural risks.

It covers the key topics of water resources engineering, from the estimation of runoff volumes and unit hydrographs to the routing of flows along rivers and through lakes, reservoirs and hydraulic structures. It deals with questions regarding basic hydrological data, hydrological modeling and the prediction and forecasting of low flows and flood discharges. This book also covers innovative topics such as hydrology in mountainous regions, regionalization techniques and the generation of meteorological scenarios for hydrological analysis.

The various topics are presented in a rigorous manner with detailed descriptions of the corresponding methods and applications, fully reflecting the vast experience of the authors in this field.

This work will interest a wide variety of readers concerned with hydrology and water resources management, including teachers, students, researchers, engineers, geographers, planners, ecologists and environmental specialists.

Benoît Hingray is a graduate of École Polytechnique (Palaiseau, France) and ENGREF (École Nationale du Génie Rural des Eaux et Forêts de Paris, France). He obtained his PhD in hydrology in 1999. From 1999 to 2006, he was a principal investigator at the Hydrology and Land Improvement laboratory of EPFL, Switzerland, in charge of research activities in hydrometeorology. Over this period, he also taught bachelors and masters level courses in this discipline. In 2007, he became a researcher of the French National Center for Scientific Research (CNRS), continuing his work on climate regionalization and the hydrological impact of climate change at LTHE (Laboratoire d'étude des Transferts en Hydrologie et Environnement) in Grenoble, France.

Cécile Picouet obtained her university education in Marseille and Montpellier (France), where she received a Masters degree in Analytical Chemistry and Environmental Sciences. She obtained her PhD in 1999 with a thesis on the Geodynamics of the Niger River in Mali. She joined the Hydrology and Land Improvement laboratory of EPFL (Switzerland) in 2001 where she took part in research and teaching in hydrology, coordinating the preparation of several E-learning platforms. She continued her research and analysis activities in the field of snow hydrology with Electricité de France and joined Hydrétudes in 2012 where she works on flood risk, water resources and regional planning projects.

André Musy is Professor Emeritus of École Polytechnique Fédérale of Lausanne (EPFL), Switzerland. He first earned a degree in Agricultural Engineering and Master's Degrees in Hydrology and Statistics and went on to obtain a PhD in Soil Physics. He then conducted several WMO hydrological projects in West Africa before returning to EPFL as full professor and chair holder in Agricultural Engineering, managing the Laboratory of Hydrology and Land Improvement as well as the Institute of Environment Science and Technology of EPFL. He also spent 5 years in Montreal as Director of Ouranos, a Quebec Consortium on regional climatology and adaptation to climate change. André Musy is recognized worldwide as an expert in hydrology and water resources management and in the field of adaptation to climate change.